Université de Montréal

Étude de complexes métalliques d^6 *à base de ligands tridentés N^N^N et de leurs processus photo-induits inusités*

par

Baptiste Laramée-Milette

Département de chimie

Faculté des arts et des sciences

Thèse présentée à la Faculté des études supérieures et postdoctorales
en vue de l'obtention du grade de Philosophiae Doctor (Ph.D.)

en chimie

08 Décembre 2017

© Baptiste Laramée-Milette, 2017

Résumé

Les trente dernières années ont vue l'apparition et l'évolution de la chimie supramoléculaire, une branche de la chimie permettant de faire le lien entre la chimie moléculaire traditionnelle et la chimie des composés macroscopiques. Le couronnement récent de pionniers de la chimie des supramolécules par le comité Nobel, Jean-Pierre Sauvage et James Fraser Stoddart, mais en évidence l'importance de ce domaine d'actualité.

Ce projet s'inscrit dans une démarche de recherche fondamentale visant à élaborer une antenne de chromophore capable d'absorber l'énergie solaire de façon optimale, et ce dans le but de la transférer à un centre réactionnel capable de convertir l'énergie lumineuse en énergie chimique. La méthodologie employée vise à exploiter divers processus photochimiques afin d'élaborer des architectures supramoléculaires discrètes et d'en étudier les propriétés optiques et électroniques.

Mots-clés : Auto-assemblage, chromophores, chimie de coordination, chimie inorganique

Abstract

The last thirty years have seen the emergence and evolution of supramolecular chemistry, a branch of chemistry that makes the link between traditional molecular chemistry and the chemistry of macroscopic compounds. The recent crowning of pioneers in supramolecular chemistry by the Nobel Committee, Jean-Pierre Sauvage and James Fraser Stoddart, but highlighting the importance of this news domain.

This project is part of a fundamental research approach aimed at developing a chromophore antenna capable of optimally absorbing solar energy, with the aim of transferring it to a reaction center capable of converting light energy into light. chemical energy. The methodology used aims at exploiting various photochemical processes in order to develop discrete supramolecular architectures and to study their optical and electronic properties.

Keywords : Self-assembly, chromophores, coordination chemistry, inorganic chemistry

Table des matières

Liste des tableaux

Liste des figures

Liste des chartes et des schémas

Liste des abréviations

Å	Angström
ADN	Acide désoxyribonucléique
ARN	Acide ribonucléique
a.u.	Arbitrary unit
BINAP	2,2'-bis(diphénylphosphino)-1,1'-binaphthyl
bpy	2,2'-bipyridine
^{tert}Bu	^{tert}butyl
Calc.	Calculated
Calcd	Calculated
CIF	Crystallographic information file
COF	Covalent organic framework
COSY	Homonuclear correlation spectroscopy
CPCM	Conductor-like polarizable continuum model
δ	Déplacement chimique
Δ	Chaleur
d	Doublet
dd	Doublet de doublet
DFT	Density functional theory
DCM	Dichloromethane
DMF	*N,N'*-Diméthylformamide
DMSO	Diméthylsulfoxide
DOSY	Diffusion-ordered spectroscopy
E	Énergie
e^-	Électron
equiv.	Équivalent
eq.	*cf.* Equiv.

ESI-MS	Electrospray ionization mass spectrometry
EtOH	Éthanol
f	Force d'oscillateur
fac-	Facial
Fc	Ferrocène
FS	Freely soluble
g	Gramme
GooF	Goodness of fit
GS	Ground state
H	Highest occupied molecular orbital
H-hpp	1,3,4,6,7,8-hexahydro-*2H*-pyrimido[1,2-α]pyrimidine
HOMO	Highest occupied molecular orbital
HR-MS	High-resolution mass spectrometry
I	Insoluble
ILCT	Intra-ligand charge transfer
IR	Infrarouge
ISC	Intersystem crossing
J	Constante de couplage
kJ	Kilojoule
λ_{ex}	Longueur d'onde d'excitation
λ_{em}	Longueur d'onde d'émission
λ_{max}	Longueur d'onde d'absorption/d'émission maximale
L	Lowest unoccupied molecular orbital
LANL2DZ	Los Alamos National Laboratory 2 double ζ
LC	Ligand-centered
LF	Ligand field state
LLCT	Ligand-to-ligand charge transfer
LMCT	Ligand-to-metal charge transfer
LUMO	Lowest unoccupied molecular orbital
m	multiplet

M	Metal
mg	Milligramme
MC	Metal-centered
Me	Méthyle
MeCN	Acétronitrile
mer-	Meridional
MLCT	Metal-to-ligand charge transfer
MO	Molecular orbital
MOF	Metal-organic framework
m/z	Ratio of mass to charge
NIR	Near infrared
nm	Nanomètre
ns	Nanoseconde
NMR	Nuclear magnetic resonance
Obs.	Observed
ORTEP	Oak Ridge thermal ellipsoid program
Ox.	Oxidation
PBE	Perdew-Burke-Ernzerhof
Ph	Phényle
phen	1,10-phénanthroline
ppm	Parties par million
PSI	Photosystème I
PSII	Photosystème II
py	Pyridine ou pyridyle
Red.	Reduction
r.t.	Room temperature
s	Singulet ou seconde
S	Soluble
Sps	Sparingly soluble
SS	Slightly soluble
SCE	Standard calomel electrode

t	Triplet
TBAP	Tetrabutylammonium hexafluorophosphate
TD-DFT	Time-dependent density functional theory
tpy	2,2':6',2"-terpyridine
UV	Ultraviolet
Vis	Visible
VS	Very soluble
VSS	Very slightly soluble
XRD	X-ray diffraction
Z	Nombre de molécule dans la maille élémentaire

Remerciements

J'aimerais tout d'abord remercier mon directeur de thèse, professeur Dr. Garry S. Hanan, pour m'avoir acceuilli au sein de son groupe de recherche. Je lui suis particulièrement reconnaissant pour le temps qu'il a investi dans ma formation académique ainsi que pour ses connaissances scientifiques et son professionnalisme. J'ai particulièrement apprécié d'avoir la liberté de travailler sur une panoplie de projets fantastiques.

Je veux également remercier chaleureusement les différents organismes subventionnaires, soit le Conseil de recherches en sciences naturelles et en génie (CRSNG), l'Université de Montréal ainsi que la Faculté des études supérieures et postdoctorales (FESP). Plus particulièrement, la Fondation Joseph-Armand Bombardier et Rosdev pour leur implication dans le financement des bourses d'excellences remises par la FESP.

Je me dois de remercier mes collègues de travail, ainsi que les différents groupes de recherches de l'Université de Montréal qui ont contribué d'une façon ou d'une autre à la réalisation de cette thèse. Plus spécifiquement, un grand merci aux membres actuel et passé du groupe Hanan : Thomas Auvray, Olivier Schott, Jessica Castro, Dr. Mihaela Cibian, Dr. Élodie Rousset, Dr. André Bessette, Dr. Amlan K. Pal et Dr. Daniel Chartrand. J'aimerais aussi remercier chaleureusement les groupes de recherche des professeurs Reber, Schaper, Skene et Zargarian.

Je veux également souligner la contribution des différents stagiaires que j'ai personnellement encadrer au cours de mes études, plus particulièrement Félix Lussier, Christophe Lachance-Brais, Samantha Tremblay et Sacha Nguyen.

Je souhaite remercier le personnel de soutien de l'Université de Montréal : Thierry Maris, Michel Simard et Francine Bélanger pour leur précieuse aide à l'acquisition des structures rayons X; Francine Bélanger et Elena Nadezhina du laboratoire d'analyse élémentaire; Antoine Hamel et Cédric Malveau du laboratoire de spectroscopie RMN; Denis Deschênes, Medgine Lindor-Ménard, Kevin Delorme des laboratoires d'enseignement ainsi que Jean-François Myre de l'atelier mécanique.

Un grand merci à tous nos collaborateurs au fil des ans, plus particulièrement aux Prof. Sebastiano Campagna, Prof. Nelsi Zaccheroni, Prof. Ilaria Ciofini, Prof. Benjamin Elias ainsi que Prof. Cécile Moucheron.

Finalement, j'aimerais remercier ma conjointe Sabrina Haslam ainsi que mes enfants Jules et Constance pour leur soutient indéfectible et leur support moral tout au long de mes études.

Chapitre 1 – Introduction

1.1. Processus photochimique

Tôt dans l'histoire contemporaine de la chimie, la photosynthèse fut reconnue comme un exemple de photochimie naturelle. Cependant, ce n'est qu'au détour des années soixante que la recherche fondamentale en photochimie s'est développée.[1] Plus particulièrement, la photochimie inorganique a connu son essor notamment grâce aux travaux de Balzani et Carassiti.[2]

La photochimie appartient à une branche particulière de la chimie s'intéressant à l'interaction entre la lumière et la matière. Ce domaine est régi par deux principes fondamentaux, qui stipulent que seule la lumière absorbée peut être à l'origine d'un processus photochimique (loi de Grotthus-Draper) et que chaque photon absorbé sera à l'origine d'un processus chimique (loi de Stark-Einstein).[3]

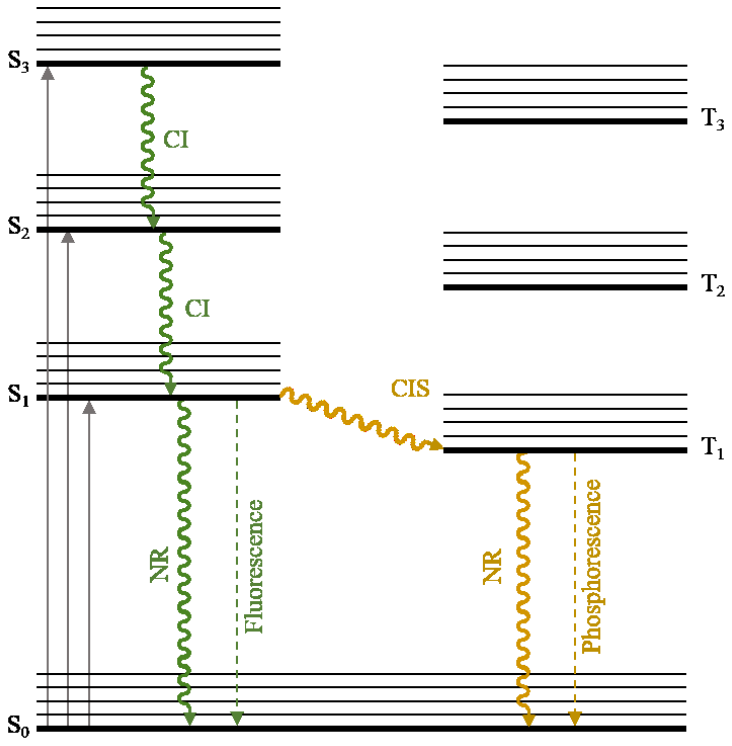

Figure 1.1 – Diagramme de Jablonski des modes de désactivation possible. CI= Conversion interne; CIS= Croisement intersystème; NR= Désactivation non-radiative.

Typiquement, tel que présenté à la Figure 1.1,[4] lorsqu'un chromophore (qu'il soit organique ou inorganique) absorbe une radiation d'une énergie spécifique, celui-ci sera promu de l'état fondamental (S) à l'état excité (S*) puis retournera à l'état fondamental via différents mécanismes. Il est important de spécifier que les propriétés de l'espèce à l'état excité sont fondamentalement différentes de son homologue à l'état fondamental, ce qui rend le domaine d'autant plus intéressant puisque la réactivité des espèces S et S* sera distincte. De façon générale, les processus de désactivation de l'état excité se différencient essentiellement par la nature radiative ou non radiative ainsi que par l'aspect intra- ou intermoléculaire de la désactivation vers l'état fondamental. Les principaux modes de désactivations sont représentés à la Figure 1.2 et certain de ces processus seront discutés en détail dans les sections à venir.[4]

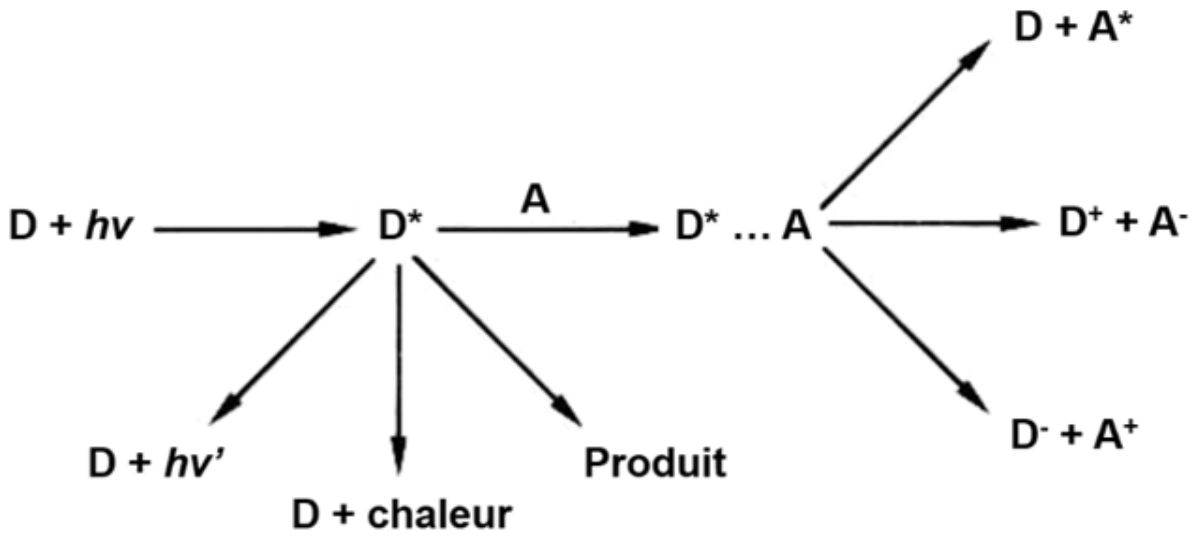

Figure 1.2 – Principaux modes de désactivation de l'état excité. D = Donneur; A = Accepteur.

1.1.1. Photosynthèse naturelle et artificielle

L'utilisation de la lumière à des fins synthétiques est un concept que la nature a développé et perfectionné au cours du temps afin de mettre au point divers mécanismes et procédés chimiques essentiels à la vie. L'exemple le plus connu de photochimie

naturelle est certainement le processus de photosynthèse mis à profit par les plantes et certaines bactéries afin de convertir l'énergie solaire et l'emmagasiner sous forme de sucres (Figure 1.3).

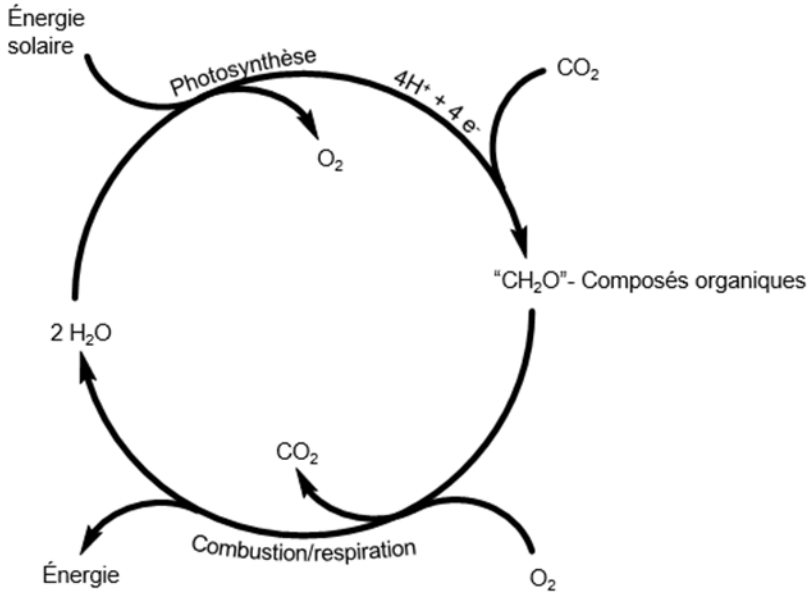

Figure 1.3 – Cycle schématique des processus impliqués dans la photosynthèse naturelle.[5]

L'antenne de chromophores utilisée par la nature est particulièrement intéressante. Tel que le démontre la structure à la Figure 1.4, chez Rhodospirillum molischianum, le complexe récolteur d'énergie est constitué de deux sections distinctes de chromophores métalliques de type porphyriniques: la partie externe (en vert) est constituée de 8 unités où la distance Mg-Mg est d'environ 22 Å tandis que la partie centrale (en rouge) est

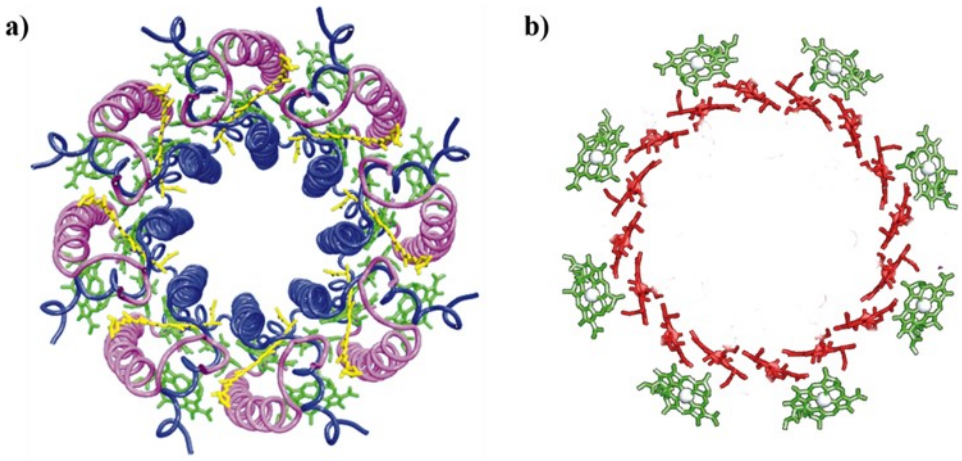

Figure 1.4 – Structure cristalline du complexe récolteur d'énergie de type II de Rhodospirillum molischianum.[7]

constituée d'un assemblage de 8 dimères de porphyrines où la distance entre les centres métalliques est d'en moyenne 9 Å. Cet assemblage cyclique illustre de façon remarquable l'habilité de la nature à manipuler la liaison non covalente (i.e. ponts hydrogènes et chimie de coordination) afin d'ériger des architectures supramoléculaires fonctionnelles complexes. Il est intéressant de se questionner sur la pertinence d'utiliser un système cyclique et l'effet sur l'efficacité du transfert électronique intra- et intermoléculaire.

L'étude des processus photo-induits à l'intérieur de systèmes supramoléculaires est donc cruciale afin de mieux comprendre les processus photochimiques naturels afin de pouvoir transposer efficacement ces propriétés aux systèmes artificiels (Figure 1.5).

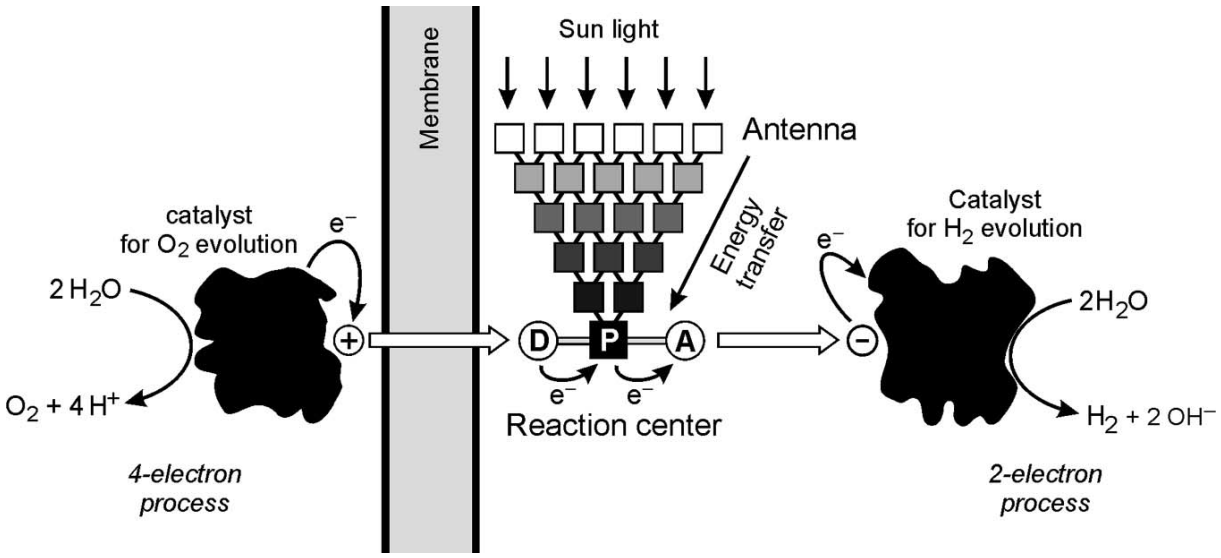

Figure 1.5 – Schéma d'un système photosynthétique artificiel.[8]

Le développement d'un système synthétique tel que proposé par Balzani *et al*. vise à imiter la fonction de la photosynthèse naturelle, c'est-à-dire la conversion de l'énergie solaire en énergie chimique.[8] Afin de simplifier la problématique reliée à l'élaboration d'un système complet, la recherche actuelle se concentre plutôt sur l'étude indépendante des demi-réactions, soit l'oxydation de l'eau et la réduction de protons en dihydrogène. Tout comme dans le modèle naturel, la première étape consiste en l'absorption de photons par une antenne de chromophore pouvant ensuite permettre le transfert efficace de l'énergie vers un centre réactionnel, soit un catalyseur, qui sera en mesure de transformer et de stocker cette énergie par la formation de liaison chimique.

Tel que décrit par Campagna *et al.*,[9] le design et l'architecture des chromophores entrants dans la composition de l'antenne doit être pensée de sorte à répondre à trois critères clés soit :

- L'espèce doit être chimiquement stable à l'état fondamental et à l'état excité
- Le chromophore choisi doit être panchromatique, c'est-à-dire pouvoir absorber une grande proportion de la radiation solaire, particulièrement dans le visible et le proche infra-rouge.
- Posséder un temps de vie de l'état excité suffisamment long pour pouvoir transférer de façon efficace l'énergie jusqu'au centre réactionnel.

En ce sens, la chimie supramoléculaire[10] et la maîtrise des interactions moléculaires plus faibles que la liaison covalente (60-100 kcal/mole)[11] est une avenue de recherche des plus pertinentes, puisqu'elle permet l'étude de composés de diverses morphologies (espèces discrètes *vs* polymères; mono- *vs* hétérométallique; mono-, bi- ou tridimensionnelle) afin d'optimiser les propriétés recherchées. Comme nous l'avons vu précédemment, la nature a adopté une approche selon laquelle une seule unité se répète de façon à former un assemblage discret. Alors que plusieurs études se sont penchées sur l'avantage de cet arrangement cyclique sur le plan de l'efficacité du transfert énergétique,[12] une question demeure : Comment la nature fait elle pour procéder à l'auto-correction nécessaire à l'assemblage de tel macrocycle ?

1.1.2. Auto-assemblage de métallacycles

Par définition, l'autoassemblage est un procédé dynamique menant à l'organisation sélective et spontanée d'une unité chimique structurée.[13] Ce phénomène est régi par plusieurs facteurs structuraux, tel que le type et le nombre de ligands, les angles de coordination, le choix du métal, etc., ainsi que par des facteurs thermodynamiques, où l'occupation maximale des sites de coordinations et l'entropie du système doivent être considérés. Plusieurs stratégies ont été mises au point afin de générer des structures macrocycliques auto-assemblées,[14] mais l'approche directionnelle (aussi nommée approche [n + n]) élaborée et popularisée par Fujita et Stang respectivement,[15] est sans conteste la technique la plus populaire (Figure 1.6).

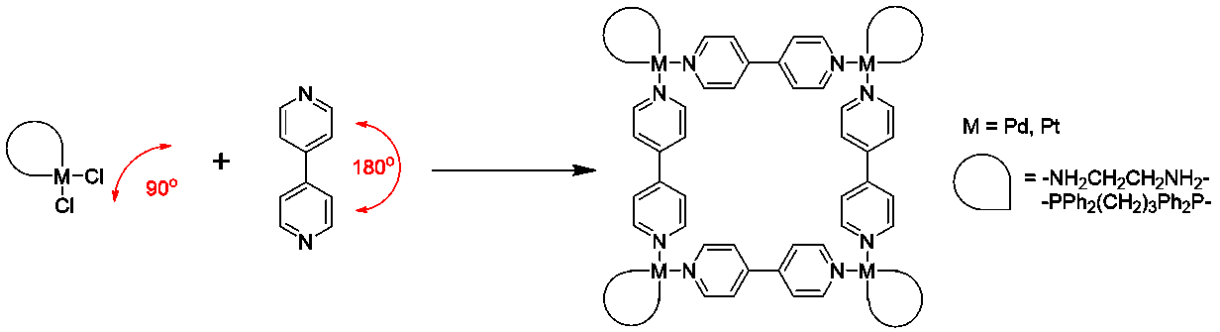

Figure 1.6 – Exemple de l'approche directionnelle de type [n + n].

Cette méthode prend avantage de la rigidité du ligand et des angles de coordination intrinsèques aux métaux et aux ligands choisis pour obtenir une espèce unique assemblée. L'application des principes de la chimie combinatoire à cette technique de synthèse permet de mener rapidement à une vaste librairie de polygones et polyèdres moléculaires.[14c]

1.1.3. Synthèse par coordination dirigée de type [n x 1]

Alors que la littérature abonde d'exemples d'assemblages obtenus grâce à la méthode de type [n + n], l'approche de type [n x 1], plus fréquemment appelée autoassemblage de type tête-à-queue, est moins répandue. Cette technique, employé autant en chimie organométallique qu'en chimie de coordination, diffère du fait que le donneur organique et l'accepteur métallique sont généralement situés sur la même entité chimique. Le précurseur réagit donc avec lui-même afin de mener à l'espèce thermodynamique la plus favorable, soit l'autoassemblage d'une espèce macrocyclique. Cette approche a notamment été popularisée par Pecoraro *et al.* à partir du début des années 1990 afin de former des dérivés des éthers couronnes, agissant comme récepteur pour différents cations métalliques (Figure 1.7).[16]

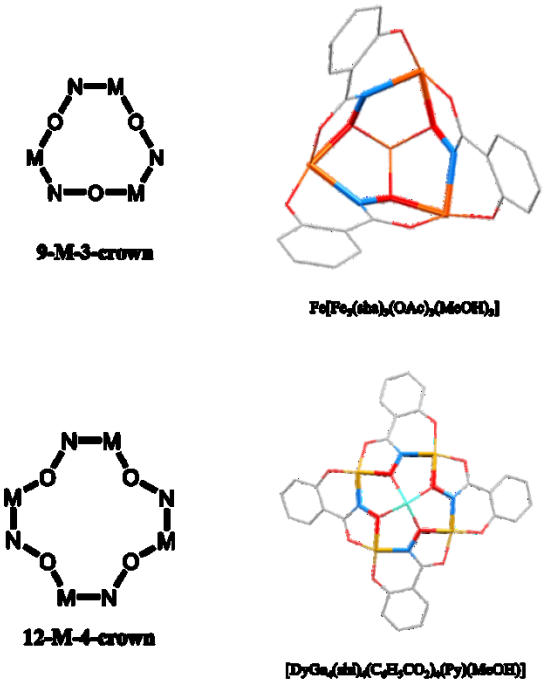

Figure 1.7 – Exemple des dérivés d'éther-couronnes obtenus par l'approche de type tête-à-queue.[16a, i]

À partir du milieu des années 1990, plusieurs auteurs ont contribué au domaine en mettant l'emphase sur des composés organométalliques de type demi-sandwich.

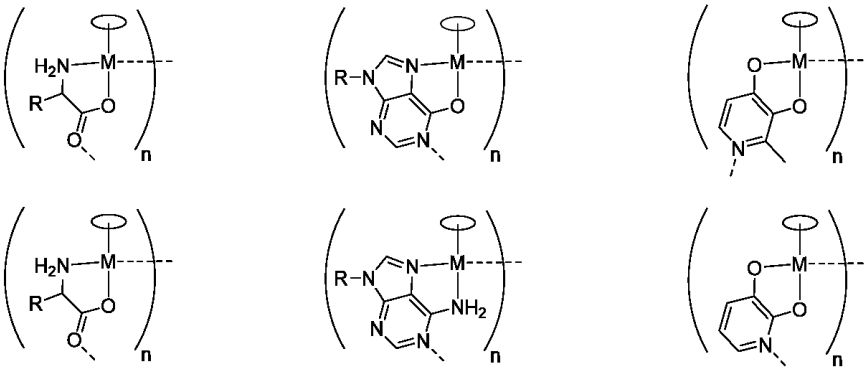

Joó *et al.*: M = Ru, Ir, Rh [12m, 20] Beck *et al.*: M = Rh[17] | Fish *et al.*: M = Rh [18] Sheldrick *et al.*: M = Ru, Ir [19] | Severin *et al.*: M = Ru, Ir [21]

Figure 1.8 – Dérivés organométalliques de type demi-sandwich menant aux assemblages de type tête-à-queue.

Beck *et al.*,[17] Fish *et al.*,[18] Sheldrick *et al.*[19] et Joó *et al*.[12m, 20] ont principalement travaillé avec des complexes métalliques à base de ligands biologiques (base azotée/nucléotide/nucléoside, acide aminé, etc.) tandis que Severin *et al.*[21] et quelques autres ont utilisé des ligands de type di-oxo (Figure 1.8).[22] Ce n'est qu'au milieu des années 2000 que les premières architectures moléculaires de type [n x 1] intégrant des ligands de type polypyridyle furent introduites, notamment par Loeb,[23] Sauvage[24] et Newkome[25] (Figure 1.9). Malheureusement, il n'existe que très peu d'informations concernant la synergie de tels systèmes et l'effet sur les propriétés optiques et électroniques.

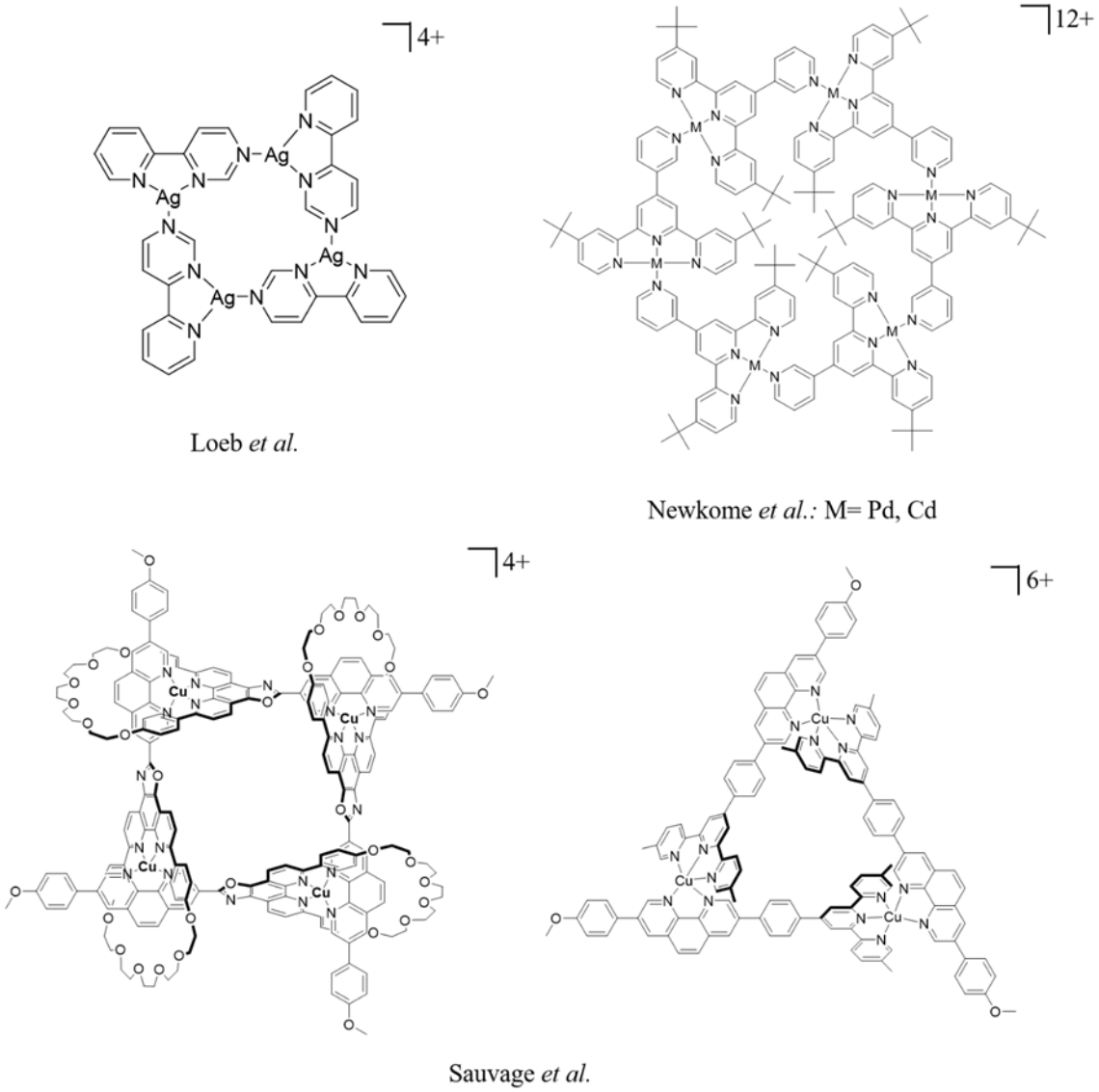

Figure 1.9 – Assemblage de coordination cyclique de type [n x 1]

1.2. Complexes métalliques de type polypyridine

La chimie des composés de type polypyridine, plus particulièrement ceux à base de 2,2'-bipyridine (bpy) et de 2,2':6',2"-terpyridine (tpy), a connu un essor fulgurant à partir du début des années 1990. L'intérêt pour ce type de composés est facile à comprendre : ces complexes métalliques sont généralement stables aux conditions

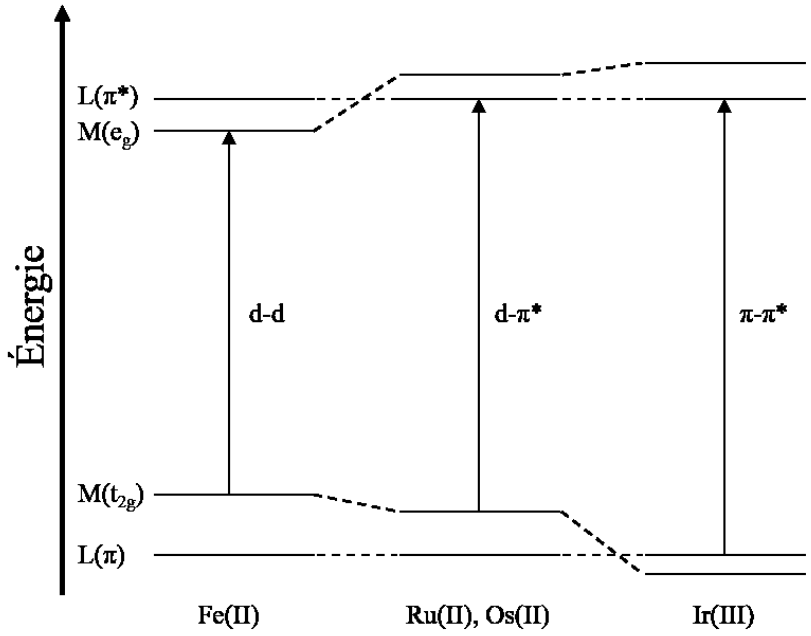

Figure 1.10 – Schéma de la disposition relatives des orbitales atomiques de complexes d6 de type [M(L^L)3]n+.[26]

ambiantes (air/eau), les ligands sont aisément modifiables et peuvent se coordonner à un vaste choix d'éléments chimiques du tableau périodique.[26] Ce faisant, suivant les principes de chimie combinatoire, le chimiste peut à loisir modifier finement les propriétés optiques et électroniques des complexes métalliques par différentes voies (par exemple en changeant l'ion métallique, voir Figure 1.10), selon les domaines d'applications désirés. Évidemment, certains métaux ont rapidement été ciblé (i.e. le ruthénium, le rhénium, l'iridium, etc.) et ce due aux propriétés optiques intéressantes de ce type de complexes métalliques.[27]

1.2.1. Ruthénium

La luminescence d'un rouge flamboyant des composés de type $[(bpy)_3Ru^{2+}][(X)_2]$ (où X représente un contre-anion, tel que PF_6^-, NO_3^-, BF_4^-, etc.) a rapidement popularisé l'utilisation du ruthénium en chimie de coordination. Le potentiel de ces complexes en photocatalyse,[28] photo-thérapie[29] ainsi que leur application dans les cellules photovoltaïques à colorants[30] et comme complexe récolteur d'énergie[31] est due aux propriétés optiques et électroniques intrinsèques de ces composés. Notamment, ceux-ci possèdent une absorption panchromatique s'étendant de l'ultraviolet jusqu'au domaine du visible (200-500 nm) ainsi qu'un état excité de longue durée de vie. Cependant, les complexes à base de bipyridines forment systématiquement des énantiomères Δ et Λ, ce qui peut être problématique lors de la préparation d'espèces polynucléaires due à la formation statistique de mélange d'isomères (i.e. un complexe binucléaire aura trois isomères, soit Δ-Δ, Δ-Λ et Λ-Λ). Le problème se complexifie davantage lorsqu'on considère le cas d'espèces hétéroleptiques ainsi que lorsque le ligand est substitué de façon non-symétrique (Figure 1.11).

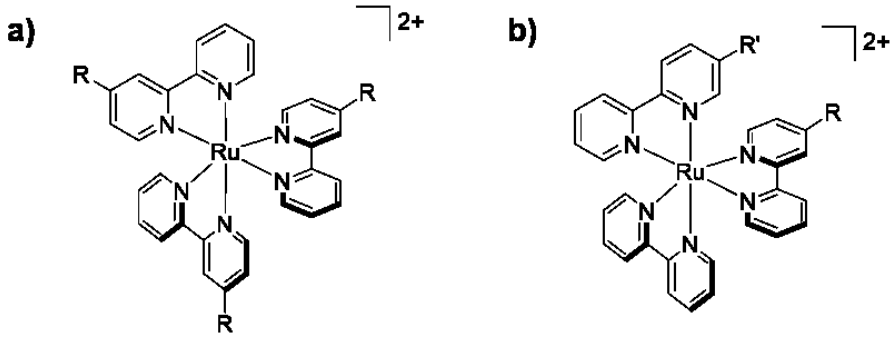

Figure 1.11 – Exemple d'un complexe de type $[Ru(N\hat{}N)_3]^{2+}$ a) homoleptique avec des ligands non-symétriques et b) hétéroleptiques.

L'utilisation des ligands tridentés de type 2,2' :6',2"-terpyridine élimine le problème de chiralité due à la présence d'un élément de symétrie C_2, à condition que le ligand soit symétrique. Cependant, les complexes de type $[(tpy)_2Ru^{2+}][(X)_2]$ sont quant

à eux très faiblement luminescent ($\Phi_{bpy} \approx 6x10^{-2}$ *vs* $\Phi_{tpy} \approx 1x10^{-6}$).[32] Cette particularité est liée principalement au recouvrement orbitalaire moins efficace entre le métal et le ligand, due notamment à la déformation de la géométrie octaédrique autour de l'ion métallique induite par le ligand. À titre d'exemple comparatif, tel que présenté à la Figure 1.12, l'angle de chélation est d'environ 159° dans le cas des complexes $[(tpy)_2Ru]^{2+}$ et de 172° pour les complexes $[(bpy)_2Ru]^{2+}$.[26]

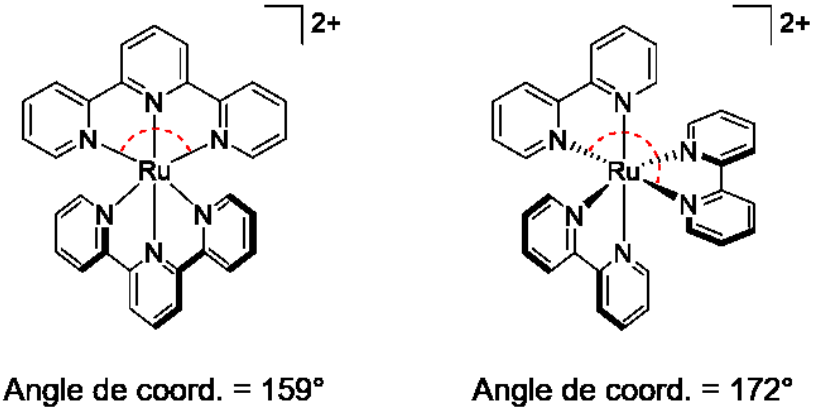

Figure 1.12 – Comparaison des angles de chélation entre les complexes de type $Ru(tpy)_2^{2+}$ et $Ru(bpy)_3^{2+}$.

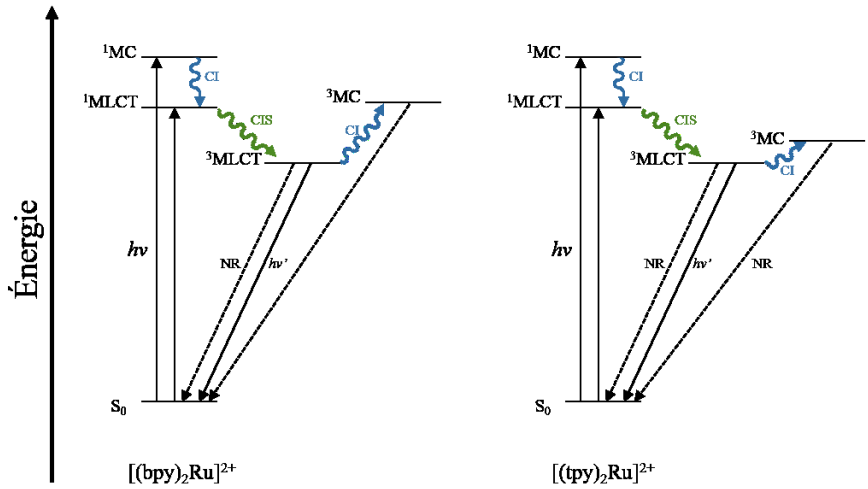

Figure 1.13 – Comparaison du niveau énergétique ^3MC entre les complexes de Ru(II) ayant des ligands bipyridines et terpyridines.

En outre, cette déformation affecte les niveaux énergétiques de l'état excité, tel que présenté à la Figure 1.13, rendant aisément possible la population thermique de l'état triplet centré sur le métal (^{3}MC) dans le cas des complexes à base de ligands terpyridine, menant à une désactivation non-radiative de l'état excité. Il existe néanmoins différentes approches afin de modifier les propriétés optiques de ces complexes, soit en stabilisant l'état ^{3}MLCT (i.e. par l'ajout de groupement électroattracteurs) ou en déstabilisant l'état ^{3}MC (i.e. par la modification de l'angle de coordination vers l'octaèdre parfait et/ou par l'introduction de groupement σ-donneur).[33]

1.2.2. Rhénium

Depuis leur première apparition au cours des années 1970, la chimie des composés de Re(I) polypyridines a abondamment été étudié en raison de leur luminescence à température ambiante. Plus particulièrement, les complexes de type *fac*-[(N^N)$Re^+(CO)_3$L] (où N^N représente l'utilisation d'un ligand bidenté diimine et L est soit un halogénure ou un ligand monodenté neutre) ont suscité l'intérêt de la communauté scientifique pour leurs applications dans une variété de domaine d'intérêts (i.e. photosensibilisateur, photocatalyse, diode électroluminescente, senseur chimique, etc.).[34] Ces complexes sont généralement caractérisés par une absorption intense dans le visible, s'étendant entre 350-450 nm et d'une luminescence dont la longueur d'onde et le temps de vie de l'état excité dépendent essentiellement du ligand (e.i. 50 ns pour 2,2'-bpy *vs* 290 ns pour 1,10-phen), de ses substituants (déplacement bathochromique par l'ajout de groupement électrodonneur) et du solvant dans lequel les composés sont étudiés (polaire *vs* non-polaire).[35] L'utilisation de ligands polypyridines tridentés est beaucoup moins répandue et n'a fait l'objet que d'une poignée d'études. Trois classes de complexes ont majoritairement été étudiées, tel que présenté à la Figure 1.14.

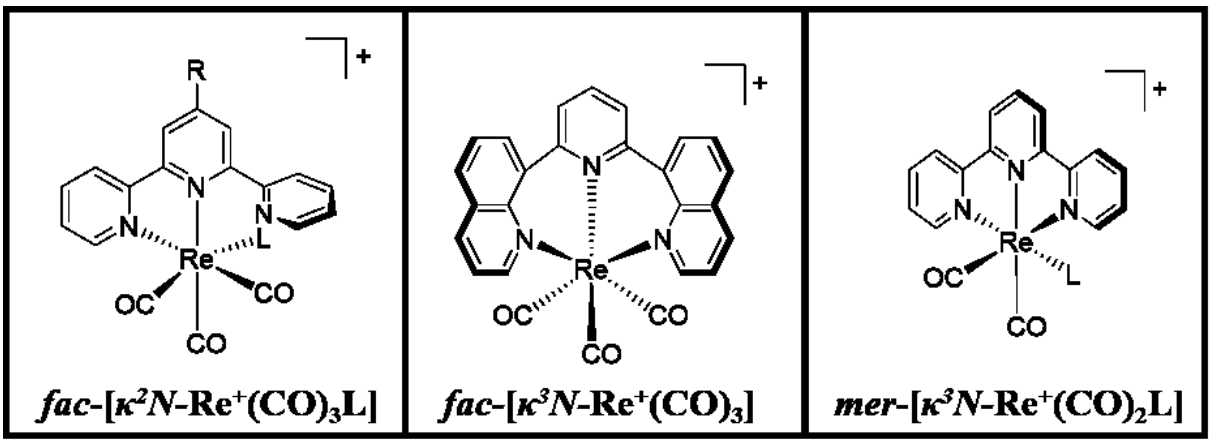

Figure 1.14 – Représentation des trois grandes classes de composés tridentés de rhénium à base de ligands polypyridines.

Les premières études sur les complexes de type *fac*-[κ^2N-$Re^+(CO)_3L$] remontent au début des années 1990 et portent principalement sur le mécanisme de la fluxionnalité du ligand terpyridine en solution, tel qu'illustré à la Figure 1.15.[36]

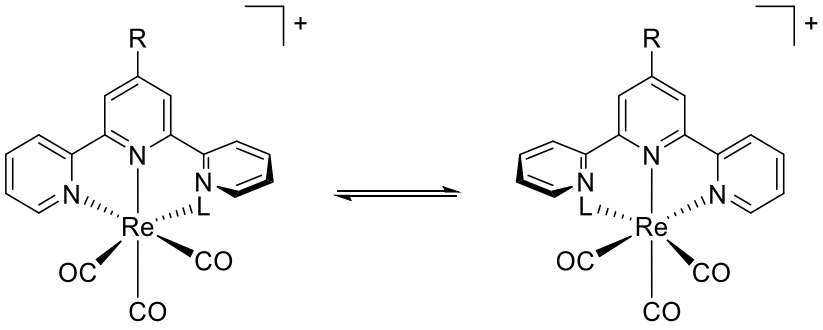

Figure 1.15 – Représentation de la fluxionnalité observée dans les complexes de type $[Re(N\text{^}N)(CO)_3L]^+$.

Les complexes de type *fac*-[κ^3N-$Re^+(CO)_3$] quant à eux ne sont apparus qu'au milieu des années 2000 et nécessitent l'utilisation d'un ligand flexible afin d'adopter la géométrie faciale.[37] Les propriétés optiques et électroniques de quelques complexes ont

été évaluées (Figure 1.16), où par exemple l'utilisation de ligands dérivés des 2-quinoline démontrent des temps de vie de l'état excité de l'ordre de plusieurs microsecondes à température ambiante.[37b] Cependant, il est difficile d'attribuer l'amélioration des propriétés optiques à la géométrie octaédrique, comme dans le cas des complexes de ruthénium, puisque d'autres complexes possédant une géométrie proche de l'octaèdre présentent des temps de vie allant de 3 à 10 ns seulement,[37h, 37i] indiquant que l'origine de la transition électronique impliquée pourrait être responsable des différences marquées entre les quelques complexes de type *fac*-[κ^3N-$Re^+(CO)_3$] étudiés jusqu'à présent (e.i. transition centrée sur les ligands *vs* transfert de charge métal-ligand) et pourrait même impliquer des processus atypiques dans certain cas, tel que la fluorescence différée activée thermiquement (de l'anglais : Thermally Activated Delayed Fluorescence, TADF).

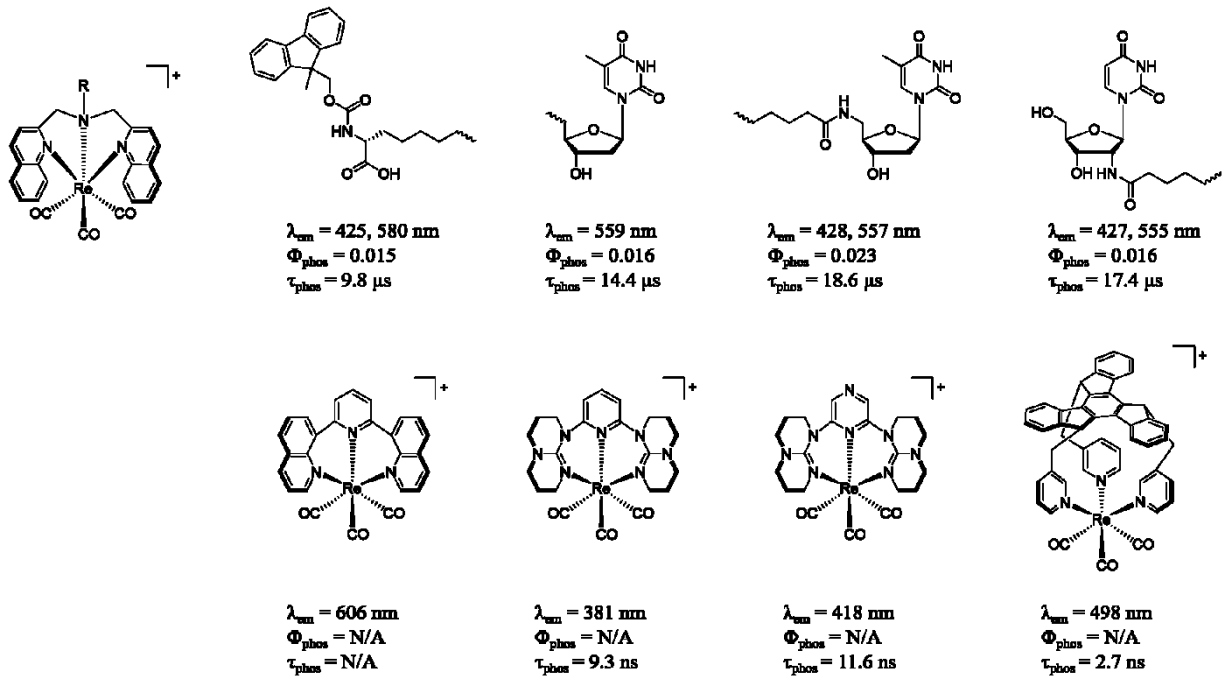

Figure 1.16 – Différents exemples de complexes de type *fac*-[κ^3N-$Re^+(CO)_3$] et leurs propriétés de luminescence.

Finalement, ce n'est que tout récemment que la chimie des complexes de type *mer*-[κ^3N-$Re^+(CO)_2L$] s'est développée, notamment grâce au travail de Hightower *et al*.[38] Les propriétés de ces complexes sont étonnantes. Tout d'abord, l'absorption des complexes de type κ^3N- couvre l'ensemble du visible, s'étendant de l'ultra-violet jusqu'au proche infrarouge (200-800 nm). Comparativement, leurs homologues de type κ^2N- n'absorbent qu'entre 200-450 nm. Les propriétés de luminescence des complexes κ^3N- sont aussi surprenantes : selon les données de la littérature, il semble que ces complexes ne soient pas émissifs à température ambiante. Toutefois, lorsqu'analysé à 77K, la luminescence fût observée à très haute énergie (400-530 nm, selon la source), ce qui à priori contrevient à la règle de Kasha.

1.2.3. Photochimie des complexes de Ru(II) et Re(I)

Comme il a été mentionné précédemment, l'absorption d'un photon par un chromophore mène à un état excité qui doit éventuellement retourner à un état fondamental. La désactivation de l'état excité peut se faire par deux voies distinctes, soit par désactivation radiative et par désactivation non-radiative (Figure 1.17). Il est important de préciser que ces processus de relaxation vers l'état fondamental sont en compétition et qu'ils ne sont pas exclusifs, c'est-à-dire que les deux procédés peuvent être observés de façon simultanée. Alors que la relaxation par voie radiative permet de retourner à l'état fondamental de l'espèce initiale, le sort de l'espèce relaxant *via* la voie non-radiative est incertain, où la distorsion de la structure originale est telle qu'il est possible d'arriver soit à l'espèce initiale, soit à une nouvelle espèce et ce par photosubstitution ou par photoisomérisation.

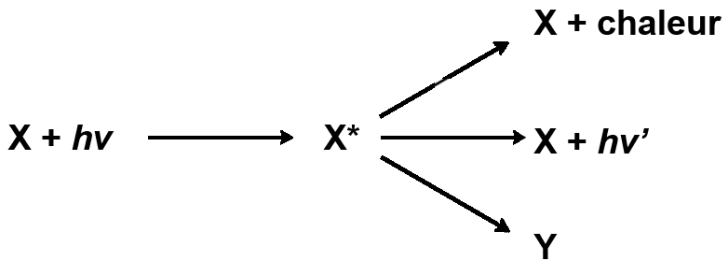

Figure 1.17 – Schéma des processus de désactivation possibles suite à l'absorption d'une onde électromagnétique.

La désactivation de l'état excité peut aussi être possible par l'interaction avec une seconde entité chimique et ce par voies intra- ou intermoléculaire. Deux types majeurs de désactivation sont rencontré, soit le transfert d'électron et le transfert d'énergie (Figure 1.18).

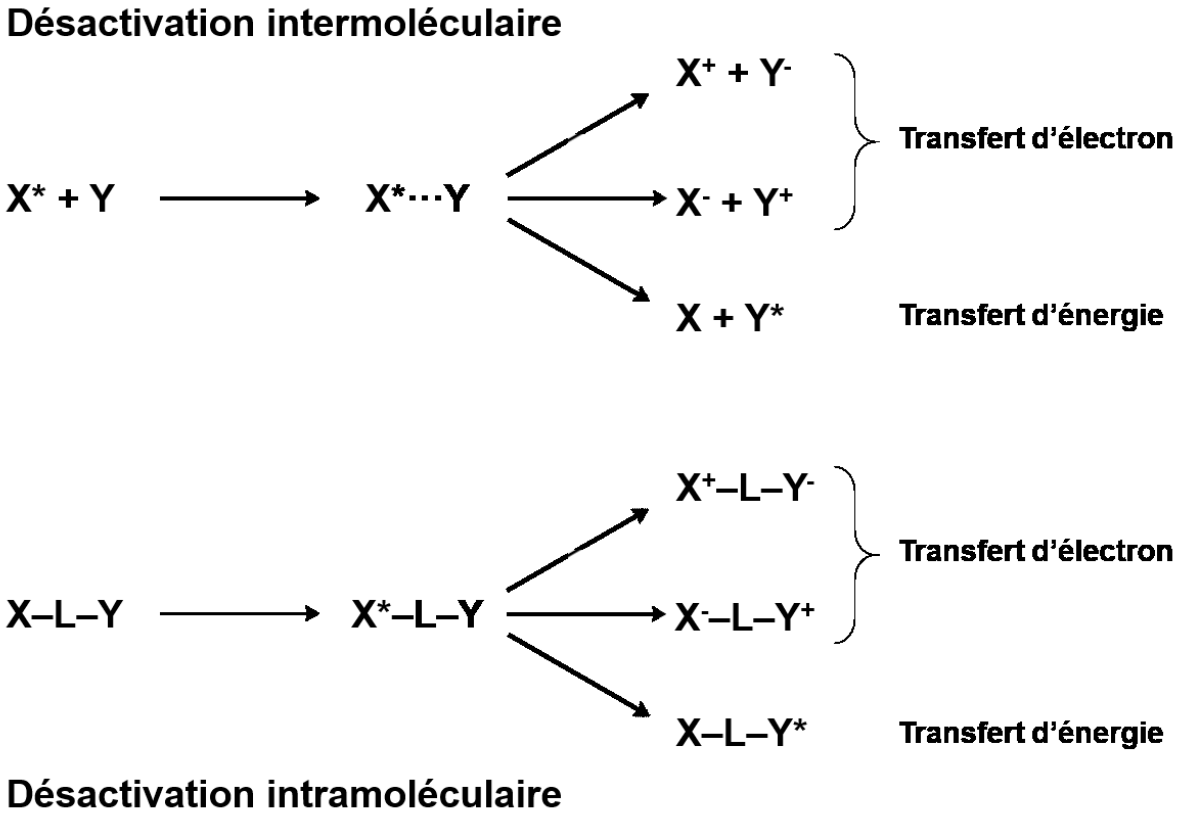

Figure 1.18 – Représentation schématique de la désactivation moléculaire par transfert électronique et transfert d'énergie.

1.2.3.1. Photosubstitution de ligands des complexes polypyridines de ruthénium

Dès le milieu des années 1970, plusieurs groupes de recherches présentèrent des études portant principalement sur la photo-réactivité des complexes de type $[(bpy)_3Ru^{2+}][(X^-)_2]$.[39] Notamment, van Houten et Watts étudièrent la dépendance du taux de la photosubstitution en fonction de la température en milieu aqueux.[40] Ils arrivèrent à la conclusion qu'en augmentant la température, le taux de désactivation de l'état excité via un mécanisme non-radiatif par population thermique de l'état excité ^{3}MC est favorisé, promouvant une photolyse adéquate. À l'opposé, à basse température l'état ^{3}MLCT est majoritairement populé et puisque cet état est photo-inerte, seulement une désactivation radiative est observée. L'étude de la photosubstitution de ligand en présence de différents solvants fût initié par Gleria *et al.*,[41] tandis que l'effet du contre-anion fût dévoilé par Hoggard et Porter,[42] suivi par d'autres groupes au courant des années 1980. La photo-réactivité de d'autres dérivés de la 2,2'-bipyridine (i.e. bipyrazine (bpz), biquinoline (bqn), etc.) furent étudiés par la suite, mettant également l'emphase sur l'effet de l'utilisation de complexes hétéroleptiques.[43] Plus récemment, l'effet stérique du ligand bidenté fût investigué, notamment par Sauvage *et al*. à la fin des années 1990.[44]

Les études sur la photochimie des complexes ayant des ligands de plus hautes denticité sont beaucoup plus rares et leur première apparition dans la littérature remonte seulement à la fin des années 1980.[45] Walsh *et al.* étudièrent la photo-réactivité des complexes de type $[(tpy)(L)_3Ru^{2+}][(X^-)_2]$ et $[(tpy)(L)_2(X)Ru^{2+}][X^-]$ en présence d'ion chlorure et/ou en présence d'un solvant coordinant (i.e. MeCN, pyridine, etc.), tandis que McMillin *et al.* mirent en évidence la photo-conversion quantitative de $[(tpy)(bpy)(MeCN)Ru^{2+}][(X^-)_2]$ en $[(tpy)(bpy)(py)Ru^{2+}][(X^-)_2]$.[46] Ce n'est d'ailleurs que tout récemment que Turro *et al.* étudièrent à nouveau ce type système, en mettant l'emphase particulièrement sur l'encombrement stérique du ligand bidenté et son effet sur le rendement quantique de la photoéjection du ligand monodenté.[29e, 47] Finalement, le groupe de Turro en collaboration avec Kodanko et Schlegel étudièrent également la photo-substitution de ligand en utilisant des complexes de coordination de ruthénium ayant des ligands tétradentates.[48]

L'intérêt de la photo-substitution de ligand a évidemment une portée synthétique non-négligeable, donnant l'opportunité de procédé à des modifications chimiques qui seraient beaucoup plus ardues, voire impossible via une voie purement thermique (tel que l'expulsion d'un groupement de type 2,2'-bipyridine). Il est également possible d'imaginer le potentiel de cette réactivité de l'état excité dans le domaine de la photo-thérapie, où il serait possible d'éjecter un composé thérapeutique à un endroit cibler simplement en irradiant l'endroit visé pour le traitement, sans affecter les organes sains.[49]

1.2.4.1. Photosubstitution de ligands des complexes polypyridines de rhénium

La photosubstitution de ligand des composés de rhénium est un domaine relativement jeune dont les intérêts de recherches actuel porte principalement sur l'aspect synthétique (molécule atteignable par voie photo-chimique uniquement)[50] ainsi que sur la portée thérapeutique potentielle des photoCORMs (de l'anglais photo CO releasing molecules).

La première étude sur le sujet remonte à 1991 où Pac *et al.* décrivirent dans une brève communication scientifique la photo-conversion du composé *fac*-[(2,2'-bpy)$Re^{+}(CO)_3Br$] en *cis,trans*-[(2,2'-bpy)$Re^{+}(CO)_2(P(OR)_3)_2$] en présence de triéthylamine.[51] Cette photo-réaction est initiée par un transfert électronique du donneur (TEA dans ce cas) au complexe de rhénium à l'état excité, tel qu'en témoigne l'absence de réactivité si la lumière ou la triéthylamine est manquante (Figure 1.19).

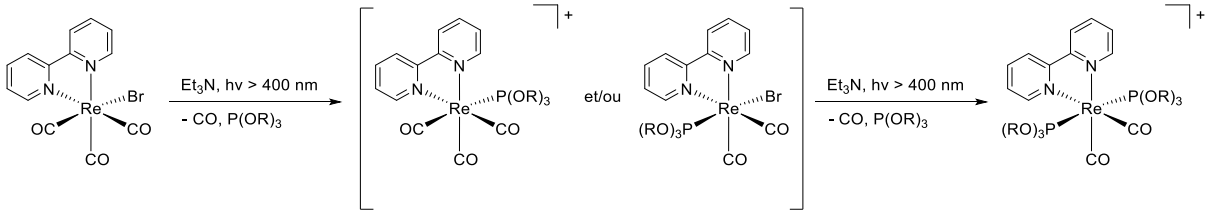

Figure 1.19 – Exemple de photo-conversion d'un composé de type (N^N)$Re(CO)_3X$.

Au début des années 2000, Ishitani proposa une voie de synthèse similaire des composés de type *cis,trans*-[(2,2'-bpy)$Re^{+}(CO)_2(PR_3)_2$] et *cis,trans*-[(2,2'-bpy)$Re^{+}(CO)_2(PR_3)(L)$], où L représente un ligand monodentate neutre ou anionique.[52] L'intérêt de cette

approche décrite en détail par Ishitani est qu'elle permet la formation d'espèces asymétriques, offrant ainsi la possibilité de modifier finement les propriétés optiques et électroniques selon les ligands utilisés. Selon le modèle proposé et illustré à la Figure 1.20, la réaction opère *via* un mécanisme dissociatif, dont la première étape consiste au passage de l'état fondamental à l'état excité, suivie d'un croisement intersystème de l'état ^{1}MLCT vers l'état ^{3}MLCT. S'ensuit une population thermique de l'état ^{3}MC (aussi dénomé ^{3}LF pour « Ligand Field »), menant à la photo-dissociation du ligand CO *trans* au ligand PR_3 exclusivement. Le site vacant est ensuite coordiné par le ligand libre en solution.

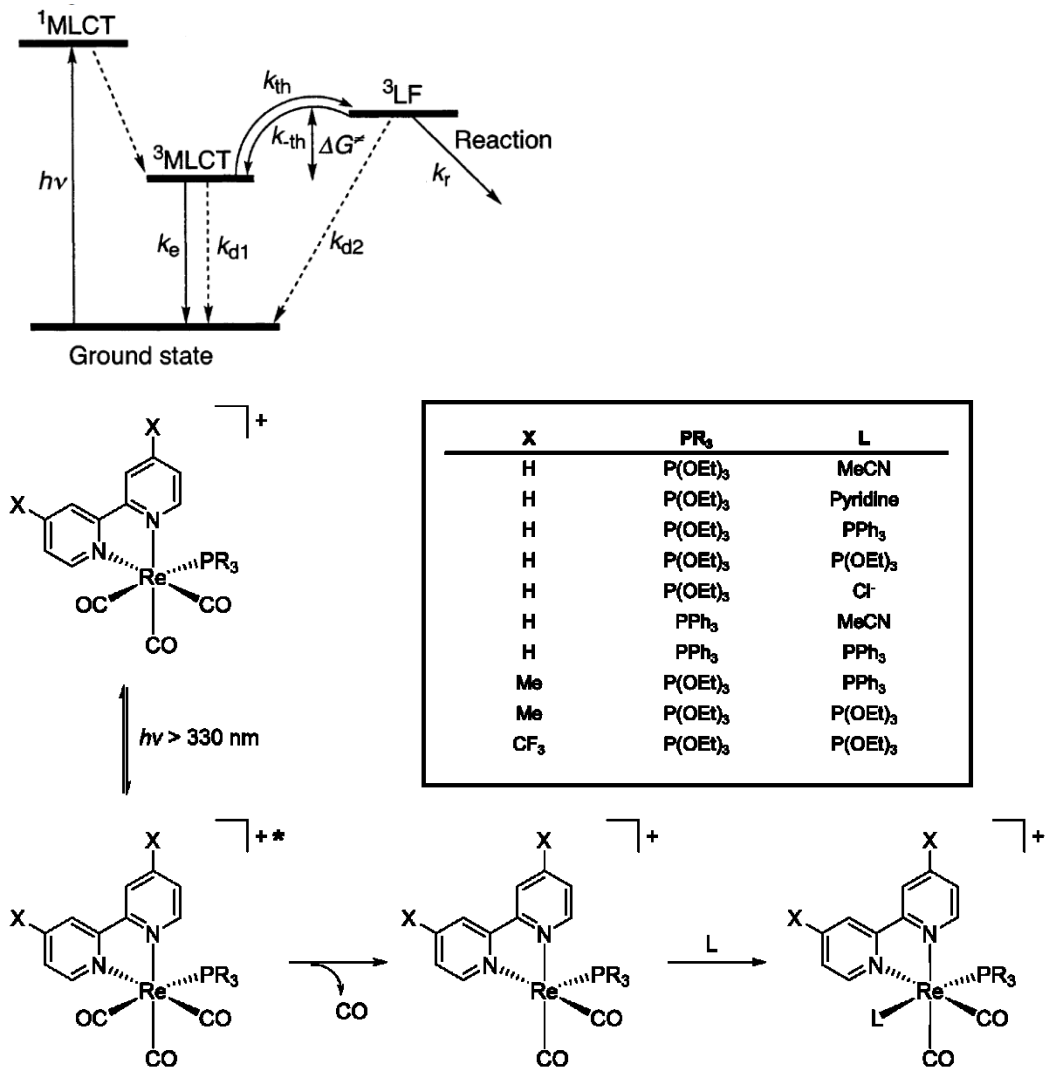

X	PR_3	L
H	$P(OEt)_3$	MeCN
H	$P(OEt)_3$	Pyridine
H	$P(OEt)_3$	PPh_3
H	$P(OEt)_3$	$P(OEt)_3$
H	$P(OEt)_3$	Cl^-
H	PPh_3	MeCN
H	PPh_3	PPh_3
Me	$P(OEt)_3$	PPh_3
Me	$P(OEt)_3$	$P(OEt)_3$
CF_3	$P(OEt)_3$	$P(OEt)_3$

Figure 1.20 – Mécanisme général impliqué lors de la photo-réaction des composés de type (N^N)Re(CO)$_3$X.

Une approche similaire développée par le même groupe permet également de travailler avec des complexes de rhénium plus commun, tel que présenté à la Figure 1.21. L'irradiation à haute énergie (*hv* = 313 nm) du précurseur *fac*-[(2,2'-bpy)$Re^{+}(CO)_3Cl$] mène à deux isomères, *trans*-[(2,2'-bpy)$Re^{+}(CO)_2(L)Cl$] et *cis*$_1$-[(2,2'-bpy)$Re^{+}(CO)_2(L)Cl$], où la dénomination *cis*/*trans* réfère à la position relative des ligands L et Cl.[53]

La formation de deux isomères est expliquée par deux mécanismes différents, en compétitions suite à la formation de l'état excité. Tout d'abord, l'isomère *cis*$_1$-[(2,2'-bpy)$Re^{+}(CO)_2(L)Cl$] est obtenu selon un mécanisme similaire à celui présenté précédemment, soit par population thermique de l'état ^{3}MC suivi d'une dissociation du ligand CO et d'une coordination d'un ligand (mécanisme dissociatif). Il est important de mentionner qu'une différence majeure survient dans ce mécanisme, soit le basculement du ligand chloro qui, selon les études DFT réalisées, survient après la dissociation du ligand carbonyle.

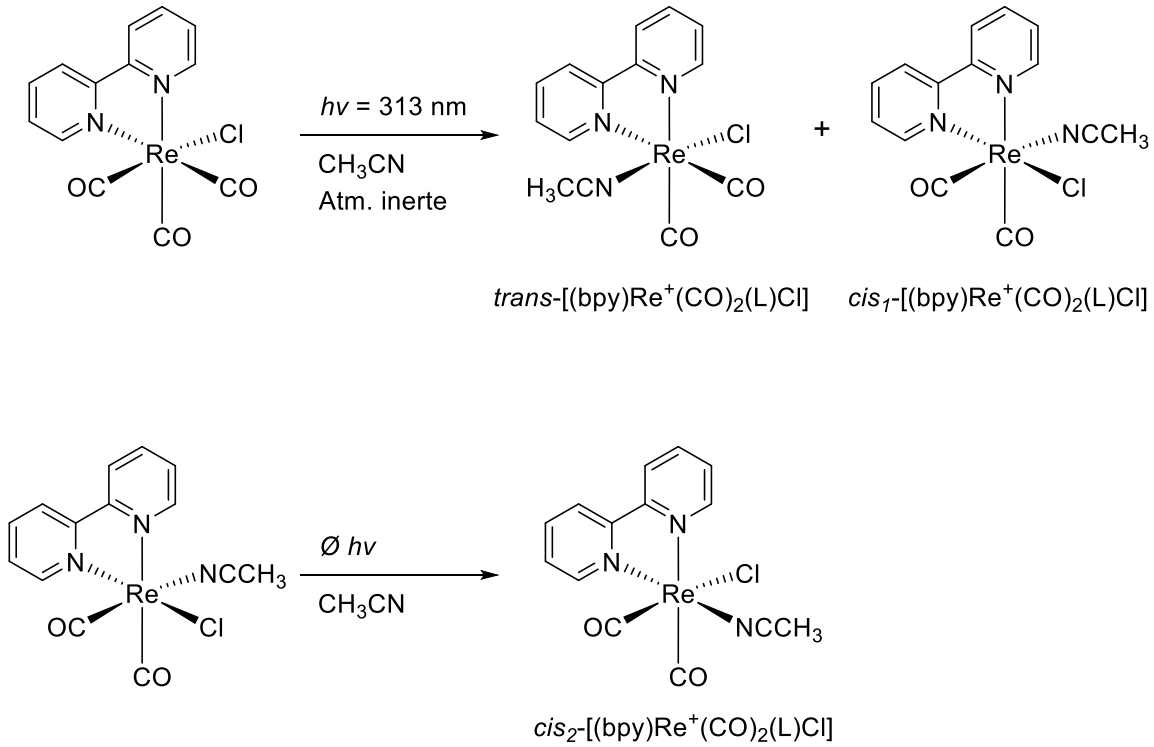

Figure 1.21 – Exemple de photo-conversion suivie d'une isomérisation.

L'origine de ce phénomène (stérique, électronique ou autre) n'est toutefois pas claire, mais pourrait être due à la géométrie adoptée de l'espèce pentacoordinnée, où le ligand bipyridine et l'atome de chlore sont pratiquement sur le même plan.[54] Il est également intéressant de noter que l'isomère *cis*$_1$- est instable à température ambiante où, même en l'absence de lumière, il s'isomérise en *cis*$_2$-[(2,2'-bpy)$Re^{+}(CO)_2$(L)Cl].

Finalement, selon les études réalisées par Ishitani, la formation de l'espèce *trans*- nécessite la population d'états vibrationnels de haute énergie (abrévié "HES" par les auteurs pour "higher excited state") accessibles seulement par l'utilisation d'une longueur d'onde d'irradiation < 330 nm. Une fois que l'états ^{1}HES est populé, une conversion intersystème vers un état ^{3}HES s'ensuit. Si un ligand (tel que l'acétonitrile) se trouve à proximité de la sphère de coordination du métal, un intermédiaire hepta-coordinné peut être formé selon un mécanisme associatif. Il s'ensuit l'éjection d'un ligand carbonyle et la formation de l'espèce *trans*.

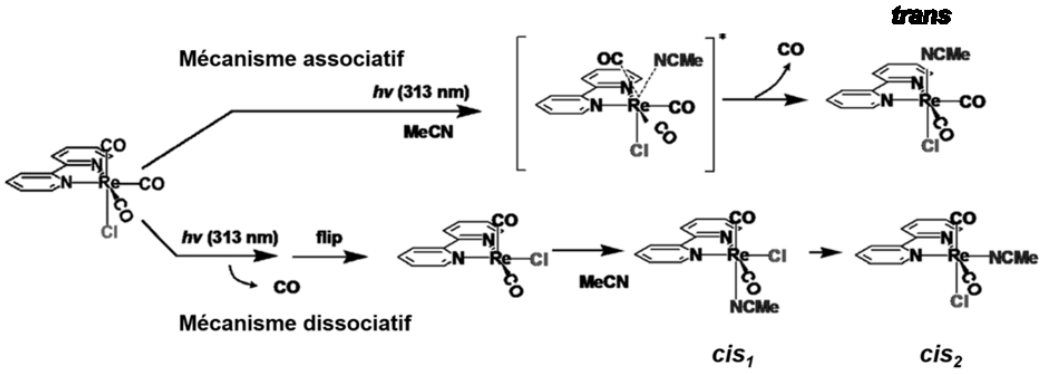

Figure 1.22 – Schématisation du mécanisme proposé par Ishitani explicant la formation de trois espèces différentes, suivant soit un mécanisme associatif ou dissociatif.[53]

1.2.3.2. Photo-isomérisation des complexes polypyridines de ruthénium

L'un des premiers exemples de photo-isomérisation de complexe de ruthénium polypyridyles fût rapporté par Meyer *et al.* au début des années 1980 (Figure 1.24), où l'irradiation du composé *cis*-[$(bpy)_2(H_2O)_2Ru^{2+}$] mena au composé *trans*-[$(bpy)_2(H_2O)_2Ru^{2+}$] et vice-versa.[55] Plus récemment, Rack *et al.* a mené plusieurs études concernant la photo-isomérisation de complexe de ruthénium ayant des ligands de type

sulfoxide capablent de former des isomères de liaison (Ru-S *vs* Ru-O).[56] Ces processus pourraient, en principe, être exploité en tant qu'interrupteur moléculaire.

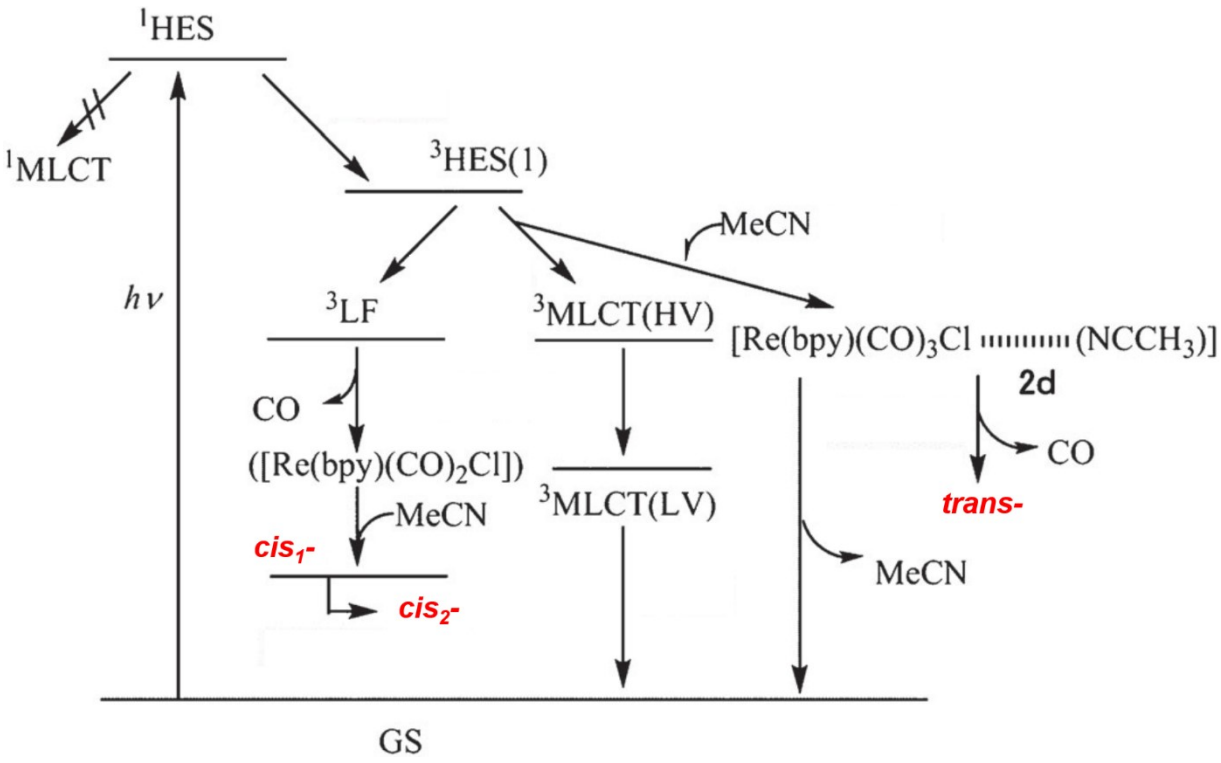

Figure 1.23 – Diagramme de Jablonski simplifié expliquant la formation simultanée des espèces *cis*$_1$-, *cis*$_2$- et *trans*-.

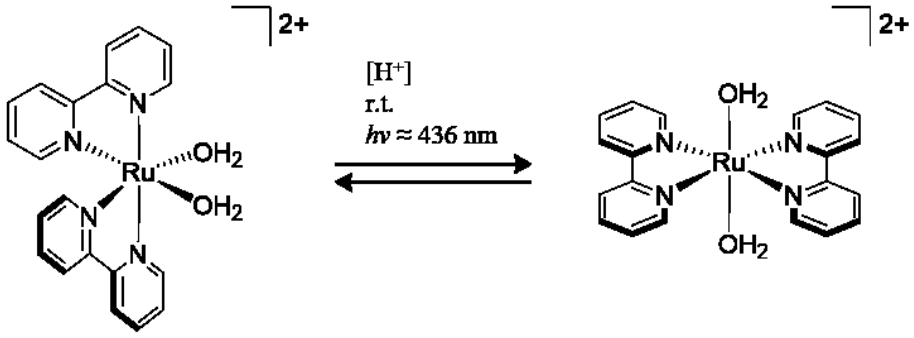

Figure 1.24 – Exemple de photo-isomérisation d'un complexe de ruthénium.

1.2.4.1. Photo-isomérisation des complexes polypyridines de rhénium

Relativement peu d'exemples de photo-isomérisation de complexes de rhénium ont été démontré jusqu'à présent (Figure 1.25). L'isomérisation du composé *fac*-[(bpy)$Re^{+}(CO)_3Cl$] en *mer*-[(bpy)$Re^{+}(CO)_3Cl$] s'effectue en irradiant un échantillon à température ambiante à l'aide d'une source lumineuse de haute énergie (313 nm) en maintenant une atmosphère de CO.[57] La photo-isomérisation s'effectue selon le mécanisme dissociatif décrit plus haut.

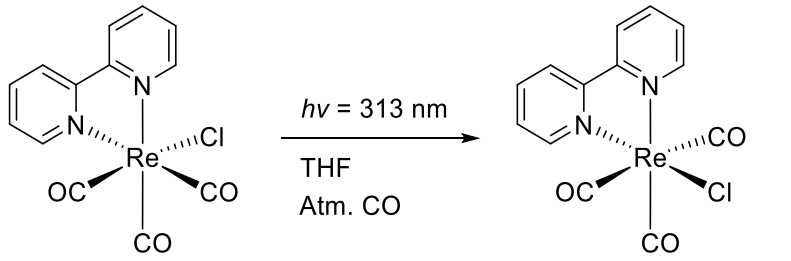

fac-[(bpy)$Re^{+}(CO)_3Cl$] *mer*-[(bpy)$Re^{+}(CO)_3Cl$]

Figure 1.25 – Exemple de photo-isomérisation d'un complexe de rhénium.

1.2.3.3. Transfer électronique

L'état excité des complexes de type $[Ru(N\hat{}N)_3]^{2+}$ et $[Re(N\hat{}N)(CO)_3L]^{+}$ a été particulièrement exploité en photocatalyse. L'exemple classique de l'utilisation des complexes de ruthénium est leur exploitation dans le cadre de la photosynthèse artificielle,[58] tel qu'illustré à la Figure 1.26, où la transformation rédox du photosensibilisateur en présence d'un catalyseur et d'un donneur sacrificiel peut s'effectuer par un mécanisme oxydatif et/ou un mécanisme réductif, selon le donneur sacrificiel utilisé. Plus récemment, suivant la vague de popularité de la chimie verte, l'utilisation de photosensibilisateurs de ruthénium en synthèse organique a permis le développement de nombreuses réactions photocatalysées.[59]

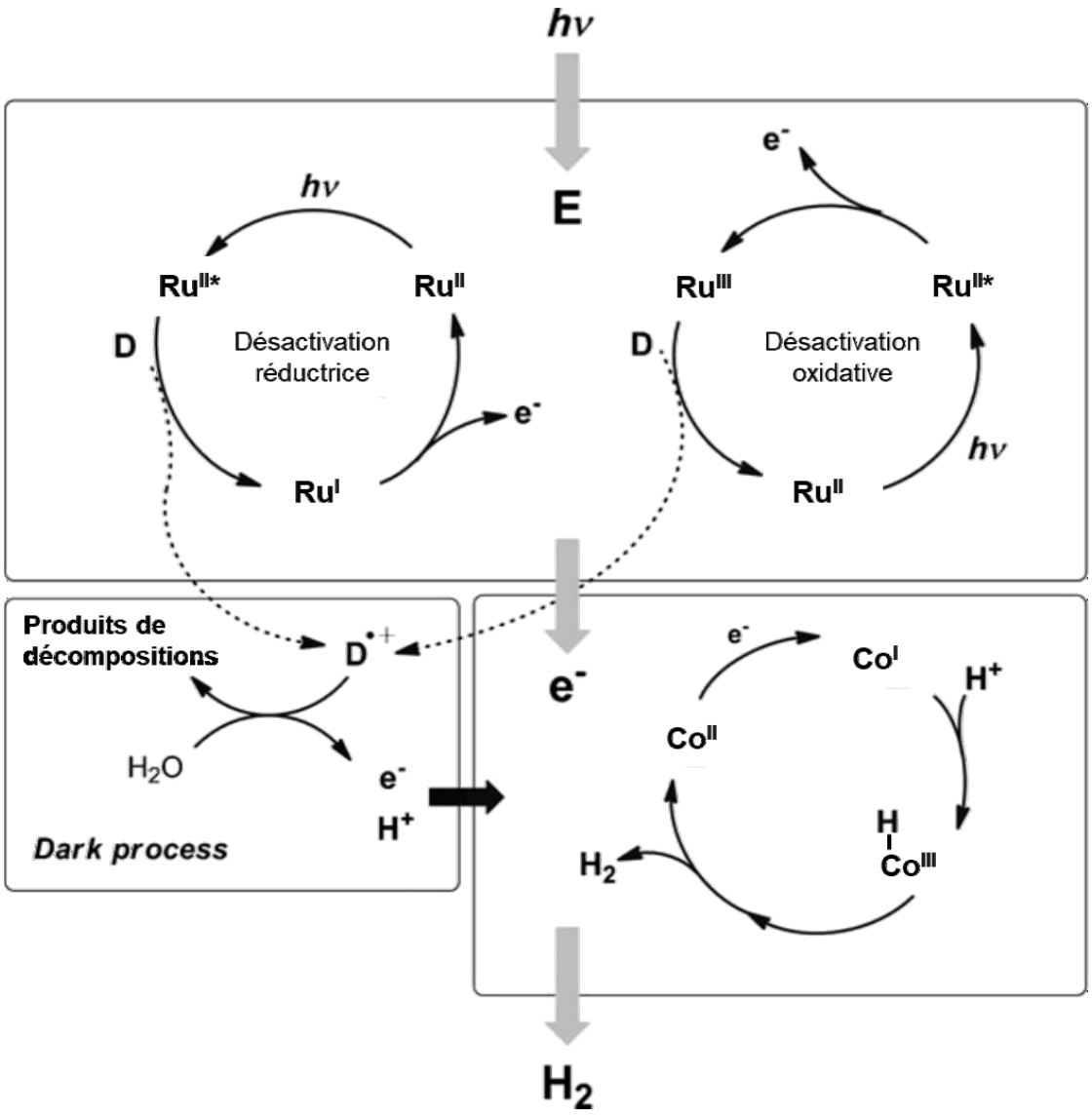

Figure 1.26 – Schéma du transfert électronique impliqué lors d'une désactivation réductrice ou oxidative dans la catalyse de formation du H_2.

Quant à eux, les composés de rhénium font l'objet d'intenses recherches en tant que photocatalyseur permettant la réduction du CO_2, une alternative intéressante pouvant, à long terme, résoudre la problématique reliée à l'exploitation des ressources non-renouvelables de combustible fossiles. Tel qu'illustré à la Figure 1.27, en présence d'un donneur sacrificiel tel que la triéthanolamine, l'état excité des complexes de type $[Re(N\text{^}N)(CO)_3L]^+$ est désactivé de façon réductive menant vers une espèce à 17 électrons permettant la capture et la conversion du CO_2 en CO.[60]

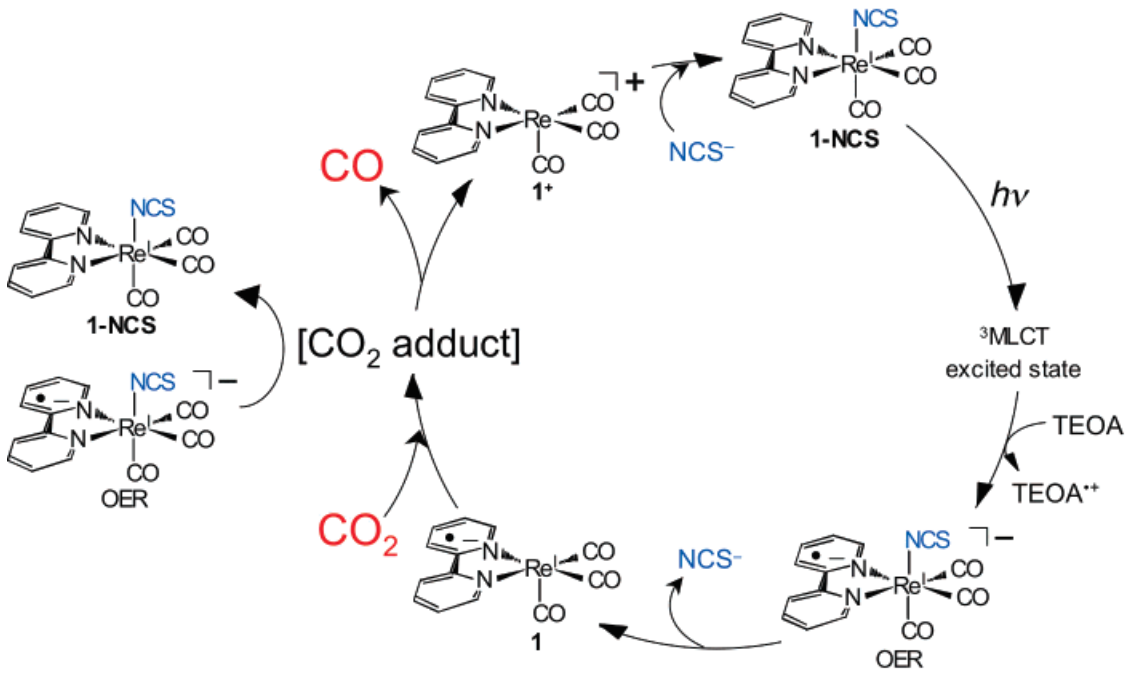

Figure 1.27 – Cycle catalytique de la conversion du CO_2 en CO impliquant un catalyseur de rhénium(I).

1.2.3.3. Transfer d'énergie

Bien que divers systèmes de type Re(I)-Ru(II) exploitent le transfert d'énergie à des fins photosynthétiques,[61] l'exemple classique le plus populaire de transfert d'énergie intramoléculaire est certainement celui de type Ru(II)-vers-Os(II), examiné à partir de la fin des années 1980 par Furue *et al.*[62] puis popularisé notamment par les groupes de Balzani[63], Constable[63g, 63h, 64], Ziessel[65] et Sauvage[63b, 63g, 63h, 66] respectivement. Ces études s'inscrivent principalement dans le cadre de la photosynthèse artificielle afin d'imiter le transfert énergétique retrouvé à l'état naturel dans l'antenne de chromophore. La majorité des composés polypyridines hétérométalliques Ru(II)/Os(II) peuvent être catégorisé en trois grandes classes: les tiges moléculaires,[63f-i, 63l, 64b, 66g, 66h, 67] les étoiles moléculaires[64b, 68] et les dendrimères[9, 63j, 63k, 69]. Les études sur le sujet sont vastes et, tel que présenté aux Figure 1.28 et Figure 1.29, se concentrent essentiellement sur la modification du ligand dont notamment: la rigidité/flexibilité, la nucléarité (diade, triade, etc.), la proximité des ions métalliques ainsi que la communication électronique et leur effet sur l'efficacité du transfert énergétique.

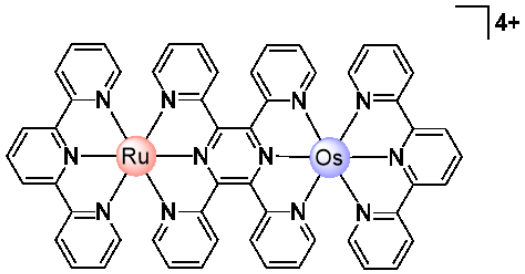

Brewer *et al.* (1996)

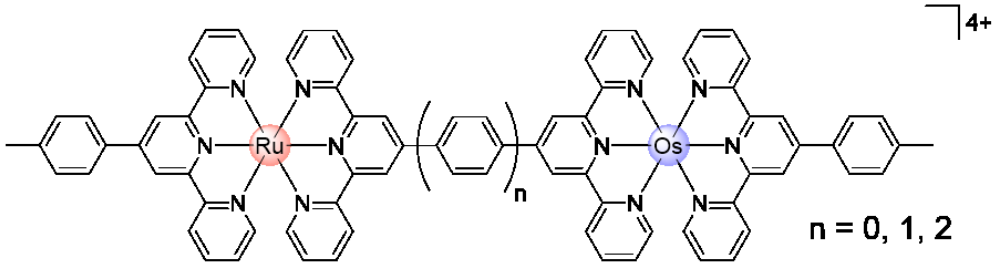

Barigelletti, Balzani, Collin, Sauvage, Constable *et al.* (1994)

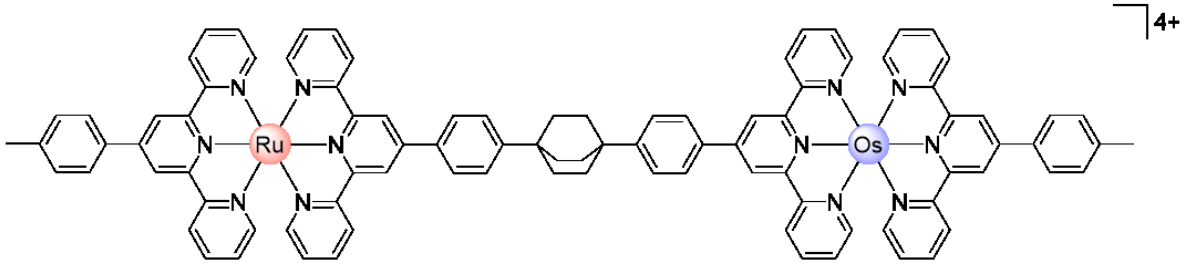

Hammarström, Barigelletti, Collin, Sauvage *et al.* (1996)

Figure 1.28 – Divers exemples de tiges moléculaires hétérométalliques.

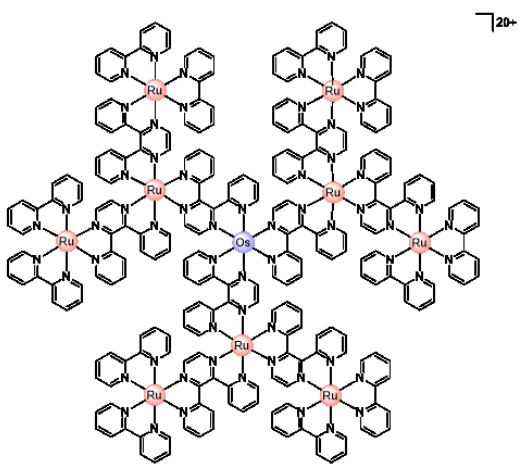

Denti, Campagna, Balzani *et al.* (1992)

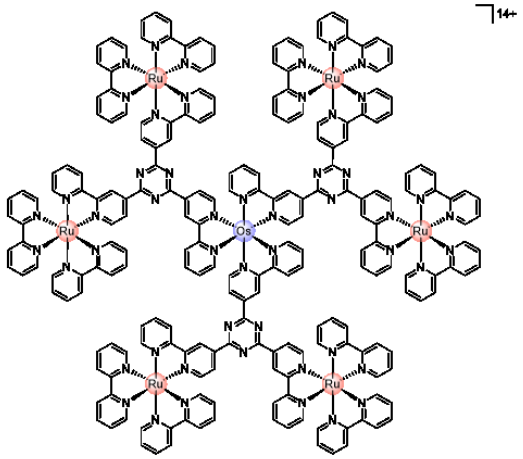

Puntoriero, Campagna *et al.* (2016)

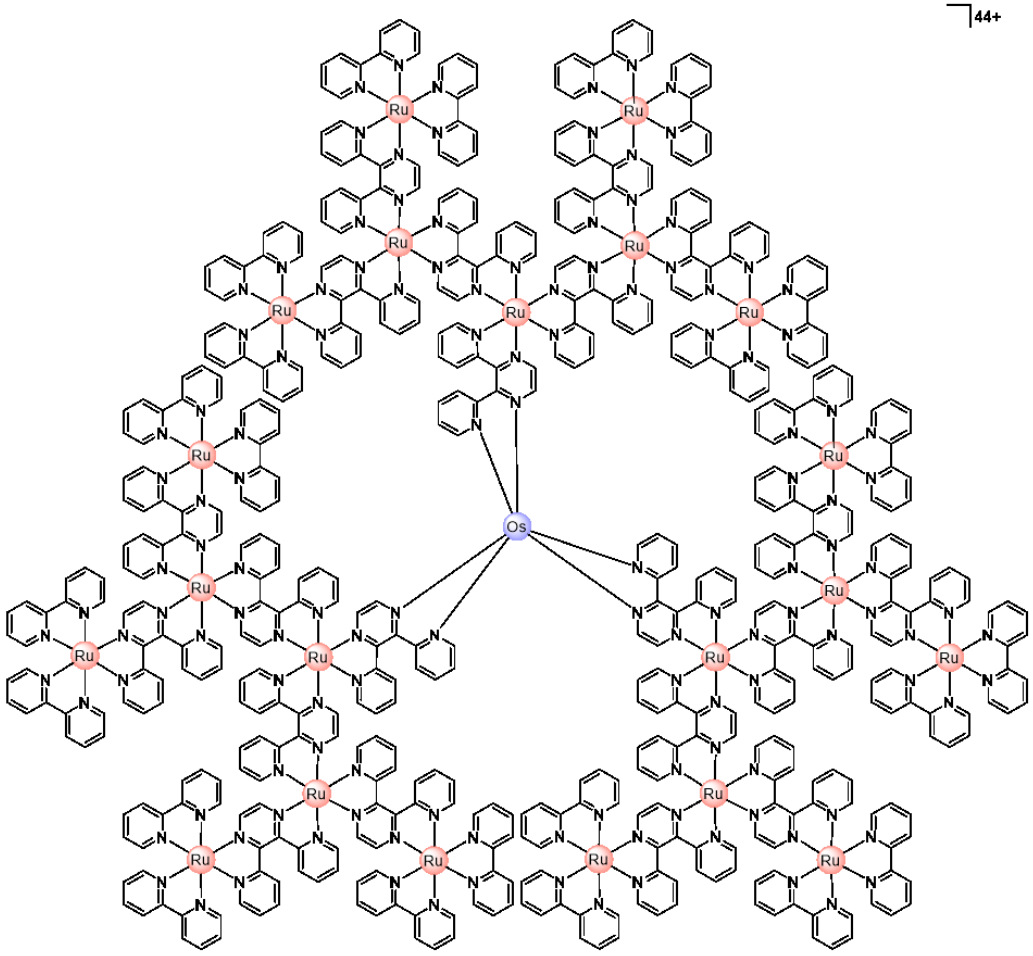

Serroni, Juris, Venturi *et al.* (1997)

Figure 1.29 – Divers exemples de dendrimères hétérométalliques de type Ru^{II}/Os^{II}.

1.3. Objectifs de recherche:

Tel que présenté au début de la section 1.1, l'un des système photo-récolteur d'énergie retrouvé dans les systèmes naturelles consiste en un assemblage de plusieurs sous-unités de type porphyrinique. Philosophiquement parlant, il est intéressant de se questionner sur la procédure utilisée par la nature afin d'arriver à ces assemblages. Pourquoi le système est-il cyclique et non polymérique ? Et surtout, comment la nature réussie-t-elle à implanter le système d'auto-correction propre aux assemblages et ce, sans ballon réactionnel, solvant organique, plaque chauffante et autres équipements auquel le chimiste a accès au laboratoire. À priori, il est donc logique d'émettre l'hypothèse selon laquelle la nature requiert donc une source externe d'énergie, en l'occurrence l'énergie lumineuse, pour lui permettre de réaliser l'exploit d'assembler ces chromophores de façon systématique en un arrangement cyclique parfait.
Les études entreprises dans cette thèse ont donc pour but d'investiguer la photo-induction de l'assemblage de métallacycles pouvant être utilisé comme antenne moléculaire afin de récolter et de convertir l'énergie solaire en énergie chimique. La thèse se divise en huit chapitres dont les thèmes sont énoncés ci-bas.

Chapitre 1: Ce chapitre introduit brièvement les principes importants de chimie supramoléculaire ainsi que les avancées récentes dans le domaine de l'assemblage en chimie de coordination et en chimie organométallique utilisant l'approche de type [n x 1].

Chapitre 2: Ce chapitre conceptuallise l'assemblage photo-induit sous divers aspects, tel que la pré-organisation photo-induite, l'assemblage photo-induit ainsi que la post-modification photo-induite d'espèces uniques métallacycliques et prismatiques.

Chapitre 3: Ce chapitre porte sur la synthèse de ligands N^N^N non-symétrique substitué avec une fonction de type hexahydro-pyrimidopyrimidine (hpp) et de leur chimie de complexation au ruthénium. Une étude détaillée des propriétés optiques et électroniques révèle notamment que l'importante donation sigma du groupement hpp

permet de moduler efficacement le potentiel d'oxydation du métal en fonction du nombre d'unité autour de ce dernier. De plus, la luminescence des complexes subit un déplacement bathochromique important, comparativement au complexe de référence de type $[Ru(tpy)_2]^{2+}$.

Chapitre 4: Ce chapitre constitue une suite logique au chapitre 2 où le contrôle des propriétés optiques et électroniques (via l'utilisation d'un ligand avec des fonctions de type hpp) est mis à profit afin d'étudier le transfert d'énergie au cœur d'un système hétérométallique Ru^{II}-Os^{II}. Bien que ce type de système soit un exemple classique d'un manuel de photochimie, où typiquement le transfert d'énergie du ruthénium vers l'atome d'osmium est observé, le composé étudié dans le cadre de ce travail représente le premier exemple de la littérature où le transfert d'énergie se fait de façon inverse, c'est-à-dire de l'osmium vers le ruthénium.

Chapitre 5: Ce chapitre porte sur la synthèse de ligand de type di-*tert*-butyle-2,2′ :6′,2"-terpyridine substitués. L'introduction des groupement *tert*-butyle améliore considérablement la solubilité des ligands et complexes dans une variété de solvant organique, une propriété non-négligeable lors de la synthèse d'espèces de taille moléculaire élevée (e.g. polymère de coordination, métallacycle, etc.).

Chapitre 6 et **Chapitre 7:** Ces chapitres portent sur l'assemblage thermique de métallacycles à base de rhénium. L'étude vise à investiguer les propriétés optiques et électroniques d'assemblage de type [n x 1] et d'évaluer leur potentiel en tant que chromophore métallique. Les résultats démontrent que la plus grande flexibilité des complexes de type k^2N-terpyridine mènent à l'assemblage de triangle et de carré moléculaire tandis que la plus grande rigidité des précurseurs de type k^3N- permet seulement la synthèse d'un carré auto-assemblé.

Chapitre 8: Ce chapitre portent sur l'assemblage photo-induit d'un métallacycle de ruthénium. Les connaissances acquises dans le cadre des chapitres 5 et 6 en trait à l'assemblage de type [n x 1] est combiné aux études sur la photo-éjection de ligand.

L'assemblage obtenu représente le premier métallacycle de ruthénium obtenu de façon photo-induite et est le second exemple d'assemblage photo-induit dans la littérature.

Chapitre 9: Ce chapitre ce veut une brève récapitulation du travail accompli et vise à élaborer brièvement sur les différentes perspectives possibles des projets en cours.

1.4. Bibliographie:

[1] a) G. S. Hammond, N. J. Turro, *Science* **1963**, *142*, 1541-1553; b) D. R. Arnold, N. C. Baird, J. R. Bolton, *Photochemistry: an introduction*, Academic Press Inc., New York, London, **1974**; c) N. J. Turro, G. Schuster, *Science* **1975**, *187*, 303-312; d) G. B. Porter, *J. Chem. Ed.* **1983**, *60*, 785-790; e) T. J. Meyer, *Pure Appl. Chem.* **1986**, *58*, 1193-1206; f) A. W. Adamson, *Coord. Chem. Rev.* **1993**, *125*, 1-12; g) T. Bitterwolf, in *Encyclopedia of Inorganic and Bioinorganic Chemistry*, John Wiley & Sons, Ltd., **2011**, pp. 1-45.

[2] V. Balzani, V. Carassiti, L. Moggi, F. Scandola, *Inorg. Chem.* **1965**, *4*, 1243-1247.

[3] B. Dinda, *Essentials of Pericyclic and Photochemical Reactions, Vol. 93*, Springer, Switzerland, **2017**.

[4] V. Balzani, P. Ceroni, A. Juris, *Photochemistry and Photophysics: Concepts, Research and Applications*, Wiley-VCH Verlag GmbH & Co. KGaA, Weinheim, **2014**.

[5] J. Barber, P. D. Tran, *J. R. Soc. Interface* **2013**, *10*, 20120984.

[6] R. J. Codgell, J. Southall, A. T. Gardiner, C. J. Law, A. Gall, A. W. Roszak, N. W. Isaacs, *C. R. Chimie* **2006**, *9*, 201-206.

[7] J. Koepke, X. Hu, C. Muenke, K. Schulten, H. Michel, *Structure* **1996**, *4*, 581-597.

[8] P. Ceroni, A. Credi, M. Venturi, V. Balzani, *Photochem. Photobiol. Sci.* **2010**, *9*, 1561-1573.

[9] A. Arrigo, G. La Ganga, F. Nastasi, S. Serroni, A. Santoro, M.-P. Santoni, M. Galletta, S. Campagna, F. Puntoriero, *C. R. Chimie* **2017**, *20*, 209-220.

[10] a) J.-P. Sauvage, P. Gaspard, *From Non-Covalent Assemblies to Molecular Machines*, Wiley-VCH Verkag GmbH & Co. KGaA, Weinheim, **2011**; b) F. Diederich, P. J. Stang, R. R. Tykwinski, *Modern Supramolecular Chemistry: Strategies for Macrocycle Synthesis*, Wiley-VCH Verlag GmbH & Co. KGaA, Weinheim, **2008**.

[11] a) M. Fujita, *Molecular Self-Assembly Organic Versus Inorganic Approaches*, Springer, Berlin, Heidelberg, **2000**; b) C. J. Bruns, J. F. Stoddart, *The Nature of the Mechanical Bond: From Molecules to Machines*, John Wiley & Sons, Inc, NJ, USA, **2017**.

[12] a) J. Yang, M.-C. Yoon, H. Yoo, P. Kim, D. Kim, *Chem. Soc. Rev.* **2012**, *41*, 4808-4826; b) J. Yang, M. Park, Z. Yoon, T. Hori, X. Peng, N. Aratani, P. Dedecker, J.-i. Hotta, H. Uji-i, M. Sliwa, J. Hofkens, A. Osuka, D. Kim, *J. Am. Chem. Soc.* **2008**, *130*, 1879-1884; c) S. Tretiak, C. Middleton, V. Chernyak, S. Mukamel, *J. Phys. Chem. B* **2000**, *104*, 9540-9553; d) T. Pullerits, V. Sundström, *Acc. Chem. Res.* **1996**, *29*, 381-389; e) M. Pajusalu, M. Rätsep, G. Trinkunas, A. Freiberg, *ChemPhysChem* **2011**, *12*, 634-644; f) N. Nagata, Y. Kuramochi, Y. Kobuke, *J. Am. Chem. Soc.* **2009**, *131*, 10-11; g) N. Krauß, *Curr. Opin. Chem. Biol.* **2003**, *7*, 540-550; h) N. W. Isaacs, R. J. Cogdell, A. A. Freer, S. M. Prince, *Curr. Opin. Struct. Biol.* **1995**, *5*, 794-797; i) A. Freer, S. Prince, K. Sauer, M. Papiz, A. Lawless, G. McDermott, R. Cogdell, N. W. Isaacs, *Structure* **1996**, *4*, 449-462; j) R. J. Cogdell, N. W. Isaacs, A. A. Freer, T. D. Howard, A. T. Gardiner, S. M. Prince, M. Z. Papiz, *FEBS Lett.* **2003**, *555*, 35-39; k) R. J. Cogdell, A. Gall, J. Köhler, *Q. Rev. Biophys.* **2006**, *39*, 227-324; l) R. J. Codgell, J. Southall, A. T. Gardiner, C. J. Law, A. Gall, A. W. Roszak, N. W. Isaacs, *C. R. Chimie* **2006**, *9*, 201-206; m) H. Cho, H. Rhee, J. Song, C.-K. Min, M. Takase, N. Aratani, S. Cho, A. Osuka, T. Joo, D. Kim, *J. Am. Chem. Soc.* **2003**, *125*, 5849-5860.

[13] a) A. Pfeil, J. M. Lehn, *J. Chem. Soc.* **1992**, 838-840 ; b) G. Ercolani, L. Mandolini, P. Mencarelli, S. Roelens, *J. Am. Chem. Soc.* **1993**, *115*, 3901-3908; c) X. Chi, A. J. Guerin, R. A. Haycock, C. A. Hunter, L. D. Sarson, *J. Chem. Soc., Chem. Commun.* **1995**, 2563-2565; d) D. Philp, J. F. Stoddart, *Angew. Chem. Int. Ed.* **1996**, *35*, 1155-1196; e) S. J. Rowan, D. G. Hamilton, P. A. Brady, J. K. M.

Sanders, *J. Am. Chem. Soc.* **1997**, *119*, 2578-2579; f) G. Ercolani, *J. Phys. Chem. B* **1998**, *102*, 5699-5703; g) G. Ercolani, M. Ioele, D. Monti, *New J. Chem.* **2001**, *25*, 783-789; h) A. V. Davis, R. M. Yeh, K. N. Raymond, *Proc. Nat. Acad. Sci. USA* **2002**, *99*, 4793-4796; i) G. Ercolani, *J. Am. Chem. Soc.* **2003**, *125*, 16097-16103; j) G. Ercolani, *J. Phys. Chem. B* **2003**, *107*, 5052-5057; k) R. M. Yeh, A. D. Davis, K. N. Raymond, *Comprehensive Coordination Chemistry II: From biology to nanotechnology, Vol. 7*, Elsevier Pergamon, Amsterdam, **2004**; l) J. D. Halley, D. A. Winkler, *Complexity* **2008**, *14*, 10-17; m) C. Piguet, *Chem. Commun.* **2010**; n) C. Piguet, *Dalton Trans.* **2011**, *40*, 8059-8071; o) V. Percec, *Hierarchical Macromolecular Structures: 60 Years after the Staudinger Nobel Prize I* **2013**; p) M. L. Saha, S. De, S. Pramanik, M. Schmittel, *Chem. Soc. Rev.* **2013**, *42*, 6860-6909; q) Y. Tsujimoto, T. Kojima, S. Hiraoka, *Chem. Sci.* **2014**, *5*, 4167-4172; r) S. Hiraoka, *Chem. Rec.* **2015**, *15*, 1144-1147.

[14] a) B. H. Northrop, Y.-R. Zheng, K.-W. Chi, P. J. Stang, *Acc. Chem. Res.* **2009**, *42*, 1554-1563; b) S. Leininger, B. Olenyuk, P. J. Stang, *Chem. Rev.* **2000**, *100*, 853-908; c) R. Chakrabarty, P. S. Mukherjee, P. J. Stang, *Chem. Rev.* **2011**, *111*, 6810-6918; d) T. R. Cook, Y. R. Zheng, P. J. Stang, *Chem. Rev.* **2013**, *113*, 734-777.

[15] a) M. Fujita, J. Yazaki, K. Ogura, *J. Am. Chem. Soc.* **1990**, *112*, 5645-5647; b) P. J. Stang, D. H. Cao, *J. Am. Chem. Soc.* **1994**, *116*, 4981-4982.

[16] a) M. S. Lah, M. L. Kirk, W. Hatfield, V. L. Pecoraro, *J. Chem. Soc., Chem. Commun.* **1989**, 1606-1608; b) V. L. Pecoraro, *Inorg. Chim. Acta.* **1989**, *155*, 171-173; c) C. R. Cornman, J. Kampf, V. L. Pecoraro, *Inorg. Chem.* **1992**, *31*, 1981-1983; d) D. P. Kessisoglou, J. Kampf, V. L. Pecoraro, *Polyhedron* **1994**, *13*, 1379-1391; e) B. R. Gibney, H. Wang, J. W. Kampf, V. L. Pecoraro, *Inorg. Chem.* **1996**, *35*, 6184-6193; f) J. J. Bodwin, A. D. Cutland, R. G. Malkani, V. L. Pecoraro, *Coord. Chem. Rev.* **2001**, *216*, 489-512; g) G. Psomas, A. J. Stemmler, C. Dendrinou-Samara, J. J. Bodwin, M. Schneider, M. Alexiou, J. W. Kampf, D. P. Kessissoglou, V. L. Pecoraro, *Inorg. Chem.* **2001**, *40*, 1562-1570; h) E. R. Trivedi, S. V. Eliseeva, J. Jankolovits, M. M. Olmstead, S. Petoud, V. L. Pecoraro, *J. Am. Chem. Soc.* **2014**, *136*, 1526-1534; i) C. Y. Chow, S. V. Eliseeva, E. R. Trivedi,

T. N. Nguyen, J. W. Kampf, S. Petoud, V. L. Pecoraro, *J. Am. Chem. Soc.* **2016**, *138*, 5100-5109.

[17] R. Krämer, K. Polborn, C. Robl, W. Beck, *Inorg. Chim. Acta.* **1992**, *198*, 415-420.

[18] a) H. Chen, M. M. Olmstead, D. P. Smith, M. F. Maestre, R. H. Fish, *Angew. Chem. Int. Ed.* **1995**, *34*, 1514-1517; b) H. Chen, S. Ogo, R. H. Fish, *J. Am. Chem. Soc.* **1996**, *118*, 4993-5001; c) S. Ogo, H. Chen, M. M. Olmstead, R. H. Fish, *Organometallics* **1996**, *15*, 2009-2013; d) R. Bakhtiar, H. Chen, S. Ogo, R. H. Fish, *Chem. Commun.* **1997**, 2135-2136; e) S. Ogo, S. Nakamura, H. Chen, K. Isobe, Y. Watanabe, R. H. Fish, *J. Org. Chem.* **1998**, *63*, 7151-7156; f) R. H. Fish, *Coord. Chem. Rev.* **1999**, *185-186*, 569-584; g) S. Ogo, O. Buriez, J. B. Kerr, R. H. Fish, *J. Organomet. Chem.* **1999**, *589*, 66-74; h) R. H. Fish, G. Jaouen, *Organometallics* **2003**, *22*, 2166-2177.

[19] a) S. Korn, W. S. Sheldrick, *J. Chem. Soc., Dalton Trans.* **1997**, 2191-2199; b) S. Korn, W. S. Sheldrick, *Inorg. Chim. Acta.* **1997**, *254*, 85-91; c) P. Annen, S. Schildberg, W. S. Sheldrick, *Inorg. Chim. Acta* **2000**, *307*, 115-124.

[20] a) D. Carmona, F. J. Lahoz, R. Atencio, L. A. Oro, M. P. Lamata, F. Viguri, E. San José, C. Vega, J. Reyes, F. Joo, A. Katho, *Chem. Eur. J.* **1999**, *5*, 1544-1564; b) Á. Kathó, D. Carmona, F. Viguri, C. D. Remacha, J. Kovács, F. Joó, L. A. Oro, *J. Organomet. Chem.* **2000**, *593*, 299-306.

[21] a) T. Habereder, M. Warchhold, H. Nöth, K. Severin, *Angew. Chem. Int. Ed.* **1999**, *38*, 3225-3228; b) H. Piotrowski, G. Hilt, A. Schulz, P. Mayer, K. Polborn, K. Severin, *Chem. Eur. J.* **2001**, *7*, 3196-3208; c) H. Piotrowski, K. Polborn, G. Hilt, K. Severin, *J. Am. Chem. Soc.* **2001**, *123*, 2699-2700; d) H. Piotrowski, K. Severin, *Proc. Nat. Acad. Sci. USA* **2002**, *99*, 4997-5000; e) K. Severin, *Coord. Chem. Rev.* **2003**, *245*, 3-10; f) T. Brasey, A. Buryak, R. Scopelliti, K. Severin, *Eur. J. Inorg. Chem.* **2004**, *2004*, 964-967; g) N. Christinat, R. Scopelliti, K. Severin, *Chem. Commun.* **2004**, *0*, 1158-1159; h) Z. Grote, R. Scopelliti, K. Severin, *J. Am. Chem. Soc.* **2004**, *126*, 16959-16972; i) M.-L. Lehaire, R. Scopelliti, L. Herdeis, K. Polborn, P. Mayer, K. Severin, *Inorg. Chem.* **2004**, *43*, 1609-1617; j) T. Brasey, R. Scopelliti, K. Severin, *Inorg. Chem.* **2005**, *44*, 160-

162; k) T. Brasey, R. Scopelliti, K. Severin, *Chem. Commun.* **2006**, *0*, 3308-3310; l) K. Severin, *Chem. Commun.* **2006**, *0*, 3859-3867; m) N. Christinat, R. Scopelliti, K. Severin, *J. Org. Chem.* **2007**, *72*, 2192-2200; n) Z. Grote, R. Scopelliti, K. Severin, *Eur. J. Inorg. Chem.* **2007**, *2007*, 694-700; o) S. Mirtschin, E. Krasniqi, R. Scopelliti, K. Severin, *Inorg. Chem.* **2008**, *47*, 6375-6381; p) W. Ang, Z. Grote, R. Scopelliti, L. Juillerat-Jeanneret, K. Severin, P. J. Dyson, *J. Organomet. Chem.* **2009**, *694*, 968-972; q) K. Severin, *Dalton Trans.* **2009**, *0*, 5254-5264; r) E. Sheepwash, K. Zhou, R. Scopelliti, K. Severin, *Eur. J. Inorg. Chem.* **2013**, *2013*, 2558-2563.

[22] a) H. Rauter, E. C. Hillgeris, A. Erxleben, B. Lippert, *J. Am. Chem. Soc.* **1994**, *116*, 616-624; b) L. Mimassi, C. Guyard-Duhayon, M. Rager, H. Amouri, *Inorg. Chem.* **2004**, *43*, 6644-6649; c) P. D. Frischmann, B. J. Sahli, S. Guieu, B. O. Patrick, M. J. MacLachlan, *Chem. Eur. J.* **2012**, *18*, 13712-13721; d) G. L. Wang, Y. J. Lin, G. X. Jin, *Chem. Eur. J.* **2011**, *17*, 5578-5587; e) C. Dendrinou-Samara, G. Psomas, L. Iordanidis, V. Tangoulis, D. P. Kessissoglou, *Chem. Eur. J.* **2001**, *7*, 5041-5051.

[23] D. A. Beauchamp, S. J. Loeb, *Chem. Commun.* **2002**, *0*, 2484-2485.

[24] a) B. Champin, V. Sartor, J.-P. Sauvage, *New J. Chem.* **2008**, *32*, 1048-1054; b) J. Voignier, J. Frey, T. Kraus, M. Buděšínský, J. Cvačka, V. Heitz, J. P. Sauvage, *Chem. Eur. J.* **2011**, *17*, 5404-5414.

[25] S. Perera, X. Li, M. Guo, C. Wesdemiotis, C. N. Moorefield, G. R. Newkome, *Chem. Commun.* **2011**, *47*, 4658-4660.

[26] K. Kalyanasundaram, *Photochemistry of polypyridine and porphyrin complexes*, Academic Press Limited, London, **1992**.

[27] a) *Photochemistry and photophysics of coordination compounds I, Vol. 280*, Springer-Verlag Berlin, Berlin, Heidelberg, New York, **2007**; b) *Photochemistry and Photophysics of Coordination Compounds II*, Springer-Verlag, Berlin, Heidelberg, New York, **2007**.

[28] a) T. Ohno, F. Tanigawa, K. Fujihara, S. Izumi, M. Matsumura, *J. Photochem. Photobiol. A* **1999**, *127*, 107-110; b) A. J. Esswein, D. G. Nocera, *Chem. Rev.* **2007**, *107*, 4022-4047; c) T. P. Yoon, M. A. Ischay, J. Du, *Nature Chem.* **2010**,

2, 527-532; d) T. S. Teets, D. G. Nocera, *Chem. Commun.* **2011**, *47*, 9268-9274; e) N. Corrigan, S. Shanmugam, J. Xu, C. Boyer, *Chem. Soc. Rev.* **2016**, *45*, 6165-6212; f) K. Teegardin, J. I. Day, J. Chan, J. Weaver, *Org. Process Res. Dev.* **2016**, *20*, 1156-1163; g) N. Elgrishi, M. B. Chambers, X. Wang, M. Fontecave, *Chem. Soc. Rev.* **2017**, *46*, 761-796.

[29] a) O. J. Stacey, S. J. A. Pope, *RSC Adv.* **2013**, *3*, 25550-25564; b) T. Storr, in *Ligand Design in Medicinal Inorganic Chemistry*, John Wiley & Sons, Ltd, **2014**; c) J. D. Knoll, C. Turro, *Coord. Chem. Rev.* **2015**, *282-283*, 110-126; d) E. Ruggiero, S. Castro, A. Habtemariam, L. Salassa, *Struct. Bond.* **2015**, *165*, 69-107; e) J. K. White, R. H. Schmehl, C. Turro, *Inorg. Chim. Acta* **2017**, *454*, 7-20.

[30] a) M. Grätzel, *J. Photochem, Photobiol. A* **2004**, *164*, 3-14; b) C. Klein, M. K. Nazeeruddin, D. D. Censo, P. Liska, M. Grätzel, *Inorg. Chem.* **2004**, *43*, 4216-4226; c) M. Grätzel, *Inorg. Chem.* **2005**, *44*, 6841-6851; d) F. Bella, C. Gerbaldi, C. Barolo, M. Grätzel, *Chem. Soc. Rev.* **2015**, *44*, 3431-3473.

[31] M. Grätzel, K. Kalyanasundaram, in *Photosensitization and photocatalysis using inorganic and organometallic compounds*, Springer Science+Business Media, Dordrecht, **1993**.

[32] J. P. Sauvage, J. P. Collin, J. C. Chambron, S. Guillerez, C. Coudret, *Chem. Rev.* **1994**, *94*, 993-1019.

[33] A. K. Pal, G. S. Hanan, *Chem. Soc. Rev.* **2014**, *43*, 6184-6197.

[34] a) A. J. Lees, in *Photophysics of organometallics, Vol. 29*, Springer, Berlin, Heidelberg, Berlin, Heidelberg, **2010**; b) H. Takeda, K. Koike, T. Morimoto, H. Inumaru, O. Ishitani, in *Inorganic Photochemistry*, **2011**, pp. 137-186.

[35] a) K. Kalyanasundaram, *J. Chem. Soc., Faraday Trans.* **1986**, *82*, 2401-2415; b) L. A. Worl, R. Duesing, P. Chen, L. Della Ciana, T. J. Meyer, *J. Chem. Soc., Dalton Trans.* **1991**, *0*, 849-858.

[36] a) P. A. Anderson, R. F. Keene, E. Horn, E. R. T. Tiekink, *Appl. Organomet. Chem.* **1990**, *4*, 523-533; b) E. W. Abel, N. J. Long, K. G. Orrell, A. G. Osborne, H. M. Pain, V. Sik, *J. Chem. Soc., Chem. Commun.* **1992**, *0*, 303-304; c) E. W. Abel, V. S. Dimitrov, N. J. Long, K. G. Orrell, A. G. Osborne, H. M. Pain, V. Sik, M. B. Hursthouse, M. A. Mazid, *J. Chem. Soc., Chem. Commun.* **1993**, *0*, 597-

603; d) E. W. Abel, A. Gelling, K. G. Orrell, A. G. Osborne, V. Sik, *Chem. Commun.* **1996**, *0*, 2329-2330; e) A. Gelling, M. D. Olsen, K. G. Orrell, A. G. Osborne, V. Sik, *J. Chem. Soc., Dalton Trans.* **1998**, *0*, 3479-3488; f) A. Gelling, K. G. Orrell, A. G. Osborne, V. Sik, *J. Chem. Soc., Dalton Trans.* **1998**, *0*, 937-945; g) A. Freyer, A. Freyer, C. DiMeglio, *J. Chem. Ed.* **2006**, *83*, 788-790; h) Q. Ge, T. C. Corkery, M. G. Humphrey, M. Samoc, T. S. Hor, *Dalton Trans.* **2009**, 6192-6200; i) A. J. Amoroso, A. Banu, M. P. Coogan, P. G. Edwards, G. Hossain, K. M. Malik, *Dalton Trans.* **2010**, *39*, 6993-7003; j) V. Fernandez-Moreira, F. L. Thorp-Greenwood, R. J. Arthur, B. M. Kariuki, R. L. Jenkins, M. P. Coogan, *Dalton Trans.* **2010**, *39*, 7493-7503; k) D. Wang, Q. L. Xu, S. Zhang, H. Y. Li, C. C. Wang, T. Y. Li, Y. M. Jing, W. Huang, Y. X. Zheng, G. Accorsi, *Dalton Trans.* **2013**, *42*, 2716-2723.

[37] a) K. A. Stephenson, S. R. Banerjee, T. Besanger, O. O. Sogbein, M. K. Levadala, N. McFarlane, J. A. Lemon, D. R. Boreham, K. P. Maresca, J. D. Brennan, J. W. Babich, J. Zubieta, J. F. Valliant, *J. Am. Chem. Soc.* **2004**, *126*, 8588-8599; b) L. Wei, J. W. Babich, W. C. Eckelman, J. Zubieta, *Inorg. Chem.* **2005**, *44*, 2198-2209; c) M. Casanova, E. Zangrando, F. Munini, E. Iengo, E. Alessio, *Dalton Trans.* **2006**, 5033-5045; d) R. S. Herrick, T. J. Brunker, C. Maus, K. Crandall, A. Cetin, C. J. Ziegler, *Chem. Commun.* **2006**, 4330-4331; e) D. V. Griffiths, Y. K. Cheong, P. Duncanson, M. Motevalli, *Dalton Trans.* **2011**, *40*, 10215-10228; f) K. Wu, D. Mukherjee, A. Ellern, A. D. Sadow, W. E. Geiger, *New J. Chem.* **2011**, *35*, 2169-2178; g) D. J. Losey, B. A. Frenzel, W. M. Smith, S. E. Hightower, C. G. Hamaker, *Inorg. Chem. Commun.* **2013**, *30*, 46-48; h) A. K. Pal, G. S. Hanan, *Dalton Trans.* **2014**, *43*, 11811-11814; i) H. Norouzi-Arasi, A. K. Pal, S. Nag, D. Chartrand, G. S. Hanan, *Chem. Commun.* **2016**, *52*, 12159-12162.

[38] a) D. R. Black, S. E. Hightower, *Inorg. Chem. Commun.* **2012**, *24*, 16-19; b) B. A. Frenzel, J. E. Schumaker, D. R. Black, S. E. Hightower, *Dalton Trans.* **2013**, *42*, 12440-12451.

[39] G. Malouf, P. C. Ford, *J. Am. Chem. Soc.* **1974**, *96*, 601-603.

[40] J. Van Houten, R. J. Watts, *J. Am. Chem. Soc.* **1976**, *98*, 4853-4858.

[41] M. Gleria, F. Minto, G. Beggiato, P. Bortolus, *J. Chem. Soc., Chem. Commun.* **1978**, *0*, 285a.

[42] P. E. Hoggard, G. B. Porter, *J. Am. Chem. Soc.* **1978**, *100*, 1457-1463.

[43] a) B. Durham, J. L. Walsh, C. L. Carter, T. J. Meyer, *Inorg. Chem.* **1980**, *19*, 860-865; b) W. M. Wallace, P. E. Hoggard, *Inorg. Chem.* **1980**, *19*, 2141-2145; c) C. R. J., A. B. P. Lever, *Inorg. Chem.* **1982**, *21*, 2276-2282; d) G. H. Allen, R. P. White, D. P. Rillema, T. J. Meyer, *J. Am. Chem. Soc.* **1984**, *106*, 2613-2620; e) D. P. Rillema, D. G. Taghdiri, D. S. Jones, K. C. D., L. A. Worl, T. J. Meyer, H. A. Levy, *Inorg. Chem.* **1987**, *26*, 578-585; f) A. von Zelewsky, G. Gremaud, *Helv. Chim. Acta* **1988**, *71*, 1108-1115; g) H. B. Ross, M. Boldaji, D. P. Rillema, C. B. Blanton, R. P. White, *Inorg. Chem.* **1989**, *28*, 1013-1021.

[44] a) A.-C. Laemmel, J. P. Collin, J. P. Sauvage, *Eur. J. Inorg. Chem.* **1999**, 383-386; b) Y. J. Tu, S. Mazumder, J. F. Endicott, C. Turro, J. J. Kodanko, H. B. Schlegel, *Inorg. Chem.* **2015**, *54*, 8003-8011.

[45] H.-F. Suen, S. W. Wilson, M. Pomerantz, J. L. Walsh, *Inorg. Chem.* **1989**, *28*, 786-791.

[46] C. R. Hecker, P. E. Fanwick, D. R. McMillin, *Inorg. Chem.* **1991**, *30*, 659-666.

[47] a) R. N. Garner, L. E. Joyce, C. Turro, *Inorg. Chem.* **2011**, *50*, 4384-4391; b) B. A. Albani, C. B. Durr, C. Turro, *J. Phys. Chem. A* **2013**, *117*, 13885-13892; c) J. D. Knoll, B. A. Albani, C. B. Durr, C. Turro, *J. Phys. Chem. A* **2014**, *118*, 10603-10610; d) J. D. Knoll, B. A. Albani, C. Turro, *Acc. Chem. Res.* **2015**, *48*, 2280-2287; e) J. K. White, R. H. Schmehl, C. Turro, *Inorg. Chim. Acta* **2017**, *454*, 7-20.

[48] A. Li, J. K. White, K. Arora, M. K. Herroon, P. D. Martin, H. B. Schlegel, I. Podgorski, C. Turro, J. J. Kodanko, *Inorg. Chem.* **2016**, *55*, 10-12.

[49] W. Sun, S. Li, B. Haupler, J. Liu, S. Jin, W. Steffen, U. S. Schubert, H. J. Butt, X. J. Liang, S. Wu, *Adv. Mater.* **2017**, *29*, 1603702.

[50] a) J. G. Vos, M. T. Pryce, *Coord. Chem. Rev.* **2010**, *254*, 2519-2532; b) J. Rohacova, A. Sekine, T. Kawano, S. Tamari, O. Ishitani, *Inorg. Chem.* **2015**, *54*, 8769-8777; c) S. Sato, O. Ishitani, *Coord. Chem. Rev.* **2015**, *282-283*, 50-59; d) K. Saita, Y. Harabuchi, T. Taketsugu, O. Ishitani, S. Maeda, *Phys. Chem. Chem.*

Phys. **2016**, *18*, 17557-17564; e) T. Mukuta, P. V. Simpson, J. G. Vaughan, B. W. Skelton, S. Stagni, M. Massi, K. Koike, O. Ishitani, K. Onda, *Inorg. Chem.* **2017**, *56*, 3404-3413.

[51] C. Pac, S. Kaseda, K. Ishii, S. Yanagida, *J. Chem. Soc., Chem. Commun.* **1991**, *0*, 787-788.

[52] K. Koike, J. Tanabe, S. Toyama, H. Tsubaki, K. Sakamoto, J. R. Westwell, F. P. A. Johnson, H. Hori, H. Saitoh, O. Ishitani, *Inorg. Chem.* **2000**, *39*, 2777-2783.

[53] S. Sato, A. Sekine, Y. Ohashi, O. Ishitani, A. M. Blanco-Rodriguez, A. Vlcek Jr., T. Unno, K. Koike, *Inorg. Chem.* **2007**, *46*, 3531-3540.

[54] S. Sato, Y. Matubara, K. Koike, M. Falkenstrom, T. Katayama, Y. Ishibashi, H. Miyasaka, S. Taniguchi, H. Chosrowjan, N. Mataga, N. Fukazawa, S. Koshihara, K. Onda, O. Ishitani, *Chem. Eur. J.* **2012**, *18*, 15722-15734.

[55] B. Durham, S. R. Wilson, D. J. Hodgson, T. J. Meyer, *J. Am. Chem. Soc.* **1980**, *102*, 600-607.

[56] a) J. J. Rack, J. R. Winkler, H. B. Gray, *J. Am. Chem. Soc.* **2001**, *123*, 2432-2433; b) J. J. Rack, N. V. Mockus, *Inorg. Chem.* **2003**, *42*, 5792-5794; c) J. J. Rack, A. A. Rachford, A. M. Shelker, *Inorg. Chem.* **2003**, *42*, 7357-7359; d) A. A. Rachford, J. L. Petersen, J. J. Rack, *Inorg. Chem.* **2005**, *44*, 8065-8075; e) D. P. Butcher, Jr., A. A. Rachford, J. L. Petersen, J. J. Rack, *Inorg. Chem.* **2006**, *45*, 9178-9180; f) A. A. Rachford, J. L. Petersen, J. J. Rack, *Inorg. Chem.* **2006**, *45*, 5953-5960; g) A. A. Rachford, J. J. Rack, *J. Am. Chem. Soc.* **2006**, *128*, 14318-14324; h) A. A. Rachford, J. L. Petersen, J. J. Rack, *Dalton Trans.* **2007**, 3245-3251; i) N. V. Mockus, D. Rabinovich, J. L. Petersen, J. J. Rack, *Angew. Chem. Int. Ed.* **2008**, *47*, 1458-1461; j) D. A. Lutterman, A. A. Rachford, J. J. Rack, C. Turro, *J. Phys. Chem. A* **2009**, *113*, 11002-11006; k) B. A. McClure, N. V. Mockus, D. P. Butcher, Jr., D. A. Lutterman, C. Turro, J. L. Petersen, J. J. Rack, *Inorg. Chem.* **2009**, *48*, 8084-8091; l) B. A. McClure, J. J. Rack, *Angew. Chem. Int. Ed.* **2009**, *48*, 8556-8558; m) T. A. Grusenmeyer, B. A. McClure, C. J. Ziegler, J. J. Rack, *Inorg. Chem.* **2010**, *49*, 4466-4470; n) D. A. Lutterman, A. A. Rachford, J. J. Rack, C. Turro, *J. Phys. Chem. Lett.* **2010**, *1*, 3371-3375; o) B. A. McClure, E. R. Abrams, J. J. Rack, *J. Am. Chem. Soc.* **2010**, *132*, 5428-5436; p)

B. A. McClure, J. J. Rack, *Eur. J. Inorg. Chem.* **2010**, *2010*, 3895-3904; q) B. A. McClure, J. J. Rack, *Inorg. Chem.* **2011**, *50*, 7586-7590; r) K. Garg, J. T. Engle, C. J. Ziegler, J. J. Rack, *Chem. Eur. J.* **2013**, *19*, 11686-11695; s) Y. Jin, J. J. Rack, *Isr. J. Chem.* **2013**, *53*, 280-287; t) A. W. King, Y. Jin, J. T. Engle, C. J. Ziegler, J. J. Rack, *Inorg. Chem.* **2013**, *52*, 2086-2093; u) K. Garg, A. W. King, J. J. Rack, *J. Am. Chem. Soc.* **2014**, *136*, 1856-1863; v) A. W. King, J. P. Malizia, J. T. Engle, C. J. Ziegler, J. J. Rack, *Dalton Trans.* **2014**, *43*, 17847-17855; w) A. W. King, B. A. McClure, Y. Jin, J. J. Rack, *J. Phys. Chem. A* **2014**, *118*, 10425-10432; x) A. W. King, L. Wang, J. J. Rack, *Acc. Chem. Res.* **2015**, *48*, 1115-1122.

[57] S. Sato, T. Morimoto, O. Ishitani, *Inorg. Chem.* **2007**, *46*, 9051-9053.

[58] V. Artero, M. Chavarot-Kerlidou, M. Fontecave, *Angew. Chem. Int. Ed.* **2011**, *50*, 7238-7266.

[59] C. K. Prier, D. A. Rankic, D. W. MacMillan, *Chem. Rev.* **2013**, *113*, 5322-5363.

[60] H. Takeda, K. Koike, H. Inoue, O. Ishitani, *J. Am. Chem. Soc.* **2008**, *130*, 2023-2031.

[61] a) B. Gholamkhass, H. Mametsuka, K. Koike, T. Tanabe, M. Furue, O. Ishitani, *Inorg. Chem.* **2005**, *44*, 2326-2336; b) G. Sahara, H. Kumagai, K. Maeda, N. Kaeffer, V. Artero, M. Higashi, R. Abe, O. Ishitani, *J. Am. Chem. Soc.* **2016**, *138*, 14152-14158; c) Y. Tamaki, O. Ishitani, *ACS Catal.* **2017**, *7*, 3394-3409; d) R. L. Cleary, K. J. Byrom, D. A. Bardwell, J. C. Jeffery, M. D. Ward, G. Calogero, N. Armaroli, L. Flamigni, Barigelletti, *Inorg. Chem.* **1997**, *36*, 2601-2609.

[62] a) M. Furue, S. Kinoshita, T. Kushida, *Chem. Lett.* **1987**, *0*, 2355-2358; b) M. Furue, T. Yoshidzumi, S. Kinoshita, T. Kushida, S. Nozakura, M. Kamachi, *Bull. Chem. Soc. Jpn.* **1991**, *64*, 1632-1640; c) M. Furue, K. Maruyama, Y. Kanematsu, T. Kushida, M. Kamachi, *Coord. Chem. Rev.* **1994**, *132*, 201-208.

[63] a) S. Campagna, G. Denti, L. S. Sabatino, S., M. Ciano, V. Balzani, *J. Chem. Soc., Chem. Commun.* **1989**, *0*, 1500-1501; b) J. P. Collin, S. Guillerez, J. P. Sauvage, F. Barigelleti, L. De Cola, L. Flamigni, V. Balzani, *Inorg. Chem.* **1991**, *30*, 4230-4238; c) G. Denti, S. Campagna, S. Serroni, M. Ciano, V. Balzani, *J. Am. Chem. Soc.* **1992**, *114*, 2944-2950; d) P. Belser, A. Von Zelewski, M. Frank, C. Seel, F. Vogtle, L. De Cola, F. Barigelleti, V. Balzani, *J. Am. Chem. Soc.* **1993**, *115*, 4076-

4086; e) L. De Cola, V. Balzani, F. Barigelleti, L. Flamigni, P. Belser, A. Von Zelewski, M. Frank, F. Vogtle, *Inorg. Chem.* **1993**, *32*, 5228-5238; f) F. Vögtle, M. Frank, P. Belser, A. von Zelewsky, V. Balzani, L. Cola, F. Barigelletti, L. Flamigni, M. Nieger, *Angew. Chem. Int. Ed.* **1993**, *32*, 1643-1646; g) F. Barigelleti, L. Flamigni, V. Balzani, J. P. Collin, J. P. Sauvage, A. Sour, E. C. Constable, A. M. W. C. Thompson, *J. Am. Chem. Soc.* **1994**, *116*, 7692-7699; h) F. Barigelletti, L. Flamigni, V. Balzani, J. P. Collin, J. P. Sauvage, A. Sour, E. C. Constable, A. M. W. Thompson, *Coord. Chem. Rev.* **1994**, *132*, 209-214; i) V. Balzani, F. Barigelletti, P. Belser, S. Bernhard, L. Cola, L. Flamigni, *J. Phys. Chem.* **1996**, *100*, 16786-16788; j) S. Serroni, A. Juris, M. Venturi, S. Campagna, I. R. Resino, G. Denti, A. Credi, V. Balzani, *J. Mater. Chem.* **1997**, *7*, 1227-1236; k) V. Balzani, S. Campagna, G. Denti, A. Juris, S. Serroni, M. Venturi, *Acc. Chem. Res.* **1998**, *31*, 26-34; l) B. Schlicke, P. Belser, L. Cola, E. Sabbioni, V. Balzani, *J. Am. Chem. Soc.* **1999**, *121*, 4207-4214; m) H. Baudin, J. Davidsson, S. Serroni, A. Juris, V. Balzani, S. Campagna, L. Hammarström, *J. Phys. Chem. A* **2002**, *106*, 4312-4319.

[64] a) E. C. Constable, A. M. W. C. Thompson, *J. Chem. Soc., Dalton Trans.* **1995**, *0*, 1615-1627; b) E. C. Constable, R. W. Handel, C. E. Housecroft, A. Farran Morales, B. Ventura, L. Flamigni, F. Barigelletti, *Chem. Eur. J.* **2005**, *11*, 4024-4034.

[65] a) V. Grosshenny, R. Ziessel, *Angew. Chem. Int. Ed.* **1995**, *34*, 1100-1102; b) V. Grosshenny, A. Harriman, M. Hissler, R. Ziessel, *J. Chem. Soc., Faraday Trans.* **1996**, *92*, 2223-2238; c) A. El-ghayoury, A. Harriman, A. Khatyr, R. Ziessel, *Angew. Chem. Int. Ed.* **2000**, *39*, 185-189; d) A. El-ghayoury, A. Harriman, R. Ziessel, *J. Phys. Chem. A* **2000**, *104*, 7906-7915; e) A. Harriman, A. Khatyr, R. Ziessel, A. C. Benniston, *Angew. Chem. Int. Ed.* **2000**, *39*, 4287-4290; f) A. Harriman, M. Hissler, A. Khatyr, R. Ziessel, *Eur. J. Inorg. Chem.* **2003**, *2003*, 955-959; g) S. Diring, R. Ziessel, F. Barigelletti, A. Barbieri, B. Ventura, *Chem. Eur. J.* **2010**, *16*, 9226-9236.

[66] a) M. Beley, J. P. Collin, J. P. Sauvage, *Inorg. Chem.* **1993**, *32*, 4539-4543; b) M. Beley, S. Chodorowski, J. P. Collin, J. P. Sauvage, L. Flamigni, F. Barigelleti,

Inorg. Chem. **1994**, *33*, 2543-2547; c) J. P. Sauvage, J. P. Collin, J. C. Chambron, S. Guillerez, C. Coudret, *Chem. Rev.* **1994**, *94*, 993-1019; d) F. Barigelleti, L. Flamigni, M. Guardigli, A. Juris, M. Beley, S. Chodorowski-Kimmes, J. P. Collin, J. P. Sauvage, *Inorg. Chem.* **1996**, *35*, 136-142; e) F. Barigelletti, L. Flamigni, M. Guardigli, A. Juris, M. Beley, S. Chodorowski-Kimmes, J.-P. Collin, J.-P. Sauvage, *Inorg. Chem.* **1996**, *35*, 136-142; f) L. Hammarström, F. Barigelletti, L. Flamigni, N. Armaroli, A. Sour, J.-P. Collin, J.-P. Sauvage, *J. Am. Chem. Soc.* **1996**, *118*, 11972-11973; g) F. Barigelleti, L. Flamigni, J. P. Collin, J. P. Sauvage, *Chem. Commun.* **1997**, *0*, 333-338.

[67] a) S. Welter, N. Salluce, A. Benetti, N. Rot, P. Belser, P. Sonar, A. C. Grimsdale, K. Müllen, M. Lutz, A. L. Spek, L. Cola, *Inorg. Chem.* **2005**, *44*, 4706-4718; b) E. Coronado, P. Gavina, S. Tatay, R. Groarke, J. G. Vos, *Inorg. Chem.* **2010**, *49*, 6897-6903.

[68] a) J. M. Haider, R. M. Williams, L. De Cola, Z. Pikramenou, *Angew. Chem. Int. Ed.* **2003**, *42*, 1830-1833; b) J. A. Faiz, R. M. Williams, M. J. Silva, L. Cola, Z. Pikramenou, *J. Am. Chem. Soc.* **2006**, *128*, 4520-4521; c) J. Otsuki, A. Imai, K. Sato, D. M. Li, M. Hosoda, M. Owa, T. Akasaka, I. Yoshikawa, K. Araki, T. Suenobu, S. Fukuzumi, *Chem. Eur. J.* **2008**, *14*, 2709-2718.

[69] a) S. Serroni, S. Campagna, F. Puntoriero, C. Di Pietro, N. D. McClenaghan, F. Loiseau, *Chem. Soc. Rev.* **2001**, *30*, 367-375; b) J. Larsen, F. Puntoriero, T. Pascher, N. McClenaghan, S. Campagna, E. Akesson, V. Sundstrom, *ChemPhysChem* **2007**, *8*, 2643-2651; c) E. La Mazza, F. Puntoriero, F. Nastasi, B. Laramée-Milette, G. S. Hanan, S. Campagna, *Dalton Trans.* **2016**, *45*, 19238-19241.

Chapitre 2 – Shedding light on photo-induced assembly of discrete ensembles

2.1. Résumé

Au cours des dernières décennies, l'auto-assemblage de molécules discrètes et polymériques basées sur la chimie organométallique et la chimie de coordination s'est révélé être un outil efficace pour générer une vaste bibliothèque de supramolécules organisées. La conception judicieuse des blocs de construction, une combinaison d'un noyau métallique et d'un ligand organique, peut conduire à des propriétés améliorées basées sur le choix des différents composants. Malgré des centaines d'espèces rapportées dans la littérature, la plupart ont été obtenues par synthèse thermique classique. Néanmoins, les supramolécules obtenues grâce à l'assemblage induit par la lumière présentent un intérêt élevé en raison de leurs propriétés exclusives inaccessibles par les réactions de chauffage classiques. Récemment, quelques groupes de recherche ont utilisé des stratégies induites par la lumière ou assistées par la lumière pour générer des architectures assemblées discrètes, ouvrant de nouvelles perspectives dans le domaine de la chimie supramoléculaire. Cet article conceptuel vise à introduire les concepts fondamentaux des réactions avec les complexes métalliques d^6 et d^8 utilisés comme bloc de construction pour les auto-assemblages d'espèces discrètes, induites par la lumière.

Contribution :

Baptiste Laramée-Milette : Rédaction de l'article.

Garry S. Hanan: supervision, revision de l'article

Shedding light on photo-induced assembly of discrete ensembles

*Baptiste Laramée-Milette and Garry S. Hanan**

Département de chimie, Université de Montréal, 5155 Ch. de la rampe, Pavillon J.-A. Bombardier, Montréal, Québec, Canada, H3T 2B1

*: E-mail: garry.hanan@umontreal.ca

Manuscript in preparation

2.2. Introduction

Early in the history of modern chemistry, light has been recognized as a crucial component of several natural processes, including vision and photosynthesis.[1] While decomposition of dyes and pigments induced by light was already observed nearly 2000 years ago, as described by Vitruvius, the first literature report of a photoreaction made on purpose was only achieved in the early 1840's by Draper.[2] It is, however, the work of Turro and Hammond as well as Balzani and Carassiti in the early 1960's which gave a decisive impulse to the fields of organic and inorganic photochemistry, respectively.[3] Since then, tremendous work has been accomplished, leading to the development of several synthetic, photo-redox and photo-catalytic processes.[4] Nowadays, light is considered as an important tool in synthetic chemistry, where reactions induced by the interaction of photons with matter are considered no more peculiar than conventional thermal reactions. More specifically, photochemical reactions involving organometallic species and coordination compounds, especially those of d^6 and d^8 transition metal complexes,[5] have been widely investigated and shows great potentials in a wide range of applications, such as photo-catalysis,[4j, 6] photo-switches[7] as well as in photo-dynamic therapy (i.e. photoCORMs, photoNORMs, photoredox catalysis and other examples).[8]

Furthermore, light has been used for a variety of structural reorganizations sometime impossible to perform with regular heating technique (or at least in a much simpler fashion), such as linkage isomerization,[9] geometrical rearrangement,[10] haptotropic rearrangement,[5e, 11] and photolysis, as schematized in Figure 2.1. It is noteworthy to mention that such rearrangement often leads to new behavior and metal complexes with modified properties, therefore giving new opportunities to fine-tune their optical, electronic as well as the magnetic properties.

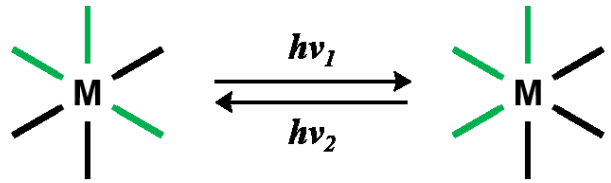

Geometrical rearrangement

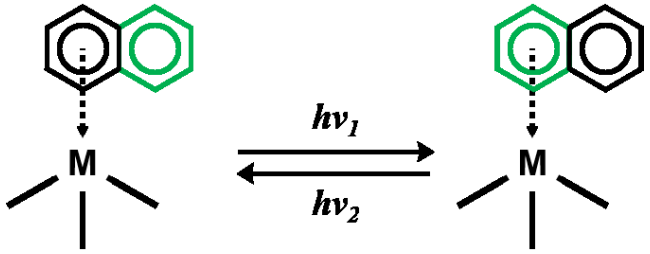

Haptotropic rearrangement

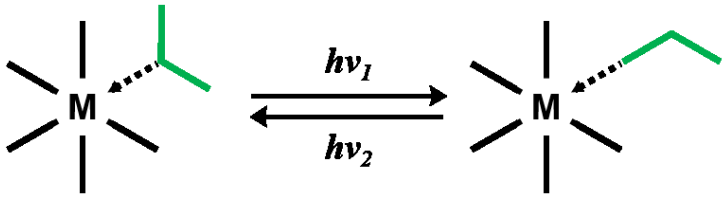

Linkage isomerization

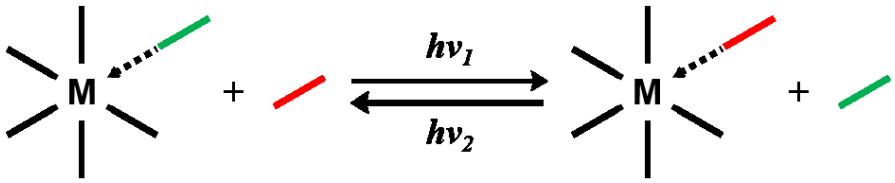

Photolysis

Figure 2.1 - Schematic photo-reactions of organometallic and coordination metal complexes.

Nevertheless, until recently the uses of light in coordination chemistry has been limited to the synthesis/modifications of low nuclearity species, mainly mononuclear metal complexes. The number of studies involving multimetallic species are scarce and research on supramolecular discrete species obtained through a photochemical approach are even more unique.

The starting point of our own research was based on a simple observation related to the chromophore antenna used in natural system to perform photosynthesis. The structure of the light-harvesting complex II (LH-II) in some species of purple bacteria, such as rhodospirillum molischianum, has been known since the mid-90's, owing to the brilliant work of Isaacs and others.[12] This work triggered several studies on both natural and synthetic analogs of the LH-II complex, mainly devoted to the comprehension and relationship activity of the energy transfer between the different parts of the system,[13] to promote the conversion of light into chemical energy.

As shown in Figure 2.2a, the structure of the LH-II unit is rather complicated, however our main interest dwell in the central part (Figure 2.2b), an assembly of 8 porphyrin dimers with an average metal-to-metal distance of 9 Å. This elegant assembly shows Nature's ability to work with non-covalent interactions to build supramolecular architectures. Nevertheless, as it will be described later, one of the key factor to a successful self-assembly process requires reversibility, therefore prompting our interest in the method used by Nature to achieve such flawless assembly without the needs of a flask. While we haven't found any thorough investigation on the subject in the literature, our main hypothesis stands on the possibility for Nature to use the sun's energy, through light irradiation, to trigger the coordination/de-coordination process to achieve reversibility and avoid the formation of long polymeric chains.

Therefore, this Concept article aim to outline the progress made in the field of light-triggered formation and modification of discrete entities and investigate possible paths to create new supramolecular architectures. While still in its infancy, we think that it is a challenging field of research with many opportunities that may perhaps not be unveiled by solely using conventional thermal reaction.

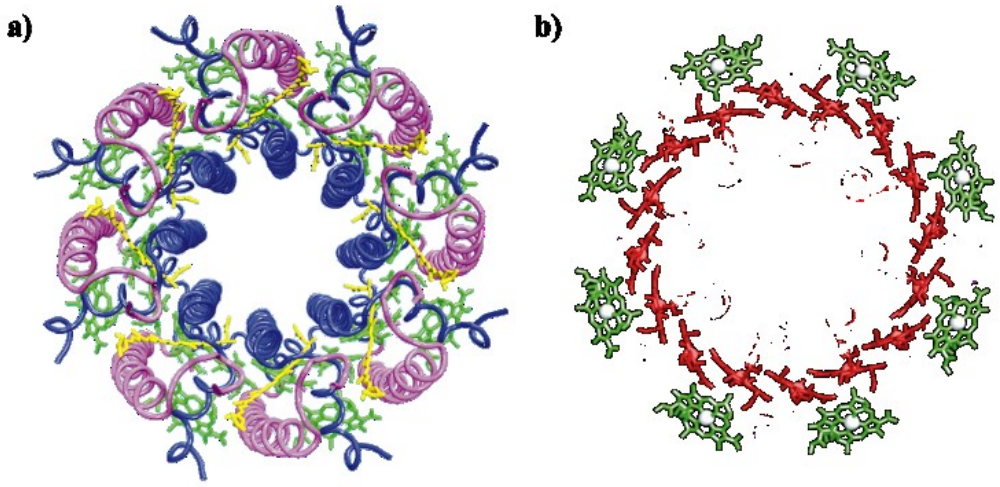

Figure 2.2 - The LH-II complex from *Rs. molischianum*. a) View from above and b) detailed view of the porphyrin assembly.

2.3. Discrete assemblies *via* light irradiation

2.3.1. General concept

The assembly of complementary building blocks into polymeric as well as discrete entities is a well-known procedure which has led to the synthesis of hundreds of bidimensional and tridimensional species over the past decades.[14] The key steps required for molecular assembly are simples and have been previously described[15]:

Intermolecular interaction: The components of the assembly are required to interact together in a perfect synergy. The building block may interact with another module of a different nature ([n + n] type assembly) or, when designed properly, with a building block of the same nature, (head-to-tail or [n x 1] type assembly).

Reversibility: The interaction must be reversible. Reversibility is essential to achieve the self-correction process required to obtain the thermodynamically favored assembly over the kinetically formed intermediates.

Complementary: The coordination vector of the precursor(s) must complete each other, in order to achieve a discrete entity.

Furthermore, in the specific case of assemblies obtained via photo-irradiation, a fourth specification can be introduced:

Photo-active or light-responsive: Either the precursor to the assembly or the assemble species itself must require light-irradiation to be formed. As depicted in Figure 2.3, the first scenario where the precursor to the assembly is created through a photochemical means is termed "light- assisted assembly" while the second situation is labeled as "light-induced assembly". Alternatively, if an assembly obtained by conventional heating procedures is photo-active and can be modified afterward with light, it will be named "post-assembly light-induced modification".

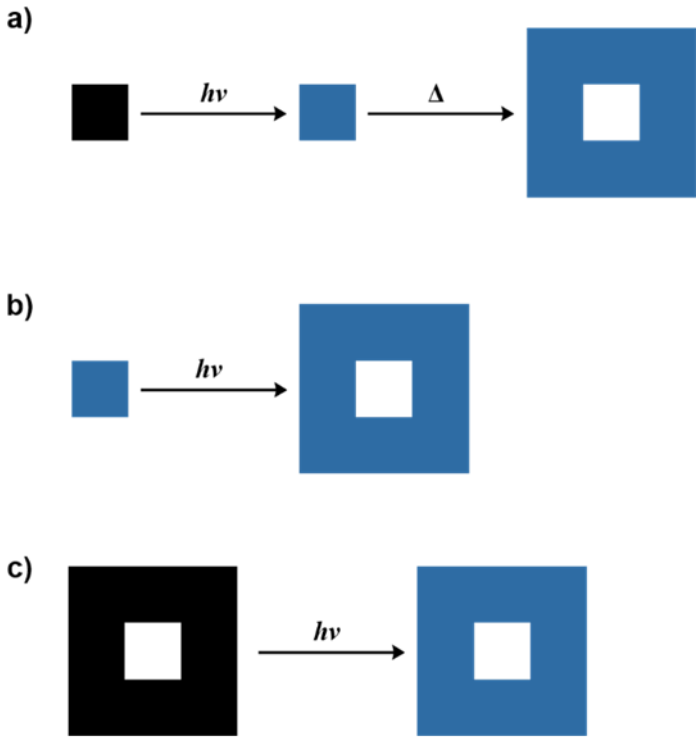

Figure 2.3 - Schematic representation of a) Light-assisted assembly, b) Light-induced self-assembly and c) light-induced post-modifications.

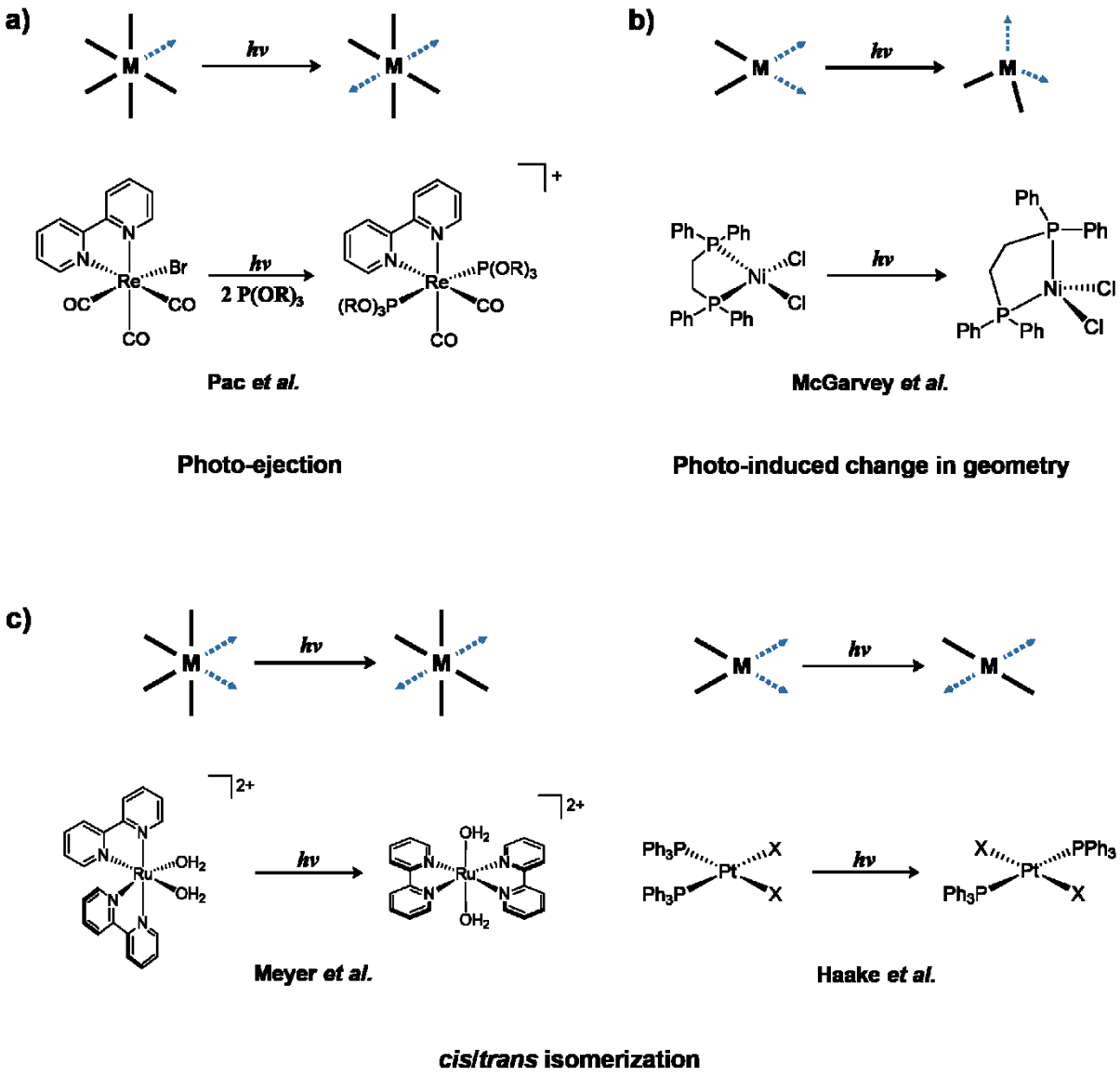

Figure 2.4a - Strategies to photochemically pre-organized the building block in light-assisted assembly: a) photo-ejection of a ligand; b) photo-induced change in the geometry; c) *cis*-/*trans*- isomerization.

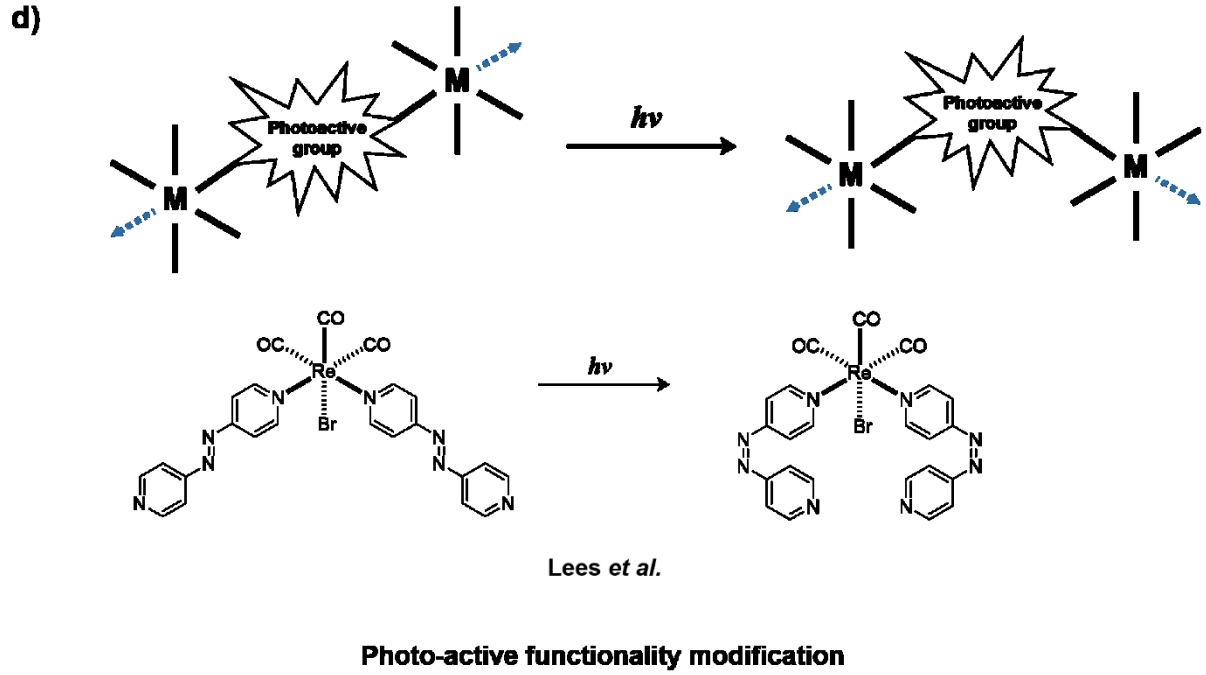

Figure 2.5b - Strategies to photochemically pre-organized the building block in light-assisted assembly: d) modification of a photo-active functionality.

2.3.2. Light-assisted assembly

As mentioned before, the first step to light-assisted assembly involves the photo-induced formation of the molecular precursor prior to the construction of the supramolecular entities. As depicted in Figure 2.4, preorganization might involve any structural rearrangement (photo-ejection,[8l, 16] *cis*-/*trans*- and *mer*-/*fac* isomerization,[17] change of geometry,[18] photo-active functionalities[19]) leading to a coordination angle suitable to further assemble the precursor into a more complex species.

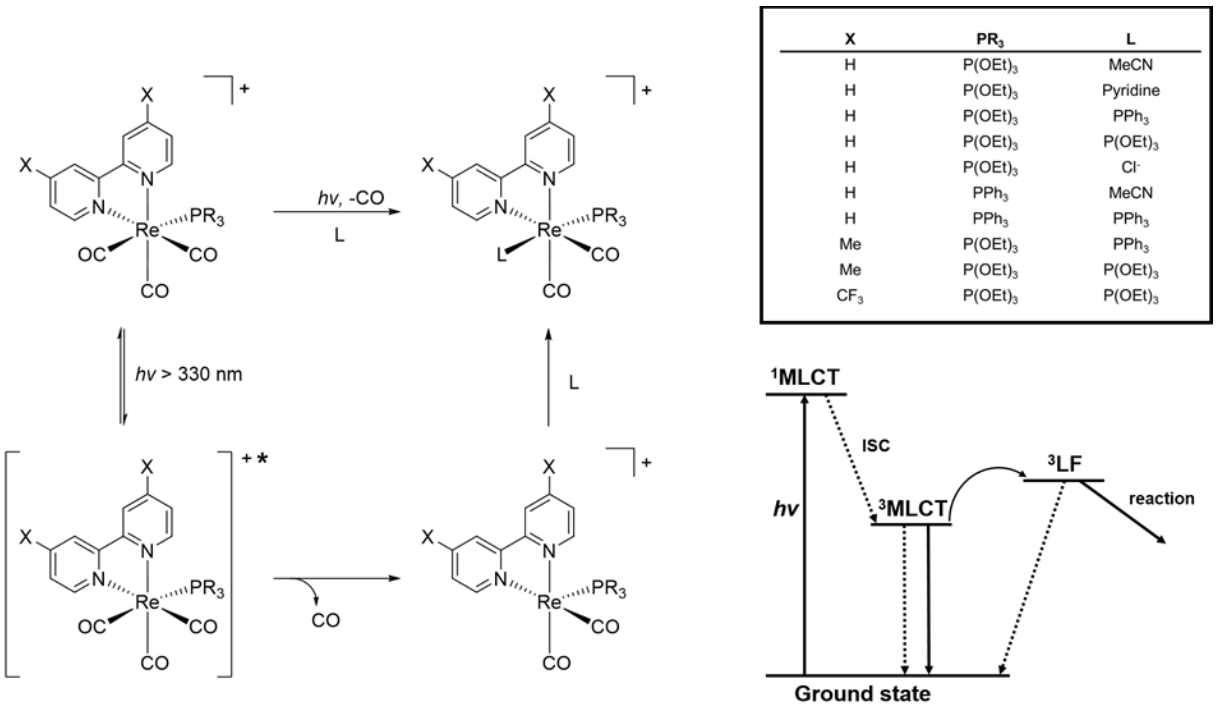

X	PR_3	L
H	$P(OEt)_3$	MeCN
H	$P(OEt)_3$	Pyridine
H	$P(OEt)_3$	PPh_3
H	$P(OEt)_3$	$P(OEt)_3$
H	$P(OEt)_3$	Cl^-
H	PPh_3	MeCN
H	PPh_3	PPh_3
Me	$P(OEt)_3$	PPh_3
Me	$P(OEt)_3$	$P(OEt)_3$
CF_3	$P(OEt)_3$	$P(OEt)_3$

Figure 2.6 - Example of pre-organization in in $[Re^{I}(N^N)(CO)_3(PR_3)]^+$ complexes leading to the photo-ejection of the ligand *trans*- to the phosphine.

Nevertheless, in the case of light-assisted assembly, the supramolecular species itself is not synthesized through a photochemical means, requiring regular thermal technique to achieve the final supramolecular structure.

An excellent example of such process was demonstrated a few years ago, by Ishitani and co-workers. The group has been active in the field of light-promoted substitution with rhenium-based metal complexes since the early 2000's, when they presented an elegant pathway to prepare *cis*,*trans*-$[Re(N^N)(CO)_2(PR_3)(L)]^+$, a new class of dicarbonyl rhenium complexes, from *fac*-$[Re(N^N)(CO)_3(PR_3)]^+$ through a photochemical means (Figure 2.6).[20]

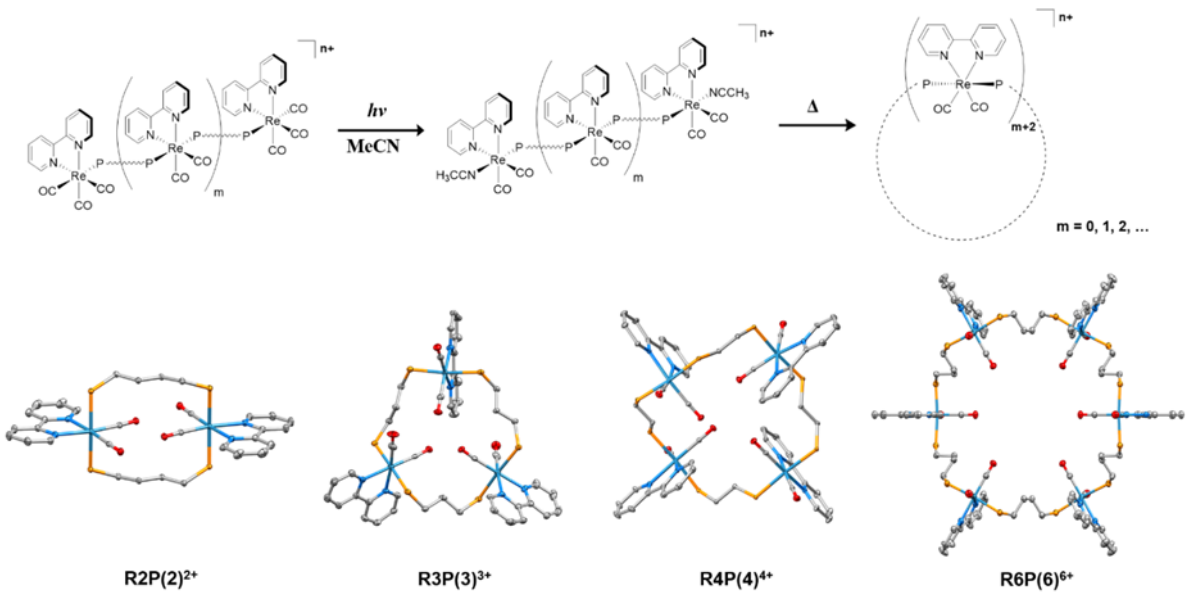

Figure 2.7 - Rhenium(I) bidimentional assemblies obtained with the light-assisted assembly strategy.

The Ishitani group later demonstrated that bisphosphine derivatives could further be used to obtain multimetallic linear species by using a "complexes as ligands" strategy, leading to a series of oligomers and polymers of up to 20 units,[21] obtained in a controlled step-wise fashion.

As depicted in Figure 2.7, the careful removal of the two terminal carbonyl ligands by light-irradiation in a coordinating solvent such as acetonitrile, leads to a flexible precursor suitable for cyclization by the same strategy, which requires a thermal approach to succeed in the preparation of polynuclear ring-shaped Re(I) species.[22]

2.3.3. Light-induced assembly

The formation of discrete assemblies through light irradiation, which is the key concept of this article, is highly fascinating and only two examples are known in the literature. The original example was presented in 2009 by the Fujita group,[23] which demonstrated an efficient way to obtain both bidimensional and tridimensional discrete entities based on the photo-labilization of a platinum(II)-pyridine bond with high-energy UV irradiation, following a [n + n] directional bonding strategy (Figure 2.8).

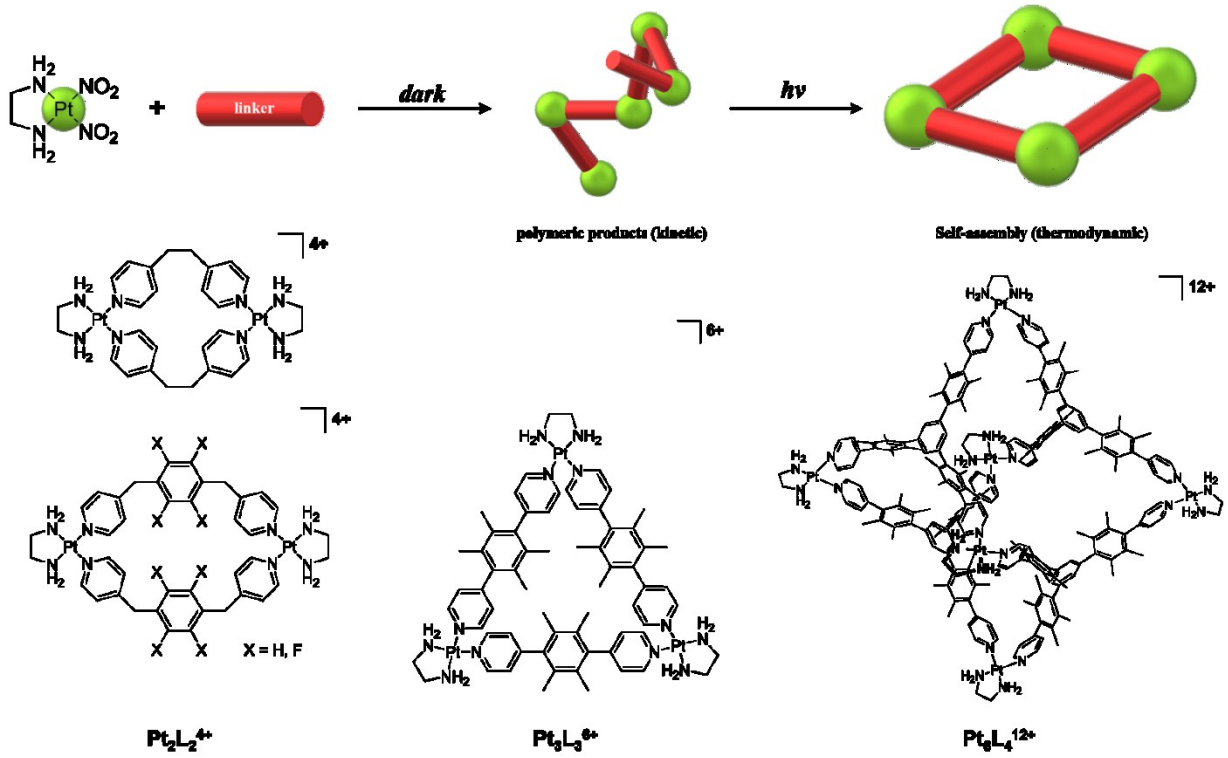

Figure 2.8 - Schematic representation of bidimensional and tridimensional [n + n] discrete species obtained through light-induced assembly.

The mechanism is similar to the one described before in the case of the Re(I) species. Nevertheless, it is important to mention that photochemically driven Pt(II) assembly cannot be generalized to all ligands. In fact, it seems that ligands with extended π-conjugation (i.e. 4,4'-bipyridine, 1,4-bis(4-pyridyl)benzene and 1,2-bis(4-pyridyl)acetylene) do not lead to their respective assembly. As suggested by DFT calculations, the photo-inactivity of these species is due to the relatively low energy of the π* orbitals, which lies below the Pt(II) antibonding d_{x2-y2} orbital. Therefore, the introduction of functionalities that disrupt the conjugation tend to destabilize the ligand π* orbitals, moving them to higher energy, above the platinum d_{x2-y2} orbitals, leading to the required photo-activity.

Recently, our group worked on the assembly and dis-assembly of a polypyridyl Ru(II) molecular square[24] (Figure 2.9) based on a complex-as-ligand polypyridyl-type precursor, following a [n x 1] bonding strategy. Photo-irradiation with visible energy

irradiation (456 nm) in a non-coordinating solvent lead to the photo-ejection of the acetonitrile solvent molecule *cis*- to the terpyridyl ligand, therefore creating a 90° angle suitable for the assembly of a molecular square. The square itself shows enhanced optical properties due to the inherent rigidity of the assembly, where the lifetime of the excited state was measured to be 40 times that of its ruthenium precursor, while the quantum yield was shown to be three orders of magnitude higher, reaching up to 1.0%. We also demonstrated that by dissolving the square in acetonitrile and upon irradiation with the exact same wavelength of irradiation used to form the square, we were also able to dis-assemble the molecule into its original starting material. We believe that the mechanism follows the same path as mentioned before, through thermal population of the ^{3}LF state, as shown by others.

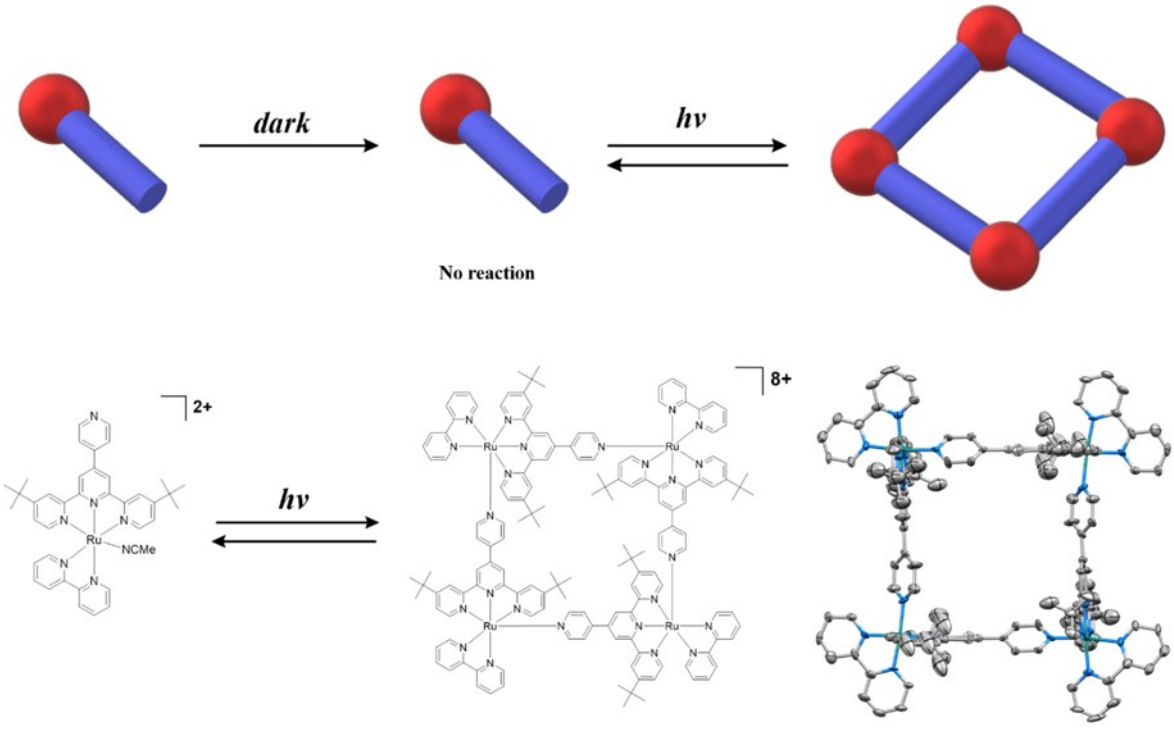

Figure 2.9 - Schematic representation of the light-induced [n x 1] tetraruthenium assembly.

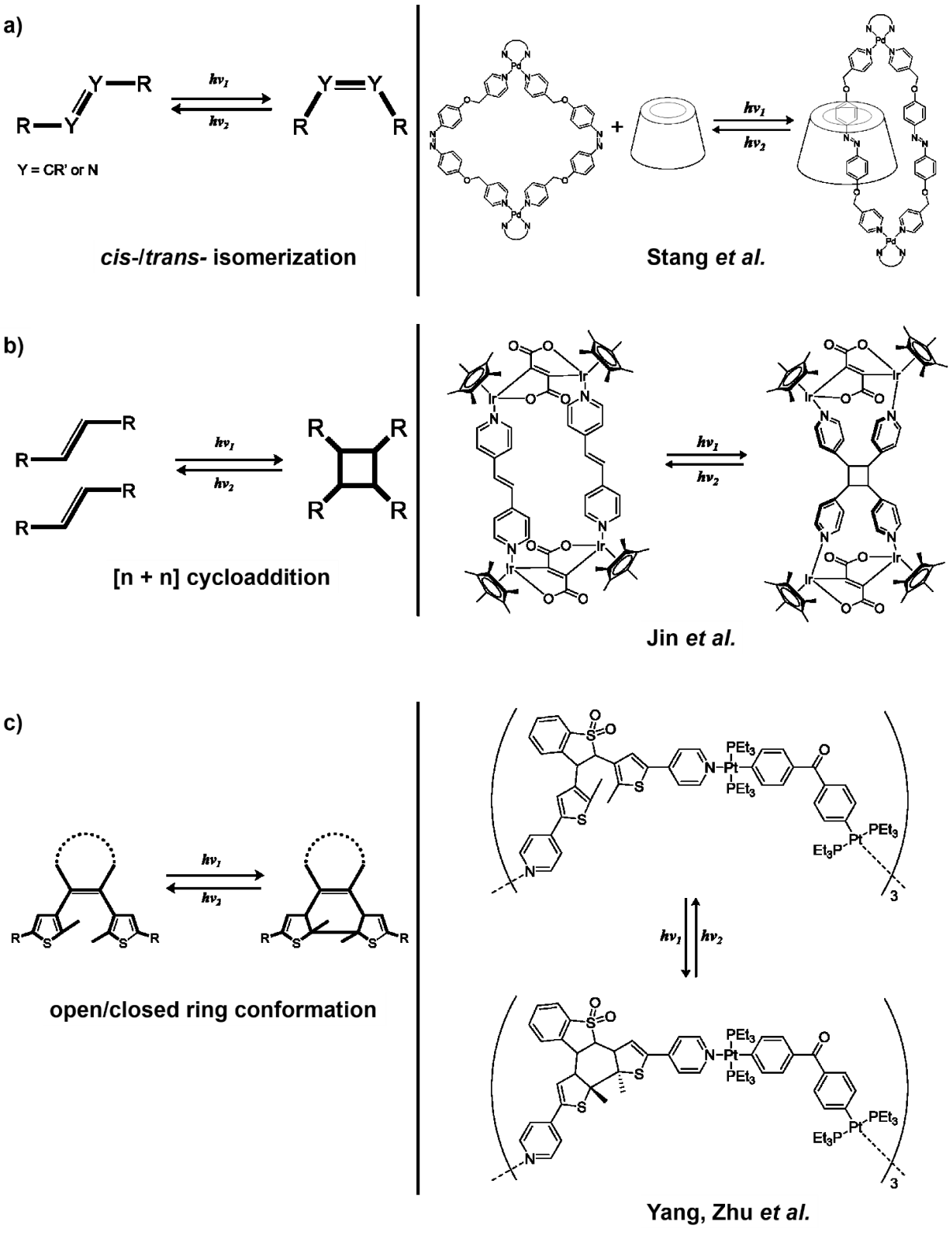

Figure 2.10 - Examples of the most common light-induced post-modification of discrete metallacycles enclosing photo-active functionnalities.

2.3.4. Post-assembly light-induced modifications

Discrete coordination assemblies made of ligands with photo-active functionalities are of interest since they can subsequently be modified. Depending on the type of functionalities, this modification can be reversible, therefore leading to molecules able to act as molecular switches. Several examples of discrete species with different categories of photo-functional groups (especially alkene, dithienylethene, as well as azobenzene derivatives, see Figure 2.10) have been exploited in the past years. While other examples involving a similar strategy with polymeric one-, two- as well as three-dimensional architectures exists in the literature,[25] our discussion will be limited to the discrete assemblies.

One of the first example of post-modification on a metallacycle was described in the early 2000's by Lees and co-workers on a mixed Pd^{II}/Re^{I} tetranuclear species involving the ligand *trans*-4,4'-azopyridine which,[19a] upon irradiation at 366 nm, isomerized to the *cis*- derivative leading to an intramolecular reorganization into a dinuclear species (Figure 2.11). Recently, a similar experiment conducted by Stang et al. (Figure 2.10) with a flexible azobenzene ligand lead to the reversible catenation of a Pd^{II} metallacycle in a photo-controllable manner.[26]

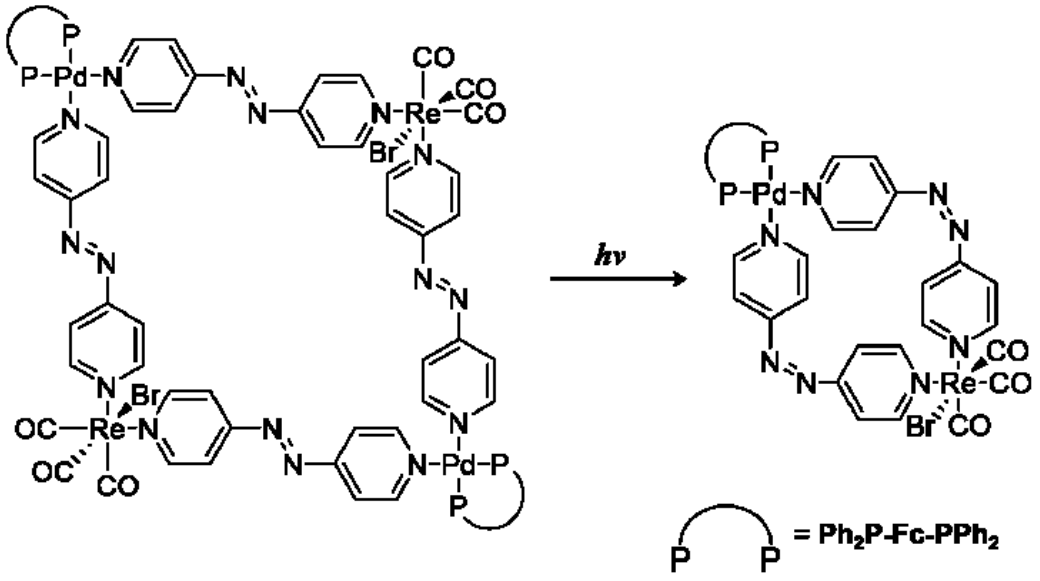

Figure 2.11 - Light-induced post-modification of a Re(I)-Pd(II) discrete metallacycle containing azopyridine linkers.

Another strategy consists in the use of a metal template which bring two olefins in close proximity, thus giving the opportunity to photo-induced a [2 + 2] cyclodimerization. MacGillivray and co-workers were the first to describe the intermolecular [2 + 2] photodimerization in coordination-driven self-assemble discrete systems,[27] where Schiff-base Zn^{II} complexes were used to bring the neighboring alkenes closer. A few other examples have been reported in the past years, especially with silver and gold, but also with copper, rhenium and iridium (Figure 2.10).[28]

A few groups have harnessed the use of dithienylethene ligands, which can display an open or closed configuration depending on the wavelength of irradiation. While the first example shown by Yang, Zhu and co-workers in 2012 dealt with bi-dimensional metallacycles (Figure 2.10),[29] more recent examples demonstrated the possibilities to use this type of ligand in three-dimensionnal architectures, such as metallacages[30] (Figure 2.12) and MOFs.[31]

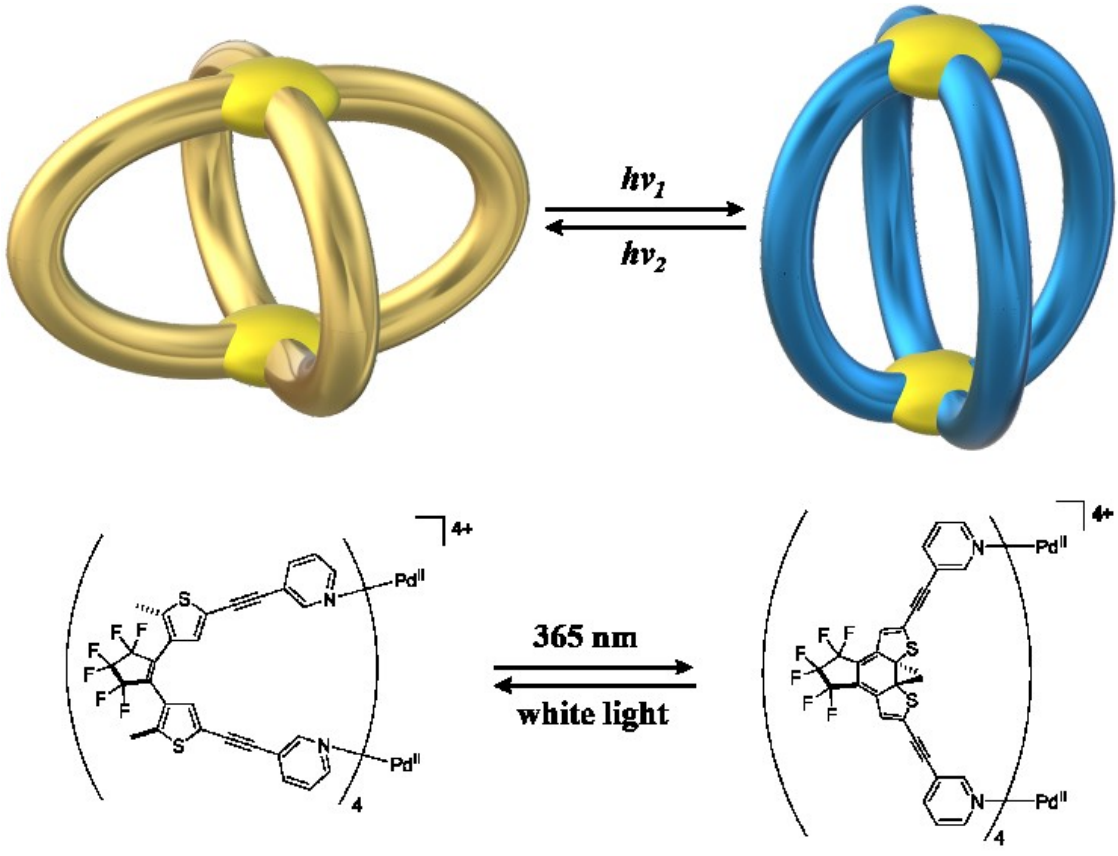

Figure 2.12 – Post-modifications of dithienylethene-based metallacage.

Although most post-assembly light-induced modifications uses photo-active ligands, there is some rare evidences of species prepared without such circumstances. The Fujita group has demonstrated that the photo-labilization of both Pt^{II}-pyridyl bond and Ru^{II}-pyridyl bond could be used to photo-trigger the selective and quantitative formation of catetanes.[32] Another example by the Lusby group has shown possible the preparation of a series of M_4L_6 Co(III) tetrahedra from M_2L_3 helicates, in a photoredox-induced fashion.[33]

2.3.5. Conclusion and outlook

Beyond a doubt, chemistry promoted by light-irradiation has entered its golden era. While photo-induced modification of mono-nuclear species has been widely explored for the past decades, uses of photochemistry in a controlled fashion to organize supramolecular entities is an exciting field of research with infinite possibilities.

2.3.6. Acknowledgements

G.S.H. and B.L.M. thank the Natural Sciences and Engineering Research Council (NSERC) of Canada, the Fondation J.A. Bombardier and the Université de Montréal for financial support.

2.3.7. References

[1] G. Ciamician, *Science* **1912**, *36*, 385-394.

[2] J. W. Draper, *Phil. Mag. Series 3* **1843**, *23*, 401-415.

[3] a) G. S. Hammond, N. J. Turro, *Science* **1963**, *142*, 1541-1553; b) V. Balzani, V. Carassiti, L. Moggi, F. Scandola, *Inorg. Chem.* **1965**, *4*.

[4] a) J. Kagan in *Organic Photochemistry: Principles and Applications*, Academic Press Limited, New York, **1993**, p; b) T. Bach, J. P. Hehn, *Angew. Chem. Int. Ed.* **2011**, *50*, 1000-1045; c) M. D. Karkas, J. A. Porco, Jr., C. R. Stephenson, *Chem. Rev.* **2016**, *116*, 9683-9747; d) M. Oelgemoller, *Chem. Rev.* **2016**, *116*, 9664-9682; e) V. Ramamurthy, J. Sivaguru, *Chem. Rev.* **2016**, *116*, 9914-9993; f) M. H. Shaw, J. Twilton, D. W. MacMillan, *J. Org. Chem.* **2016**, *81*, 6898-6926; g) X. Deng, Z. Li, H. Garcia, *Chem. Eur. J.* **2017**, *23*, 11189-11209; h) J. Twilton, C. Le, P. Zhang,

M. H. Shaw, R. W. Evans, D. W. C. MacMillan, *Nat Rev. Chem.* **2017**, *1*; i) C. K. Prier, D. A. Rankic, D. W. MacMillan, *Chem. Rev.* **2013**, *113*, 5322-5363; j) A. J. Esswein, D. G. Nocera, *Chem. Rev.* **2007**, *107*, 4022-4047; k) A. KudoY. Miseki, *Chem. Soc. Rev.* **2009**, *38*, 253-278; l) V. Artero, M. Chavarot-Kerlidou, M. Fontecave, *Angew. Chem. Int. Ed.* **2011**, *50*, 7238-7266; m) T. S. Teets, D. G. Nocera, *Chem. Commun.* **2011**, *47*, 9268-9274; n) R. N. Perutz, B. Procacci, *Chem. Rev.* **2016**, *116*, 8506-8544; o) N. Elgrishi, M. B. Chambers, X. Wang, M. Fontecave, *Chem. Soc. Rev.* **2017**, *46*, 761-796; p) S. Y. Tee, K. Y. Win, W. S. Teo, L. D. Koh, S. Liu, C. P. Teng, M. Y. Han, *Adv. Sci.* **2017**, *4*, 1600337.

[5] a) A. W. Adamson, W. L. Waltz, E. Zinato, D. W. Watts, P. D. Fleishauer, R. D. Lindholm, *Chem. Rev.* **1968**, *68*, 541-585; b) E. J. Baerends, A. Rosa, *Coord. Chem. Rev.* **1998**, *177*, 97-125; c) A. Vlcek Jr., *Coord. Chem. Rev.* **1998**, *177*, 219-256; d) A. Kumar, S.-S. Sun, A. J. Lees in *Photophysics and Photochemistry of Organometallic Rhenium Diimine Complexes*, **2009**, pp. 37-71; e) H. Nakai, K. Isobe, *Coord. Chem. Rev.* **2010**, *254*, 2652-2662; f) H. Takeda, K. Koike, T. Morimoto, H. Inumaru, O. Ishitani in *Photochemistry and photocatalysis of rhenium(I) diimine complexes*, **2011**, pp. 137-186; g) J. J. Vittal, H. S. Quah, *Dalton Trans.* **2017**, *46*, 7120-7140.

[6] a) P. Chowdhury, G. MalekshoarA. Ray, *Inorganics* **2017**, *5*, 34; b) J. I. Day, K. Teegardin, J. Weaver, J. Chan, *Org. Process Res. Dev.* **2016**, *20*, 1156-1163; c) P. Kumar, C. Joshi, A. K. Srivastava, P. Gupta, R. Boukherroub, S. L. Jain, *ACS Sustain. Chem. Eng.* **2016**, *4*, 69-75; d) C. K. Prier, D. A. Rankic, D. W. MacMillan, *Chem. Rev.* **2013**, *113*, 5322-5363; e) D. M. Schultz, T. P. Yoon, *Science* **2014**, *343*, 1239176.

[7] a) S. Decurtins, P. Gutlich, K. M. Hasselbach, A. Hauser, H. Spiering, *Inorg. Chem.* **1985**, *24*, 2174-2178; b) P. Natarajan, M. Schmittel, *Inorg. Chem.* **2013**, *52*, 8579-8590; c) B. Rosner, M. Milek, A. Witt, B. Gobaut, P. Torelli, R. H. Fink, M. M. Khusniyarov, *Angew. Chem. Int. Ed.* **2015**, *54*, 12976-12980; d) C.-C. Wu, J. Jung, P. K. Gantzel, P. Gutlich, D. N. Hendrickson, *Inorg. Chem.* **1997**, *36*, 5339-5347.

[8] a) K. L. Haas, K. J. Franz, *Chem. Rev.* **2009**, *109*, 4921-4960; b) R. D. Rimmer, A. E. Pierri, P. C. Ford, *Coord. Chem. Rev.* **2012**, *256*, 1509-1519; c) O. J. Stacey, S. J.

A. Pope, *RSC Adv.* **2013**, *3*; d) T. R. deBoer-Maggard, P. K. Mascharak in *Photoactivatable metal complexes and their use in biology and medicine*, (Ed. T. Storr), John Wiley & Sons, Hoboken, **2014**; e) M. A. GonzalesP. K. Mascharak, *J. Inorg. Biochem.* **2014**, *133*, 127-135; f) A. E. Pierri, D. A. Muizzi, A. D. Ostrowski, P. C. Ford in *Photo-Controlled Release of NO and CO with Inorganic and Organometallic Complexes*, **2014**, pp. 1-45; g) E. Ruggiero, S. Alonso-de Castro, A. Habtemariam, L. Salassa in *The Photochemistry of Transition Metal Complexes and Its Application in Biology and Medicine*, **2014**, pp. 69-107; h) J. D. Knoll, C. Turro, *Coord. Chem. Rev.* **2015**, *282-283*, 110-126; i) C. Mari, V. Pierroz, S. Ferrari, G. Gasser, *Chem. Sci.* **2015**, *6*, 2660-2686; j) K. Mitra, *Dalton Trans.* **2016**, *45*, 19157-19171; k) E. Üstün, A. Özgür, K. A. Coşkun, S. Demir Düşünceli, İ. Özdemir, Y. Tutar, *Transit. Met. Chem.* **2017**, *42*, 331-337; l) J. K. White, R. H. Schmehl, C. Turro, *Inorg. Chim. Acta* **2017**, *454*, 7-20.

[9] a) F. Akhter, M. Kojima, M. Hirotsu, S. Kashino, Y. Yoshikawa, *Chem. Lett.* **1994**, 2393-2396; b) F. Akhter, M. Kojima, T. Yoshi, S. Kashino, Y. Yoshikawa, *Chem. Lett.* **1994**, 171-174; c) F. Akhter, M. Hirotsu, I. Sugimoto, M. Kojima, *Bull. Chem. Soc. Jpn.* **1996**, *69*, 643-653; d) J. J. Rack, J. R. Winkler, H. B. Gray, *J. Am. Chem. Soc.* **2001**, *123*, 2432-2433; e) E. Alessio, B. Serli, E. Zangrando, M. Calligaris, Natalia S. Panina, *Eur. J. Inorg. Chem.* **2003**, *2003*, 3160-3166; f) J. J. Rack, N. V. Mockus, *Inorg. Chem.* **2003**, *42*, 5792-5794; g) J. J. Rack, A. A. Rachford, A. M. Shelker, *Inorg. Chem.* **2003**, *42*, 7357-7359; h) T. T. To, C. E. Barnes, T. J. Burkey, *Organometallics* **2004**, *23*, 2708-2714; i) A. A. Rachford, J. L. Petersen, J. J. Rack, *Inorg. Chem.* **2005**, *44*, 8065-8075; j) D. P. Butcher, Jr., A. A. Rachford, J. L. Petersen, J. J. Rack, *Inorg. Chem.* **2006**, *45*, 9178-9180; k) T. Hosoya, H. Uekusa, Y. Ohashi, T. Ohhara, R. Kuroki, *Bull. Chem. Soc. Jpn.* **2006**, *79*, 692-701; l) N. V. Mockus, J. L. Petersen, J. J. Rack, *Inorg. Chem.* **2006**, *45*, 8-10; m) A. A. Rachford, J. L. Petersen, J. J. Rack, *Inorg. Chem.* **2006**, *45*, 5953-5960; n) A. A. Rachford, J. J. Rack, *J. Am. Chem. Soc.* **2006**, *128*, 14318-14324; o) A. A. Rachford, J. L. Petersen, J. J. Rack, *Dalton Trans.* **2007**, 3245-3251; p) N. V. Mockus, D. Rabinovich, J. L. Petersen, J. J. Rack, *Angew. Chem. Int. Ed.* **2008**, *47*, 1458-1461; q) D. A. Lutterman, A. A. Rachford, J. J. Rack, C. Turro, *J. Phys. Chem. A* **2009**,

113, 11002-11006; r) B. A. McClure, N. V. Mockus, D. P. Butcher, Jr., D. A. Lutterman, C. Turro, J. L. Petersen, J. J. Rack, *Inorg. Chem.* **2009**, *48*, 8084-8091; s) B. A. McClure, J. J. Rack, *Angew. Chem. Int. Ed.* **2009**, *48*, 8556-8558; t) S. Ng, M. B. Walker, P. J. Farmer, *Inorg. Chim. Acta* **2009**, *362*, 4013-4016; u) T. A. Grusenmeyer, B. A. McClure, C. J. Ziegler, J. J. Rack, *Inorg. Chem.* **2010**, *49*, 4466-4470; v) D. A. Lutterman, A. A. Rachford, J. J. Rack, C. Turro, *J. Phys. Chem. Lett.* **2010**, *1*, 3371-3375; w) B. A. McClure, E. R. Abrams, J. J. Rack, *J. Am. Chem. Soc.* **2010**, *132*, 5428-5436; x) B. A. McClure, J. J. Rack, *Eur. J. Inorg. Chem.* **2010**, *2010*, 3895-3904; y) E. S. Kelbysheva, M. G. Ezernitskaya, T. V. Strelkova, Y. A. Borisov, A. F. Smol'yakov, Z. A. Starikova, F. M. Dolgushin, A. N. Rodionov, B. V. Lokshin, N. M. Loim, *Organometallics* **2011**, *30*, 4342-4353; z) B. A. McClure, J. J. Rack, *Inorg. Chem.* **2011**, *50*, 7586-7590; aa) M. Nishikawa, K. Nomoto, S. Kume, H. Nishihara, *J. Am. Chem. Soc.* **2012**, *134*, 10543-10553; ab) M. R. Warren, S. K. Brayshaw, L. E. Hatcher, A. L. Johnson, S. Schiffers, A. J. Warren, S. J. Teat, J. E. Warren, C. H. Woodall, P. R. Raithby, *Dalton Trans.* **2012**, *41*, 13173-13179; ac) K. Garg, J. T. Engle, C. J. Ziegler, J. J. Rack, *Chem. Eur. J.* **2013**, *19*, 11686-11695; ad) K. Garg, S. I. M. Paris, J. J. Rack, *Eur. J. Inorg. Chem.* **2013**, *2013*, 1142-1148; ae) Y. Jin, J. J. Rack, *Isr. J. Chem.* **2013**, *53*, 280-287; af) A. W. King, Y. Jin, J. T. Engle, C. J. Ziegler, J. J. Rack, *Inorg. Chem.* **2013**, *52*, 2086-2093; ag) M. Nishikawa, Y. Takara, Y. Hattori, K. Nomoto, T. Kusamoto, S. Kume, H. Nishihara, *Inorg. Chem.* **2013**, *52*, 8962-8970; ah) K. Garg, A. W. King, J. J. Rack, *J. Am. Chem. Soc.* **2014**, *136*, 1856-1863; ai) A. W. King, J. P. Malizia, J. T. Engle, C. J. Ziegler, J. J. Rack, *Dalton Trans.* **2014**, *43*, 17847-17855; aj) A. W. King, B. A. McClure, Y. Jin, J. J. Rack, *J. Phys. Chem. A* **2014**, *118*, 10425-10432; ak) X. Liu, X. Wang, B. Xu, L. Andrews, *Phys. Chem. Chem. Phys.* **2014**, *16*, 2607-2620; al) M. R. Warren, T. L. Easun, S. K. Brayshaw, R. J. Deeth, M. W. George, A. L. Johnson, S. Schiffers, S. J. Teat, A. J. Warren, J. E. Warren, C. C. Wilson, C. H. Woodall, P. R. Raithby, *Chem. Eur. J.* **2014**, *20*, 5468-5477; am) A. W. King, L. Wang, J. J. Rack, *Acc. Chem. Res.* **2015**, *48*, 1115-1122; an) H. Li, L. Zhang, Y. Wang, X. Fan, *RSC Adv.* **2015**, *5*, 58580-58586; ao) J. M. Skelton, R. Crespo-Otero, L. E. Hatcher, S. C. Parker, P. R. Raithby, A. Walsh, *CrystEngComm* **2015**, *17*, 383-394; ap) M. Hirahara, A.

Tsukamoto, H. Goto, S. Tada, M. Yagi, Y. Umemura, *Chem. Eur. J.* **2016**, *22*, 2590-2594; aq) H. Li, L. Zhang, L. Zheng, X. Li, X. Fan, Y. Zhao, *Chem. Eur. J.* **2016**, *22*, 14285-14292.

[10] a) M. Okazaki, Y. Kawano, H. Tobita, S. Inomata, H. Ogino, *Chem. Lett.* **1995**, 1005-1006; b) A. J. Deeming, A. E. Vassos, *J. Chem. Soc., Dalton Trans.* **1997**, *1997*, 3519-3524; c) S. Özkar, C. Kayran, N. Demir, *J. Organomet. Chem.* **2003**, *688*, 62-67; d) A. R. McDonald, M. Lutz, L. S. von Chrzanowski, G. P. M. van Klink, *Inorg. Chem.* **2008**, *47*, 6681-6691; e) K. Tsuchiya, E. Ito, S. Yagai, A. Kitamura, T. Karatsu, *Eur. J. Inorg. Chem.* **2009**, *2009*, 2104-2109; f) P. Li, B. de Bruin, J. N. H. Reek, W. I. Dzik, *Organometallics* **2015**, *34*, 5009-5014.

[11]a) H. Nagashima, T. Fukahori, M. Nobata, A. Suzuki, M. Nakazawa, K. Itoh, *Organometallics* **1994**, *13*, 3427-3433; b) H. C. Jahr, M. Nieger, K. Heinz Dötz, *Chem. Commun.* **2003**, 2866-2867; c) K. H. Dotz, H. C. Jahr, *Chem. Rec.* **2004**, *4*, 61-71; d) H. C. Jahr, M. Nieger, K. H. Dotz, *Chem. Eur. J.* **2005**, *11*, 5333-5342; e) T. A. Albright, P. I. Dosa, T. N. Grossmann, V. N. Khrustalev, O. A. Oloba, R. Padilla, R. Paubelle, A. Stanger, T. V. Timofeeva, K. P. Vollhardt, *Angew. Chem. Int. Ed.* **2009**, *48*, 9853-9857; f) T. A. Albright, R. Drissi, V. Gandon, S. Oldenhof, O. A. Oloba-Whenu, R. Padilla, H. Shen, K. P. Vollhardt, V. Vreeken, *Chem. Eur. J.* **2015**, *21*, 4546-4550.

[12]a) S. Karrasch, P. A. Bullough, R. Ghosh, *EMBO J.* **1995**, *14*, 631-638; b) G. McDermott, S. M. Prince, A. A. Freer, A. M. Hawthornthwaite-Lawless, M. Z. Papiz, R. J. Codgell, N. W. Isaacs, *Nature* **1995**, *374*, 517-521; c) J. Koepke, X. Hu, C. Muenke, K. Schulten, H. Michel, *Structure* **1996**, *4*, 581-597; d) H. Savage, M. Cyrklaff, G. Montoya, W. Kuhlbrandt, I. Sinning, *Structure* **1996**, *4*, 243-252; e) M. Z. Papiz, S. M. Prince, T. Howard, R. J. Cogdell, N. W. Isaacs, *J. Mol. Biol.* **2003**, *326*, 1523-1538.

[13]a) N. W. Isaacs, R. J. Codgell, A. A. Freer, S. M. Prince, *Curr. Opin. Struct. Biol.* **1995**, *5*, 794-797; b) A. A. Freer, S. M. Prince, K. Sauer, M. Z. Papiz, A. M. Hawthornthwaite-Lawless, G. McDermott, R. J. Cogdell, N. W. Isaacs, *Structure* **1996**, *4*, 449-462; c) T. Pullerits, V. Sundstrom, *Acc. Chem. Res.* **1996**, *29*, 381-389; d) S. Tretiak, C. Middleton, V. Chernyak, S. Mukamel, *J. Phys. Chem. B* **2000**, *104*,

9540-9553; e) H. S. Cho, H. Rhee, J. K. Song, C.-K. Min, M. Takase, N. Aratani, S. Cho, A. Osuka, T. Joo, D. Kim, *J. Am. Chem. Soc.* **2003**, *125*, 5849-5860; f) R. J. Cogdell, N. W. Isaacs, A. A. Freer, T. D. Howard, A. T. Gardiner, S. M. Prince, M. Z. Papiz, *FEBS Lett.* **2003**, *555*, 35-39; g) N. Krauß, *Curr. Opin. Chem. Biol.* **2003**, *7*, 540-550; h) R. J. Codgell, J. Southall, A. T. Gardiner, C. J. Law, A. Gall, A. W. Roszak, N. W. Isaacs, *C. R. Chimie* **2006**, *9*, 201-206; i) R. J. Cogdell, A. Gall, J. Kohler, *Q. Rev. Biophys.* **2006**, *39*, 227-324; j) P. K. Wawrzyniak, A. Alia, R. G. Schaap, M. M. Heemskerk, H. J. de Groot, F. Buda, *Phys. Chem. Chem. Phys.* **2008**, *10*, 6971-6978; k) J. Yang, M. Park, Z. S. Yoon, T. Hori, X. Peng, N. Aratani, P. Dedecker, J.-i. Hotta, H. Uji-i, M. Sliwa, J. Hofkens, A. Osuka, D. Kim, *J. Am. Chem. Soc.* **2008**, *130*, 1879-1884; l) N. Nagata, Y. Kuramochi, Y. Kobuke, *J. Am. Chem. Soc.* **2009**, *131*, 10-11; m) M. Pajusalu, M. Ratsep, G. Trinkunas, A. Freiberg, *ChemPhysChem* **2011**, *12*, 634-644; n) J. Yang, M. C. Yoon, H. Yoo, P. Kim, D. Kim, *Chem. Soc. Rev.* **2012**, *41*, 4808-4826.

[14] a) D. Philp, J. F. Stoddart, *Angew. Chem. Int. Ed.* **1996**, *35*, 1154-1196; b) M. Fujita in *Molecular Self-Assembly Organic Versus Inorganic Approaches*, Springer, Berlin, Heidelberg, **2000**, p; c) G. F. Swiegers, T. J. Malefetse, *Chem. Eur. J.* **2001**, *7*, 3637-3643; d) R. M. Yeh, A. V. Davis, K. N. Raymond in *Supramolecular Systems: Self-Assembly*, *Vol. 7.8*, Elsevier Ltd., **2004**; e) J.-P. Sauvage, P. Gaspard in *From Non-Covalent Assemblies to Molecular Machines*, Wiley-VCH Verlag GmbH & Co. KGaA, Weinheim, **2011**, p; f) R. Chakrabarty, P. S. Mukherjee, P. J. Stang, *Chem. Rev.* **2011**, *111*, 6810-6918.

[15] a) X. Chi, A. J. Guerin, R. A. Haycock, C. A. Hunter, L. D. Sarson, *J. Chem. Soc., Chem. Commun.* **1995**, 2563-2565; b) P. J. Stang, *Chem. Eur. J.* **1998**, *4*, 19-27; c) G. Ercolani, *J. Am. Chem. Soc.* **2003**, *125*, 16097-16103; d) S. J. Rowan, D. G. Hamilton, P. A. Brady, J. K. M. Sanders, *J. Am. Chem. Soc.* **1997**, *119*, 2578-2579; e) G. Ercolani, *J. Phys. Chem. B* **1998**, *102*, 5699-5703; f) A. V. Davis, R. M. Yeh, K. N. Raymond, *Proc. Nat. Acad. Sci. USA* **2002**, *99*, 4793-4796; g) J. D. Halley, D. A. Winkler, *Complexity* **2008**, *14*, 10-17; h) C. Piguet, *Chem. Commun.* **2010**, *46*, 6209-6231; i) M. M. Safont-Sempere, G. Fernandez, F. Würthner, *Chem. Rev.* **2011**, *111*, 5784-5814.

[16] a) A. Vlcek Jr., *Coord. Chem. Rev.* **2002**, *230*, 225-242; b) S. Sato, A. Sekine, Y. Ohashi, O. Ishitani, A. M. Blanco-Rodriguez, A. Vlcek Jr., T. Unno, K. Koike, *Inorg. Chem.* **2007**, *46*, 3531-3540; c) S. Sato, Y. Matubara, K. Koike, M. Falkenstrom, T. Katayama, Y. Ishibashi, H. Miyasaka, S. Taniguchi, H. Chosrowjan, N. Mataga, N. Fukazawa, S. Koshihara, K. Onda, O. Ishitani, *Chem. Eu. J.* **2012**, *18*, 15722-15734; d) S. Sato, O. Ishitani, *Coord. Chem. Rev.* **2015**, *282-283*, 50-59.

[17] a) S. H. Mastin, P. Haake, *Chem. Commun.* **1970**, 202; b) D. Strauss, P. C. Ford, *J. Chem. Soc., Chem. Commun.* **1977**, 194-195; c) N. W. Alcock, T. J. Kemp, F. L. Wimmer, *Inorg. Chim. Acta* **1980**, *44*, L245-L246; d) B. Durham, S. R. Wilson, D. J. Hodgson, T. J. Meyer, *J. Am. Chem. Soc.* **1980**, *102*, 600-607; e) L. H. Skibsted, W. Weber, R. van Eldik, H. Kelm, P. C. Ford, *Inorg. Chem.* **1983**, *22*, 541-546; f) A. Ross, P. R. Sharp, *Inorg. Chem.* **2013**, *52*, 12645-12654; g) A. B. Tamayo, B. D. Alleyne, P. I. Djurovich, S. Lamansky, I. Tsyba, N. N. Ho, R. Bau, M. E. Thompson, *J. Am. Chem. Soc.* **2003**, *125*, 7377-7387; h) T. Karatsu, E. Ito, S. Yagai, A. Kitamura, *Chem. Phys. Lett.* **2006**, *424*, 353-357.

[18] J. H. Worrell, Genova, *J. Am. Chem. Soc.* **1970**, *92*, 5282-5284.

[19] a) S.-S. Sun, A. J. Lees, *J. Am. Chem. Soc.* **2000**, *122*, 8956-8967; b) D. M. Dattelbaum, M. K. Itokazu, N. Y. M. Iha, T. J. Meyer, *J. Phys. Chem. A* **2003**, *107*, 4092-4095; c) A. O. T. Patrocinio, N. Y. M. Iha, *Inorg. Chem.* **2008**, *47*, 10851-10857; d) Y. Hasegawa, S. Kume, H. Nishihara, *Dalton. Trans.* **2009**, 280-284; e) K. P. M. Frin, M. K. Itokazu, N. Y. M. Iha, *Inorg. Chim. Acta* **2010**, *363*, 294-300.

[20] K. Koike, J. Tanabe, S. Toyama, H. Tsubaki, K. Sakamoto, J. R. Westwell, F. P. A. Johnson, H. Hori, H. Saitoh, O. Ishitani, *Inorg. Chem.* **2000**, *39*, 2777-2783.

[21] Y. Yamamoto, S. Sawa, Y. Funada, T. Morimoto, M. Falkenstrom, H. Miyasaka, S. Shishido, T. Ozeki, K. Koike, O. Ishitani, *J. Am. Chem. Soc.* **2008**, *130*, 14659-14674.

[22] a) T. Morimoto, C. Nishiura, M. Tanaka, J. Rohacova, Y. Nakagawa, Y. Funada, K. Koike, Y. Yamamoto, S. Shishido, T. Kojima, T. Saeki, T. Ozeki, O. Ishitani, *J. Am. Chem. Soc.* **2013**, *135*, 13266-13269; b) T. Asatani, Y. Nakagawa, Y. Funada, S. Sawa, H. Takeda, T. Morimoto, K. Koike, O. Ishitani, *Inorg. Chem.* **2014**, *53*, 7170-7180; c) J. Rohacova, A. Sekine, T. Kawano, S. Tamari, O. Ishitani, *Inorg. Chem.*

2015, *54*, 8769-8777; d) J. Rohacova, O. Ishitani, *Chem. Sci.* **2016**, *7*, 6728-6739; e) T. Morimoto, O. Ishitani, *Acc. Chem. Res.* **2017**, DOI: 10.1021/acs.accounts.7b00244; f) J. Rohacova, O. Ishitani, *Dalton. Trans.* **2017**, *46*, 8899-8919.

[23] K.-i. Yamashita, K.-i. Sato, M. Kawano, M. Fujita, *New J. Chem.* **2009**, *33*, 264-270.

[24] B. Laramée-Milette, F. Nastasi, F. Puntoriero, S. Campagna, G. S. Hanan, *Chem. Eur. J.* **2017**, DOI: 10.1002/chem.201702714.

[25] a) A. Modrow, D. Zargarani, R. Herges, N. Stock, *Dalton. Trans.* **2011**, *40*, 4217-4222; b) J. Park, D. Yuan, K. T. Pham, J. R. Li, A. Yakovenko, H. C. Zhou, *J. Am. Chem. Soc.* **2012**, *134*, 99-102; c) J. W. Brown, B. L. Henderson, M. D. Kiesz, A. C. Whalley, W. Morris, S. Grunder, H. Deng, H. Furukawa, J. I. Zink, J. F. Stoddart, O. M. Yaghi, *Chem. Sci.* **2013**, *4*; d) J. Park, L. B. Sun, Y. P. Chen, Z. Perry, H. C. Zhou, *Angew. Chem. Int. Ed.* **2014**, *53*, 5842-5846; e) S. Castellanos, F. Kapteijn, J. Gascon, *CrystEngComm* **2016**, *18*, 4006-4012; f) S.-L. Huang, T. S. A. Hor, G.-X. Jin, *Coor. Chem. Rev.* **2017**, *346*, 112-122; g) G. K. Kole, A. M. Peedikakkal, B. M. Toh, J. J. Vittal, *Chem. Eur. J.* **2013**, *19*, 3962-3968; h) A. Michaelides, S. Skoulika, M. G. Siskos, *Chem. Commun.* **2013**, *49*, 1008-1010; i) J. M. Chen, Y. X. Hou, Q. K. Zhou, H. ZhangD. Liu, *Dalton Trans* **2017**, *46*, 9755-9759; j) J. H. Lee, S. Park, S. Jeoung, H. R. Moon, *CrystEngComm* **2017**, *19*, 3719-3722.

[26] D. Zhang, Y. Nie, M. L. Saha, Z. He, L. Jiang, Z. Zhou, P. J. Stang, *Inorg. Chem.* **2015**, *54*, 11807-11812.

[27] G. S. Papaefstathiou, Z. Zhong, L. Geng, L. R. MacGillivray, *J. Am. Chem. Soc.* **2004**, *126*, 9158-9159.

[28] a) M. Nagarathinam, A. M. Peedikakkal, J. J. Vittal, *Chem. Commun.* **2008**, 5277-5288; b) M. H. Mir, J. X. Ong, G. K. Kole, G. K. Tan, M. J. McGlinchey, Y. Wu, J. J. Vittal, *Chem. Commun.* **2011**, *47*, 11633-11635; c) W. B. Yu, Y. F. Han, Y. J. Lin, G. X. Jin, *Chem. Eur. J.* **2011**, *17*, 1863-1871; d) Z. Z. Lu, C. C. Lee, M. Velayudham, L. W. Lee, J. Y. Wu, T. S. Kuo, K. L. Lu, *Chem. Eur. J.* **2012**, *18*, 15714-15721; e) Y. F. Han, G. X. Jin, C. G. Daniliuc, F. E. Hahn, *Angew. Chem. Int.*

Ed. **2015**, *54*, 4958-4962; f) C.-X. Wang, Y. Gao, Y.-X. Deng, Y.-J. Lin, Y.-F. Han, G.-X. Jin, *Organometallics* **2015**, *34*, 5801-5806.

[29] S. Chen, L. J. Chen, H. B. Yang, H. Tian, W. Zhu, *J. Am. Chem. Soc.* **2012**, *134*, 13596-13599.

[30] a) M. Han, R. Michel, B. He, Y. S. Chen, D. Stalke, M. John, G. H. Clever, *Angew. Chem. Int. Ed.* **2013**, *52*, 1319-1323; b) M. Han, Y. Luo, B. Damaschke, L. Gomez, X. Ribas, A. Jose, P. Peretzki, M. Seibt, G. H. Clever, *Angew. Chem. Int. Ed.* **2016**, *55*, 445-449.

[31] a) F. Luo, C. B. Fan, M. B. Luo, X. L. Wu, Y. Zhu, S. Z. Pu, W. Y. Xu, G. C. Guo, *Angew. Chem. Int. Ed.* **2014**, *53*, 9298-9301; b) V. I. Nikolayenko, S. A. Herbert, L. J. Barbour, *Chem. Commun.* **2017**, *53*, 11142-11145.

[32] K.-i. Yamashita, M. Kawano, M. Fujita, *J. Am. Chem. Soc.* **2007**, *129*, 1850-1851.

[33] M. J. Burke, G. S. Nichol, P. J. Lusby, *J. Am. Chem. Soc.* **2016**, *138*, 9308-9315.

Chapitre 3 – Ruthenium bistridentate complexes with non-symmetrical hexahydro-pyrimidopyrimidine ligands: a structural and theoretical investigation of their optical and electrochemical properties

3.1. Résumé

Six complexes de ruthénium ont été synthétisés sur la base de trois ligands tridentés non-symétriques portant le groupement fortement donneur d'électrons 1,3,4,6,7,8-hexahydro-*2H*-pyrimido [1,2-α] pyrimidine (hpp), **bpyG** (bpyG = 2,2'-bipyridyl-6-hpp), **phenG** (phenG = 2-hpp-1,10-phénanthroline) et **QpyG** (**QpyG** = 2-hpp-6-quinolylpyridyle). La conformation *fac*-/*mer*- des espèces homoleptiques a un effet dramatique sur les propriétés optiques, où l'absorption des isomères *fac*- est décalée vers le rouge par 150 nm, atteignant ainsi le proche IR à environ 850 nm. En raison des effets structuraux intéressant sur les propriétés optiques, la théorie de la densité fonctionnelle (DFT) et les calculs DFT dépendants du temps ont été mis en place pour jeter un éclairage sur les données expérimentales et prouver que le couplage excitonique est à l'origine du déplacement bathochrome observé. Les propriétés électroniques ont été étudiées et tel que corroborées par des données électrochimiques, la présence du groupement hpp affecte fortement le potentiel d'oxydation de l'ion métallique de ruthénium, ce qui permet un ajustement facile des propriétés électroniques. Les propriétés de luminescences de tous les composés ont également été étudiées (λ_{max} = 781-817 nm) et les complexes ont une durée de vie de l'état excité plus longue (10 à 30x) comparativement à la durée de vie du composé de référemce de type bis(2,2': 6',2"-terpyridine)ruthénium(II).

Contribution :

Baptiste Laramée-Milette : Synthèse et caractérisation complète des ligands et des complexes homo- et hétéroleptiques. Analyse structurelle par diffraction des rayons X, étude computationnelle, analyse des propriétés optiques et électroniques. Rédaction de l'article.

Garry S. Hanan: supervision, revision de l'article

Ruthenium bistridentate complexes with non-symmetrical hexahydro-pyrimidopyrimidine ligands: a structural and theoretical investigation of their optical and electrochemical properties

*Baptiste Laramée-Milette and Garry S. Hanan**

Département de chimie, Université de Montréal, 5155 Ch. de la rampe, Pavillon J.-A. Bombardier, Montréal, Québec, Canada, H3T 2B1

*: E-mail: garry.hanan@umontreal.ca

Full paper

Received: 16th June 2016; Published online: 12th July 2016; Published Online

DOI:10.1039/C6DT02408D

Reproduced with permission from *Dalton Trans.* **2016**, *45*, 12507-12517

Copyright 2016 The Royal Society of Chemistry

3.2. Table of content graphic

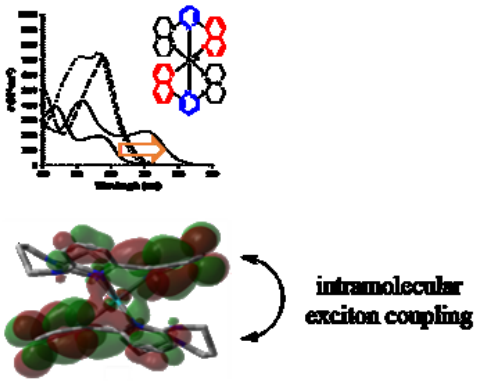

3.3. Abstract

Six ruthenium complexes were synthesized based on three non-symmetrical tridentate ligands bearing the strongly electron-donating group 1,3,4,6,7,8-hexahydro-2H-pyrimido[1,2-α]pyrimidine (hpp), bpyG (bpyG = 2,2'-bipyridyl-6-hpp), phenG (phenG = 2-hpp-1,10-phenanthroline) and QpyG (QpyG = 2-hpp-6-quinolylpyridyl). The fac-/mer-conformation of the homoleptic species has a dramatic effect on the optical properties, where the fac-isomer absorption is red-shifted by 150 nm, thus reaching the near-IR at approximately 850 nm. Owing to the interesting structural effect on the optical properties, density functional theory (DFT) and time-dependent DFT calculations have been implemented to enlighten the experimental data and prove that exciton coupling is at the origin of the observed shift. The electronic properties have been investigated and, as corroborated by electrochemical data, the presence of the hpp ligand strongly affects the oxidation potential of the ruthenium metal ion, which allows facile fine-tuning of the electronic properties. The luminescence properties of all the compounds have also been investigated (λmax emission = 781–817 nm) and the complexes have longer excited-state lifetimes at room temperature than the parent bis(2,2':6',2''-terpyridine)ruthenium(II) by 10 to 30 times.

3.4. Introduction

Polypyridyl metal complexes have received considerable attention during the past decades, essentially due to their unique properties such as luminescence at room temperature, moderate- to long-lived triplet excited-states lifetimes, good chemical stability, ease of synthesis, as well as their ability to undergo rapid electron or energy transfer.[1] As an example, the tris(2,2'-bipyridine)ruthenium(II) ($[Ru(bpy)_3]^{2+}$) and the bis(2,2':6',2"-terpyridine)ruthenium(II) ($[Ru(tpy)_2]^{2+}$) complexes and their derivatives have found applications in several technological areas, including photosensitization,[2] photocatalysis,[3] chemi-[4] and electro-luminescence,[5] photochemical energy conversion,[6] ion-sensing[7] as well as a few biological application (e.g. fluorescent probes,[8] anti-cancer agents,[9] enzyme inhibitors,[10] cytotoxic agents[11]).

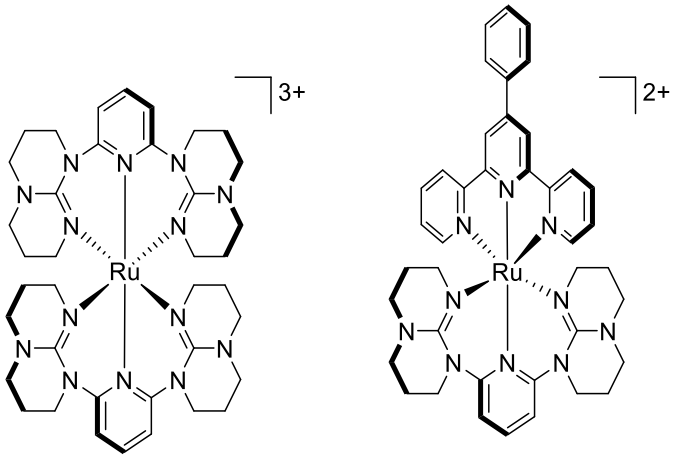

***fac*-Ru(pyG$_2$)$_2$** ***mer*-Ru(Phtpy)(pyG$_2$)**

Chart 3.1 - Ruthenium complexes bearing the ligand dgpy.

Despite the fact that complexes of the $[Ru(bpy)_3]^{2+}$ type exhibit a long-lived excited-state lifetime (~860 ns) at room temperature, the absence of stereospecificity in their synthesis leads to both Λ- and Δ-enantiomers. As a consequence, the achiral nature of the terpyridine motif (D_{2d} instead of D_3) is more attractive for their incorporation in

supramolecular complexes, although their photophysical properties are less appealing, with excited-state lifetime usually shorter than 1 ns.[12] To overcome this problem, several approaches have been developed over the past few years, via judicious modification of the ligand, in order to improve the photophysical properties of terdentate Ru^{II} complexes.[13] More specifically, strategies invoking the stabilization of the ^{3}MLCT state or the destabilization of the ^{3}MC state have been found to be effective for the reduction of the non-radiative deactivation pathway by increasing the ^{3}MLCT-^{3}MC gap. Among the most promising approach are the reduction of the angular strain around the metal center,[14] and the incorporation of strong σ-donor moiety.[14f, 14g, 15]

In a recent publication, our group has demonstrated a simple route for the synthesis of di(hpp)-substituted N-heterocyclic ligands capable of forming six-membered chelate rings with various transition metals (Chart 3.1). Upon complexation with Ru^{II} or Re^{I}, the bite angle around the metal core is found to be closer to 180°, thus improving the octahedral geometry, which is critical in the improvement of the photophysical properties of the metal complexes.[16] Following these results, we decided to investigate the optical and electrochemical properties of several ruthenium metal complexes (Chart 3.2) synthesized from non-symmetrical polypyridyl-hpp ligands, with the aim of combining the most promising approaches in order to obtain chromophores with enhanced optical properties, such as panchromatic absorption and long-lived excited states.

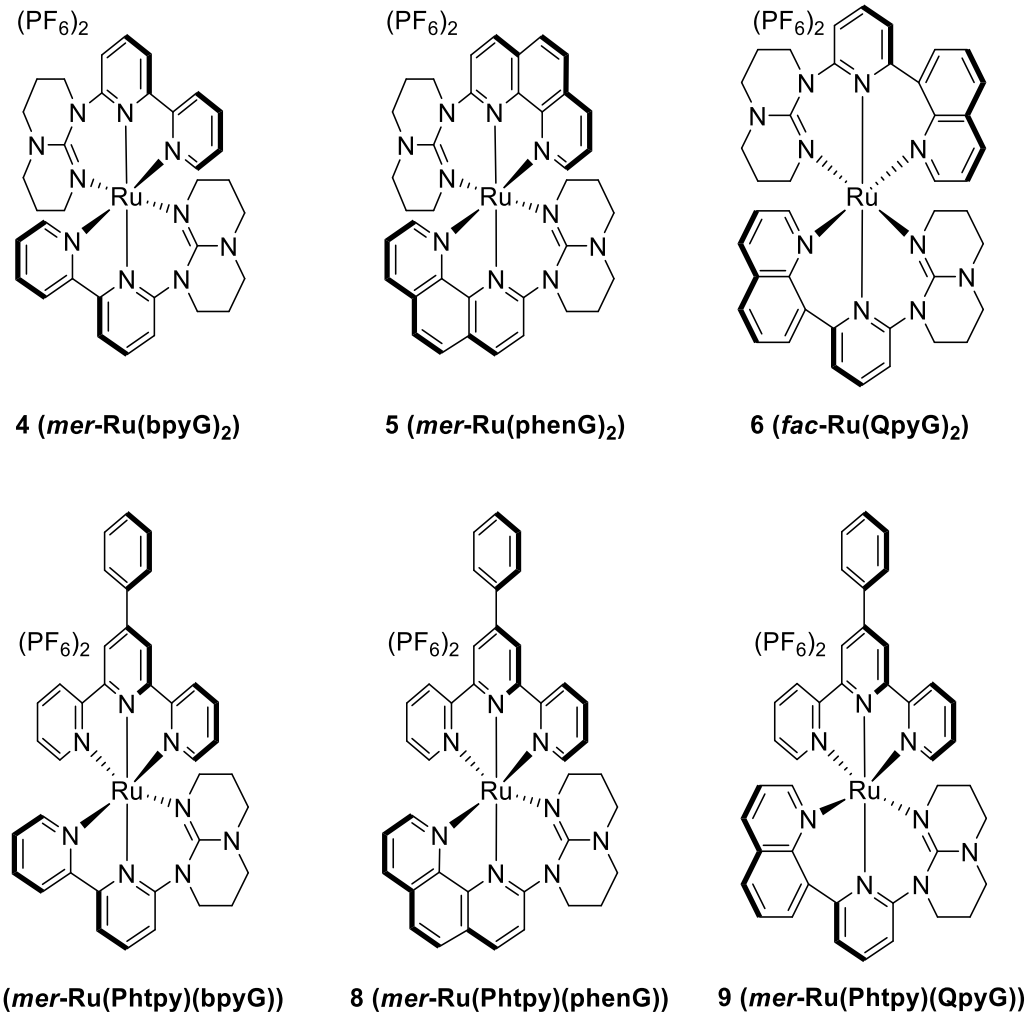

Chart 3.2 - Homoleptic and heteroleptic ruthenium complexes bearing non-symmetrical tridentate N^N^N type ligands in this study.

3.5. Results and discussion

3.5.1. Synthesis of the ligands

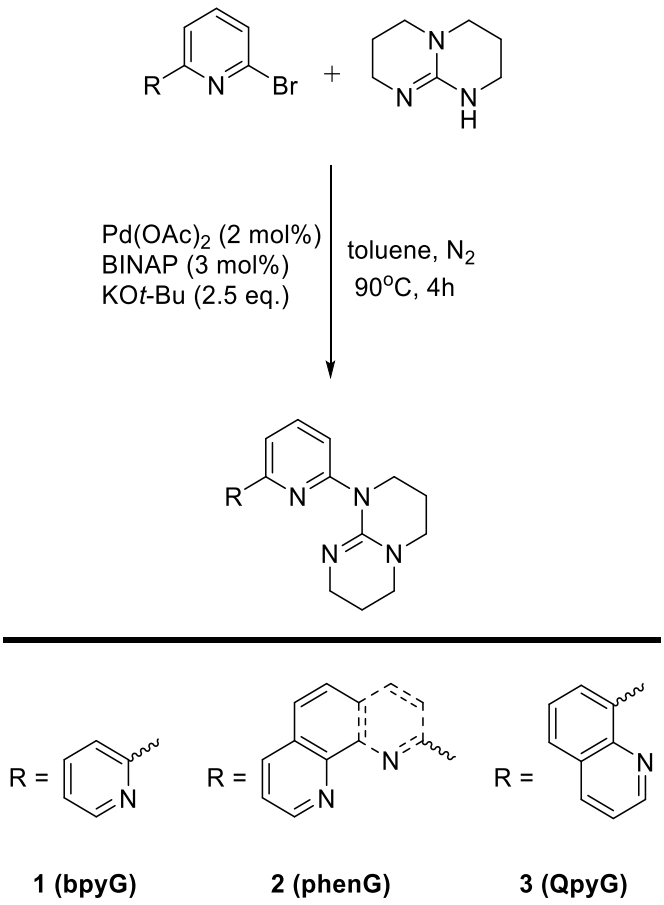

Scheme 3.1 - Synthesis of the non-symmetrical tridentates ligands.

The N-heterocycle-guanidyl ligand **1** (see Scheme 3.1) was synthesized in two steps, where the first step involved the reaction of 2,6-dibromopyridine and 2-pyridylzinc bromide in a 1:1 ratio following a standard Negishi heterocoupling protocol in order to obtain 6-bromo-2,2'-bipyridine.[17] The resulting product was then reacted with 1,3,4,6,7,8-hexahydro-2*H*-pyrimido[1,2-α]pyrimidine (H-hpp) in a 1:1 ratio via a Pd-catalyzed C-N bond forming reaction.[18] Ligand **2** was synthesized in 4 steps, starting with the methylation of 1,10-phenanthroline, followed by oxidation and chlorination according to literature procedures.[19] The resulting 2-chloro-1,10- phenanthroline was finally reacted with H-hpp in the same ratio as described above to yield ligand **2**. Ligand

3 was synthesized in a similar way compared to ligand **1**, with the only difference being that the first step implied a Suzuki-Miyaura heterocoupling reaction between 2,6-dibromopyridine and 8-quinoline boronic acid in a 4:1 ratio.[20] Purification of all the ligands was achieved by the elution over a deactivated neutral alumina column, using a solvent mixture of methylene chloride and ethanol in a 95:5 ratio. The resulting products were recrystallized from slow evaporation of a chloroform solution.

3.5.2. Synthesis and characterization of the ruthenium complexes

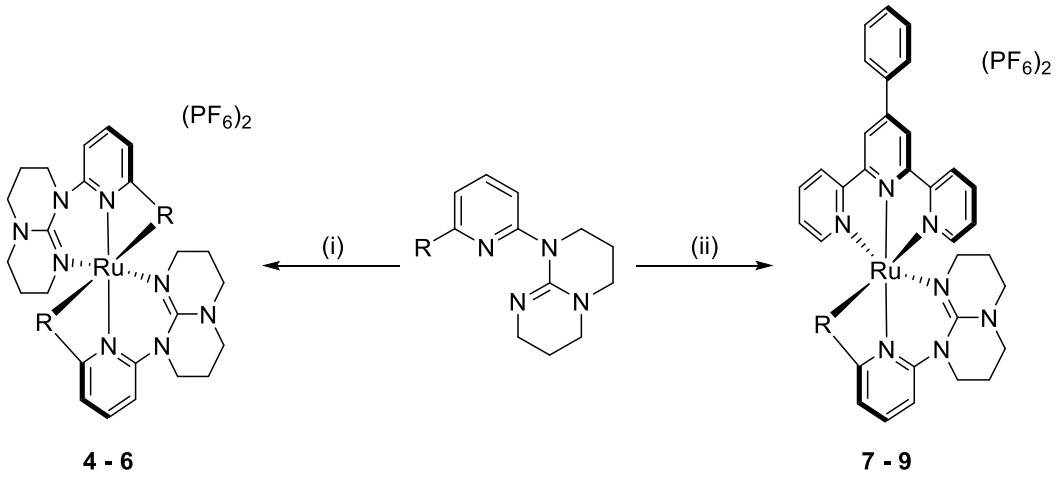

Scheme 3.2 - Synthesis of the homoleptic and heteroleptic ruthenium complexes (See Scheme 3.1 for the definition of R groups). (i) $RuCl_3.H_2O$ (0.5 eq.), ethylene glycol, microwave (400W, 200°C), 20 minutes; (ii) 4-phtpy$RuCl_3$ (1.1 eq.), ethylene glycol, microwave (400W, 200°C), 20 minutes.

As depicted in Scheme 3.2, the homoleptic metal complexes were synthesized by reacting the ligands and the ruthenium source ($Ru(DMSO)_4Cl_2$ or $RuCl_3.3H_2O$) in a 2:1 ratio. The reaction took place under microwave irradiation in ethylene glycol in the presence of few drops of 4-ethylmorpholine, added as a reducing agent, in order to obtain complexes **4-6** in low to good yield. The heteroleptic complexes **7-9** were synthesized in a similar fashion. The isolated crude materials were all subjected to further purification in order to remove any homoleptic bis-terpyridine metal complexes formed during the reaction. The complexes were purified by flash column chromatography over silica using

a mixture of acetonitrile:water:KNO_3 as the eluent (7:2:1 ratio in the case of complexes **4-5** and **7-8** while complex **9** required a 14:1:1 mixture). The purification procedure of complex **6** was more difficult to deal with compared to all the other complexes. It appears that due to several parameters (such as the flexible nature of the aliphatic backbone of the hpp moiety, the non-symmetrical properties of the ligand and the formation of a 6-membered ring by the quinoline moiety part of ligand **3**), several diastereoisomers are obtained. Nonetheless, a major deep purple band was isolated after purification over a silica column using a 7:2:1 ratio of the eluent mixture mentioned above. As shown by ^{1}H NMR analysis, this fraction displayed two set of peaks in a 9:1 ratio. The purple product was rechromatographed over SP-Sephadex C25 cation exchanger following the experimental procedure developed by Keene and coworkers to manage diastereoisomeric separations.[21] All the ruthenium complexes were isolated as their PF_6 salts.

3.5.3. Single-crystal X-ray crystallography and DFT calculations

Since previously reported ruthenium complexes bearing more flexible ligands are known to form both *mer* and *fac* isomers,[22] we decided to verify the coordination geometry of a few complexes by crystallography. Single crystals of metal complexes **4**$(PF_6)_2$ and **7**$(PF_6)_2$ were obtained by slowly diffusing diethyl ether into a concentrated solution of acetone over 1-3 days, while complex **6**$(PF_6)_2$ crystallized from the slow diffusion of diethyl ether into a concentrated acetonitrile solution. Their X-ray crystallographic structures are shown in Figure 3.1 to
Figure 3.3 and their data collected in Table 3.1. Select geometric parameters as well as theoretical DFT calculation results from geometry optimization are listed in

Table 3.2.

As expected, in all cases the ruthenium ion adopts a hexa-coordinate octahedral configuration. For complexes **4** and **7**, the ligands are found to be in a *mer*- conformation while complex **6** display a *fac*- conformation. These results suggest that releasing the strain around the metal center by increasing the chelate ring size from five-chelate/five-chelate to five-chelate/six-chelate does not lead to the formation of *fac*- isomers.

However, as it was already observed for similar ligands such as 2,6-bis(8'-quinolinyl)pyridine (bqp),[22c, 23] 2,6-diguanidylpyridine (dgpy) and 2,6-diguanidylpyrazine (dgpz),[15f] extending the ring size to a six-chelate/six-chelate is more

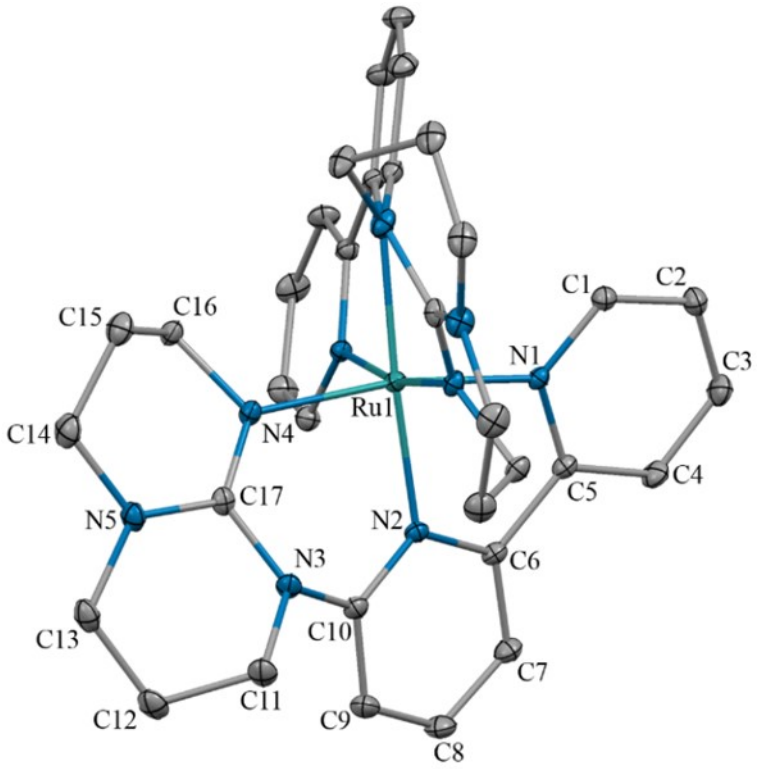

Figure 3.1 - Thermal ellipsoid diagram (30% probability) of the single-crystal structure of **4**. Solvent molecules, hydrogens atoms and counter-anions are omitted for clarity.

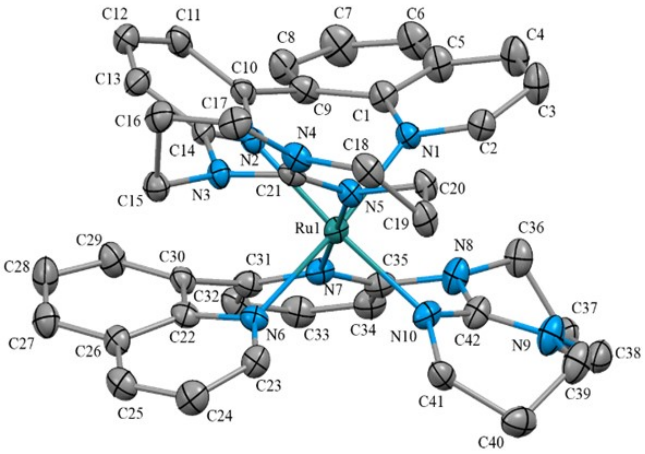

Figure 3.2 - Thermal ellipsoid diagram (30% probability) of the single-crystal structure of **6**. Solvent molecules, hydrogens atoms and counter-anions are omitted for clarity.

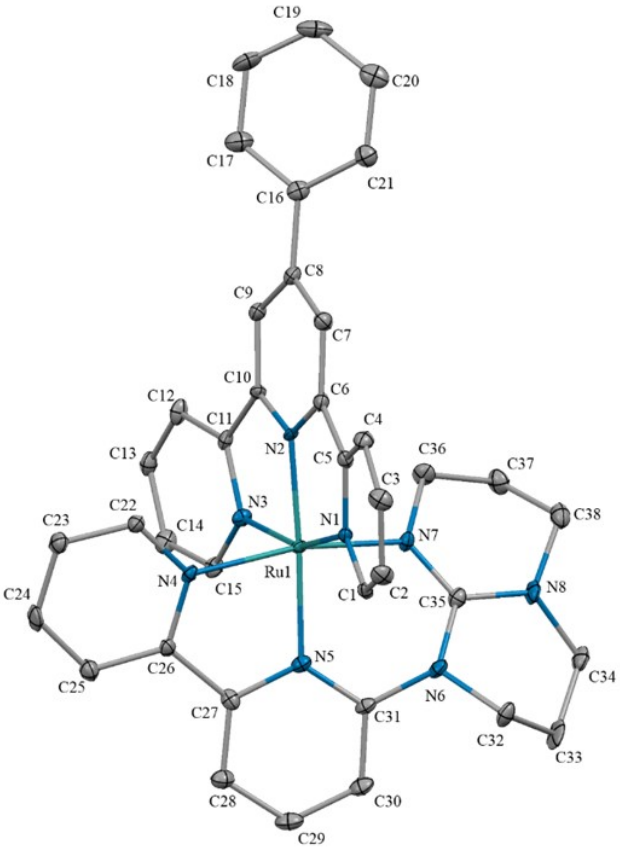

Figure 3.3 - Thermal ellipsoid diagram (30% probability) of the single-crystal structure of **7**, showing one entity present in the asymmetric unit. Solvent molecules, hydrogens atoms and counter-anions are omitted for clarity.

apt to lead to *fac*-isomers due to an increase in flexibility. More specifically, from the experimental data for complex **6**, the major species is found to be the *fac*-(*cis*-hpp-*cis*-pyridine-*trans*-quinoline)$_2$Ru^{II} complex. As shown in Figure 10.5, due to the presence of an inversion center in the space group (P2$_1$/c), the species is not enantiopure and both (Λ)-*fac*- and (Δ)-*fac*-(**QpyG**)Ru^{II} metal complex can be found in the unit cell.

As illustrated in Figure 3.4, a detailed analysis of the Ru-N bonds lengths for the homoleptic and heteroleptic complexes bearing the bpyG ligand revealed that the distance between the ruthenium ion and the peripheral pyridyl ring is regular with a bond length varying between 2.05-2.06 Å while the distance between the metal and the central pyridyl ring is somewhat shorter at 2.00-2.04 Å. The distance to the peripheral hpp ligand ranges from 2.06-2.08 Å, which is a distance similar to other ruthenium complexes with a guanidyl moiety (2.07-2.09 Å). Besides, the Ru-N$_{hpp}$ distance does not seem to be affected by the *mer*-/*fac*- isomerism, since a bond length of 2.09 Å is observed in complex **6**.

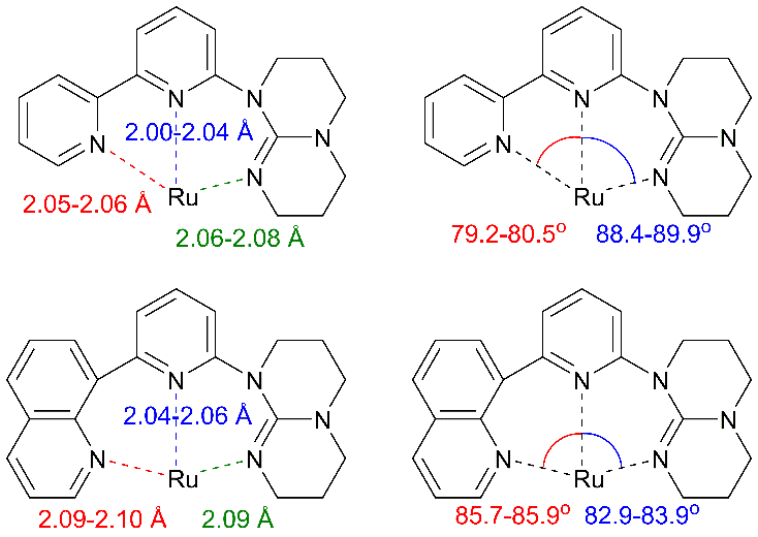

Figure 3.4 - Selected Ru-N bond lengths and angles in homo- and heteroleptic complexes bearing the non-symmetrical bpyG and QpyG ligands.

Table 3.1 - Solid-state structure and refinement data for complexes **4**, **6** and **7**.

	4	6	7
Formula	$[C_{34}H_{38}N_{10}Ru][(PF_6)_2] \cdot ((CH_3CH_2)_2O)$	$[C_{42}H_{42}N_{10}Ru][(PF_6)_2] \cdot (CH_3CN)$	$[C_{38}H_{34}N_8Ru][(PF_6)_2] \cdot ((CH_3)_2CO)$
Color/form	purple/needle	purple/block	red/block
M_w [gmol^{-1}]	1047.84	1118.92	1051.74
Temperature [K]	100	100	100
Wavelength [Å]	1.3418	1.54178	1.3418
Crystal system	Monoclinic	Monoclinic	Triclinic
a [Å]	11.3080(4)	22.1907(6)	13.4632(3)
b [Å]	26.7172(8)	8.1133(2)	17.4582(5)
c [Å]	14.0045(5)	24.9115(6)	19.4702(5)
α [°]	90	90	69.392(1)
β [°]	99.477(1)	104.456(2)	80.492(1)
γ [°]	90	90	79.524(1)
V [Å^3]	4173.3(2)	4343.1(2)	4186.6(2)
Space group	C_2/c	$P2_1/c$	P-1
Z	4	4	1
$d_{calcd.}$ [gcm^{-3}]	1.668	1.711	1.669
μ [mml^{-1}]	3.042	4.524	3.066
F(000)	2128	2272	2128
Reflection collected	47209	105462	18299
Independent reflections	4598	8562	18299
GoF	1.076	1.067	1.037
R_1(F) [$I > 2\sigma(I)$]	0.0354	0.0621	0.0331
$wR(F^2)$ [$I > 2\sigma(I)$]	0.0944	0.1554	0.0835
R_1(F) (all data)	0.0358	0.0770	0.0357
wR(F^2) (all data)	0.0947	0.1659	0.0857
Largest diff. peak/hole [eÅ^{-3}]	0.967	1.559	1.176

Table 3.2 - Selected bond lengths and angles obtained from X-ray diffraction for **4**, **6** and **7** and DFT results from geometry optimizations.[a]

	4		5	6	
	X-ray	DFT	DFT	X-ray	DFT
N_{het}-Ru (Å)	2.054(2)	2.065	2.060	2.085(3) 2.097(3)	2.098
N_{py}-Ru (Å)	2.016(2)	2.031	2.027	2.056(3) 2.035(3)	2.067
N_{hpp}-Ru (Å)	2.062(2)	2.083	2.075	2.091(3) 2.094(3)	2.127
N_{het}-Ru-N_{hpp} (deg)	169.3(1)	169.7	168.0	95.3(1) 93.5(1)	93.6
Dihedral angles (deg)	67.7(1)	72.1	71.2	29.6(1) 31.6(1)	40.4 40.7

	7[b]		8	9
	X-ray	DFT	DFT	DFT
N_{het}-Ru (Å)	2.048(2) 2.056(2)	2.066	2.071	2.100
N_{py}-Ru (Å)	2.026(2) 2.032(2)	2.044	2.045	2.078
N_{hpp}-Ru (Å)	2.072(2) 2.084(2)	2.090	2.075	2.092
N_{het}-Ru-N_{hpp} (deg)	166.9(1) 166.6(1)	168.5	167.4	176.1
Dihedral angles (deg)	74.8(1) 74.3(1)	78.3	79.6	56.7[c] 64.7[d]

[a] Where N_{het} is the nitrogen atom on the peripheral heterocycle (bipyridine, phenanthroline or quinoline), N_{py} is the nitrogen on the central pyridine and N_{hpp} is the nitrogen on the hexahydropyrimidopyrimidine moiety. [b]Parameters where measured for the two molecules displayed in the assymetric unit. [c]Calculated dihedral angle between the pyridyl unit of ligand **3** and the terpyridine motif. [d]Calculated dihedral angle between the quinolyl unit of ligand **3** and the terpyridine motif.

The Ru-N_{quin} bond length range between 2.09-2.10 Å, which is similar to the experimental Ru-N_{quin} bond length in *fac*-(2,6-bisquinolylpyridine)$_2$Ru^{II} complexes (2.09-2.12 Å). As in the other example cited before, the Ru-N_{py} distance in complex **6** is slightly shorter (2.04-2.06 Å) compared to both Ru-N_{hpp} and Ru-N_{quin} bond distances. For heteroleptic complex **7**, the Ru-N bond length between the ruthenium and the pyridyl units of the terpyridine are normal (Ru-$N_{peripheral}$: 2.07-2.08 Å; Ru-$N_{central}$: 1.96 Å).

As mentioned earlier, by enhancing the octahedral geometry around the metal core we should improve the photophysical properties of the complexes. As displayed in Figure 3.4, for metal complexes bearing the **bpyG** ligand, the angle formed by the peripheral pyridyl ring, the metal and the central pyridyl ring range from 79º to 81º, which is expected for regular bipyridyl Ru^{II} complexes (79º).[24] The improvement of the octahedral geometry is achieved by the hpp ligand, where the angle formed by the central pyridyl ring, the ruthenium ion and the hpp ring is almost ideal, ranging from 88º to 90º. Nevertheless, a change from a meridional to a facial conformation affects this angle to a small extent. For example, the N_{hpp}-Ru-N_{py} angles in complex **6** ranges from 83º to 84º, which is similar to the angles found in the previously reported *fac*-$(dgpy)_2Ru^{III}$ complex (83-84º). The dihedral angle between the chromophores of a same metal complex is of importance in this study since it can greatly affect the optical properties, which will be discuss below in greater detail. As shown in Table 10.2, Table 10.15 and Table 10.19, the experimental angle measured for complex **4** (67.7º) and **7** (74.3º and 74.8º) are in good agreement with their theoretical values calculated by density functional theory (72º and 71º, respectively). The values found by DFT (40-41º) for complex **6** are slightly over-estimated, with experimental values of 30-32º. In all the cases, both calculated and experimental values display a more acute dihedral angle compared to the typical dihedral angle observe for bis(terpyridine)Ru^{II} type complexes (90º). This is a direct consequence of the greater flexibility of the ligands used in this study, where the dihedral angle of the complexes having a *mer*- conformation are closer to the angle observed in Ru^{II} complexes with 6-(2-picolyl)-2,2'-bipyridine type ligand (63º).

3.5.4. Electrochemical studies

The redox properties of the ligands and the metal complexes were investigated by cyclic voltammetry and the data are summarized in Table 3.3. The homoleptic complexes **4-6** display a reversible mono-electronic oxidation wave at $E_{1/2} \approx 0.3$ V *vs* SCE, which is assigned to the Ru^{II}/Ru^{III} metal-centered oxidation. It is worth mentioning that the oxidation of the ruthenium metal ion is independent of the isomer conformation, where both *mer*- and *fac*- isomers are oxidized at similar potentials.

Table 3.3 – Electrochemical data for the ligands and the Ru(II) complexes.[a]

Cmpd	Oxidation potential (V) (ΔE_p (mV))		Reduction potential (V) (ΔE_p (mV))			
$py(G)_2$	1.11 (308)	0.77 (irr.)	–	–	–	–
bpyG	–	–	-1.74 (irr.)	–	-2.36 (77)	–
phenG	1.11 (irr.)	–	-1.71 (irr.)	-1.83 (134)[b]	-2.48 (146)[b]	–
QpyG	1.08 (irr.)	–	-1.62 (irr.)	-1.97 (49)	-2.48 (129)[b]	–
4	1.47 (73)[b]	0.28 (71)	-1.48 (66)	-1.72 (67)	-2.26 (165)[b]	–
5	1.40 (155)[b]	0.28 (94)	-1.53 (72)	-1.71 (190)[b]	–	–
6	–	0.31 (121)	-1.48 (90)	-1.80 (90)	-2.29 (irr.)[c]	–
7	–	0.70 (68)	-1.31 (67)	-1.61 (74)	-2.01 (116)[b]	-2.09 (56)[b]
8	–	0.71 (76)	-1.31 (81)	-1.63 (68)	-1.93 (104)[b]	-2.08 (141)[b]
9	–	0.76 (116)	-1.31 (123)[b]	-1.63 (155)	-1.98 (59)	2.27 (162)[b]
fac-$(py(G)_2)_2Ru$[d]	1.18	–	-0.29	–	–	–
mer-$(py(G)_2)(Phtpy)Ru$[d]	–	0.50	-1.47	-2.01	–	–
mer-$(phtpy)_2Ru$[e]	–	1.29	-1.26	–	–	–

[a]Potentials are in volts *vs* SCE. Cyclic voltammetry was performed in MeCN/*t*-$Bu_4N(PF_6)$ (0.1M), recorded at 25 ± 1°C with a sweep rate of 50 mV s^{-1}. All potentials are corrected *vs* Fc/Fc^+=0.40 V. [b] Quasi-reversible.[c] Irreversible. [d] From ref. 15f. [e] From ref. 12a.

The heteroleptic complexes bearing a 2,2':6',2''-terpyridine ligand (complexes **7**-**9**) exhibits a metal-based oxidation around 0.7 V. The observed cathodic shift of the Ru^{II}/Ru^{III} wave by *ca.* 0.6 – 1.2 V compared to the reference $[Ru(phtpy)_2]^{2+}$ ($E_{1/2}$ = 1.3 V) is ascribed to the strong electron-donating ability of the bicyclic guanidine based hpp ligands, and it is interesting to note the simplicity of the fine-tuning of the electrochemical properties by adding or removing an hpp-moiety from the metal complex. As a matter of comparison, a series of several similar homoleptic and heteroleptic ruthenium complexes featuring *N*-heterocyclic carbene (NHC) based ligands[25] as well as few cyclometalated Ru^{II} species[14m, 15a, 15b, 26] with their respective redox potential for the Ru^{II}/Ru^{III} couple can be found in Figure 10.12. It is worth mentioning that following Lever's ligand electrochemical parameter (E_L) series, the hpp ligands range have E_L between -0.4 to -0.6 V, which makes them the strongest donating neutral ligand reported.[27]

A second quasi-reversible oxidation process is observed for complexes **4** and **5**. Detailed DFT calculations were performed on the first and second oxidized states of the complexes through the PBE0 functional with inclusion of solvent (acetonitrile) by the

conductor-like polarization continuum model (CPCM), using an unrestricted formalism for the open shell systems. In the case of the first oxidation, the geometry of the metal complexes was optimized in the doublet state (S = 1/2) while it was optimized in the triplet (S = 1) geometry for the second oxidation. For the first oxidation, as depicted in Figure 3.5, the results are consistent with the unpaired electrons being mainly located on the ruthenium core, where the Ru ion has larger contribution relative to the hpp-moiety of the **bpyG** and **phenG** ligands (complex **4**: 0.782 *vs* 0.226; complex **5**: 0.879 *vs* 0.126), which confirm the assignment of the first oxidation toward the $Ru^{III/II}$ process. In the case of the second oxidation, the spin density distribution of the triplet $\mathbf{4}^{4+}$and $\mathbf{5}^{4+}$ are delocalized on both the metal and the hpp-moiety of the ligand. From the DFT calculations, the contributions are 0.023/1.213/0.764 for 2,2'-bpy/hpp/Ru, respectively, in complex $\mathbf{4}^{4+}$, which establishes a greater influence from the ligand compared to the metal ion while the contribution is almost the same in complex $\mathbf{5}^{4+}$ with 0.015/1.006/0.979 for 1,10-phen/hpp/Ru, respectively.

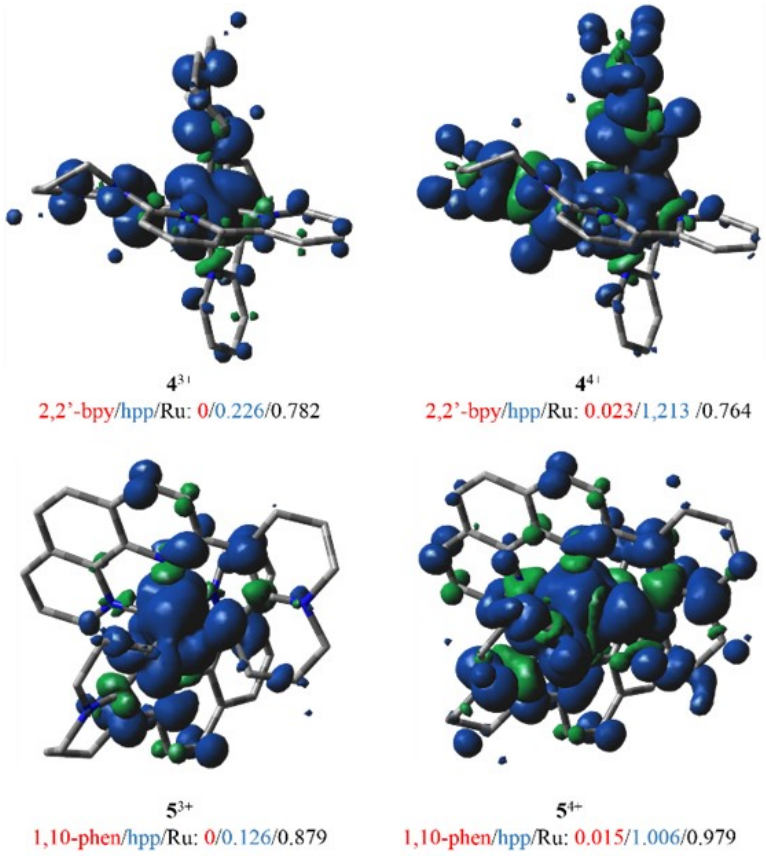

Figure 3.5 – DFT-calculated spin density distributions.

3.5.5. Spectroscopic studies

The UV-visible spectra of the metal complexes and the reference $[Ru(Phtpy)_2][(PF_6)_2]$ are displayed in Figure 3.6 and their data are collected in Table 3.4. The electronic absorption spectra were recorded in dry, degassed acetonitrile at room temperature (r.t.). All the complexes exhibit strong ligand-centered (LC) $\pi \rightarrow \pi^*$ transitions between 200 and 300 nm with extinction coefficients ranging from 3.0 to 6.0 x 10^4 $M^{-1}cm^{-1}$. The absorption bands between 300 and 400 nm consist of a mixture of $\pi \rightarrow \pi^*$ LC and metal-to-ligand charge-transfer transitions (MLCT), whereas the bands observed at lower energy are mainly MLCT transitions. It is worth mentioning that due to the introduction of the strongly donating hpp moiety, both the homoleptic and heteroleptic complexes displays a bathochromic shift of about 100-150 nm of the lowest energy ^{1}MLCT maxima compared to $[(phtpy)_2Ru][(PF_6)_2]$. This red-shift have been attributed to a better interaction between the ligand and the t_2 [d(Ru)] orbitals of the ruthenium metal ion, which reduces the HOMO-LUMO energy-gap.

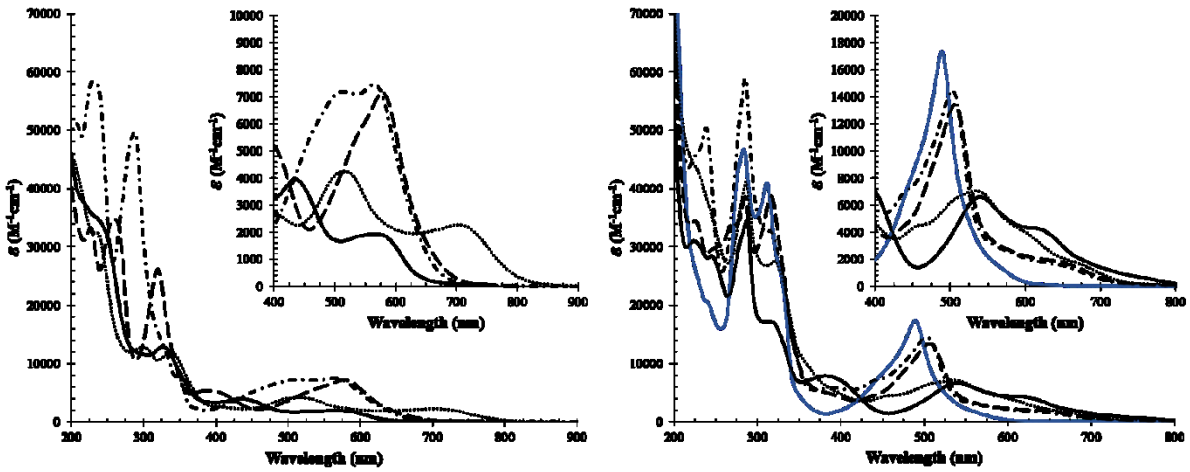

Figure 3.6 - Absorption spectra of the homoleptic (left: **4** (dash), **5** (dash-dots), **6** (dots) and $[(dgpy)_2Ru^{3+}][(PF_6)_3]$ (plain)) and heteroleptic (right: **7** (dash), **8** (dash-dots), **9** (dots), $[(dgpy)(phtpy)Ru^{2+}][(PF_6)_2]$ (plain, black) and $[(phtpy)_2Ru^{2+}][(PF_6)_2]$ (plain, blue)) ruthenium complexes in MeCN solutions at room temperature.

All the results are consistent with the calculated electronic transitions by TD-DFT using the PBE0 functional with inclusion of solvent (acetonitrile) by the conductor-like polarization continuum model (CPCM). The spectra displayed in Figure 10.13 were simulated by convolution of computed vertical excitation using a Gaussian broadening. The area of the bands is proportional to the calculated oscillator strength.

When looking at the spectra of the homoleptic complexes **4**, one can observe that there is a significant difference in the shape of the spectra between the facial and the meridional isomers. Moreover, complexes **4-5** as well as the reference $[(dgpy)_2Ru^{3+}][(PF_6)_3]$ absorb light up to 700 nm, while complex **6** displays non-negligible absorptivity up to 850 nm, consisting in a red-shift of about 150 nm compare to the other species (Figure 3.6). As mentioned earlier, the dihedral angle between the chromophore of the same metal complex has been investigated by both single crystal X-ray diffraction study as well as by DFT optimization calculations. Correlated with the assignment of the transitions seen in UV-vis spectroscopy by TD-DFT calculations, we can conclude that this phenomenon arise from intramolecular exciton coupling interaction.[28]

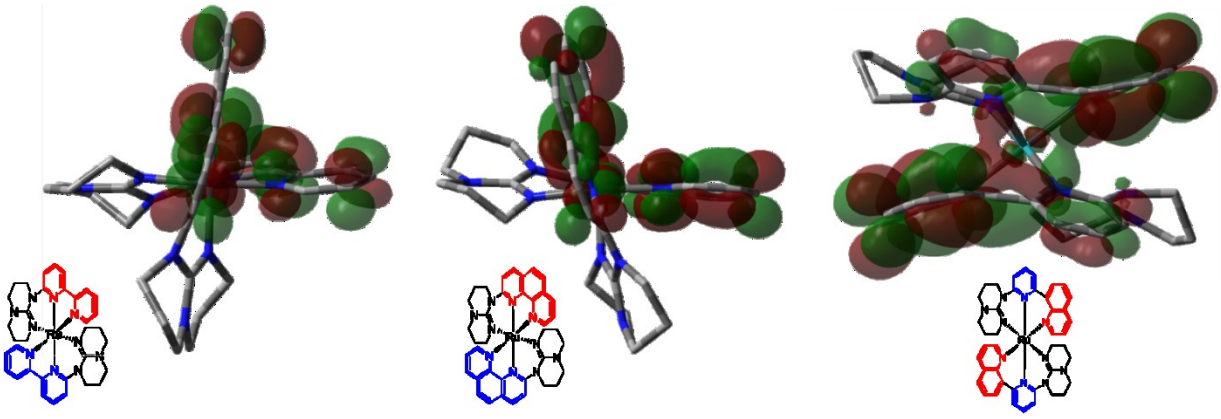

Figure 3.7 - Kohn-Sham electron density sketches of the LUMO of $\mathbf{4}^{2+}$, $\mathbf{5}^{2+}$ and $\mathbf{6}^{2+}$ in (S = 0) ground state.

From TD-DFT calculation, we determined that for all the homoleptic complexes, the lowest transition consists of a ^{1}MLCT from the highest occupied molecular orbital

(HOMO) to the lowest unoccupied molecular orbital (LUMO). As shown in Figure 3.7, the LUMO of complexes **4**-**6** is delocalized, respectively, on the 2,2'-bipyridyl unit, the 1,10-phenanthroline unit and on the quinoline-pyridyl part of the different ligands. The meridional configuration of metal complex **4** and **5** lead to a dihedral angle of approximately 70° which, following the exciton coupling theory developed by Kasha,[28-29] is not favorable for strong interactions in the excited state via dipolar coupling and this exciton coupling for these two complexes is expected to be either weak or non-existent. The scenario is rather different in the case of complex **6**. As shown, the *fac*-isomerism bring the two ligands very close one to the other (centroid distance between the central pyridine and quinoline ring = 3.67-3.72 Å) in which the two ligands are held by the Ru^{II} metal ion in a slipped-cofacial conformation with an orientation (dihedral angle = 29.6-31.6°) suitable for the exciton to be delocalized over the two QpyG ligands.

Table 3.4 – Optical properties of the metal complexes and the references in acetonitrile[a]

Cmpd	Absorption λ_{max}/nm	Luminescence 298 K (77K)	Lifetime 298 K
	λ_{max}/nm (ε, x10^4 M^{-1} cm^{-1})	λ_{max}/nm	τ, ns (χ^2)
4	227 (3.33), 261 (3.47), 320 (2.62), 388 (0.53), 544 (0.58), 578 (0.71)	811	7.5
5	230 (5.84), 288 (4.95), 348 (0.79), 513 (0.72), 564 (0.75)	781	2.6
6	225 (3.44), 269 (3.41), 285 (3.85), 316 (3.87), 388 (0.47), 437 (0.44), 506 (1.34), 645 (0.18)	No luminescence detected	
7	235 (3.25), 299 (1.28), 338 (1.21), 409 (0.26), 516 (0.42), 706 (0.23)	813	4.4
8	238 (5.04), 285 (5.89), 315 (3.28), 389 (0.58), 442 (0.71), 503 (1.45), 564 (0.75	817	4.9
9	228 (4.31), 286 (4.11), 321 (2.75), 454 (0.44), 510 (0.66), 534 (0.71), 605 (0.38), 676 (0.16)	No luminescence detected	
fac-$(dgpy)_2Ru$[b]	234 (3.52), 326 (1.28), 433 (0.39), 564 (0.19)	No luminescence detected	
mer-(dgpy)(Phtpy)Ru[b]	225 (2.62), 244 (2.26), 289 (2.69), 317 (1.33), 379 (0.61), 541 (0.50), 622 (0.33)	901	129
mer-$(Phtpy)_2Ru$[c]	283 (4.68), 311 (4.09), 330 (2.37), 489 (1.73)	715	1.0

[a]Due to low signal intensity, emission quantum yields were not determined. [b] From ref. 14g and 15f. [c] From ref. 12a.

3.5.6. Luminescence studies

The emission properties of **4-9** as well as related complexes are found in Table 3.4. The complexes were analyzed in diluted acetonitrile solution and each sample was degassed with argon for at least 5 minutes prior to the analysis. All the spectra were

corrected for detector response. While complexes **4-5** and **7-8** were found to be emissive around 785-825 nm, no emission was detected in the case of complex **6** up to 900 nm, most likely due to an instrumental limitation (the limited spectral range of the detector). In the case of complex **9**, the TD-DFT calculations revealed that the nature of the lowest energy level is not a MLCT but rather a LMCT, which is known to deactivate the luminescence through radiationless decay processes. All the emissive species are red-shifted compared to the luminescence of reference complex $[Ru(tpy)_2][(PF_6)_2]$ (640 nm)[27] by 150-175 nm. When comparing the complexes bearing the same non-symmetrical ligand, the homoleptic complexes are blue-shifted by 10-25 nm compare to their heteroleptic analog. The excited state lifetimes of the complexes mentioned above are 10 to 30 times longer lived than the archetypical $[Ru(tpy)_2]^{2+}$ complexes (0.25 ns) [12,13], ranging from 2.6 to 7.5 ns. We believe that this is a direct consequence of the destabilization of the ^{3}MC state, which is due to the presence of the strong σ-donating hexahydropyrimidopyrimidine moiety as well as the formation of 6-membered rings, therefore leading to a geometry around the metal core closer to a typical octahedral geometry. Accordingly, the probability of non-radiative decay induced by a thermally-activated internal conversion from the ^{3}MLCT state to the ^{3}MC state is decreased at ambient temperature, leading to a slightly longer excited state lifetime.

3.5.7. Conclusions

A series of ruthenium homoleptic and heteroleptic complexes bearing non-symmetrical ligands having an hpp-moiety have been prepared and characterized. Their optical and electrochemical properties were investigated and when possible, the results were compared with structural and theoretical data. The strong donating ability of the hpp units induced a red-shift of the ^{1}MLCT band of most metal complexes, compared to the $[Ru(phtpy)_2]^{2+}$ complex, and a definite ML-LCT character. More specifically, homoleptic complex **6** covers the entire visible portion of the electromagnetic spectrum up to the near infrared. As shown by theoretical calculations, the low-energy transition is the result of intramolecular exciton coupling interactions. In term of the electrochemical properties, we demonstrated that the redox potential of the Ru^{II}/Ru^{III} couple can be easily modulated: when there are more hpp- units around the metal core,

the easier it is to oxidize the species, leading to a facile means of fine-tuning the electronical properties of the ruthenium complexes. The excited state lifetimes of the new red-absorbing complexes are 10 to 30 times longer lived than the archetypical $[Ru(tpy)_2]^{2+}$ complex. The use of these ruthenium complexes for photocatalytic water-splitting is underway.

3.5.8. Acknowledgements

BLM and GSH thank the Natural Sciences and Engineering Research Council (NSERC) of Canada as well as the Fondation J.A. Bombardier and the Université de Montréal for financial support. The authors are also grateful to Compute Canada and UdeM NMR, EA and XRD facilities and staff for their help.

3.5.9. Experimental

3.5.9.1 Crystal Structure Determination

X-Ray diffraction data collection for the metal complexes **4** and **7** was carried out on a Bruker Venture Metaljet diffractometer equipped with an Oxford Cryosystem liquid N_2 device, using a Ga-Kα radiation (λ = 1.34139 Å), while data collection for the metal complex **6** was carried out on a Bruker APEX II DUO Kappa-CCD diffractometer equipped with an Oxford Cryosystem liquid N2 device, using Kα radiation (λ = 1.54178 Å). The crystal-detector distance was 38 mm for complex **6**. In all the cases, the cell parameters were determined (APEX2 software) from reflections taken from three sets of 100 frames. The structure was solved by direct methods using the program Olex2. The H-atoms were included in calculated positions and treated as riding atoms using Olex2 default parameters. The non-H atoms were refined anisotropically, using weighted full-matrix least-squares on F2. More details are provided in the Supporting Information. CCDC 1472077, CCDC 1472078 and CCDC 1472079 contain the supplementary crystallographic data for this paper. These data can be obtained free of charge from The Cambridge Crystallographic Data Centre via www.ccdc.ac.uk/data_request/cif.

3.5.9.2 Computational Methods

Gaussian 09, Revision D.01 was used for all theoretical calculations discussed herein. The molecular structure of the metal complexes was fully optimized with CPCM acetonitrile solvation model in absence of constraints at Density Functional Theory (DFT) level, using the crystallographic data as the starting point for the optimization. In particular, the hybrid PBE0 functional, casting 25% of HF exchange in the PBE functional was applied. A double zeta valence basis set was used for all atoms but the Ru ones which were described by the Los Alamos pseudo potential and corresponding basis set. Details of optimized structures are given in the Supporting Informations. No imaginary frequencies were obtained when frequency calculations on optimized geometries were performed. The molecular structure of the oxidized complexes was fully optimized at the same level of theory but using unrestricted formalism in the case of open shell systems. The values of $<S^2>$ were monitored and did not show major spin contamination. GaussView 5.0.8 and Chemissian 2.200 software were used for data analysis, visualization and surface plots.

3.5.10. References

[1] (a) K. Kalyanasundaram, *Photochemistry of Polypyridine and Porphyrin Complexes*, 1st edn., Academic Press Inc., New York, USA, 1991; (b) U. S. Schubert, H. Hofmeier and G. R. Newkome, *Modern Terpyridine Chemistry*, 1st edn., Wiley-VCH Verlag GmbH & Co. KGaA, Weingeim, Germany, 2006; (c) U. S. Schubert, A. Winter and G. R. Newkome, *Terpyridine-based Materials For Catalytic, Optoelectronic and Life Science Applications*, 1st edn., Wiley-VCH Verlag GmbH & Co. KGaA, Weinheim, Germany, 2011; (d) S. Campagna, F. Puntoriero, F. Nastasi, G. Bergamini and V. Balzani, Springer-Verlag, New York, USA, 2007 edn., 2007.

[2] (a) F. Puntoriero, A. Sartorel, M. Orlandi, G. La Ganga, S. Serroni, M. Bonchio, F. Scandola and S. Campagna, *Coord. Chem. Rev.*, 2011, **255**, 2594; (b) M. Natali, M. Orlandi, S. Berardi, S. Campagna, M. Bonchio, A. Sartorel and F. Scandola, *Inorg. Chem.*, 2012, **51**, 7324; (c) D. G. Brown, P. A. Schauer, J. Borau-Garcia, B. R. Fancy and C. P. Berlinguette, *J. Am. Chem. Soc.*, 2013, **135**, 1692; (d) N. S. Murray, J. A. Rudd, A.-C. Chamayou, E. C. Constable, C. E. Housecroft, M. Neuburger and J. A.

Zampese, *RSC Adv.*, 2014, **4**, 11766; (e) K. Heussner, K. Peuntinger, N. Rockstroh, S. Rau and C. Streb, *Dalton Trans.*, 2015, **44**, 330; (f) B. Laramee-Milette, F. Lussier, I. Ciofini and G. S. Hanan, *Dalton Trans.*, 2015, **44**, 11551; (g) E. K. Pefkianakis, T. A. Theodossiou, D. K. Toubanaki, E. Karagouni, P. Falaras, K. Papadopoulos and G. C. Vougioukalakis, *Photochem. Photobiol.*, 2015, **91**, 1191.

[3] (a) Y. Gao, X. Ding, J. Liu, L. Wang, Z. Lu, L. Li and L. Sun, *J. Am. Chem. Soc.*, 2013, **135**, 4219; (b) J. Huang, D. Wang, Z. Yue, X. Li, D. Chu and P. Yang, *J. Phys. Chem. C*, 2015, **119**, 27892; (c) A. Jana, J. Mondal, P. Borah, S. Mondal, A. Bhaumik and Y. Zhao, *Chem. Commun.*, 2015, **51**, 10746; (d) E. Kato, H. Takeda, K. Koike, K. Ohkubo and O. Ishitani, *Chem. Sci.*, 2015, **6**, 3003; (e) G. Pratsch and L. E. Overman, *J. Org. Chem.*, 2015, **80**, 11388; (f) S. Zhang, L. Li, S. Zhao, Z. Sun and J. Luo, *Inorg. Chem.*, 2015, **54**, 8375.

[4] (a) B. A. Gorman, P. S. Francis and N. W. Barnett, *Analyst*, 2006, **131**, 616; (b) E. Kerr, E. H. Doeven, G. J. Barbante, C. F. Hogan, D. J. Bower, P. S. Donnelly, T. U. Connell and P. S. Francis, *Chem. Sci.*, 2015, **6**, 472; (c) P. Li, Z. Jin, M. Zhao, Y. Xu, Y. Guo and D. Xiao, *Dalton Trans.*, 2015, **44**, 2208; (d) M. Sentic, S. Arbault, L. Bouffier, D. Manojlovic, A. Kuhn and N. Sojic, *Chem. Sci.*, 2015, **6**, 4433; (e) K. N. Swanick, M. Sandroni, Z. Ding and E. Zysman-Colman, *Chem. Eur. J.*, 2015, **21**, 7435; (f) C.-Y. Xiong, H.-J. Wang, W.-B. Liang, Y.-L. Yuan, R. Yuan and Y.-Q. Chai, *Chem. Eur. J.*, 2015, **21**, 9825.

[5] (a) J. K. Lee, D. S. Yoo, E. S. Handy and M. F. Rubner, *Appl. Phys. Lett.*, 1996, **69**, 1686; (b) A. Paul, R. A. Bartels, R. Tobey, H. Green, S. Weiman, I. P. Christov, M. M. Murnane, H. C. Kapteyn and S. Backus, *Nature*, 2003, **421**, 51; (c) Y. Chuai, D. N. Lee, C. Zhen, J. H. Min, B. H. Kim and D. Zou, *Synth. Met.*, 2004, **145**, 259; (d) J. Yang and K. C. Gordon, *Chem. Phys. Lett.*, 2004, **385**, 481; (e) H. Shahroosvand, P. Abbasi, A. Faghih, E. Mohajerani, M. Janghouri and M. Mahmoudi, *RSC Adv.*, 2014, **4**, 1150; (f) H. Shahroosvand, S. Rezaei, E. Mohajerani, M. Mahmoudi, M. A. Kamyabi and S. Nasiri, *New J. Chem.*, 2014, **38**, 5312; (g) H. Shahroosvand, S. Rezaei, E. Mohajerani and M. Mahmoudi, *New J. Chem.*, 2015, **39**, 3035.

[6] (a) A. Mishra, N. Pootrakulchote, M. K. Fischer, C. Klein, M. K. Nazeeruddin, S. M. Zakeeruddin, P. Bauerle and M. Gratzel, *Chem. Commun.*, 2009, 7146; (b) A. Abbotto

and N. Manfredi, *Dalton Trans.*, 2011, **40**, 12421; (c) A. Abbotto, F. Sauvage, C. Barolo, F. De Angelis, S. Fantacci, M. Graetzel, N. Manfredi, C. Marinzi and M. K. Nazeeruddin, *Dalton Trans.*, 2011, **40**, 234; (d) G. C. Vougioukalakis, A. I. Philippopoulos, T. Stergiopoulos and P. Falaras, *Coord. Chem. Rev.*, 2011, **255**, 2602; (e) M. García-Iglesias, L. Pellejà, J.-H. Yum, D. González-Rodríguez, M. K. Nazeeruddin, M. Grätzel, J. N. Clifford, E. Palomares, P. Vázquez and T. Torres, *Chem. Sci.*, 2012, **3**, 1177; (f) J.-F. Yin, M. Velayudham, D. Bhattacharya, H.-C. Lin and K.-L. Lu, *Coord. Chem. Rev.*, 2012, **256**, 3008; (g) K.-L. Wu, W.-P. Ku, S.-W. Wang, A. Yella, Y. Chi, S.-H. Liu, P.-T. Chou, M. K. Nazeeruddin and M. Grätzel, *Adv. Funct. Mater.*, 2013, **23**, 2285; (h) Q. Wang, W. Wu, C.-L. Ho, L. Xue, Z. Lin, H. Li, Y. H. Lo and W.-Y. Wong, *Eur. J. Inorg. Chem.*, 2014, **2014**, 5322; (i) M. Urbani, M. Medel, S. A. Kumar, M. Ince, A. N. Bhaskarwar, D. González-Rodríguez, M. Grätzel, M. K. Nazeeruddin and T. Torres, *Chem. Eur. J.*, 2015, **21**, 16252.

[7] (a) C. Bhaumik, S. Das, D. Saha, S. Dutta and S. Baitalik, *Inorg. Chem.*, 2010, **49**, 5049; (b) D. Saha, S. Das, C. Bhaumik, S. Dutta and S. Baitalik, *Inorg. Chem.*, 2010, **49**, 2334; (c) C. Bhaumik, D. Saha, S. Das and S. Baitalik, *Inorg. Chem.*, 2011, **50**, 12586; (d) D. A. Jose, P. Kar, D. Koley, S. Ganguly, W. Thiel, H. N. Ghosh and A. Das, *Inorg. Chem.*, 2007, **46**, 5576; (e) Y. Cui, Y.-L. Niu, M.-L. Cao, K. Wang, H.-J. Mo, Y.-R. Zhong and B. H. Ye, *Inorg. Chem.*, 2008, **47**, 5616.

[8] (a) Q. Shao and B. Xing, *Chem. Commun.*, 2012, **48**, 1739; (b) P. Zhou, Z. Zheng, W. Lu, F. Zhang, Z. Zhang, D. Pang, B. Hu, Z. He and H. Wang, *Angew. Chem. Int. Ed.*, 2012, **51**, 670; (c) P. Zhang, L. Pei, Y. Chen, W. Xu, Q. Lin, J. Wang, J. Wu, Y. Shen, L. Ji and H. Chao, *Chem. Eur. J.*, 2013, **19**, 15494; (d) R. Zhang, Z. Ye, B. Song, Z. Dai, X. An and J. Yuan, *Inorg. Chem.*, 2013, **52**, 10325; (e) F. Liu, Y. Gao, J. Wang and S. Sun, *Analyst*, 2014, **139**, 3324; (f) W. Xu, J. Zuo, L. Wang, L. Ji and H. Chao, *Chem. Commun.*, 2014, **50**, 2123; (g) A. Byrne, C. Dolan, R. D. Moriarty, A. Martin, U. Neugebauer, R. J. Forster, A. Davies, Y. Volkov and T. E. Keyes, *Dalton Trans.*, 2015, **44**, 14323; (h) Y. Ding, Q. Wu, K. Zheng, L. An, X. Hu and W. Mei, *RSC Adv.*, 2015, **5**, 63330; (i) D. Hara, H. Komatsu, A. Son, S. Nishimoto and K. Tanabe, *Bioconjug. Chem.*, 2015, **26**, 645; (j) Z. Ye, Q. Gao, X. An, B. Song and J. Yuan, *Dalton Trans.*, 2015, **44**, 8278; (k) B. Yu, C. Ouyang, K. Qiu, J. Zhao, L. Ji and H. Chao,

Chem. Eur. J., 2015, **21**, 3691; (l) P. Zhang, H. Huang, Y. Chen, J. Wang, L. Ji and H. Chao, *Biomaterials*, 2015, **53**, 522.

[9] (a) V. Pierroz, T. Joshi, A. Leonidova, C. Mari, J. Schur, I. Ott, L. Spiccia, S. Ferrari and G. Gasser, *J. Am. Chem. Soc.*, 2012, **134**, 20376; (b) N. Iizuka, S.-i. Motoki, M. Nakai and Y. Nakabayashi, *Inorg. Chem. Commun.*, 2014, **46**, 145; (c) T. Joshi, V. Pierroz, C. Mari, L. Gemperle, S. Ferrari and G. Gasser, *Angew. Chem. Int. Ed.*, 2014, **53**, 2960; (d) W. Li, B.-J. Han, J.-H. Yao, G.-B. Jiang, G.-J. Lin, Y.-Y. Xie, H.-L. Huang and Y.-J. Liu, *Spectrochim. Acta, Part A*, 2015, **150**, 127; (e) C. Mari, V. Pierroz, S. Ferrari and G. Gasser, *Chem. Sci.*, 2015, **6**, 2660; (f) C. Mari, V. Pierroz, A. Leonidova, S. Ferrari and G. Gasser, *Eur. J. Inorg. Chem.*, 2015, **2015**, 3879.

[10] (a) S. P. Mulcahy, S. Li, R. Korn, X. Xie and E. Meggers, *Inorg. Chem.*, 2008, **47**, 5030; (b) S. Sharma, S. K. Singh and D. S. Pandey, *Inorg. Chem.*, 2008, **47**, 1179; (c) C. M. Che and F. M. Siu, *Curr. Opin. Chem. Biol.*, 2010, **14**, 255; (d) X. Chen, F. Gao, Z. X. Zhou, W. Y. Yang, L. T. Guo and L. N. Ji, *J. Inorg. Biochem.*, 2010, **104**, 576; (e) J. F. Kou, C. Qian, J. Q. Wang, X. Chen, L. L. Wang, H. Chao and L. N. Ji, *J. Biol. Inorg. Chem.*, 2012, **17**, 81; (f) N. A. Vyas, S. S. Bhat, A. S. Kumbhar, U. B. Sonawane, V. Jani, R. R. Joshi, S. N. Ramteke, P. P. Kulkarni and B. Joshi, *Eur. J. Med. Chem.*, 2014, **75**, 375; (g) K. Traven, N. Eleftheriadis, S. Seršen, J. Kljun, J. Bezenšek, B. Stanovnik, I. Turel and F. J. Dekker, *Polyhedron*, 2015, **101**, 306; (h) W. Zhang, H. Y. Zhang, Y. H. Zhang and Y. Liu, *Chem. Commun.*, 2015, **51**, 16127.

[11] (a) B.-J. Han, G.-B. Jiang, J. Wang, W. Li, Q.-S. Dai, Y.-Y. Xie, G.-J. Lin, H.-L. Huang and Y.-J. Liu, *Trans. Met. Chem.*, 2014, **40**, 153; (b) G.-B. Jiang, J.-H. Yao, J. Wang, W. Li, B.-J. Han, Y.-Y. Xie, G.-J. Lin, H.-L. Huang and Y.-J. Liu, *New J. Chem.*, 2014, **38**, 2554; (c) X.-L. Hong and W.-G. Lu, *J. Coord. Chem.*, 2015, **68**, 4408; (d) S. H. Lai, G. B. Jiang, J. H. Yao, W. Li, B. J. Han, C. Zhang, C. C. Zeng and Y. J. Liu, *J. Inorg. Biochem.*, 2015, **152**, 1; (e) C. Zhang, C.-C. Zeng, S.-H. Lai, D.-G. Xing, W. Li, B.-J. Han and Y.-J. Liu, *Polyhedron*, 2016.

[12] (a) M. Maestri, N. Armaroli, V. Balzani, E. C. Constable and A. M. W. Cargill Thompson, *Inorg. Chem.*, 1995, **34**, 2759; (b) J.-P. Sauvage, J.-P. Collin, J.-C. Chambron, S. Guillerez and C. Coudret, *Chem. Rev.*, 1994, **94**, 993.

[13] (a) A. K. Pal and G. S. Hanan, *Chem. Soc. Rev.*, 2014, **43**, 6184; (b) E. A. Medlycott and G. S. Hanan, *Chem. Soc. Rev.*, 2005, **34**, 133.

[14] (a) H. Wolpher, O. Johansson, M. Abrahamsson, M. Kritikos, L. Sun and B. Åkermark, *Inorg. Chem. Commun.*, 2004, **7**, 337; (b) M. Abrahamsson, H.-C. Becker, L. Hammarström, C. Bonnefous, C. Chamchoumis and R. P. Thummel, *Inorg. Chem.*, 2007, **46**, 10354; (c) M. Abrahamsson, M. Jäger, R. J. Kumar, T. Österman, P. Persson, H.-C. Becker, O. Johansson and L. Hammarström, *J. Am. Chem. Soc.*, 2008, **130**, 15533; (d) F. Schramm, V. Meded, H. Fliegl, K. Fink, O. Fuhr, Z. Qu, W. Klopper, S. Finn, T. E. Keyes and M. Ruben, *Inorg. Chem.*, 2009, **48**, 5677; (e) G. A. Parada, L. A. Fredin, M.-P. Santoni, M. Jäger, R. Lomoth, L. Hammarström, O. Johansson, P. Persson and S. Ott, *Inorg. Chem.*, 2013, **52**, 5128; (f) A. R. Naziruddin, C.-L. Kuo, W.-J. Lin, W.-H. Lo, C.-S. Lee, B.-J. Sun, A. H. H. Chang and W.-S. Hwang, *Organometallics*, 2014, **33**, 2575; (g) A. K. Pal, S. Serroni, N. Zaccheroni, S. Campagna and G. S. Hanan, *Chem. Sci.*, 2014, **5**, 4800; (h) M. Jäger, R. J. Kumar, H. Göris, J. Bergquist and O. Johansson, *Inorg. Chem.*, 2009, **48**, 3228; (i) A. Breivogel, C. Forster and K. Heinze, *Inorg. Chem.*, 2010, **49**, 7052; (j) A. Breivogel, M. Meister, C. Forster, F. Laquai and K. Heinze, *Chem. Eur. J.*, 2013, **19**, 13745; (k) A. Breivogel, S. Wooh, J. Dietrich, T. Y. Kim, Y. S. Kang, K. Char and K. Heinze, *Eur. J. Inorg. Chem.*, 2014, **2014**, 2720; (l) A. Breivogel, M. Park, D. Lee, S. Klassen, A. Kühnle, C. Lee, K. Char and K. Heinze, *Eur. J. Inorg. Chem.*, 2014, **2014**, 288; (m) C. Kreitner, E. Erdmann, W. W. Seidel and K. Heinze, *Inorg. Chem.*, 2015, **54**, 11088.

[15] (a) C. Bonnefous, A. Chouai and R. P. Thummel, *Inorg. Chem.*, 2001, **40**, 5851; (b) S. H. Wadman, M. Lutz, D. M. Tooke, A. L. Spek, F. Hartl, R. W. A. Havenith, G. P. M. van Klink and G. van Koten, *Inorg. Chem.*, 2009, **48**, 1887; (c) D. G. Brown, N. Sanguantrakun, B. Schulze, U. S. Schubert and C. P. Berlinguette, *J. Am. Chem. Soc.*, 2012, **134**, 12354; (d) H. Kisserwan, A. Kamar, T. Shoker and T. H. Ghaddar, *Dalton Trans.*, 2012, **41**, 10643; (e) Y. M. Zhang, J. Y. Shao, C. J. Yao and Y. W. Zhong, *Dalton Trans.*, 2012, **41**, 9280; (f) A. K. Pal, N. Zaccheroni, S. Campagna and G. S. Hanan, *Chem. Commun.*, 2014, **50**, 6846.

[16] A. K. Pal and G. S. Hanan, *Dalton Trans.*, 2014, **43**, 11811.

[17] Y. Q. Fang and G. S. Hanan, *Synlett*, 2003, **6**, 852.

[18] G. Hanan, D. Chand, A. Pal and P. Mandali, *Synlett*, 2015, **26**, 1408.

[19] M. Böttger, B. Wiegmann, S. Schaumburg, P. G. Jones, W. Kowalsky and H.-H. Johannes, *Beilstein J. Org. Chem.*, 2012, **8**, 1037.

[20] M. Abrahamsson, M. Jäger, T. Österman, L. Eriksson, P. Persson, H.-C. Becker, O. Johansson and L. Hammarström, *J. Am. Chem. Soc.*, 2006, **128**, 12616.

[21] (a) T. J. Rutherford, O. Van Gijte, A. Kirsch-De Mesmaeker and F. R. Keene, *Inorg. Chem.*, 1997, **36**, 4465; (b) N. C. Fletcher, P. C. Junk, D. A. Reistma and F. R. Keene, *J. Chem. Soc., Dalton Trans.*, 1998, 133; (c) N. C. Fletcher and F. R. Keene, *J. Chem. Soc., Dalton Trans.*, 1999, 683; (d) D. M. D'Alessandro and F. R. Keene, *Chem. Phys.*, 2006, **324**, 8.

[22] (a) I. Romero, M. Rodríguez, A. Llobet, M.-N. Collomb-Dunand-Sauthier, A. Deronzier, T. Parella and H. Stoeckli-Evans, *J. Chem. Soc., Dalton Trans.*, 2000, 1689; (b) Y. Shimizu, S. Fukui, T. Oi and H. Nagao, *Bull. Chem. Soc. Jpn.*, 2008, **81**, 1285; (c) M. Jäger, R. J. Kumar, H. Görls, J. Bergquist and O. Johansson, *Inorg. Chem.*, 2009, **48**, 3228.

[23] D. J. Losey, B. A. Frenzel, W. M. Smith, S. E. Hightower and C. G. Hamaker, *Inorg. Chem. Commun.*, 2013, **30**, 46.

[24] D. P. Rillema and D. S. Jones, *J. Chem. Soc., Chem. Commun.*, 1979, 849.

[25] (a) J. Dinda, S. Liatard, J. Chauvin, D. Jouvenot and F. Loiseau, *Dalton Trans.*, 2011, **40**, 3683; (b) H. J. Park and Y. K. Chung, *Dalton Trans.*, 2012, **41**, 5678; (c) W. Yang and Y. Zhong, *Chin. J. Chem.*, 2013, **31**, 329.

[26] (a) P. G. Bomben, K. C. Robson, P. A. Sedach and C. P. Berlinguette, *Inorg. Chem.*, 2009, **48**, 9631; (b) B. D. Koivisto, K. C. Robson and C. P. Berlinguette, *Inorg. Chem.*, 2009, **48**, 9644.

[27] A. B. P. Lever, *Inorg. Chem.*, 1990, **29**, 1271.

[28] S. G. Telfer, T. M. McLean and M. R. Waterland, *Dalton Trans*, 2011, **40**, 3097.

[29] M. Kasha, H. R. Rawls and M. A. El-Bayoumi, *Pure Appl. Chem.*, 1965, **11**, 371.

Chapitre 4 – *Going against the flow: Os(II)-to-Ru(II) energy transfer in rod-like polypyridyl chromophore*

4.1. Résumé

Le design judicieux d'une tige moléculaire hétérométallique de type Ru-Os a conduit au premier transfert d'énergie photo-induit d'osmium-à-ruthénium dans un complexe de type polypyridyle. La lumière absorbée est dirigée du centre métallique d'osmium vers la périphérie du complexe, où seule la luminescence à faible énergie du complexe phen-hpp hétéropétique du ruthénium a été observée.

Contribution :

Baptiste Laramée-Milette : Synthèse et caractérisation complète des ligands et des complexes homo- et hétéroleptiques. Analyse structurelle par diffraction des rayons X, étude computationnelle, analyse des propriétés optiques et électroniques. Rédaction de l'article.

Garry S. Hanan: Supervision, révision de l'article

Going against the flow: Os(II)-to-Ru(II) energy transfer in rod-like polypyridyl chromophore

*Baptiste Laramée-Milette and Garry S. Hanan**

Département de chimie, Université de Montréal, 5155 Ch. de la rampe, Pavillon J.-A. Bombardier, Montréal, Québec, Canada, H3T 2B1

*: E-mail: garry.hanan@umontreal.ca

Communication

Received: 07th May 2017; Accepted and published Online: 02nd August 2017

DOI:10.1039/C7CC03541A

Reproduced with permission from *Chem. Commun.* **2017**, *53*, 10496-10499

Copyright 2017 The Royal Society of Chemistry

4.2. Front cover

4.3. Table of content graphic

4.4. Abstract

The judicious design of a unique mixed-metal Ru-Os molecular rod led to the first photoinduced energy transfer from osmium-to-ruthenium in a polypyridyl complex. The absorbed light is directed from the osmium metal center to the peripheral ruthenium moieties, where only the low energy luminescence from the heteroleptic ruthenium phen-hpp complex was observed.

4.5. Introduction

Over the last three decades, intercomponent energy transfer has been extensively studied by the scientific community, with the goal of achieving thorough control on the directionality of energy transfer at the molecular level.[1-12] Among all examples, the Ru(II)-to-Os(II) energy transfer in polypyridyl systems can certainly be considered as a classic textbook case, where several examples of molecular rods,[13-32] dendrimers/dendrons[33-40] and star-shaped molecules[41-46] have been studied by different groups for their possible applications in opto-electronic and light-harvesting devices. Interestingly, despite the wide availability of polypyridyl ligands in the literature which, in theory, should allow facile fine-tuning of the optical as well as the electrochemical properties of the complexes, to the best of our knowledge, the opposite example, where an osmium chromophore transfers its energy to a ruthenium chromophore, has yet to be demonstrated.

In our effort to harvest NIR-radiation, our group[47-55] recently described a new type of symmetrical and non-symmetrical ligand incorporating the electron-donating hexahydro-pyrimidopyrimidine (hpp) moiety.[47-55] Considering our results with non-symmetrical mono-substituted hpp ligands,[54] the strong donation of the hpp ligand led to a large red-shift in the luminescence of its ruthenium complexes, with their emission maxima centered around 810 nm in the case of the heteroleptic species, being red-shifted by approximately 75 nm as compared to the archetypical $Os(tpy)_2^{2+}$ complexes (tpy = 2,2':6',2"terpyridine). This atypical relationship piqued our interest, so we investigated the properties of a system designed on the closely related rod-like chromophores reported in the mid-90's by Sauvage[15, 16] and Ziessel.[17, 56] We herein report the synthesis of a

heterometallic rod and its precursor (**Chart 1**), their optical as well as their electrochemical properties along with theoretical density functional theory (DFT) and time-dependent DFT (TD-DFT) calculations to support the experimental observations.

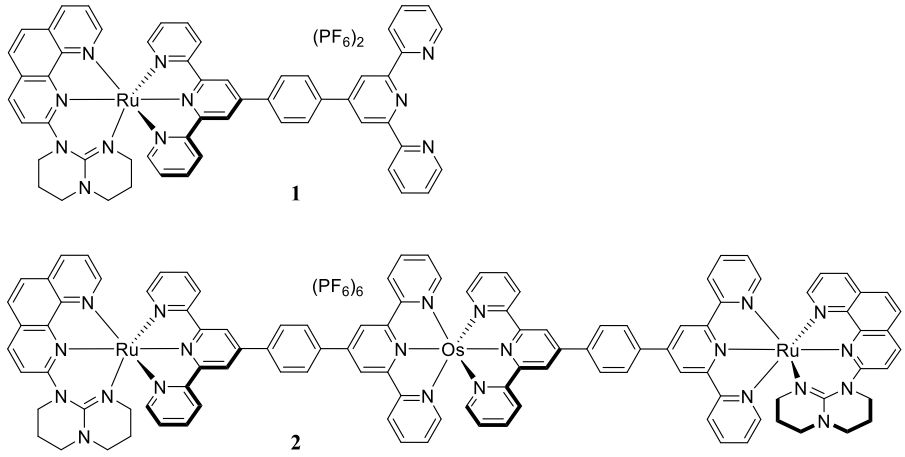

Chart 4.1 - Structure of the mononuclear Ru(II) complex 1 and the corresponding mixed-metal Ru(II)/Os(II) species 2.

4.6. Synthesis of the metal complexes

Metal complex **1** was readily prepared in a two-step reaction. First, the 2-(hexahydro-pyrimidopyrimidine)-1,10-phenanthroline ligand (phen-hpp) was reacted with an equimolar amount of $RuCl_3.3H_2O$ at reflux in ethanol for 2 hours to afford (phen-hpp)$RuCl_3$ as a burgundy precipitate. The precursor was then suspended in ethylene glycol in a 1:1 ratio with 1’’’,4’’’-bis(4’-(2,2’:6’,2”-terpyridine)-benzene (bistpy) ligand and reacted in a sealed microwave vial for 15 minutes at 205°C, affording a deep purple solution. The addition of a KPF_6 aqueous solution to the resulting mixture led to the precipitation of a deep brownish precipitate, which was further isolated by centrifugation. Purification of the residue on silica gel (20:1:1 $MeCN:H_2O:KNO_3$, with 1% Et_3N) led to the isolation of the mononuclear species **1**.

The heterometallic species **2** was prepared in similar conditions, were the Ru(II) complex **1** was suspended in ethylene glycol with an equimolar amount of K_2OsCl_6 in a

microwave vial equipped with a magnetic bar. The suspension was left under microwave irradiation at 205°C for 15 minutes. After this time, the resulting deep purple solution was poured into an aqueous KPF_6 solution, resulting in the instant precipitation of a near-black precipitate. The precipitate was centrifuged for 15 minutes and further subjected to gel chromatography on silica, using a mixture of MeCN:H_2O:KNO_3 sat. with 1 % Et_3N in a 15:1:1 ratio, leading to the isolation of species **2** in a 46 % yield.

4.7. Results and discussion

Small crystals of **1** suitable for single-crystal X-ray crystallography experiment were grown from the slow diffusion of diethyl ether into an acetonitrile solution. The connectivity of the atoms clearly demonstrated the nature of the metal complex, as depicted in Figure 11.13. The octahedral geometry is slightly enhanced around the metal core, where the N_{hpp}-Ru-$N_{centerphen}$ angle formed by the phen-hpp ligand is of 88° and the N_{hpp}-Ru-$N_{sidephen}$ angle is of 166° compared to the typical N_{side}-Ru-N_{center} and the N_{side}-Ru-N_{side} angles in the terpyridine ligand (≈75-80° and 158°, respectively).

Table 4.1 – Electrochemical data for the homo- and heterometallic Ru(II)/Os(II) metal complexes in DMF[a]

Cmpd	$E_{1/2}^{Ox}$ (V) (ΔE_p (mV))			$E_{1/2}^{Red}$ (V) (ΔE_p (mV))			
1	–	–	0.72 (63)	-1.23 (85)	-1.58 (76)	-1.80 (98)	–
2	–	0.92 (53)	0.72 (64)	-1.11 (51)	-1.26 (100)	-1.44 (47)	-1.60[b]
$(ttpy)_2Ru$	1.25	–	–	-1.24	-1.46	–	–
$(ttpy)_2Os$	–	0.93	–	-1.23	-1.54	–	–
$((ttpy)Ru(bistpy))_2Os$	1.25	0.90	–	-1.20	-1.43	–	–
(phtpy)(phen-hpp)Ru	–	–	0.71	-1.31	-1.63	-1.93	–

[a] Potentials are in volts vs SCE. Cyclic voltammetry was performed in DMF/*t*-Bu4N(PF_6) (0.1M), recorded at 25±1 °C with a sweep rate of 50 mV s^{-1}. All potentials are corrected vs. Fc/Fc^+ = 0.45V. ttpy = 4'-*p*-tolyl-2,2':6',2"-terpyridine. phtpy = 4'-phenyl-2,2':6',2"-terpyridine. [b] Due to absorption at the electrode, a striping peak was observed; the potential is given for the cathodic wave.

The redox properties of the metal complexes **1**-**2** were examined by cyclic and square-wave voltammetry and the details are presented in Table 4.1. As previously described for similar heteroleptic Ru(II) species, the mononuclear ruthenium complex **1**

display a single monoelectronic reversible wave at +0.72 V, ascribed to the oxidation of Ru(II) to Ru(III). It is worth mentioning that the oxidation on the metal-core is severely affected by the strongly electron-donating hpp moiety (Lever's ligand electrochemical parameter (E_L) ≈ -0.4 to -0.6 V)[54] when compared to conventional $Ru(tpy)_2^{2+}$ complexes, where the oxidation potential is of approximatively +1.25 V. Interestingly, the oxidation of the ruthenium core is 200 mV less positive than osmium terpyridine-based complexes, which usually display an Os(II)/Os(III) reversible oxidation wave at about 0.9 V.[57] On the other hand, the ligand-centered reductions in **1** are not affected by the electron-donation of the non-symmetrical phen-hpp ligand as compared to the $Ru(tpy)_2^{2+}$ analog. All three reductions are mono-electronic events and, as a first approximation by DFT calculations (Figure 11.14), are attributed to the reduction of the terpyridine closest to the ruthenium center (-1.23 V), followed by the reduction of the phenanthroline ligand (-1.58 V)) and the free terpyridine moiety (-1.80 V).

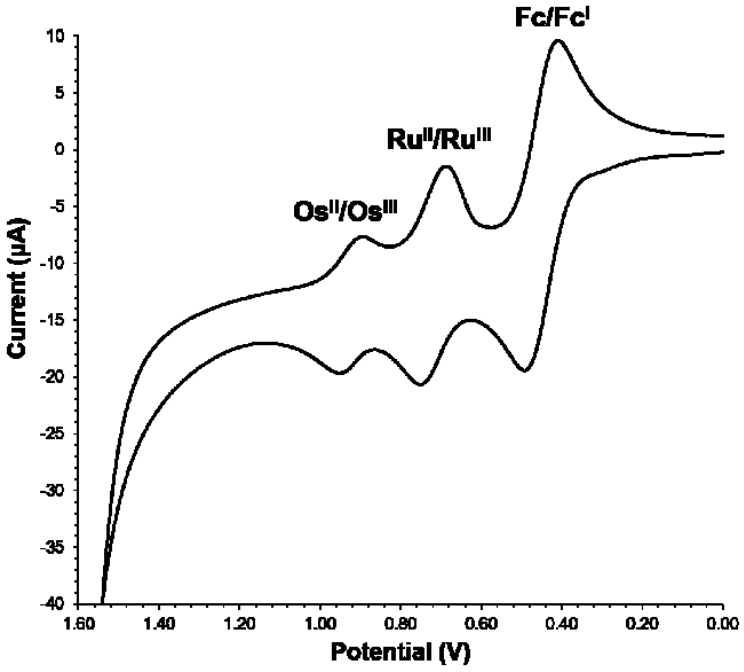

Figure 4.1 - Cyclic voltammogram of complex 2 displaying the reversible Os(II)/Os(III) and Ru(II)/Ru(III) oxidations, with ferrocene as internal standard.

The heterometallic species **2** displays two well resolved reversible oxidation waves at 0.92 V and 0.72 V (Figure 4.1), assigned to the mono-electronic oxidation of the osmium core and two coincidental mono-electronic oxidations of the ruthenium cores, respectively. The resolution of the waves and the absence of shift in the oxidation potential of both metal ions is an indication of a lack of communication between the metal centers. In the experimental conditions, up to four reduction processes were observed. The first three processes are fully reversible (Figure 11.16) while the fourth one is ill-defined due to adsorption and stripping on the electrode.[46] Nevertheless, square-wave voltammetry experiment (Figure 11.17) revealed that the first and third processes are mono- electronic while the second and fourth processes are the results of two coincidental mono-electronic processes. As depicted in Figure 4.2, we assigned the reduction as follows: the first reduction at -1.11 V is located on one of the terpyridine moiety coordinated to the osmium core. The following two coincidental mono-electronic processes at -1.26 V are due to the quasi-simultaneous reduction of the terpyridine units coordinated to the ruthenium cores while the third mono-electronic reduction at -1.44 V is ascribed to the reduction of the remaining terpyridine unit. Finally, the external phenanthroline units are simultaneously reduced at -1.60 V.

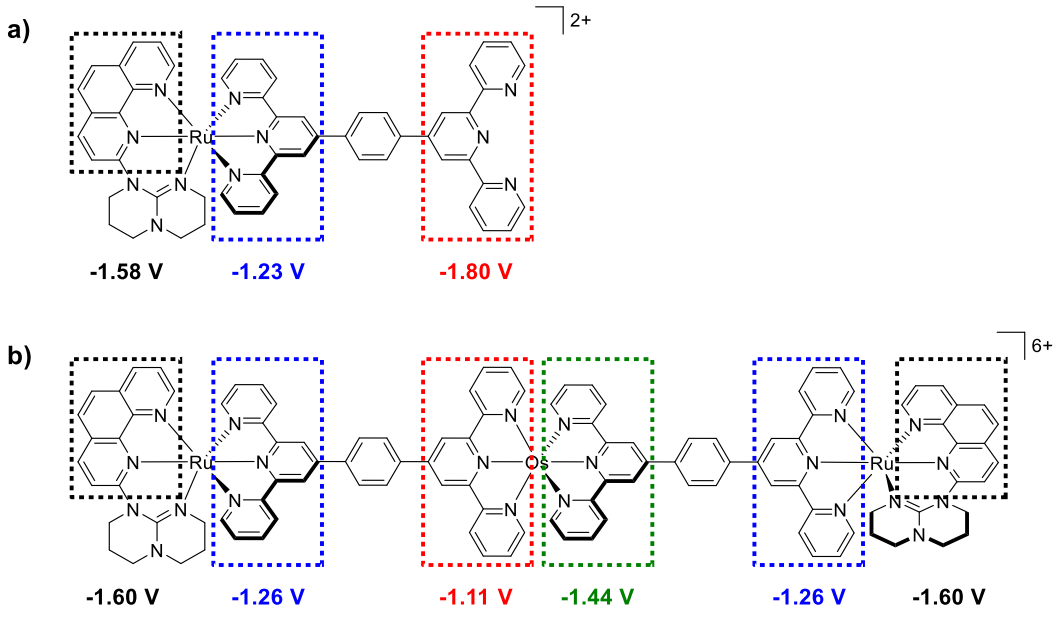

Figure 4.2 - Attribution of the ligand-based reduction processes observed in a) metal complex **1** and b) hetero-metallic complex **2**.

This assignment is in good agreement with the DFT approximation, where the electron-rich phen-hpp ligand only slightly contributes to the LUMO+6 and its major contribution was observed in LUMO+8.

The UV-visible absorption spectra of **1** and **2** were acquired in diluted dry degassed acetonitrile at ambient temperature (Figure 4.3). As determined by TD-DFT using the PBE0 functional with inclusion of acetonitrile solvent by the conductor-like polarization continuum model (CPCM), the two complexes exhibit strong ligand-centered (LC) $\pi \rightarrow \pi^*$ transitions between 200-250 nm. The intense absorption band found between 250-350 nm consist of a mixture of $\pi \rightarrow \pi^*$ LC transitions and metal-to-ligand charge-transfer (MLCT) transitions while the lower energy transition between 350-550 nm are mainly ^{1}MLCT transitions. The heteroleptic species **2** display enhanced spin-forbidden ^{3}MLCT between 550-700 nm, mainly due to strong spin-orbit coupling interaction as well as $^1MLCT_{tpy}$ and ligand-to-ligand charge transfer (LLCT) from the phen-hpp ligand to the tpy unit. Complex **1** displays a weak tailing absorption in the same portion of the spectra owing to the $^1MLCT_{tpy}$ and $LLCT_{phen\text{-}hpp \rightarrow tpy}$ transitions.

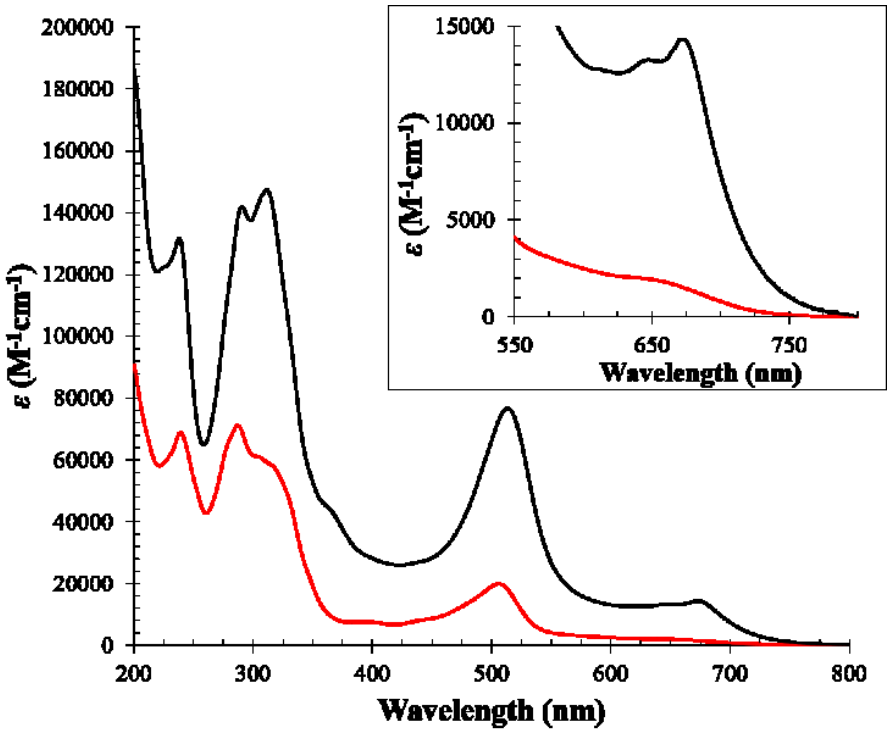

Figure 4.3 - Absorption spectra of 1 (red) and 2 (black) in acetonitrile solution at r.t.

The luminescence properties of the complexes were obtained in deareated spectroscopic grade acetonitrile solution. As depicted in Figure 11.20, the mono ruthenium and heterometallic species are emissive under these conditions, with their λ_{max} centered at 805 nm and 807 nm, respectively. It is worth mentioning that the emission maximum in **2** displays a bathochromic shift of 50-60 nm compared to both Os(II) references (mononuclear and heterometallic complexes). The Ru(II) species showed a 5.1 ns lifetime following a mono-exponential lifetime decay. Very interestingly, the lifetime value measured for the trinuclear species was of 5.6 ns, and also has mono-exponential decay, therefore indicating that the energy transfer from the Os(II) to the Ru(II) part of the metal complex is complete. Accordingly, as depicted in Figure 4.4, we propose that following excitation of the metal complex **2**, there is a rapid energy transfer from the ^{3}MLCT level of the Os(II) species to the ^{3}MLCT of the Ru(II), followed by radiative decay to the ground state of the molecule.

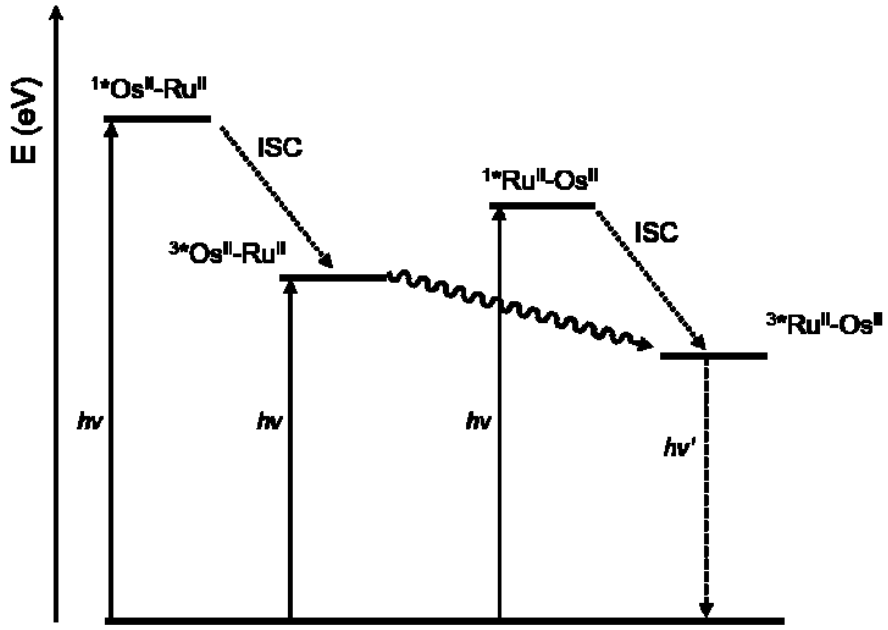

Figure 4.4 - Schematic Jablonski diagram of the energy transfer between the Os(II) and Ru(II) moieties. ISC = intersystem crossing.

4.8. Conclusion

In summary, we have designed and prepared a new type of molecular rod where the strong donation of the non-symmetrical phen-hpp ligand severely affects the optical as well as electrochemical properties of the ruthenium moiety, leading to a bathochromic shift in its emission. The heterometallic species is, to the best of our knowledge, the first Ru(II)-Os(II) polypyridyl system capable of osmium-to-ruthenium energy transfer. As this bridging ligand is also used in metallosupramolecular polymers,[58-59] fine control over energy transfer with the hpp unit may have further applications in other fields.

4.9. References

[1] J. P. Collin, P. Gaviña, V. Heitz and J. P. Sauvage, *Eur. J. Inorg. Chem.*, 1998, 1-14.

[2] S. Serroni, S. Campagna, F. Puntoriero, C. Di Pietro, N. D. McClenaghan and F. Loiseau, *Chem. Soc. Rev.*, 2001, **30**, 367-375.

[3] S. Serroni, S. Campagna, F. Puntoriero, F. Loiseau, V. Ricevuto, R. Passalacqua and M. Galletta, *C. R. Chim.*, 2003, **6**, 883-893.

[4] H. Hofmeier and U. S. Schubert, *Chem. Soc. Rev.*, 2004, **33**, 373-399.

[5] L. Cola and P. Belser, in *Electron Transfer in Chemistry*, ed. V. Balzani, Wiley-VCH Verlag GmbH, Weinheim, Germany, 2008.

[6] P. P. Laine, S. Campagna and F. Loiseau, *Coord. Chem. Rev.*, 2008, **252**, 2552-2571.

[7] J. Otsuki, T. Akasaka and K. Araki, *Coord. Chem. Rev.*, 2008, **252**, 32-56.

[8] A. Barbieri, B. Ventura and R. Ziessel, *Coord. Chem. Rev.*, 2012, **256**, 1732-1741.

[9] M. Gilbert and B. Albinsson, *Chem. Soc. Rev.*, 2014, **44**, 845-862.

[10] A. Arrigo, A. Santoro, F. Puntoriero, P. P. Laine and S. Campagna, *Coord. Chem. Rev.*, 2015, **304-305**, 109-116.

[11] A. Arrigo, L. G. Ganga, F. Nastasi and S. Serroni, *C. R. Chim.*, 2017.

[12] F. Barigelletti and L. Flamigni, *Chem. Soc. Rev.*, 2000, **29**, 1-12.

[13] L. De Cola, V. Balzani, F. Barigelletti, L. Flamigni, P. Belser, A. von Zelewsky, M. Frank and F. Vögtle, *Inorg. Chem.*, 1993, **32**, 5228-5238.

[14] F. Vögtle, M. Frank, P. Belser, A. von Zelewsky, V. Balzani, L. De Cola, F. Barigelletti, L. Flamigni and M. Nieger, *Angew. Chem. Int. Ed.*, 1993, **32**, 1643-1646.

[15] F. Barigelletti, L. Flamigni, V. Balzani, J. P. Collin, J. P. Sauvage, A. Sour, E. C. Constable and A. M. W. C. Thompson, *J. Am. Chem. Soc.*, 1994, **116**, 7692-7699.

[16] M. Beley, S. Chodorowski, J. P. Collin, J. P. Sauvage, L. Flamigni and F. Barigelletti, *Inorg. Chem.*, 1994, **33**, 2543-2547.

[17] V. Grosshenny, A. Harriman and R. Ziessel, *Angew. Chem. Int. Ed.*, 1995, **34**, 1100-1102.

[18] V. Balzani, F. Barigelletti, P. Belser, S. Bernhard, L. De Cola and L. Flamigni, *J. Phys. Chem.*, 1996, **100**, 16786-16788.

[19] F. Barigelletti, L. Flamigni, M. Guardigli, A. Juris, M. Beley, S. Chodorowski-Kimmes, J. P. Collin and J. P. Sauvage, *Inorg. Chem.*, 1996, **35**, 136-142.

[20] V. Grosshenny, A. Harriman, M. Hissler and R. Ziessel, *J. Chem. Soc., Farad. Trans.*, 1996, **92**, 2223-2238.

[21] L. Hammarstrom, F. Barigelletti, L. Flamigni, N. Armaroli, A. Sour, J. P. Collin and J. P. Sauvage, *J. Am. Chem. Soc.*, 1996, **118**, 11972-11973.

[22] F. Barigelletti, L. Flamigni, J. P. Collin and J. P. Sauvage, *Chemical Communications*, 1997, 333-338.

[23] B. Schlicke, P. Belser, L. De Cola, E. Sabbioni and V. Balzani, *J. Am. Chem. Soc.*, 1999, **121**, 4207-4214.

[24] A. El-Ghayoury, A. Harriman, A. Khatyr and R. Ziessel, *Angew. Chem. Int. Ed.*, 2000, **39**, 185-189.

[25] A. El-ghayoury, A. Harriman and R. Ziessel, *J. Phys. Chem. A*, 2000, **104**, 7906-7915.

[26] A. Harriman, A. Khatyr, R. Ziessel and A. C. Benniston, *Angew. Chem. Int. Ed.*, 2000, **39**, 4287-4290.

[27] T. Akasaka, T. Mutai, J. Otsuki and K. Araki, *Dalton Trans.*, 2003, 1537-1544.

[28] A. Harriman, M. Hissler, A. Khatyr and R. Ziessel, *Eur. J. Inorg. Chem.*, 2003, **2003**, 955-959.

[29] C. Chiorboli, M. T. Indelli and F. Scandola, *Top. Curr. Chem.*, 2005, **257**, 63-102.

[30] S. Welter, N. Salluce, A. Benetti, N. Rot, P. Belser, P. Sonar, A. C. Grimsdale, K. Mullen, M. Lutz, A. L. Spek and L. De Cola, *Inorg. Chem.*, 2005, **44**, 4706-4718.

[31] D. Maity, C. Bhaumik, S. Mardanya, S. Karmakar and S. Baitalik, *Chem. Eur. J.*, 2014, **20**, 13242-13252.

[32] M. Wachtler, J. Kubel, K. Barthelmes, A. Winter, A. Schmiedel, T. Pascher, C. Lambert, U. S. Schubert and B. Dietzek, *Phys. Chem. Chem. Phys.*, 2016, **18**, 2350-2360.

[33] S. Campagna, G. Denti, L. Sabatino, S. Serroni, M. Ciano and V. Balzani, *J. Chem. Soc., Chem. Commun.*, 1989, 1500-1501.

[34] V. Balzani, S. Campagna, G. Denti, A. Juris, S. Serroni and M. Venturi, *Acc. Chem. Res.*, 1998, **31**, 26-34.

[35] F. Puntoriero, S. Serroni, A. Licciardello, M. Venturi, A. Juris, V. Ricevuto and S. Campagna, *J. Chem. Soc., Dalton Trans.*, 2001, 1035-1042.

[36] S. Serroni, S. Campagna, F. Puntoriero, C. Di Pietro, N. D. McClenaghan and F. Loiseau, *Chem. Soc. Rev.*, 2001, **30**, 367-375.

[37] H. B. Baudin, J. Davidsson, S. Serroni, A. Juris, V. Balzani, S. Campagna and L. Hammarström, *J. Phys. Chem. A*, 2002, **106**, 4312-4319.

[38] J. Andersson, F. Puntoriero, S. Serroni, A. Yartsev, T. Pascher, T. Polivka, S. Campagna and V. Sundstrom, *Farad. Discuss.*, 2004, **127**, 295-305.

[39] J. Andersson, F. Puntoriero, S. Serroni, A. Yartsev, T. Pascher, T. Polivka, S. Campagna and V. Sundstrom, *Chem. Phys. Lett.*, 2004, **386**, 336-341.

[40] A. Arrigo, L. G. Ganga, F. Nastasi, S. Serroni, A. Santoro, M.-P. Santoni, M. Galletta, S. Campagna and F. Puntoriero, *C. R. Chim.*, 2017, **20**, 209-220.

[41] P. Belser, A. von Zelewsky, M. Frank, C. Seel, F. Vögtle, L. De Cola, F. Barigelletti and V. Balzani, *J. Am. Chem. Soc.*, 1993, **115**, 4076-4086.

[42] J. M. Haider, R. M. Williams, L. De Cola and Z. Pikramenou, *Angew. Chem. Int. Ed.*, 2003, **42**, 1830-1833.

[43] J. A. Faiz, R. M. Williams, M. J. Silva, L. De Cola and Z. Pikramenou, *J Am Chem Soc*, 2006, **128**, 4520-4521.

[44] J. Otsuki, A. Imai, K. Sato, D. M. Li, M. Hosoda, M. Owa, T. Akasaka, I. Yoshikawa, K. Araki, T. Suenobu and S. Fukuzumi, *Chem. Eur. J.*, 2008, **14**, 2709-2718.

[45] E. La Mazza, F. Puntoriero, F. Nastasi, B. Laramée-Milette, G. S. Hanan and S. Campagna, *Dalton Trans.*, 2016, **45**, 19238-19241.

[46] A. K. Bilakhiya, B. Tyagi and P. Paul, *Inorg. Chem.*, 2002, **41**, 3830-3842.

[47] A. K. Pal, P. D. Ducharme and G. S. Hanan, *Chem. Commun.*, 2014, **50**, 3303-3305.

[48] A. K. Pal and G. S. Hanan, *Dalton Trans.*, 2014, **43**, 6567-6577.

[49] A. K. Pal and G. S. Hanan, *Dalton Trans.*, 2014, **43**, 11811-11814.

[50] A. K. Pal, S. Nag, J. G. Ferreira, V. Brochery, G. La Ganga, A. Santoro, S. Serroni, S. Campagna and G. S. Hanan, *Inorg. Chem.*, 2014, **53**, 1679-1689.

[51] A. K. Pal, S. Serroni, N. Zaccheroni, S. Campagna and G. S. Hanan, *Chem. Sci.*, 2014, **5**, 4800-4811.

[52] A. K. Pal, N. Zaccheroni, S. Campagna and G. S. Hanan, *Chem. Commun.*, 2014, **50**, 6846-6849.

[53] A. Pal, P. Mandali, D. Chand and G. S. Hanan, *Synlett*, 2015, **26**, 1408-1412.

[54] B. Laramée-Milette and G. S. Hanan, *Dalton Trans.*, 2016, **45**, 12507-12517.

[55] R. J. Schwamm, R. Vianello, A. Marsavelski, M. A. Garcia, R. M. Claramunt, I. Alkorta, J. Saame, I. Leito, C. M. Fitchett, A. J. Edwards and M. P. Coles, *J. Org. Chem.*, 2016, **81**, 7612-7625.

[56] V. Grosshenny, A. Harriman, F. M. Romero and R. Ziessel, *J. Phys. Chem.,* 1996, **100**, 17472-17484.

[57] J. P. Collin, S. Guillerez, J. P. Sauvage, F. Barigelletti, L. De Cola, L. Flamigni and V. Balzani, *Inorg. Chem.*, 1992, **31**, 4112-4117.

[58] U. Kolb, K. Büscher, C. A. Helm, A. Lindner, A. F. Thünemann, M. Menzel, M. Higuchi and G. G. Kurth, *Proc. Natl. Acad. Sci. U. S. A.*, 2006, **103**, 10202-10206.

[59] G. Schwarz, T. K. Sievers, Y. Bodenthin, I. Hasslauer, Té Geue, J. Koetz and D. G. Kurth, *J. Mater. Chem.*, 2010, **20**, 4142-4148.

Chapitre 5 - *Simple solubilisation of the traditional 2,2':6',2"-terpyridine ligand in organic solvents by substitution with 4,4"-di-tert-butyl groups*

5.1. Résumé

Une procédure simple à une étape est décrite pour la synthèse et la purification de 4,4"-di-*tert*-butyl-2,2':6',2"-terpyridine 4'-substitué ligands. La nouvelle série de ligands affiche une solubilité améliorée dans la plupart des solvants organiques par rapport au ligand traditionnelle de type 2,2':6',2"- terpyridine non-substitué.

Contribution :

Baptiste Laramée-Milette : Synthèse et caractérisation complète de la plupart des ligands et analyse partielle des complexes métalliques. Analyse structurelle par diffraction des rayons X, analyse des propriétés optiques et électroniques. Rédaction de l'article.

Thomas Auvray: Synthèse, purification et caractérisation partielle d'un ligand.

Sacha Nguyen: Synthèse, purification et caractérisation partielle du complexe de Fe(II).

Samantha Tremblay: Synthèse, purification et caractérisation partielle du complexe de Cu(II).

Christophe Lachance-Brais: Synthèse, purification et caractérisation partielle du complexe de Ni(II).

Mélanie Donguy: Synthèse, purification et caractérisation partielle d'un ligand.

Valeska Taylor: Synthèse, purification et caractérisation partielle d'un ligand.

Denis Deschênes: Développement de la méthode de purification du précurseur.

Garry S. Hanan: Supervision, révision de l'article.

Simple solubilisation of the traditional 2,2':6',2"-terpyridine ligand in organic solvents by substitution with 4,4"-di-*tert*-butyl groups

*Baptiste Laramée-Milette,[a] Thomas Auvray,[a] Sacha Nguyen,[a] Samantha Tremblay,[a] Christophe Lachance-Brais,[a] Mélanie Donguy,[b] Valeska Taylor,[a] Denis Deschênes[a] and Garry S. Hanan[a]**

a) Département de chimie, Université de Montréal, 5155 Ch. de la rampe, Pavillon J.-A. Bombardier, Montréal, Québec, Canada, H3T 2B1

b) Département de Chimie, 1 Rue de la Technologie, UT Lyon 1, 69622 Villeurbanne cedex, France

*: E-mail: garry.hanan@umontreal.ca

Full paper

Received: 17th July 2015; Published online: 22nd September 2015

DOI:10.1055/s-0035-1560324

Reproduced with permission from *Synthesis.* **2015**, *47*, 3849-3858

Copyright 2015 Georg Thieme Verlag Stuttgart · New York

5.2. Table of content graphic

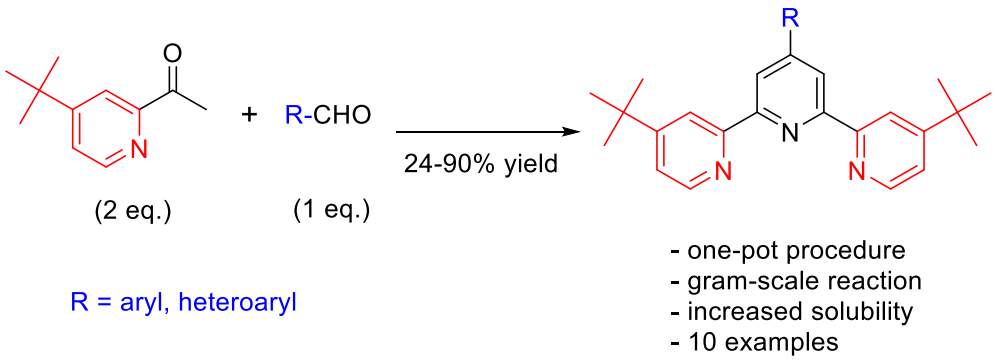

5.3. Abstract

A simple one-pot procedure is described for the synthesis and purification of 4′-substituted 4,4″-di-*tert*-butyl-2,2′:6′,2″-terpyridine ligands. The new series of ligand display improved solubility in most organic solvents in comparison to traditional 2,2′:6′,2″-terpyridine ligands.

5.3.1. Introduction

For the past few decades, the 2,2':6',2"-terpyridine (tpy) motif has been the ligand of choice of coordination chemists due to its ability to bond to a vast variety of metal ions.[1] The metal complexes generated via the coordination of tridentate ligands are more appealing as compared to their bidentate analogs since there is no possibility of diastereomer formation in their octahedral complexes[2] and they have found applications in several areas of research, such as anion-sensing,[3] bio-medical applications,[4] catalysis,[5] and dye-sensitized solar cells.[6]

A number of strategies have been developed over the years for the synthesis of both symmetrical and non-symmetrical terpyridine ligands. Among the most utilized techniques, the Tschitschibabin and Kröhnke-type syntheses allow the easy preparation of 4'-aryl and 4'-heteroaryl-2,2':6',2"-terpyridines by a ring-assembly methodology.[7] As

shown by several authors, the substitution in the 4'-terpyridine position by an aryl substituent can have a major influence on the properties of the metal complexes (Chart 5.1 a)).[8] Also, the careful design and introduction of the substituents into the 4'-position and further coordination to metal ions can give rise to one-, two- and three-dimensional polymers and assemblies.[9] One major drawback of this approach is that as the size of the supramolecular species become larger, its solubility usually decreases.

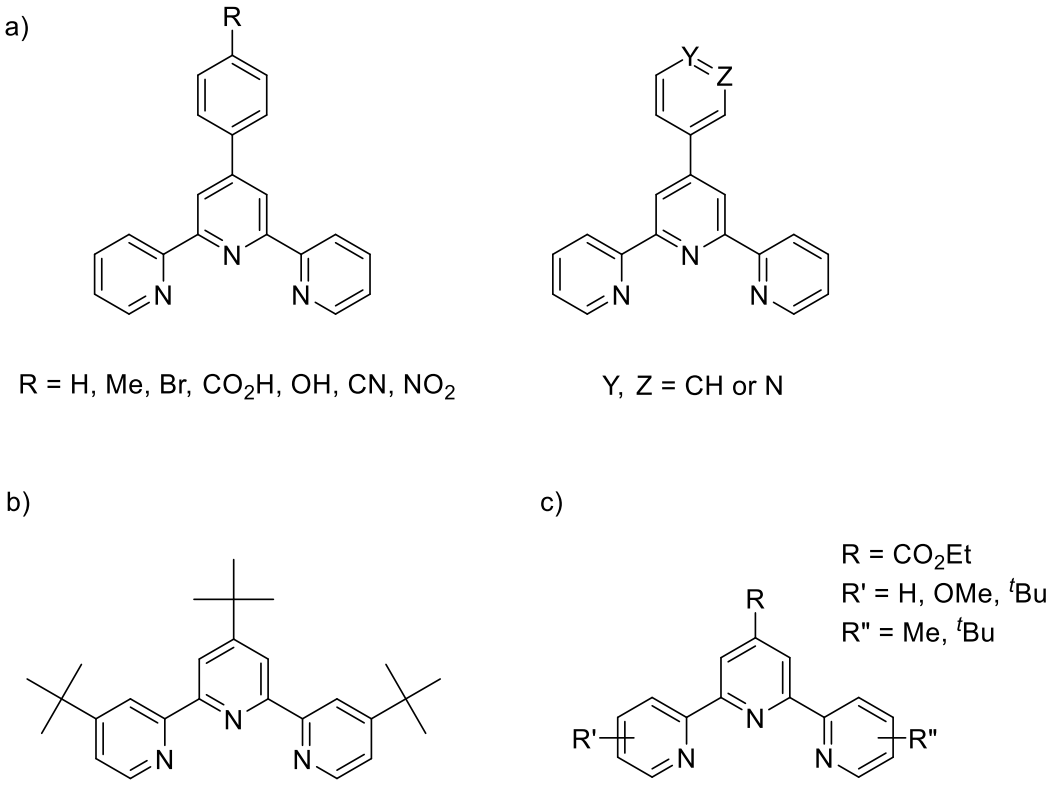

Chart 5.1 - Substitutions patterns of a) regular 4'-aryl and 4'-heteroaryl terpyridine ligands, b) Le Bozec's 4,4',4"-tri-tert-butyl terpyridine ligand and c) Tzschucke's non-symmetric alkylated terpyridine ligands.

To overcome such problems, several groups have used solubilizing groups such as tert-butyl units in order to maintain a modicum of solubility in most organic solvents.[10] As an example, there are numerous references relating to 4,4',4"-tri-*tert*-butyl-2,2':6',2"-terpyridine ligand since it was first synthesized by Le Bozec in the early 1990's (Chart

5.1 b)).[10] It is somewhat surprising that aside from Le Bozec's ligand, there are only a few reports of the use of tert-butyl-terpyridine ligands in supramolecular coordination chemistry.[11] A few years ago, Tzschucke et al. reported the preparation of symmetrically and non-symmetrically alkylated terpyridines (R= Me, tBu), however this methodology required multi-step reaction conditions involving inert atmosphere conditions and expensive Pd(II) catalysts (Chart 5.1 c)).[12] Only a handful of other examples of 4,4"-bi-tert-butyl-terpyridine ligand have been synthesized in which the 4'-position of the central pyridine is fully accessible for functionalization.[12,13] A strategy that allows easy access to solubilized 4'-aryl and 4'-heteroaryl terpyridine ligands would lead to the synthesis of supramolecular materials and assemblies not otherwise accessible with regular 2,2':6',2"-terpyridine units.[14] Herein, we report the one-pot synthesis of several 4'-aryl and 4'-heteroaryl-bi-4,4"-tert-butyl-2,2':6',2"-terpyridine ligands as well as three metal complexes (Fe(II), Ni(II), Cu(II)) in order to demonstrate their metal ion coordination ability.

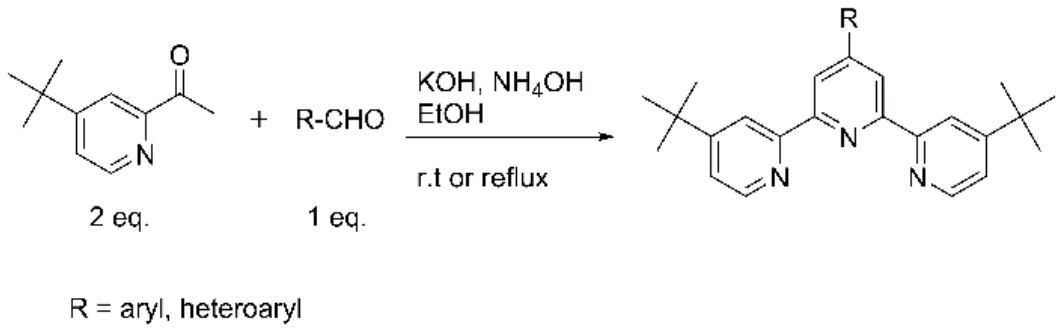

Scheme 5.1 - One-pot synthesis of 4'-aryl and 4'-heteroaryl-bi-4,4"-tert-butyl-2,2':6',2"-terpyridine.

5.3.2. Synthesis of the ligands

The synthetic procedure is similar to the previously mentioned one-pot synthesis,[15] however, the isolation and purification of the ligand had to be adapted due to the greater solubility of the ligands in most organic solvents (Table 12.1).

Table 5.1 – List of the various ligands synthesized in refluxing ethanol and their yields.

Ligand	R	Yield %
1	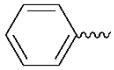	27
2	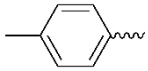	25
3	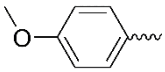	38
4	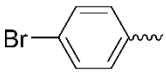	40
5	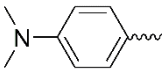	27
6	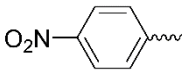	71
7	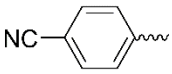	47
8	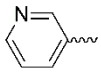	50 (15)[a]
9	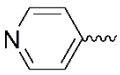	90
10		24

[a] Yield of the previously published mechanically ground two-step reaction.[14]

The 2-acetyl-4-*tert*-butylpyridine precursor was obtained via the acetylation of 4-*tert*-butylpyridine,[13] however the maximum yield that we obtained for this reaction was 25 %. The enolate of 2-acetyl-4-*tert*-butylpyridine was obtained by the addition of KOH at ambient temperature in ethanolic solution. The aldol condensation and Michael addition proceed at room temperature in most cases. The cyclization of the central pyridine was accomplished in ethanol at reflux, so the diketone intermediate would still be solubilized. After a few hours at reflux a small amount of precipitate appeared on the wall of the flask, however, most of the product remained in solution. The solvent was reduced to a minimum volume (~25 mL) under vacuum and saturation of the remaining solution with water led to the precipitation of a brown-beige compound. Filtration of the aqueous suspension over a bed of celite was followed by an aqueous wash to remove

excess KOH and NH_4OH as well as water-soluble impurities. The precipitate was then dissolved in a minimum amount of acetone and the ligand was precipitate by the addition of hexanes. Recrystallization of the ligand in a minimum amount of hot methanol afforded pure material. In all of the cases, the ^{1}H NMR, ^{13}C NMR as well as the COSY NMR supported the formation of the desired ligands and their purity. In terms of the solubility in organic solvent, it appears that the bis-*tert*-butylterpyridine ligands have an increased solubility in a wide range of organic solvents in which their homologues without the *tert*-butyl group are only sparingly soluble or insoluble. In fact, almost any organic solvent except hexanes (and presumably other aliphatic solvents) can be used to dissolve the new ligands with the *tert*-butyl units.

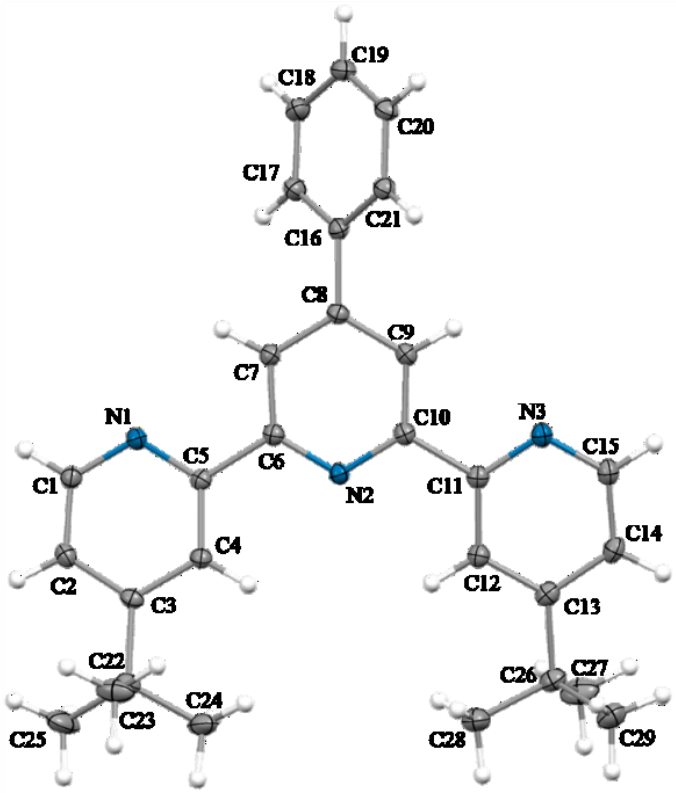

Figure 5.1 - ORTEP diagram of 1 complex with anisotropic displacement ellipsoids at 50% probability.

X-Ray quality crystals of **1** were grown by slow evaporation of a mixture of water and ethanol. As depicted in Figure 5.1, diffraction analyses reveal that the three pyridyl rings are almost coplanar ($\theta_{plane} < 10^o$), which is explain by the presence of four weak C-H···N hydrogen bonds (C-H···N distance < 2.55 Å). Intramolecular H···H repulsion force the plane of the 4'-phenyl ring to adopt an angle of approximately 50° compare to the central pyridyl ring.

Among various combinations of metals and ligands **1**-**10**, we investigated the coordination of three 1st row transition metal ions, Fe(II), Ni(II) and Cu(II) to ligand **4** (see Table 5.2). It is worth noting that other terpyridine metal complexes using these metals ions are known to catalyse several types of organic reactions.[16] The presence of the bromine atom on the backbone of the molecules is also of interest for further post-coordination modification (e.g. Suzuki-Miyaura, Negishi, Heck and other coupling reactions), thus potentially giving access to symmetrical, non-symmetrical and also poly-terpyridines ligands for the synthesis of supramolecular materials.[17]

Table 5.2 – Synthesis of the 1st row transition metal complexes.

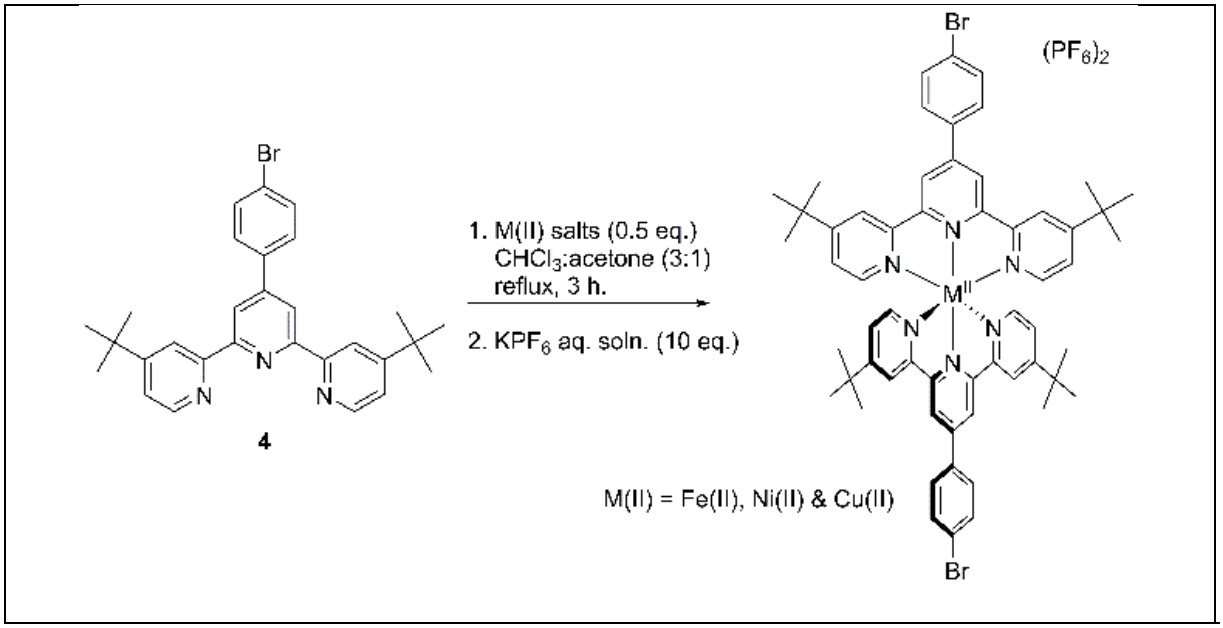

Complex	Reaction Conditions	Yield (%)
4Fe	$CHCl_3$:Acetone (3:1) Reflux, 3 h	46
4Ni		63
4Cu		52

The complexation was achieved by mixing the ligand (2 equivalents) and the metal precursor (1 equivalent) in a mixture of chloroform:acetone (3:1) and refluxing for 3 hours. The metal-ligand coordination was confirmed by a strong color change during the reaction (Fe(II)=deep purple; Ni(II)= pale yellow; Cu(II)= cyan). The reaction process was followed by thin layer chromatography (silica, hexane:ethyl acetate 7:3). The solvent was removed under reduced pressure and the resulting material was dissolved in a minimum amount of acetonitrile. The resulting complex was then subjected to metathesis by pouring it into an aqueous solution with an excess of KPF_6 (10 equivalents). The precipitate was then collected by filtration.

The ^1H NMR spectra were obtained in CD_3CN for all of the compounds and they supported the formation of the complexes. While **4Fe** is diamagnetic, complexes **4Ni** and **4Cu** are paramagnetic and signals observed in ^1H NMR spectra are shifted and broadened when compared to characteristic diamagnetic metal complexes. Due to this behavior, proton count and assignments of the observed peaks were impossible in both cases. However, we were able to grow X-ray quality crystals of all of the complexes.

Crystals of **4Fe** were obtained by the slow evaporation of an acetone/toluene solution over few days while **4Ni** crystallized from the slow evaporation of an acetone/hexane solution. As displayed in Figure 5.2 and Figure 5.3, the iron and nickel compounds are homoleptic complexes where the two ligands adopt a meridional arrangement and are almost perpendicular one to the other (88° and 82° for the Fe(II) and Ni(II) complexes, respectively). In both cases, the metal ions adopt a distorted octahedral geometry. The Fe-N as well as the Ni-N bond distances and the average of bites angles ($N\text{-}M^{II}\text{-}N$) are analogous to those found in similar metal complexes.[18, 19]

The copper compound crystallized from the slow evaporation of a chloroform solution at ambient temperature. To our surprise, it appeared that complexation of the Cu(II) metal ion did not give the expected homoleptic complex.[18] Instead, as depicted inFigure 5.4, a rare binuclear centrosymmetric Cu(II) dimer was obtained, where the copper ions adopt a slightly distorted square-pyramidal geometry.[20]

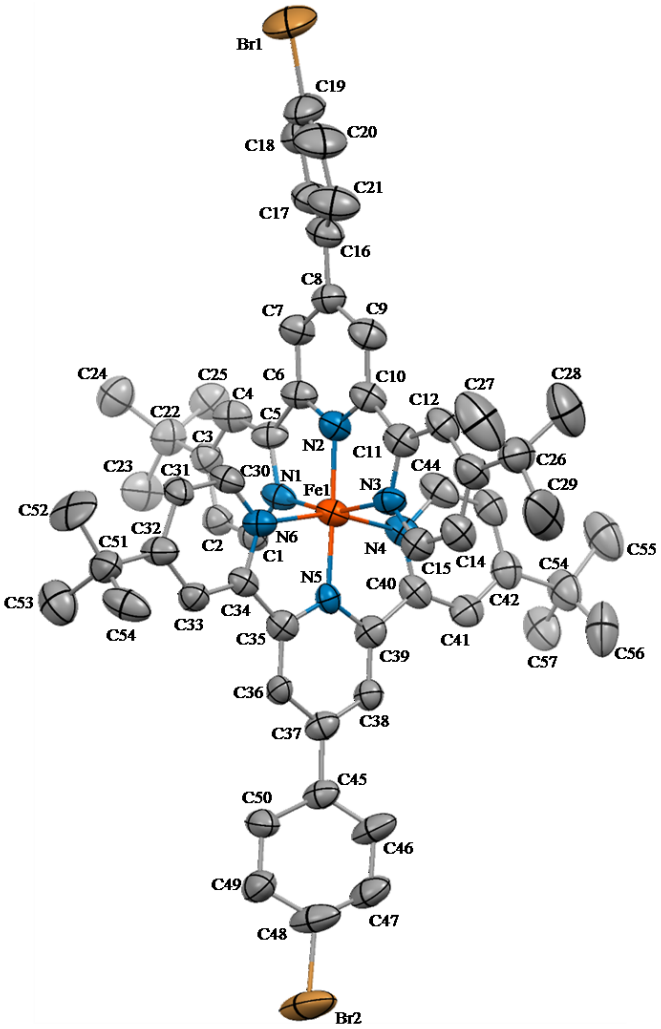

Figure 5.2 - ORTEP diagram of **4Fe** complex with anisotropic displacement ellipsoids at 50% probability. The hydrogen atoms, toluene solvent molecules and PF_6 counter-anion were omitted for clarity.

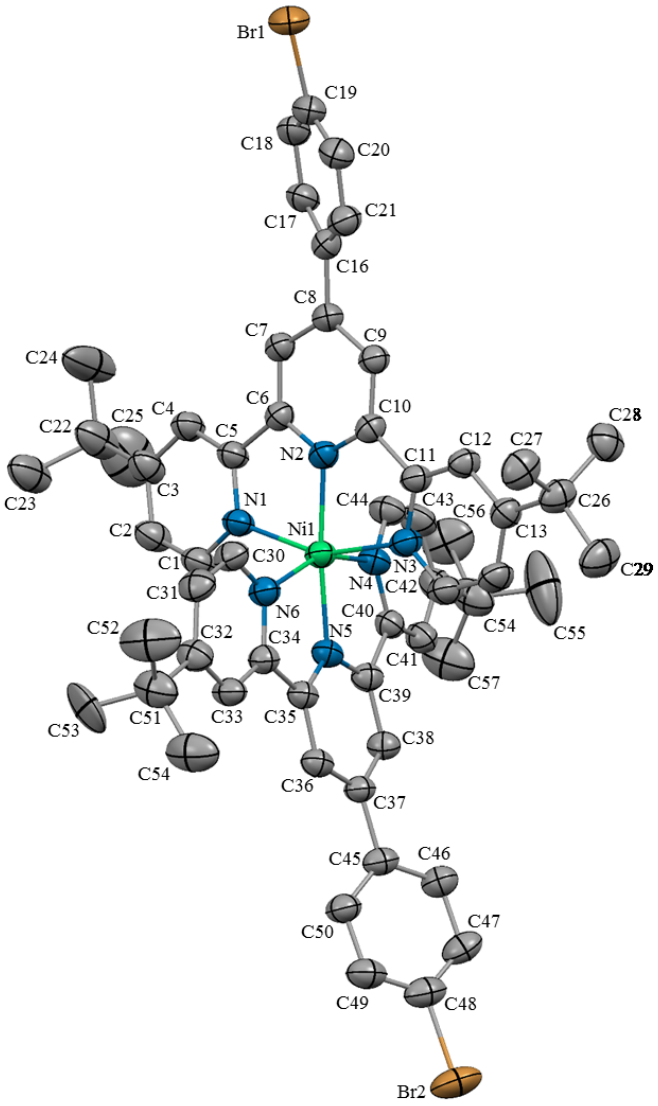

Figure 5.3 - ORTEP diagram of **4Ni** complex with anisotropic displacement ellipsoids at 50% probability. The hydrogen atoms, acetone solvent molecules and PF_6 counter-anion were omitted for clarity.

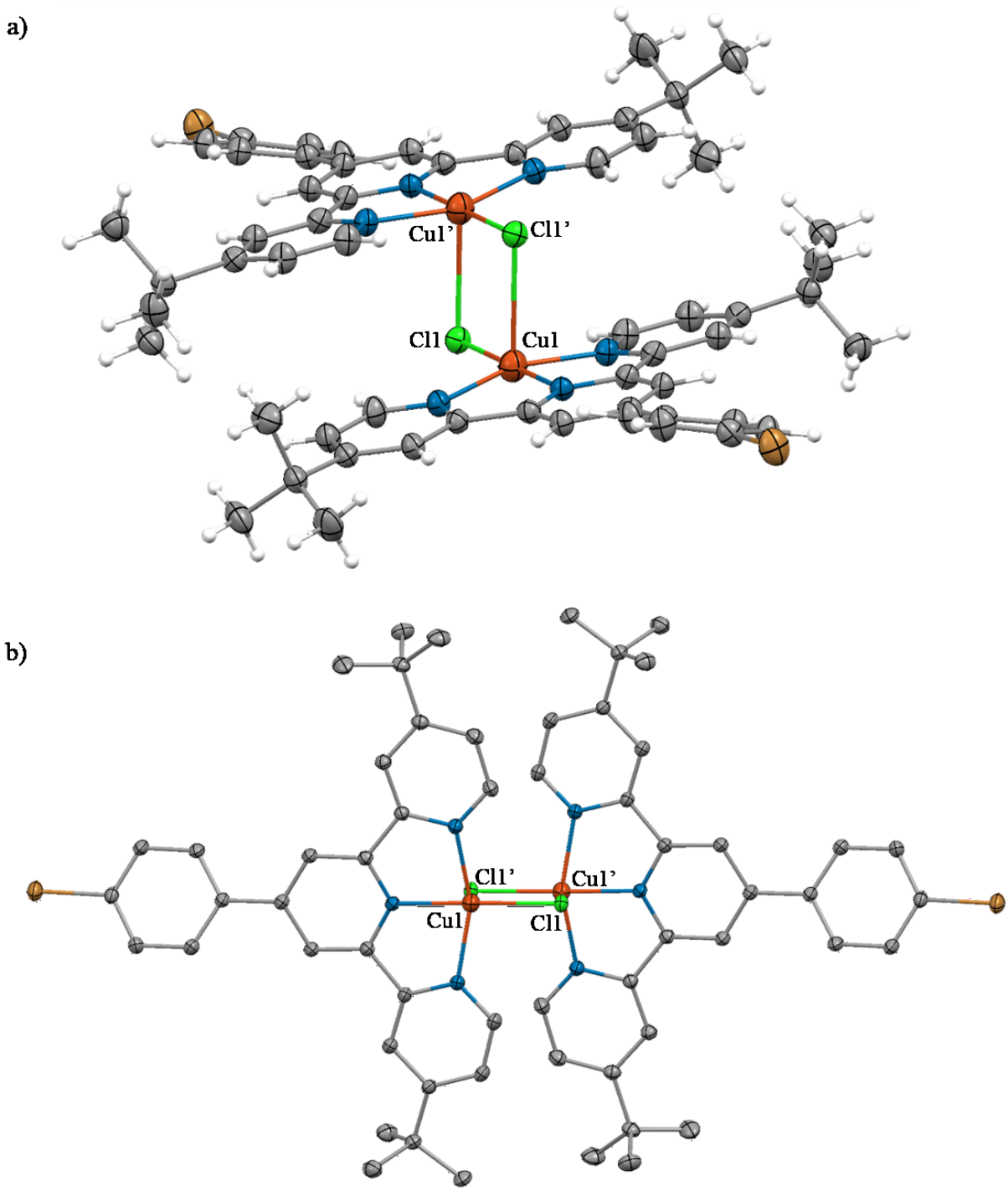

Figure 5.4 - ORTEP diagram of **4Cu** complex with anisotropic displacement ellipsoids at 50% probability. The hydrogen atoms, chloroform solvent molecule and PF_6 counter-anion were omitted for clarity.

Table 5.3 – Solid-state structure and refinement data for ligand **2** and complexes 4Fe, 4Ni and 4Cu.

	2	**4Fe**
Formula	$C_{29}H_{31}N_3$	$[C_{54}H_{60}N_6Br_2Fe][(PF_6)_2]\cdot(C_7H_8)_2$
Color/form	Colorless block	Purple needle
M_w [gmol^{-1}]	438.70	1346.73
Temperature [K]	100	150
Wavelength [Å]	0.71073	1.54178
Crystal system	monoclinic	Monoclinic
Unit cell dimension		
a [Å]	14.7283(5)	14.5883(6)
b [Å]	6.2151(2)	25.7565(10)
c [Å]	26.2221(9)	19.6856(8)
α [°]	90	90
β [°]	91.6740(1)	107.436(2)
γ [°]	90	90
V [Å^3]	2399.29(14)	7056.9(5)
Space group	$P2_1/n$	$P2_1/c$
Z	4	4
$d_{calcd.}$ [gcm^{-3}]	1.214	1.441
μ [mml^{-1}]	0.070	4.132
F(000)	972	3136
Reflection collected	45580	13410
Independent reflections	4794	13410
Goodness-of-fit (GOF) on F^2	1.038	1.038
R_1(F) [$I > 2\sigma(I)$]	0.0392	0.0977
$wR(F^2)$ [$I > 2\sigma(I)$]	0.1013	0.1148
R_1(F) (all data)	0.0414	0.2539
wR(F^2) (all data)	0.1036	0.2666
Largest difference peak/hole [e Å^{-3}]	0.2180	0.802

Table 5.4 – Solid-state structure and refinement data for ligand **2** and complexes 4Fe, 4Ni and 4Cu.

	4Ni	**4Cu**
Formula	$[C_{54}H_{60}N_6Br_2Ni][(PF_6)_2]\cdot(C_3H_6O)$	$[C_{54}H_{60}N_6Br_2Cu_2Cl_2][(PF_6)_2]\cdot(CHCl_3)$
Color/form	Yellow needle	Cyan needle
M_w [gmol^{-1}]	1392.75	833.05
Temperature [K]	150	100
Wavelength [Å]	1.54178	0.71073
Crystal system	Tetragonal	Triclinic
Unit cell dimension		
a [Å]	32.2042(13)	9.1227(3)
b [Å]	32.2042(13)	13.7546(4)
c [Å]	24.5290(11)	15.4580(6)
α [°]	90	99.306(2)
β [°]	90	107.1230(1)
γ [°]	90	104.4900(1)
V [Å^3]	25439(2)	1735.68(10)
Space group	I 4_1 c d	P-1
Z	16	2
$d_{calcd.}$ [gcm^{-3}]	1.455	1.653
μ [mml^{-1}]	3.074	2.193
F(000)	11345	866
Reflection collected	223250	31419
Independent reflections	11995	7509
Goodness-of-fit (GOF) on F^2	1.037	1.111
R_1(F) [$I > 2\sigma(I)$]	0.0468	0.0515
$wR(F^2)$ [$I > 2\sigma(I)$]	0.1198	0.1386
R_1(F) (all data)	0.0537	0.0531
wR(F^2) (all data)	0.1259	0.1399
Largest difference peak/hole [e Å^{-3}]	0.776	1.126

The length of the Cu-Cl bond with the apical chlorine of the pyramid (2.78 Å) is significantly longer than the Cu-Cl bond with the chlorine atom pseudo-planar to the terpyridine ligand (2.23 Å). It is worth mentioning that under high-resolution mass spectrometry conditions, only half of the dimer was observed, even when the mildest possible conditions were used for the ionisation (applied potential = 30-50 V). It is difficult to speculate on the fate of the dimeric complex once in solution since it is unclear if the dimer is unstable only under the ionisation conditions used for the HR-MS experiment or if the Cu-Cl bond with the chlorine in the apical position of the square-based pyramid is broken once the complex is solubilized.

5.3.3. Conclusion

In conclusion, we have demonstrated a simple one-pot reaction for the synthesis of bis-4,4”-*tert*-butyl-2,2’:6’,2”-terpyridine units with several 4’-aryl and 4’-heteroaryl substituents. Further complexation with different 1st row transition metal ions lead to the synthesis of a dimeric Cu(II) species as well as two homoleptic Fe(II) and Ni(II) metal complexes. Both ligands and complexes show much greater solubility in most common organic solvents. Based on this research, new metallo-supramolecular one-dimensional polymer species as well as two- and three-dimensional assembly are now under investigation.

5.3.4. Experimental

5.3.4.1. Materials and Instrumentations

Nuclear magnetic resonance (NMR) spectra were recorded in $CDCl_3$ and CD_3CN at 25ºC on a Bruker AV-400 spectrometer at 400 MHz for ^{1}H NMR and 100 MHz for ^{13}C NMR. Chemical shifts (δ) are reported in part per million (ppm) relative to TMS, and are referenced to the residual solvent signal (δ = 1.94 ppm for acetonitrile-d_3 and 7.26 ppm for chloroform-d_1). Absorption spectra were measured in deaerated spectroscopic grade solvent at room temperature on a Cary 300 UV-Vis-NIR Spectrophotometer from Agilent Technologies. The high-resolution mass spectrometry (HR-MS) experiments were performed on a Bruker Daltonics microTOF spectrometer using electrospray ionization. Infrared spectra were recorded on a Bruker alpha-p FT-IR spectrometer equipped with a single reflection diamond ATR module.

5.3.4.2. X-ray Structure Determination

X-Ray diffraction data collection for ligand 2 and the metal complex 4Cu were carried out on a Bruker APEX II area detector diffractometer equipped with graphite monochromated Mo-Kα radiation (λ = 0.71073 Å). Data collection for the metal complexes 4Fe and 4Ni were carried out on a Bruker APEX II DUO Kappa-CCD diffractometer equipped with an Oxford Cryosystem liquid N2 device, using Cu-Kα

radiation (λ = 1.54178 Å). The crystal–detector distance was 38 mm. The cell parameters were determined (APEX2 software) from reflections taken from three sets of 100 frames. The structures were solved by direct methods using the program SHELXS-97. The refinement and all further calculations were carried out using SHELXL-97. The H-atoms were included in calculated positions and treated as riding atoms using SHELXL default parameters. The non-H atoms were refined anisotropically, using weighted full-matrix least-squares on F2.

5.3.4.3. Procedures

4,4”-di-*tert*-butyl-2,2’:6’,2”-terpyridines; General procedure

2-Acetyl-4-*tert*-butylpyridine (2.50 g, 14 mmol) was added into a solution of benzaldehyde (0.75 g, 7 mmol) in EtOH (100 mL). KOH pellets (1.1 g, 20 mmol) and aq NH_3 (25 mL, 29.3%, 30 mmol) were then added to the solution. The solution was stirred at room temperature for 4 h.

The solvent was reduced to 20 mL and saturated with 200 mL of water. The off-white solid was filtered over Celite, was washed with water, and was dissolved in a minimum amount of acetone. The solvent was reduced to 5-10 mL and was saturated with hexanes. The precipitate was collected by filtration. Recrystallization from hot MeOH afforded 4’-phenyl-4,4”-di-*tert*-butyl-2,2’:6’,2”-terpyridine (1) in 27% yield (800 mg).

4’-phenyl-4,4”-di-*tert*-butyl-2,2’:6’,2”-terpyridine (1)

Yield: 800 mg (27%); white crystalline solid; mp 157-159 ºC.

IR (neat): 2955, 2923, 2867, 1585, 1546, 1370, 891, 840, 695 cm^{-1}.

^1H NMR (400 MHz, $CDCl_3$): δ (ppm) = 8.81 (d, *J* = 2 Hz, 2H), 8.75 (s, 2H), 8.65 (d, *J* = 5 Hz, 2H), 7.93 (d, *J* = 7 Hz, 2H), 7.51 (t, *J* = 7 Hz, 2H), 7.44 (t, *J* = 7 Hz, 2H), 7.37 (dd, *J* = 5 Hz, 2H), 1.45 (s, 18H).

^{13}C NMR (100 MHz, $CDCl_3$): δ (ppm) = 161.2, 160.9, 156.0, 155.8, 150.4, 148.9, 138.5, 135.7, 128.9, 127.4, 121.1, 118.8, 118.3, 35.0, 30.5.

HRMS (ESI): *m/z* $[M + H]^+$ calcd for $C_{29}H_{31}N_3$: 422.25907; found: 422.25969; difference: 1.46 ppm.

4’-(4-methylphenyl)-4,4”-di-*tert*-butyl-2,2’:6’,2”-terpyridine (2)

Following the general procedure:

2-acetyl-4-*tert*Butylpyridine : 1.0 g; 4-methylbenzaldehyde: 340 mg

Yield: 310 mg (25%); white solid; mp 135-137 ºC.

IR (neat): 2959, 2866, 1585, 1542, 1370, 818 cm^{-1}.

^{1}H NMR (400 MHz, $CDCl_3$): δ (ppm) = 8.80 (d, *J* = 2 Hz, 2H), 8.72 (s, 2H), 8.64 (d, *J* = 6 Hz, 2H), 7.83 (d, *J* = 8 Hz, 2H), 7.36 (dd, *J* = 5 Hz, 2H), 7.31 (d, *J* = 8 Hz, 2H), 2.43 (s, 3H), 1.45 (s, 18H).

^{13}C NMR (100 MHz, $CDCl_3$): δ (ppm) = 160.7, 156.2, 155.9, 150.2, 149.0, 139.0, 135.6, 129.6, 127.2, 121.0, 118.4, 118.2, 35.0, 30.5, 21.3.

HRMS (ESI): *m/z* $[M + H]^+$ calcd for $C_{30}H_{33}N_3$: 436.27472; found: 436.27393; difference: 1.81 ppm.

4’-(4-methoxyphenyl)-4,4”-di-*tert*-butyl-2,2’:6’,2”-terpyridine (3)

Following the general procedure:

2-acetyl-4-*tert*Butylpyridine : 2.5 g; 4-methoxybenzaldehyde: 960 mg

Yield: 1.21 g (38%); white solid; mp 145-147 ºC.

IR (neat): 2961, 2901, 2867, 1583, 1542, 1370, 824 cm^{-1}.

^{1}H NMR (400 MHz, $CDCl_3$): δ (ppm) = 8.80 (d, *J* = 2 Hz, 2H), 8.70 (s, 2H), 8.64 (d, *J* = 5 Hz, 2H), 7.89 (d, *J* = 9 Hz, 2H), 7.36 (dd, *J* = 5 Hz, 2H), 7.03 (d, *J* = 9 Hz, 2H), 3.87 (s, 3H), 1.45 (s, 18H).

^{13}C NMR (100 MHz, $CDCl_3$): δ (ppm) = 160.8, 160.4, 156.2, 155.8, 149.8, 149.0, 130.8, 128.5, 121.0, 118.2, 118.0, 114.2, 55.3, 34.9, 30.5.

HRMS (ESI): *m/z* $[M + Na]^+$ calcd for $C_{30}H_{33}N_3O$: 474.25158; found: 474.24922; difference: 4.98 ppm.

4’-(4-bromophenyl)-4,4”-di-*tert*-butyl-2,2’:6’,2”-terpyridine (4)

Following the general procedure:

2-acetyl-4-*tert*Butylpyridine : 2.5 g; 4-bromobenzaldehyde: 1.3 g

Yield: 1.40 g (40%); white solid; mp 174-177 ºC.

IR (neat): 2961, 2902, 2866, 1583, 1542, 1370, 893, 824 cm^{-1}.

^{1}H NMR (400 MHz, $CDCl_3$): δ (ppm) = 8.80 (d, *J* = 2 Hz, 2H), 8.70 (s, 2H), 8.64 (d, *J* = 5 Hz, 2H), 7.79 (d, *J* = 9 Hz, 2H), 7.63 (t, *J* = 9 Hz, 2H), 7.38 (dd, *J* = 5 Hz, 2H), 1.45 (s, 18H).

^{13}C NMR (100 MHz, $CDCl_3$): δ (ppm) = 161.0, 156.0, 155.8, 149.1, 149.0, 137.5, 132.0, 128.9, 123.4, 121.2, 118.4, 118.3, 35.0, 30.5.

HRMS (ESI): *m/z* $[M + H]^+$ calcd for $C_{29}H_{30}N_3Br$: 502.16770; found: 502.16668; difference: 2.03 ppm.

4'-(4-dimethylaminephenyl)-4,4"-di-*tert*-butyl-2,2':6',2"-terpyridine (5)

Following the general procedure:

2-acetyl-4-*tert*Butylpyridine : 1.0 g; 4-(dimethylamino)benzaldehyde: 420mg

Yield: 355 mg (27%); yellow solid; mp 143-145 ºC.

IR (neat): 2955, 2867, 1583, 1528, 1359, 813 cm^{-1}.

^{1}H NMR (400 MHz, $CDCl_3$): δ (ppm) = 8.79 (d, *J* = 2 Hz, 2H), 8.70 (s, 2H), 8.65 (d, *J* = 5 Hz, 2H), 7.90 (d, *J* = 9 Hz, 2H), 7.35 (dd, *J* = 5 Hz, 2H), 6.82 (d, *J* = 9 Hz, 2H), 3.04 (s, 6H), 1.45 (s, 18H).

^{13}C NMR (100 MHz, $CDCl_3$): δ (ppm) = 160.6, 156.5, 155.7, 151.1, 150.0, 149.0, 128.1, 125.6, 120.9, 118.2, 117.3, 112.2, 40.3, 34.9, 30.5.

HRMS (ESI): *m/z* $[M + H]^+$ calcd for $C_{31}H_{36}N_4$: 465.30127; found: 465.29973; difference: 3.11 ppm.

4'-(4-nitrophenyl)-4,4"-di-*tert*-butyl-2,2':6',2"-terpyridine (6)

Following the general procedure:

2-acetyl-4-*tert*Butylpyridine : 2.5 g; 4-nitrobenzaldehyde: 1.1 g

Yield: 2.33 g (71%); beige solid; mp 210-214 ºC.

IR (neat): 2961, 2901, 2867, 1583, 1542, 1370, 824 cm^{-1}.

^{1}H NMR (400 MHz, $CDCl_3$): δ (ppm) = 8.79 (s (broad), 2H), 8.71 (s (broad), 2H), 8.63 (s (broad), 2H), 8.33 (d (broad), *J* = 7 Hz, 2H), 8.02 (d (broad), *J* = 7Hz, 2H), 7.38 (s (broad), 2H), 3.87, 1.45 (s, 18H).

^{13}C NMR (100 MHz, $CDCl_3$): δ (ppm) = 161.4, 156.8, 155.9, 149.5, 148.5, 148.2, 145.4, 128.7, 124.5, 121.9, 119.1, 118.7, 35.4, 30.9.

HRMS (ESI): *m/z* $[M + Na]^+$ calcd for $C_{29}H_{30}N_4O_2$: 489.22610; found: 489.22777; difference: 3.41 ppm.

4’-(4-cyanophenyl)-4,4”-di-*tert*-butyl-2,2’:6’,2”-terpyridine (7)

Following the general procedure:

2-acetyl-4-*tert*Butylpyridine : 2.5 g; 4-formylbenzonitrile: 925 mg

Yield: 1.71 g (47%); beige solid; mp 205-208 ºC.

IR (neat): 2962, 2903, 2868, 1586, 1542, 1371, 894, 840 cm^{-1}.

^{1}H NMR (400 MHz, $CDCl_3$): δ (ppm) = 8.79 (d, *J* = 1 Hz, 2H), 8.74 (s, 2H), 8.64 (d, *J* = 5 Hz, 2H), 8.00-7.94 (m, 4H), 7.38 (d, *J* = 4 Hz, 2H), 1.45 (s, 18H).

^{13}C NMR (100 MHz, $CDCl_3$): δ (ppm) = 168.8, 161.0, 156.1, 155.7, 149.1, 149.0, 142.1, 133.5, 128.0, 127.6, 121.3, 118.7, 118.3, 35.0, 30.5.

HRMS (ESI): *m/z* $[M + H]^+$ calcd for $C_{30}H_{30}N_4$: 447.25432; found: 447.25335; difference: 2.17 ppm.

4’-(3-pyridinyl)-4,4”-di-*tert*-butyl-2,2’:6’,2”-terpyridine (8)

Following the general procedure:

2-acetyl-4-*tert*Butylpyridine : 2.5 g; nicotinaldehyde: 755 mg

Yield: 1.49 g (50%); white solid; mp 197-200 ºC.

IR (neat): 2963, 2868, 1587, 1543, 1371, 1024 cm^{-1}.

^{1}H NMR (400 MHz, $CDCl_3$): δ (ppm) = 9.05 (d, *J* = 2 Hz, 1H), 8.71 (d, *J* = 2 Hz, 1H), 8.60 (s, 2H), 8.59 (dd, *J* = 5 Hz, 1H), 8.56 (d, *J* = 5 Hz, 2H), 8.22 (dt, *J* = 8 Hz, 1H), 7.46 (dd, *J* = 8 Hz, 1H), 7.36 (dd, *J* = 5 Hz, 2H), 1.39 (s, 18H).

^{13}C NMR (100 MHz, $CDCl_3$): δ (ppm) = 161.4, 156.0, 155.4, 149.4, 148.8, 147.7, 146.9, 135.2, 134.4, 124.0, 121.4, 118.6, 118.5, 34.9, 30.3.

HRMS (ESI): *m/z* $[M + H]^+$ calcd for $C_{28}H_{30}N_4$: 423.25432; found: 423.25314; difference: 2.79 ppm.

4’-(4-pyridinyl)-4,4”-di-*tert*-butyl-2,2’:6’,2”-terpyridine (9)

Following the general procedure:

2-acetyl-4-*tert*Butylpyridine : 2.5 g; isonicotinaldehyde: 755 mg

Yield: 2.66 g (90%); white solid; mp 161-165 ºC.

IR (neat): 2962, 2868, 1585, 1540, 1371, 821 cm^{-1}.

^{1}H NMR (400 MHz, $CDCl_3$): δ (ppm) = 8.81 (d, *J* = 2 Hz, 2H), 8.81-8.77 (m, 4H), 8.66 (d, *J* = 5 Hz, 2H), 7.82 (d, *J* = 5 Hz, 2H), 7.40 (dd, *J* = 5 Hz, 2H), 1.47 (s, 18H).

^{13}C NMR (100 MHz, $CDCl_3$): δ (ppm) = 161.4, 156.9, 156.0, 150.9, 149.5, 147.9, 146.5, 122.1, 121.8, 118.8, 118.7, 35.4, 30.9.
HRMS (ESI): *m/z* $[M + H]^+$ calcd for $C_{28}H_{30}N_4$: 423.25432; found: 423.25272; difference: 3.78 ppm.

4'-(2-furanyl)-4,4"-di-*tert*-butyl-2,2':6',2"-terpyridine (10)
Following the general procedure:
2-acetyl-4-*tert*Butylpyridine : 2.5 g; 2-furancarbaldehyde: 677 mg
Yield: 280 mg (24%); beige solid; mp 158-161 ºC.
IR (neat): 2961, 2902, 2866, 1582, 1544, 1370, 893, 839 cm^{-1}.
^{1}H NMR (400 MHz, $CDCl_3$): δ (ppm) = 8.77 (s, 2H), 8.71 (s, 2H), 8.65 (d, *J* = 5 Hz, 2H), 7.58 (s, 1H), 7.37 (dd, *J* = 5 Hz, 2H), 7.12 (d, *J* = 3 Hz, 1H), 6.56 (dd, *J* = 3 Hz, 1H), 1.44 (s, 18H).
^{13}C NMR (100 MHz, $CDCl_3$): δ (ppm) = 160.8, 155.9, 149.0, 143.6, 139.6, 121.1, 118.2, 114.9, 112.1, 109.1, 35.0, 30.5.
HRMS (ESI): *m/z* $[M + H]^+$ calcd for $C_{27}H_{29}N_3O$: 412.23834; found: 412.23756; difference: 1.89 ppm.

Metal complexes; Typical procedure
In a 100 mL round-bottomed flask charged with 4'-(4-bromophenyl)-4,4"-di-tert-butyl-2,2':6',2"-terpyridine (100 mg, 0.20 mmol) was added $CHCl_3$ (25 mL). To the clear solution was added an acetone solution (25 mL) of the metal salt (0.10 mmol). An instant change in coloration was observed. The mixture was left under reflux for 3 hours. After this time, the solvent was removed under vacuum and the residue was dissolve in a minimum amount of acetone. The metathesis of the counter-anion was then achieved by the addition of an aqueous solution of KPF_6 (10 eq.), leading to the instant precipitation of a colored precipitate in 45-65% yield.

4Fe (11)
Following the general procedure:
$Fe(SO_4)(H_2O)_7$: 27.8 mg, 4Fe precipitated as a purple solid.
Yield: 60 mg (46%); decomp. > 245 ºC.

IR (neat): 2965, 2909, 2872, 1615, 832, 556 cm^{-1}.

^{1}H NMR (400 MHz, CD_3CN): δ (ppm) = 9.23 (s, 2H), 8.59 (s, 2H), 8.29 (d, *J* = 9 Hz, 2H), 8.01 (d, *J* = 9 Hz, 2H), 7.08 (dd, *J* = 6 Hz, 2H), 7.02 (d, *J* = 6 Hz, 2H), 1.27 (s, 18H).

^{13}C NMR (100 MHz, $CDCl_3$): δ (ppm) = 164.7, 161.5, 158.5, 153.1, 149.8, 136.9, 133.7, 130.8, 125.4, 122.5, 122.1, 36.1, 30.3.

HRMS (ESI): *m/z* $[M\text{-}PF_6]^+$ calcd for $C_{29}H_{30}N_3BrFePF_6$: 1201.22216; found: 1201.21883; difference: 2.77 ppm; $[M\text{-}2PF_6]^{2+}$ calcd for $C_{29}H_{30}N_3BrFe$: 528.12872; found: 528.12949; difference: 1.46 ppm.

4Ni (12)

Following the general procedure:

$Ni(OAc)_2(H_2O)_4$: 28.5 mg, 4Ni precipitated as a beige solid.

Yield: 85 mg (63%); decomp. > 225 ºC.

IR (neat): 2966, 2908, 2872, 1611, 1288, 1137, 823, 739, 482 cm^{-1}.

^{1}H NMR (400 MHz, CD_3CN): δ (ppm) = 76.05 (s, broad), 71.56 (s, broad), 41.80 (m, broad), 11.03 (s, broad), 10.72(s, broad), 7.40 (s, broad) 1.03 (s, broad).

^{13}C NMR (100 MHz, $CDCl_3$): δ (ppm) = No peak was observed due to the paramagnetic nature of the compound.

HRMS (ESI): *m/z* $[M\text{-}PF_6]^+$ calcd for $C_{29}H_{30}N_3BrNiPF_6$: 1203.22167; found: 1203.21858; difference: 2.57 ppm; $[M\text{-}2PF_6]^{2+}$ calcd for $C_{29}H_{30}N_3BrNi$: 529.12857; found: 529.12845; difference: 0.23 ppm.

4Cu (13)

Following the general procedure:

$Cu(OAc)_2$: 18.2 mg, 4Cu precipitated as a cyan solid.

Yield: 75 mg (52%); decomp. > 285 ºC.

IR (neat): 2962, 2906, 2872, 1612, 1409, 1394, 1255, 1009, 821 cm^{-1}.

^{1}H NMR (400 MHz, CD_3CN): δ (ppm) = 9.05 (s, broad), 7.15 (s, broad), 1.06 (s, broad).

^{13}C NMR (100 MHz, $CDCl_3$): δ (ppm) = No peak was observed due to the paramagnetic nature of the compound.

HRMS (ESI): *m/z* $[M]^+$ calcd for $C_{29}H_{30}N_3BrCuCl$: 599.05821; found: 599.05988; difference: 2.79 ppm.

5.3.5. Acknowledgment

The authors thank the Natural Sciences and Engineering Research Council (NSERC) of Canada and the Université de Montréal's Direction des Relations Internationales for financial aid. MD and SN thank the Ministère de l'Enseignement Supérieur et de la Recherche for funding. We are grateful to UdeM NMR and XRD services for their help.

5.3.6. References

[1] (a) Schubert, U. S.; Hofmeier, H.; Newkome, G. R., Modern Terpyridine Chemistry. 1st ed.; Wiley-VCH Verlag GmbH & Co. KGaA: Weingeim, Germany, 2006. (b) Schubert, U. S.; Winter, A.; Newkome, G. R., Terpyridine-based Materials For Catalytic, Optoelectronic and Life Science Applications. 1st ed.; Wiley-VCH Verlag GmbH & Co. KGaA: Weinheim, Germany, 2011. (c) Constable, E. C. *Chem. Soc. Rev.* 2007, **36**, 246.

[2] Sauvage, J.-P.; Collin, J.-P.; Chambron, J.-C.; Guillerez, S.; Coudret, C. *Chem. Rev.* 1994, **94**, 993.

[3] (a) Fan, Y.; Zhu, Y. M.; Dai, F. R.; Zhang, L. Y.; Chen, Z. N. *Dalton Trans.* 2007, 3885. (b) Bhaumik, C.; Das, S.; Saha, D.; Dutta, S.; Baitalik, S. *Inorg. Chem.* 2010, **49**, 5049. (c) Bhaumik, C.; Saha, D.; Das, S.; Baitalik, S. *Inorg. Chem.* 2011, **50**, 12586. (d) Maity, D.; Das, S.; Mardanya, S.; Baitalik, S. *Inorg. Chem.* 2013, **52**, 6820. (e) Maity, D.; Bhaumik, C.; Mondal, D.; Baitalik, S. *Dalton Trans.* 2014, **43**, 1829. (f) Karmakar, S.; Maity, D.; Mardanya, S.; Baitalik, S. *J. Phys. Chem. A* 2014, **118**, 9397. (g) Zhang, Z. H.; Liu, J.; Wan, L. Q.; Jiang, F. R.; Lam, C. K.; Ye, B. H.; Qiao, Z.; Chao, H. Y. *Dalton Trans.* 2015, **44**, 7785.

[4] (a) Zhao, L.-X.; Kim, T. S.; Ahn, S.-H.; Kim, T.-H.; Kim, E.-K.; Cho, W.-J.; Choi, H.; Lee, C.-S.; Kim, J.-A.; Jeong, T. C.; Chang, C.-J.; Lee, E.-S. Bioorg. Med. *Chem. Lett.* 2001, **11**, 2659. (b) Wong, K. M. C.; Tang, W. S.; Chu, B. W. K.; Zhu, N.; Yam, V. W. W. *Organometallics* 2004, **23**, 3459. (c) Ma, D. L.; Shum,

T. Y.; Zhang, F.; Che, C. M.; Yang, M. *Chem. Commun.* 2005, 4675. (d) Eryazici, I.; Moorefield, C. N.; Newkome, G. R. *Chem. Rev.* 2008, **108**, 1834. (e) Jain, A.; Wang, J.; Mashack, E. R.; Winkel, B. S.; Brewer, K. J. *Inorg. Chem.* 2009, **48**, 9077. (f) Wang, P.; Leung, C. H.; Ma, D. L.; Lu, W.; Che, C. M. *Chem. Asian J.* 2010, **5**, 2271. (g) Husson, J.; Knorr, M. *J. Org. Chem.* 2012, **8**, 379. (h) Ma, D. L.; He, H. Z.; Leung, K. H.; Chan, D. S.; Leung, C. H. *Angew. Chem. Int. Ed.* 2013, **52**, 7666. (i) Li, K.; Zou, T.; Chen, Y.; Guan, X.; Che, C. M. *Chem. Eur. J.* 2015, **21**, 7441.

[5] (a) Anka-Lufford, L. L.; Prinsell, M. R.; Weix, D. J. *J. Org. Chem.* 2012, **77**, 9989. (b) Dai, Y.; Wu, F.; Zang, Z.; You, H.; Gong, H. *Chem. Eur. J.* 2012, **18**, 808. (c) Kaveevivitchai, N.; Chitta, R.; Zong, R.; El Ojaimi, M.; Thummel, R. P. *J. Am. Chem. Soc.* 2012, **134**, 10721. (d) Yi, J.; Liu, J.-H.; Liang, J.; Dai, J.-J.; Yang, C.-T.; Fu, Y.; Liu, L. *Adv. Synth. Catal.* 2012, **354**, 1685. (e) Shrestha, R.; Dorn, S. C.; Weix, D. J. *J. Am. Chem. Soc.* 2013, **135**, 751.

[6] (a) Saap, S. A.; Elliott, C. M.; Contado, C.; Caramori, S.; Bignozzi, C. A. *J. Am. Chem. Soc.* 2002, **124**, 11215. (b) Ardo, S.; Sun, Y.; Staniszewski, A.; Castellano, F. N.; Meyer, G. J. *J. Am. Chem. Soc.* 2010, **132**, 6696. (c) Onicha, A. C.; Castellano, F. N. *J. Phys. Chem. C* 2010, **114**, 6831. (d) Gibson, E. A.; Smeigh, A. L.; Le Pleux, L. C.; Hammarström, L.; Odobel, F.; Boschloo, G.; Hagfeldt, A. *J. Phys. Chem. C* 2011, **115**, 9772. (e) Feldt, S. M.; Lohse, P. W.; Kessler, F.; Nazeeruddin, M. K.; Grätzel, M.; Boschloo, G.; Hagfeldt, A. *Phys. Chem. Chem. Phys.* 2013, **15**, 7087. (f) Ocakoglu, K.; Sogut, S.; Sarica, H.; Guloglu, P.; Erten-Ela, S. *Synth. Met.* 2013, **174**, 24.

[7] (a) Tschitschibabin, A. E.; Oparina, M. P. *J. Prakt. Chem.* 1924, **107**, 145. (b) Krohnke, F. *Synthesis* 1976, 1, 1.

[8] (a) Constable, E. C.; Neuburger, M.; Smith, D. R.; Zehnder, M. *Inorg. Chim. Acta* 1998, **275-276**, 359. (b) Beves, J. E.; Constable, E. C.; Housecroft, C. E.; Neuburger, M.; Schaffner, S.; Zampese, J. A. *Eur. J. Org. Chem.* 2008, **2008**, 3569. (c) Constable, E. C.; Figgemeier, E.; Housecroft, C. E.; Kokatam, S. L.; Medlycott, E. A.; Neuburger, M.; Schaffner, S.; Zampese, J. A. *Dalton Trans.* 2008, 6752. (d) Serroni, S.; Campagna, S.; Nascone, R. P.; Hanan, G. S.; Davidson, G. J. E.; Lehn, J.-M. *Chem. Eur. J.* 1999, **5**, 3523. (e) Loiseau, F.; Passalacqua, R.; Campagna, S.; Polson, M. I. J.; Fang, Y.-Q.; Hanan, G. S.

Photochem. Photobiol. Sci. 2002, **1**, 982. (f) Wang, J.; Hanan, G. S.; Loiseau, F.; Campagna, S. *Chem. Commun.* 2004, 2068. (g) Cooke, M. W.; Hanan, G. S.; Loiseau, F.; Campagna, S.; Watanabe, M.; Tanaka, Y. *Angew. Chem. Int. Ed.* 2005, **44**, 4881. (h) Ioachim, E.; Medlycott, E. A.; Hanan, G. S. *Inorg. Chim. Acta* 2006, **359**, 2599. (i) Wang, J.; Fang, Y. Q.; Bourget-Merle, L.; Polson, M. I.; Hanan, G. S.; Juris, A.; Loiseau, F.; Campagna, S. *Chem. Eur. J.* 2006, **12**, 8539. (j) Medlycott, E. A.; Hanan, G. S.; Loiseau, F.; Campagna, S. *Chem. Eur. J.* 2007, **13**, 2837. (k) Wang, J.; Medlycott, E. A.; Hanan, G. S.; Loiseau, F.; Campagna, S. *Inorg. Chim. Acta* 2007, **360**, 876.

[9] (a) Beves, J. E.; Bray, D. J.; Clegg, J. K.; Constable, E. C.; Housecroft, C. E.; Jolliffe, K. A.; Kepert, C. J.; Lindoy, L. F.; Neuburger, M.; Price, D. J.; Schaffner, S.; Schaper, F. *Inorg. Chim. Acta* 2008, **361**, 2582. (b) Constable, E. C.; Housecroft, C. E.; Neuburger, M.; Schaffner, S.; Schaper, F. *Inorg. Chem. Commun.* 2006, **9**, 433. (c) Constable, E. C.; Housecroft, C. E.; Neuburger, M.; Schaffner, S.; Schaper, F. *Inorg. Chem. Commun.* 2006, **9**, 616. (d) Constable, E. C.; Dunphy, E. L.; Housecroft, C. E.; Neuburger, M.; Schaffner, S.; Schaper, F.; Batten, S. R. *Dalton Trans.* 2007, 4323. (e) Yang, J.; Bhadbhade, M.; Donald, W. A.; Iranmanesh, H.; Moore, E. G.; Yan, H.; Beves, J. E. *Chem. Commun.* 2015, **51**, 4465. (f) Constable, E. C.; Housecroft, C. E.; Tao, Y. *Synthesis* 2004, 869.

[10] (a) Ben Hadda, T.; Le Bozec, H. *Inorg. Chim. Acta* 1993, **204**, 103. (b) Daniel, T.; Suzuki, N.; Tanaka, K.; Nakamura, A. *J. Organomet. Chem.* 1995, **505**, 109.

[11] (a) Constable, E. C.; Harverson, P.; Smith, D. R.; Whall, L. A. *Tetrahedron* 1994, **50**, 7799. (b) Constable, E. C.; Harverson, P.; Smith, D. R.; Whall, L. A. *Polyhedron* 1997, **16**, 3615. (c) de Pater, B. C.; Zijp, E. J.; Fruhauf, H.-W.; Ernsting, J. M.; Elsevier, C. J.; Vrieze, K. *Organometallics* 2004, **23**, 269. (d) de Pater, B. C.; Frühauf, H.-W.; Goubitz, K.; Fraanje, J.; Budzelaar, P. H. M.; Gal, A. W.; Vrieze, K. *Inorg. Chim. Acta* 2005, **358**, 431. (e) Constable, E. C.; Hostettler, N.; Housecroft, C. E.; Kopecky, P.; Neuburger, M.; Zampese, J. A. *Dalton Trans.* 2012, **41**, 2890. (f) Choudhuri, M. M.; Kaim, W.; Sarkar, B.; Crutchley, R. J. *Inorg. Chem.* 2013, **52**, 11060. (g) Pu, A.-T.; Yang, J.; Kan, W.-Q.; Yang, Y.; Ma, J.-F. *Polyhedron* 2013, **50**, 556.

[12] Duric, S.; Sypaseuth, F. D.; Hoof, S.; Svensson, E.; Tzschucke, C. C. *Chem. Eur. J.* 2013, **19**, 17456.

[13] (a) Díaz, D. J.; Storrier, G. D.; Bernhard, S.; Takada, K.; Abruña, H. D. *Langmuir* 1999, **15**, 7351. (b) Díaz, D. J.; Bernhard, S.; Storrier, G. D.; Abruña, H. D. *J. Phys. Chem. B* 2001, **105**, 8746. (c) Bernhard, S.; Goldsmith, J. I.; Takada, K.; Abruña, H. D. *Inorg. Chem.* 2003, **42**, 4389. (d) Cooke, M. W.; Tremblay, P. M.; Hanan, G. S. *Inorg. Chem. Commun.* 2007, **10**, 1365. (e) Cooke, M. W.; Tremblay, P.; Hanan, G. S. *Inorg. Chim. Acta* 2008, **361**, 2259. (g) Liu, R.; Li, Z.; Zhu, H.; Sun, W. *Inorg. Chim. Acta* 2012, **387**, 383. (h) Wang, M.; Wang, C.; Hao, X. Q.; Li, X.; Vaughn, T. J.; Zhang, Y. Y.; Yu, Y.; Li, Z. Y.; Song, M. P.; Yang, H. B.; Li, X. *J. Am. Chem. Soc.* 2014, **136**, 10499. (i) Wang, C.; Hao, X.-Q.; Wang, M.; Guo, C.; Xu, B.; Tan, E. N.; Zhang, Y.-Y.; Yu, Y.; Li, Z.-Y.; Yang, H.-B.; Song, M.-P.; Li, X. *Chem. Sci.* 2014, **5**, 1221. (j) Chan, A. K.-W.; Lam, W. H.; Tanaka, Y.; Wong, K. M.-C.; Yam, V. W.-W. *Proc. Nat. Acad. Sci. USA* 2015, **112**, 690.

[14] Perera, S.; Li, X.; Guo, M.; Wesdemiotis, C.; Moorefield, C. N.; Newkome, G. R. *Chem. Commun.* 2011, **47**, 4658.

[15] (a) Hanan, G. S.; Wang, J. Synlett 2005, 1251. (b) Cahamchoumis, C.; Potvin, P. G. *J. Chem. Res.* 1998, 180.

[16] (a) Nakayama, Y.; Baba, Y.; Yasuda, H.; Kawakita, K.; Ueyama, N. *Macromolecules* 2003, **36**, 7953. (b) Gong, H.; Gagné, M. R. *J. Am. Chem. Soc.* 2008, **130**, 12177. (c) Jones, G. D.; Martin, J. L.; McFarland, C.; Allen, O. R.; Hall, R. E.; Haley, A. D.; Brandon, R. J.; Konovalova, T.; Desrochers, P. J.; Pulay, P.; Vicic, D. A. *J. Am. Chem. Soc.* 2006, **128**, 13175. (d) Enthaler, S.; Hagemann, B.; Erre, G.; Junge, K.; Beller, M. *Chem. Asian J.* 2006, **1**, 598. (e) Prinsell, M. R.; Everson, D. A.; Weix, D. J. *Chem. Commun.* 2010, **46**, 5743. (f) Jones, G. D.; McFarland, C.; Anderson, T. J.; Vicic, D. A. *Chem. Commun.* 2005, 4211. (g) Suzuki, H.; Matsumura, S. I.; Satoh, Y.; Sogoh, K.; Yasuda, H. *React. Funct. Polym.* 2004, **59**, 253. (h) Kwong, H.-L.; Lee, W.-S. *Tetrahedron: Asymmetry* 2000, **11**, 2299.

[17] (a) Grosshenny, V.; Ziessel, R. J. Organomet. Chem. 1993, **453**, C19. (b) Grosshenny, V.; Romero, F. M.; Ziessel, R. *J. Org. Chem.* 1997, **62**, 1491. (c) Siemeling, U.; Vorfeld, U.; Neumann, B.; Stammler, H.-G.; Zanello, P.; Biani, F. d. Eur. J. *Inorg. Chem.* 1999, 1. (d) Aspley, C. J.; Gareth Williams, J. A. *New J. Chem.* 2001, 25, 1136. (e) Hovinen, J.; Hakala, H. Org. Lett. 2001, **3**, 2473. (f)

Goodall, W.; Wild, K.; Arm, K. J.; Williams, J. A. G. *J. Chem. Soc., Perkin Trans. 2* 2002, 1669. (g) Baranoff, E.; Griffiths, K.; Collin, J.-P.; Sauvage, J.-P.; Ventura, B.; Flamigni, L. *New J. Chem.* 2004, **28**, 1091. (h) Hinderberger, D.; Schmelz, O.; Rehahn, M.; Jeschke, G. *Angew. Chem. Int. Ed.* 2004, **43**, 4616. (i) Duprez, V.; Biancardo, M.; Spanggaard, H.; Krebs, F. C. *Macromolecules* 2005, **38**, 10436. (j) YuN, S.-C.; Chen, H.-B.; Zhang, Y.; Pei, *J. Org. Lett.* 2006, **8**, 5701. (k) Han, F. S.; Higuchi, M.; Kurth, D. G. *Org. Lett.* 2007, **9**, 559. (l) Popović, Z.; Busby, M.; Huber, S.; Calzaferri, G.; De Cola, L. *Angew. Chem. Int. Ed.* 2007, **46**, 8898. (m) Vrábel, M.; Hocek, M.; Havran, L.; Fojta, M.; Votruba, I.; Klepetářová, B.; Pohl, R.; Rulíšek, L.; Zendlová, L.; Hobza, P.; Shih, I. h.; Mabery, E.; Mackman, R. Eur. J. *Inorg. Chem.* 2007, **2007**, 1752. (n) Han, F. S.; Higuchi, M.; Kurth, D. G. *J. Am. Chem. Soc.* 2008, **130**, 2073. (o) Han, F.-S.; Higuchi, M.; Kurth, D. G. *Tetrahedron* 2008, **64**, 9108. (p) Golubkov, G.; Weissman, H.; Shirman, E.; Wolf, S. G.; Pinkas, I.; Rybtchinski, B. *Angew. Chem. Int. Ed.* 2009, **48**, 926. (q) Piao, X.; Zou, Y.; Wu, J.; Li, C.; Yi, T. Org. Lett. 2009, **11**, 3818. (r) Qiu, D.; Cheng, Y.; Wang, L. *Dalton Trans.* 2009, 3247. (s) Murphy, F. A.; Draper, S. M. J. Org. Chem. 2010, **75**, 1862. (t) Rühl, T.; Stulz, E. *Supramol. Chem.* 2010, **22**, 103. (u) Wang, W.; Wang, S.; Li, X.; Collin, J.-P.; Liu, J.; Liu, P. N.; Lin, N. *J. Am. Chem. Soc.* 2010, **132**, 8774. (v) Yu, L.; Wang, Z.; Wu, J.; Tu, S.; Ding, K. *Angew. Chem. Int. Ed.* 2010, **49**, 3627. (w) Eryazici, I.; Farha, O. K.; Compton, O. C.; Stern, C.; Hupp, J. T.; Nguyen, S. T. *Dalton Trans.* 2011, **40**, 9189. (x) Higuchi, M.; Li, J.; Sato, T.; Li, H. *Synthesis* 2011, **2011**, 1361. (y) Huang, Z.; Chen, X.; Zhang, J.; Yu, X.-Q.; Pu, L. *Tetrahedron* Lett. 2011, **52**, 5497. (z) Nie, H.-J.; Yao, J.; Zhong, Y.-W. *J. Org. Chem.* 2011, **76**, 4771. (aa) Vilà, N.; Royal, G.; Loiseau, F.; Deronzier, A. *Inorg Chem.* 2011, **50**, 10581. (ab) Xu, B.; Chi, Z.; Zhang, X.; Li, H.; Chen, C.; Liu, S.; Zhang, Y.; Xu, J. *Chem. Commun.* 2011, **47**, 11080. (ac) Fillaud, L.; Trippé-Allard, G.; Lacroix, J. C. *Org. Lett.* 2013, **15**, 1028. (ad) Katagiri, S.; Sakamoto, R.; Maeda, H.; Nishimori, Y.; Kurita, T.; Nishihara, H. *Chem. Eur. J.* 2013, **19**, 5088. (ae) Tan, Y.; Gao, J.; Yu, J.; Wang, Z.; Cui, Y.; Yang, Y.; Qian, G. *Dalton Trans.* 2013, **42**, 11465. (af) Yao, C.-J.; Zhong, Y.-W.; Yao, J. *Inorg. Chem.* 2013, **52**, 10000. (ag) Ghosh, B. N.; Bhowmik, S.; Mal, P.; Rissanen, K. *Chem. Commun.* 2014, **50**, 734. (ah) Hossain, M. D.; Zhang, J.; Pandey, R. K.; Sato, T.; Higuchi,

M. Eur. J. *Inorg. Chem.* 2014, **2014**, 3763. (ai) Jing, S.; Zheng, C.; Pu, S.; Fan, C.; Liu, G. *Dyes Pigments* 2014, **107**, 38. (aj) Nie, H.-J.; Yao, C.-J.; Sun, M.-J.; Zhong, Y.-W.; Yao, J. *Organometallics* 2014, **33**, 6223. (ak) Rajwar, D.; Liu, X.; Lim, Z. B.; Cho, S. J.; Chen, S.; Thomas, J. M. H.; Trewin, A.; Lam, Y. M.; Sum, T. C.; Grimsdale, A. C. *RSC Adv.* 2014, **4**, 17680. (al) Wu, D.; Shao, T.; Men, J.; Chen, X.; Gao, G. *Dalton Trans.* 2014, **43**, 1753. (am) Ghosh, B. N.; Topić, F.; Sahoo, P. K.; Mal, P.; Linnera, J.; Kalenius, E.; Tuononen, H. M.; Rissanen, K. *Dalton Trans.* 2015, **44**, 254. (an) Liu, C.-L.; Zheng, C.-J.; Liu, X.-K.; Chen, Z.; Yang, J.-P.; Li, F.; Ou, X.-M.; Zhang, X.-H. *J. Mater. Chem. C* 2015, **3**, 1068.

[18] Pal, A. K.; Laramée-Milette, B.; Hanan, G. S. *Inorg. Chim. Acta* 2014, **418**, 15.

[19] (a) Ollagnier, C. M.; Nolan, D.; Fitchett, C. M.; Draper, S. M. *Inorg. Chem. Commun.* 2007, **10**, 1045. (b) Beves, J. E.; Dunphy, E. L.; Constable, E. C.; Housecroft, C. E.; Kepert, C. J.; Neuburger, M.; Price, D. J.; Schaffner, S. *Dalton Trans.* 2008, 386. (c) Gou, L.; Xu, L.-F.; Hu, H.-M.; Wang, B.-C.; Wu, Q.-R.; Chen, X.-L.; Tang, Z.-X. Z. *Anorg. Allg. Chem.* 2008, **634**, 1215.

[20] (a) Rojo, T.; Arriortua, M. I.; Ruiz, J.; Darriet, J.; Villeneuve, G.; Beltran-Porter, D. J. Chem. Soc., *Dalton Trans.* 1987, 285. (b) Valdéz-Martinez, J.; Salazar-Mendoza, D.; Toscano, R. A. *Acta Cryst.* 2002, E58, m712. (c) Jin, X.-H.; Cai, L.-X.; Sun, J.-K.; Ju, Z.-F.; Zhang, J. *Inorg. Chem. Commun.* 2010, **13**, 86. (d) Thornley, P. A.; Starkey, J. C.; Zibaseresht, R.; Polson, M. I. J.; Wikaira, J. L.; Hartshorn, R. M. J. *Coord. Chem.* 2011, **64**, 145.

Chapitre 6 – Synthesis of a discrete Re(I) di- and tricarbonyl assemblies using a [4 x 1] directional bonding strategy

6.1. Résumé

L'auto-assemblage discret de deux carrés de Re(I) a été réalisé par une stratégie simple et efficace où les complexes, [Re(4-pytpy-κ^2N)$(CO)_3$Br] et [Re(4-pytpy-κ^3N)$(CO)_2$Br], agissent comme leur propre ligands. Les propriétés photophysiques et électrochimiques des assemblages et leurs précurseurs sont décrits ainsi que l'étude par diffraction des rayons X.

Contribution :

Baptiste Laramée-Milette : Synthèse et caractérisation complète du ligand et analyse partielle des complexes métalliques. Analyse structurelle par diffraction des rayons X, analyse des propriétés optiques et électroniques. Rédaction de l'article.

Christophe Lachance-Brais: Synthèse, purification et caractérisation partielle d'un complexe précurseur de Re(I).

Garry S. Hanan: Supervision, révision de l'article.

Synthesis of discrete Re(I) di- and tricarbonyl assemblies using a [4 x 1] directional bonding strategy

*Baptiste Laramée-Milette, Christophe Lachance-Brais and Garry S. Hanan**

Département de chimie, Université de Montréal, 5155 Ch. de la rampe, Pavillon J.-A. Bombardier, Montréal, Québec, Canada, H3T 2B1

*: E-mail: garry.hanan@umontreal.ca

Communication

Received: 20th August 2014; Published online: 08th October 2014

DOI:10.1039/c4dt03077j

Reproduced with permission from *Dalton Trans.* **2015**, *44*, 41-45

Copyright 2015 The Royal Society of Chemistry

6.2. Table of content graphic

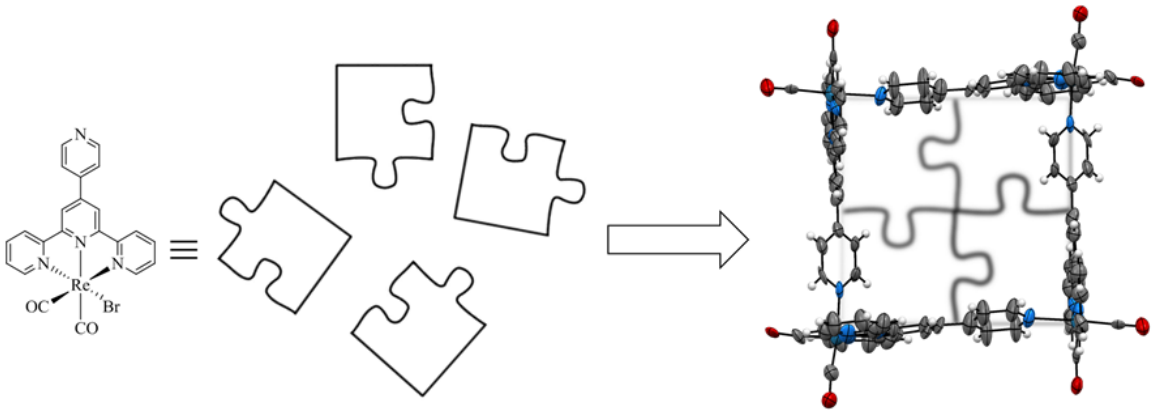

6.3. Abstract

Discrete self-assembly of two Re(I) squares was achieved by a simple and efficient strategy where the complexes, [Re(4-pytpy-κ^2*N*)$(CO)_3$Br] and [Re(4-pytpy-κ^3*N*)$(CO)_2$Br], act as their own ligands. The photophysical and electrochemical properties of the assemblies and their precursors are described along with solid-state X-ray diffraction studies.

6.4. Introduction

Over the past few decades, self-assembly of simple components has led to the synthesis of remarkable materials such as molecular cages,[1] macrocycles,[2] helices,[3] grids,[4] and MOFs.[5] Although there are several ways to build complex assemblies, the directional bonding approach is quite straightforward and probably the most useful for the construction of rigid assemblies.[6] However, it usually requires two separate entities, an organic donor ligand and a metallic acceptor, reacting together in perfect symbiosis in order to arrive at the final assembly.

A key building block for such complex assemblies is the 2,2':6',2''-terpyridine (tpy) motif since its metal complexes are chemically stable and have quite rich electrochemical and photophysical properties that are used for photosensitization in DSSC devices,[7] catalysis,[8] ion-sensing,[9] bioimaging[10] and chemotherapy.[11]

Additionally, there are a large variety of metal ions that bind to terpyridine ligands, including main group, transition, lanthanide and actinide metal ions.[12]

Recently rhenium ions, more specifically the tricarbonylrhenium(I)X (where X= Br, Cl or I) has been used to organize and link several pyridine-functionalized ligands into squares, rectangles and dimers with interesting photoluminescences properties.[13] More recently, Hightower *et. al.* have prepared a series of meridionally-coordinated tridentate terpyridine Re(I) dicarbonyl complexes, which showed enhanced absorption through the entire visible portion of the electromagnetic spectrum.[14]

Extrapolation of the binding motif mentioned above leads to the self-assembly of two novel Re(I) squares using the directional bonding approach in which the donor and acceptor are located on the same building block,[15] leading to [4 x 1] assemblies instead of the traditional [2 + 2] or [4 + 4] squares. Both the 4-pytpy (4-pytpy = 4'-(4'-pyridyl)-2,2':6',2''-terpyridine) ligand and Re(I) complexes 1-4 were prepared in average to good yield using methodologies described in the literature (Scheme 6.1).[14]

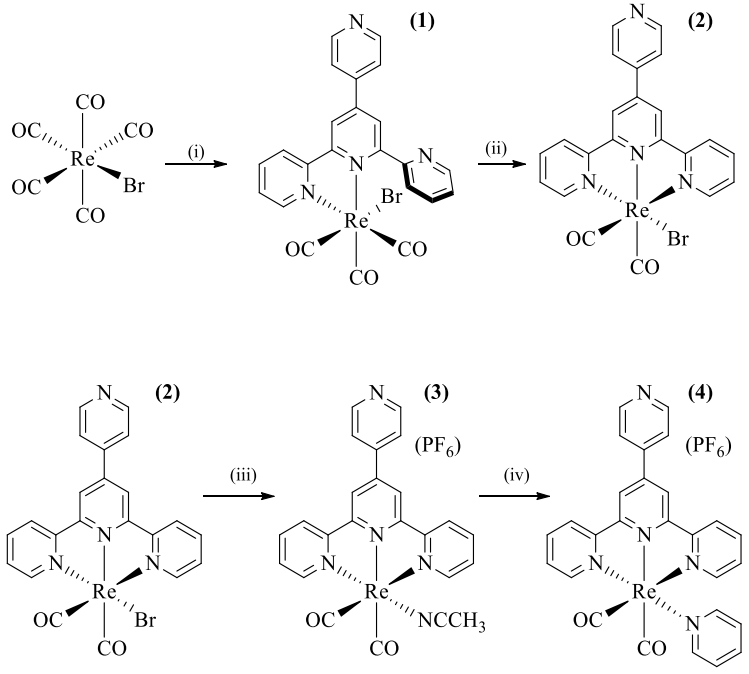

Scheme 6.1 - Synthesis of bi- and tridentate terpyridine rhenium complexes. (Reagents and conditions :(i) 1.1 eq. 4-pytpy, toluene, reflux, 5 h; (ii) Sealed tube, 280ºC, N_2, 8 h; (iii) AgOTf (1.1 eq), acetonitrile, reflux, 5-8 h; (iv) pyridine (excess), reflux, 4 h.)

6.5. Results and discussion

Compound **4** was prepared as a model of the self-assembled square. Although DFT calculations and other analyses support the *cis* configuration of the carbonyl moieties on the rhenium core, this is the first structural evidence to confirm the geometry.[14,16] Single crystals of **4** suitable for X-ray analysis were grown from the slow evaporation of an acetone:water (1:1) solution. To the best of our knowledge, this is the first crystallographic report of a $[Re(tpy\text{-}\kappa^3N)(CO)_2(L)]^+$ complex.

The data obtained by solid-state analysis confirmed that the two carbonyls are lying in a perpendicular fashion, with an experimental angle of 85.5(1)° while the pyridyl unit is at an 84.44(7)° angle to the tpy-κ^3N moiety, suggesting that [4x1] self-assembly of a square should be possible (Figure 6.1).

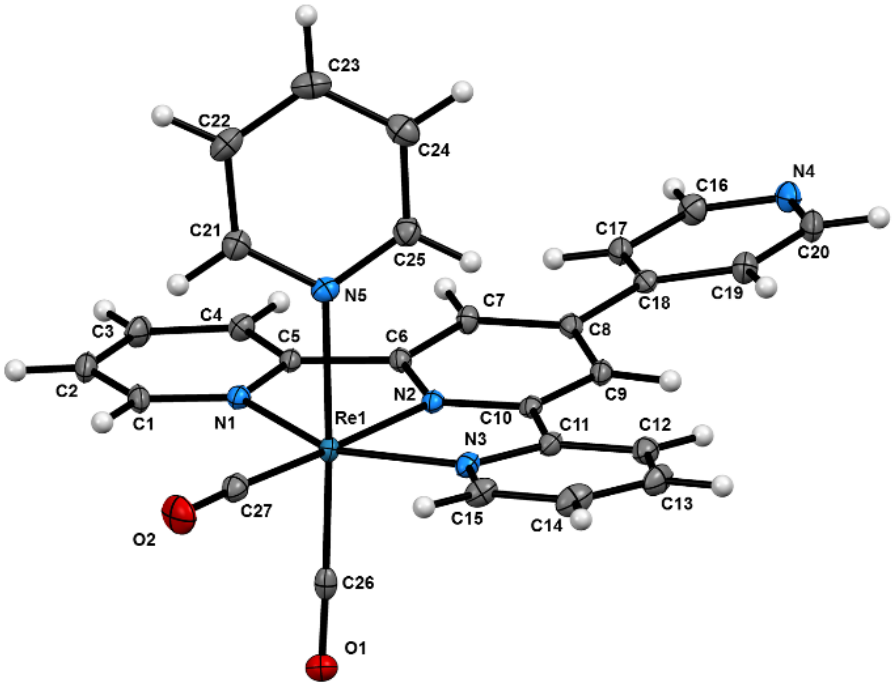

Figure 6.1 - X-Ray crystal structure of 4 showing the *cis* configuration of the CO ligand as well as the coordination angle between the 2,2':6',2''-terpyridine unit and the pyridine ligand. The counter-anion (PF_6^-) and solvent molecule (H_2O) were omitted for clarity. The ellipsoids are drawn with a 50% probability.

The squares were synthesized in a two-step one-pot reaction, where [Re-(4-pytpy-κ^2*N*)(CO)$_3$(MeCN)]$^+$ and [Re-(4-pytpy-κ^3*N*)(CO)$_2$(MeCN)]$^+$ were generated in-situ. Due to the excess of acetonitrile competing for the binding site on the metal ion, none of the assembly was generated after the first step. However, after replacement of the MeCN by a less coordinating solvent mixture of acetone:toluene (1:1), the desired assemblies were obtained in good yield (Scheme 6.2). The assemblies were confirmed by ^{1}H NMR, HR-MS, and elemental analyses. DOSY experiments also confirmed the larger size of the [4 x 1] assemblies compared to the starting complexes.

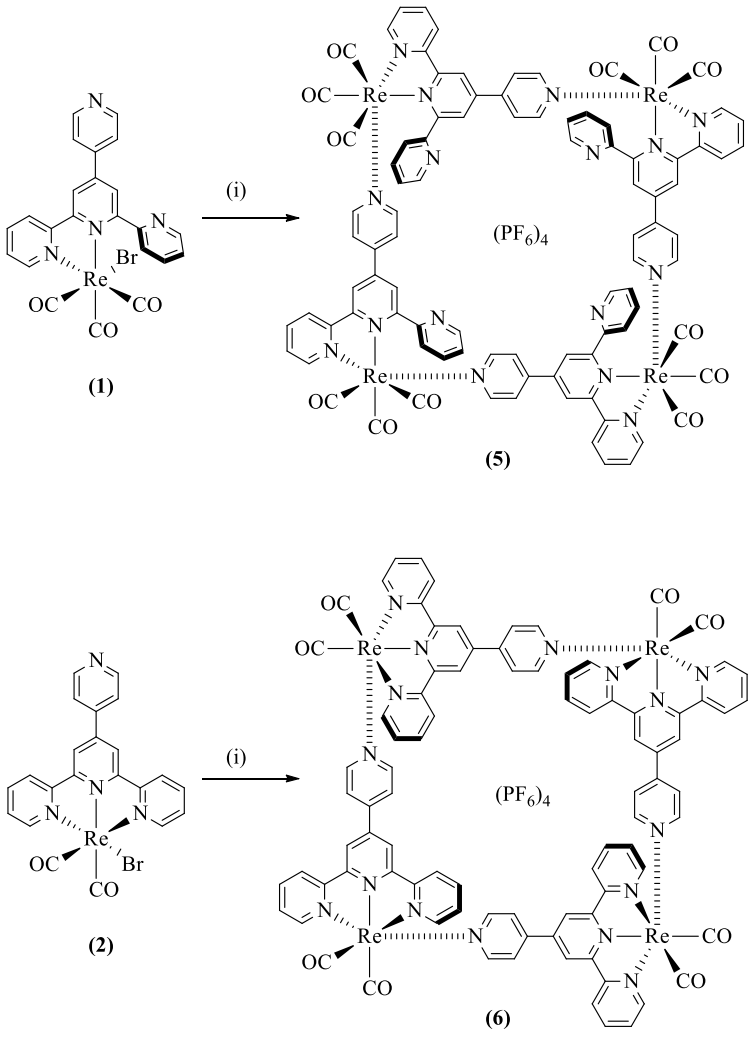

Scheme 6.2 - [4 x 1] Self-assembly of the Re(I) squares. (Reagents and conditions: (i) AgOTf (1.1 eq), MeCN, reflux, 5h followed by reflux in acetone/toluene (1:1), N_2, 10-12 h.).

Single crystals of 6 were obtained by slow evaporation of acetone-methanol-water (45:45:10) over a few weeks. Although precise interatomic distances are not available for this structure, the atom connectivity confirms without any doubt that a [4 x 1] self-assembled structure is obtained, as confirmed by other analyses.

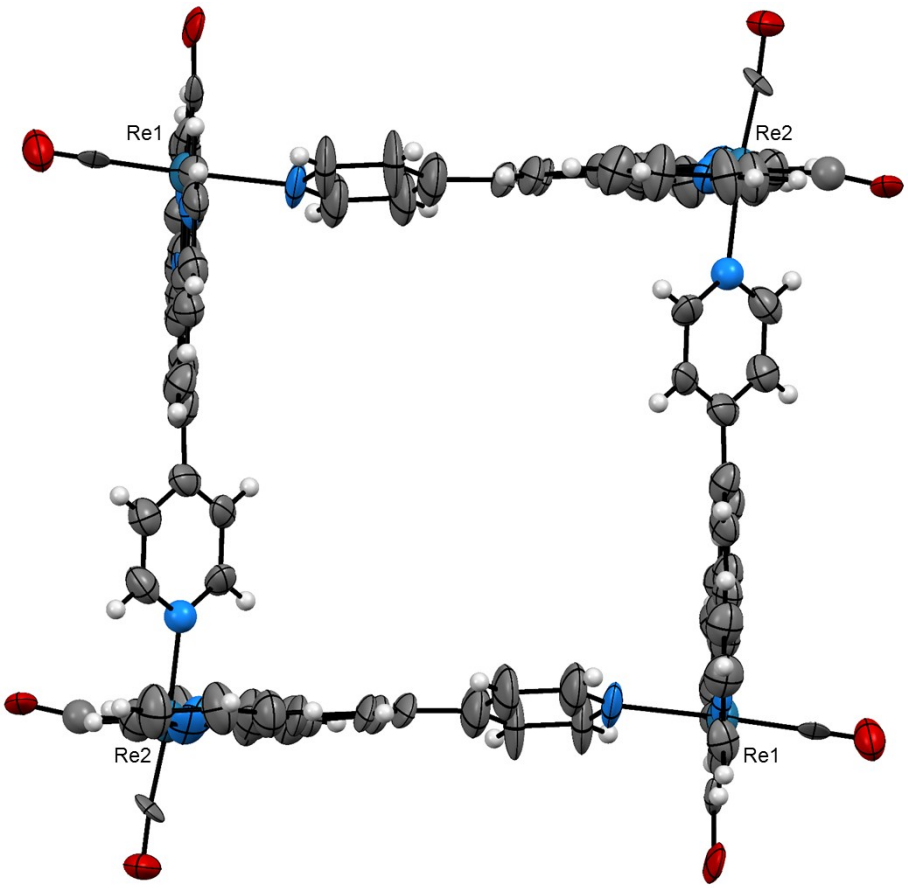

Figure 6.2 - X-ray crystal structure of 6 showing the self-assembled molecular square. The four counter-anion (PF_6^-) were omitted for clarity. The ellipsoids are drawn with a 50% probability.

The electronic absorption spectra for 1, 2 and 4-6 were recorded in dry, degassed acetonitrile, at room temperature (r.t.). All of the complexes exhibit ligand-centered (LC) $\pi \rightarrow \pi^*$ transitions between 200 and 300 nm. The absorptions between 300 and 350 nm consist of a mixture of $\pi \rightarrow \pi^*$ LC and metal-to-ligand charge-transfer transitions (MLCT), whereas the bands observed between 350 and 800 nm are mainly MLCT transitions. It is worth noting the red-shift of the [Re-(4-pytpy-$\kappa^3 N$)$(CO)_2]_4[(PF_6)_4]$ absorption, which also absorbs throughout the visible region with

low to moderate absorption ($\varepsilon \approx 26000\ M^{-1}cm^{-1}$ at 470 nm, $\varepsilon \approx 1800\ M^{-1}cm^{-1}$ between 625 and 725 nm) (Figure 6.3).

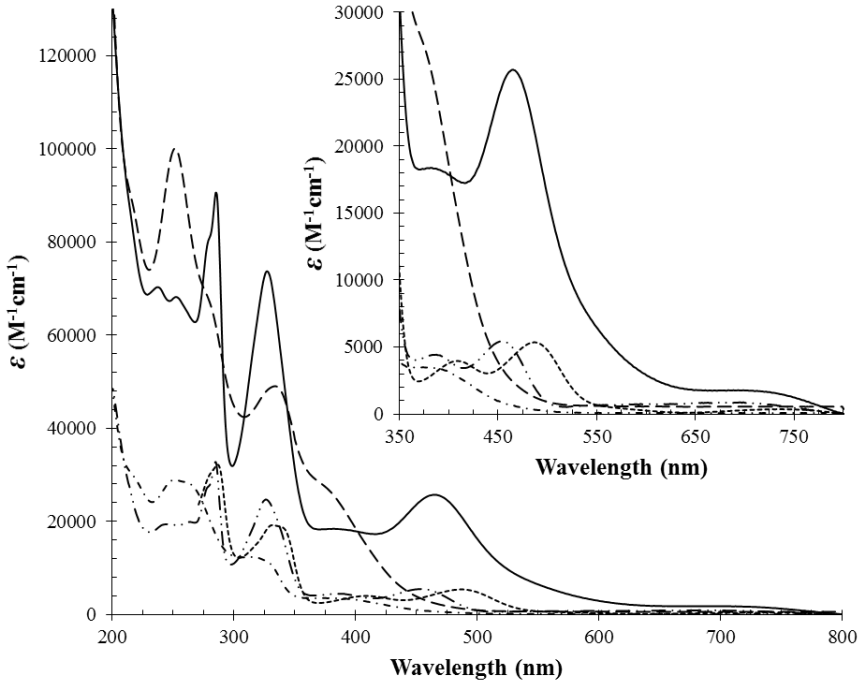

Figure 6.3 - Absorption spectra of the rhenium squares and their precursors recorded in MeCN solution at r. t.: 1 (dash·dot), 2 (short dash), 4 (dash·dot·dot), 5 (long dash), 6 (solid line).

The emission spectra for complexes 1, 2, 5 and 6 were recorded in dry, degassed acetonitrile at room temperature. Since 2 and 6 were found to be non-emissive at room temperature, we also recorded the emission spectra at 77 K in a 1:1 toluene-acetonitrile glass matrix. However, even though similar compounds were reported to have an emission maximum centered at 522 nm,[14] complexes 2 and 6 were not emissive under similar conditions. Both complexes 1 and 5 emit at room temperature, with a maximum centered at 625 nm (λ_{ex} = 370 nm; $\Phi=7.2x10^{-5}$ *vs* Re(2,2'-bpy)$(CO)_3Cl$) in the case of 1 and a maximum centered at 600 nm (λ_{ex} = 365 nm; $\Phi=1.7x10^{-4}$ *vs* Re(2,2'-bpy)$(CO)_3Cl$) for 5.

Table 6.1 – Electrochemical data for the tpy-κ^2*N* and tpy-κ^3*N* complexes.

Cmpd	$E_{1/2}^{Ox}$ [a]			$E_{1/2}^{Red}$ [a]							
1	1.41[b]	0.76	-	-0.88[b]	-0.97	-1.13[c]	-1.30	-1.43	-1.63[b]	-1.72	-1.98[c]
2	-	0.71	0.53	-0.85	-1.15[b]	-1.21	-1.74[b]	-2.15	-	-	-
5	-	-	-	-0.69	-0.78	-0.86	-1.31	-1.43	-1.58	-1.70[b]	-
6	0.87[c]	0.71	0.53	-0.81[b]	-0.85	-1.11[b]	-1.20	-2.15[c]	-	-	-
$[Re(bpy)(py)(CO)_3]^+$ [d]	1.74	-	-	-1.09	-1.39	-	-	-	-	-	-
Re(tpy-κ^2*N*)$(CO)_3Cl$ [e]	-	0.79[b]	-	-1.74	-	-	-	-	-	-	-
Re(tpy-κ^3*N*)$(CO)_2Cl$ [f]	1.22	-	0.48	-1.17[b]	-1.34[b]	-	-	-	-	-	-
$[Re(tpy\text{-}\kappa^3N)(py)(CO)_2]^+$ [f]	1.35[b]	0.86	-	-1.21[b]	-	-	-	-	-	-	-

[a] Potentials are in volt *vs* SCE. Cyclic voltammetry was performed in DMF/t-$Bu_4N(PF_6)$ (0.1M), recorded at 25 ± 1°C with a sweep rate of 50mV s^{-1}. All potentials are corrected *vs* Fc/Fc^+. A more detailed table is available in the ESI. [b] Irreversible; potential is given for the cathodic wave. [c] Quasi-reversible process. [d] In MeCN from ref. 16. [e] In MeCN, from ref. 17. [f] In MeCN, from ref. 14.

The electrochemical behaviour of complexes 1, 2, 5 and 6 is presented in Table 6.1 – Electrochemical data for the tpy-κ^2*N* and tpy-κ^3*N* complexes.. The complexes were examined by cyclic voltammetry, differential pulse voltammetry as well as by square-wave voltammetry. Due to solubility issues, dimethylformamide (DMF) was selected for the electrochemical analyses. The observed electronic processes are all monoelectronic. Among all of the complexes, only 5 lacks accessible oxidation potentials. The oxidation potential of the model compound $[Re(bpy)(py)(CO)_3]^+$ in acetonitrile is reported at 1.74 V, which is at a slightly more positive potential compare to the oxidation of DMF itself, which occurred near 1.7 V. All the other complexes showed at least two metal-based oxidations, with three oxidation processes being observed in the case of 6. All of the compounds presented ligand-based reductions. It is worth mentioning the electron-reservoir properties of 5, in which the first six reduction processes are fully reversible, while in all other cases irreversible reduction processes are observed at low potential.

6.6. Conclusion

In summary, we described the use of a [4 x 1] directional bonding approach for the construction of supramolecular Re(I) assemblies. The *cis* configuration of the $[Re(tpy\text{-}\kappa^3N)(CO)_2L]^+$ complexes was also confirmed by solid state crystallographic measurements which opened the door to discrete assemblies. The synthesis and characterization of the novel square assemblies show quite different photophysical and electrochemical properties from their precursor compounds. We envision that complexes **5** and **6** could be used as electronic reservoirs and as photosensitizers, respectively.[19]

6.7. References

[1] (*a*) D. L. Caulder and K. N. Raymond, *Acc. Chem. Res.*, 1999, **32**, 975; (*b*) F. Hof, S. L. Craig, C. Nuckolls and J. Rebek Jr, *Angew. Chem. Int. Ed.*, 2002, **41**, 1488; (*c*) A. J. Baer, B. D. Koivisto, A. P. Côté, N. J. Taylor, G. S. Hanan, H. Nierengarten, A. Van Dorsselaer *Inorg. Chem.*, 2002, **41**, 4987; (*d*) D. K. Chand, K. Biradha, M. Kawano, S. Sakamoto, K. Yamaguchi and M. Fujita, *Chem. Asian J.*, 2006, **1**, 82; (*e*) S. J. Lee, K. L. Mulfort, X. Zuo, A. J. Goshe, P. J. Wesson, T. S. Nguyen, J. T. Hupp and D. M. Tiede, *J. Am. Chem. Soc.*, 2008, **130**, 836; (*f*) T. Schröder, R. Brodbeck, M. C. Letzel, A. Mix, B. Schnatwinkel, M. Tonigold, D. Volkmer and J. Mattay, *Tetrahedron Lett.*, 2008, **49**, 5939; (*g*) M. Yoshizawa, J. K. Klosterman and M. Fujita, *Angew. Chem.*, 2009, **48**, 3418; (*h*) Q. F. Sun, J. Iwasa, D. Ogawa, Y. Ishido, S. Sato, T. Ozeki, Y. Sei, K. Yamaguchi and M. Fujita, *Science*, 2010, **328**, 1144; (*i*) N. Kishi, Z. Li, K. Yoza, M. Akita and M. Yoshizawa, *J. Am. Chem. Soc.*, 2011, **133**, 11438; (*j*) H. Amouri, C. Desmarets and J. Moussa, *Chem. Rev.*, 2012, **112**, 2015; (*k*) Q. F. Sun, S. Sato and M. Fujita, *Nature Chem.*, 2012, **4**, 330; (*l*) D. Tripathy, A. K. Pal, G. S. Hanan and D. K. Chand, *Dalton Trans.*, 2012, **41**, 11273; (*m*) R. Custelcean, *Chem. Soc. Rev.*, 2014, **43**, 1813; (*n*) S. Durot, J. Taesch and V. Heitz, *Chem. Rev.*, 2014, DOI: 10.1021/cr400673y; (*o*) A. Mishra, A. Dubey, J. W. Min, H. Kim, P. J. Stang and K. W. Chi, *Chem. Commun.*, 2014, **50**, 7542; (*p*) S. Mukherjee and P. S. Mukherjee, *Chem. Commun.*, 2014, **50**, 2239; (*q*) C. Wang, X.-Q. Hao, M. Wang, C. Guo, B. Xu, E. N. Tan, Y.-Y. Zhang, Y. Yu, Z.-Y. Li, H.-B. Yang, M.-P. Song and X. Li, *Chem. Sci.*, 2014, **5**, 1221; (*r*) M. Yoshizawa and J. K. Klosterman, *Chem. Soc. Rev.*, 2014, **43**, 1885; (*s*) K. Li, L.-Y. Zhang, C. Yan, S.-C. Wei, M. Pan, L. Zhang and C.-Y. Su, *J. Am. Chem. Soc.*, 2014, **136**, 4456; (*t*) C. Klein, C. Gütz, M. Bogner, F. Topić, K. Rissanen and A. Lützen, *Angew. Chem. Int. Ed.*, 2014, **53**, 3739.

[2] (*a*) E. C. Constable, K. Harris, C. E. Housecroft and M. Neuburger, *Dalton Trans.*, 2011, **40**, 1524; (*b*) E. C. Constable, C. E. Housecroft, S. Vujovic and J. A. Zampese, *CrystEngComm*, 2014, **16**, 328; (*c*) X. Lu, X. Li, Y. Cao, A. Schultz, J. L. Wang, C. N. Moorefield, C. Wesdemiotis, S. Z. Cheng and G. R. Newkome, *Angew. Chem.*, 2013, **52**, 7728; (*d*) G. R. Newkome, T. J. Cho, C. N.

Moorefield, G. R. Baker, Cush and P. S. Russo, *Angew. Chem. Int. Ed.*, 1999, **38**, 3717; (*e*) G. R. Newkome, P. Wang, C. N. Moorefield, T. J. Cho, P. P. Mohapatra, S. Li, S. H. Hwang, O. Lukoyanova, L. Echegoyen, J. A. Palagallo, V. Iancu and S. W. Hla, *Science*, 2006, **312**, 1782; (*f*) A. K. Pal, B. Laramée-Milette and G. S. Hanan, *RSC Advances*, 2014, **4**, 21262; (*g*) M. P. Santoni, A. K. Pal, G. S. Hanan, M. C. Tang, K. Venne, A. Furtos, P. Menard-Tremblay, C. Malveau and B. Hasenknopf, *Chem. Commun.*, 2012, **48**, 200; (*h*) R. Trokowski, S. Akine and T. Nabeshima, *Chem. Commun.*, 2008, 889; (*i*) P. Wang, C. N. Moorefield and G. R. Newkome, *Angew. Chem.*, 2005, **44**, 1679; (*j*) J. Xu, R. Wang, Y. Li, Z. Gao, R. Yao, S. Wang and B. Wu, *Eur. J. Inorg. Chem.*, 2012, **2012**, 3349; (*k*) P. D. Frischmann, S. Guieu, R. Tabeshi and M. J. MacLachlan, *J. Am. Chem. Soc.*, 2010, **132**, 7668.

[3] (*a*) S. Bala, A. Goswami, S. Sengupta, S. Ganguly, S. Bhattacharya, S. Khanra and R. Mondal, *Cryst. Growth Des.*, 2013, **13**, 5068; (*b*) E. C. Constable, S. M. Elder, J. Healy, M. D. Ward and D. A. Tocher, *J. Am. Chem. Soc.*, 1990, **112**, 4590; (*c*) E. C. Constable, M. D. Ward and D. A. Tocher, *J. Am. Chem. Soc.*, 1990, **112**, 1256; (*d*) C. Jia, B. P. Hay and R. Custelcean, *Inorg. Chem.*, 2014, **53**, 3893; (*e*) A. M. Johnson, M. C. Young, X. Zhang, R. R. Julian and R. J. Hooley, *J. Am. Chem. Soc.*, 2013, **135**, 17723; (*f*) C. Piguet, J. C. G. Buenzli, G. Bernardinelli, G. Hopfgartner and A. F. Williams, *J. Am. Chem. Soc.*, 1993, **115**, 8197; (*g*) F. Puntoriero, S. Campagna, A. Stadler and J. Lehn, *Coord. Chem. Rev.*, 2008, **252**, 2480; (*h*) S. Ruettimann, C. Piguet, G. Bernardinelli, B. Bocquet and A. F. Williams, *J. Am. Chem. Soc.*, 1992, **114**, 4230; (*i*) Y. Wei, K. Wu, J. He, W. Zheng and X. Xiao, *CrystEngComm*, 2011, **13**, 52; (*j*) R. Zong and R. P. Thummel, *Inorg. Chem.*, 2005, **44**, 5984.

[4] (*a*) G. S. Hanan, D. Volkmer and J.-M. Lehn, *Can. J. Chem.*, 2004, **82**, 1428; (*b*) G. S. Hanan, D. Volkmer, U. S. Schubert, J.-M. Lehn, G. Baum and D. Fenske, *Angew. Chem. Int. Ed.*, 1997, **36**, 1842; (*c*) Y. S. Moroz, K. Kulon, M. Haukka, E. Gumienna-Kontecka, H. Kozlowski, F. Meyer and I. O. Fritsky, *Inorg. Chem.*, 2008, **47**, 5656; (*d*) M. Moustapha-Sow, O. Diouf, M. Gaye, A. Salam-Sall, G. Castro, P. Pérez-Lourido, L. Valencia, A. Caneschi and L. Sorace, *Cryst. Growth Des.*, 2013, **13**, 4172.

[5] (*a*) T. R. Cook, Y. R. Zheng and P. J. Stang, *Chem. Rev.*, 2013, **113**, 734; (*b*) R. J. Kuppler, D. J. Timmons, Q.-R. Fang, J.-R. Li, T. A. Makal, M. D. Young, D. Yuan, D. Zhao, W. Zhuang and H.-C. Zhou, *Coord. Chem. Rev.*, 2009, **253**, 3042; (*c*) S. T. Meek, J. A. Greathouse and M. D. Allendorf, *Adv. Mater.*, 2011, **23**, 249; (*d*) J. L. C. Rowsell and O. M. Yaghi, *Microporous Mesoporous Mater.*, 2004, **73**, 3.

[6] R. Chakrabarty, P. S. Mukherjee and P. J. Stang, *Chem. Rev*, 2011, **111**, 6810.

[7] (*a*) M. Beley, C.-A. Bignozzi, G. Kirsch, M. Alebbi and J.-C. Raboin, *Inorg. Chim. Acta*, 2000, **318**, 197; (*b*) M. K. Nazeeruddin, P. Péchy and M. Grätzel, *Chem. Commun.*, 1997, 1705; (*c*) M. K. Nazeeruddin, P. Péchy, T. Renouard, S. M. Zakeeruddin, R. Humphry-Baker, P. Comte, P. Liska, L. Cevey, E. Costa, V. Shklover, L. Spiccia, G. B. Deacon, C. A. Bignozzi and M. Grätzel, *J. Am. Chem. Soc.*, 2001, **123**, 1613.

[8] (*a*) C.-T. Yeung, W.-S. Lee, C.-S. Tsang, S.-M. Yiu, W.-T. Wong, W.-Y. Wong and H.-L. Kwong, *Polyhedron*, 2010, **29**, 1497; (*b*) H.-L. Kwong and W.-S. Lee, *Tetrahedron: Asymmetry*, 2000, **11**, 2299; (*c*) E. P. Kelson and P. Phengsy, *J. Chem. Soc., Dalton Trans.*, 2000, 4023.

[9] (*a*) S. Yin, J. Zhang, H. Feng, Z. Zhao, L. Xu, H. Qiu and B. Tang, *Dyes and Pigments*, 2012, **95**, 174; (*b*) Q.-Y. Cao, M. Li, L. Zhou and Z.-W. Wang, *RSC Adv.*, 2014, **4**, 4041; (*c*) Y. H. Lee, N. V. Nghia, M. J. Go, J. Lee, S. U. Lee and M. H. Lee, *Organometallics*, 2014, **33**, 753.

[10] (*a*) U. Basu, I. Khan, D. Koley, S. Saha, P. Kondaiah and A. R. Chakravarty, *J. Inorg. Biochem.*, 2012, **116**, 77; (*b*) Y. Tan, M. Liu, J. Gao, J. Yu, Y. Cui, Y. Yang and G. Qian, *Dalton Trans.*, 2014, **43**, 8048.

[11] (*a*) A. Hussain, S. Gadadhar, T. K. Goswami, A. A. Karande and A. R. Chakravarty, *Eur. J. Med. Chem.*, 2012, **50**, 319; (*b*) V. M. Manikandamathavan, V. Rajapandian, A. J. Freddy, T. Weyhermüller, V. Subramanian and B. U. Nair, *Eur. J. Med. Chem.*, 2012, **57**, 449.

[12] (*a*) M. E. Gallina, G. Bergamini, S. Di Motta, J. Sakamoto, F. Negri and P. Ceroni, *Photochem. Photobiol. Sci.*, 2014, **13**, 997; (*b*) A. K. Pal, B. Laramée-Milette and G. S. Hanan, *Inorg. Chim. Acta*, 2014, **418**, 15; (*c*) A. K. Pal, N. Zaccheroni, S. Campagna and G. S. Hanan, *Chem. Commun.*, 2014, **50**, 6846-6849; (*d*) S. G. Thangavelu, M. B. Andrews, S. J. Pope and C. L. Cahill, *Inorg.*

Chem., 2013, **52**, 2060; (*e*) A. Wild, A. Winter, F. Schlutter and U. S. Schubert, *Chem. Soc. Rev.*, 2011, **40**, 1459; (*f*) A. Winter, M. D. Hager, G. R. Newkome and U. S. Schubert, *Adv. Mater.*, 2011, **23**, 5728; (*g*) V. Bekiari and P. Lianos, *Adv. Mater.*, 2000, **12**, 1603; (*h*) M. G. B. Drew, P. B. Iveson, M. J. Hudson, J. O. Liljenzin, L. Spjuth, P.-Y. Cordier, Å. Enarsson, C. Hill and C. Madic, *J. Chem. Soc., Dalton Trans.*, 2000, 821; (*i*) L. Gou, Q.-R. Wu, H.-M. Hu, T. Qin, G.-L. Xue, M.-L. Yang and Z.-X. Tang, *Inorg. Chim. Acta*, 2008, **361**, 1922; (*j*) F. W. Lewis, L. M. Harwood, M. J. Hudson, M. G. Drew, M. Sypula, G. Modolo, D. Whittaker, C. A. Sharrad, V. Videva, V. Hubscher-Bruder and F. Arnaud-Neu, *Dalton Trans.*, 2012, **41**, 9209; (*k*) J. Lhoste, A. Perez-Campos, N. Henry, T. Loiseau, P. Rabu and F. Abraham, *Dalton Trans.*, 2011, **40**, 9136; (*l*) Q.-R. Wu, J.-J. Wang, H.-M. Hu, Y.-Q. Shangguan, F. Fu, M.-L. Yang, F.-X. Dong and G.-L. Xue, *Inorg. Chem.Commun.*, 2011, **14**, 484; (*m*) A. K. Pal, S. Serroni, N. Zaccheroni, S. Campagna and G. S. Hanan, *Chem. Sci.*, 2014, DOI: 10.1039/c4sc01604a.

[13] (*a*) K. D. Benkstein, J. T. Hupp and C. L. Stern, *J. Am. Chem. Soc.*, 1998, **120**, 12982; (*b*) R. Nagarajaprakash, D. Divya, B. Ramakrishna and B. Manimaran, *Organometallics*, 2014, **33**, 1367; (*c*) P. Thanasekaran, C.-C. Lee and K.-L. Lu, *Acc. Chem. Res.*, 2012, **45**, 1403; (*d*) R. V. Slone, J. T. Hupp, C. L. Stern and T. E. Albrecht-Schmitt, *Inorg, Chem.*, 1996, **35**, 4096; (*e*) K. D. Benkstein, C. L. Stern, K. E. Span, R. C. Johnson, K. A. Walters, F. W. M. Vanhelmont and J. T. Hupp, *Eur. J. Inorg. Chem.*, 2002, 2818; (*f*) S.-S. Sun and A. J. Lees, *Inorg. Chem.*, 2001, **40**, 3154; (*g*) B. Manimaran, A. Vanitha, M. Karthikeyan, B. Ramakrishna and S. M. Mobin, *Organometallics*, 2014, **33**, 465; J. T. Hupp, *Struct. Bond*, 2006, **121**, 145.

[14] (*a*) D. R. Black and S. E. Hightower, *Inorg. Chem. Commun.*, 2012, **24**, 16; (*b*) B. A. Frenzel, J. E. Schumaker, D. R. Black and S. E. Hightower, *Dalton Trans.*, 2013, **42**, 12440.

[15] L. H. Tong, S. Clifford, A. Gomila, S. Duval, L. Guénée and A. F. Williams, *Chem. Commun.*, 2012, **48**, 9891.

[16] (*a*) A. Juris, S. Campagna, I. Bidd, J.-M. Lehn and R. Ziessel, *Inorg. Chem.*, 1988, **27**, 4007; (*b*) E. W. Abel, V. S. Dimitrov, N. J. Long, K. G. Orrell, A. G.

Osborne, H. M. Pain, V. Šik, M. B. Hursthouse and M. A. Mazid, *J. Chem. Soc., Dalton Trans.*, 1993, 597.

[17] L. Sacksteder, A. P. Zipp, E. A. Brown, J. Streich, J. N. Demas and B. A. DeGraff, *Inorg. Chem.*, 1990, **29**, 4335.

[18] A. J. Amoroso, A. Banu, M. P. Coogan, P. G. Edwards, G. Hossain and K. M. A. Malik, *Dalton Trans.*, 2010, **39**, 6993.

[19] (*a*) D. Astruc, *Bull. Chem. Soc. Jpn*, 2007, **80**, 1658; (*b*) M.-P. Santoni, G. S. Hanan, B. Hasenknopf, A. Proust, F. Nastasi, S. Serroni and S. Campagna, *Chem. Commun.*, 2011, **47**, 3586; (*c*) M. P. Santoni, A. K. Pal, G. S. Hanan, A. Proust and B. Hasenknopf, *Inorg. Chem.*, 2011, **50**, 6737 (*d*) M. P. Santoni, F. Nastasi, S. Campagna, G. S. Hanan, B. Hasenknopf and I. Ciofini, *Dalton Trans,* 2013, **42**, 5281; (*e*) M.-P. Santoni, G. S. Hanan, B. Hasenknopf, *Coord. Chem. Rev.*, 2014, **281**, 64–85.

Chapitre 7 – Visible and near-IR emissions from k^2N- and k^3N-terpyridine rhenium(I) assemblies obtained by an [n x 1] head-to-tail bonding strategy

7.1. Résumé

Une stratégie de type tête-à-queue [n × 1] a été utilisée pour la synthèse des métallocycles de Re(I). À partir d'un précurseur de type *k*^{3}*N*-dicarbonyle, un seul ensemble discret [4 × 1] a été isolé et caractérisé, alors que le précurseur de type *k*^{2}*N*-tricarbonyle a conduit à deux ensembles majeurs, un carré et un triangle de type [3 × 1]. Une étude de diffraction des rayons X à l'état solide a confirmé la distorsion angulaire élevée (71° à 96°) des précurseurs de type *k*^{2}*N*-. La réversibilité électrochimique de l'assemblage triangulaire (5) et des carrés (6, 7) est augmentée par rapport à celle de leurs précurseurs. L'étude photophysique a confirmé des déplacements prononcés vers le rouge dans les émissions des complexes de type *k*^{3}*N*-dicarbonyle **4** (935 nm) et **7** (980 nm), confirmées par la théorie fonctionnelle de la densité (DFT) et les calculs DFT en fonction du temps (TD-DFT).

Contribution :

Baptiste Laramée-Milette : Synthèse et caractérisation complète du ligand et des complexes métalliques. Analyse structurelle par diffraction des rayons X, étude computationnelle, analyse des propriétés optiques et électroniques. Rédaction de l'article.

Francesco Palomba: Analyse de la luminescence dans le proche IR.

Nelsi Zaccheroni: Analyse de la luminescence dans le proche IR, révision de l'article.

Garry S. Hanan: Supervision, révision de l'article.

Visible and near-IR emissions from k^2N- and k^3N-terpyridine rhenium(I) assemblies obtained by an [nx1] head-to-tail bonding strategy

Baptiste Laramée-Milette,[a] *Nelsi Zaccheroni,*[b] *Francesco Palomba*[b] *and Garry S. Hanan*[a]*

[a]Département de chimie, Université de Montréal, 5155 Ch. de la rampe, Pavillon J.-A. Bombardier, Montréal, Québec, Canada, H3T 2B1

[b]Dipartimento di chimica, « Giacomo Ciamician », Università di Bologna, Via Selmi 2, 40126, Bologna, Italy

*: E-mail: garry.hanan@umontreal.ca

Full paper

Published online: 12th April 2017

DOI: 10.1002/chem.201700077

Reproduced with permission from *Chem. Eur. J.* **2017**, *23*, 6370-6379

Copyright 2017 Wiley-VCH Verlag GmbHH & Co. kGaA, Weinheim

7.2. Table of content graphic

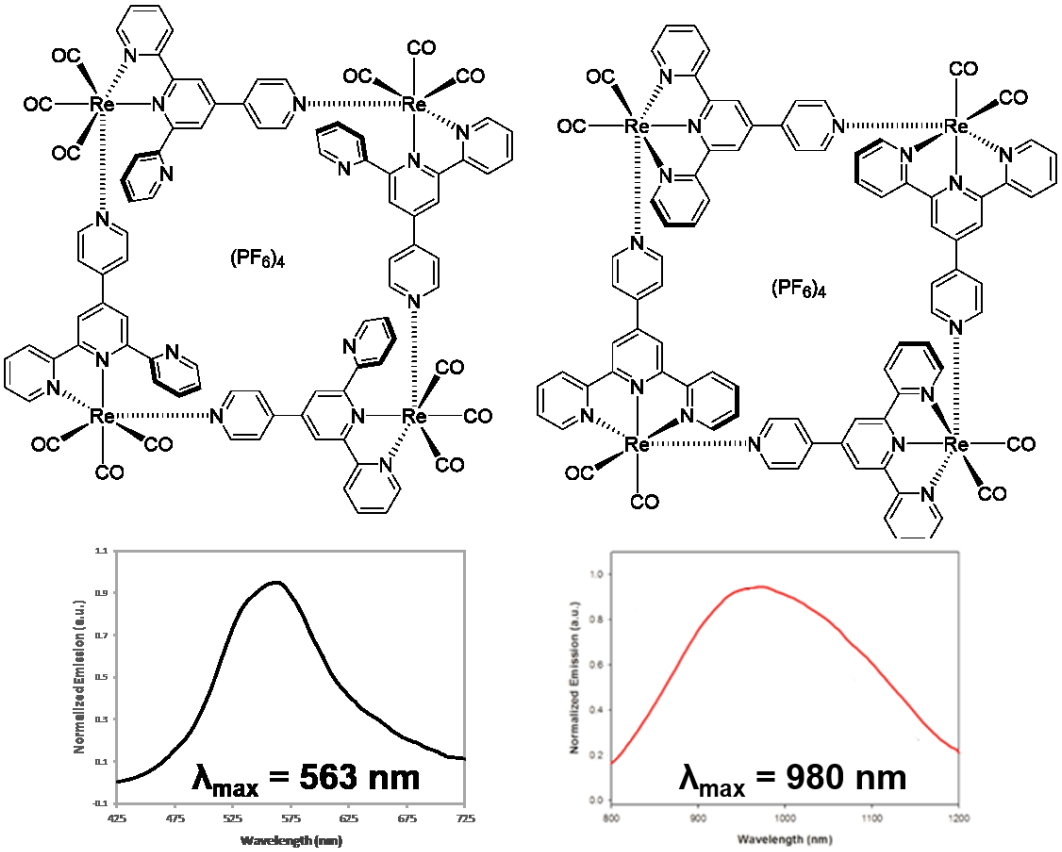

7.3. Abstract

An [n × 1] head-to-tail bonding strategy has been used for the synthesis of Re(I) metallacycles. From a k^3N-dicarbonyl precursor, a single discrete [4 × 1] square assembly was isolated and characterized, whereas a k^2N-tricarbonyl precursor led to two major species, a square and a [3 × 1] triangular assembly. Solid-state X-ray diffraction study has confirmed the high angular distortion (71° to 96°) of the k^2N precursors. The electrochemical reversibility of the triangular (5) and square (6, 7) assemblies is increased with respect to that of their precursors. Photophysical investigation has confirmed pronounced red-shifts in the emissions of the k^3N-dicarbonyl species **4** (935 nm) and **7** (980 nm), as confirmed by density functional theory (DFT) and time-dependent DFT (TD-DFT) calculations.

7.4. Introduction

Since their first report in the early 1970s,[1] emissive low-spin d^6 polypyridyl rhenium(I) carbonyl complexes have drawn intense interest from the scientific community. Over the last decades, most attention has been devoted to the study of the photoluminescence properties of the *fac*-Re(I)(NN)$(CO)_3$X species (where NN is a bidentate-diimine ligand and X is a halogen or a monodentate ligand such as a pyridine or phosphine derivative)[2] and their use as potential chemosensors,[3] OLEDs,[4] biological probes,[5] catalysts[6] and photocatalysts.[7] Moreover, the well-defined coordination angle formed by the *fac*-triscarbonyl species have been exploited for the self-assembly of several metallacycles[8] as well as metallaprisms.[9] The simplicity of the synthesis of the Re precursors and their supramolecular assemblies as well as the facile tuning of their optical properties by varying the bidentate ligand certainly contributed to the rise in popularity of this class of compound.

Surprisingly, there are few studies that have emphasized the closely related *cis*-dicarbonyl rhenium species. As shown in Figure 7.1, one of the earliest examples is a tris-phosphine derivative reported in the early 1970s by Moelwyn-Hughes and co-workers[1a] while *cis*-dicarbonyl Re(I) complexes with nitrogen donor ligands (such as 2,2'-bipyridine, 2,2':6',2''-terpyridine, bisiminopyridine, thioarylazoimidazole as well as PNN pincer ligand)[2g, 10] have only been reported in the past decade. Even though there is no evidence that these types of complexes display photoluminescence in ambient conditions, their inherent absorption properties through the entire visible portion of the electromagnetic spectrum is of interest and could lead to the development of chromophores able of efficient light-harvesting for energy conversion/storages purposes.

In that light, our group has recently presented the synthesis and characterization of both k^2N- and k^3N-terpyridine rhenium(I) building blocks which,[10e] owing to the inherent rigidity of the 4'-(pyridin-4-yl)-2,2':6',2''-terpyridine (4-pytpy) ligand, could further self-assemble using a [n x 1] head-to-tail bonding strategy in which the metal complexes acted as their own ligand.[11] Our interest in using this simple procedure derived from the fact that the conventional [n + n] approach required a perfect synergy between the metallic acceptor and the organic donor moiety in order to synthesise the desired assemblies[12] while the [n x

1] approach needs a single component to react with itself. Moreover, due to the harsh synthetic conditions (sealed tube at 280ºC for 8 hours under inert gas) for the key k^3N-derivative building block, one could not envisage the conversion of k^2N to k^3N post-self-assembly of the k^2N-metallasquare.

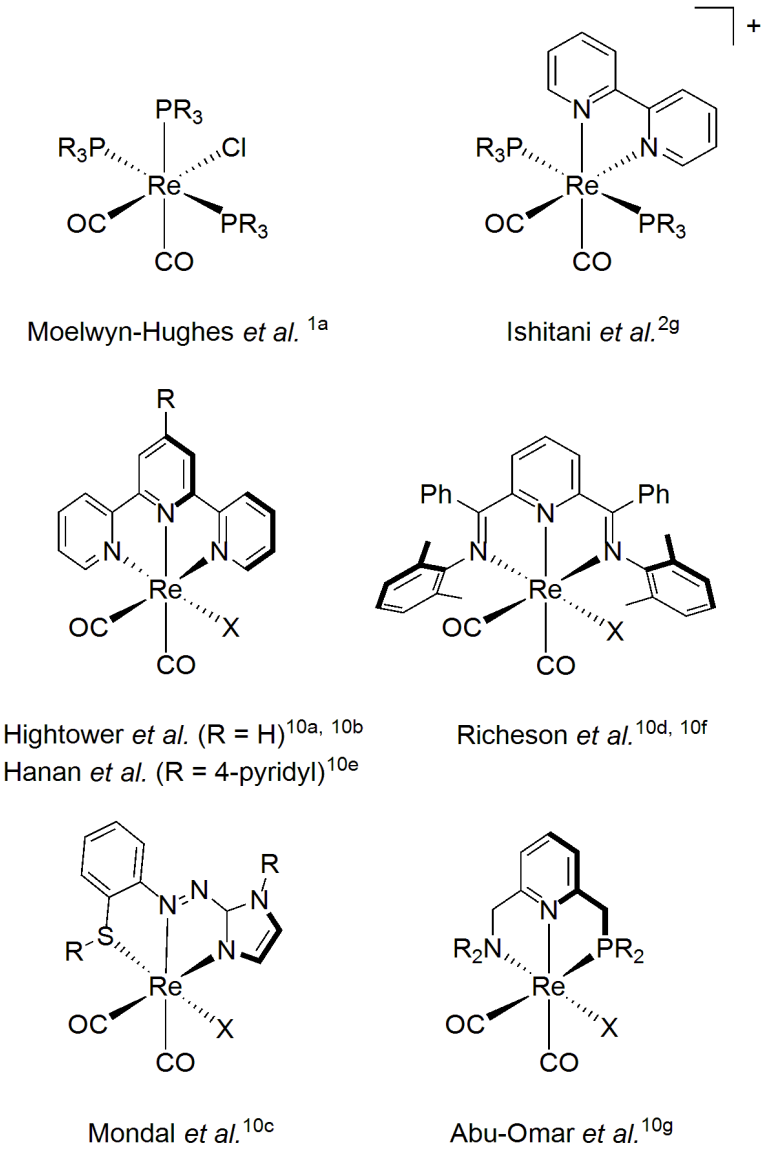

Figure 7.1 - Selected examples of *cis*-dicarbonyl Re(I) complexes.

As expected, the resulting k^3N-Re(I) dicarbonyl species displays extended absorption through the visible spectrum, reaching up to 800 nm, which is red-shifted by nearly 300 nm compared to its k^2N- analogue. Nevertheless, the k^2N-assembly caught our attention since it appears that the metallomacrocycle is quite stable electrochemically as compared to its halogenated precursor, as experiments showed

that up to six fully reversible reduction processes could be observed without signs of decomposition (such as quasi- or irreversible processes) of the aforementioned species.

Considering the interesting properties of both the k^2N- and k^3N-metal complexes, including near-IR emission, there is great interest in pursuing the investigation of the Re(I) terpyridyl chromophores in more depth. In this paper, we report the synthesis of a triangular-shaped k^2N-metallacycle and its optical and electrochemical properties. We also compare the properties of the k^2N- and k^3N-assemblies to their respective model complexes. The single-crystal X-ray diffraction study of the triangle macrocycle is also presented along with density functional theory (DFT) and time-dependant density functional theory (TD-DFT) calculations.

7.5. Results and discussion

7.5.1. Synthesis

The ligand 4-pytpy and metal complexes **1**-**4** were prepared according to previously published literature procedures (Scheme 7.1).[10a, b, 13] The species were isolated in average to good yields and were purified by recrystallization. The k^2N-assemblies (Scheme 7.2, top) were prepared in average yield using the methodology described in the literature, where precursor **1** was first reacted in a 1:1 ratio with silver triflate, used as a dehalogenating agent. Due to the coordinating nature and large excess of acetonitrile in which the reaction is taking place, the formation of the desired assemblies was not observed. After a few hours, the mixture was cooled to ambient temperature, filtered to remove the AgBr precipitate, and was evaporated to dryness.

A solvent mixture consisting of less coordinating solvents, such as acetone:toluene in a 1:1 ratio, was added to the flask and the solution was left at reflux for several hours. After the reaction, the solvent was removed under vacuum and the residue was subject to a column purification by size-exclusion chromatography, taking place over a 2 meter long Sephadex LH-20 column with an inner diameter of 5 cm, using a solvent combination of acetonitrile:methanol:water in a 45:45:10 ratio. Special care has to be taken during the elution, since the first and second band to elute (the square and triangle metallacycles, respectively) are very close due to their similar size.

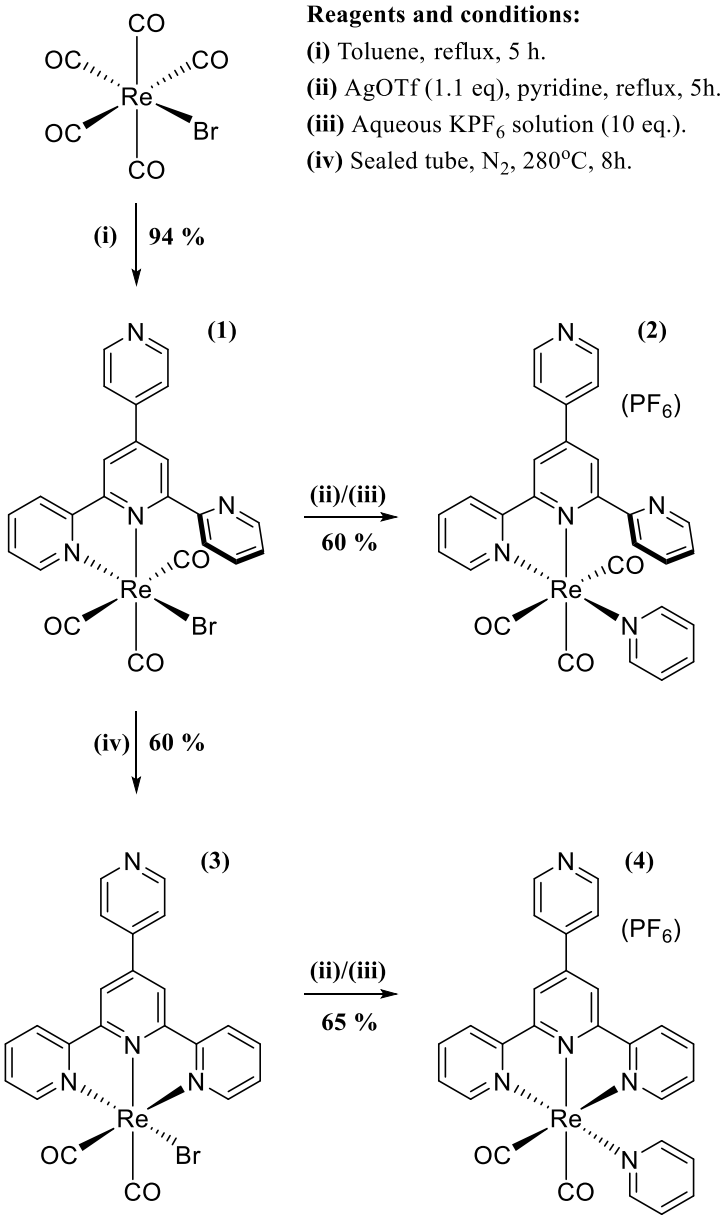

Scheme 7.1 - Synthesis of the Re(I) precursors and model complexes.

A second purification using the same elution conditions was done with some of the fractions in order to obtain the pure compounds. Despite all our efforts, the Re(I) k^2N-metallasquare did not crystallize, presumably due to the presence of four isomers induced by the free pyridyl moiety of the terpyridine ligand (up-up-up-up, up-up-up-down, up-up-down-down and up-down-up-down). Nonetheless, the k^2N-metallatriangle did crystallize, even though two different isomers (up-up-up and up-up-down) can co-exist for the same reasons mentioned above. The fractions collected

after the size-exclusion chromatography column were left to slowly evaporate over a few days, leading to the formation of small crystals which were suitable for single-crystal X-ray diffraction studies. In a similar fashion, the k^3N-metallasquare was synthesized in a two-step one-pot procedure, using the same experimental procedure as described for the k^2N-assemblies (Scheme 7.2, bottom). The macrocycle was obtained in very good yield. Single crystals of the k^3N-square were obtained after slow evaporation of a mixture of an acetone:MeOH:H_2O (45:45:10) over several days. Despite the fact that a k^3N-triangular species was detected by high-resolution mass spectrometry (HR-MS), we were not able to isolate and characterize it, even after scaling up the reaction.

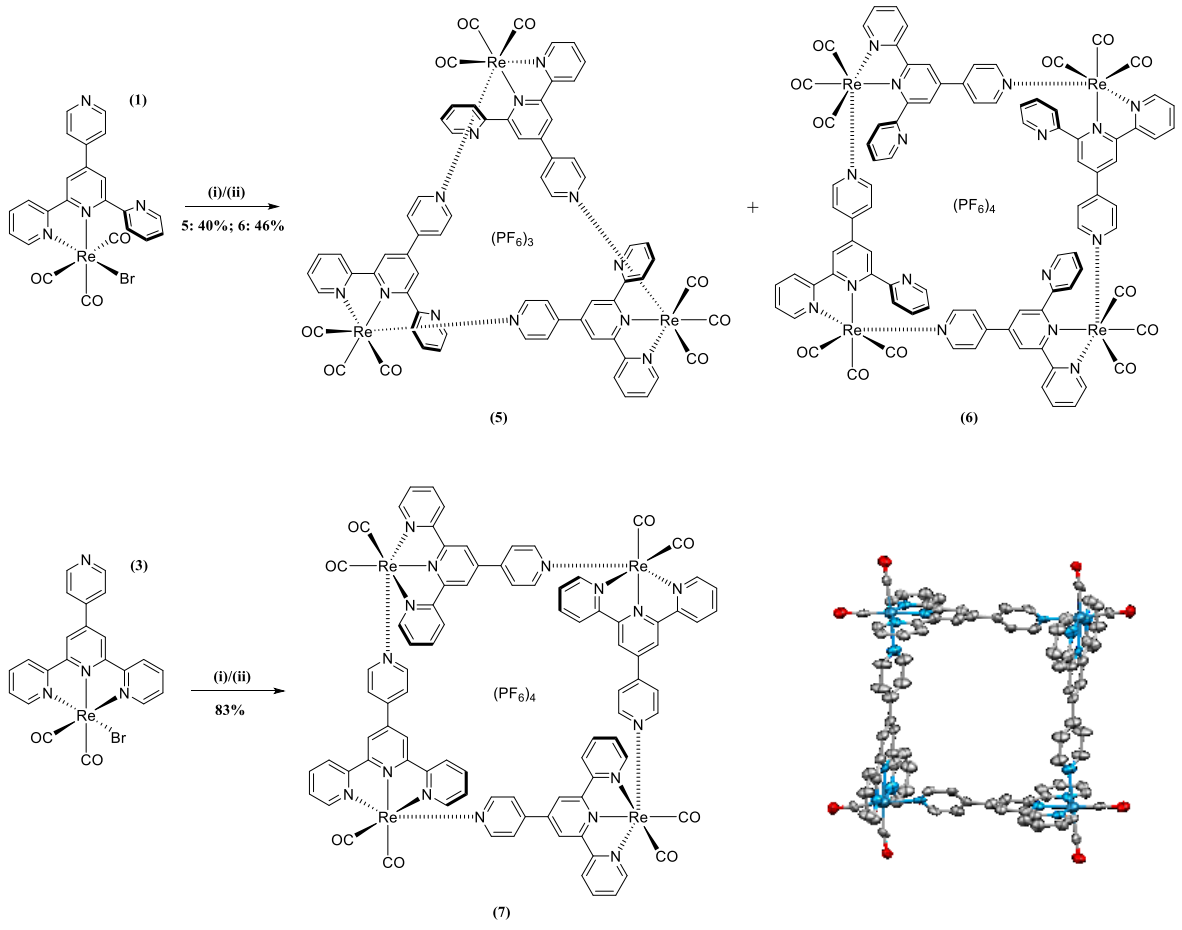

Scheme 7.2 - Synthesis of the self-assembled Re(I) [n x 1]-metallacycles from the k^2N- and k^3N-terpyridine precursor (Reagents and conditions: (i) AgOTf (1.1 eq), MeCN, reflux, 5h; (ii) Reflux in acetone/toluene (1:1), N_2, 10-12 h) and X-ray structure of **7**. The counter-anions and the hydrogen atoms were omitted for clarity.

7.5.2. ^{1}H and DOSY NMR spectroscopy

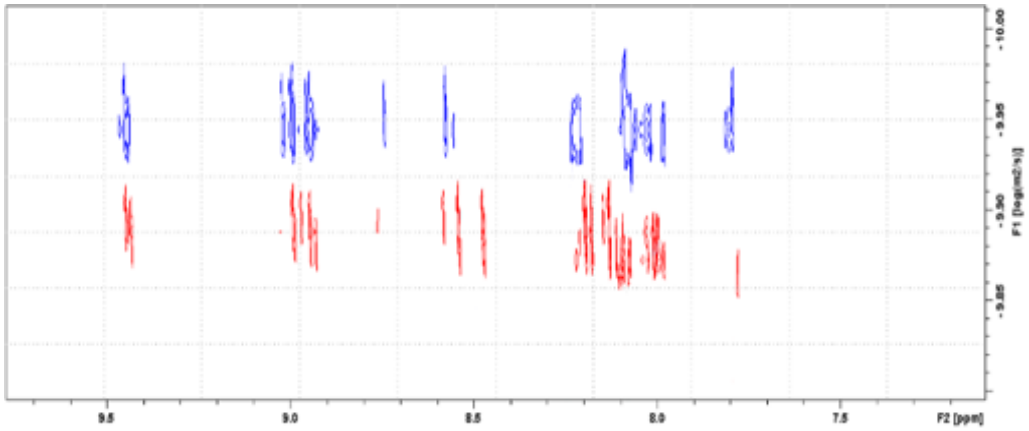

Figure 7.2 - Representative DOSY NMR spectroscopy comparison of the k^3N-metallatriangle **5** (red) and the k^2N-metallasquare **6** (blue) in DMSO-d_6.

As expected, due to the formation of several isomers during the synthesis of the k^2N-species (two isomers for a k^2N-triangle and four isomers for a k^2N-square), it is difficult to obtain insight on the nature of the k^2N-metallcycles by ^{1}H NMR analysis considering that the ^{1}H NMR spectra of both species are virtually identical. Therefore, diffusion-ordered NMR spectroscopy experiments were conducted on both isolated fractions (Figure 7.2), since it is known that the size of a species and its diffusion coefficient in solution are correlated through the use of the Stokes-Einstein equation ($D = k_BT/6\pi\eta r_H$), assuming near-spherical entities.[14] As expected, the first species to elute displays a lower diffusion coefficient, $D_1 = 1.14\text{x}10^{-10}$ m^2/s, compared to the second species, which exhibit a diffusion coefficient of $D_2 = 1.35\text{x}10^{-10}$ m^2/s. Further identification of the species by high-resolution mass spectrometry revealed that the first species to elute from the sephadex column was assigned as a k^2N-metallasquare while the second species was found to be a k^2N-metallatriangle.

From a mathematical point of view, we know that the circumcircle radius of a square (r_s) and an equilateral triangle (r_t) are defined as:

$r_s = a/\sqrt{2}$

$r_t = a/\sqrt{3}$

Where "a" is the length of the sides.

From these formulas, the ratio between the two circumcircle radii is found to be:

$r_t/r_s = (a/\sqrt{3})/(a/\sqrt{2}) = 0.82$.[15]

Therefore, one can expect that the ratio of the diffusion coefficient of the triangular and square species found by DOSY NMR to be approximately equal to the previously mentioned value. In our specific example, we have found that $D_2/D_1 = 0.84$, which is in excellent agreement with the theoretical value. The case of the k^3N-square assembly is more straightforward in the analysis of the ^{1}H NMR data, which due to the symmetry of the molecule (C_{4h}), considerably simplifies the NMR spectrum where only a few broadened peaks were observed. The DOSY NMR of the single fraction obtained after purification displayed a diffusion coefficient of 0.97×10^{-10}, close to the value obtained for the k^2N-square.

7.5.3. Solid state X-ray characterization

Detailed analysis of the crystallographic data was performed with the goal of rationalizing the formation of both the metallatriangle and metallasquare when starting with the k^2N-precursor, while only the metallasquare is obtained from the k^3N- building block. Detailed crystallographic parameters as well as selected bond distances are tabulated in Table 14.1 and Table 7.1, respectively.

Crystals suitable for X-ray diffraction studies were obtained for the model complex **2** (Figure 7.3). As expected, the metal complex adopts a distorted octahedral geometry around the metal core with the three carbonyls in a *facial* configuration. The uncoordinated pyridyl ring of the terpyridine ligand is significantly out-of-plane compared to the other part of the ligand, with a N(2)-C(13)-C(14)-N(3) torsion angle of -83.8 (4)°. The loss of co-planarity is mainly due to steric hindrance between the free

pyridyl ring and the C(2)-O(2) carbonyl ligand lying under it, where a careful analysis of the solid-state data reveals a strong metal-carbonyl···π(aryl) interaction.[16] The centroid-to-centroid distance between the free pyridyl ring and the CO ligand is 3.05(1) Å.

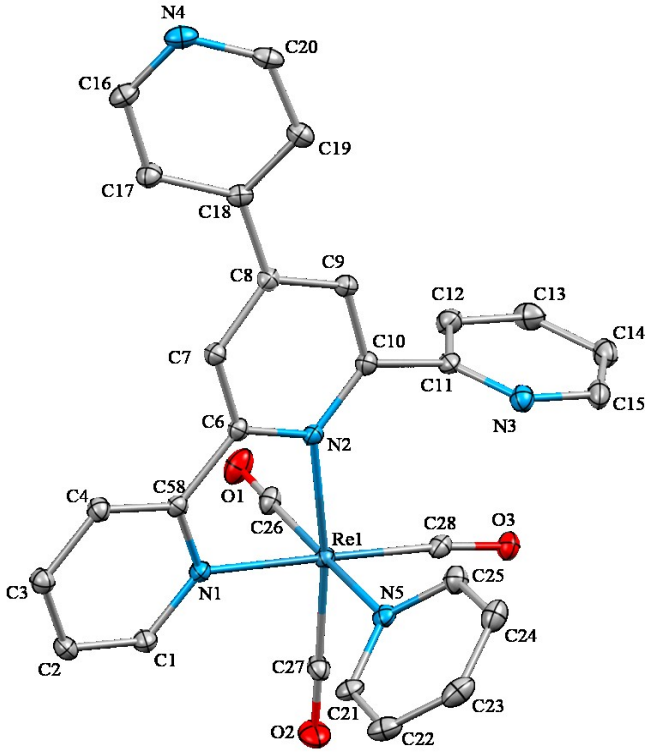

Figure 7.3 - X-ray crystal structure of 2. The counter-anion (PF6) and the hydrogen atoms were omitted for clarity. The ellipsoids are drawn at a 30% probability.

As shown in Table 7.1, the removal of the carbonyl ligand at the equatorial position (*cis* to the pyridine ligand) does not affect the CO ligand in the axial position, however, all the other ligands linked to the metal core are significantly influenced. More precisely, a longer C(26)-O(1) bond distance is observed in the k^3N- complex (1.171(4) Å *vs* 1.146(4) Å in **2**), indicating a reduced carbon-oxygen bond strength, while an increase of the pi-backbonding is confirmed by a smaller C(26)-Re(1) bond distance with 1.883(3) Å and 1.938(3) Å in the k^3N- and k^2N- complexes, respectively. Accordingly, the Re(1)-N(5) bond between the rhenium core and the pyridine ligand *trans*- to C(26)-O(1) is longer in **4**. As depicted in Figure 7.4, the solid state data shows that the tpy-Re-

py plane angle in both model complexes is almost perfect for the synthesis of a molecular square, with 96º and 81º in the k^2N- and k^3N- complexes, respectively. However, the steric hindrance found in complex **2** severely affects the coordination angle (71º),[17] which is closer to the angle required for achieving a molecular triangle, while the k^3N-species displays a coordination angle of 89º.

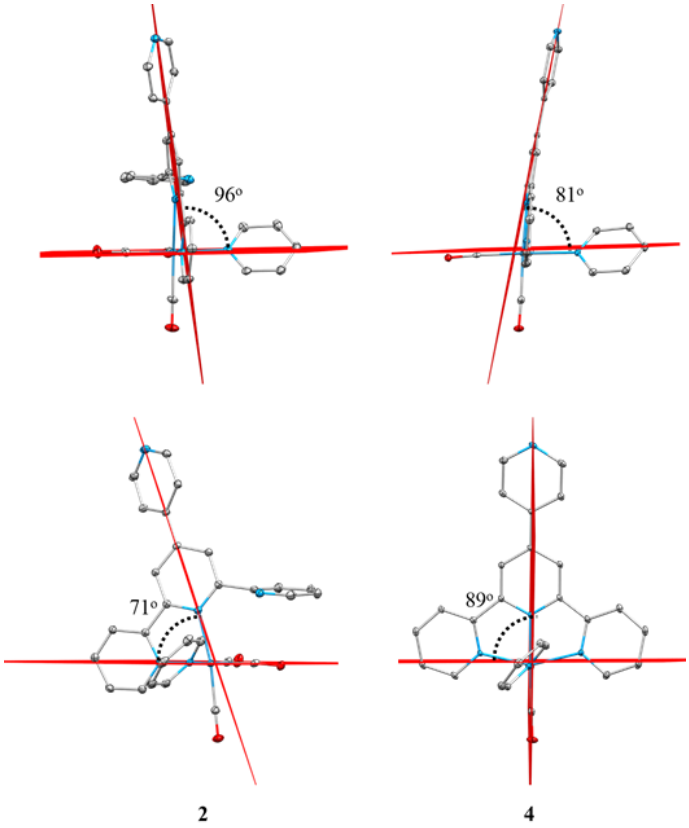

Figure 7.4 - Comparison of the tpy-Re-py plane angle (top) and the coordination angle (bottom) in model complexes 2 and 4.

It is worth mentioning that in contrast to the k^3N-type complexes' rigidity, the coordination angle found in **2** is far from being static: the fluxionality in solution of terpyridine ligands (through either associative "tick-tock" twist or isomerisation mechanisms) in k^2N-rhenium complexes is well known.[18] Therefore, due to the flexibility of the k^2N-building blocks, one can expected a mixture of k^2N-assemblies while the more rigid k^3N-species should lead to a single preferred species.

Despite the fact that two different isomers can co-exist owing to the position of the free pyridyl group (up or down), we obtained crystals of the triangular-shaped k^2N-macrocycle. It is interesting to note that regardless of the statistical probability of finding the up-up-down (UUD) isomer as the major species, only the up-up-up (UUU) species crystallized in the conditions mentioned earlier. Nevertheless, we cannot exclude the probability that the UUD isomer was also synthesized.

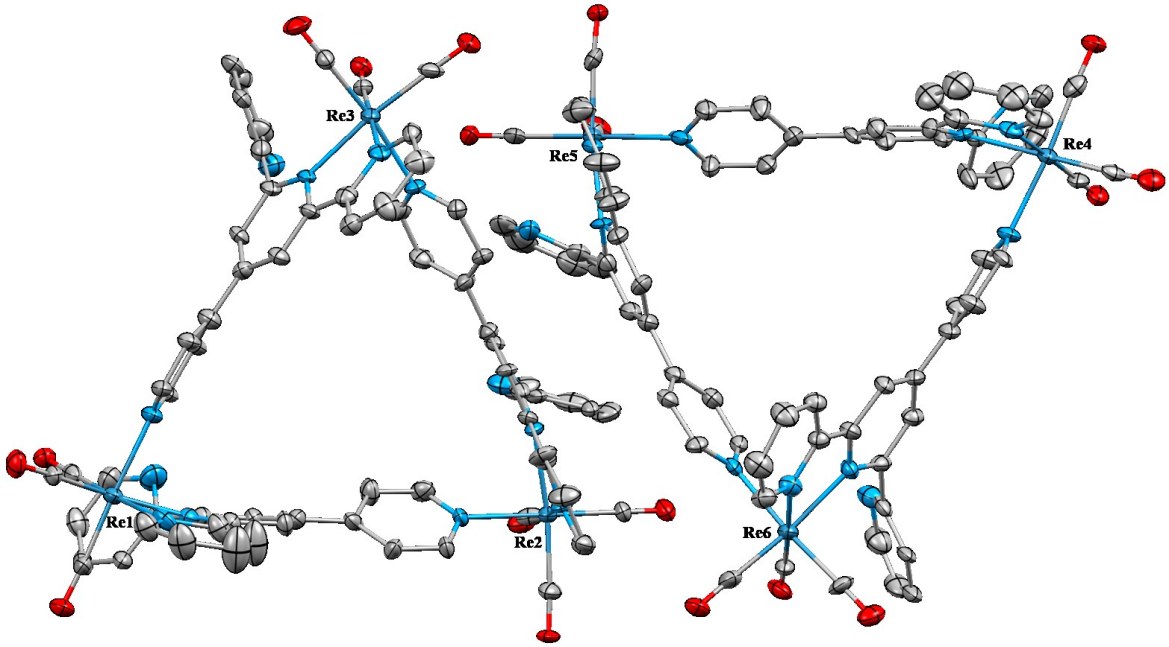

Figure 7.5 - X-ray crystal structure of 5 depicting the self-assembled k^2N-metallatriangle. The counter-anions (NO_3^-) and the hydrogen atoms were omitted for clarity. The ellipsoids are drawn with a 30% probability.

As depicted in Figure 7.5, the asymmetric unit is occupied by two metallacycles. Due to significant disorder in the crystal structure (twinning) and since the counter-anions were not exchanged before crystallization, we assigned the residual electronic density to NO_3^- counter-anions. Despite much effort, we failed in growing better quality crystals with other counter-anions.

As expected, the coordination geometry around the rhenium centers can be described as slightly distorted octahedral. The angles formed by the central pyridyl ring of the terpyridine units, the metals and the pyridyl rings from the backbone of the ligands (N_{tpy}-Re-N_{4py}) in metal complex **5** range between 79.8-82.2º, which a priori would not suggest the formation of a molecular triangle. It is worth mentioning that the same angles found in the k^3N-square are slightly wider, ranging between 82.9-85.1º. As in the case of model complex **2**, the coordination angle in the triangular assemblies are more acute, with values oscillating between 52.3-66.9º. These values are significantly different from those of the k^3N-square, where the measured angles range between 80.1-84.3º. As in the case of model complex **2**, the observed angular differences are primarily due to steric hindrance between the free pyridyl groups and the carbonyl ligand *trans* to the peripheral pyridyl coordinated to the rhenium center. Therefore, we established that a loss of rigidity in the building block when going from the k^3N- to the k^2N- adduct as well as steric influences and an entropic factor could explain the formation of a molecular triangle. Nevertheless, since the angular parameters are also propitious for the synthesis of a square assembly, both species were obtained.

Table 7.1 - Selected bond lengths obtained from X-ray diffraction and DFT results from geometry optimizations.

Bond type	**2**		**4**	
	X-ray (Å)	DFT (Å)	X-ray (Å)	DFT (Å)
N(1)-Re(1)	2.169(2)	2.147	2.129(1)	2.112
N(2)-Re(1)	2.213(2)	2.187	2.056(1)	2.068
N(5)-Re(1)	2.210(3)	2.194	2.242(3)	2.227
C(26)-Re(1)	1.938(3)	1.913	1.883(3)	1.887
C(27)-Re(1)	1.915(3)	1.906	1.911(4)	1.886
C(26)-O(1)	1.146(4)	1.183	1.171(4)	1.199
C(27)-O(2)	1.150(4)	1.185	1.159(4)	1.200

7.5.4. Infrared spectroscopy

The characteristic carbonyl stretching vibration was probed by infrared spectroscopy and the data are tabulated in Table 7.2 along with their calculated frequencies values obtained via density functional theory (DFT) computational studies. The calculated values for both k^2N-metallacycles were obtained for all their structural isomers (up/down variations of the free pyridyl units). While the tabulated values are an average of the frequencies obtained by the DFT method, the difference observed among the isomers of the same species was < 2 cm^{-1} and thus considered negligible. As expected, the k^2N- complex **1** exhibit three distinct stretching vibrations between ca. 1880-2020 cm^{-1} while only two bands are observed for model complex **2** and the metallacycles **5-6**. Nevertheless, it is worth mentioning that the band found at ca. 1910-1920 cm^{-1} is broad compared to the other one.

The calculated infrared data correlate very well this observation, where in the case of complex **2**, two bands are found in close proximity around 1883-1891 cm^{-1} while complexes **5-6** show a broad calculated band at ca. 1880-1900 cm^{-1}. The results found for the k^2N-species are in good agreement with the values reported for other k^2N-terpyridine *fac*-rhenium tricarbonyl species.[18g, 19] In a similar fashion, the experimental infrared spectrum of the k^3N-species displays two strong stretching vibrations between ca. 1800-1900 cm^{-1}, which is consistent with the theoretical data as well as with previously studied rhenium dicarbonyl species.[10a, 20]

Table 7.2 - Infrared ν(C≡O) frequencies and comparison to their DFT calculated values.

Cmpd	exp. ν(C≡O)[a] / cm^{-1}	calc. ν(C≡O) / cm^{-1}
2	2033, 1918 (br.)	2013, 1891, 1883
4	1905, 1834	2004, 1936
5	2033, 1917 (br.)	2014, 1894-1888 (br.)
6	2030, 1909 (br.)	2015, 1897-1883 (br.)
7	1907, 1834	1891, 1814

[a]Infrared spectra were acquired in the solid state.

7.5.4. Spectroscopic and theoretical studies

The absorption spectra of model complexes **2** and **4** as well as their corresponding assemblies **5**-**7** are shown in Figure 7.6 and their data are summarized in Table 7.3. In order to understand the nature of the electronic transitions, theoretical calculations at the density functional theory (DFT) and time-dependent DFT (TD-DFT) level were performed, using the PBE0 functional with inclusion of acetonitrile solvent by the conductor-like polarization continuum model (CPCM). The calculated spectra (see supporting information) were simulated by convolution of computed vertical excitation using Gaussian broadening, where the area of the bands are proportional to the calculated oscillator strength. It is worth mentioning that minor differences were observed between the isomers of the k^2N-assemblies. Therefore, the calculated spectra are depicted as a combination of all the isomers, where the ratio of each isomer has been determined via a probabilistic reasoning of their occurrence in solution.

Table 7.3 - Optical properties of the metal complexes and the references in acetonitrile.

#	Absorption	Luminescence		Lifetime
		Exp. (298K)	Calcd.	
	λ_{max}/nm (ε, x10^4 $M^{-1}cm^{-1}$)	λ_{max}/nm	λ_{AE}/nm	τ/ns
2	254 (3.42), 278 (2.59), 330 (1.31), 381 (0.40)	564	611	3.5
4	237 (1.85), 252 (1.92), 280 (2.78), 285 (3.27) 326 (2.47), 387 (0.44), 487 (0.54), 713 (0.08)	940	993	ND[a]
5	252 (6.53), 278 (4.42), 331 (3.04), 381 (1.59)	546	617	3.6
6	252 (9.96), 278 (6.79), 334 (4.85), 381 (2.53)	563	629	3.4
7	237 (7.03), 252 (6.82), 280 (8.10), 285 (9.06), 327 (7.37), 387 (1.83), 466 (2.57), 712 (0.17)	980	1040	ND[a]

[a]ND = the response of our NIR detector is too slow to allow time resolved measurements.

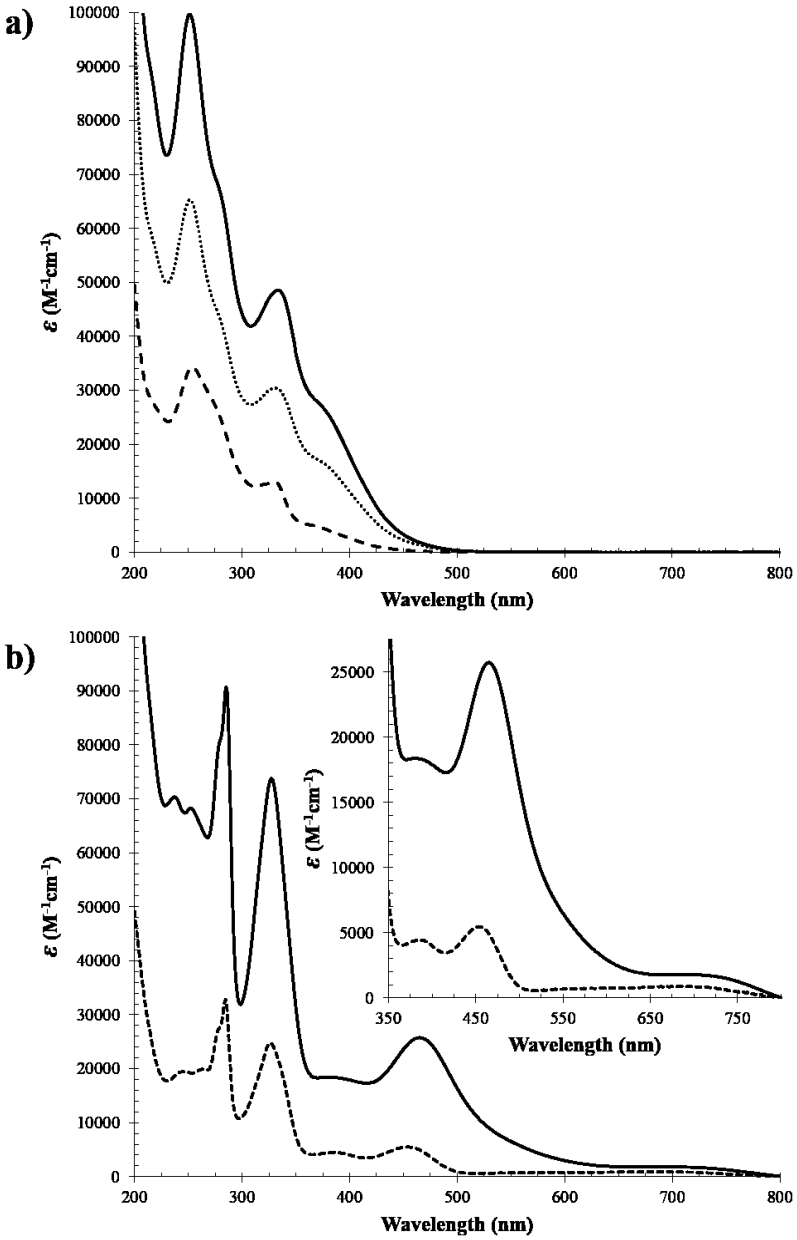

Figure 7.6 - UV-visible spectra of the a) k^2N-series (complex 2 (dash); metallatriangle 5 (dot); metallasquare 6 (plain)) as well as b) the k^3N-series (complex 4 (dash); metallasquare 7 (plain)) recorded in dilute acetonitrile solution.

As depicted in Figure 7.7, it is interesting to note how the simple removal of one carbonyl ligand from the metal core affects the energy level of the highest occupied molecular orbital (HOMO). In the case of the rhenium tricarbonyl species **2**, **5** and **6**, the

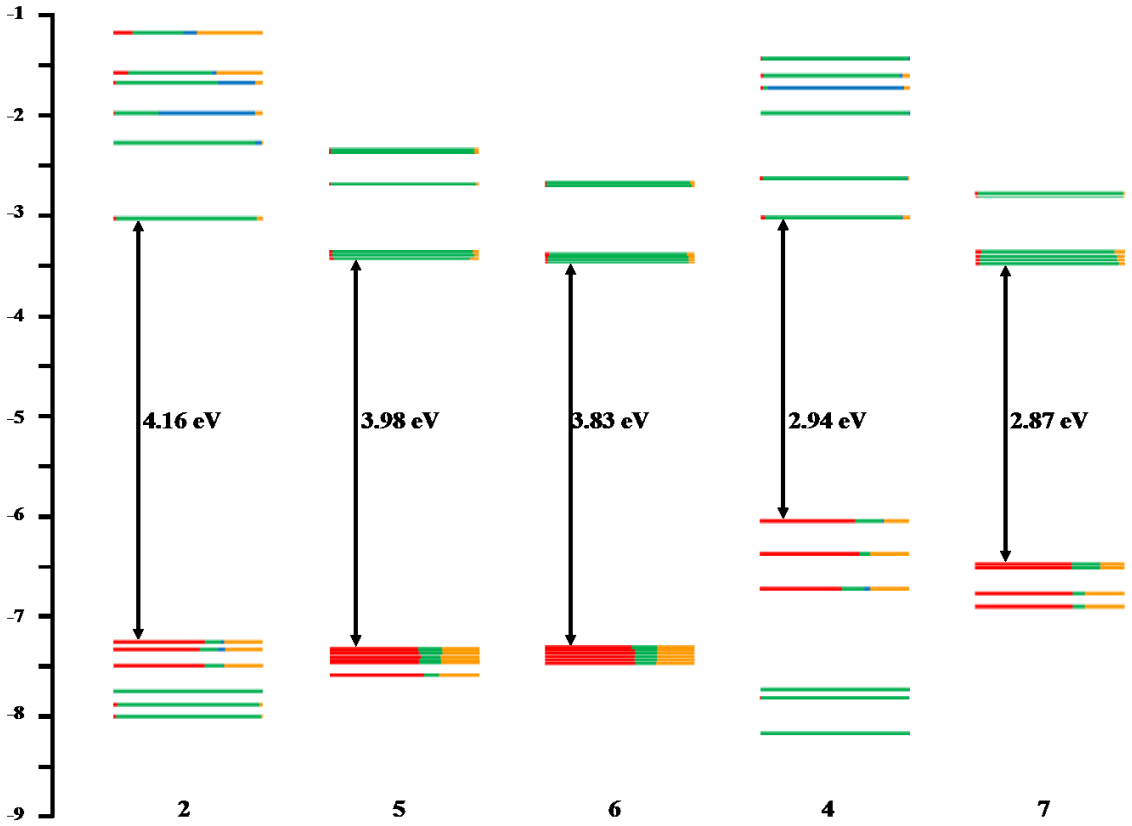

Figure 7.7 - Molecular orbital energy diagram comparing the k^2N- and the k^3N- species along with their HOMO-LUMO gap. The colour code defines the total contribution to the orbital from the rhenium (red), the 4-pytpy (green), the pyridine (blue) as well as the carbonyl ligands (yellow). In the case of the k^2N-metallotriangle and square, the average contribution of the different isomers is reported, since no major difference were observed between each isomers of a same species.

energy of the HOMO ranges from -7.3 to -7.4 eV, which is stabilized by more than 1 eV compared to the rhenium dicarbonyl equivalent, where the energy of the HOMO ranges between -6.1 and -6.2 eV. This observation is in good agreement with the spectrochemical series since strong-field ligands such as CO are known to efficiently stabilize the metal ion through π-backbonding, which is not as strong in the case of a pyridine-type ligand. The first distinguishable low-lying singlet-singlet absorption bands in the k^2N-complexes range between 350-500 nm and have as an origin the

HOMO→LUMO (91%) and HOMO-1→LUMO (85%) transitions (HOMO = highest-occupied molecular orbital, LUMO = lowest-unoccupied molecular orbital). It is best described as a combination of $^1MLCT_{tpy}$ (MLCT = metal-to-ligand charge-transfer) and $^1LLCT_{CO\rightarrow tpy}$ (LLCT = ligand-to-ligand charge-transfer).

The higher energy absorption band observed between 300-350 nm originates from HOMO-4→LUMO (85%), HOMO-5→LUMO (90%) and HOMO-1→LUMO-1 (80%) transitions and can be defined as a combination of $^1MLCT_{tpy}/^1MLCT_{CO}/^1LLCT_{CO\rightarrow tpy}$ character. The shoulder found around 275-300 nm as well as 200-225 nm are mainly constituted of a mixture of $^1MLCT_{tpy}/^1MLCT_{py}/\ ^1LLCT_{CO\rightarrow tpy}/^1LLCT_{CO\rightarrow py}$ character while the main transition found between 225-275nm is purely defined by $^1MLCT_{py/tpy/CO}$ character. The origin of the first band is not as clear in the case of the metallacycles, where several orbitals (ranging from the HOMO-8 up to LUMO+2) are found to be responsible for the observed transitions. As in the model complex, the absorption band can be described as a mixture of $^1MLCT_{tpy}$ and $LLCT_{CO\rightarrow tpy}$. The structure of the second band is slightly different compared to the model complex. While there is evidence of both $^1MLCT_{tpy}$ and $^1LLCT_{CO\rightarrow tpy}$ character, there is no sign of contribution from the metal core to the carbonyl ligands. It is also interesting to note some intra-ligand charge transfer (^{1}ILCT) from the terpyridine part of the ligand to the pyridyl backbone, which was not observed in the k^2N-model. The shoulder found between 275-300 nm possesses $^1MLCT_{tpy}$ and $^1LLCT_{CO\rightarrow tpy}$ character. Finally, the transition between 225-275 nm is only $^1MLCT_{tpy}$ character, without contribution of the CO ligands.

Similarly, the character of the lowest-lying absorption band found in k^3N-complexes around 600-800 nm is best described as a mixture of $^1MLCT_{tpy}/^1LLCT_{co\rightarrow tpy}$. It is worth noting the important difference in the molar absorbance between 500-600 nm (defined as a mixture of $^1MLCT_{tpy}/^1LLCT_{co\rightarrow tpy}$ character) in the metallasquare ($1x10^4$ $M^{-1}cm^{-1}$) compared to the model complex ($1x10^3$ $M^{-1}cm^{-1}$), which is ascribed to the synergy among the components of the self-assembly. Finally, the three main bands found between 300-500 nm are also a combination of $^1MLCT_{tpy}/^1LLCT_{co\rightarrow tpy}$ character while the feature around 275 nm is mostly $^1MLCT_{tpy}/^1MLCT_{CO}/\ ^1LLCT_{CO\rightarrow tpy}$ character.

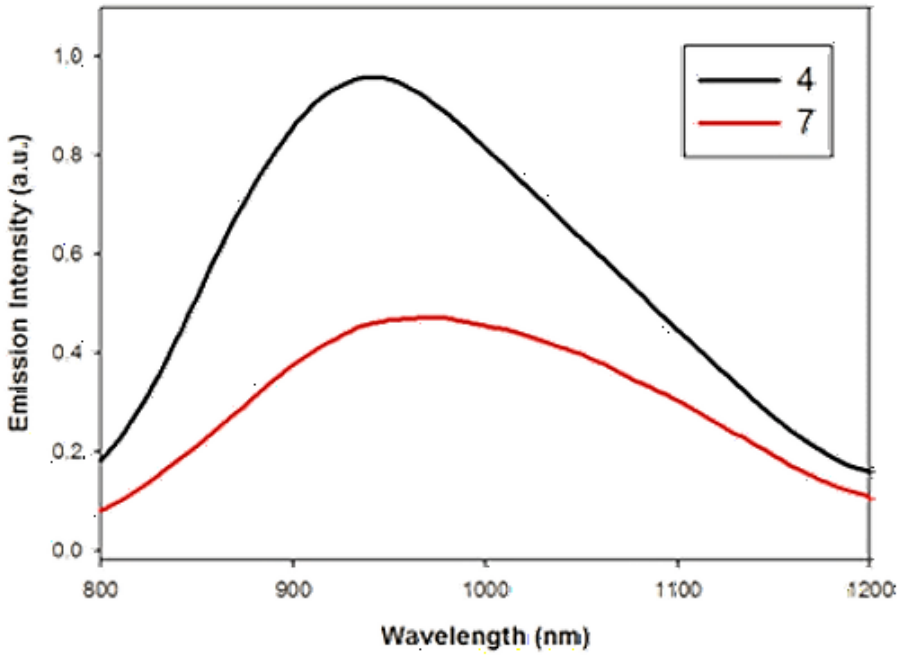

Figure 7.8 - Emission spectra of the k^3N-series compound **4** and **7** recorded in acetonitrile solutions at room temperature.

7.5.5. Luminescence spectroscopy

The emission properties of the Re(I) complexes were thoroughly investigated in degassed acetonitrile solution at ambient temperature and the data are tabulated in Table 7.3. All the k^2N-species are found to be luminescent in these experimental conditions. The luminescence of all the complexes is broad and tails up to 600-650 nm. The maximum of luminescence (λ_{max}) of the k^2N-model is found around 565 nm. Similarly, the luminescence of the metallatriangle is centred at 545 nm, slightly blue-shifted compared to the metallasquare with $\lambda_{max} \approx 565$ nm. As shown in Table 7.3, the calculated adiabatic electronic emission (λ_{AE}), which correspond to the energy gap between the optimized T_1 geometry and the ground state S_0, slightly overestimate the luminescence wavelength by about 50-70 nm. As reported earlier, the k^3N-species were not found to be emissive at room temperature up to 800 nm.[10a, b, e] Therefore, we conducted luminescence studies on the k^3N-species in the infrared region (Figure 7.8, Figure 14.16 and Table 14.25). The experimental λ_{max} measured for complex **4** and the assembly **7** are 940 nm and 980 nm, respectively, which is in good agreement with theoretical

approximation obtained on the triplet states of the k^3N-complexes (Table 7.3 and Table 14.26). Theoretical adiabatic emission (λ_{AE}) calculated by DFT predict that the luminescence for both the precursor and the square assembly should occur at wavelength near 993 nm and 1040 nm, respectively.

Table 7.4 – Optical properties of the metal complexes and the references in acetonitrile.

Cmpd	Absorption	Luminescence		Lifetime
		Exp. (298K)	Calcd.	
	λ_{max}/nm (ε, x10^4 M^{-1}cm^{-1})	λ_{max}/nm	λ_{AE}/nm	τ/ns
2	254 (3.42), 278 (2.59), 330 (1.31), 381 (0.40)	564	611	3.5
4	237 (1.85), 252 (1.92), 280 (2.78), 285 (3.27), 326 (2.47), 387 (0.44), 487 (0.54), 713 (0.08)	940	993	ND[a]
5	252 (6.53), 278 (4.42), 331 (3.04), 381 (1.59)	546	617	3.6
6	252 (9.96), 278 (6.79), 334 (4.85), 381 (2.53)	563	629	3.4
7	237 (7.03), 252 (6.82), 280 (8.10), 285 (9.06), 327 (7.37), 387 (1.83), 466 (2.57), 712 (0.17)	980	1040	ND[a]

[a]Not detected: the response of our NIR detector is too slow to allow time resolved measurements.

7.5.6. Electrochemical studies

The cyclic voltammetry study on the assemblies and their precursors was carried out in dry degassed DMF solutions at ambient temperature, using NBu_4PF_6 (0.1M) as the electrolyte. The peak potential (E_p) and peak potential difference (Δ) are tabulated in Error! Reference source not found.. A first reversible reduction wave was observed at -0.92 V in complex **2** which is attributable to the one-electron reduction of the tpy ligand. The second reduction process at -1.43 V, also assigned to the reduction of the tpy ligand, have limited chemical reversibility and further decomposition of the species is observed when returning to the initial potential. A single irreversible oxidation wave, assigned to the Re(I)/Re(II) couple was seen at 1.50 V. The $Re^{1+/2+}$ redox process was not observed in both complex **5** and **6** due to the limited working window of the solvent (1.7 V to -2.3 V). The striking difference between **2** and both triangular and square-shaped assemblies stand on the reversibility of the first six reduction waves observed in both macrocycles **5** and **6** (Figure 7.9).

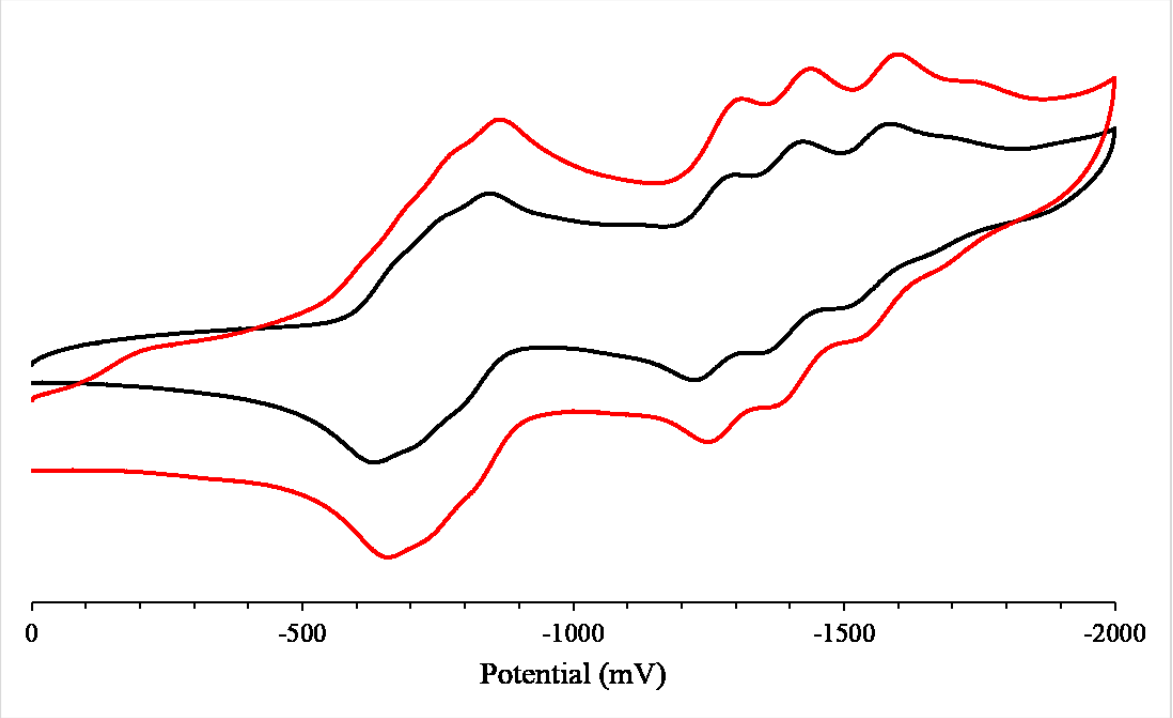

Figure 7.9 - Comparison of the cyclic voltammograms of the k^2N-square (red) and the triangle (black) at a 1 mM concentration, recorded in deaerated DMF in the presence of NBu_4PF_6 (0.1 M) at a sweep rate of 50 mV/s.

As in complex **2**, the consecutive reduction waves are assigned to the progressive reduction of the terpyridine ligands, however, strong delocalization throughout the assemblies allow enhanced electrochemical stabilities. Interestingly, the same trend is not observed in the k^3N-series where both model **4** and assembly **7** displays limited chemical reversibility or an irreversible reduction process at -0.94 V and -0.81 V, respectively. An irreversible $Re^{1+/2+}$ oxidation process is observed at 0.86 V in the model metal complex **4**. It is somewhat surprising that complex **7** exhibits two reversible oxidation waves (0.53 V and 0.71 V), followed by a third irreversible process at 0.87 V. As observed in the reduction of the k^2N-assemblies, we postulate that the stability within the k^3N-macrocycle differs substantially compared to the model complex alone. Therefore, it is possible that the oxidation of the metal ions at low potential does not instantly lead to further degradation of the species.

7.5.7. Conclusions

The [n x 1] head-to-tail bonding strategy was successfully applied in the synthesis of three Re(I) assemblies. A comprehensive investigation of the solid-state structure of the model complexes was conducted. We have determined that the steric hindrance in the k^2N-building blocks is responsible for a more acute coordination angle. Nevertheless, we postulated that this angle is far from being variable due to the fluxionality of the ligand, therefore allowing the synthesis of both a metallasquare and a metallatriangle. The structure of the k^2N-triangle was confirmed by solid-state crystallographic measurements. The k^3N-building block, however, displays a more rigid skeleton, and only a self-assembled square was obtained. It is worth mentioning that the self-assemblies exhibit remarkable stability, where they preserved their integrity even in strong polar solvents such as DMSO, DMF and MeCN. The optical properties were investigated for all the complexes and compared to theoretical calculations. The k^2N-species were all emissive in ambient conditions, with their maximum of emission around 545-565 nm, tailing up to 650 nm and their luminescence lifetime ranging between 3-4 ns. The k^3N-complexes **4** and **7** were found emissive in the near-IR portion of the electromagnetic spectrum, with their maxima of 940 and 980 nm, respectively, close to the predicted values obtained by DFT calculations. Finally, the electrochemical properties of the complexes were investigated. Interestingly, the assemblies resulting from the k^2N-building blocks proved to have greater electrochemical stability than the k^3N ones. We believe that the metallacycles analyzed in this study are of interest for photosensitizing applications as well as playing the role of electron reservoirs in hydrogen evolution reactions.

7.5.8. Acknowledgements

BLM and GSH thank the Natural Sciences and Engineering Research Council (NSERC) of Canada as well as the Fondation J.A. Bombardier and the Université de Montréal for financial support. The authors are also grateful to Compute Canada and UdeM NMR, EA and XRD facilities and staff for their help. NZ thanks the financial support by the Università degli Studi di Bologna (Progetto Studi di fattibilità FARB (NANOX)) and

also the program ERASMUS-MUNDUS Action 2 with the project NOVA DOMUS-CHEMEDPHO for the scholarship award that has helped this collaboration.

7.5.9. References

[1] a) J. T. Moelwyn-Hughes and A. W. B. Garner, *J. Chem. Soc.* **1971**, 2361-2370; b) M. Wrighton and D. L. Morse, *J. Am. Chem. Soc.* **1974**, *96*, 998-1003.

[2] a) K. Kalyanasundaram, *J. Chem. Soc., Faraday Trans. 2* **1986**, *82*, 2401-2415; b) L. A. Worl, R. Duesing, P. Chen, L. Ciana and T. J. Meyer, *J. Chem. Soc., Dalton Trans.* **1991**, 849; c) A. Coleman, C. Brennan, J. Vos and M. Pryce, *Coord. Chem. Rev.* **2008**, *252*, 2585-2595; d) A. Kumar, S.-S. Sun and A. J. Lees, *Photophysics and photochemistry of organometallic Rhenium diimine complexes*, Spinger GmbH, **2010**, p. 35; e) A. Juris, S. Campagna, I. Bidd, J. M. Lehn and R. Ziessel, *Inorg. Chem.* **1988**, *27*, 4007; f) P. J. Wright, M. G. Affleck, S. Muzzioli, B. W. Skelton, P. Raiteri, D. S. Silvester, S. Stagni and M. Massi, *Organometallics* **2013**, *32*, 3728-3737; g) H. Tsubaki, A. Sekine, Y. Ohashi, K. Koike, H. Takeda and O. Ishitani, *J. Am. Chem. Soc.* **2005**, *127*, 15544-15555.

[3] C. Wang, H. C. Lam, N. Zhu and K. M. Wong, *Dalton Trans.* **2015**, *44*, 15250-15263.

[4] a) G. Velmurugan and P. Venuvanalingam, *Dalton Trans.* **2015**, *44*, 8529-8542; b) T. Klemens, A. Switlicka-Olszewska, B. Machura, M. Grucela, E. Schab-Balcerzak, K. Smolarek, S. Mackowski, A. Szlapa, S. Kula, S. Krompiec, P. Lodowski and A. Chrobok, *Dalton Trans.* **2016**, *45*, 1746-1762.

[5] a) C. Metcalfe, C. Rajput and J. A. Thomas, *J. Inorg. Biochem.* **2006**, *100*, 1314-1319; b) F. L. Thorp-Greenwood, V. Fernández-Moreira, C. O. Millet, C. F. Williams, J. Cable, J. B. Court, A. J. Hayes, D. Lloyd and M. P. Coogan, *Chem. Commun.* **2011**, *47*, 3096-3098; c) Z.-B. Zheng, Y.-Q. Wu, K.-Z. Wang and F. Li, *Dalton Trans.* **2014**, *43*, 3273-3284.

[6] a) T. Yoshida, K. Tsutsumida, S. Teratani, K. Yasufuku and M. Kaneko, *J. Chem. Soc., Chem. Commun.* **1993**, 631; b) V. Yempally, W. Y. Fan, B. A. Arndtsen and A. A. Bengali, *Inorg. Chem.* **2015**, *54*, 11441-11449.

[7] a) J. Hawecker, J. M. Lehn and R. Ziessel, *Helv. Chim. Acta* **1986**, *69*, 1990-2012; b) H. Takeda and O. Ishitani, *Coord. Chem. Rev.* **2010**, *254*, 346-354; c) A. J. Huckaba, E. A. Sharpe and J. H. Delcamp, *Inorg. Chem.* **2016**, *55*, 682-690; d) Y. Ueda, H. Takeda, T. Yui, K. Koike, Y. Goto, S. Inagaki and O. Ishitani, *ChemSusChem* **2015**, *8*, 439-442; e) G. Sahara and O. Ishitani, *Inorg. Chem.* **2015**, *54*, 5096-5104.

[8] a) R. V. Slone, J. T. Hupp, C. L. Stern and T. E. Albrecht-Schmitt, *Inorg. Chem.* **1996**, *35*, 4096-4097; b) S. M. Woessner, J. B. Helms, Y. Shen and P. B. Sullivan, *Inorg. Chem.* **1998**, *37*, 5406-5407; c) S.-S. Sun and A. J. Lees, *Inorg. Chem.* **1999**, *38*, 4181-4182; d) S.-S. Sun and A. J. Lees, *J. Am. Chem. Soc.* **2000**, *122*, 8956-8967; e) T. Rajendran, B. Manimaran, F.-Y. Lee, P.-J. Chen, S.-C. Lin, G.-H. Lee, S.-M. Peng, Y.-J. Chen and K.-L. Lu, *J. Chem. Soc., Dalton Trans.* **2001**, 3346; f) S.-S. Sun, J. A. Anspach, A. J. Lees and P. Y. Zavalij, *Organometallics* **2002**, *21*, 685-693; g) S.-S. Sun, J. A. Anspach and A. J. Lees, *Inorg. Chem.* **2002**, *41*, 1862-1869; h) P.-H. Huang, J. T. Lin and M.-C. P. Yeh, *J. Organomet. Chem.* **2006**, *691*, 975-982; i) J. T. Hupp, *Struct. Bond.* **2006**, *121*, 145-165; j) M. Sathiyendiran, R.-T. Liao, P. Thanasekaran, T.-T. Luo, N. S. Venkataramanan, G.-H. Lee, S.-M. Peng and K.-L. Lu, *Inorg. Chem.* **2006**, *45*, 10052-10054; k) J.-Y. Wu, P. Thanasekaran, Y.-W. Cheng, C.-C. Lee, B. Manimaran, T. Rajendran, R.-T. Liao, G.-H. Lee, S.-M. Peng and K.-L. Lu, *Organometallics* **2008**, *27*, 2141-2144; l) R.-T. Liao, W.-C. Yang, P. Thanasekaran, C.-C. Tsai, M. Sathiyendiran, Y.-H. Liu, T. Rajendran, H.-M. Lin, T.-W. Tseng and K.-L. Lu, *Chem. Commun.* **2008**, 3175-3177; m) M. P. Coogan, V. Fernández-Moreira, B. M. Kariuki, S. J. A. Pope and F. L. Thorp-Greenwood, *Angew. Chem. Int. Ed.* **2009**, *48*, 4965-4968; n) Z.-Z. Lu, C.-C. Lee, M. Velayudham, L.-W. Lee, J.-Y. Wu, T.-S. Kuo and K.-L. Lu, *Chem. Eur. J.* **2012**, *18*, 15714-15721; o) D. Bhattacharya, *Inorg. Chem. Commun.* **2013**, *36*, 159-162; p) R. Nagarajaprakash, D. Divya, B. Ramakrishna and B. Manimaran, *Organometallics* **2014**, *33*, 1367-1373; q) B. Shankar, S. Sahu, N. Deibel, D. Schweinfurth, B. Sarkar, P. Elumalai, D. Gupta, F. Hussain, G. Krishnamoorthy and M. Sathiyendiran, *Inorg. Chem.* **2014**; r) R. Govindarajan, R. Nagarajaprakash and B. Manimaran, *Inorg. Chem.* **2015**, *54*, 10686-10694; s) J. Chen, K. H. Lee, H.

H. Y. Sung, I. D. Williams, Z. Lin and G. Jia, *Angew. Chem. Int. Ed.* **2016**, *128*, 7310-7314.

[9] a) B. Manimaran, P. Thanasekaran, T. Rajendran, R.-T. Liao, Y.-H. Liu, G.-H. Lee, S.-M. Peng, S. Rajagopal and K.-L. Lu, *Inorg. Chem.* **2003**, *42*, 4795-4797; b) D. Bhattacharya, C. H. Chang, Y. H. Cheng, L. L. Lai, H. Y. Lu, C. Y. Lin and K. L. Lu, *Chem. Eur. J.* **2012**, *18*, 5275-5283; c) P. Thanasekaran, C.-C. Lee and K.-L. Lu, *Acc. Chem. Res.* **2012**, *45*, 1403-1418; d) B. Shankar, P. Elumalai, S. Deval Sathiyashivan and M. Sathiyendiran, *Inorg. Chem.* **2014**, *53*, 10018-10020; e) B. Manimaran, A. Vanitha, M. Karthikeyan, B. Ramakrishna and S. M. Mobin, *Organometallics* **2014**, *33*, 465-472; f) R. Nagarajaprakash, R. Govindarajan and B. Manimaran, *Dalton Trans.* **2015**, *44*, 11732-11740; g) R. Nagarajaprakash, C. Kumar, S. M. Mobin and B. Manimaran, *Organometallics* **2015**, *34*, 724-730.

[10] a) D. R. Black and S. E. Hightower, *Inorg. Chem. Commun.* **2012**, *24*, 16-19; b) B. A. Frenzel, J. E. Schumaker, D. R. Black and S. E. Hightower, *Dalton Trans.* **2013**, *42*, 12440-12451; c) M. S. Jana, A. K. Pramanik, D. Sarkar, S. Biswas and T. K. Mondal, *J. Mol. Struct.* **2013**, *1047*, 73-79; d) T. Jurca, W. C. Chen, S. Michel, I. Korobkov, T. G. Ong and D. S. Richeson, *Chem. Eur. J.* **2013**, *19*, 4278-4286; e) B. Laramée-Milette, C. Lachance-Brais and G. S. Hanan, *Dalton Trans.* **2015**, *44*, 41-45; f) P. Bulsink, A. Al-Ghamdi, P. Joshi, I. Korobkov, T. Woo and D. Richeson, *Dalton Trans.* **2016**, *45*, 8885-8896.

[11] a) T. Kajiwara and T. Ito, *J. Chem. Soc., Chem. Commun.* **1994**, 1773-1774; b) N. Matsumoto, Y. Motoda, T. Matsuo, T. Nakashima, N. Re, F. Dahan and J.-P. Tuchagues, *Inorg. Chem.* **1999**, *38*, 1165-1173; c) R. F. Carina, A. F. Williams and G. Bernardinelli, *Inorg. Chem.* **2001**, *40*, 1826-1832; d) T. Brasey, R. Scopelliti and K. Severin, *Inorg. Chem.* **2005**, *44*, 160-162; e) J. J. Fernández, A. Fernández, D. Vázquez-García, M. López-Torres, A. Suárez, N. Gómez-Blanco and J. M. Vila, *Eur. J. Inorg. Chem.* **2007**, *2007*, 5408-5418; f) S.-B. Zhao, R.-Y. Wang and S. Wang, *J. Am. Chem. Soc.* **2007**, *129*, 3092-3093; g) J. Aimi, Y. Nagamine, A. Tsuda, A. Muranaka, M. Uchiyama and T. Aida, *Angew. Chem. Int. Ed.* **2008**, *47*, 5153-5156; h) R. A. Jensen, R. F. Kelley, S. Lee, M. R. Wasielewski, J. T. Hupp and D. M. Tiede, *Chem. Commun.* **2008**, 1886-1888; i) S. A. Willison, J. A. Krause

and W. B. Connick, *Inorg. Chem.* **2008**, *47*, 1258-1260; j) R. Lomoth and S. Ott, *Dalton Trans.* **2009**, 9952-9959; k) P. D. Frischmann, S. Guieu, R. Tabeshi and M. J. MacLachlan, *J. Am. Chem. Soc.* **2010**, *132*, 7668-7675; l) S. Perera, X. Li, M. Guo, C. Wesdemiotis, C. N. Moorefield and G. R. Newkome, *Chem. Commun.* **2011**, *47*, 4658-4660; m) P. D. Frischmann, B. J. Sahli, S. Guieu, B. O. Patrick and M. J. MacLachlan, *Chemistry - A European Journal* **2012**, *18*, 13712-13721; n) L. H. Tong, S. Clifford, A. Gomila, S. Duval, L. Guénée and A. F. Williams, *Chem. Commun.* **2012**, *48*, 9891-9893; o) P. J Wright, S. Muzzioli, B. W. Skelton, P. Raiteri, J. Lee, G. Koutsantonis, D. S. Silvester, S. Stagni, M. Massi, *Dalton Trans.*, **2013**, *42*, 8188; p) A. Behnia, P. D. Boyle, M. A. Fard, J. M. Blacquiere and R. J. Puddephatt, *Dalton Trans.* **2016**, *45*, 19485-19490.

[12] a) R. Chakrabarty, P. S. Mukherjee and P. J. Stang, *Chem. Rev.* **2011**, *111*, 6810-6918; b) T. R. Cook and P. J. Stang, *Chem. Rev.* **2015**, *115*, 7001-7045.

[13] G. S. Hanan and J. Wang, *Synlett* **2005**, 1251-1254.

[14] W. H. Otto, M. H. Keefe, K. E. Splan, J. T. Hupp and C. K. Larive, *Inorg. Chem.* **2002**, *41*, 6172-6174.

[15] S. Goeb, S. Bivaud, P. I. Dron, J. Y. Balandier, M. Chas and M. Salle, *Chem. Commun.* **2012**, *48*, 3106-3108.

[16] a) J. Zukerman-Schpector, I. Haiduc and E. R. Tiekink, *Chem. Commun.* **2011**, *47*, 12682-12684; b) C. Murcia-García, A. Bauzá, G. Schnakenburg, A. Frontera and R. Streubel, *CrystEngComm* **2015**, *17*, 1769-1772; c) C. Murcia-García, A. Bauzá, A. Frontera and R. Streubel, *CrystEngComm* **2015**, *17*, 6736-6743.

[17] a) E. R. Civitello, P. S. Dragovich, T. B. Karpishin, S. G. Novik, G. Bierach, J. F. O'Connell and T. D. Westmoreland, *Inorg. Chem.* **1993**, *32*, 237; b) Q. Ge, T. C. Corkery, M. G. Humphrey, M. Samoc and T. S. Hor, *Dalton Trans.* **2009**, 6192-6200.

[18] a) E. W. Abel, V. S. Dimitrov, N. J. Long, K. G. Orrell, A. G. Osborne, H. M. Pain, V. Sik, M. B. Hursthouse and M. A. Mazid, *J. Chem. Soc., Dalton Trans.* **1993**, 597; b) P. A. Anderson, R. F. Keene, E. Horn and E. R. T. Tiekink, *Appl. Organomet. Chem.* **1990**, *4*, 523-533; c) E. W. Abel, A. Gelling, K. G. Orrell, A. G. Osborne and V. Sik, *Chem. Commun.* **1996**, 2329; d) A. Gelling, K. G. Orrell,

A. G. Osborne and V. Šik, *J. Chem. Soc., Dalton Trans.* **1998**; e) A. Gelling, M. D. Olsen, K. G. Orrell and A. G. Osborne, *J. Chem. Soc., Dalton Trans.* **1998**, 3479; f) E. W. Abel, N. J. Long, K. G. Orrell, A. G. Osborne, H. M. Pain and V. Sik, *J. Chem. Soc. , Chem. Commun.* **1992**, 303; g) V. Fernandez-Moreira, F. L. Thorp-Greenwood, R. J. Arthur, B. M. Kariuki, R. L. Jenkins and M. P. Coogan, *Dalton Trans.* **2010**, *39*, 7493-7503.

[19] a) Q. Ge, C. T. Corkery, M. G. Humphrey, M. Samoc and A. T. S. Hor, *Dalton Trans.* **2009**, 6192-6200; b) A. J. Amoroso, A. Banu, M. P. Coogan, P. G. Edwards, G. Hossain and A. K. M. Malik, *Dalton Trans.* **2010**, *39*, 6993-7003.

[20] B. A. Frenzel, J. E. Schumaker, D. R. Black and S. E. Hightower, *Dalton Trans.* **2013**, *42*, 12440-12451.

Chapitre 8 – Light-induced self-assembly of a luminescent tetraruthenium square

8.1. Résumé

L'auto-assemblage est un puissant outil synthétique qui a conduit au développement d'architectures multi-dimensionnelles. Des MOFs aux flacons moléculaires, les matériaux auto-assemblés se sont révélés très intéressants pour la communauté scientifique. Par la présente, nous décrivons une stratégie pour la construction et la déconstruction d'une structure supramoléculaire grâce à l'auto-assemblage et au désassemblage induit par la lumière. La combinaison de deux approches, une stratégie de liaison directrice [n x 1] et une stratégie de photo-dissociation du ligand, permet l'auto-assemblage induit par la lumière d'un précurseur de type polypyridyle Ru(II) en un carré moléculaire unique. La spectroscopie RMN DOSY confirme la synthèse d'une espèce de volume élevé, tandis que l'identité de l'espèce a été clairement établie par spectrométrie de masse à haute résolution et études de diffraction des rayons X sur un monocristal. Il est à noter que le carré auto-assemblé n'est pas obtenu par des techniques thermiques classiques dans des conditions similaires, mais n'est obtenu que par une simple irradiation lumineuse. Le carré de tetraruthenium a une durée de vie de l'état excitée (135 ns) 40 fois celle de son précurseur mononucléaire et son rendement quantique (1,0%) est supérieur de trois ordres de grandeur. Ces propriétés de luminescence remarquables sont étroitement liées à la structure carrée relativement rigide de l'assemblage de tétraruthénium, comme le suggère la spectroscopie d'absorption transitoire. Les résultats décrits ici sont un exemple rare de processus d'auto-assemblage et de désassemblage induits par la lumière, et peuvent ouvrir la voie à une nouvelle branche de la chimie supramoléculaire, conduisant à la préparation de supermolécules structurellement organisées par des techniques photochimiques.

Contribution :

Baptiste Laramée-Milette : Synthèse et caractérisation complète du ligand et des complexes métalliques. Analyse structurelle par diffraction des rayons X, étude computationnelle, analyse des propriétés optiques et électroniques. Rédaction de l'article.

Francesco Nastasi and Fausto Puntoriero: Analyse par absorption transitoire et écriture de la section associée dans l'article.

Sebastiano Campagna: Révision de l'article.

Garry S. Hanan: Supervision, révision de l'article.

Photo-induced assembly of a luminescent tetraruthenium square

Baptiste Laramée-Milette,[a] Francesco Nastasi,[b] Fausto Puntoriero,[b] Sebastiano Campagna[b] and Garry S. Hanan[a]**

[a]Département de chimie, Université de Montréal, 5155 Ch. de la rampe, Pavillon J.-A. Bombardier, Montréal, Québec, Canada, H3T 2B1

[b]Dipartimento di Scienze Chimiche, Biologiche, Farmaceutiche ed Ambientali, Università di Messina, and Centro di ricerca interuniversitario per la conversione chimica dell'energia solare (SOLAR-CHEM), 98166, Messina, Italy

*: E-mail: garry.hanan@umontreal.ca

*: E-mail: campagna@unime.it

Full paper

Published online: 18th september 2017

DOI: 10.1002/chem.201702714

Reproduced with permission from *Chem. Eur. J.* **2017**, *23*, 16497-16504

Copyright 2017 Wiley-VCH Verlag GmbHH & Co. kGaA, Weinheim

8.2. Front cover

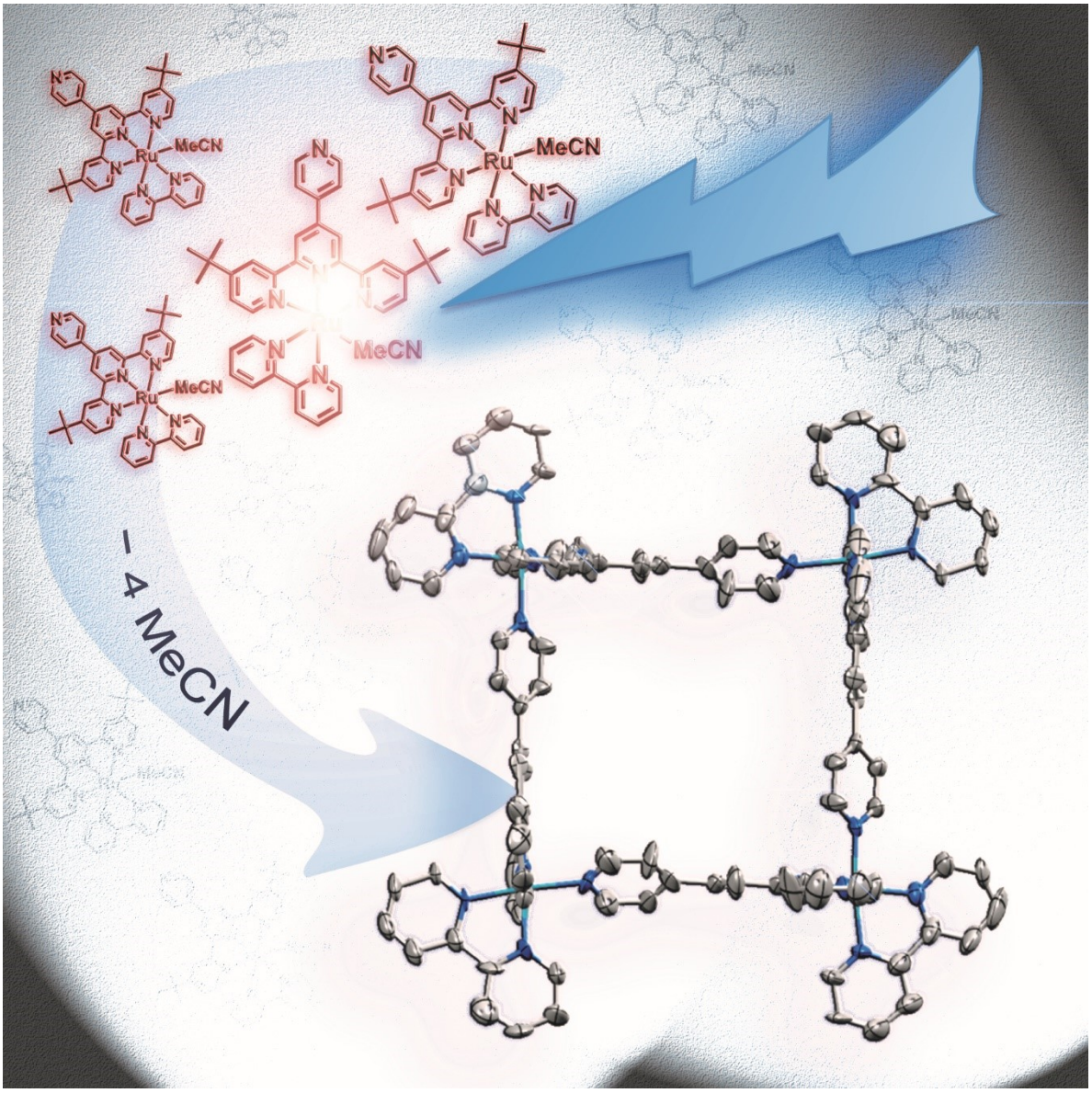

8.3. Table of content graphic

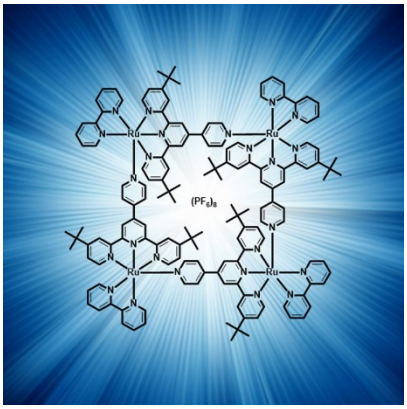

8.4. Abstract

Self-assembly is a powerful synthetic tool that has led to the development of one-, two- and three-dimensional architectures. From MOFs to molecular flasks, self-assembled materials have proven to be of great interest to the scientific community. Here we describe a strategy for the construction and de-construction of a supramolecular structure through unprecedented photo-induced assembly and dis-assembly. The combination of two approaches, a [n x 1]-directional bonding strategy and a ligand photo-dissociation strategy, allows the photo-induced assembly of a polypyridyl Ru^{II} precursor into a discrete molecular square. Diffusion-ordered NMR spectroscopy confirmed the synthesis of a higher volume species, while the identity of the species was established by high-resolution mass spectrometry and single-crystal X-ray diffraction studies. The self-assembled square is not obtained by classical thermal techniques in similar conditions, but is obtained only by light-irradiation. The tetraruthenium square has an excited-state lifetime (135 ns) 40 times that of its mononuclear precursor and its luminescence quantum yield (1.0%) is three orders of magnitude higher. These remarkable luminescence properties are closely related to the relatively rigid square structure of the tetraruthenium assembly, as suggested by slow radiationless decay and transient absorption spectroscopy. The results described herein are a rare example of photo-induced assembly and dis-assembly processes, and can open the way to a new avenue in supramolecular chemistry, leading to the preparation of structurally-organized supermolecules by photochemical techniques.

8.5. Introduction

Since the pioneering work of Pederson, Cram and Lehn in the 1960's and 70's,[1, 2] the field of supramolecular chemistry has attracted considerable interest from the scientific community, where the judicious design of simple building blocks has led to the synthesis of a wide library of supramolecular assemblies. More specifically, the work performed in the early 1990's by Fujita and Stang furthered the concept of metal-directed self-assembly,[3, 4] which led to the development of one, two- and three-dimensional architectures.[4d, 5] Surprisingly, despite the tremendous amount of discrete structures in the literature, the main way to achieve self-assembly is through thermally activated processes. In this work, we present another route in the synthesis of ruthenium polypyridyl discrete assemblies,[6] that of photo-induced assembly.

The mechanism of photo-ejection of a ligand is well known in the literature[7] and has been applied for several purposes, such as the induction of geometrical changes,[8] photochromic switching,[9] photosubstitution reactions,[7b, 10] and light-driven motions.[11] As an alternative to the classical thermal synthesis of discrete assemblies, Fujita *et al.* briefly investigated the photo-induced assembly of Pt^{II} macrocyles through the photo-labilization of a monodentate ligand (Chart 8.1). The discrete species, however, were only observed in the case of non-conjugated ligands and no reversibility of the assembly was shown.[3f] In a similar fashion, Ishitani *et al.* recently worked on ring-shaped rhenium(I) complexes which required the photo-irradiation of the precursor to induce the photo-ejection of a carbonyl ligand.[12] Nevertheless, the precursor had to be heated at reflux to achieve the desired discrete assemblies, with no disassembly process possible.

a)

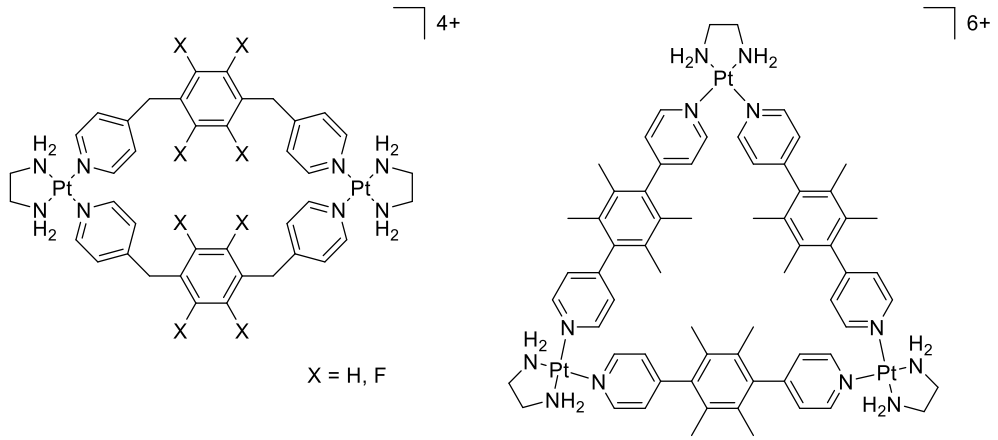

Fujita *et al.* [11]

b)

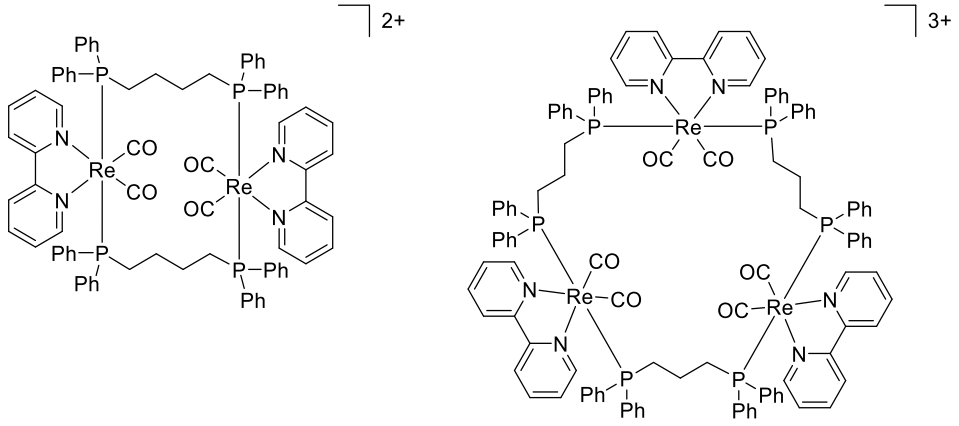

Ishitani *et al.* [12]

Chart 8.1 - Selected examples of metallacycles obtained by a) light-induced self-assembly and b) light-assisted synthesis.

With the goal of extending the available synthetic pathways to achieve self-assembly, we have combined our recent work on head-to-tail assemblies with the photo-ejection of monodentate ligands through light irradiation.[10j, 13] We report herein the rare assembly and dis-assembly of a discrete metallocyclic structure exclusively through light-irradiation of the precursor, a simple ruthenium polypyridyl complex.

8.6. Results and Discussion

8.6.1. Synthetic procedures

The synthesis of the precursor for the assembly was obtained in three straightforward steps (Scheme 8.1). The substituted di-*tert*-butyl-terpyridine ligand was used to maintain solubility during the photo-assembly process. Initially, 1 equivalent of $RuCl_3.3H_2O$ was heated in the presence of 1 equivalent of 4,4”-di-*t*Bu-4’-pyridin-4’”-yl-2,2’:6’,2”-terpyridine ligand (4-pytpy)[14] in refluxing mixture of DCM/EtOH (9:1) for 3 hours to

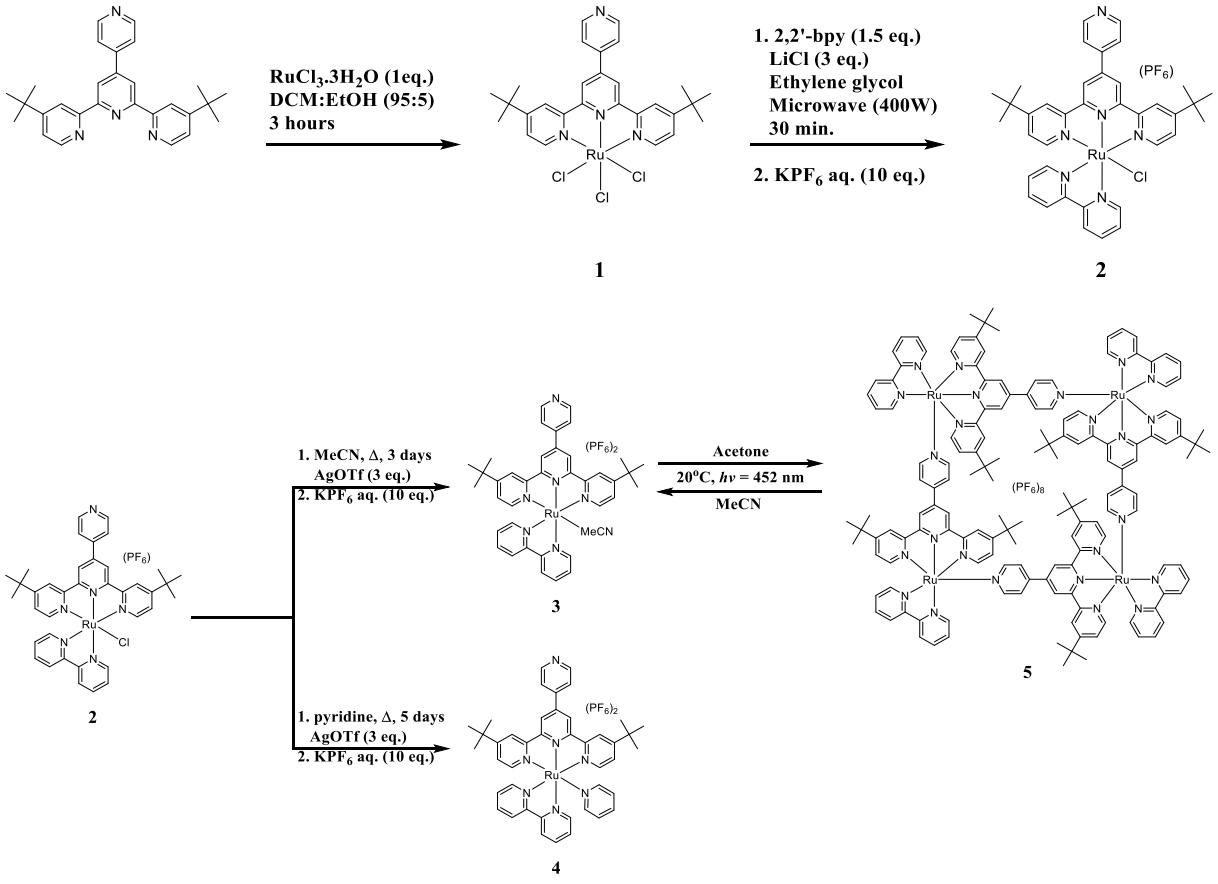

Scheme 8.1 – Reaction scheme for the synthesis of precursors 1-3, model complex 4 and metallosquare 5.

afford **1,** (4-pytpy)$RuCl_3$, as a dark brown precipitate in 87% yield. The ruthenium precursor was then mixed with a slight excess of 2,2'-bipyridine (1.5 equiv) in the presence of an excess amount of LiCl (5 equiv) in ethylene glycol into a 20 mL micro-wave vial. The vial was heated under micro-wave irradiation (400 W, 200°C) for 30 minutes. The deep-purple solution was subject to counter-ion metathesis (aqueous KPF_6, 10 equiv) before purification over neutral deactivated alumina column with a mixture of toluene:MeCN in a 7:3 ratio. The first purple band to elute contained the desired species **2** in 30% yield. Finally, **2** was left under reflux in acetonitrile with 3 equivalents of silver triflate for 3 days, leading to **3** in a quantitative yield. The model complex **4** was obtained

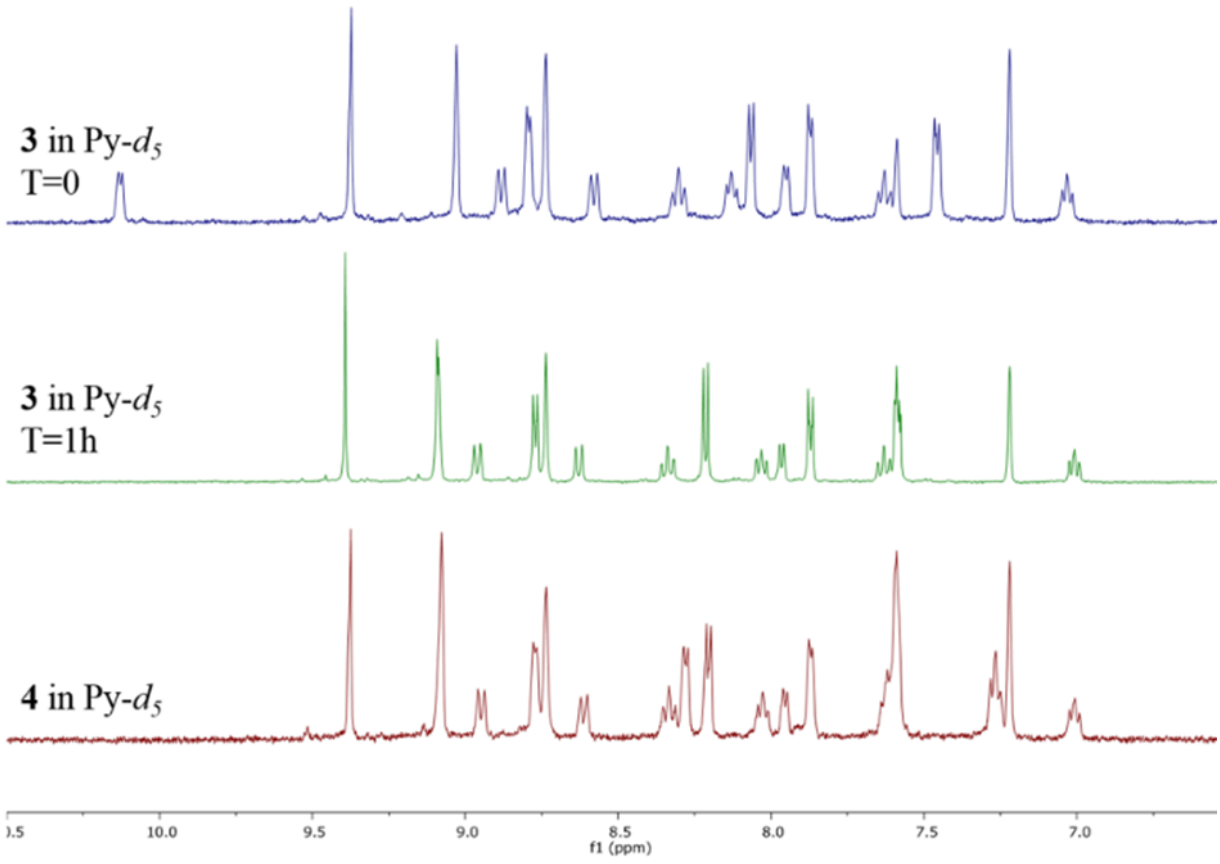

Figure 8.1 - ^1H NMR study over time of the photo-induced conversion of **3** into **4** in pyridine-d_5 at 20°C (λ = 452 nm). Note that the signals at ~8.3 ppm and ~7.3 ppm are missing after 1h of irradiation since pyridine-d_5 was used.

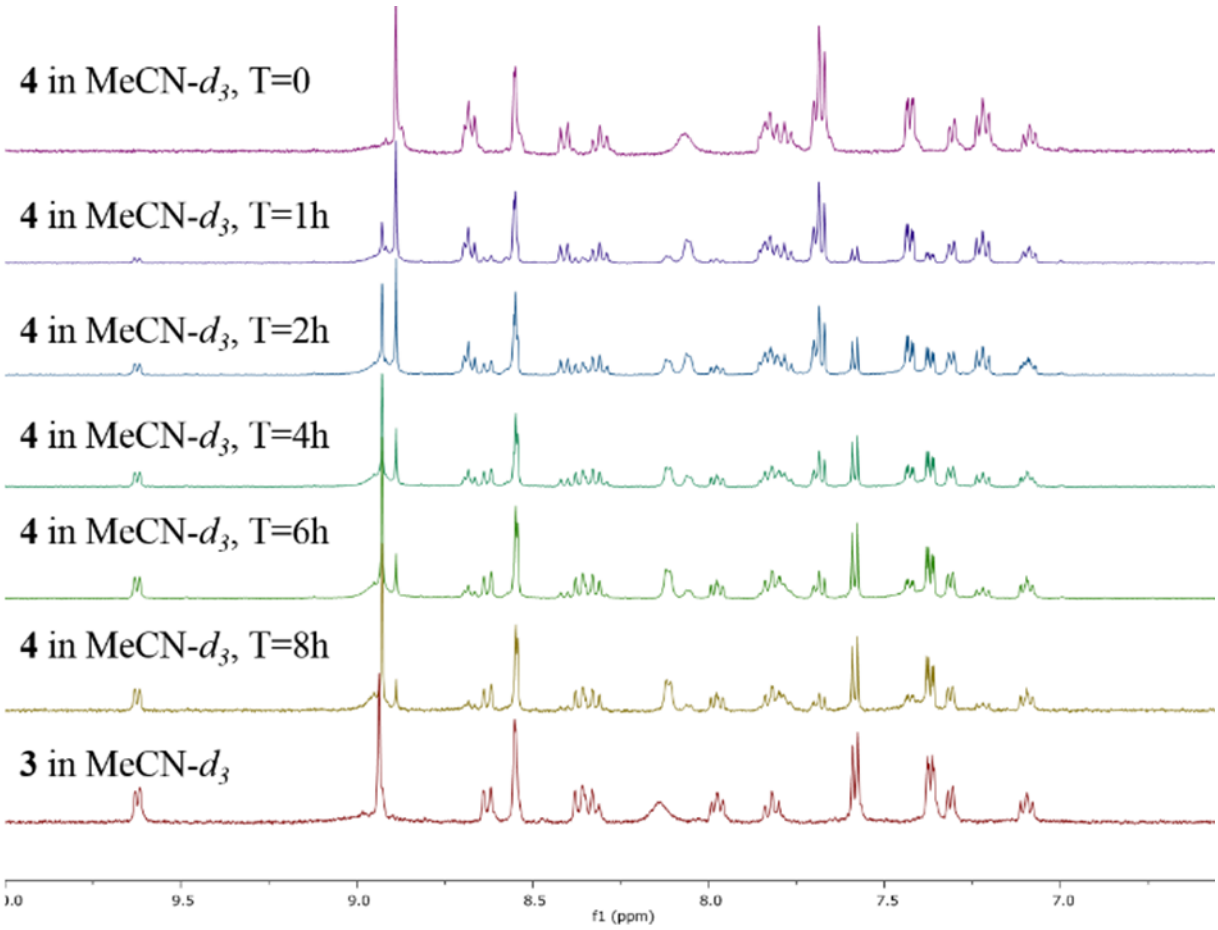

Figure 8.2 - ^{1}H NMR study over time of the photo-induced conversion of **4** into **3** in acetonitrile-d_3 at 20°C (λ = 452 nm).

in a similar way to **3**, where it was refluxed in pyridine for a period of 5 days. Complex **4** was isolated as an ochre precipitate in near-quantitative yield.

The photo-ejection of acetonitrile and pyridine ligands coordinated to a ruthenium core are already known in literature,[10b, g, i, j] so we decided to investigate the reversibility of the ligand exchange by ^{1}H NMR spectroscopy before attempting the photo-induced assembly. Precursor **3** was dissolved in pyridine-d_5 and was irradiated at 452 nm at 20°C. As depicted in

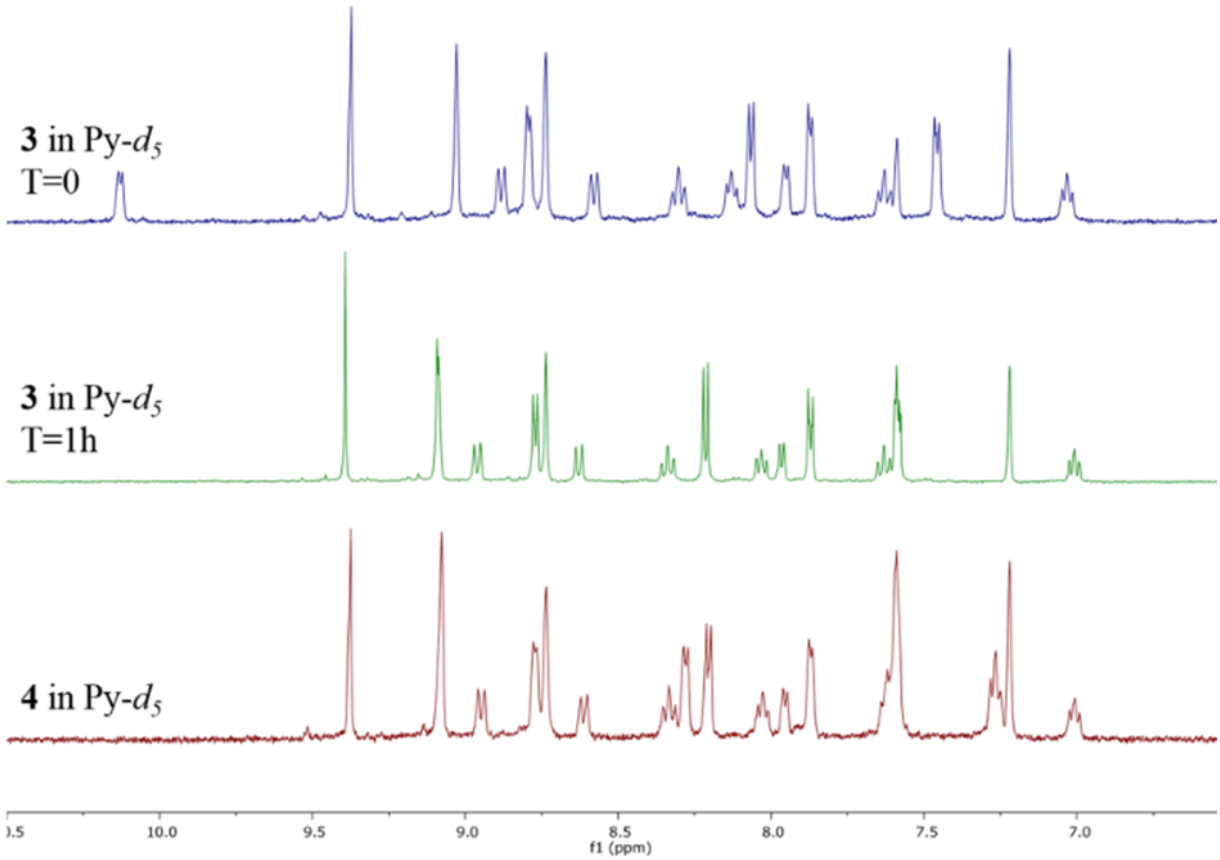

Figure 8.1, within 1 hour of light irradiation complex **3** was entirely converted to complex **4**. Similarly, model complex **4** was dissolved in acetonitrile-d_3 and left under light-irradiation in the exact same conditions as mentioned before. The lability of the pyridine ligand is less pronounced, since it took an average of 8 hours to convert most of metal complex **4** to precursor **3** (Figure 8.2). Nevertheless, the experiment constituted a very good indication of the reversibility of ligand coordination. Therefore, one could expect that the kinetic product (oligomers) can rearrange over the course of the experiment to generate the more thermodynamically stable product, the square assembly.[15] Despite the very good solubility of precursor **3** in a variety of solvents, we decided to conduct the photo-induced assembly in non-coordinating solvents (acetone) to avoid any competition for the binding site.[16] The experiment was conducted in deuterated solvent to follow the reaction over time by ^{1}H NMR. Ruthenium assembly **5** was synthesized in a NMR tube, charged with 5 mg of **3** dissolved in 0.5 mL of acetone-d_6. The tube was left under light irradiation (hv = 452 nm) and the temperature was controlled at 20°C throughout the

course of the experiment. As shown in Figure 8.3, after 1 hour the characteristic doublet at 9.90 ppm had completely disappeared, indicating that the starting material had been consumed. After 24 hours, a single major species was obtained with traces amount of intermediates, however, no more changes in the ^{1}H NMR spectrum were observed after this time. The reaction mixture was purified by size-exclusion chromatography over a Sephadex LH-20 column (70x1 cm) with acetone/MeOH/H_2O in a 45:45:10 ratio as eluent. Further metathesis of the counter-anion with aqueous KPF_6 solution led to the precipitation of a red-orange precipitate in 80% yield.

Diffusion-ordered NMR spectroscopy experiments were conducted on precursor **2** and **3** as well as on model complex **4** and assembly **5** (Figure 15.4 and Table 15.2). It is well known that following Stokes-Einstein equation, the diffusion coefficient in solution of a species is correlated to its size ($D = k_B T/6\pi\eta r_H$) assuming a near-spherical species, where D is the diffusion coefficient, k_B is the Boltzmann constant, T is the temperature in kelvin, η the viscosity of the medium and r_H the hydrodynamic radii of the species.[17] The measured diffusion coefficient for **2**, **3** and **4** were essentially identical with values of 10.0×10^{-10} m^2/s, 9.93×10^{-10} m^2/s and 9.99×10^{-10} m^2/s respectively, while the metallacycle **5** has a lower diffusion coefficient of 5.19×10^{-10} m^2/s, which is very good sign that a species of higher volume was synthesized. From a mathematical point of view, we can assume that the precursors adopt a rectangular-type shape with an height

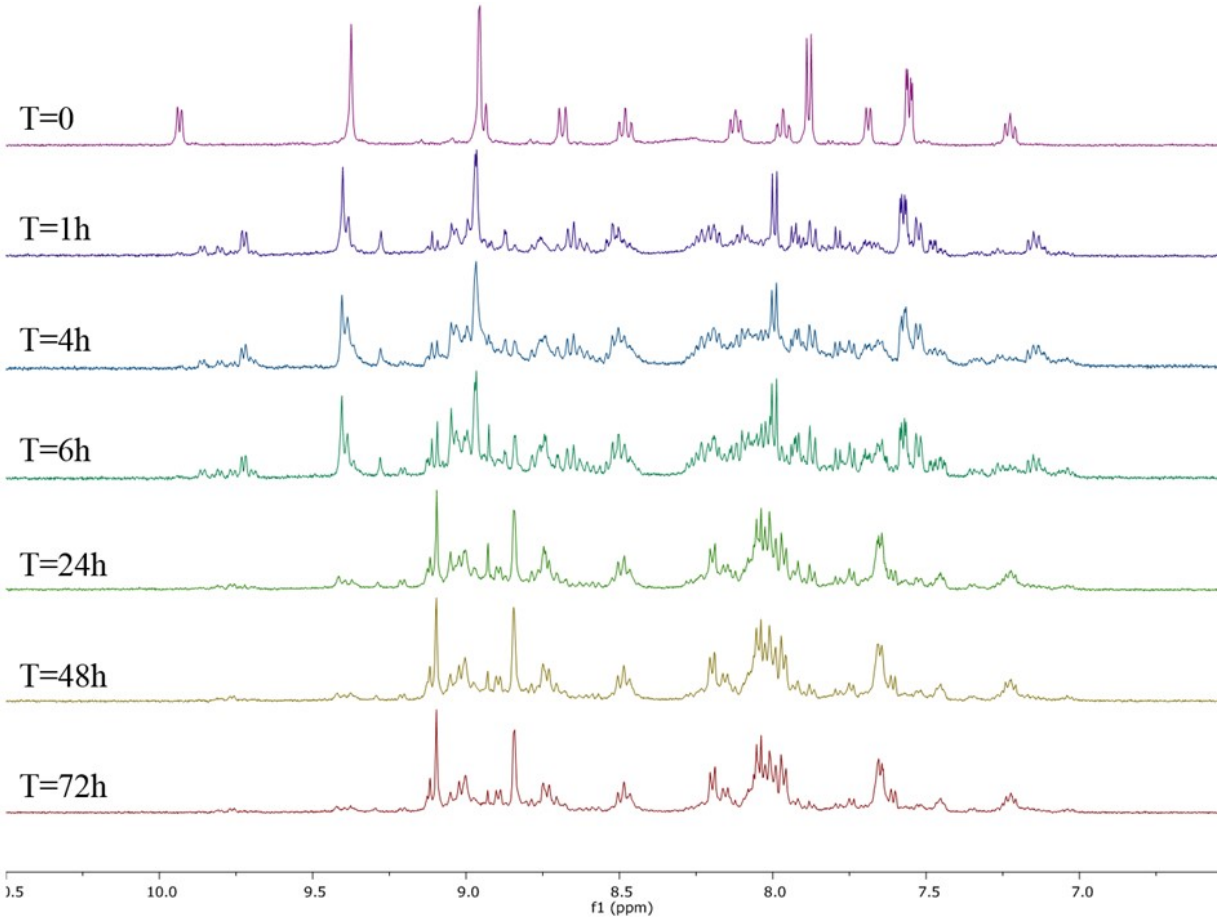

Figure 8.3 - ^{1}H NMR study over time of the photo-induced conversion of **3** into **5** in acetone-d_6 at 20°C (hv=452 nm).

and width of approximately 14 and 9 Å, respectively, while the square's side are nearly 21 Å. The circumcircle radius of a square (r_s) and a rectangle (r_t) are defined as:

$r_s = a/\sqrt{2}$

$r_t = \sqrt{(b^2 + c^2)}/2$

Where "a", "b" and "c" are the length of the sides. Accordingly, the ratio between the two circumcircle radii is found to be:

$r_t/r_s = 8/15 = 0.53$

In our specific example, we have found that the diffusion coefficient of the precursors is approximatively twice the diffusion recorded for the square, therefore in good agreement with the expected values.

The identity of the species was confirmed by high-resolution electron-spray ionization mass spectrometry (HR-ESI-MS), where the doubly-charged $[C_{152}H_{152}N_{24}Ru_4P_6F_{36}]^{2+}$ (exp. 1794.8362 *m/z*, calcd. 1794.8377, diff. 0.84 ppm) and the triply-charged species $[C_{152}H_{152}N_{24}Ru_4P_5F_{30}]^{3+}$ (exp. 1148.2343 *m/z*, calcd. 1148.2359, diff. 1.39 ppm) were detected. Finally, small crystals of **5** were obtained by slow diffusion of diisopropyl ether into an acetone solution of the square over several weeks.

The crystals were analyzed by single-crystal X-ray diffraction studies, which confirmed the nature of the species without a doubt (Figure 8.4, Figure 8.5). A detailed analysis of the bond length and angles and a comparison to optimized values obtained by density functional theory (DFT) calculations is presented in Table 15.11. The synthesis of the square was further repeated under dark conditions, to validate that only light was responsible for the induction of the self- assembly. The sample was covered in aluminum foil and irradiated under the same conditions as mentioned before. As can be observed in Figure 15.1, no changes were observed by ^{1}H NMR spectroscopy after 24 hours, which confirmed that the reaction was only driven by light-irradiation.

On the other hand, we were also interested to know if the metallosquare could be obtained through regular thermal synthetic conditions. We kept acetone as the solvent for precursor **3** and heated the solution at 60°C over 72 hours. As shown in Figure 15.2, it appeared that **3** barely reacted, leading to only trace amounts of unidentified intermediate species. The reversibility of the self-assembly was also investigated by ^{1}H NMR (Figure 15.3). The square assembly was dissolved in CD_3CN (1 mg/mL) and the sample was left under light irradiation (452 nm) as described before. The changes were monitored and we observed that after approximately 7 hours, the metal complex has been completely converted back to precursor **3**.

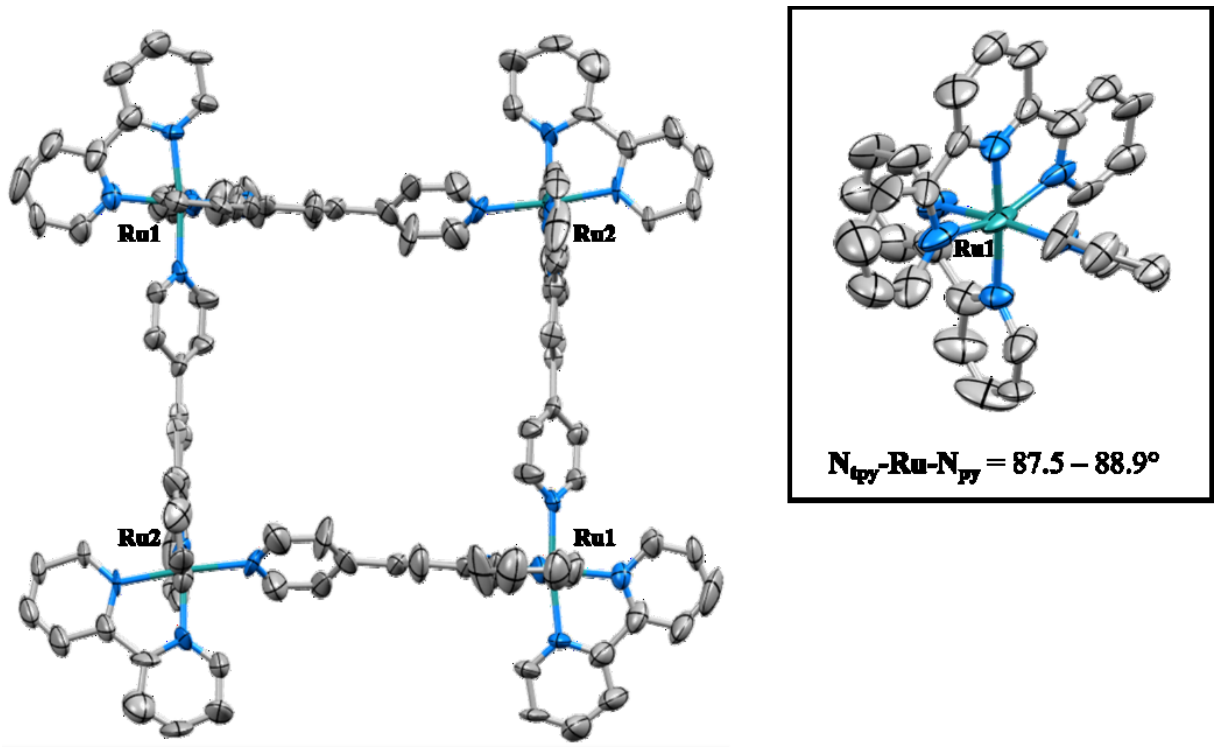

Figure 8.4 - X-ray crystal structure of metal complex **5** with ellipsoids plotted at a 30% probability level. The counter-anions, hydrogen atoms and tertbutyl moieties were omitted for clarity. The inset focusses on the coordination angle around the metal core.

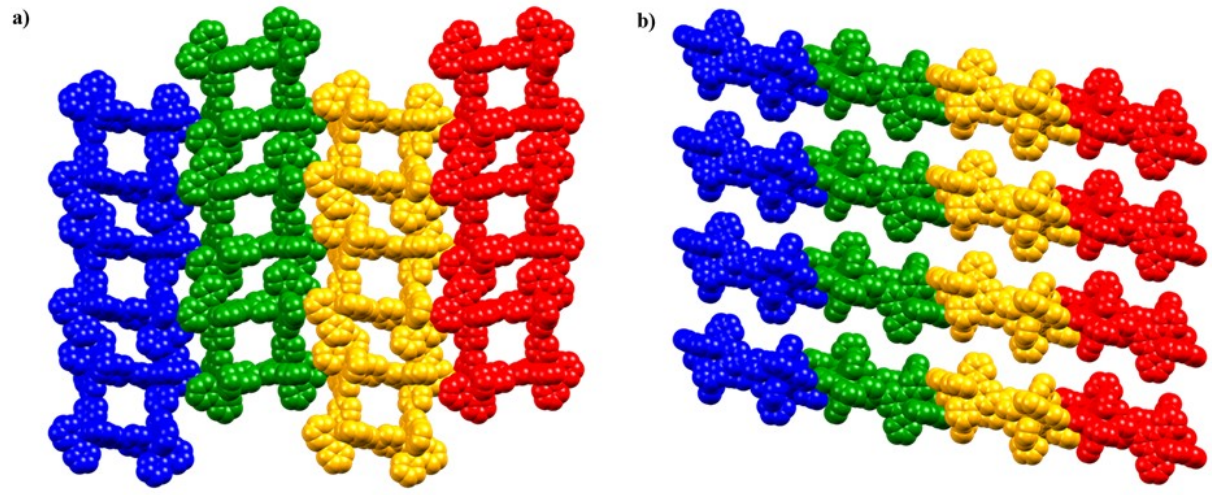

Figure 8.5 - Space filling view along a) the a axis showing the crystal packing of the molecular square forming infinite channels and b) along the b axis displaying the lamellar staking motif. The hydrogen atoms, the *tert*-butyl units as well as the PF_6 counter-anions have been omitted for clarity.

8.6.2. Electrochemical properties

The electrochemical behaviour of all the complexes are summarized in Table 8.1 and characteristic cyclovoltammograms of the complexes are presented in Figure 15.5-Figure 15.13. The complexes were examined by cyclic voltammetry and square-wave voltammetry in dimethylformamide (*t*-Bu_4NPF_6 0.1M) solution at ambient temperature. Metal complexes **2-4** exhibits a reversible one-electron ligand-based reduction at potential ranging from -1.1 to -1.3 V *vs.* SCE, followed by an irreversible reduction process near-1.4 to -1.6 V. Interestingly, it appears that the formation of the discrete assembly significantly increases the chemical stability compared to precursor **3** and model complex **4**, where up to four-reversible reduction waves were observed in the square assembly **5**. According to the Randles-Sevcik equation, we have found that the first two ligand-based reduction processes observed for **5**, E_1^{red} and E_2^{red}, are coincidental and have two monoelectronic processes. In both cases, the experimental peak separation (ΔE_p) between the anodic and cathodic peak indicates that each process implies two coincidental one-electron reductions. Also, the 0.1 V difference between E_1^{red} and E_2^{red} demonstrates that both processes are mostly localized. Therefore, we can propose that the first ligand-based reduction observed at -0.92 V constitutes the coincidental reduction of the terpyridine ligand on opposite sides of the ruthenium assembly. Similarly, the second reduction process at -1.02 V involves the synchronous reduction of the two remaining terpyridine ligands on opposite sides of the square. The attribution of the remaining reduction waves (E_3^{red} to E_5^{red}) is still ambiguous: E_3^{red} and E_5^{red} are both monoelectronic processes, while E_4^{red} is composed of four indistinguishable monoelectronic processes. The Kohn-Sham electron density (Figure 15.20) representation of the molecular orbitals obtained by DFT calculation in the ground state (*S*=0) suggest that the monoelectronic processes could be delocalized throughout the entire system, therefore reducing the charge density and electrostatic repulsions.[20] It is unlikely for the four electrons observed in E_4^{red} to be also located on the main macrocycle, which is particularly true considering the resolution between both two-electron processes combined in E_4^{red}. Consequently, we propose that the external 2,2'-bipyridine ligands could be successively reduced at potential reaching -1.52 V, while the

addition of an extra electron (E_5^{red}) within the ninthly reduced system leads to the irreversible reduction of the square assembly. Finally, the oxidative process occurring at +1.26 V consist of four coincidental one-electron oxidations of the four Ru(II) centers.

Table 8.1 – Electrochemical data for the RuII complexes in DMF.[a]

Compound	$E_{1/2}^{Ox}$ (V) (ΔE_p (mV))	$E_{1/2}^{Red}$ (V) (ΔE_p (mV))				
2	0.79 (69)	-1.32 (75)	-1.55 (irr.)[b]	–	–	–
3	1.26 (99)	-1.15 (71)	-1.39 (irr.)[b]	–	–	–
4	1.20 (81)	-1.13 (70)	-1.49 (irr.)[b]	–	–	–
5	1.26 (147)	-0.92 (84)[c]	-1.02 (81)[c]	-1.14 (71)	-1.52 (135)[d]	-1.76 (irr.)[b]
$Ru(ttpy)_2$ [18]	1.30	-1.22	-1.46	–	–	–

[a] All Cyclic voltammetry measurements were performed in DMF/*t*-$Bu_4N(PF_6)$ (0.1M), recorded at 25±1 °C with a sweep rate of 50 mV s^{-1}. Potentials reported are *vs* SCE, using the Fc^+/Fc (0.45 V) as internal reference.[19] [b] Irreversible; the potential is given for the cathodic wave. [c] Two-electron process. [d] Four-electron process.

8.6.3. Photophysical properties

The optical properties of the metal complexes were investigated in diluted acetonitrile solution at ambient temperature. It is worth mentioning that the timescale of the experiments was too fast to observe any effects that could arise due to photo-ejection of a ligand. The absorption spectra are shown in Figure 8.6 and the photophysical data are gathered in Table 8.2. The 300-700 nm region is predominantly composed of absorption bands due to spin-allowed metal-to-ligand charge transfer (^{1}MLCT) transitions. The UV region (200-300 nm) shows an important contribution of π→π* bands, along with minor contributions from ^{1}MLCT bands around 215 nm and 270 nm (Table 15.6, Table 15.9 and Table 15.13). As expected, the intensity of the square's absorption is approximately four times the one observed for the model and the precursor, reaching up to 40 000 $M^{-1}cm^{-1}$ in the visible portion of the spectra (500 nm). Compounds **3-5** exhibit the typical ^{3}MLCT emission of Ru(II) polypyridine complexes, not far from that of a model species, $Ru(ttpy)^{2+}$ (ttpy = 4'-tolyl-2,2':6',2''-terpyridine),[21] see Table 8.2.

Table 8.2 - Photophysical properties of the Ru(II) complexes in MeCN solution.

Compound	Luminescence 298K	Lifetime 298K	Φ
	λ_{max}/nm	τ/ns	
3	735	1.2	$6x10^{-5}$
4	690	7.7	$2x10^{-4}$
5	745	135	$1x10^{-2}$
$Ru(ttpy)_2^{2+}$ [21]	640	1.0	$3x10^{-5}$

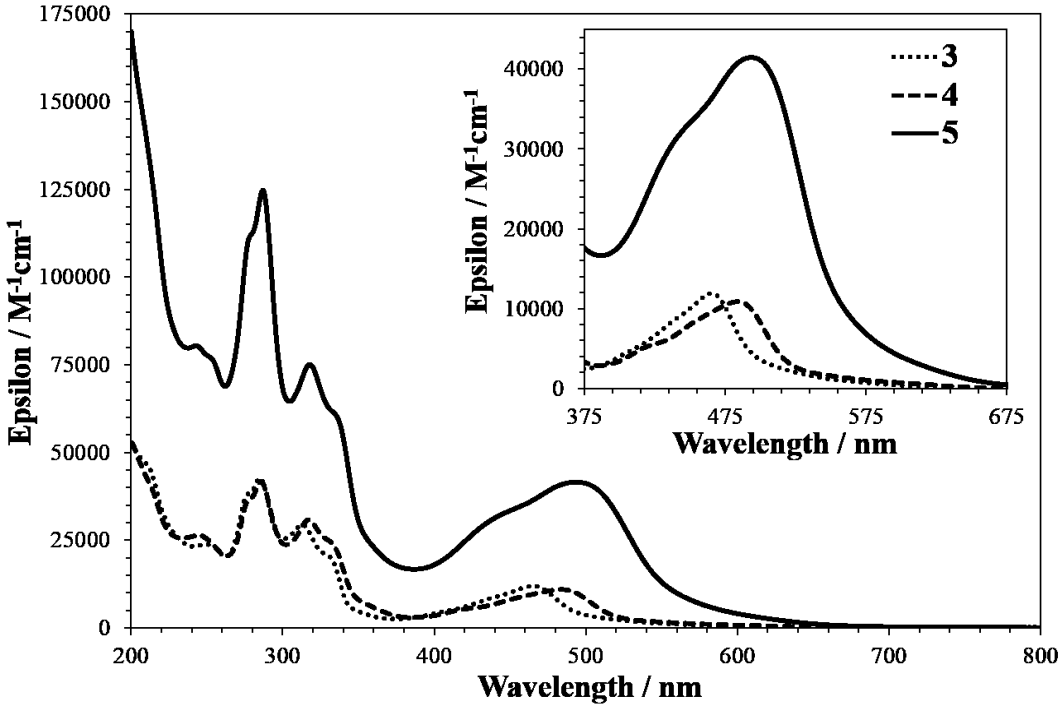

Figure 8.6 - Absorption spectra of precursor **3** (dot), model complex **4** (dash) and assembly **5** (plain), recorded in acetonitrile solution at ambient temperature.

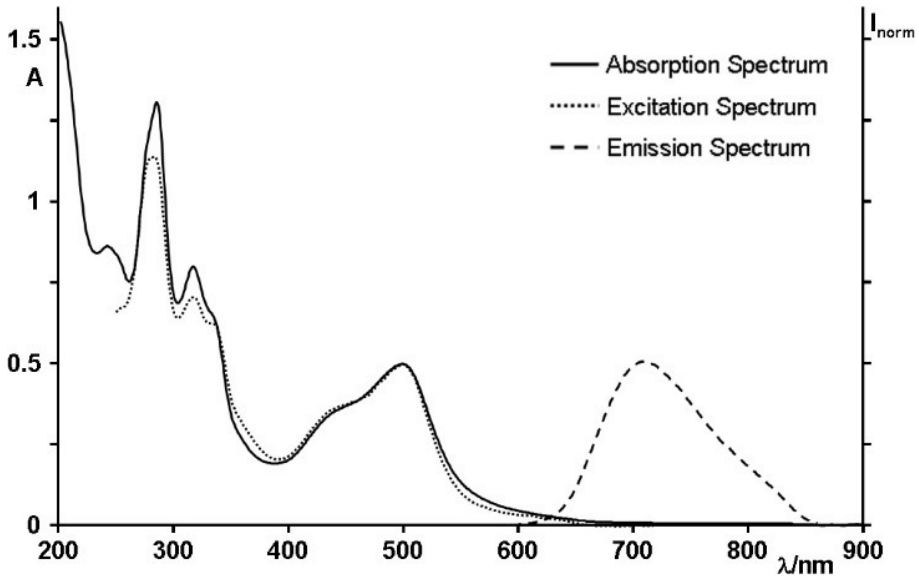

Figure 8.7 - Absorption (enclosed for comparison), excitation, and emission spectra of **5** in acetonitrile solution at room temperature.

The emission and excitation spectra of the metallosquare **5** are shown in Figure 8.7. A major deactivation pathway of the MLCT emissive level(s) of Ru^{II} polypyridine complexes is via thermally-activated surface crossing to a low-lying metal centered (MC) state, which is structurally-distorted compared to the ground state, so that radiationless decays are quite fast due to favourable Franck-Condon factors.[7d, 22] This explains the relatively short emission lifetimes and very low quantum yields of **3**, **4**, and the model $Ru(ttpy)^{2+}$. Quite interestingly, emission lifetime (135 ns) and quantum yield (1 %) of the metallosquare **5** are much longer and intense, respectively, than **3**, **4**, and $Ru(ttpy)^{2+}$. A quick analysis of the data indicates that the reason is the relatively slow rate constant for radiationless decay of the ^{3}MLCT emissive state in **5**, which is at least one order of magnitude slower than those of the other species. Such a difference can neither be attributed to the energy gap between MLCT and MC levels (expected to be similar in **5** and **4** or $Ru(ttpy)^{2+}$) nor to the energy gap law, related to the emission energy (emission energy of the various compounds in Table 8.2 is too similar one to another to justify the differences). We suggest that the MC state of **5** can be less distorted compared to the corresponding level of the monomeric species, due to rigidity of the square, therefore

reducing the Franck-Condon factors for radiationless decay via the MC state. Consequently, the relatively long-lived and moderately intense emission of **5** is proposed to be directly connected to its self-assembled and organized square structure.

Finally, to shine some light on the early events of the photo-induced assembly process, we performed pump-probe transient absorption (TA) spectroscopy (excitation wavelength, 400 nm) on **3**, **4**, and **5** in acetonitrile and acetone. Excitation of these compounds in acetonitrile leads to very similar results: in all cases, the TA spectrum initially shows a bleach peaking at about 465 nm and a broad transient at wavelengths longer than 500 nm. Such a spectrum, apart from very small changes, directly decays to the ground state on the ns timescale, without appreciable spectral changes (see Figure 8.8). This result could seem to disagree with the above-mentioned results of photo-irradiation of **4** and **5** in acetonitrile, both leading to **3**. However, as also discussed above, these photoreactions are quite slow, and probably they are not appreciable by pump-probe TA experiments, which are not able to identify the formation of tiny amounts of photoproducts.

The situation is different for **3** in acetone (see Figure 8.9): the initial bleach at 465 nm evolves with time and a new bleach peaking around 500 nm appears. The new transient absorption spectrum does not tend to decay towards the ground state, but a more or less stable photoproduct is formed, which is assumed to be due to the formation of a precursor of **5**. Compound **4** in acetone exhibits a quite puzzling behavior: the initial bleach at 490 nm moves to shorter wavelengths and increases in about 270 ps, suggesting relaxed (very weakly) emissive state, probably an equilibrated MLCT/MC state.

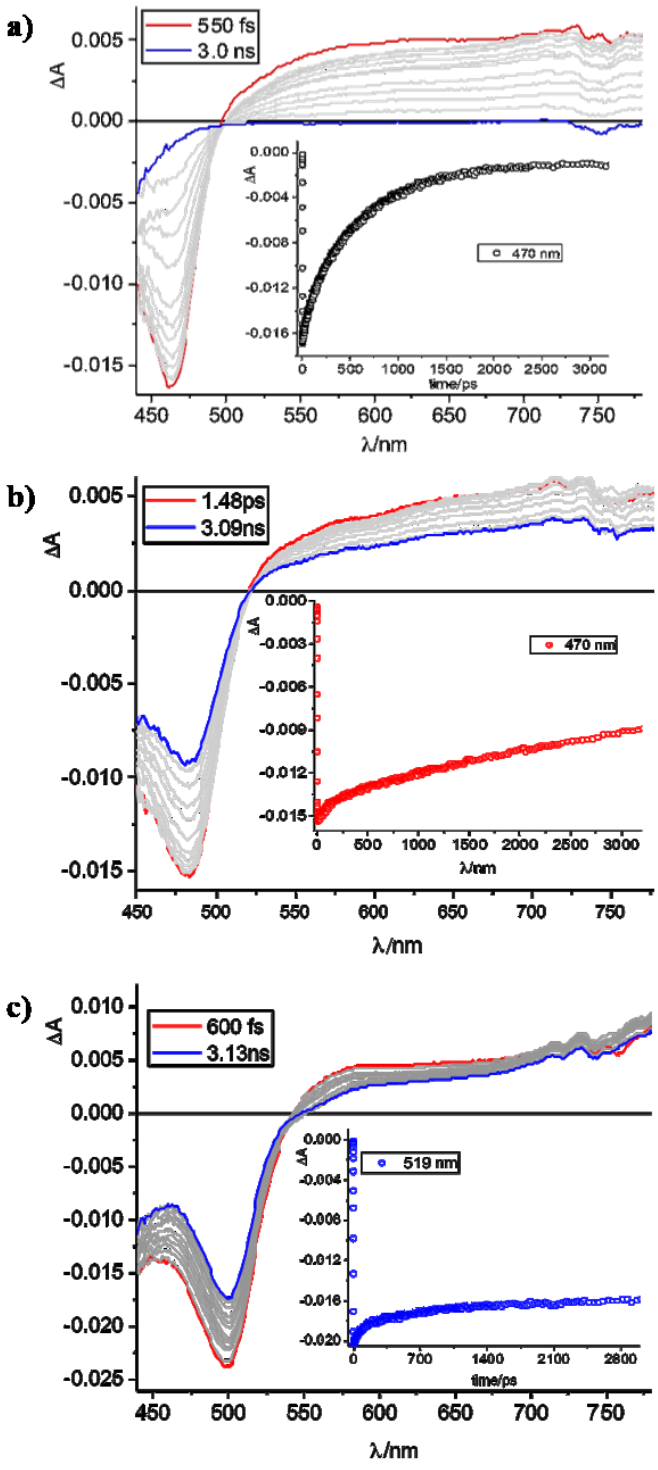

Figure 8.8 - Pump-probe transient absorption spectra and decays of a) **3**, b) **4** and c) **5** in acetonitrile, with light excitation at 400 nm.

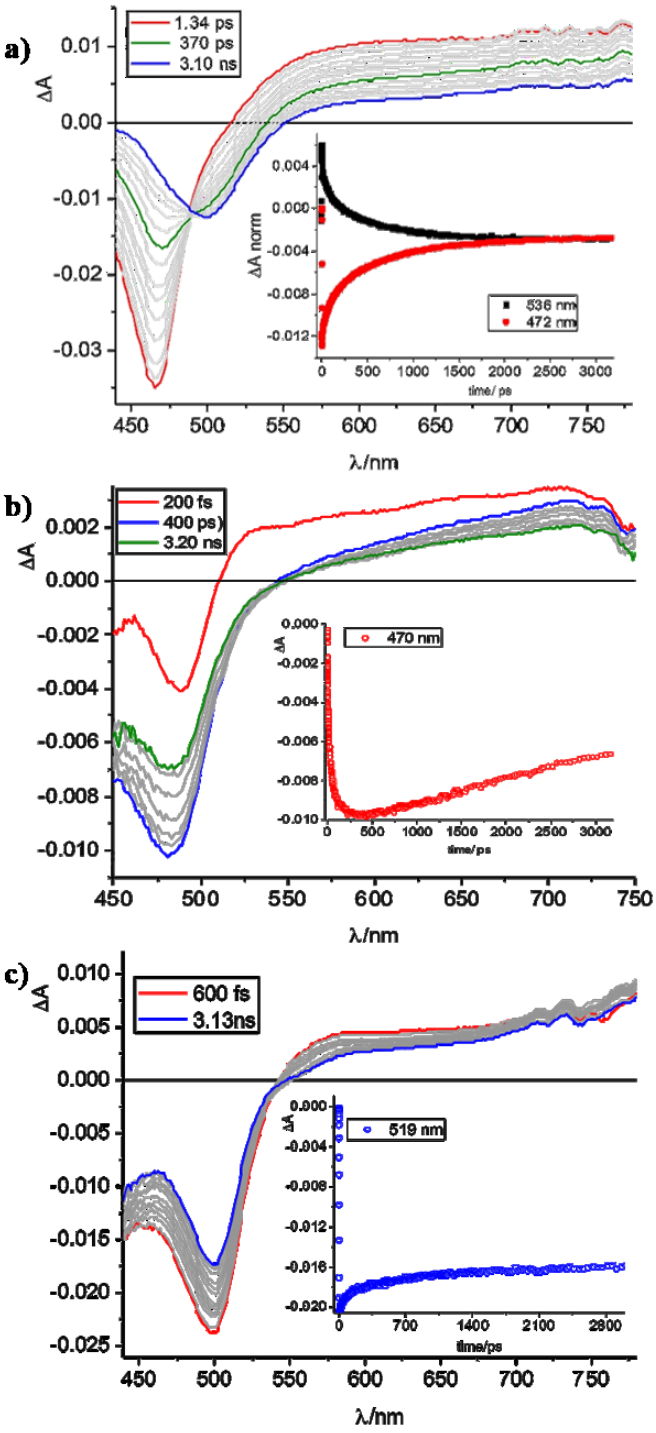

Figure 8.9 - Pump-probe transient absorption spectra and decays of a) **3**, b) **4** and c) **5** in acetone, with light excitation at 400 nm.

Such a relaxed state is evidently highly distorted with respect to the ground state, thereby justifying the short lifetime and very low quantum yield of **4**, as already discussed. The metallacycle **5** in acetone does not behave differently than in acetonitrile: the initial TA spectrum apparently decays to the ground state, without exhibiting significant spectral changes. In particular, the spectral changes occurring in **4** in acetone do not occur in **5** in the same solvent, although the first coordination sphere of both compounds is essentially identical, that is formed by a terpyridine-like ligand, a bipyridine-like ligand, and a pyridine-like ligand. The difference is that the pyridine of **4** is replaced in **5** by a pyridine connected to a much larger and bulkier group (indeed, it is the whole square), so that any structural rearrangement, for example rotation of the pyridine with respect to the metal-pyridine axes, would be extremely energy demanding, and possibly inhibited. The excited-state of **5** has, therefore, a geometry relatively similar to that of the ground state, a consequence of its square structure, confirming that the efficient and relatively long-lived emission can be directly connected to its molecular shape, as proposed above.

8.6.4. Conclusion

A rare example of a light-induced assembly process allows the preparation of a luminescent tetranuclear Ru^{II} species, **5**. Interestingly, **5** cannot be synthesized by thermal reactions in similar conditions. The tetraruthenium square **5** has a much longer excited-state lifetime and higher emission quantum yield compared to its mononuclear components as well as in comparison with other Ru^{II} polypyridine compounds emitting at comparable energy: such interesting photophysical properties are proposed to be related to the structurally-organized and increased rigidity of its square structure. The light-induced synthetic methodology opens the way to a new avenue in supramolecular chemistry and we envision that supermolecules that can be obtained by photochemical techniques will grow in importance in the future. We are currently extending this light-induced synthetic strategy to one-, two- and three-dimensional systems with different combinations of metal-ions and ligands to improve the overall properties of the metal complexes.

8.6.5. Acknowledgements

G.S.H. and B.L.M. thank the Natural Sciences and Engineering Research Council (NSERC) of Canada, the Fondation J.A. Bombardier and the Université de Montréal for financial support. The authors are also grateful to UdeM NMR and XRD facilities and staff for their help. F.N, F.P. and S.C. thank the Ministry of Foreign Affairs and International Cooperation (MAECI) of Italy for support via the Italy-Japan bilateral cooperation (project: A supramolecular approach to artificial photosynthesis).

8.6.6. References

[1] E. P. Kyba, R. C. Helgeson, K. Madan, G. W. Gokel, T. L. Tarnowski, S. S. Moore, D. J. Cram, *J. Am. Chem. Soc.* **1977**, *99*, 2564-2571.

[2] J. M. Lehn, *Pure Appl. Chem.* **1978**, *50*, 871-892.

[3] a) M. Fujita, J. Yazaki, K. Ogura, *J. Am. Chem. Soc.* **1990**, *112*, 5645-5647; b) M. Fujita, *Chem. Soc. Rev.* **1998**, *27*, 417; c) M. Fujita, K. Umemoto, M. Yoshizawa, N. Fujita, T. Kusukawa, K. Biradha, *Chem. Commun.* **2001**, 509-518; d) W. Y. Sun, M. Yoshizawa, T. Kusukawa, M. Fujita, *Curr. Opin. Chem. Biol.* **2002**, *6*, 757-764; e) M. Yoshizawa, M. Fujita, *Pure Appl. Chem.* **2005**, *77*, 1107-1112; f) K.-I. Yamashita, K.-I. Sato, M. Kawano, M. Fujita, *New J. Chem.* **2009**, *33*, 264-270; g) M. Fujita, T. Murase, *From Non-Covalent Assemblies to Molecular Machines* **2010**, 7-30.

[4] a) P. J. Stang, D. H. Cao, *J. Am. Chem. Soc.* **1994**, *116*, 4981-4982; b) S. Leininger, B. Olenyuk, P. J. Stang, *Chem. Rev.* **2000**, *100*, 853-908; c) B. H. Northrop, Y. R. Zheng, K. W. Chi, P. J. Stang, *Acc. Chem. Res.* **2009**, *42*, 1554-1563; d) T. R. Cook, Y. R. Zheng, P. J. Stang, *Chem. Rev.* **2012**, *113*, 734-777; e) T. R. Cook, P. J. Stang,, *Coordination-Driven Supramolecular Macromolecules via the Directional Bonding Approach*, Springer-Verlag, Berlin Heidelberg, **2013**; f) T. R. Cook, V. Vajpayee, M. H. Lee, P. J. Stang, K. W. Chi, *Acc. Chem. Res.* **2013**, *46*, 2464-2474; g) R. Chakrabarty, P. S. Mukherjee, P. J. Stang, *Chem. Rev.* **2011**, *111*, 6810-6918.

[5] a) G. R. Newkome, C. N. Moorefield, *Chem. Soc. Rev.*, **2015**, *44*, 3954–3967; b) C. Wang, X.-Q. Hao, M. Wang, C. Guo, B. Xu, E. Tan, Y. Zhang, Y. Yu, Z. Li, H.-B. Yang, P. Song and X. Li, *Chem. Sci.*, **2014**, *5*, 1221–1226; c) J. M. Lodlow III, T.-Z. Xie, Z. Guo, K. Guo, M. J. Saunders, C. N. Moorefield, C. Wesdemiotis and G. R. Newkome, *Chem. Commun.*, **2015**, *51*, 3820–3823; d) T.-Z. Xie, K. Guo, Z. Guo, W.-Y. Gao, L. Wojtas, G.-H. Ning, M. Huang, X. Lu, J.-Y. Li, S.-Y. Liao, Y.-S. Chen, C. N. Moorefield, M. J. Saunders, S. Z. D. Cheng, C. Wesdemiotis, G. R. Newkome, *Angew. Chem., Int. Ed.*, **2015**, *54*, 9224–9229; e) T. Habereder, M. Warchhold, H. Noth, K. Severin, *Angew. Chem. Int. Ed.* **1999**, *38*, 3225; f) H. Piotrowski, K. Polborn, G. Hilt, K. Severin, *J. Am. Chem. Soc.* **2001**, *123*, 2699; g) H. Piotrowski, G. Hilt, A. Schulz, P. Mayer, K. Polborn, K. Severin, *Chem. Eur. J.* **2001**, *7*, 3196; h) K. Severin, *Coord. Chem. Rev.* **2003**, *245*, 3; i) J. A. Thomas *Chem. Soc. Rev.* **2007**, *36*, 856–868; j) V. Croué, S. Goeb, M. Sallé *Chem. Commun.* **2015**, ***51***, 7275-7289

[6] a) S.-S. Sun, A. J. Lees, *Inorg. Chem.* **2001**, *40*, 3154-3160; b) K. Li, L. Y. Zhang, C. Yan, S. C. Wei, M. Pan, L. Zhang, C. Y. Su, *J. Am. Chem. Soc.* **2014**, *136*, 4456-4459; c) A. J. Metherell, M. D. Ward, *Chem. Commun.* **2014**, *50*, 6330-6332; d) T. Z. Xie, S. Y. Liao, K. Guo, X. Lu, X. Dong, M. Huang, C. N. Moorefield, S. Z. Cheng, X. Liu, C. Wesdemiotis, G. R. Newkome, *J. Am. Chem. Soc.* **2014**, *136*, 8165-8168; e) J. Yang, M. Bhadbhade, W. A. Donald, H. Iranmanesh, E. G. Moore, H. Yan, J. E. Beves, *Chem. Commun.* **2015**, *51*, 4465-4468; f) A. J. Metherell, M. D. Ward, *RSC Adv.* **2016**, *6*, 10750-10762; g) K. Wu, K. Li, Y. J. Hou, M. Pan, L. Y. Zhang, L. Chen, C. Y. Su, *Nat. Commun.* **2016**, *7*, 10487; h) N. Shan, S. J. Vickers, H. Adams, M. D. Ward, J. A. Thomas *Angew. Chem. Int. Ed.* **2004**, *43*, 3938 –3941; i) L. A. Berben, M. C. Faia, N. R. Crawford, J. R. Long, *Inorg. Chem.*, **2006**, *45*, 6378.

[7] a) G. Malouf, P. C. Ford, *J. Am. Chem. Soc.* **1974**, *96*, 601-603; b) H. B. Ross, M. Boldaji, P. D. Rillema, C. B. Blanton, R. P. White, *Inorg. Chem.* **1989**, *28*, 1013-1021; c) L. Salassa, C. Garino, G. Salassa, R. Gobetto, C. Nervi, *J. Am. Chem. Soc.* **2008**, *130*, 9590-9597; d) T. J. Meyer, *Pure Appl. Chem.* **1986**, *58*, 1193-1206; e) L. Salassa, C. Garino, G. Salassa, C. Nervi, R. Gobetto, C. Lamberti, D. Gianolio,

R. Bizzarri, P. J. Sadler, *Inorg. Chem.* **2009**, *48*, 1469-1481; f) R. N. Garner, L. E. Joyce, C. Turro, *Inorg. Chem.* **2011**, *50*, 4384-4391; g) S. E. Greenough, G. M. Roberts, N. A. Smith, M. D. Horbury, R. G. McKinlay, J. M. Żurek, M. J. Paterson, P. J. Sadler, V. G. Stavros, *Phys. Chem. Chem. Phys.* **2014**, *16*, 19141-19155; h) J. D. Knoll, B. A. Albani, C. Turro, *Acc. Chem. Res.* **2015**, *48*, 2280-2287; i) J. D. Knoll, B. A. Albani, C. Turro, *Chem. Commun.* **2015**, *51*, 8777-8780; j) Y.-J. Tu, S. Mazumder, J. F. Endicott, C. Turro, J. J. Kodanko, B. H. Schlegel, *Inorg. Chem.* **2015**, *54*, 8003-8011; k) C. Moucheron, A. Mesmaeker, J. M. Kelly, *J. Photochem. Photobiol. B* **1997**, *40*, 91-106; l) R. Blasius, C. Moucheron, A. Kirsch-De Mesmaeker, *Eur. J. Inorg. Chem.* **2004**, *2004*, 3971-3979; m) R. Blasius, H. Nierengarten, M. Luhmer, J. F. Constant, E. Defrancq, P. Dumy, A. van Dorsselaer, C. Moucheron, A. Kirsch-Demesmaeker, *Chem. Eur. J.* **2005**, *11*, 1507-1517.

[8] a) J. G. Vos, M. T. Pryce, *Coord. Chem. Rev.* **2010**, *254*, 2519-2532; b) D. Unjaroen, J. B. Kasper, W. R. Browne, *Dalton Trans.* **2014**, *43*, 16974-16976; c) S. Bonnet, J.-P. Collin, J.-P. Sauvage, *Inorg. Chem.* **2007**, *46*, 10520-10533; d) S. Bonnet, J.-P. Collin, J.-P. Sauvage, *Chem. Commun.* **2005**, 3195-3197.

[9] a) E. Wachter, D. K. Heidary, B. S. Howerton, S. Parkin, E. C. Glazer, *Chem. Commun.* **2012**, *48*, 9649-9651; b) E. Wachter, B. S. Howerton, E. C. Hall, S. Parkin, E. C. Glazer, *Chem. Commun.* **2013**, *50*, 311-313; c) E. Wachter, E. C. Glazer, *J. Phys. Chem. A* **2014**, *118*, 10474-10486.

[10] a) B. Durham, J. L. Walsh, C. L. Carter, T. J. Meyer, *Inorg. Chem.* **1980**, *19*, 860-865; b) H. Suen, S. W. Wilson, M. Pomerantz, J. L. Walsh, *Inorg. Chem.* **1989**, *28*, 786-791; c) S. Sato, Y. Matubara, K. Koike, M. Falkenström, T. Katayama, Y. Ishibashi, H. Miyasaka, S. Taniguchi, H. Chosrowjan, N. Mataga, N. Fukazawa, S. Koshihara, K. Onda, O. Ishitani, *Chem. Eur. J.* **2012**, *18*, 15722-15734; d) M. Hirahara, S. Nagai, K. Takahashi, K. Saito, T. Yui, M. Yagi, *Inorg. Chem.* **2015**, *54*, 7627-7635; e) S. Sato, O. Ishitani, *Coord. Chem. Rev.* **2015**, *282*, 50-59; f) A. Li, J. K. White, K. Arora, M. K. Herroon, P. D. Martin, B. H. Schlegel, I. Podgorski, C. Turro, J. J. Kodanko, *Inorg. Chem.* **2016**, *55*, 10-12; g) J. K. White, R. H. Schmehl, C. Turro, *Inorg. Chim. Acta* **2017**, *454*, 7-20; h) S. Bonnet, J.-P. Collin, J.-P. Sauvage, E. Schofield, *Inorg. Chem.* **2004**, *43*, 8346-8354; i) C. R. Hecker, P.

E. Fanwick, D. R. McMillin, *Inorg. Chem.* **1991**; 659-666; j) J. D. Knoll, B. A. Albani, C. B. Durr, C. Turro, *J. Phys. Chem. A* **2014**, *118*, 10603-10610.

[11] a) J.-P. Collin, J.-P. Sauvage, *Chem. Lett.* **2005**, *34*, 742-747; b) J. P. Collin, D. Jouvenot, M. Koizumi, J. P. Sauvage, *Eur. J. Inorg. Chem.* **2005**, *2005*, 1850-1855; c) P. Mobian, J.-M. Kern, J.-P. Sauvage, *Angew. Chem. Int. Ed.* **2004**, *43*, 2392-2395.

[12] a) T. Morimoto, C. Nishiura, M. Tanaka, J. Rohacova, Y. Nakagawa, Y. Funada, K. Koike, Y. Yamamoto, S. Shishido, T. Kojima, T. Saeki, T. Ozeki, O. Ishitani, *J. Am. Chem. Soc.* **2013**, *135*, 13266-13269; b) T. Asatani, Y. Nakagawa, Y. Funada, S. Sawa, H. Takeda, T. Morimoto, K. Koike, O. Ishitani, *Inorg. Chem.* **2014**, *53*, 7170-7180; c) J. Rohacova, A. Sekine, T. Kawano, S. Tamari, O. Ishitani, *Inorg. Chem.* **2015**, *54*, 8769-8777.

[13] a) B. Laramée-Milette, C. Lachance-Brais, G. S. Hanan, *Dalton Trans.* **2015**, *44*, 41-45; b) B. Laramee-Milette, N. Zaccheroni, F. Palomba, G. S. Hanan, *Chem. Eur. J.* **2017**, 6370-6379.

[14] B. Laramée-Milette, T. Auvray, S. Nguyen, S. Tremblay, C. Lachance-Brais, M. Donguy, V. Taylor, D. Deschênes, G. S. Hanan, *Synthesis* **2015**, *47*, 3849-3858.

[15] a) G. Ercolani, *J. Phys. Chem. B* **1998**, *102*, 5699-5703; b) G. Ercolani, M. Ioele, D. Monti, *New J. Chem.* **2001**, *25*, 783-789.

[16] R. Díaz-Torres, S. Alvarez, *Dalton Trans.* **2011**, *40*, 10742.

[17] W. H. Otto, M. H. Keefe, K. E. Splan, J. T. Hupp, C. K. Larive, *Inorg. Chem.* **2002**, *41*, 6172-6174.

[18] M. Beley, J. P. Collin, J. P. Sauvage, H. Sugihara, F. Heisel, A. Miehé, *J. Chem. Soc., Dalton Trans.* **1991**, 3157-3159.

[19] N. G. Connelly, W. E. Geiger, Chem. Rev. **1996**, *96*, 877-910.

[20] P. H. Dinolfo, M. E. Williams, C. L. SternJ. T. Hupp, *J. Am. Chem. Soc.* **2004**, *126*, 12989-13001.

[21] J. P. Sauvage, J. P. Collin, J. C. Chambron, S. Guillerez, C. Coudret, V. Balzani, F. Barigelletti, L. De Cola, L. Flamigni, *Chem. Rev.* **1994**, *94*, 993-919.

[22] a) S. Campagna, F. Puntoriero, F. Nastasi, G. Bergamini, V. Balzani, *Top. Curr. Chem.* **2007**, *280*, 117-214; b) M. Natali, F. Puntoriero, C. Chiorbolli, G. La Ganga,

A. Sartorel, M. Bonchio, S. Campagna, F. Scandola, *J. Chem. Phys. C.* **2015**, *119*, 2371-2379; b) M. Natali, F. Puntoriero, C. Chiorbolli, G. La Ganga, A. Sartorel, M. Bonchio, S. Campagna, F. Scandola, *J. Chem. Phys. C.* **2015**, *119*, 2371-2379.

Chapitre 9 - Conclusion

Cette thèse s'inscrit dans un contexte où la recherche fondamentale tente par tous les moyens de diminuer notre dépendance aux énergies fossiles. S'inspirant de la nature, nous voulons trouver une alternative inspirée par la photosynthèse naturelle.

L'objectif initial de la thèse visait à étudier la photo-labilisation de ligands afin de permettre l'auto-assemblage de complexe de coordination simple en objet supramoléculaire ordonné pouvant jouer le rôle de chromophore aux propriétés améliorées. Plus particulièrement, nous cherchions à dévellopper des molécules panchromatiques possédant une photo-stabilité accrue pouvant permettre le transfert d'énergie, tel qu'observé dans les systèmes photo-synthétiques naturels.

Plusieurs étapes fondamentales, tel que le développement de nouveaux ligands ayant des fonctions solubilisante (chapitre 2, chapitre 4) ainsi que l'étude de l'auto-assemblage de type tête-à-queue, aussi appelé [*n x 1*] (chapitre 5 et chapitre 6), ont finalement permises l'atteinte des objectifs initiaux, soit la photo-induction de l'auto-assemblage (chapitre 7).

Les lignes suivantes résument brièvement les avancées accomplies ainsi que les perspectives (parfois ambitieuses) des projets abordés au cours des dernières années.

9.1. Conclusion et perspectives : Chapitre 2 et 3

Principe bien connu en chimie de coordination, le design de ligand permet de modifier de façon contrôlé les propriétés optiques et électroniques des complexes de coordinations formés. Les ligands et complexes métalliques présentés au chapitre 2 font suite au travail amorcé par le Dr. Amlan K. Pal dans notre groupe de recherche. En introduisant des groupements très fortements σ-donneurs et en améliorant la géométrie autour du cœur métallique, Dr. Pal a démontré que des complexes de Ru(II) à base de ligands symétriques de type hpp étaient fort prometteur dans le but de récolter l'énergie solaire dans le proche infrarouge.

L'étude présenté au chapitre 2 a permis de démontrer la facilité avec laquelle nous pouvons modifier les propriétés électroniques des composés de ruthénium en ajoutant

successivement 1-, 2-, 3- ou 4- groupement hpp autour de l'atome métallique central.

Subséquemment, nous avons utilisé ce principe afin de démontrer qu'il est possible de contrôler de façon précise le transfert d'énergie entre deux entitées. Typiquement, les composés hétérométalliques à base de ruthénium et d'osmium démontrent un tranfert d'énergie efficace allant du complexe de ruthénium (donneur) vers le complexe d'osmium (accepteur) avec émission d'énergie (sous forme de lumière) provenant de ce dernier. L'introduction d'un seul groupement de type hpp dans la sphère de coordination du ruthénium permet d'abaisser suffisament les niveaux énergétiques, comparativement aux niveaux énergétiques d'un composé de type $Os(tpy)_2$, de sorte que le transfert d'énergie du centre métallique d'osmium vers le ruthénium a été observé pour la première fois dans la littérature.

Les ligands à base de fonctions hpp présentes plusieurs opportunités de synthèses. Un aspect important négligé dans le cadre de ce projet consiste en la fonctionnalisation de ces ligands, de sortes à obtenir des dérivés tridentates analogues aux terpyridines conventionnelles. L'introduction de groupements électro-donneur ou électro-accepteur pourrait permettre de moduler davantage les propriétés des complexes métalliques, en plus de donner la possibilité de construire des architectures supramoléculaires élaborées.

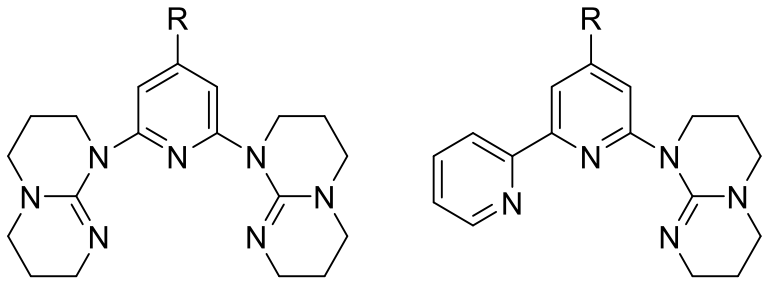

Malheureusement, pour le moment cette chimie semble limité puisqu'avec les connaissances actuelles, elle nécessiterait des précurseurs coûteux (e.i. 2,4,6-tribromopyridine) et serait peu sélective (rendement faible des produits désirés). Alternativement, il pourrait être souhaitable de tenter une approche similaire à la synthèse des 2,2' :6',2''-terpyridine.

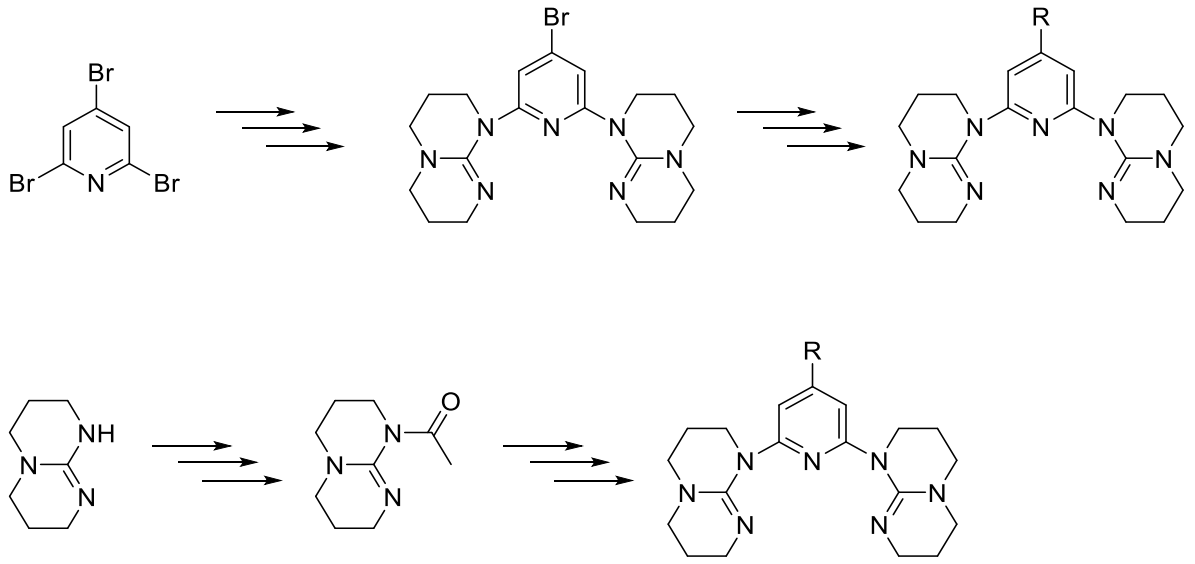

Figure 9.1 – Voies de synthèse proposées pour l'obtention de ligand tridentate symétrique de type 1,1'-(4-R-pyridine)-2,6-(hpp).

Alternativement, un précurseur intéressant dans cette optique est probablement le ligand non-symmétrique de type phen-hpp, puisqu'il serait possible d'oxyder la phenanthroline pour ensuite y installer diverse fonctionnalité avant de procéder finalement au couplage, tel que présenté à la Figure 9.2.

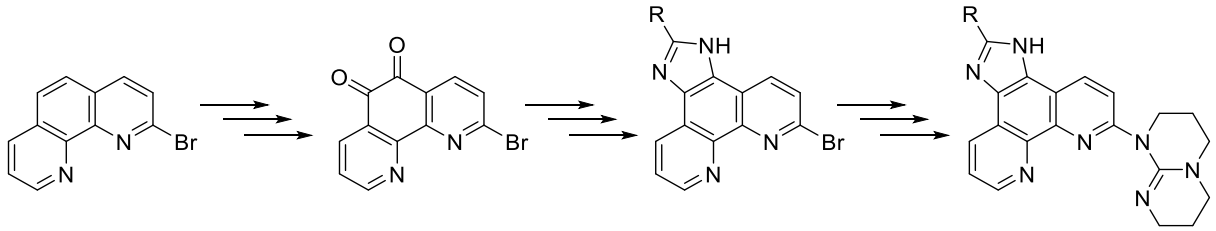

Figure 9.2 – Voie de synthèse proposée pour la fonctionalisation du ligand assymétrique de type phen-hpp.

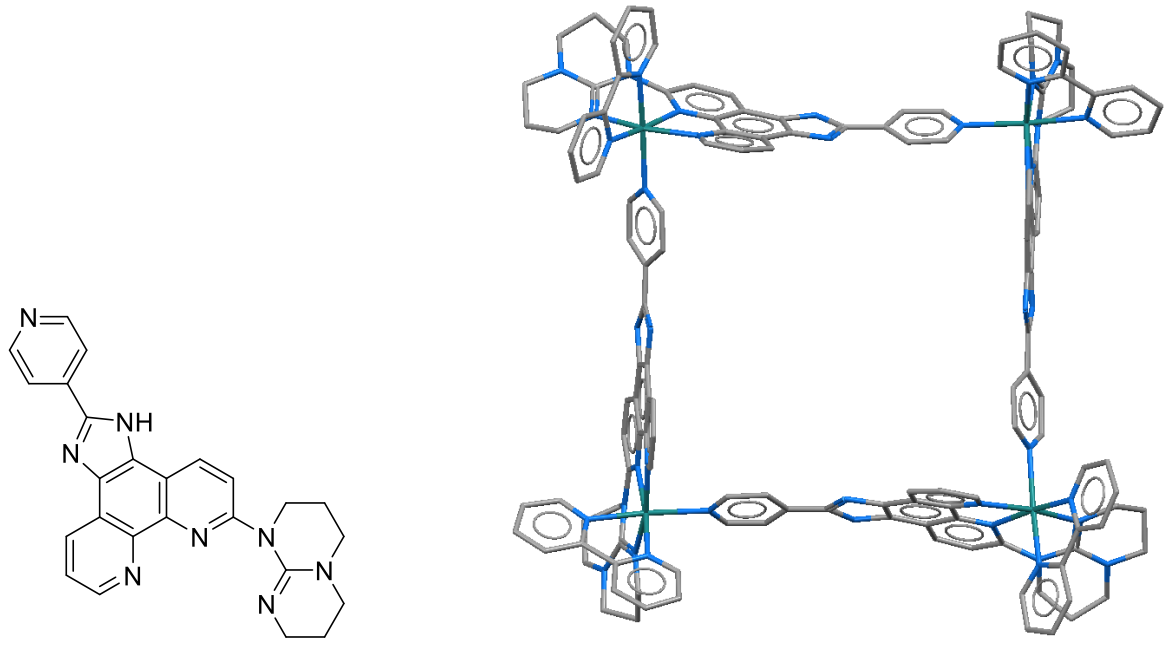

Figure 9.3 – Exemple d'un ligand de type phen-hpp fonctionnalisé et son application dans l'auto-assemblage d'un carré moléculaire.

9.2. Conclusion et perspectives : Chapitre 4

Les ligands tridentates de type 2,2':6',2''-terpyridine ont fait l'objet d'un grand nombre d'études, tant en chimie de coordination qu'en chimie supramoléculaire. Le problème souvent rencontré dans ce dernier domaine demeure la solubilité médiocre des complexes obtenus en milieu aqueux et organique. Cette problématique peut facilement être résolue par l'ajout de groupement solubilisant, souvent via la fonctionnalisation avec des chaines alkyles de tailles variées. Le travail présenté au chapitre 4 est donc très fondamental et vise à étendre la portée d'utilisation de ce type de ligands, plus particulièrement en chimie supramoléculaire, en améliorant la solubilité des espèces macromoléculaires. Nous avons choisi de fonctionnalisé les ligands avec des unités de type ^{tert}butyle pour des raisons pratiques, puisque la 4-*tert*-butylepyridine est disponible commercialement et qu'il est raisonnablement facile de procéder à l'acétylation. Alternativement, d'autres fonctionnalitées (i.e. méthyle, isopropyle, cyclohexyle, adamantyle, …) pourraient être utilisées.

9.3. Conclusion et perspectives : Chapitre 5 et 6

Ces chapitres présentent l'assemblage par voie thermique de divers auto-assemblage à base de rhénium(I). Outre la plus grande stabilité chimique des espèces de types k^2N-, les propriétés optiques des composés étudiés sont fort étonnantes. Par exemple, nous avons été les premiers à démontrés que les espèces de type k^3N- luminescent dans l'infra-rouge à température ambiante, contrairement à ce qui avait été rapporté préalablement par d'autres groupe de recherche.

Tel que présenté au chapitre 7, il serait fort intéressant de travaillé sur la photo-induction de l'assemblage d'espèces macrocycliques à base de rhénium (Figure 9.4) et également sur la photochimie des espèces de type k^2N- et leur photo-conversion en espèce k^3N- (Figure 9.5).

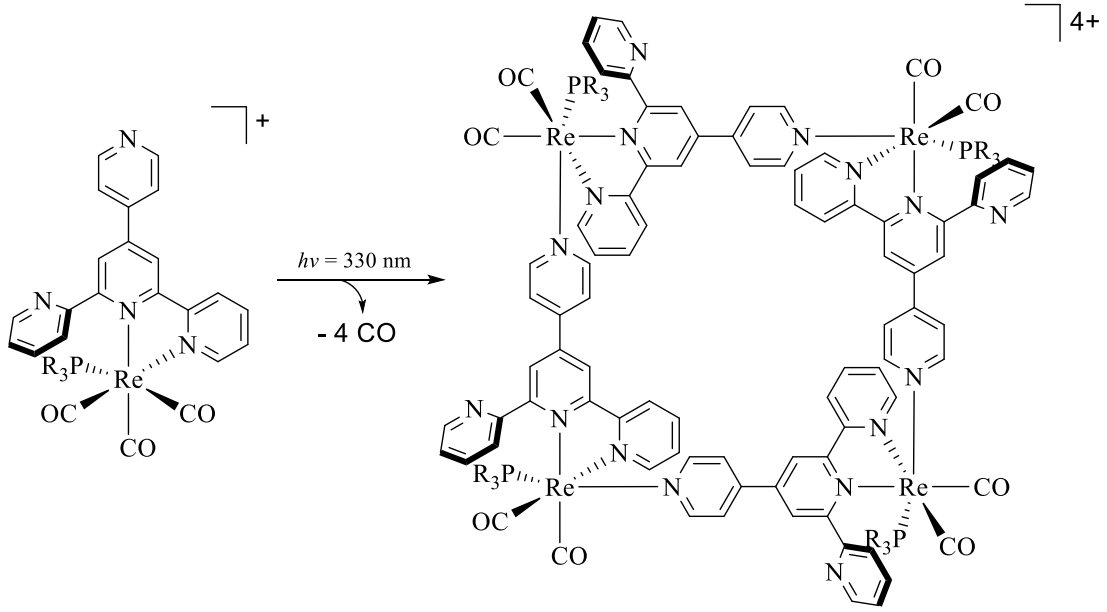

Figure 9.4 – Exemple d'un assemblage photo-induit à base de rhénium.

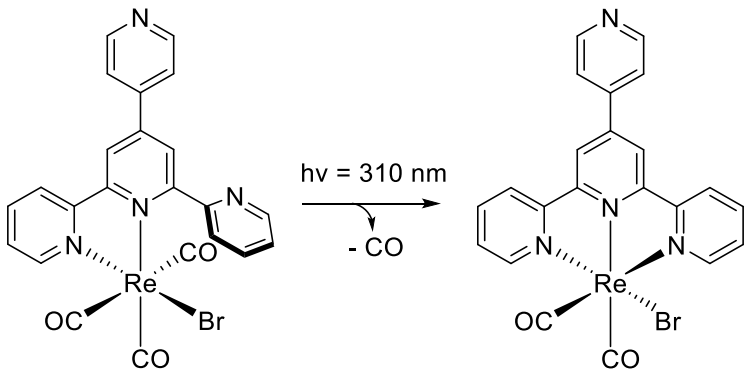

Figure 9.5 – Exemple théorique de la photo-conversion d'une espèce k^2N- en k^3N-.

9.4. Conclusion et perspectives : Chapitre 7

Le travail présenté au chapitre 7 a permis d'approfondir davantage le domaine de l'auto-assemblage photo-induit. À ce jour, ormis les travaux présentés dans le cadre de cette thèse, un seul autre exemple de ce type de chimie a été démontré par le passé par le groupe de recherche du professeur Makoto Fujita. Les briques à bases de dérivés polypyridyles de ruthénium sont nombreuses et plusieurs études sont possibles dans ce domaine. Par exemple, bien que nous ayons une idée globale du mécanisme de l'auto-assemblage présenté au chapitre 7, certaines questions demeures au niveau de la réactivité des espèces intermédiaires (dimère et trimère). D'autre part, toujours en se basant sur la base des travaux réalisés, nous pourrions penser à utiliser la cavité afin de faire de l'inclusion moléculaire. Nous pourrions étudier de nouveaux angles de coordinations, de sorte à obtenir des entités supramoléculaire unusuelle de plus grande taille. De plus, d'autres métaux sont envisageables, notamment des composés de rhénium, d'osmium, de palladium, de platine et d'iridium.

Cas isolé ou prémices d'un nouveau domaine en chimie de coordination/chimie supramoléculaire, seul le temps nous le dira. Une chose est certaine : ce domaine offre la possibilité d'étudier des molécules jusqu'ici inaccessibles par voie classique thermique. Alors que cette thèse s'achève, un univers de possibilités s'ouvre à nous.

Chapitre 10 - Informations supplémentaires: Ruthenium Bistridentate Complexes with Non-Symmetrical Hexahydro-pyrimidopyrimidine Ligands: A Structural and Theoretical Investigation of their Optical and Electrochemical Properties

10.1. Experimental

10.1.1. Materials and Instrumentations

All solvents and reagents were used as purchased without further purification before the reactions. $RuCl_3.3H_2O$ was purchased from Pressure Chemical Corporation. All other reagents were purchased from Sigma-Aldrich. ACS grade solvents were purchased from VWR and Fisher. Nuclear magnetic resonance (NMR) spectra were recorded in CD_2Cl_2, $CDCl_3$ and CD_3CN at 25ºC on a Bruker AV-400 spectrometer at 400 MHz for ^1H NMR and at 100 MHz for ^{13}C NMR. Chemical shifts (δ) are reported in parts per million (ppm) relative to TMS, and are referenced to the residual solvent signal (δ = 1.94 ppm for acetonitrile-d_3, 5.32 ppm for methylene chloride-d_2 and 7.26 ppm for chloroform-d_1). The high-resolution mass spectrometry (HR-MS) experiments were performed on a Bruker Daltonics microTOF spectrometer using electrospray ionization. Absorption and emission spectra were measured in deaerated spectrograde solvent at room temperature on a Cary 300 UV-Vis-NIR Spectrophotometer from Agilent Technologies and a Cary Eclipse Fluorescence Spectrophotometer, respectively. For the luminescence lifetimes, an Edinburgh OB 900 single-photon-counting spectrometer was used, employing a Hamamatsu PLP2 laser diode as pulse (wavelength output, 408 nm; pulse width, 59 ps).

Electrochemical measurements were carried out in argon-purged acetonitrile at room temperature with a BAS CV50W multipurpose potentiostat. The working electrode was

a glassy carbon electrode. The counter electrode was a Pt wire, and the pseudo-reference electrode was a silver wire. The reference was set using an internal 1 mM ferrocene/ferrocenium sample at $E_{1/2}$ = 400 mV vs SCE in dry acetonitrile.[1]

The concentration of the compounds was of about 1 mM. Tetrabutylammonium hexafluorophosphate (TBAP) was used as the supporting electrolyte and its concentration was 0.10 M. Cyclic voltammograms were obtained at scan rates of 50, 100, 200, and 500 mV/s. For reversible processes, half-wave potentials (vs SCE) were measured with square-wave voltammetry (SW) experiments performed with a step rate of 4 mV, an amplitude of 25 mV and a frequency of 15 Hz. For irreversible reduction processes, the cathodic peak was used as *E*. The criteria for reversibility were the close to unity ratio of the intensities of the cathodic and anodic currents, and the constancy of the peak potential on changing scan rate. Experimental uncertainties are as follows: absorption maxima, ± 2 nm; molar absorption coefficient, 10%; emission maxima, ± 5 nm; excited state lifetimes, 10%; redox potentials, ± 10 mV. The microanalyses were performed at the Elemental Analysis Service of the Université de Montréal.

10.1.2. Synthesis of the ligands and metal complexes

$Ru(DMSO)_4Cl_2$,[2] 6-bromo-2,2'-bipyridine,[3] 2-chloro-1,10-phenanthroline[4] and (4'-phenyl-2,2':6',2"-terpyridine)$RuCl_3$[5] were synthesized as previously described. Solvents were removed under reduced pressure using a rotary evaporator unless otherwise stated.

10.1.2.1. 2,2'-bipyridyl-6-hpp (bpyG, 1)

A 100 mL oven-dried round-bottomed flask was charged with (±)BINAP (16 mg, 3 mol% with respect to 6-bromo-2,2'-bipyridine) under an inert N_2-atmosphere. Dry toluene (10 mL) was added to the flask and the resulting mixture was left at 60°C to give a clear colourless solution. The solution was cooled to room temperature and $Pd(OAc)_2$ catalyst (3.8 mg, 2 mol% with respect to 6-bromo-2,2'-bipyridine) was added to the flask, leading to a clear dark red solution after 5-10 minutes. To this solution was added 6-

bromo-2,2'-bipyridine (200 mg, 0.85 mmol) and the mixture was heated at 60ºC for 20 minutes, while a color change from red to yellow could be observed. To the resulting solution was added H-hpp (130 mg, 0.94 mmol) and potassium *tert*-butoxide (240 mg, 2.13 mmol) and the resulting brownish-green solution was heated at 90ºC for 3 hours. After this time, the reaction mixture was cooled to room temperature and the solvent was evaporated to dryness. The residue was suspended in 25 mL of an ether:toluene (60:10 v/v) mixture and filtered. The filtrate was evaporated to dryness. The residue was subject to a purification over deactivated neutral alumina, using a mixture of methylene chloride and ethanol in a 95:5 ratio, affording a pure white solid (110 mg, 45%).

^{1}H NMR (400 MHz, CD_2Cl_2): δ (ppm) = 8.64 (d, J = 5 Hz, 1H), 8.15 (m, 2H), 7.97 (t, J = 8 Hz, 1H), 7.82 (t, J = 7 Hz, 1H), 7.48 (d, J = 8 Hz, 1H), 7.32 (d, J = 8 Hz, 1H), 3.97 (t, J = 6 Hz, 2H), 3.62 (m, 4H), 3.50 (t, J=6 Hz, 2H), 2.27 (quint, J = 6 Hz, 2H), 2.07 (quint, J = 6 Hz, 2H).
^{13}C NMR (100 MHz, CD_2Cl_2): δ (ppm) = 153.9, 153.7, 152.5, 150.2, 148.8, 140.3, 136.7, 123.7, 120.6, 118.5, 117.5, 47.7, 47.3, 46.3, 38.2, 20.6, 19.5.
HRMS (ESI): m/z $[M+H]^+$ calcd for $C_{17}H_{19}N_5$: 294.17132; found: 294.17265; difference: 4.52 ppm

10.1.2.2. 2-hpp-1,10-phenanthroline (phenG, 2)

Synthesized from 2-chloro-1,10-phenanthroline by following the procedure described above for 1. (825 mg, 87%).

^{1}H NMR (400 MHz, $CDCl_3$): δ (ppm) = 12.60 (s, 1H), 9.05 (dd, J = 4.3 Hz, 1H), 8.40 (d, J = 8.8 Hz, 1H), 8.26 (dd, J = 8.2 Hz, 1H), 7.94 (d, J = 8.8 Hz, 1H), 7.76 (q, J = 8.8 Hz, 2H), 7.65 (dd, J = 8.1 Hz, 1H), 4.31 (t, J = 6.0 Hz, 2H), 3.80 (t, J = 6.0 Hz, 2H), 3.72 (t, J = 6.0 Hz, 2H), 2.38 (quin, J = 6.0 Hz, 2H), 2.20 (quin, J = 6.0 Hz, 2H), 1.21 (t, J = 7.0, 1H).
^{13}C NMR (100 MHz, $CDCl_3$): δ (ppm) = 153.7, 151.6, 150.6, 144.4, 142.4, 140.5, 136.4, 129.4, 126.6, 125.8, 123.8, 115.8, 49.0, 48.2, 46.9, 39.2, 21.4, 20.1.

HRMS (ESI): m/z $[M+H]^+$ calcd for $C_{19}H_{19}N_5$: 318.17132; found: 318.17161; difference: 0.91 ppm

10.1.2.3. 8-(6-bromo-2-pyridinyl)quinolone

A 20 mL microwave vial was charged with 8-quinolinylboronic acid (75 mg, 0.43 mmol), 2,6-dibromopyridine (405 mg, 1.71 mmol), potassium carbonate (340 mg, 2.45 mmol), $Pd_2(dba)_3$ (7.5 mg, 2 mol%), SPhos (6.6 mg, 4 mol%) and 20 mL of a MeCN:H_2O (2:1) solution. The biphasic mixture was degassed for 5 minutes with argon. The mixture was left under microwave heating (400W, 80ºC) for 10 minutes. The resulting yellowish solution was extracted 4 times with methylene chloride and the organic layer was evaporated to dryness. The residue was subject to a purification by flash chromatography, using a mixture of hexanes:ethyl acetate (90:10) as the eluent. The fraction containing the desired product were combined and evaporated under reduced pressure, yielding a white solid (25 mg, 20%)

^{1}H NMR (400 MHz, $CDCl_3$): δ (ppm) = 8.95 (dd, J = 2 Hz, 1H), 8.21 (t, J = 8 Hz, 3H), 7.89 (dd, J = 1 Hz, 1H), 7.66 (t, J = 8 Hz, 2H), 7.49 (d, J = 8 Hz, 1H), 7.44 (dd, J = 4 Hz, 1H).
^{13}C NMR (100 MHz, CD_2Cl_2): δ (ppm) = 157.8, 150.3, 145.6, 141.5, 137.8, 136.9, 136.5, 131.6, 129.3, 128.5, 126.5, 126.3, 125.9, 121.1.

10.1.2.4. 2-hpp-6-quinolylpyridine (QpyG, 3)

Synthesized from 8-(6-bromo-2-pyridinyl)quinolone by following the procedure described above for 1. (825 mg, 87%)

^{1}H NMR (400 MHz, CDCl3): δ (ppm) = 8.89 (dd, J = 2 Hz, 1H), 8.27 (dd, J = 2 Hz, 1H), 8.05 (t, J = 8 Hz, 1H), 7.95 (dd, J = 1 Hz, 1H), 7.91 (dd, J = 1 Hz, 1H), 7.66 (t, J = 7 Hz, 1H), 7.62 (d, J = 7 Hz, 1H), 7.55 (d, J = 8 Hz, 1H), 7.48 (dd, J = 4 Hz, 1H), 4.08 (t, J = 6 Hz, 2H), 3.68 (t, J = 6 Hz, 2H), 3.60 (t, J = 6 Hz, 2H), 3.51 (dt, J = 6 Hz, 2H), 2.29 (quint, J = 6 Hz, 2H), 2.11 (quint, J = 6 Hz, 2H).

^{13}C NMR (100 MHz, CD2Cl2): δ (ppm) = 156.1, 153.4, 151.0, 150.7, 145.6, 141.0, 137.2, 136.9, 131.1, 130.0, 129.1, 126.6, 123.2, 121.7, 115.8, 48.5, 48.2, 47.4, 46.9, 21.2, 20.1.

HRMS (ESI): m/z $[M+H]^+$ calcd for $C_{21}H_{21}N_5$: 344.18697; found: 344.18649; difference: 1.39 ppm

10.1.2.5. *mer*-[Ru(bpyG)$_2$][(PF$_6$)$_2$] (4)

A 20 mL microwave vial was charged with ligand 1 (50 mg, 0.17 mmol), $Ru(DMSO)_4Cl_2$ (40.5 mg, 0.083 mmol), 4-ethylmorpholine (12 drops) and ethylene glycol (15 mL). The vial was then subjected to microwave irradiation (400W, 200ºC) for 20 minutes. After this time, the resulting deep purple solution was poured into an aqueous KPF_6 solution (10 eq.). The resulting precipitate was filtered over paper. Recrystallization from slow diffusion of ether into an acetone solution afforded purple needles (40 mg, 50%).

^{1}H NMR (400 MHz, CD_3CN): δ (ppm) = 8.37 (d, J = 8 Hz, 2H), 8.29 (d, J = 8 Hz, 2H), 8.14 (t, J = 8 Hz, 2H), 7.80 (t, J = 8 Hz, 2H), 7.67 (d, J = 5 Hz, 2H), 7.62 (d, J = 8 Hz, 2H), 7.16(t, J = 6 Hz, 2H), 4.04 (dt, J = 4 Hz, 2H), 4.04 (dt, J = 4 Hz, 2H), 3.37-3.30 (m, 4H), 3.14 (dt, J = 9 Hz, 2H), 3.00 (q, J = 6 Hz, 2H), 2.93 (quint, J = 6 Hz, 2H), 2.55 (dq, J = 4 Hz, 2H), 2.38 (m, 2H), 2.15 (m, 2H), 1.83 (dq, J = 4 Hz, 2H), 1.12 (m, 2H).

^{13}C NMR (100 MHz, CD_3CN): δ (ppm) = 158.5, 156.5, 156.1, 153.3, 151.8, 137.0, 135.6, 125.5, 123.9, 119.0, 117.1, 49.9, 49.7, 49.1, 47.8, 30.8, 24.1, 23.7.

Elemental analysis: Calc. for $C_{34}H_{38}N_{10}RuP_2F_{12}\cdot(C_2H_5)_2O$: C, 43.39%; H, 4.60%; N, 13.32%. Found: C, 43.09%; H, 4.45%; N, 13.24%.

HRMS (ESI): m/z $[M-PF_6]^+$ calcd for $C_{34}H_{38}N_{10}RuPF_6$: 833.19695; found: 833.19864; difference: 2.03 ppm; $[M-2PF_6]^{2+}$ calcd for $C_{34}H_{38}N_{10}Ru$: 344.11611; found: 344.11664; difference: 1.54 ppm.

10.1.2.6. *mer*-[Ru(phenG)$_2$][(PF$_6$)$_2$] (5)

A 20 mL microwave vial was charged with ligand 2 (100 mg, 0.32 mmol), $RuCl_3.3H_2O$ (37 mg, 0.14 mmol), 4-ethylmorpholine (12 drops) and ethylene glycol (15 mL). The vial was then subjected to microwave irradiation (400W, 200ºC) for 20 minutes. After this

time, the resulting deep purple solution was poured into an aqueous KPF_6 solution (10 eq.). The resulting precipitate was filtered over celite, washed with ethyl acetate and dissolve with a minimum amount of acetonitrile. The solvent were removed under vacuum. Recrystallization from slow diffusion of ether into an acetone solution afforded purple block (85 mg, 52%).

^{1}H NMR (400 MHz, CD_3CN): δ (ppm) = 8.73 (d, J = 9.0 Hz, 2H), 8.34 (d, J = 8.1 Hz, 2H), 8.23 (d, J = 8.8 Hz, 2H), 8.05 (d, J = 8.8 Hz, 2H), 7.97 (m, 4H), 7.45 (dd, J = 8.2 Hz, 2H), 4.30 (dt, J = 5.0 Hz, 2H), 3.60 (m, 2H), 3.42 (m, 2H), 3.14 (m, 2H), 2.95 (m, 2H), 2.81 (m, 2H), 2.71 (m, 2H), 2.46 (m, 2H), 2.22 (m, 2H), 1.84 (m, 2H), 1.31 (m, 2H), 0.78 (m, 2H).
^{13}C NMR (100 MHz, CD_3CN): δ (ppm) = 154.7, 153.6, 151.3, 148.5, 147.2, 135.9, 134.9, 131.0, 127.5, 127.4, 126.9, 124.5, 117.4, 49.6, 49.5, 49.0, 48.7, 24.1, 23.1.
Elemental analysis: Calc. for $C_{38}H_{38}N_{10}RuP_2F_{12}\cdot C_4H_8O_2$: C, 45.29%; H, 4.16%; N, 12.57%. Found: C, 45.36%; H, 4.50%; N, 12.07%.
HRMS (ESI): m/z $[M\text{-}PF_6]^+$ calcd for $C_{38}H_{38}N_{10}RuPF_6$: 881.19706; found: 881.19717; difference: 0.12 ppm.

10.1.2.7. *fac*-[Ru(QpyG)$_2$][(PF$_6$)$_2$] (6)

A 20 mL microwave vial was charged with ligand 3 (50 mg, 0.15 mmol), $RuCl_3.3H_2O$ (19 mg, 0.073 mmol), 4-ethylmorpholine (12 drops) and ethylene glycol (15 mL). The vial was then subjected to microwave irradiation (400W, 200°C) for 20 minutes. After this time, the resulting deep purple solution was poured into an aqueous KPF_6 solution (10 eq.). The resulting precipitate was filtered over paper. The crude mixture was purified over silica using a MeCN:H_2O:NaCl sat. mixture in a 7:2:1 ratio. The major deep purple fraction was then evaporated to dryness and dissolved in a minimum amount of water. The fraction was rechromatographed using SP-Sephadex C25 cation exchanger column (1.5 cm x 35 cm) with 0.15M sodium (-)-*O*,*O'*-dibenzoyl-L-tartrate solution (pH adjusted between 8 – 9 with NaOH 4M). The major purple band was recovered and a saturated KPF_6 solution (10-15 mL) was added to the fraction. The product was extracted thrice with dichloromethane. The organic layer was then washed with three portions of diluted

NaOH 2M in order to remove the remaining excess of (-)-*O*,*O'*-dibenzoyl-L-tartrate. Recrystallization from slow diffusion of ether into a concentrated acetonitrile solution afforded purple needles (15 mg, 19%).

^{1}H NMR (400 MHz, CD_3CN): δ (ppm) = 9.67 (d, J = 8 Hz, 2H), 8.31 (d, J = 8 Hz, 2H), 7.96 (dd, J = 8 Hz, 4H), 7.61 (dd, J = 8 Hz, 2H), 7.47 (t, J = 8 Hz, 2H), 7.39 (t, J = 8 Hz, 2H), 7.31 (d, J = 8 Hz, 2H), 6.15 (d, J = 8 Hz, 2H), 4.11 (dd, J = 13 Hz, 2H), 3.69 (dt, J = 11 Hz, 2H), 3.50-3.44 (m, 4H), 3.36-3.29 (m, 4H), 3.15-3.08 (m, 6H), 1.84-1.78 (m, 3H), 1.71-1.54 (m, 3H).

^{13}C NMR (100 MHz, CD_3CN): δ (ppm) =160.2, 159.3, 159.0, 151.4, 148.2, 137.8, 137.6, 134.7, 131.4, 130.1, 129.3, 128.3, 123.2, 123.0, 109.8 50.4, 49.4, 48.8, 45.9, 23.8, 22.0.

Elemental analysis: Calc. for $C_{42}H_{42}N_{10}RuP_2F_{12}\cdot 2H_2O$: C, 45.29%; H, 4.16%; N, 12.57%. Found: C, 45.09%; H, 4.01%; N, 12.83%.

HRMS (ESI): m/z $[M\text{-}PF_6]^+$ calcd for $C_{42}H_{42}N_{10}RuPF_6$: 933.22847; found: 933.23303; difference: 4.89 ppm; $[M\text{-}2PF_6]^{2+}$ calcd for $C_{42}H_{42}N_{10}Ru$: 394.13187; found: 394.13134; difference: 1.34 ppm.

10.1.2.8. *mer*-[Ru(bpyG)(phtpy)][$(PF_6)_2$] (7)

A 20 mL microwave vial was charged with ligand 1 (35 mg, 0.12 mmol), (4'-phenyl-2,2':6',2"-terpyridine)$RuCl_3$ (66.5 mg, 0.129 mmol), 4-ethylmorpholine (12 drops) and ethylene glycol (15 mL). The vial was then subjected to microwave irradiation (400W, 200ºC) for 20 minutes. After this time, the resulting orange-red solution was poured into an aqueous KPF_6 solution (10 eq.). The resulting precipitate was filtered over paper. The residue was purified on a silica column with a mixture of MeCN:H_2O:KNO_3 sat. in a 7:2:1 ratio. The isolated species was subjected to a second metathesis with KPF_6 solution (10 eq.). The precipitate was extracted with dichloromethane and the solvent was removed under vacuum. The resulting precipitate was recrystallized by slow diffusion of ether into an acetone solution to afforded orange needles (70 mg, 60%).

^{1}H NMR (400 MHz, CD_3CN): δ (ppm) = 8.84 (s, 2H), 8.56 (d, J = 8 Hz, 2H), 8.42 (d, J = 8 Hz, 1H), 8.35 (d, J = 8 Hz, 1H), 8.31 (t, J = 8 Hz, 1H), 8.15 (d, J = 7 Hz, 2H), 7.97 (t, J = 8 Hz, 2H), 7.79 (d, J = 8 Hz, 1H), 7.75-7.70 (m, 3H), 7.66 (t, J = 7 Hz, 1H), 7.60

(d, J = 5 Hz, 2H), 7.33 (t, J = 7 Hz, 2H), 7.11 (d, J = 5 Hz, 1H), 7.03 (t, J = 7 Hz, 1H), 3.91 (d, J = 6 Hz, 2H), 3.30 (t, J = 7 Hz, 2H), 2.96 (t, J = 6 Hz, 2H), 2.36 (dd, J = 4 Hz, 2H), 2.14 (dd, J = 6 Hz, 2H), 1.23 (dd, J = 6 Hz, 2H).

^{13}C NMR (100 MHz, CD_3CN): δ (ppm) = 159.2, 158.0, 157.8, 155.5, 153.5, 151.9, 147.6, 138.7, 138.3, 137.9, 136.9, 133.1, 131.1, 130.5, 130.3, 128.6, 128.4, 127.2, 124.8, 124.4, 122.3, 119.6, 49.8, 49.7, 48.9, 46.5, 30.8, 24.0, 23.1.

Elemental analysis: Calc. for $C_{38}H_{34}N_8RuP_2F_{12}\cdot C_3H_6O$: C, 46.82%; H, 3.83%; N, 10.65%. Found: C, 46.86%; H, 3.88%; N, 10.60%.

HRMS (ESI): m/z $[M\text{-}PF_6]^+$ calcd for $C_{38}H_{34}N_8RuPF_6$: 849.15962; found: 849.15829; difference: 1.57 ppm.

10.1.2.9. *mer*-[Ru(phenG)(phtpy)][$(PF_6)_2$] (8)

Synthesized from ligand 2 by following the procedure described above for metal complex 7. (97 mg, 48%).

^{1}H NMR (400 MHz, CD_3CN): δ (ppm) = 8.90 (s, 2H), 8.87 (d, J = 9.1 Hz, 1H), 8.58 (d, J = 7.6 Hz, 2H), 8.30 (t, J = 8.4 Hz, 2H), 8.21 (dd, J = 8.2 Hz, 2H), 8.13 (d, J = 8.1 Hz, 1H), 8.04 (d, J = 8.0 Hz, 1H), 7.92 (dt, J = 8.1 Hz, 2H), 7.74 (tt, J = 7.3 Hz, 2H), 7.68 (tt, J = 7.4 Hz, 1H), 7.53 (m, 2H), 7.47 (dd, J = 5.3 Hz, 1H), 7.36 (dd, J = 8.2 Hz, 1H), 7.20 (m, 2H), 4.11 (t, J = 5.7 Hz, 2H), 3.37 (t, J = 7.4 Hz, 2H), 3.04 (t, J = 6.2 Hz, 2H), 2.46 (m, 2H), 2.32 (t, J = 5.7 Hz, 2H), 1.30 (m, 2H).

^{13}C NMR (100 MHz, CD_3CN): δ (ppm) = 161.0, 159.4, 158.2, 154.4, 153.7, 152.9, 152.3, 147.7, 147.5, 146.2, 138.3, 138.1, 137.8, 136.3, 131.3, 131.1, 130.6, 128.7, 128.4, 1128.3, 128.0, 127.0, 125.5, 124.9, 122.3, 49.8, 49.5, 49.2, 47.7, 24.2, 23.1.

Elemental analysis: Calc. for $C_{40}H_{34}N_8RuP_2F_{12}\cdot(C_2H_5)_2O$: C, 48.40%; H, 4.06%; N, 10.26%. Found: C, 47.97%; H, 3.92%; N, 10.20%.

HRMS (ESI): m/z $[M\text{-}PF_6]^+$ calcd for $C_{40}H_{34}N_8RuPF_6$: 873.15968; found: 873.16233; difference: 3.03 ppm.

10.1.2.10. *mer*-[Ru(QpyG)(phtpy)][$(PF_6)_3$] (9)

Synthesized from ligand 3 by following the procedure described above for metal complex 7. (14.5 mg, 10%).

^{1}H NMR (400 MHz, CD_3CN): δ (ppm) = 8.70-60 (m, broad), 8.55-8.47 (m, broad), 8.43 (d, broad), 8.30-8.19 (m, broad), 8.16-8.04 (m, broad), 8.01 (d, broad), 7.96-7.90 (m, broad), 7.88-7.83 (m, broad), 7.77 (d, broad), 7.72-7.66 (m, broad), 7.65-7.57 (m, broad), 3.27-3.14 (m, broad), 2.91-2.83 (m, broad), 2.41-2.25 (m, broad), 1.82-1.72 (m, broad), 1.33-1.25 (m, broad), 1.20-1.10 (m, broad).

^{13}C NMR (100 MHz, CD_3CN): δ (ppm) = No peak was observed due to the paramagnetic nature of the compound.

HRMS (ESI): m/z $[M-PF_6]^+$ calcd for $C_{42}H_{36}N_8RuPF_6$: 899.17538; found: 899.17326; difference: 2.36 ppm

10.1.3. X-ray, DFT and TD-DFT results

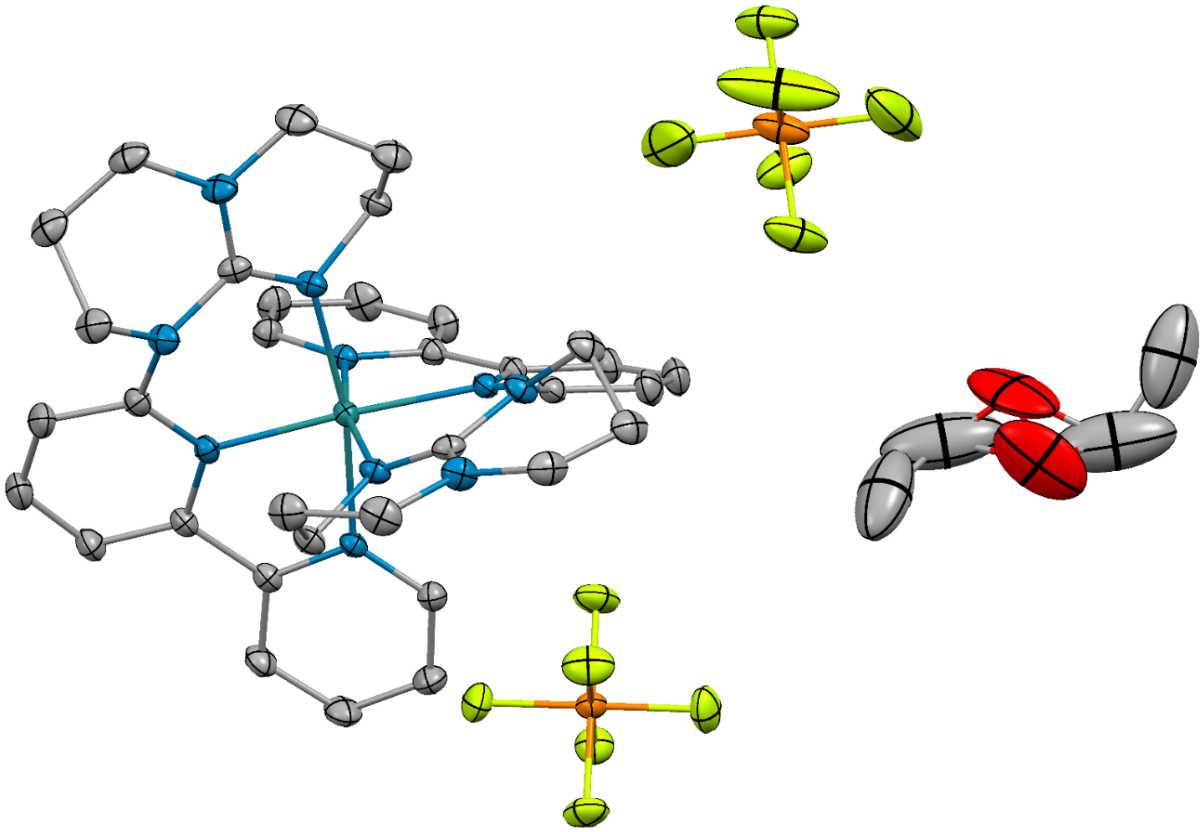

Figure 10.1 - Thermal ellipsoid diagram (30% probability) of the single crystal of 4 with the counter-anions (PF_6) and a disordered diethyl ether co-crystallization solvent molecule. The hydrogens atoms are omitted for clarity.

Table 10.1 - Atomic coordinates for DFT optimization of 4^{2+} in ($S = 0$) PBE0/LANL2DZ, CPCM(CH_3CN).

Standard orientation					
Center Number	Atomic Number	Atomic Type	Coordinates (Angstroms)		
			X	Y	Z
1	44	0	-0.000219	0.479713	0.000006
2	7	0	1.824154	0.623289	0.881213
3	7	0	-0.370106	1.980844	1.368745
4	7	0	0.732269	-0.946179	-1.330792
5	7	0	2.202619	-2.710516	-1.909561

6	7	0	2.622483	-1.465294	0.031346
7	6	0	1.999801	1.734069	1.674596
8	6	0	2.855581	-0.235586	0.671366
9	6	0	0.763061	2.475503	1.966180
10	6	0	-1.566647	2.552917	1.647821
11	1	0	-2.434813	2.121020	1.167853
12	6	0	1.808133	-1.674940	-1.096102
13	6	0	3.248772	2.061351	2.203444
14	1	0	3.381175	2.940160	2.820592
15	6	0	3.555970	-3.305096	-1.955585
16	1	0	4.028198	-3.039252	-2.910380
17	1	0	3.420044	-4.393939	-1.950455
18	6	0	-1.689282	3.643334	2.510613
19	1	0	-2.667983	4.066763	2.703077
20	6	0	0.090745	-1.166319	-2.643524
21	1	0	0.710671	-0.728541	-3.440544
22	1	0	-0.868072	-0.653469	-2.652103
23	6	0	-0.534752	4.168995	3.108832
24	1	0	-0.595120	5.019389	3.778617
25	6	0	0.700533	3.573166	2.835155
26	1	0	1.599045	3.957228	3.301747
27	6	0	1.301793	-3.296669	-2.923002
28	1	0	1.247031	-4.379027	-2.748427
29	1	0	1.758323	-3.146425	-3.910710
30	6	0	3.490233	-2.610703	0.393615
31	1	0	2.847993	-3.479191	0.581858
32	1	0	4.011831	-2.388504	1.323466
33	6	0	4.430302	-2.894267	-0.770761
34	1	0	5.018274	-1.999214	-1.000381
35	1	0	5.129725	-3.700083	-0.530339

36	6	0	4.143861	0.076520	1.155301
37	1	0	4.986336	-0.561335	0.923594
38	6	0	-0.082809	-2.664326	-2.884267
39	1	0	-0.686609	-3.090466	-2.075204
40	1	0	-0.600744	-2.858007	-3.828805
41	6	0	4.338198	1.231160	1.912020
42	1	0	5.329263	1.479792	2.274371
43	7	0	-1.824717	0.621765	-0.881189
44	7	0	0.368411	1.981126	-1.368770
45	7	0	-0.731519	-0.946756	1.330818
46	7	0	-2.200255	-2.712447	1.909516
47	7	0	-2.621271	-1.467504	-0.031331
48	6	0	-2.001300	1.732405	-1.674557
49	6	0	-2.855426	-0.237967	-0.671316
50	6	0	-0.765174	2.474848	-1.966186
51	6	0	1.564475	2.554174	-1.647882
52	1	0	2.433008	2.122999	-1.167928
53	6	0	-1.806725	-1.676477	1.096097
54	6	0	-3.250557	2.058679	-2.203348
55	1	0	-3.383699	2.937380	-2.820491
56	6	0	-3.553043	-3.308305	1.955500
57	1	0	-4.025495	-3.043038	2.910345
58	1	0	-3.416101	-4.397021	1.950209
59	6	0	1.686197	3.644677	-2.510697
60	1	0	2.664547	4.068904	-2.703189
61	6	0	-0.089836	-1.166348	2.643562
62	1	0	-0.710217	-0.729210	3.440579
63	1	0	0.868488	-0.652577	2.652208
64	6	0	0.531223	4.169381	-3.108899
65	1	0	0.590879	5.019810	-3.778703

66	6	0	-0.703567	3.572545	-2.835180
67	1	0	-1.602405	3.955858	-3.301762
68	6	0	-1.298852	-3.297883	2.922863
69	1	0	-1.243041	-4.380160	2.748121
70	1	0	-1.755530	-3.148230	3.910592
71	6	0	-3.487996	-2.613684	-0.393631
72	1	0	-2.844978	-3.481590	-0.581908
73	1	0	-4.009805	-2.391941	-1.323469
74	6	0	-4.427782	-2.898136	0.770756
75	1	0	-5.016511	-2.003602	1.000464
76	1	0	-5.126521	-3.704537	0.530309
77	6	0	-4.143992	0.073133	-1.155147
78	1	0	-4.985955	-0.565367	-0.923357
79	6	0	0.085147	-2.664201	2.884225
80	1	0	0.689391	-3.089708	2.075163
81	1	0	0.603226	-2.857447	3.828774
82	6	0	-4.339301	1.227623	-1.911846
83	1	0	-5.330589	1.475476	-2.274119

Table 10.2 - Selected bond distances and angles of 4.

Bond Length			Angle		
	Obs. (X-ray)	Calc. (DFT)		Obs. (X-ray)	Calcl. (DFT)
N1-Ru1 N1'-Ru1	2.0542 (17)	2.06487	N1-Ru1-N1'	86.59 (9)	86.720
			N1-Ru1-N2	79.63 (7)	79.742
			N1-Ru1-N2'	94.03 (7)	94.350
			N1-Ru1-N4	169.27 (7)	169.715
N2-Ru1 N2'-Ru1	2.0165 (18)	2.03113	N1-Ru1-N4'	91.98 (7)	90.656
			N2-Ru1-N1'	94.03 (7)	94.349

			N2-Ru1-N2’	171.35 (10)	171.936
			N2-Ru1-N4	89.88 (7)	90.556
N4-Ru1 N4’-Ru1	2.0621 (18)	2.08343	N2-Ru1-N4’	96.16 (7)	94.965
			N4-Ru1-N1’	91.98 (7)	90.656
			N4-Ru1-N2’	96.17 (7)	94.965
			N4-Ru1-N4’	91.36 (10)	93.602

Table 10.3 - Total energy values for the optimized structure of the first and second oxidation on complex 4 (uPBE1PBE, LANL2DZ, CPCM: Acetonitrile).

4	S	2S+1	Total Energy			Exp.
			a. u.	eV	ΔeV	eV
Neutral	0	1	-1957.34027912	-53261.96169984	-	-
1st ox.	1/2	2	-1957.17249935	-53257.39617805	4.57	4.68
2nd ox.	1	3	-1956.92448050	-53250.67723888	6.72	5.87

Table 10.4 - Spin contamination monitoring for the DFT calculation of 4 oxidized species.

4	S	2S+1	S**2		
			Before annihilation	After annihilation	% change
1st oxidation	1/2	2	0.7549	0.7500	1
2nd oxidation	1	3	2.0162	2.0002	1

Table 10.5 - Mulliken spin density values for each of the oxidized 4 species.

4	Mulliken spin density		
	Ruthenium	2,2'-bpy	hpp
1st ox.	0.782 (78%)	-0.008 (0%)	0.228 (23%)
2nd ox.	0.764 (38%)	0.013 (1%)	1.318 (66%)

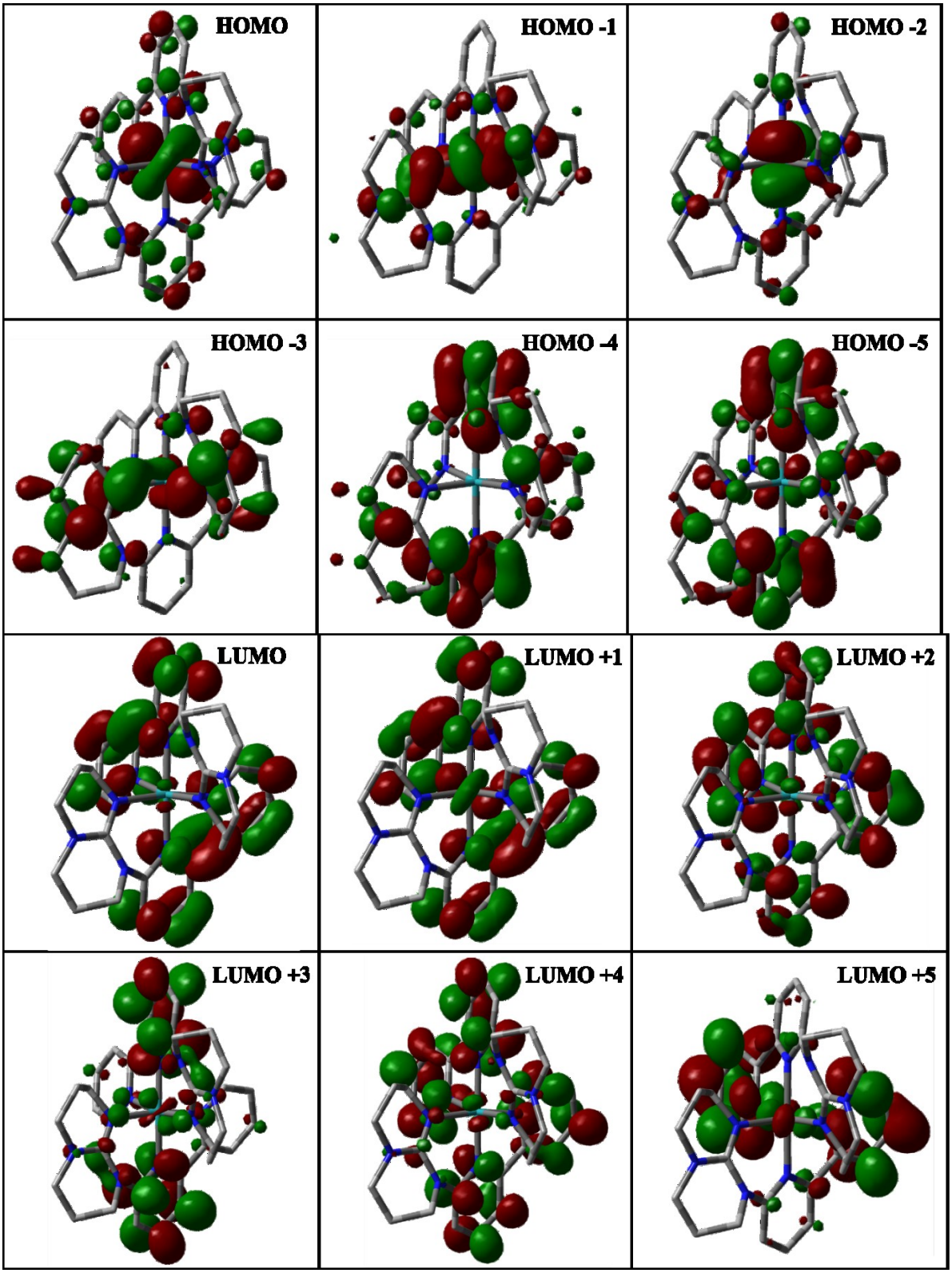

Figure 10.2 - Kohn-Sham electron density illustration of the the molecular orbitals for 42+ in (S = 0) ground state.

Table 10.6 - MO composition of 4^{2+} in (*S=0*) ground state.

MO	Energy (eV)	Composition		
		Ruthenium	bpyG	
			2,2'-bpy	hpp
LUMO+5	-0.125	1	92	6
LUMO+4	-1.348	5	94	1
LUMO+3	-1.389	2	88	9
LUMO+2	-1.551	2	94	4
LUMO+1	-2.295	9	90	1
LUMO	-2.589	1	98	1
HOMO	-5.259	59	29	9
HOMO-1	-6.073	69	24	7
HOMO-2	-6.173	78	12	9
HOMO-3	-6.752	4	6	79
HOMO-4	-7.126	0	51	44
HOMO-5	-7.175	5	54	37

Table 10.7 - Selected transitions from TD-DFT calculations of 4^{2+} in the singlet ground state (PBE0), CPCM (CH_3CN).

Energy (eV)	λ (nm)	f	Transition	Character
1.69	735	0.0064	H→L (99%)	hpp to bpy ; Ru to bpy
1.84	674	0.0070	H→L+1 (97%)	hpp to bpy ; Ru to bpy
2.53	491	0.0671	H-2→L+1 (17%) H-1→L (79%)	Ru to bpy
2.66	466	0.0617	H-2→L+1 (77%) H-1→L (16%)	Ru to bpy
2.97	418	0.0456	H→L+4 (87%)	hpp to bpy ; Ru to bpy
3.17	391	0.0891	H-1→L+1 (30%)	hpp to bpy ; Ru to bpy

			H→L+5 (52%)	
3.88	320	0.1271	H-4→L (68%) H-1→L+5 (17%)	hpp to bpy ; Ru to bpy
3.93	316	0.2899	H-5→L (70%) H-1→L+4 (15%)	hpp to bpy ; Ru to bpy
4.76	261	0.1792	H-7→L (55%) H-4→L+2 (22%)	hpp to bpy
4.84	256	0.1748	H-8→L (11%) H-2→L+13 (11%) H-1→L+10 (14%) H→L+8 (33%)	Ru to bpy
4.91	252	0.1307	H-8→L (57%) H-5→L+2 (15%)	hpp to bpy ; Ru to bpy
5.05	246	0.1337	H-7→L+1 (81%)	hpp to bpy
5.21	238	0.1147	H-6→L+2 (67%)	hpp to bpy ; Ru to bpy
5.76	215	0.1089	H-12→L (23%) H-10→L+1 (16%) H-7→L+2 (31%)	hpp to bpy

Table 10.8 - Atomic coordinates for DFT optimization of 5^{2+} in ($S = 0$) PBE0/LANL2DZ, CPCM(CH_3CN).

Standard orientation					
Center Number	Atomic Number	Atomic Type	Coordinates (Angstroms)		
			X	Y	Z
1	6	0	4.191292	-1.082350	0.240532
2	6	0	4.804589	-0.032138	-0.418386
3	7	0	2.015209	-0.204226	-0.245035
4	6	0	4.018412	0.946975	-1.074387
5	6	0	2.768678	-1.178829	0.306427

6	6	0	2.621094	0.814674	-0.952485
7	6	0	4.554143	2.031224	-1.850277
8	6	0	3.722542	2.906120	-2.504708
9	6	0	2.293287	2.758382	-2.433076
10	6	0	1.383366	3.592520	-3.129534
11	6	0	1.753766	1.717125	-1.638711
12	6	0	0.019054	3.346784	-3.018575
13	6	0	-0.441392	2.288469	-2.209091
14	7	0	0.397909	1.492271	-1.522812
15	7	0	2.173594	-2.323440	0.884214
16	6	0	2.370252	-4.788521	1.355119
17	7	0	0.696402	-3.402798	2.395472
18	6	0	1.741568	-4.395031	2.682630
19	6	0	0.915968	-2.360064	1.529936
20	6	0	3.046686	-3.540781	0.817460
21	7	0	0.000000	-1.418016	1.356200
22	6	0	-1.733222	-2.830319	2.363815
23	6	0	-0.660498	-3.799129	2.846000
24	6	0	-1.108007	-1.438450	2.330228
25	44	0	0.000000	0.000000	-0.159238
26	6	0	-4.191292	1.082350	0.240532
27	6	0	-4.804589	0.032138	-0.418386
28	7	0	-2.015209	0.204226	-0.245035
29	6	0	-4.018412	-0.946975	-1.074387
30	6	0	-2.768678	1.178829	0.306427
31	6	0	-2.621094	-0.814674	-0.952485
32	6	0	-4.554143	-2.031224	-1.850277
33	6	0	-3.722542	-2.906120	-2.504708
34	6	0	-2.293287	-2.758382	-2.433076
35	6	0	-1.383366	-3.592520	-3.129534

36	6	0	-1.753766	-1.717125	-1.638711
37	6	0	-0.019054	-3.346784	-3.018575
38	6	0	0.441392	-2.288469	-2.209091
39	7	0	-0.397909	-1.492271	-1.522812
40	7	0	-2.173594	2.323440	0.884214
41	6	0	-2.370252	4.788521	1.355119
42	7	0	-0.696402	3.402798	2.395472
43	6	0	-1.741568	4.395031	2.682630
44	6	0	-0.915968	2.360064	1.529936
45	6	0	-3.046686	3.540781	0.817460
46	7	0	0.000000	1.418016	1.356200
47	6	0	1.733222	2.830319	2.363815
48	6	0	0.660498	3.799129	2.846000
49	6	0	1.108007	1.438450	2.330228
50	1	0	-1.598682	5.166934	0.675873
51	1	0	-3.128707	5.567051	1.479149
52	1	0	-4.812243	1.820563	0.725370
53	1	0	-3.364484	3.669858	-0.221796
54	1	0	-5.887444	-0.033048	-0.441543
55	1	0	-5.632456	-2.137898	-1.919756
56	1	0	-4.131709	-3.717504	-3.098862
57	1	0	-1.755436	-4.404517	-3.746056
58	1	0	0.704963	-3.957838	-3.544710
59	1	0	1.499312	-2.079442	-2.116493
60	1	0	-3.935633	3.372322	1.432446
61	1	0	-2.495053	3.983333	3.366214
62	1	0	-1.270568	5.244623	3.180060
63	1	0	0.860385	4.815741	2.483539
64	1	0	0.642489	3.835170	3.941620
65	1	0	2.594654	2.867904	3.037848

66	1	0	2.080134	3.093068	1.358431
67	1	0	0.726495	1.179899	3.329943
68	1	0	1.830667	0.677071	2.048188
69	1	0	-1.830667	-0.677071	2.048188
70	1	0	-0.726495	-1.179899	3.329943
71	1	0	-2.594654	-2.867904	3.037848
72	1	0	-2.080134	-3.093068	1.358431
73	1	0	-0.860385	-4.815741	2.483539
74	1	0	-0.642489	-3.835170	3.941620
75	1	0	1.270568	-5.244623	3.180060
76	1	0	2.495053	-3.983333	3.366214
77	1	0	1.598682	-5.166934	0.675873
78	1	0	3.128707	-5.567051	1.479149
79	1	0	3.935633	-3.372322	1.432446
80	1	0	3.364484	-3.669858	-0.221796
81	1	0	4.812243	-1.820563	0.725370
82	1	0	5.887444	0.033048	-0.441543
83	1	0	5.632456	2.137898	-1.919756
84	1	0	4.131709	3.717504	-3.098862
85	1	0	1.755436	4.404517	-3.746056
86	1	0	-0.704963	3.957838	-3.544710
87	1	0	-1.499312	2.079442	-2.116493

Table 10.9 - Total energy values for the optimized structure of the first and second oxidation on complex 5 (uPBE1PBE, LANL2DZ, CPCM: Acetonitrile).

5	S	2S+1	Total Energy			Experimental
			a. u.	eV	ΔeV	eV
Neutral	0	1	-2109.61215483	-57405.498080329	-	-
1st ox.	1/2	2	-2109.42863809	-57400.504333094	4.99	4.68
2nd ox.	1	3	-2109.20775581	-57394.493817241	6.01	5.80

Table 10.10 - Spin contamination monitoring for the DFT calculation of 5 oxidized species.

5	S	2S+1	S**2		
			Before annihilation	After annihilation	% change
1st ox.	1/2	2	0.7576	0.7500	1
2nd ox.	1	3	2.0157	2.0001	1

Table 10.11 - Mulliken spin density values for each of the oxidized 5 species.

5	Mulliken spin density		
	Ruthenium	1,10-phenanthroline	hpp
1st ox.	0.879 (88%)	-0.004 (0%)	0.126 (13%)
2nd ox.	0.979 (49%)	0.015 (1%)	1.006 (50%)

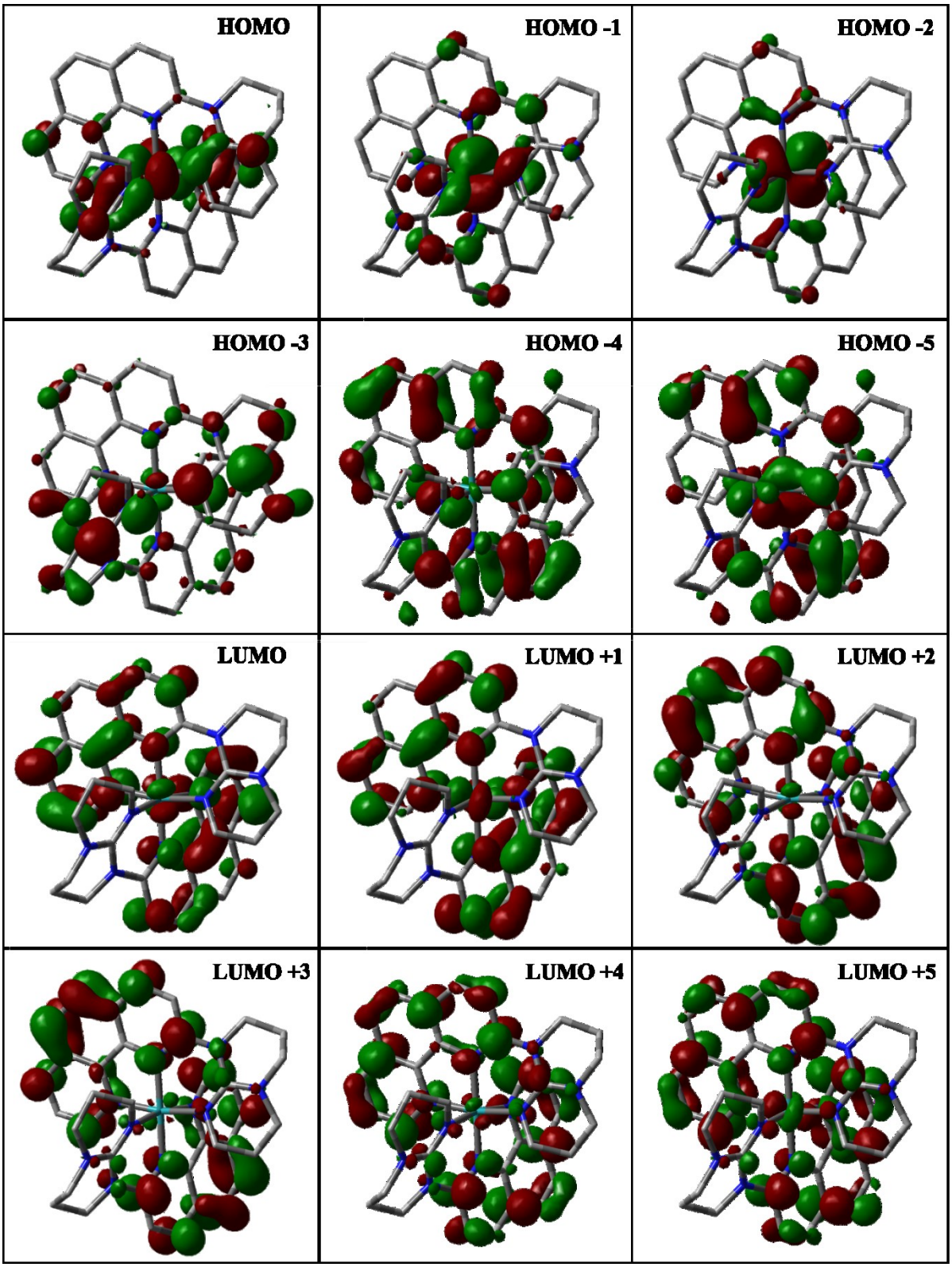

Figure 10.3 - Kohn-Sham electron density illustration of the the molecular orbitals for 52+ in (S = 0) ground state

Table 10.12 - MO composition of 5^{2+} in (*S=0*) ground state.

MO	Energy (eV)	Composition		
		Ruthenium	phenG	
			1,10-phenanthroline	hpp
LUMO+5	-0.848	4	83	13
LUMO+4	-0.923	4	81	15
LUMO+3	-2.185	2	97	1
LUMO+2	-2.206	2	95	3
LUMO+1	-2.302	4	92	4
LUMO	-2.322	2	92	6
HOMO	-5.362	58	8	33
HOMO-1	-5.443	63	14	23
HOMO-2	-6.021	86	9	6
HOMO-3	-6.706	8	9	83
HOMO-4	-6.948	7	55	38
HOMO-5	-7.078	9	57	34

Table 10.13 - Selected transitions from TD-DFT calculations of 5^{2+} in the singlet ground state (PBE0), CPCM (CH_3CN).

Energy (eV)	λ (nm)	f	Transition	Character
2,32	533	0,1311	H-1→L+1 (74%) HOMO→LUMO (21%)	Ru to phen; hpp to phen
4,01	309	0,0942	H-4→L+3 (11%) H-3→LUMO (10%) H-3→L+2 (69%)	hpp to phen
4,04	307	0,2253	H-4→L+2 (29%) H-3→L+3 (49%)	hpp to phen

4,37	283	0,0863	HOMO→L+7 (75%)	Ru to phen; hpp to phen
4,47	278	0,0907	H-1→L+6 (60%) HOMO→L+7 (11%)	Ru to phen; hpp to phen
4,55	273	0,2552	H-8→L+1 (13%) H-7→LUMO (49%)	hpp to phen
4,59	270	0,1672	H-1→L+7 (37%) HOMO→L+6 (20%)	Ru to phen; hpp to phen
4,74	262	0,2009	H-8→L+1 (14%) H-8→L+3 (12%) H-7→L+2 (39%)	Ru to phen; hpp to phen
5,02	247	0,1802	H-1→L+8 (16%) HOMO→L+9 (38%) HOMO→L+10 (14%)	Ru to phen; Ru to hpp
5,16	240	0,1464	H-9→L+1 (56%) H-4→L+4 (13%)	hpp to phen
5,31	233	0,1793	H-10→LUMO (27%) H-9→L+1 (27%) H-9→L+3 (13%) H-3→L+5 (13%)	hpp to phen
5,38	230	0,1556	H-10→LUMO (10%) H-9→L+3 (68%)	hpp to phen
5,44	228	0,4247	H-10→LUMO (29%) H-4→L+4 (47%)	hpp to phen
5,55	224	0,1228	H-10→L+2 (56%) H-5→L+5 (17%)	hpp to phen
5,58	222	0,0769	H-12→LUMO (15%) H-11→L+1 (35%) H-5→L+5 (22%)	hpp to phen
5,60	222	0,1420	H-12→LUMO (14%) H-11→L+1 (12%)	Ru to phen; hpp to phen

			H-2→L+9 (25%) H-2→L+10 (11%)	
5,61	221	0,1716	H-10→L+2 (26%) H-6→L+4 (16%) H-5→L+5 (16%)	Ru to phen; hpp to phen
5,71	217	0,1114	H-12→L (32%) H-11→L+1 (35%)	hpp to phen
593	209	0,0981	H-1→L+13 (22%) H-1→L+15 (60%)	Ru to phen; hpp to phen

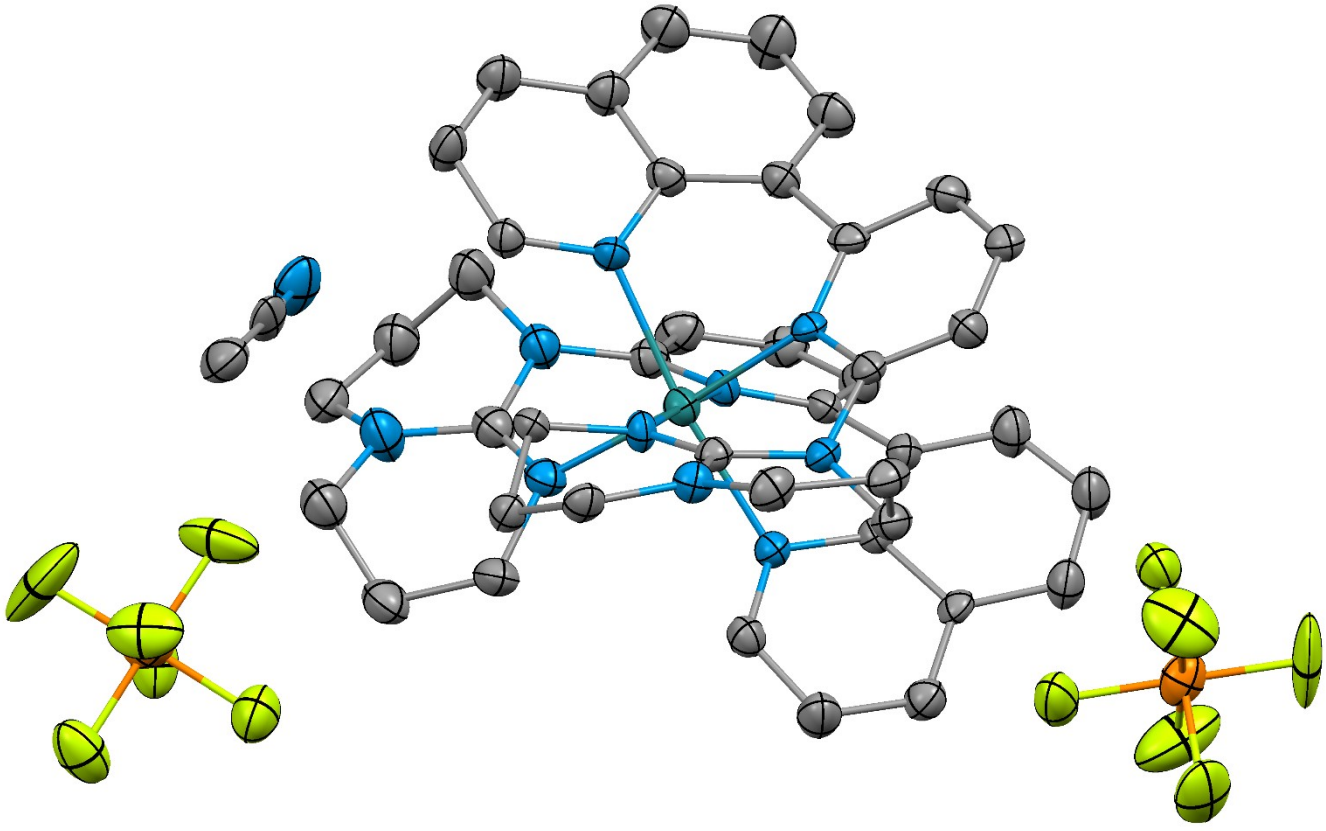

Figure 10.4 - Thermal ellipsoid diagram (30% probability) of the single crystal of 62+ with the counter-anions (PF6) and an acetonitrile solvent molecule. The hydrogens atoms are omitted for clarity.

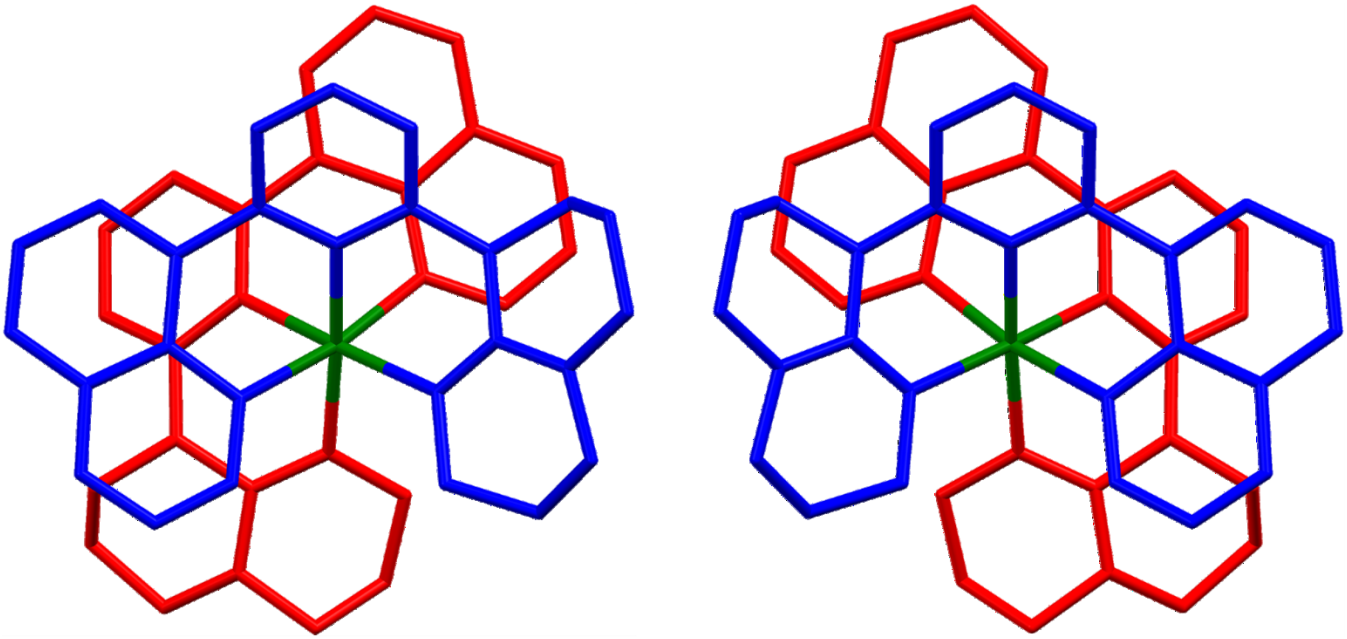

Figure 10.5 - Capped stick view of both delta and lambda enantiomers found in the unit cell of metal complex 6^{2+}. The hydrogens atoms, the counter-anions (PF_6) and the solvent molecule (acetonitrile) are omitted for clarity.

Table 10.14 - Atomic coordinates for DFT optimization of 6^{2+} in (S = 0) PBE0/LANL2DZ, CPCM(CH_3CN).

Standard orientation					
Center Number	Atomic Number	Atomic Type	Coordinates (Angstroms)		
			X	Y	Z
1	6	0	0.426807	2.472986	-3.443585
2	6	0	0.103038	4.060480	-1.169455
3	6	0	0.705446	1.898296	-2.200980
4	6	0	-0.009757	3.810972	-3.579900
5	6	0	-0.098554	4.618467	-2.462187
6	6	0	0.389181	2.662016	-1.025896

7	6	0	1.531297	0.665515	-2.161308
8	6	0	3.394571	-1.381815	-2.000737
9	6	0	2.429041	0.446574	-3.219510
10	7	0	1.513365	-0.174220	-1.074845
11	6	0	2.482279	-1.132636	-0.960940
12	6	0	3.339395	-0.607987	-3.155932
13	7	0	2.568805	-1.886208	0.223273
14	6	0	4.629646	-3.060381	0.811601
15	6	0	4.445928	-2.649908	2.273800
16	6	0	3.235797	-3.206099	0.206122
17	6	0	2.447853	-1.297260	1.489987
18	7	0	3.217716	-1.852653	2.475163
19	7	0	1.578762	-0.323490	1.709640
20	6	0	1.766092	0.546328	2.895764
21	6	0	2.857353	0.092808	3.872890
22	6	0	2.925692	-1.430938	3.851801
23	1	0	-0.344314	5.672713	-2.547857
24	1	0	-0.217799	4.206233	-4.568316
25	1	0	0.573168	1.888921	-4.345831
26	1	0	2.457942	1.127352	-4.058808
27	1	0	4.040373	-0.781125	-3.964833
28	1	0	4.164280	-2.133325	-1.894953
29	1	0	3.245219	-3.595370	-0.811059
30	1	0	2.638998	-3.897309	0.809783
31	1	0	4.352896	-3.543298	2.902533
32	1	0	5.310614	-2.078305	2.634704
33	1	0	5.183335	-4.002363	0.760700
34	1	0	5.201051	-2.306959	0.258571
35	1	0	3.714873	-1.811111	4.503478
36	1	0	1.973007	-1.866923	4.181055

37	1	0	2.632980	0.466581	4.876934
38	1	0	3.835080	0.492029	3.579067
39	1	0	0.805244	0.615422	3.415526
40	1	0	2.014510	1.549929	2.536112
41	6	0	0.000000	4.862933	-0.000278
42	6	0	0.093760	4.263774	1.240364
43	6	0	0.197784	2.858984	1.306862
44	7	0	0.328858	2.069466	0.227951
45	1	0	-0.172903	5.930015	-0.100168
46	1	0	0.022180	4.833231	2.159179
47	1	0	0.105735	2.360268	2.259260
48	44	0	0.000000	0.000000	0.321625
49	6	0	-0.426807	-2.472986	-3.443585
50	6	0	-0.103038	-4.060480	-1.169455
51	6	0	-0.705446	-1.898296	-2.200980
52	6	0	0.009757	-3.810972	-3.579900
53	6	0	0.098554	-4.618467	-2.462187
54	6	0	-0.389181	-2.662016	-1.025896
55	6	0	-1.531297	-0.665515	-2.161308
56	6	0	-3.394571	1.381815	-2.000737
57	6	0	-2.429041	-0.446574	-3.219510
58	7	0	-1.513365	0.174220	-1.074845
59	6	0	-2.482279	1.132636	-0.960940
60	6	0	-3.339395	0.607987	-3.155932
61	7	0	-2.568805	1.886208	0.223273
62	6	0	-4.629646	3.060381	0.811601
63	6	0	-4.445928	2.649908	2.273800
64	6	0	-3.235797	3.206099	0.206122
65	6	0	-2.447853	1.297260	1.489987
66	7	0	-3.217716	1.852653	2.475163

67	7	0	-1.578762	0.323490	1.709640
68	6	0	-1.766092	-0.546328	2.895764
69	6	0	-2.857353	-0.092808	3.872890
70	6	0	-2.925692	1.430938	3.851801
71	1	0	0.344314	-5.672713	-2.547857
72	1	0	0.217799	-4.206233	-4.568316
73	1	0	-0.573168	-1.888921	-4.345831
74	1	0	-2.457942	-1.127352	-4.058808
75	1	0	-4.040373	0.781125	-3.964833
76	1	0	-4.164280	2.133325	-1.894953
77	1	0	-3.245219	3.595370	-0.811059
78	1	0	-2.638998	3.897309	0.809783
79	1	0	-4.352896	3.543298	2.902533
80	1	0	-5.310614	2.078305	2.634704
81	1	0	-5.183335	4.002363	0.760700
82	1	0	-5.201051	2.306959	0.258571
83	1	0	-3.714873	1.811111	4.503478
84	1	0	-1.973007	1.866923	4.181055
85	1	0	-2.632980	-0.466581	4.876934
86	1	0	-3.835080	-0.492029	3.579067
87	1	0	-0.805244	-0.615422	3.415526
88	1	0	-2.014510	-1.549929	2.536112
89	6	0	0.000000	-4.862933	-0.000278
90	6	0	-0.093760	-4.263774	1.240364
91	6	0	-0.197784	-2.858984	1.306862
92	7	0	-0.328858	-2.069466	0.227951
93	1	0	0.172903	-5.930015	-0.100168
94	1	0	-0.022180	-4.833231	2.159179
95	1	0	-0.105735	-2.360268	2.259260

Table 10.15 - Selected bond distances and angles of 6

Bond Length			Angle		
	Obs. (X-ray)	Calc. (DFT)		Obs. (X-ray)	Calcl. (DFT)
N1-Ru1	2.085 (3)	2.09753	N1-Ru1-N2	85.84 (13)	86.456
			N1-Ru1-N5	95.29 (14)	93.602
N2-Ru1	2.056 (3)	2.06658	N1-Ru1-N6	172.21 (12)	174.881
			N1-Ru1-N7	88.93 (13)	90.084
N5-Ru1	2.091 (3)	2.12690	N1-Ru1-N10	91.52 (12)	89.740
			N2-Ru1-N5	82.93 (13)	83.373
N6-Ru1	2.097 (3)	2.09753	N2-Ru1-N6	89.24 (13)	90.084
			N2-Ru1-N7	96.75 (12)	94.977
N7-Ru1	2.035 (3)	2.06658	N2-Ru1-N10	177.26 (13)	175.855
			N5-Ru1-N6	90.09 (14)	89.740
N10-Ru1	2.094 (3)	2.12690	N5-Ru1-N7	175.73 (14)	175.855
			N5-Ru1-N10	96.62 (12)	98.524
			N6-Ru1-N7	85.65 (13)	86.456
			N6-Ru1-N10	93.46 (12)	93.602
			N7-Ru1-N10	83.90 (12)	83.373

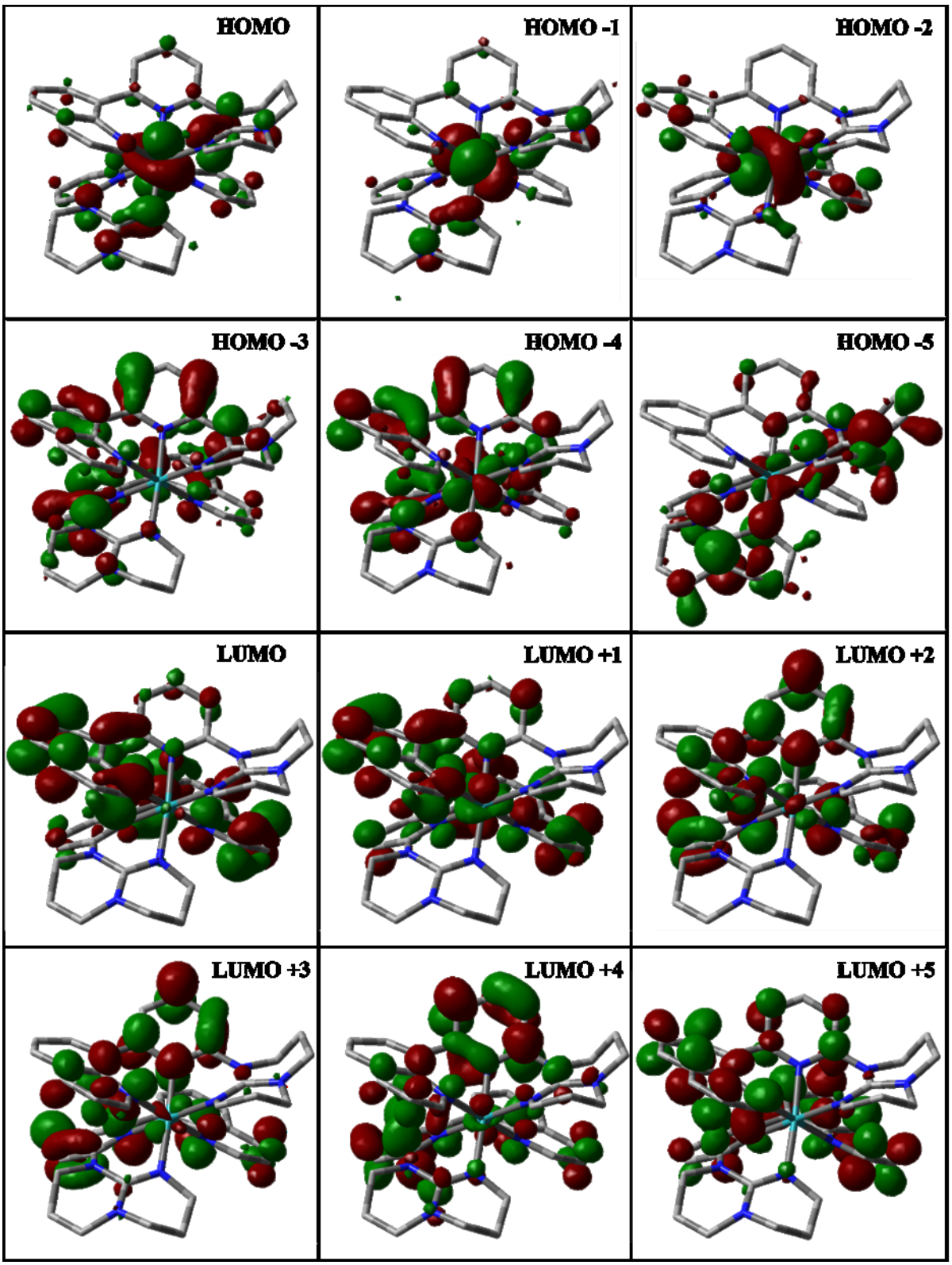

Figure 10.6 - Kohn-Sham electron density illustration of the the molecular orbitals for 6^{2+} in (S = 0) ground state.

Table 10.16 - MO composition of 6 in (*S=0*) ground state.

MO	Energy (eV)	Composition			
		Ruthenium	QpyG		
			Quinolyl	pyridyl	hpp
LUMO+5	-1.146	0	32	60	7
LUMO+4	-1.241	3	45	46	6
LUMO+3	-1.432	3	15	75	7
LUMO+2	-1.437	2	28	66	4
LUMO+1	-2.450	4	76	20	1
LUMO	-2.559	1	80	18	1
HOMO	-5.225	65	3	5	28
HOMO-1	-5.634	72	4	3	21
HOMO-2	-5.872	84	12	2	3
HOMO-3	-6.762	19	6	6	70
HOMO-4	-6.782	1	35	26	38
HOMO-5	-6.791	15	21	9	55

Table 10.17 - Selected transitions from TD-DFT calculations of 6^{2+} in the singlet ground state (PBE0), CPCM (CH_3CN).

Energy (eV)	λ (nm)	f	Transition	Character
1.77	699	0.0697	H→L (98%)	Ru to quino; hpp to quino
2.50	496	0.1017	H-2→L (87%)	Ru to quino; Ru to py
2.58	480	0.0758	H→L+2 (87%)	hpp to py and/or quino; Ru to py and/or quino
3.64	341	0.3708	H-4→L (35%) H-3→L+1 (40%) H-1→L+4 (15%)	Ru to quino; hpp to quino
4.26	291	0.1118	H-3→L+3 (78%)	hpp to py
4.39	282	0.0679	H-8→L (29%)	hpp to py and/or quino; Ru to py and/or quino

			H→L+8 (33%)	
4.81	258	0.0898	H→L+11 (44%) H→L+15 (23%)	Ru to py; Ru to hpp; Ru to quino
5.10	243	0.1071	H-11→L (44%) H-5→L+4 (12%) H-3→L+7 (16%)	hpp to quino
5.23	237	0.1199	H-11→L (11%) H-6→L+5 (31%) H-4→L+6 (15%) H-3→L+7 (11%)	Ru to quino; hpp to quino
5.25	236	0.1895	H-6→L+5 (44%)	hpp to py; hpp to quino
5.33	232	0.1281	H-8→L+3 (13%) H-7→L+2 (36%) H-1→L+11 (22%)	Ru to py; hpp to py
5.35	232	0.1111	H-7→L+3 (11%) H-1→L+9 (11%) H-1→L+10 (29%) H-1→L+14 (26%)	Ru to py; Ru to quino
5.47	227	0.1088	H-10→L+2 (44%) H-9→L+3 (28%)	quino to py
5.48	226	0.0656	H-9→L+2 (10%) H-5→L+7 (57%)	hpp to py; hpp to quino
5.71	217	0.0687	H-8→L+4 (79%)	hpp to py and/or quino ; Ru to py and/or quino
5.86	212	0.1836	H-16→L+1 (10%) H-7→L+5 (52%)	hpp to py; hpp to quino
5.99	207	0.0650	H-12→L+3 (32%) H-8→L+6 (35%)	hpp to py; hpp to quino
6.01	206	0.1207	H-16→L+1 (14%) H-12→L+3 (35%) H-8→L+6 (28%)	hpp to quino

6.14	202	0.4772	H-10→L+5 (29%) H-7→L+7 (25%)	hpp to py

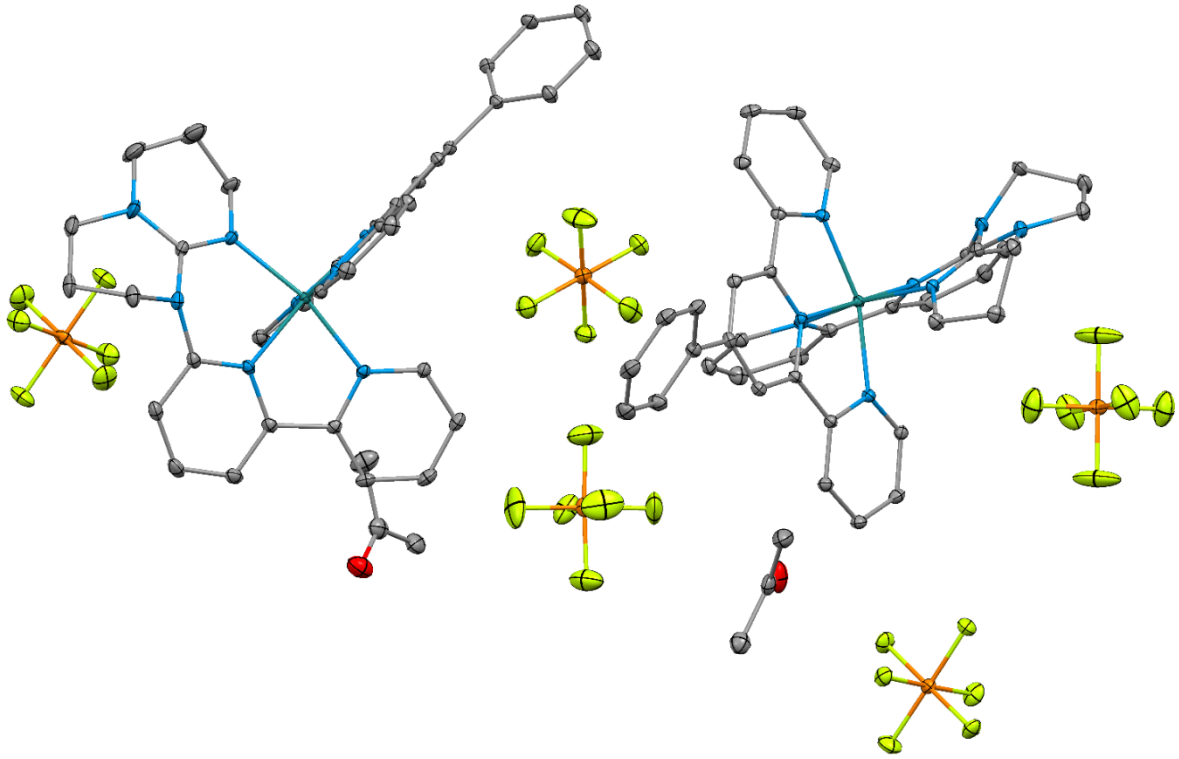

Figure 10.7 - Thermal ellipsoid diagram (30% probability) of the single crystal of 7 with the counter-anions (PF_6) and co-crystallized acetone solvent molecules. The hydrogens atoms are omitted for clarity.

Table 10.18 - Atomic coordinates for DFT optimization of 7^{2+} in (S = 0) PBE0/LANL2DZ, CPCM(CH_3CN).

Standard orientation					
Center Number	Atomic Number	Atomic Type	Coordinates (Angstroms)		
			X	Y	Z
1	44	0	-0.654055	0.368963	0.124550

2	7	0	-2.633813	0.863454	0.239355
3	7	0	-0.375048	-0.609646	1.922699
4	7	0	1.291900	0.057585	0.058551
5	7	0	-0.528905	2.273126	0.915780
6	7	0	-0.189507	1.220156	-1.724807
7	7	0	-1.152294	-1.427787	-0.820646
8	7	0	-3.398286	-1.383749	-0.021375
9	6	0	1.887209	-0.594997	1.095246
10	6	0	1.161977	1.205931	-2.005646
11	6	0	2.005797	0.539397	-0.996201
12	6	0	-3.655385	-0.001670	0.022735
13	6	0	0.934355	-0.987725	2.147107
14	7	0	-2.580005	-3.300934	-1.081470
15	6	0	-1.315417	-0.913535	2.847914
16	1	0	-2.325256	-0.590261	2.630817
17	6	0	-2.891712	2.188589	0.496701
18	6	0	-1.710734	2.970264	0.890040
19	6	0	3.388568	0.357189	-1.042263
20	1	0	3.956128	0.712250	-1.893614
21	6	0	0.599067	2.895723	1.337308
22	1	0	1.505715	2.305425	1.351199
23	6	0	-2.327531	-2.017185	-0.675497
24	6	0	1.293504	-1.682705	3.307442
25	1	0	2.323205	-1.977148	3.470940
26	6	0	0.767835	2.365076	-4.091755
27	1	0	1.140144	2.811446	-5.006942
28	6	0	-1.010453	-1.603675	4.023285
29	1	0	-1.798375	-1.824940	4.733402
30	6	0	-1.759970	4.318060	1.271393
31	1	0	-2.695421	4.862619	1.244320

32	6	0	-4.442908	-2.298440	0.500426
33	1	0	-5.184583	-1.718746	1.048124
34	1	0	-3.970885	-2.982041	1.216513
35	6	0	1.656301	1.778382	-3.181990
36	1	0	2.719065	1.766060	-3.391466
37	6	0	-3.912797	-3.917926	-1.264522
38	1	0	-3.876706	-4.895787	-0.769771
39	1	0	-4.078215	-4.094472	-2.334999
40	6	0	0.314809	-1.997101	4.256929
41	1	0	0.581580	-2.536355	5.158821
42	6	0	-1.042706	1.780956	-2.610518
43	1	0	-2.093932	1.756881	-2.351417
44	6	0	-4.190120	2.698238	0.453616
45	1	0	-4.387120	3.742220	0.658421
46	6	0	-4.978167	0.475774	-0.075956
47	1	0	-5.785737	-0.198162	-0.329822
48	6	0	-0.603314	2.362573	-3.803714
49	1	0	-1.324083	2.800870	-4.483560
50	6	0	-0.592812	4.959299	1.696453
51	1	0	-0.619162	6.001552	1.993624
52	6	0	4.044902	-0.321642	0.008094
53	6	0	3.269391	-0.796420	1.088132
54	1	0	3.750811	-1.291705	1.922587
55	6	0	7.478854	-1.863964	0.534329
56	1	0	7.906397	-2.757801	0.978258
57	6	0	-0.587117	-3.244208	-2.477318
58	1	0	0.275145	-3.805430	-2.850506
59	1	0	-1.181386	-2.923348	-3.340916
60	6	0	0.605888	4.232126	1.737365
61	1	0	1.531861	4.686846	2.068510

62	6	0	5.512071	-0.524029	-0.020070
63	6	0	-1.448926	-4.109396	-1.566071
64	1	0	-1.854356	-4.972241	-2.098474
65	1	0	-0.862247	-4.481427	-0.715720
66	6	0	-0.105159	-2.046077	-1.665976
67	1	0	0.716548	-2.356612	-1.009094
68	1	0	0.288931	-1.276745	-2.336131
69	6	0	-5.039054	-3.076980	-0.664319
70	1	0	-5.452185	-2.380843	-1.402123
71	1	0	-5.850431	-3.730184	-0.330590
72	6	0	6.091724	-1.671923	0.560752
73	1	0	5.460756	-2.433453	1.009969
74	6	0	-5.240187	1.829728	0.130942
75	1	0	-6.254298	2.203558	0.047765
76	6	0	7.746809	0.235950	-0.651980
77	1	0	8.384116	0.982961	-1.115250
78	6	0	6.359458	0.426999	-0.627546
79	1	0	5.943488	1.333526	-1.058052
80	6	0	8.312988	-0.910564	-0.071615
81	1	0	9.388380	-1.058868	-0.091165

Table 10.19 - Selected bond distances and angles of 7

Bond Length			Angle		
	Obs. (X-ray)	Calc. (DFT)		Obs. (X-ray)	Calcl. (DFT)
N1-Ru1	2.072 (2)	2.06612	N1-Ru1-N2	79.55 (8)	79.692
			N1-Ru1-N3	159.00 (8)	159.035
N2-Ru1	1.957 (2)	1.97181	N1-Ru1-N4	83.87 (8)	87.134
			N1-Ru1-N5	100.39 (8)	101.333
N3-Ru1	2.059 (2)	2.08817	N1-Ru1-N7	91.61 (8)	91.065

			N2-Ru1-N3	79.87 (8)	79.349
N4-Ru1	2.048 (2)	2.06580	N2-Ru1-N4	97.31 (8)	95.658
			N2-Ru1-N5	176.59 (8)	174.903
N5-Ru1	2.026 (2)	2.04381	N2-Ru1-N7	93.95 (8)	94.839
			N3-Ru1-N4	94.63 (8)	95.455
N7-Ru1	2.076 (2)	2.09044	N3-Ru1-N5	99.91 (8)	99.591
			N3-Ru1-N7	93.95 (8)	90.168
N9-Ru2	2.071 (2)	2.06612	N4-Ru1-N5	79.31 (9)	79.920
			N4-Ru1-N7	166.89 (8)	168.485
N10-Ru2	1.960 (2)	1.97181	N5-Ru1-N7	89.46 (9)	90.142
			N9-Ru2-N10	79.73 (8)	79.692
N11-Ru2	2.066 (2)	2.08817	N9-Ru2-N11	159.38 (8)	159.035
			N9-Ru2-N12	86.30 (8)	87.134
N12-Ru2	2.056 (2)	2.06580	N9-Ru2-N13	100.02 (8)	101.333
			N9-Ru2-N15	88.65 (8)	91.065
N13-Ru2	2.032 (2)	2.04381	N10-Ru2-N11	79.65 (9)	79.349
			N10-Ru2-N12	96.19 (8)	95.658
N15-Ru2	2.084 (2)	2.09044	N10-Ru2-N13	175.40 (8)	174.903
			N10-Ru2-N15	95.10 (8)	94.839
			N11-Ru2-N12	95.57 (8)	95.455
			N11-Ru2-N13	100.50 (8)	99.591
			N11-Ru2-N15	93.53 (8)	90.168
			N12-Ru2-N13	79.22 (9)	79.920
			N12-Ru2-N15	166.61 (8)	168.485
			N13-Ru2-N15	89.48 (9)	90.142

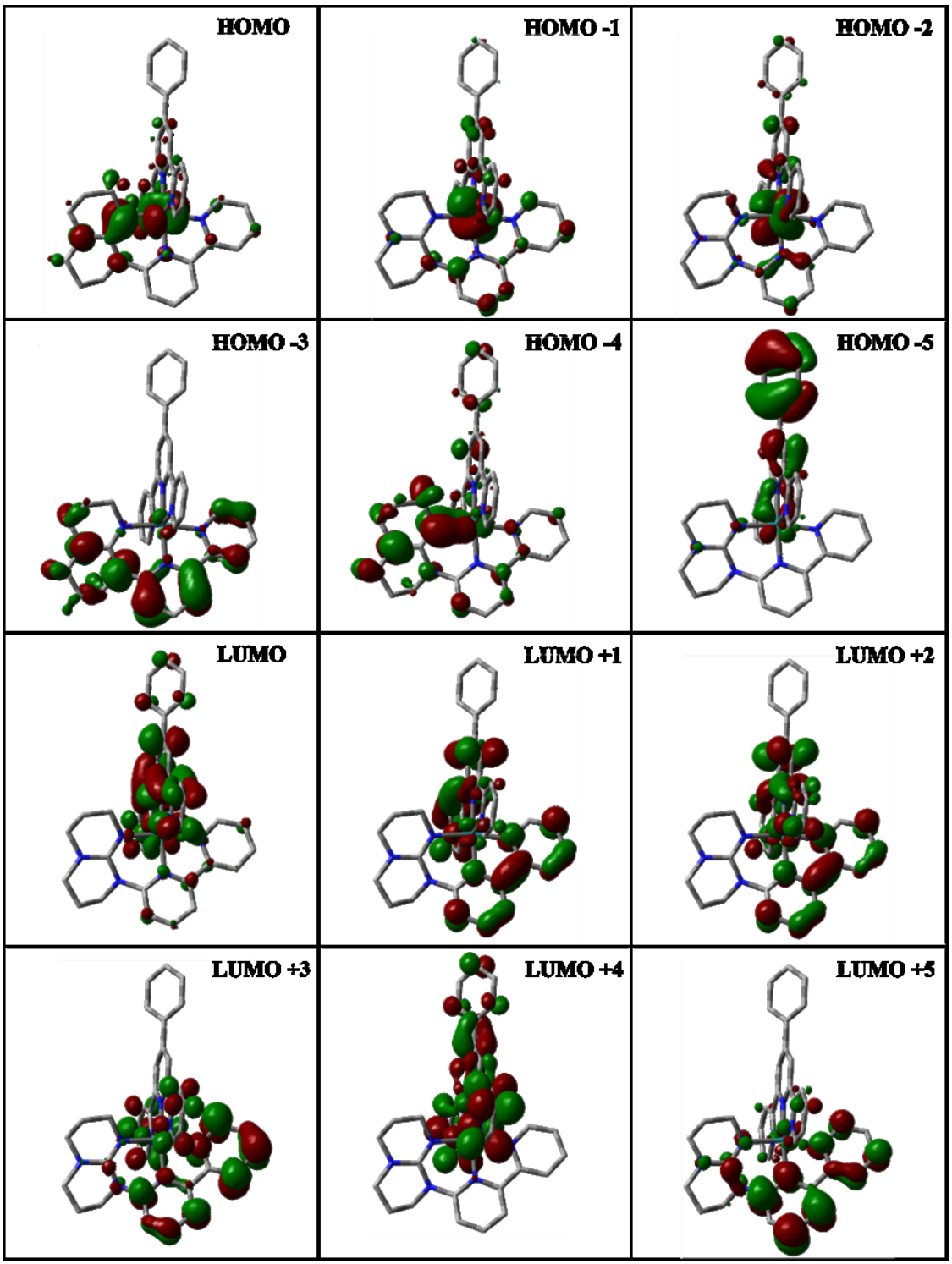

Figure 10.8 - Kohn-Sham electron density illustration of the the molecular orbitals for 7^{2+} in (S = 0) ground state.

Table 10.20 - MO composition of 7 in (*S=0*) ground state.

MO	Energy (eV)	Composition			
		Ruthenium	Phtpy	bpyhpp	
				2,2'-bpy	hpp
LUMO+5	-1.442	2	10	82	6
LUMO+4	-1.592	0	97	2	0
LUMO+3	-1.613	1	31	65	2
LUMO+2	-2.444	6	53	41	0
LUMO+1	-2.554	3	53	44	0
LUMO	-2.731	7	83	9	1
HOMO	-5.822	54	13	5	26
HOMO-1	-6.302	67	17	13	4
HOMO-2	-6.425	74	17	6	3
HOMO-3	-7.203	3	1	45	46
HOMO-4	-7.247	13	16	10	52
HOMO-5	-7.620	8	87	2	3

Table 10.21 - Selected transitions from TD-DFT calculations of 7^{2+} in the singlet ground state (PBE0), CPCM (CH_3CN).

Energy (eV)	λ (nm)	f	Transition	Character
2.03	609	0.0232	H→L (89%)	hpp to tpy ; Ru to tpy
2.42	512	0.0201	H→L+1 (30%) H→L+2 (58%)	hpp to bpy &/or hpp to tpy ; Ru to bpy &/or Ru to tpy
2.69	461	0.1855	H-2→L (45%) H-1→L (22%) H-1→L+2 (20%)	Ru to bpy ; Ru to tpy

2.83	439	0.0901	H-2→L+1 (18%) H-1→L+1 (63%)	Ru to bpy ; Ru to tpy
3.05	407	0.0232	H-2→L (10%) H-1→L+2 (62%)	Ru to bpy ; Ru to tpy
3.39	366	0.0782	H→L+4 (80%)	hpp to bpy &/or hpp to tpy ; Ru to bpy &/or Ru to tpy
4.13	300	0.1472	H-6→L (19%) H-3→L+2 (35%)	hpp to bpy &/or hpp to tpy ; Ru to bpy &/or Ru to tpy
4.18	296	0.2858	H-6→L (15%) H-5→L (39%)	hpp to bpy &/or hpp to tpy ; Ru to bpy &/or Ru to tpy
4.26	291	0.2005	H-6→L (18%) H-5→L (48%)	Ru to bpy ; Ru to tpy
4.64	267	0.1589	H-6→L+2 (22%) H-5→L+1 (10%) H-5→L+2 (33%)	tpy to bpy
4.65	267	0.1825	H-6→L+2 (37%) H-5→L+1 (18%) H-5→L+2 (20%)	tpy to bpy
4.99	249	0.1126	H-8→L+1 (34%)	hpp to tpy ; bpy to tpy

			H-3→L+4 (41%)	
4.99	248	0.1285	H-8→L+1 (11%) H-4→L+5 (29%) H-3→L+4 (27%) H-3→L+5 (11%)	hpp to tpy ; hpp to bpy
5.21	238	0.1311	H-9→L+1 (47%)	hpp to bpy ; tpy to bpy

Table 10.22 - Atomic coordinates for DFT optimization of 8^{2+} in (S = 0) PBE0/LANL2DZ, CPCM(CH_3CN).

Standard orientation					
Center Number	Atomic Number	Atomic Type	Coordinates (Angstroms)		
			X	Y	Z
1	44	0	-0.556957	-0.178514	0.005764
2	6	0	-4.908829	-0.001579	0.266023
3	6	0	-5.249301	-1.316149	0.011031
4	7	0	-2.580600	-0.470827	-0.047601
5	6	0	-4.245547	-2.248727	-0.350821
6	6	0	-3.549328	0.432086	0.201168
7	6	0	-2.919753	-1.772429	-0.354237
8	6	0	-4.502477	-3.614354	-0.713516
9	6	0	-3.478637	-4.446249	-1.094029
10	6	0	-2.122171	-3.970853	-1.137518
11	6	0	-1.026395	-4.766692	-1.557393

12	6	0	-1.853483	-2.635031	-0.751971
13	6	0	0.246583	-4.210110	-1.581209
14	6	0	0.434773	-2.871233	-1.180983
15	7	0	-0.585143	-2.097297	-0.771964
16	7	0	-3.255893	1.807769	0.317106
17	6	0	-4.045833	4.162413	-0.092440
18	7	0	-2.084967	3.663978	1.218529
19	6	0	-3.331050	4.444760	1.218359
20	6	0	-2.051806	2.353527	0.816320
21	6	0	-4.405826	2.689112	-0.072842
22	7	0	-0.943331	1.633865	0.940331
23	6	0	0.410060	3.661483	1.221395
24	6	0	-0.859916	4.483630	1.392320
25	6	0	0.115288	2.263043	1.755951
26	1	0	-3.395675	4.418399	-0.935866
27	1	0	-4.968882	4.742306	-0.182972
28	1	0	-5.690678	0.692884	0.533096
29	1	0	-4.769177	2.351632	-1.047901
30	1	0	-6.286117	-1.629138	0.077514
31	1	0	-5.526728	-3.973570	-0.691338
32	1	0	-3.678429	-5.475210	-1.376534
33	1	0	-1.189637	-5.796288	-1.859005
34	1	0	1.105808	-4.787097	-1.901599
35	1	0	1.420898	-2.425086	-1.193056
36	1	0	-5.209855	2.565927	0.659697
37	1	0	-3.961237	4.174812	2.075276
38	1	0	-3.065085	5.498236	1.319994
39	1	0	-0.894876	5.308526	0.669332
40	1	0	-0.899885	4.919819	2.397309
41	1	0	1.232624	4.133538	1.767195

42	1	0	0.700165	3.591799	0.167425
43	1	0	-0.214773	2.328866	2.803520
44	1	0	1.002786	1.636185	1.729465
45	7	0	-0.254170	0.747060	-1.817727
46	6	0	0.478384	2.015954	-4.206064
47	6	0	1.077153	0.979791	-2.102876
48	6	0	-1.195819	1.137919	-2.708518
49	6	0	-0.870124	1.773304	-3.909032
50	6	0	1.457897	1.612432	-3.291613
51	7	0	1.409990	-0.053251	-0.004063
52	6	0	4.187434	0.041451	-0.067968
53	6	0	2.026750	0.511247	-1.079441
54	6	0	2.113867	-0.579073	1.038053
55	6	0	3.509212	-0.541879	1.024913
56	6	0	3.421398	0.569304	-1.129834
57	7	0	-0.108989	-1.015436	1.863224
58	6	0	0.815162	-2.138095	4.252852
59	6	0	-0.981314	-1.453085	2.798346
60	6	0	1.245865	-1.117621	2.102450
61	6	0	1.723488	-1.679600	3.291069
62	6	0	-0.558981	-2.019707	4.004429
63	6	0	5.667371	0.095982	-0.099561
64	6	0	8.492061	0.203663	-0.159721
65	6	0	6.439455	-0.924906	0.494432
66	6	0	6.333914	1.171691	-0.723563
67	6	0	7.733173	1.225780	-0.752352
68	6	0	7.838815	-0.872097	0.463267
69	1	0	8.417204	-1.671134	0.916942
70	1	0	9.576795	0.244949	-0.182677
71	1	0	8.229083	2.066123	-1.228498

72	1	0	5.763505	1.984734	-1.163315
73	1	0	5.952186	-1.778121	0.957778
74	1	0	4.072754	-0.934795	1.862430
75	1	0	3.917119	0.995178	-1.993717
76	1	0	2.789040	-1.756904	3.469751
77	1	0	1.174531	-2.575450	5.177540
78	1	0	-2.033275	-1.341339	2.566931
79	1	0	-1.294237	-2.358010	4.724702
80	1	0	2.505195	1.790389	-3.504271
81	1	0	0.762368	2.508253	-5.129289
82	1	0	-1.659992	2.068776	-4.589369
83	1	0	-2.224762	0.929796	-2.444207

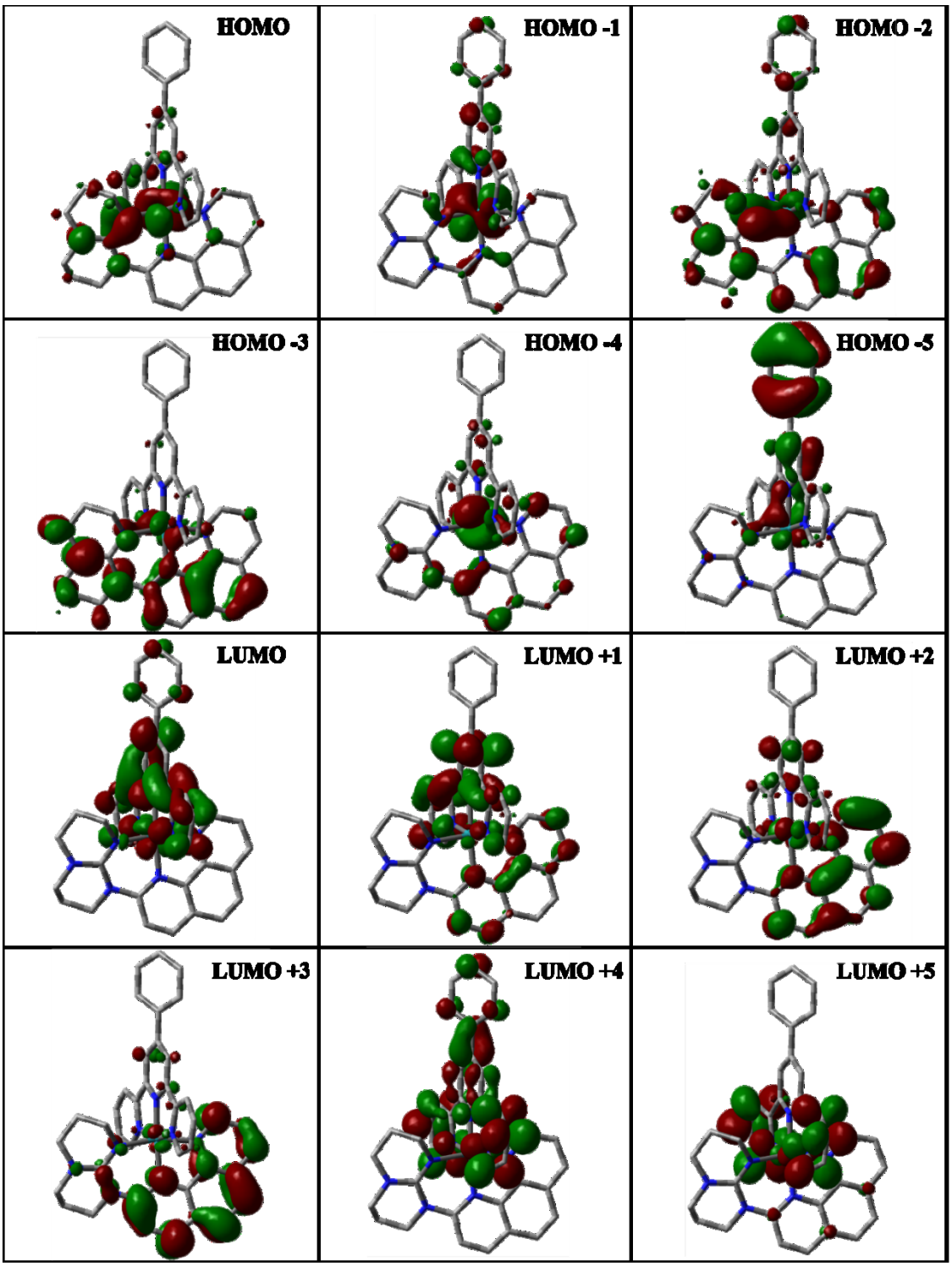

Figure 10.9 - Kohn-Sham electron density illustration of the the molecular orbitals for 8^{2+} in (S = 0) ground state.

Table 10.23 - MO composition of 8 in (*S=0*) ground state.

MO	Energy (eV)	Composition			
		Ruthenium	Phtpy	phenG	
				1,10-phenanthroline	hpp
LUMO+5	-1.205	2	90	7	1
LUMO+4	-1.238	1	98	1	0
LUMO+3	-2.261	3	14	82	0
LUMO+2	-2.308	2	59	37	3
LUMO+1	-2.325	3	64	32	1
LUMO	-2.421	1	58	38	2
HOMO	-5.599	61	8	3	28
HOMO-1	-6.080	71	8	14	7
HOMO-2	-6.284	83	10	4	3
HOMO-3	-7.129	9	2	39	49
HOMO-4	-7.193	19	5	22	54
HOMO-5	-7.621	0	92	5	2

Table 10.24 - Selected transitions from TD-DFT calculations of 8^{2+} in the singlet ground state (PBE0), CPCM (CH_3CN).

Energy (eV)	λ (nm)	f	Transition	Character
2,00	620	0,0222	H→L (92%)	hpp to tpy ; Ru to tpy
2,31	536	0,0106	H→L+1 (47%) H→L+2 (38%)	hpp to tpy and/or phen ; Ru to tpy and/or phen
2,38	520	0,0174	H-1→L (34%) H→L+1 (19%) H→L+2 (41%)	hpp to tpy and/or phen ; Ru to tpy and/or phen

2,62	474	0,0023	H→L+3 (88%)	hpp to phen ; Ru to phen
2,68	463	0,1446	H-2→L (53%) H-1→L+2 (19%)	Ru to tpy; Ru to phen
2,80	443	0,1314	H-1→L+1 (86%)	Ru to tpy
2,85	435	0,0165	H-2→L+1 (37%) H-2→L+2 (52%)	Ru to tpy; Ru to phen
2,89	428	0,0244	H-2→L+1 (56%) H-2→L+2 (36%)	Ru to tpy; Ru to phen
3,03	409	0,0762	H-2→L (10%) H-1→L+2 (62%)	Ru to tpy; Ru to phen
3,13	396	0,0351	H-2→L+3 (10%) H-1→L+3 (81%)	Ru to phen
3,22	386	0,0291	H-2→L+3 (74%)	Ru to phen
3,35	370	0,0810	H→L+4 (91%)	Ru to tpy; hpp to tpy
4,63	268	0,1625	H-6→L+1 (15%) H-6→L+2 (52%)	tpy to phen
4,67	265	0,1307	H→L+9 (60%)	Ru to phen; hpp to phen
5,43	228	0,2827	H-11→L (15%)	hpp to phen; hpp to tpy

			H-9→L+3 (52%)	
5,56	223	0,2513	H-4→L+7 (10%) H-3→L+7 (38%)	hpp to phen

Table 10.25 - Atomic coordinates for DFT optimization of 9^{3+} in (S = 1) PBE0/LANL2DZ, CPCM(CH_3CN).

Standard orientation					
Center Number	Atomic Number	Atomic Type	Coordinates (Angstroms)		
			X	Y	Z
1	44	0	0.658189	0.062898	-0.036072
2	7	0	2.735650	0.051053	-0.076768
3	7	0	0.297281	-1.107042	-1.744856
4	7	0	-1.330971	0.034689	-0.052956
5	7	0	0.230981	1.339338	1.561271
6	7	0	0.739799	-1.508696	1.202729
7	7	0	2.622982	-2.343027	0.038204
8	6	0	-1.958201	-0.775320	-0.944918
9	6	0	-1.119328	1.573103	1.727383
10	6	0	-2.005560	0.810749	0.831877
11	6	0	3.378470	-1.148977	-0.020384
12	6	0	-1.034055	-1.435070	-1.892343
13	7	0	1.368654	-3.782316	1.393727
14	6	0	1.197911	-1.547027	-2.648547
15	6	0	3.463765	1.209734	-0.188394
16	6	0	-3.401166	0.778763	0.855057

17	6	0	1.564971	-2.541556	0.913169
18	6	0	-1.450624	-2.276652	-2.924000
19	6	0	-0.656370	3.076160	3.561798
20	6	0	0.833215	-2.379391	-3.711511
21	6	0	3.164418	-3.569485	-0.602666
22	6	0	-1.577878	2.448240	2.714402
23	6	0	2.307632	-4.923647	1.263255
24	6	0	-0.506106	-2.764314	-3.838826
25	6	0	1.114181	1.928318	2.397240
26	6	0	4.861444	1.151241	-0.301601
27	6	0	4.777226	-1.238380	-0.057044
28	6	0	0.707688	2.801385	3.410074
29	6	0	-4.096972	-0.064568	-0.038153
30	6	0	-3.348369	-0.846627	-0.950559
31	6	0	-7.639705	-1.381909	-0.373294
32	6	0	-0.025880	-2.889694	3.168024
33	6	0	-5.573104	-0.128459	-0.028720
34	6	0	0.157458	-4.048770	2.198554
35	6	0	-0.187110	-1.607186	2.358389
36	6	0	3.565201	-4.562850	0.480640
37	6	0	-6.241534	-1.319443	-0.385792
38	6	0	5.522771	-0.074793	-0.214727
39	6	0	-7.737896	0.937120	0.342106
40	6	0	-6.339645	0.998790	0.337156
41	6	0	-8.393446	-0.253618	-0.011275
42	6	0	-0.613157	3.362784	-2.571450
43	6	0	0.155462	4.421510	-2.129625
44	7	0	0.693927	1.814184	-1.247978
45	6	0	1.273098	4.174998	-1.286938
46	6	0	-0.332826	2.076355	-2.070563

47	6	0	1.586280	2.823128	-0.927287
48	6	0	2.079149	5.244392	-0.811984
49	6	0	3.180304	4.977589	-0.021863
50	6	0	3.559806	3.637788	0.218091
51	6	0	2.821989	2.548554	-0.255777
52	1	0	-0.986797	1.255471	-2.329871
53	1	0	-1.453554	3.500019	-3.239733
54	1	0	-0.075122	5.441290	-2.421053
55	1	0	1.811492	6.262796	-1.075853
56	1	0	3.784099	5.782870	0.380605
57	1	0	4.465620	3.458953	0.787189
58	1	0	5.427274	2.055471	-0.477155
59	1	0	6.604330	-0.120342	-0.267214
60	1	0	5.271527	-2.194282	0.048315
61	1	0	3.990730	-3.294463	-1.255724
62	1	0	3.989014	-5.467977	0.038112
63	1	0	4.324386	-4.123668	1.135812
64	1	0	2.375191	-3.991887	-1.235331
65	1	0	2.555662	-5.266099	2.273384
66	1	0	1.758871	-5.728437	0.761310
67	1	0	0.308807	-4.993470	2.722631
68	1	0	-0.709112	-4.159593	1.535721
69	1	0	-0.916157	-3.038509	3.785064
70	1	0	0.840827	-2.832640	3.835285
71	1	0	-1.210106	-1.550227	1.971511
72	1	0	-0.024323	-0.735680	2.997585
73	1	0	2.157753	1.682698	2.258408
74	1	0	1.450809	3.248686	4.058460
75	1	0	-1.001006	3.756523	4.331847
76	1	0	-2.637682	2.636505	2.830847

77	1	0	2.220132	-1.217276	-2.520827
78	1	0	1.587334	-2.710898	-4.414301
79	1	0	-0.818410	-3.418681	-4.644494
80	1	0	-2.494776	-2.543948	-3.027835
81	1	0	-3.859268	-1.468675	-1.674020
82	1	0	-8.139057	-2.308259	-0.638948
83	1	0	-5.676208	-2.210254	-0.643655
84	1	0	-3.948253	1.371059	1.577164
85	1	0	-5.851483	1.935945	0.587679
86	1	0	-8.314057	1.815914	0.613830
87	1	0	-9.477979	-0.301505	-0.004997

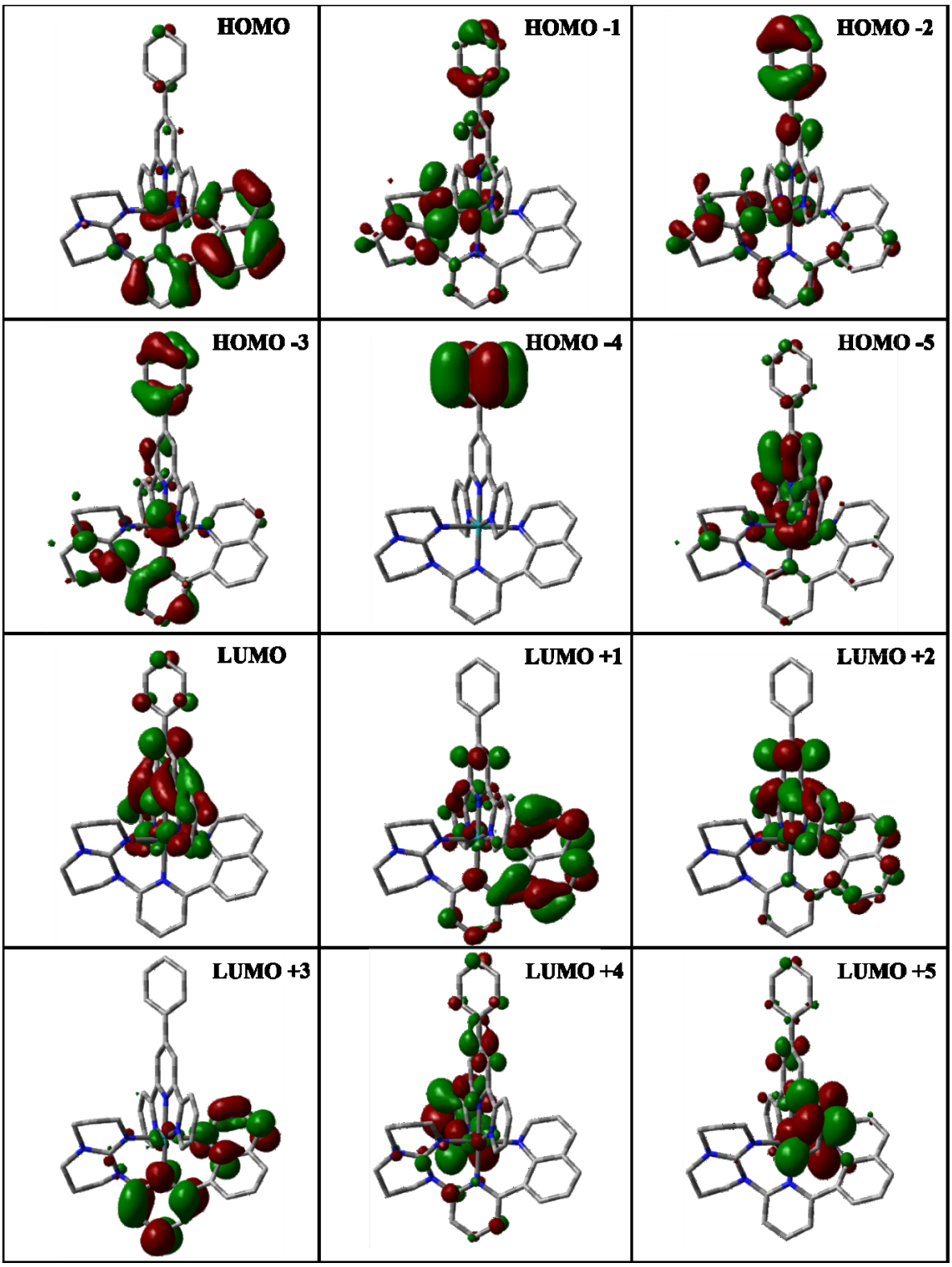

Figure 10.10 - Kohn-Sham electron density illustration of the the molecular orbitals for 9^{3+} in ($S = 1$) ground state in α-spin

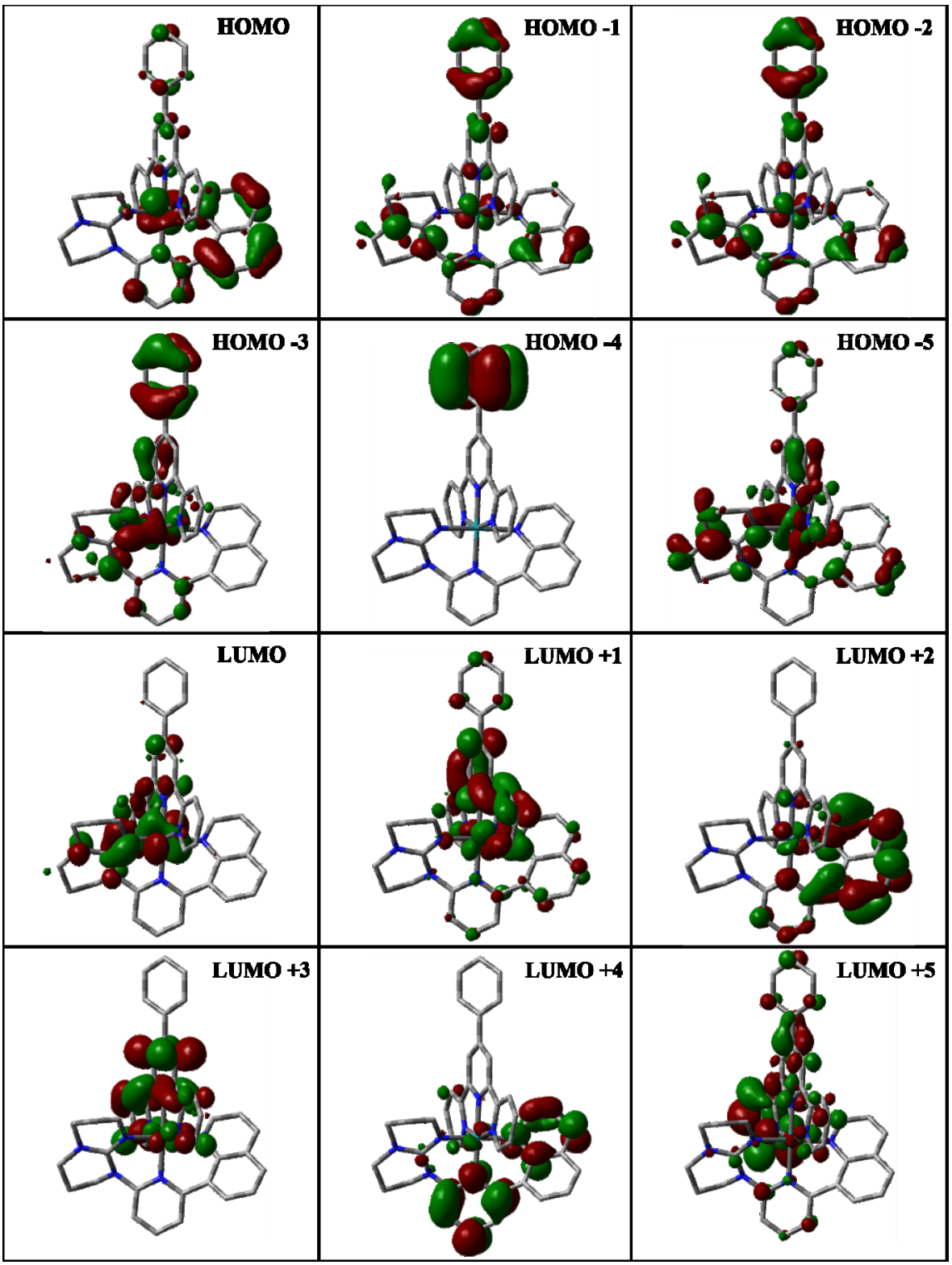

Figure 10.11 - Kohn-Sham electron density illustration of the the molecular orbitals for 9^{3+} in (S = 1) ground state in β-spin

Table 10.26 - MO composition of 9 in (*S=1*) ground state in α-spin.

MO	Energy (eV)		Composition				
			Ruthenium	Phtpy	QpyG		
					Quino	py	hpp
LUMO+5	-2.061		42	7	18	21	11
LUMO+4	-2.083		2	2	13	72	11
LUMO+3	-2.686		55	34	4	4	3
LUMO+2	-2.853		3	87	7	2	0
LUMO+1	-2.949		6	91	2	0	0
LUMO	-3.089		3	13	65	19	1
HOMO	-7.398		4	1	58	26	10
HOMO-1	-7.556		12	3	0	0	84
HOMO-2	-7.748		6	83	1	3	7
HOMO-3	-7.822		100	0	0	0	0
HOMO-4	-7.909		16	21	13	15	35
HOMO-5	-8.069		1	95	1	1	2

Table 10.27 - MO composition of 9 in (*S=1*) ground state in β-spin.

MO	Energy (eV)	Composition				
		Ruthenium	Phtpy	QpyG		
				Quino	py	hpp
LUMO+5	-2.047	2	2	15	72	9
LUMO+4	-2.373	60	29	4	3	4
LUMO+3	-2.833	4	81	13	2	0
LUMO+2	-2.864	4	94	1	0	1
LUMO+1	-3.079	1	16	64	18	1
LUMO	-4.758	67	10	1	3	19
HOMO	-7.321	17	3	45	17	17
HOMO-1	-7.447	14	3	9	15	60

HOMO-2	-7.746	15	81	0	1	2
HOMO-3	-7.820	0	100	0	0	0
HOMO-4	-7.898	29	26	9	9	25
HOMO-5	-8.013	29	51	5	2	13

Table 10.28 - Selected transitions from TD-DFT calculations of 9^{3+} in (*S=1*) ground state (PBE0), CPCM (CH_3CN).

Energy (eV)	λ (nm)	f	Transition	Character
2.02	614	0.0079	H-3(β)→L(β) (12%) H-1(β)→L(β) (59%) H(β)→L(β) (22%)	tpy to Ru; py to Ru; Q to Ru
2.13	581	0.1432	H-5(β)→L(β) (30%) H-3(β)→L(β) (32%) H-1(β)→L(β) (13%)	tpy to Ru; py to Ru; Q to Ru; hpp to Ru
2.44	508	0.0224	H-5(β)→L(β) (30%) H-3(β)→L(β) (12%) H-2(β)→L(β) (13%)	py to Ru; Q to Ru; hpp to Ru
2.54	488	0.0325	H-6(β)→L(β) (56%) H-3(β)→(β) (18%)	tpy to Ru
3.14	394	0.0675	H(α)→L(α) (24%) H(β)→L+1(β) (19%)	Ru to tpy; py to tpy; Q to tpy; hpp to tpy
3.75	331	0.1043	H-3(β)→L+1(β) (22%)	Ru to tpy; hpp to tpy
4.01	309	0.0305	H-5(β)→L+1(β) (20%) H-1(β)→L+3(β) (17%)	Ru to tpy; hpp to tpy

4.02	309	0.0499	H-6(β)→L+1(β) (12%)	Ru to tpy and/or Ru to Q; hpp to tpy and/or hpp to Q
4.08	304	0.0444	H-12(β)→L(β) (14%) H-6(β)→L+1(β) (16%) H-3(β)→L+3(β) (16%)	hpp to tpy
4.16	298	0.0602	H-12(β)→L(β) (31%) H-3(β)→L+2(β) (12%)	tpy to Ru and/or tpy to Q; hpp to Ru and/or hpp to Q
4.32	287	0.0368	H-8(α)→L(α) (30%)	Ru to tpy; hpp to tpy; Q to tpy
4.55	272	0.0434	H-1(α)→L+4(α) (12%)	Ru to tpy and/or Ru to Q and/or Ru to py; hpp to tpy and/or hpp to Q and/or hpp to py
4.59	270	0.0737	H-1(α)→L+5(α) (13%) H(α)→L+4(α) (11%)	Ru to tpy; hpp to tpy; Q to tpy
4.64	267	0.0324	H-8(α)→L+1(α) (21%) H-8(β)→L+2(β) (30%)	Ru to py and/or hpp to py; Ru to Q and/or hpp to Q
4.66	266	0.0364	H-16(β)→L(β) (13%) H-2(β)→L+5(β) (26%)	Ru to tpy; hpp to tpy; Q to tpy
4.67	265	0.0569	H-16(β)→L(β) (15%) H-2(β)→L+5(β) (13%)	Q to tpy; hpp to tpy
4.70	264	0.0295	H-5(α)→L+3(α) (12%)	Ru to py; tpy to py; hpp to py

4.71	263	0.0868	H-2(β)→L+6(β) (10%)	Ru to tpy; hpp to tpy; Q to tpy
4.91	253	0.119	H(β)→L+8(β) (15%)	Ru to tpy and/or hpp to tpy; Ru to py and/or hpp to py
4.96	250	0.0311	H-3(α)→L+4(α) (10%)	Ru to tpy; hpp to tpy
4.98	249	0.0291	H-2(α)→L+5(α) (12%) HOMO(β)→L+8(β) (14%)	Ru to tpy; Q to tpy; hpp to tpy
5.02	247	0.0455	H-9(β)→L+1(β) (12%)	Ru to tpy and/or hpp to tpy ; Ru to py and/or hpp to py
5.04	246	0.0339	H-5(α)→L+5(α) (14%) H-3(α)→L+5(α) (17%) H-1(α)→L+7(α) (23%)	Ru to py; hpp to py
5.11	242	0.0811	H-2(α)→L+6(α) (23%)	Ru to tpy; QpyG to tpy
5.13	242	0.0319	H-9(α)→L+2(α) (12%) H(α)→L+7(α) (16%)	Ru to Q; hpp to Q
5.15	241	0.0557	H-3(β)→L+6(β) (11%) H(β)→L+9(β) (18%)	py to hpp; Q to hpp

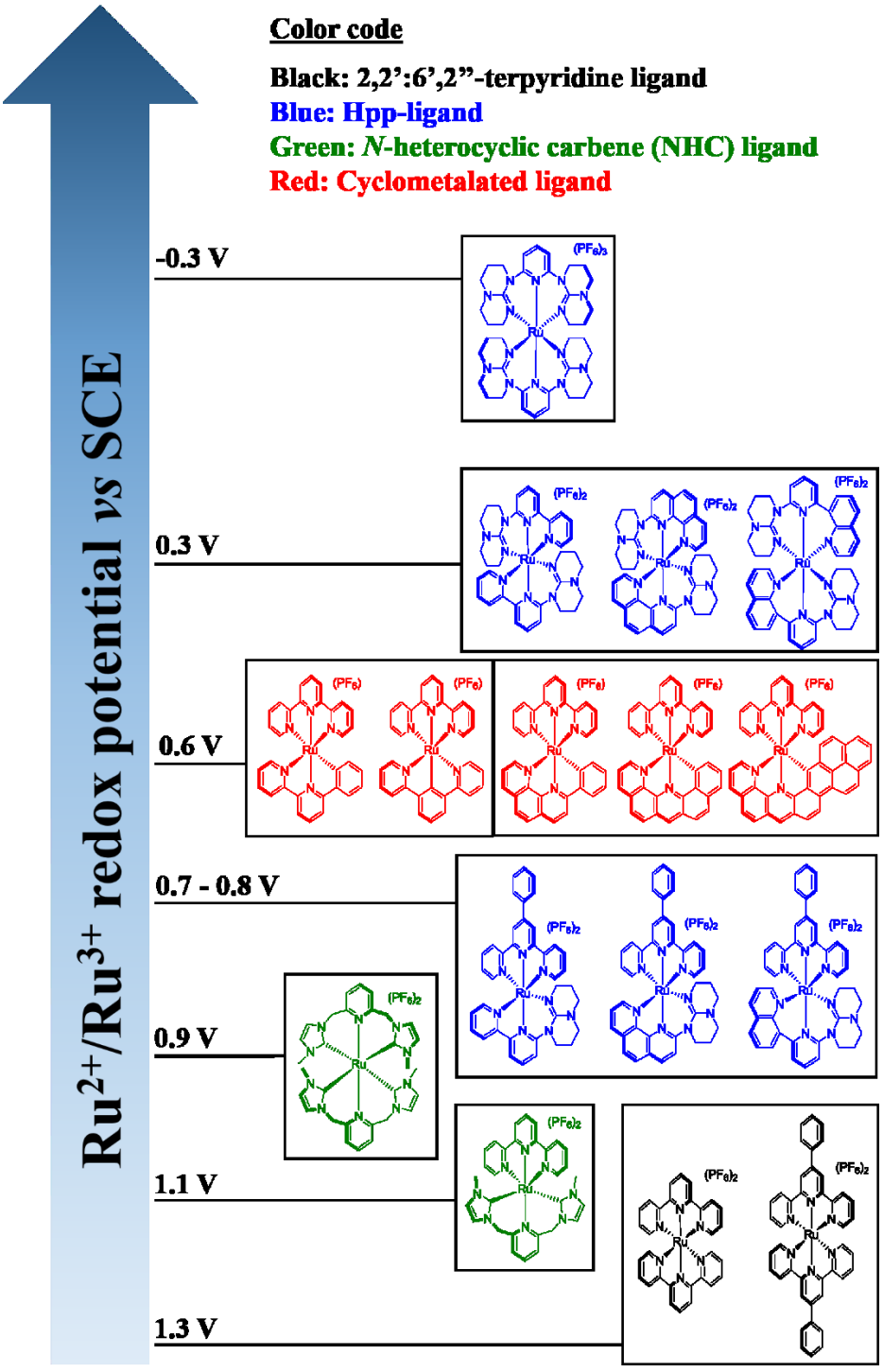

Figure 10.12 - Ru^{2+}/Ru^{3+} redox potentials comparison.

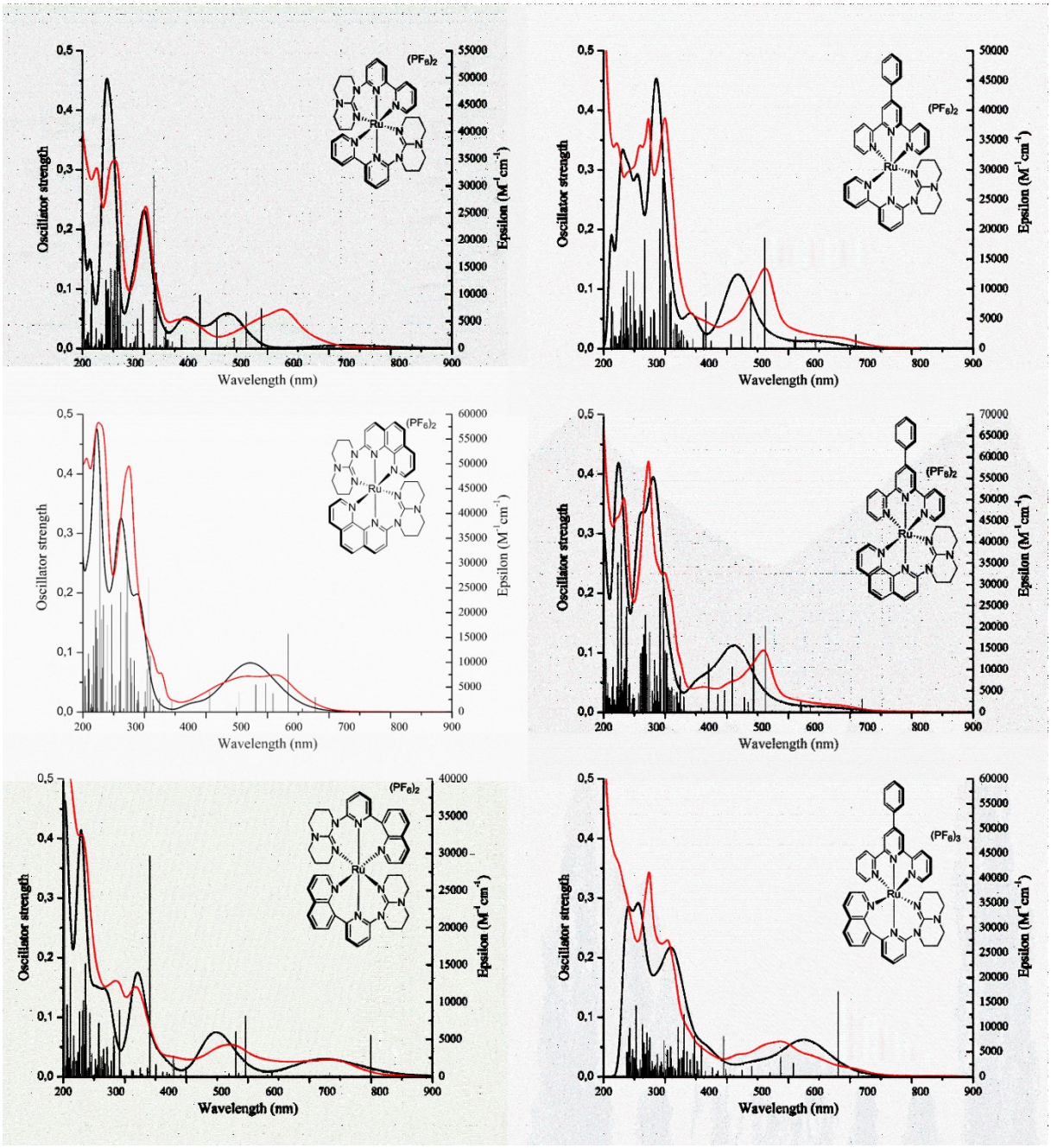

Figure 10.13 - Comparison of the experimental (red) absorption spectra recorded in acetonitrile and the TD-DFT (black) simulated (PBE0/LANL2DZ; CPCM: CH_3CN) absorption spectrum for the homoleptic complexes 4-6 (left) and heteroleptic complexes 7-9 (right).

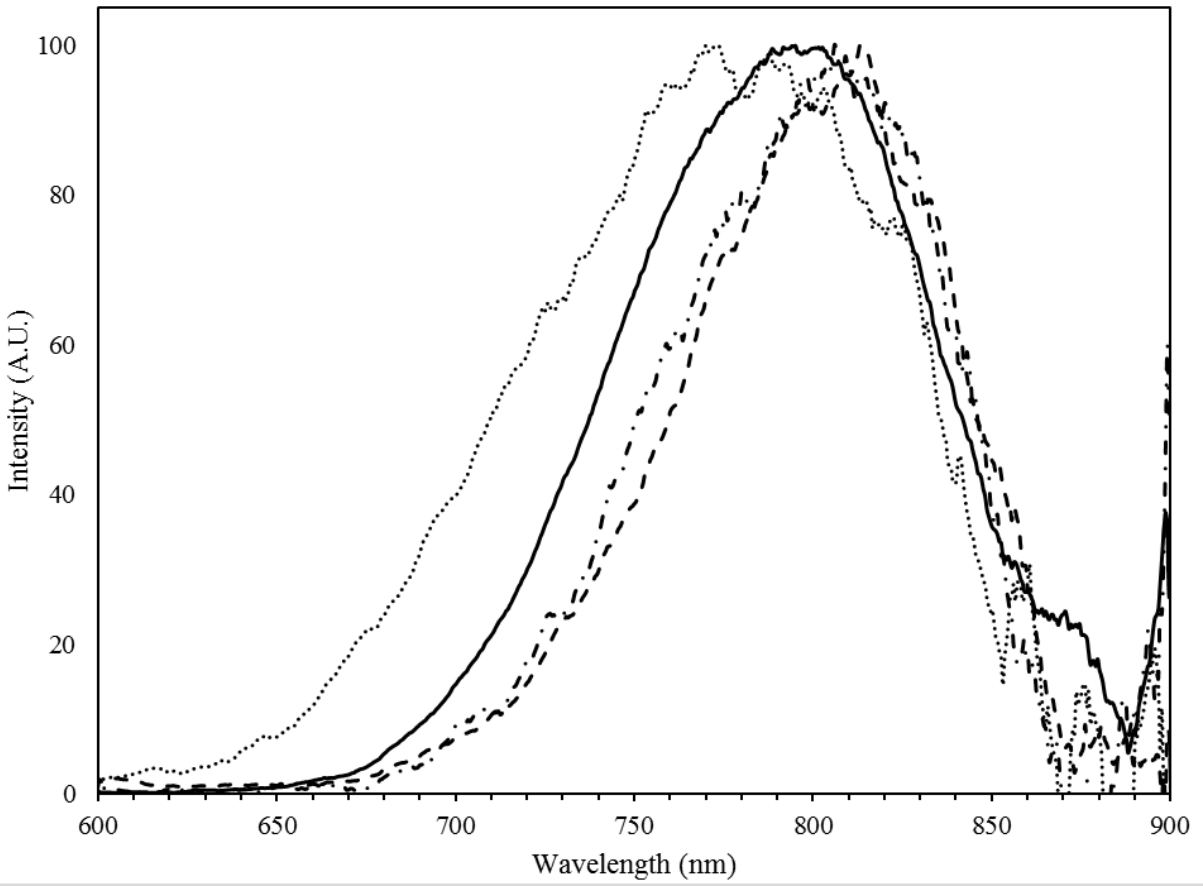

Figure 10.14 - Normalized luminescence spectra of the homoleptic complexes 4 (plain) and 5 (dots) as well as the heteroleptic complexes 7 (dash) and 8 (dash-dots) obtained in deaerated MeCN solution at ambient temperature.

10.1.5. References

[1] N. G. Connelly, W. E. Geiger, *Chem. Rev.* 1996, *96*, 877-910.

[2] I. P. Evans, A. Spencer, G. Wilkinson, *J. Chem. Soc., Dalton Trans.* 1973, 204-209.

[3] Y. Q. Fang, G. S. Hanan, *Synlett* 2003, *6*, 852-854.

[4] F. Ferretti, E. Gallo, F. Ragaini, *J. Organomet. Chem.* 2014, *771*, 59-67.

[5] D. J. Wasylenko, C. Ganesamoorthy, B. D. Koivisto, M. A. Henderson, C. P. Berlinguette, *Inorg. Chem.* 2010, *49*, 2202-2209.

Chapitre 11 – Informations supplémentaires : Going against the flow: Os(II)-to-Ru(II) energy transfer in a rod-like polypyridyl chromophore

11.1. Experimental Procedures

11.1.1. Materials and instrumentation

All solvent and reagents were used as purchased without further purification before the reactions. OsO_4 and $RuCl_3.3H_2O$ was purchased from Pressure Chemical Corporation. All other reagents were purchased from Sigma-Aldrich. ACS grade solvents were purchased from VWR and Fisher.

Nuclear magnetic resonance (NMR) spectra were recorded in acetonitrile-d_3 and DMSO-d_6 at room temperature (r.t.) on a Bruker AV400 (400 MHz) spectrometer for ^{1}H NMR, at 100 MHz for ^{13}C NMR and 600 MHz for DOSY experiment, respectively. Chemical shifts (δ) are reported in part per million (ppm) relative to TMS, and are referenced to the residual solvent protons (δ = 1.94 ppm for acetonitrile-d_3 and 2.50 ppm for DMSO-d_6) and the carbon resonance (δ = 118.26 ppm for acetonitrile-d_3 and 39.52 ppm for DMSO-d_6) of the solvent.

All the photophysical measurements were carried out in deaerated acetonitrile at r.t. in sealed quartz cells. Absorption spectra were measured on a Cary 500i UV-Vis-NIR Spectrophotometer from Agilent Technologies. For luminescence spectra a Perkin Elmer LS 55 was used. The luminescence lifetime measurement was performed on an Edinburgh OB 900 single-photon counting spectrometer equipped with a Hamamatsu PLP2 laser diode as pulse (wavelength output: 408 nm; pulse width: 59 ps). Deconvolution of the luminescence spectra was performed by using PeakFit V. 4.12.00. In all the cases, the fit correlation (r^2) was ≥ 0.99, considering an interval of 95% confidence.

Accurate high-resolution mass spectrometry experiments (HR-MS) was performed on a micrOTOF-Q II mass spectrometer from Bruker Daltonics, in positive electrospray mode. Appropriate $[M\text{-}PF_6]^{n+}$ species were used for empirical formula determination, and exact masses were calculated using the Compass DataAnalysis V4.0 SP5 software package from Bruker Daltonics.

Electrochemical measurements were carried out in argon-purged purified dimethylformamide at room temperature with a BAS CV50W multipurpose potentiostat. The working electrode was a 3-mm diameter glassy carbon electrode from CH Instruments. The counter electrode was a Pt wire, and the pseudo-reference electrode was a silver wire. The reference was set using an internal 1 mM ferrocene/ferrocinium sample at 0.450 mV vs. SCE in dimethylformamide. The concentration of the compounds was about 1 mM. Tetrabutylammonium hexafluorophosphate (TBAP) was used as supporting electrolyte and its concentration was 0.10 M. Cyclic voltammograms of were obtained at scan rates of 50, 100, 200 and 500 mVs^{-1}, respectively. The criteria for reversibility were the separation between cathodic and anodic peaks, the close to unity ratio of the intensities of the cathodic and anodic currents, and the constancy of the peak potential on changing scan rate. Square wave voltammetry was conducted with a sweep rate of 20 mVs^{-1} and a pulse amplitude, width and period of 50 mV, 50 ms and 200 ms, respectively.

Experimental uncertainties are as follows: absorption maxima, ±2 nm; molar absorption coefficient, 10%; redox potentials, ± 10 mV, emission maxima, ±2 nm; Diffusion-ordered spectroscopy, ±10 %. The microanalyses were performed at the Elemental Analysis Service of the Université de Montréal.

11.1.2. X-ray Structure Determination

X-Ray diffraction data collection for the metal complex **1** was carried out on a Bruker Venture Metaljet diffractometer equipped with an Oxford Cryosystem liquid N2 device, using Ga-Kα radiation (λ = 1.34139 Å). The cell parameters were determined (APEX2 software) from reflections taken from three sets of 100 frames, each at 1 s exposure. The structure was solved by direct methods using the program Olex2. The H-atoms were included in calculated positions and treated as riding atoms using Olex2 default parameters. The non-H atoms were refined anisotropically, using weighted full-matrix least-squares on F2. More details are provided in the Supporting Information. CCDC 1545195 contain the supplementary crystallographic data for this paper. These data can be obtained free of charge from The Cambridge Crystallographic Data Centre via www.ccdc.cam.ac.uk/data_request/cif.

11.1.3. Computational Details

Gaussian 09, Revision E.01 was used for all theoretical calculations discussed herein.[1] The molecular structure of the metal complexes was fully optimized with CPCM acetonitrile solvation model in absence of constraints at Density Functional Theory (DFT) level, using, when possible, the crystallographic data as the starting point for the optimization. In particular, the hybrid PBE0 functional,[2] casting 25% of HF exchange in the PBE functional was applied.[3] The double zeta valence basis set LANL2DZ was used for all atoms but the Re ones which were described by the Los Alamos pseudo potential and corresponding basis set.[4] No imaginary frequencies were obtained when frequency calculations on optimized geometries were performed. GaussView 5.0.9,[5] GaussSum 3.0[6] and Chemissian 4.30 software were used for data analysis, visualization and surface plots.[7]

11.2. Synthesis of the ligands and the metal complexes

The benzene-1,4-di-2,2':6',2"-terpyridin-4'-yl ligand (bistpy), the 1,10-phenanthroline-hpp (phen-hpp) ligand and the K_2OsCl_6 precursor were synthesized as previously described.[8] Unless otherwise stated, the solvents were removed under reduced pressure using a rotary evaporator.

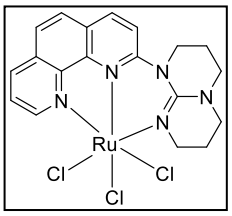

11.2.1. phen-hppRuCl$_3$

A 100 mL round-bottomed flask charged with ligand phen-hpp (315 mg, 1 mmol) and $RuCl_3.3H_2O$ (260 mg, 1 mmol) in EtOH (50 mL). The reaction mixture was left under reflux for 2 hours. After this time, the solution was cooled at -20°C. The resulting suspension was filtered over a 0.45 µm PTFE membrane, washed with EtOH (25 mL), acetone (25 mL) and diethyl ether (50 mL). The burgundy precipitate was dried under vacuum for 1 hour and was used without further purification (273 mg, 52%).

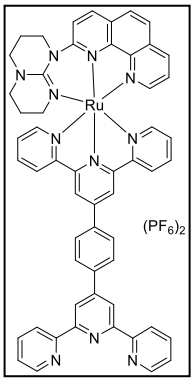

11.2.2. [bistpy(phen-hppRu)][(PF6)2] (1)

A 20-mL microwave vial was charged with precursor **phen-hppRuCl$_3$** (50 mg, 0.10 mmol) and ligand bistpy (80 mg, 0.15 mmol) in ethylene glycol (20 mL) with 4-ethylmorpholine (16 drops). The reaction mixture was left under microwave irradiation (400W) for 15 minutes. The resulting purple solution was poured into an aqueous solution of KPF_6 (10 eq.) leading to instant precipitation of a deep purple precipitate. The heterogeneous solution was filtered over Celite®. The precipitate was washed with plenty of water and then dissolve in a minimum amount of acetonitrile. The organic fraction was then evaporated to dryness. The residue was purified on silica column, using a MeCN:H_2O:KNO_3 sat. mixture in a 20:1:1 ratio containing 1% of triethylamine. The brown band was recovered and the volume reduced under vacuum to ± 10 mL. Metathesis with aqueous KPF_6 solution was performed. The precipitate was extracted with methylene chloride (4 x 25 mL). The organic fraction was dried over anhydrous $MgSO_4$ and filtered over paper. The resulting solution was evaporated to dryness and the residue

dissolved in a minimum amount of acetonitrile (5 mL). Addition of diethyl ether led to the precipitation of the mononuclear species **2**. The brown precipitate was recovered by filtration over a 0.45 µm PTFE membrane (24 mg, 22 %).

^{1}H NMR (400 MHz, CD_3CN): δ (ppm) = 8.97 (s, 2H), 8.93 (s, 2H), 8.86 (d, *J* = 9 Hz, 1H), 8.79-8.76 (m, 4H), 8.60 (d, *J* = 8 Hz, 2H), 8.39 (d, *J* = 8 Hz, 2H), 8.32-8.28 (m, 4H), 8.10 (d, *J* = 9 Hz, 1H), 8.06-8.01 (m, 3H), 7.93 (t, *J* = 8 Hz, 2H), 7.53-7.47 (m, 5H), 7.37 (dd, *J* = 7 Hz, 1H), 7.20 (t, *J* = 7 Hz, 2H), 4.09 (t, *J* = 6 Hz, 2H), 3.37 (t, *J* = 7 Hz, 2H), 3.04 (t, *J* = 6 Hz, 2H), 2.46 (m, 2H), 2.32 (m, 2H), 1.31 (m, 2H).
^{13}C NMR (100 MHz, CD_3CN): δ (ppm) = 159.3, 158.3, 154.3, 153.7, 146.1, 138.3, 137.7, 136.4, 131.3, 128.34, 128.26, 127.9, 127.0, 125.5, 124.9, 122.2, 49.7, 49.4, 49.2, 47.9, 47.7, 24.1, 23.1, 9.2.
HR-MS (ESI): m/z $[M\text{-}PF_6]^+$ calcd for $C_{55}H_{43}N_{11}RuPF_6$: 1104.23973; found: 1104.23885; difference: 0.80 ppm.
Elemental analysis: Calc. for $C_{55}H_{43}N_{11}RuP_2F_{12}.CH_2Cl_2$: C, 50.42; H, 3.40; N, 11.55. Found: C, 50.24; H, 3.67; N, 11.92%.

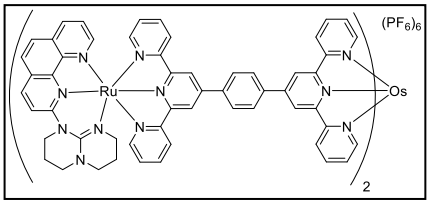

11.2.3 [(bistpy(Phen-hppRu))2Os][(PF6)6] (2)

A 20-mL microwave vial was charged with precursor **1** (50 mg, 0.04 mmol) and K_2OsCl_6 (9.6 mg, 0.02 mmol) in ethylene glycol (20 mL) with 4-ethylmorpholine (16 drops). The reaction mixture was left under microwave irradiation (400W) for 15 minutes. The resulting deep purplish solution was poured into an aqueous solution of KPF_6 (10 eq.) leading to instant precipitation of a deep colored precipitate. The heterogeneous solution was filtered over Celite®. The precipitate was washed with plenty of water and then dissolve in a minimum amount of acetonitrile. The organic fraction was then evaporated to dryness. The residue was purified on silica column, using a $MeCN:H_2O:KNO_3$ sat. mixture in a 20:1:1 ratio containing 1% of triethylamine. The purplish band was recovered and the volume reduced under vacuum to ± 10 mL. Metathesis with aqueous KPF_6 solution was performed. The precipitate was extracted with methylene chloride (4 x 25 mL). The organic fraction was dried over

anhydrous $MgSO_4$ and filtered over paper. The resulting solution was evaporated to dryness and the residue dissolved in a minimum amount of acetonitrile (5 mL). Addition of diethyl ether led to the precipitation of the trinuclear species **2**. The black precipitate was filtered over a PTFE membrane (25 mg, 42 %).

^{1}H NMR (400 MHz, CD_3CN): δ (ppm) = 9.22 (s, 4H), 9.05 (s, 4H), 8.89 (d, *J* = 9 Hz, 2H), 8.76 (d, *J* = 8 Hz, 4H), 8.67 (d, *J* = 8 Hz, 4H), 8.57 (d, *J* = 3 Hz, 8H), 8.33 (d, *J* = 9 Hz, 4H), 8.13 (d, *J* = 9 Hz, 2H), 8.07 (d, *J* = 9 Hz, 2H), 7.97 (t, *J* = 8 Hz, 4H), 7.89 (t, *J* = 8 Hz, 4H), 7.56 (d, *J* = 6 Hz, 4H), 7.52 (d, *J* = 5 Hz, 2H), 7.42-7.40 (m, 6H), 7.22 (dt, *J* = 7 Hz, 8H), 4.16-4.07 (m, 4H), 3.39 (t, *J* = 7 Hz, 4H), 3.07 (t, *J* = 6 Hz, 4H), 2.47 (m, 4H), 2.36 (t, *J* = 6 Hz, 4H), 1.34 (m, 4H).
^{13}C NMR (100 MHz, CD_3CN): δ (ppm) = 160.9, 159.3, 158.3, 156.1, 154.3, 153.6, 153.5, 152.8, 152.2, 147.4, 147.1, 146.1, 138.9, 138.5, 138.3, 136.3, 131.2, 130.1, 129.5, 128.7, 128.4, 127.9, 127.0, 125.8, 125.4, 124.9, 122.3, 121.3, 49.7, 49.4, 49.2, 48.0, 47.6, 24.1, 23.0, 9.1.
HR-MS (ESI): m/z $[M\text{-}4PF_6]^{+4}$ calcd for $C_{110}H_{86}N_{22}Ru_2OsP_2F_{12}$: 599.60983; found: 599.60976; difference: 0.12 ppm; $[M\text{-}2PF_6]^{+2}$ calcd for $C_{110}H_{86}N_{22}Ru_2OsP_4F_{24}$: 1344.18439; found: 1344.18690; difference: 1.87 ppm; $[M\text{-}PF_6]^{+}$ calcd for $C_{110}H_{86}N_{22}Ru_2OsP_5F_6$: 2833.33350; found: 2833.33132; difference: 0.77 ppm
Elemental analysis: Calc. for $C_{110}H_{86}N_{22}Ru_2OsP_6F_{36}.CH_2Cl_2$: C, 43.53; H, 2.90; N, 10.06. Found: C, 43.72; H, 3.29; N, 9.98%.

11.3. ^{1}H NMR, ^{13}C NMR and COSY NMR

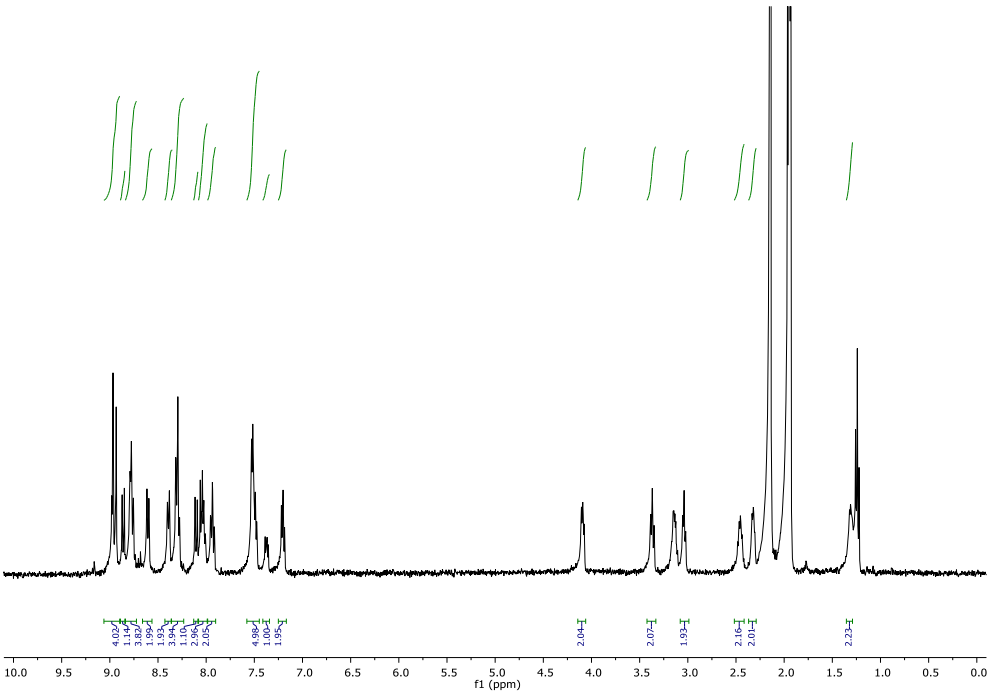

Figure 11.1 - ^{1}H NMR spectra of **1** in acetonitrile-d_3.

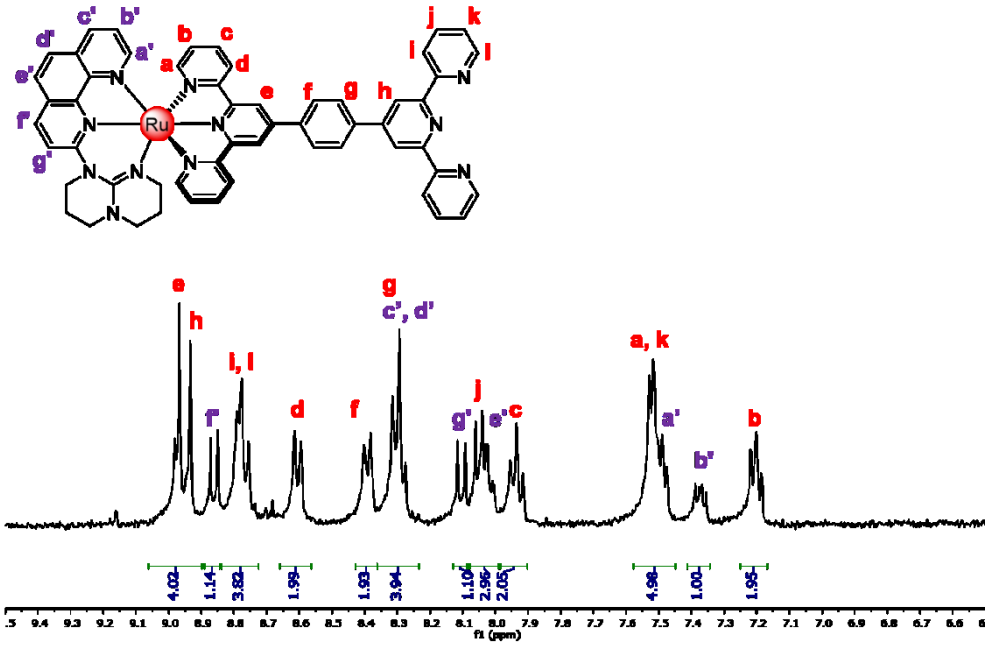

Figure 11.2 ^{1}H NMR spectra of the aromatic region of **1** in acetonitrile-d_3 with assignation of the signals.

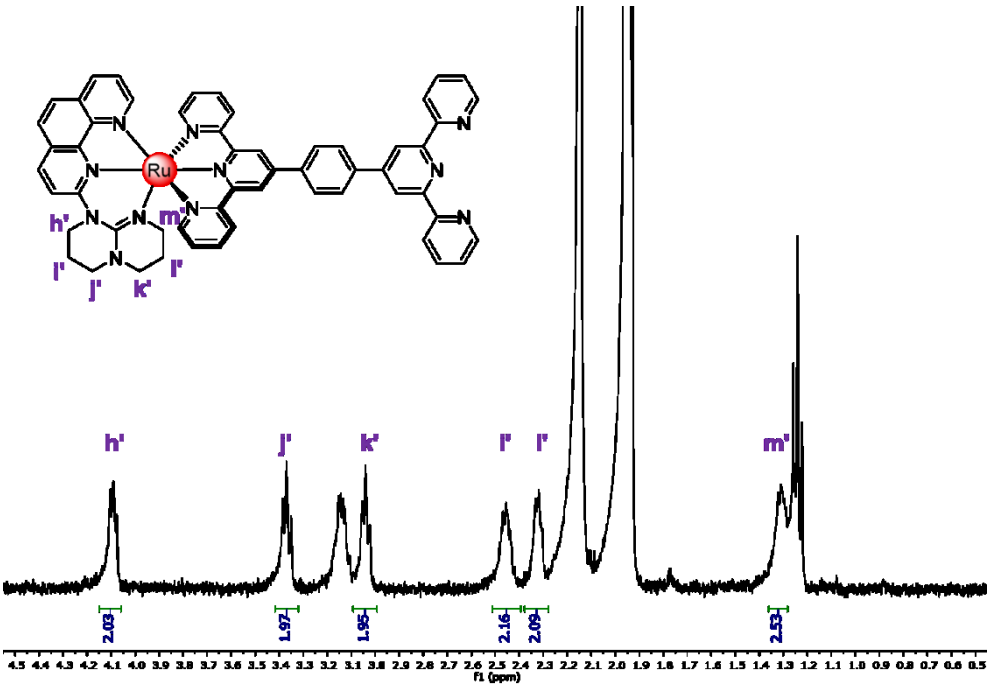

Figure 11.3 - ^{1}H NMR spectra of the aliphatic region of **1** in acetonitrile-d_3 with assignation of the signals.

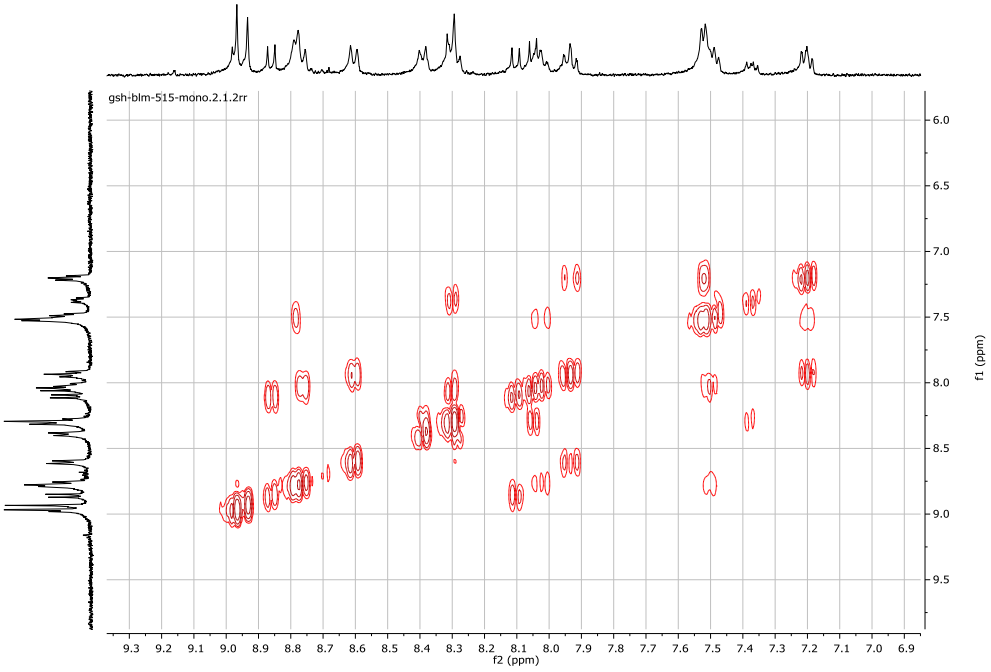

Figure 11.4 - COSY spectra of the aromatic region of **1** in acetonitrile-d_3.

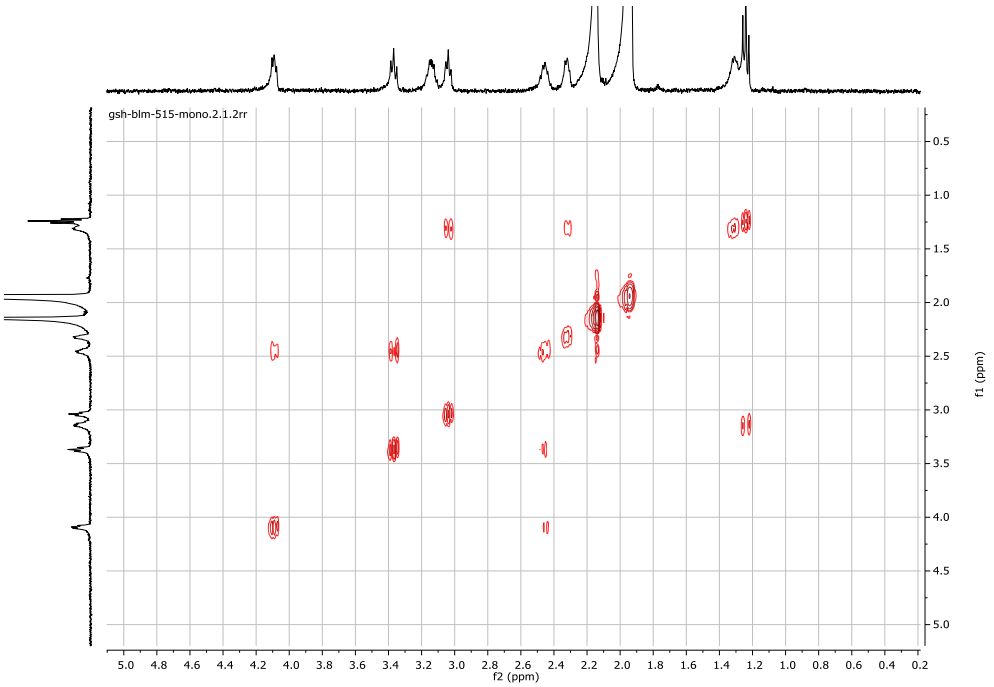

Figure 11.5 - COSY spectra of the aliphatic region of **1** in acetonitrile-d_3.

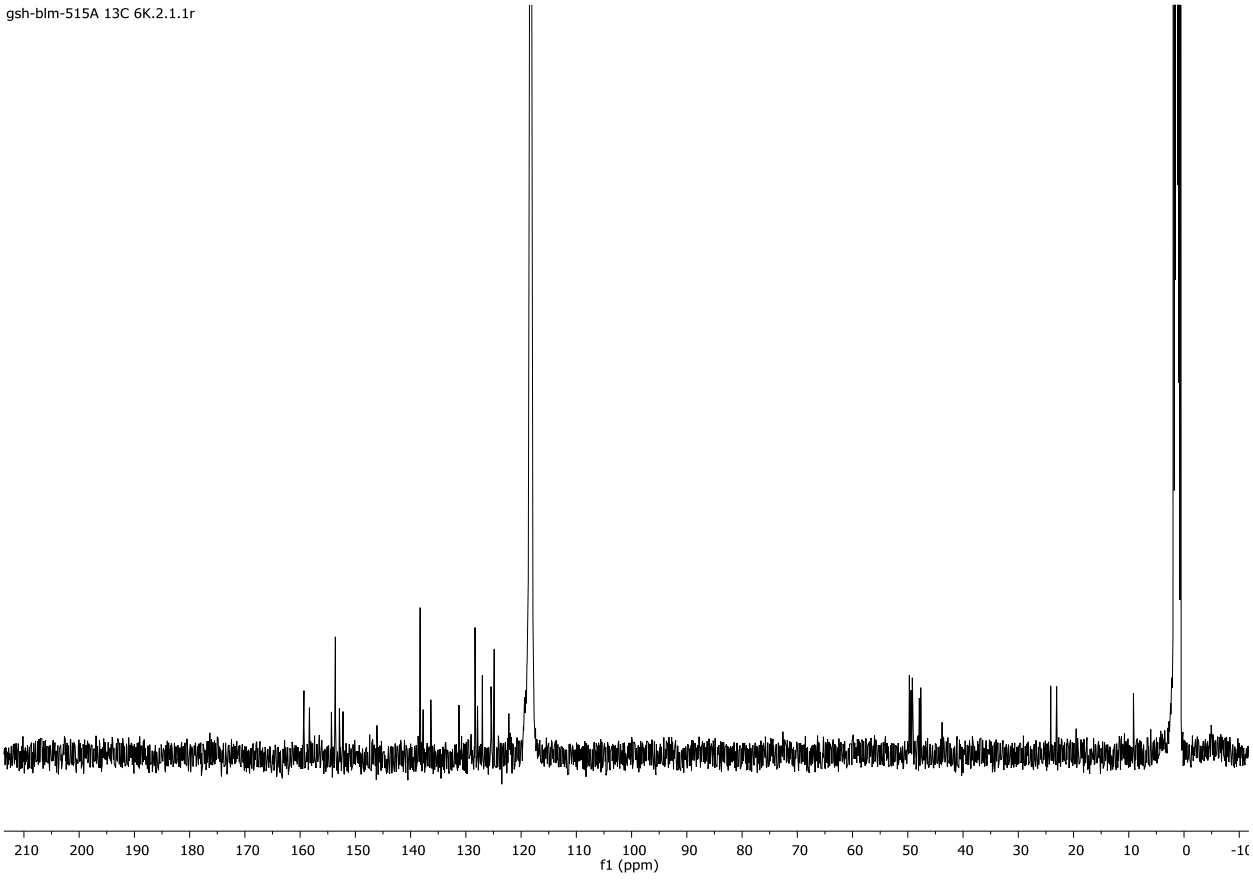

Figure 11.6 - ^{13}C NMR spectra of **1** in acetonitrile-d_3.

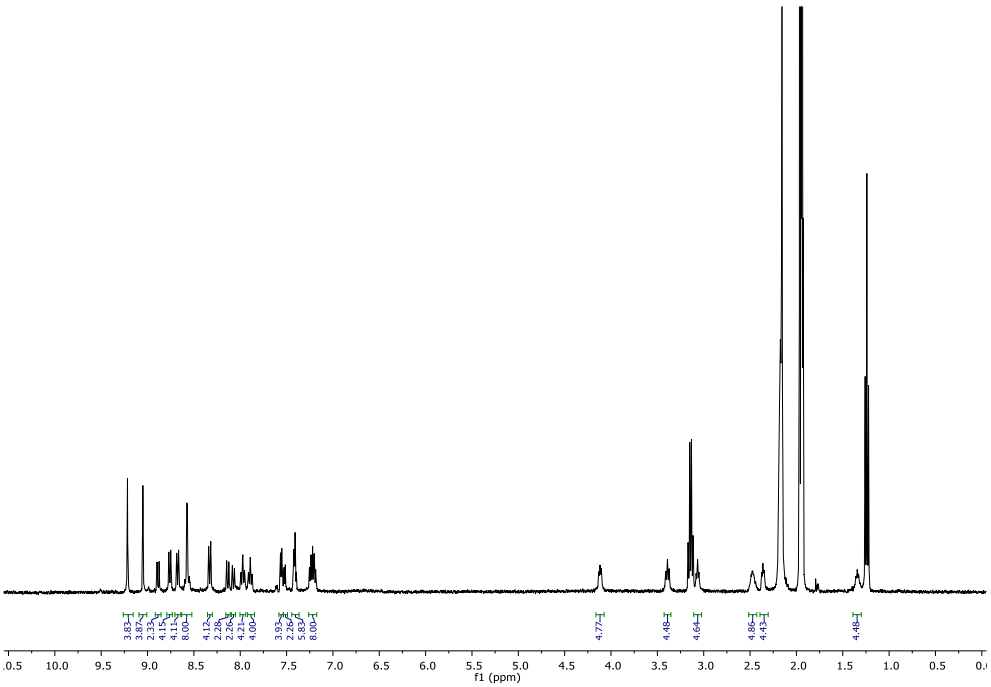

Figure 11.7 - ^{1}H NMR spectra of **2** in acetonitrile-d_3.

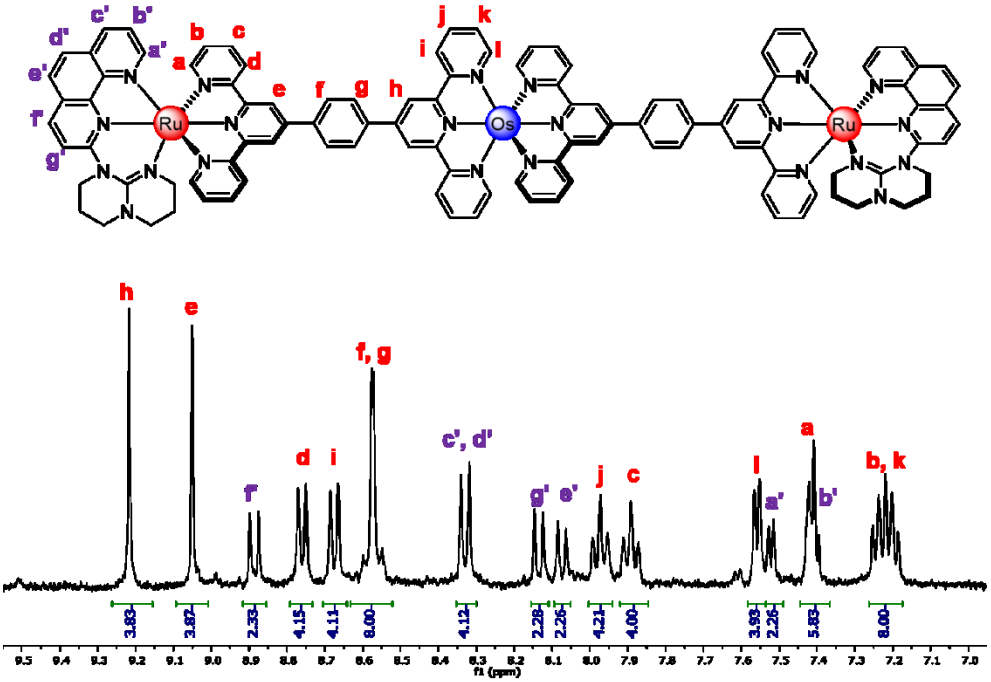

Figure 11.8 - ^{1}H NMR spectra of the aromatic region of **2** in acetonitrile-d_3.

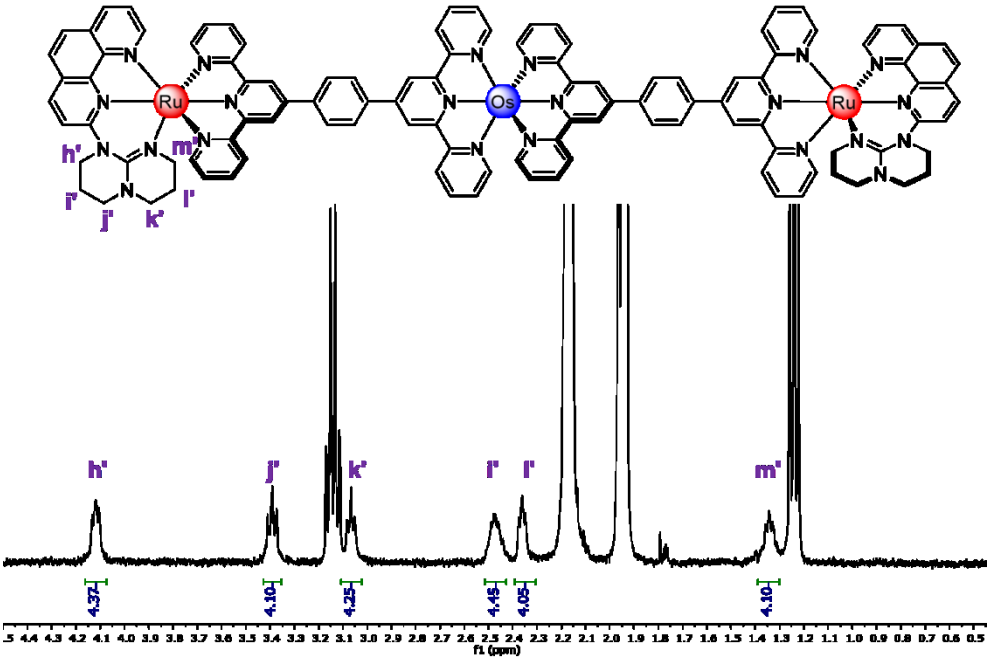

Figure 11.9 - 1H NMR spectra of the aliphatic region of 2 in acetonitrile-d3.

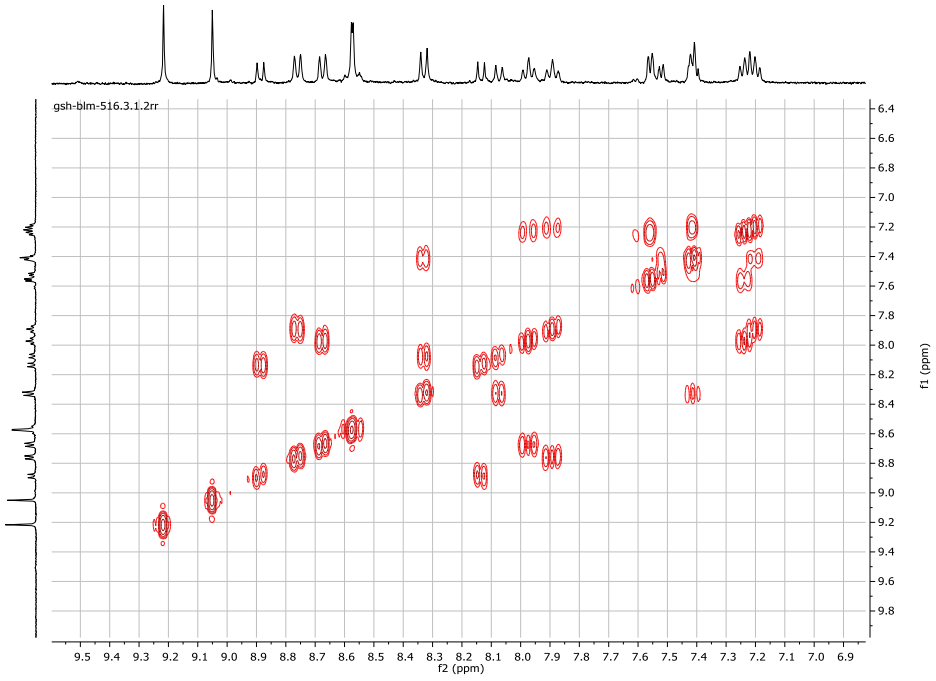

Figure 11.10 - COSY spectra of the aromatic region of **2** in acetonitrile-d_3.

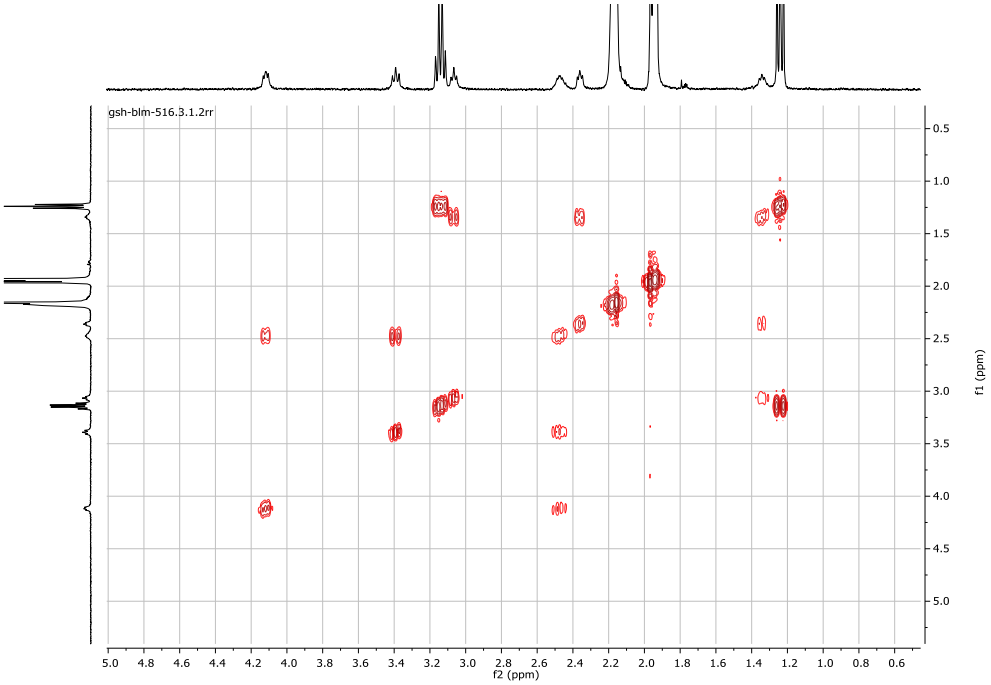

Figure 11.11 - COSY spectra of the aliphatic region of **2** in acetonitrile-d_3.

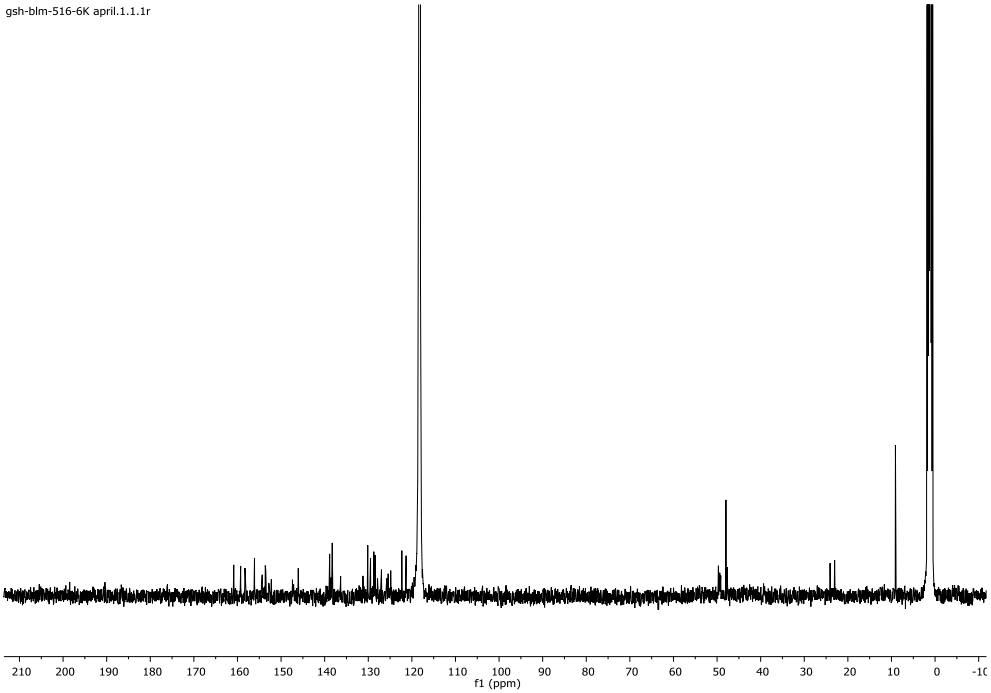

Figure 11.12 - ^{13}C NMR spectra of **2** in acetonitrile-d_3.

11.4. Crystallographic parameters

Table 11.1 - Solid-state structure and refinement data for complex **1**.

	1
Formula	$[C_{55}H_{43}N_{11}Ru][(PF_6)_2]$
Color/form	Red/block
M_w [gmol^{-1}]	1249.01
Temperature [K]	150.0
Wavelength [Å]	1.341139
Crystal system	Triclinic
a [Å]	9.335(2)
b [Å]	12.808(3)
c [Å]	23.398(5)
α [º]	97.096(4)
β [º]	100.183(5)
γ [º]	92.627(4)
V [Å^3]	2725.9(9)
Space group	*P*-1
Z	2
$d_{calcd.}$ [gcm^{-3}]	1.522
μ [mml^{-1}]	2.422
F(000)	1264
Reflection collected	6455
Independent reflections	2473
GoF	1.076
R_1(F) [$I > 2\sigma(I)$]	0.1470
$wR(F^2)$ [$I > 2\sigma(I)$]	0.3280
R_1(F) (all data)	0.2783
wR(F^2) (all data)	0.4138
Largest diff. peak/hole [eÅ^{-3}]	1.152

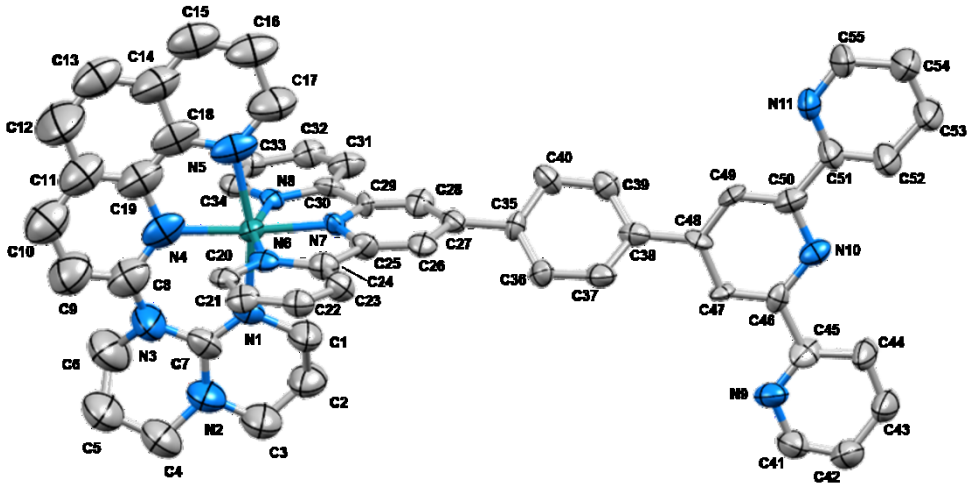

Figure 11.13 - Thermal ellipsoid diagram (30% probability) of X-ray structure of **1** with atoms' numbering. Hydrogen atoms and counter-anions are omitted for clarity.

11.5. DFT and TD-DFT results

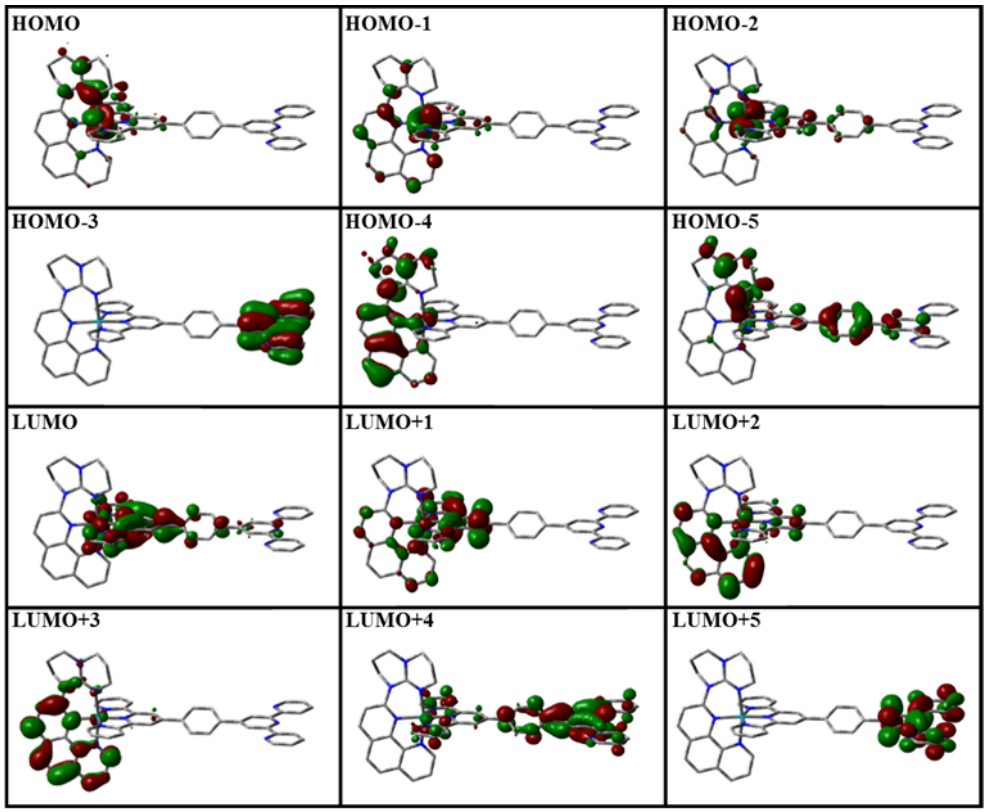

Figure 11.14 - Kohn-Sham electron density illustration of the molecular orbitals for **1** in ($S = 0$) the ground-state.

Table 11.2 - MO composition of **1** in (*S=0*) ground state.

MO	Energy (eV)	Composition (%)		
		Ruthenium	phen-hpp	phenyl-1,4-bistpy
LUMO+5	-1.903	0	0	100
LUMO+4	-2.049	0	0	99
LUMO+3	-2.281	1	94	4
LUMO+2	-2.434	5	77	18
LUMO+1	-2.529	1	20	79
LUMO	-2.773	8	3	89
HOMO	-5.843	55	32	13
HOMO-1	-6.256	62	24	14
HOMO-2	-6.409	71	8	21
HOMO-3	-7.016	0	0	100
HOMO-4	-7.211	9	86	5
HOMO-5	-7.230	9	50	41

Table 11.3 – Selected transitions from TD-DFT calculations of **1** in the singlet ground state (PBE0), CPCM (CH_3CN).

Energy (eV)	**λ (nm)**	**f**	**Transition**	**Character**
2.01	615	0.0269	H→L (90%)	$^1MLCT_{Ru\rightarrow bistpy}$ (maj.) $LLCT_{phen\text{-}hpp\rightarrow bistpy}$
2.35	525	0.0096	H-1→L (58%)H→L+1 (10%), H→L+2 (15%)	$^1MLCT_{Ru\rightarrow bistpy}$
2.38	518	0.0072	H-1→L (21%), H→L+1 (24%), H→L+2 (42%)	$^1MLCT_{Ru\rightarrow bistpy}$ (maj.) $^1MLCT_{Ru\rightarrow phen\text{-}hpp}$
2.41	512	0.0148	H→L+1 (57%), H→L+2 (30%)	
2.67	463	0.2461	H-2→L (51%), H-1→L+2 (19%)	
2.68	461	0.0021	H→L+3 (91%)	$^1MLCT_{Ru\rightarrow phen\text{-}hpp}$
2.81	440	0.1574	H-1→L+1 (88%)	$^1MLCT_{Ru\rightarrow bistpy}$

2.86	431	0.0124	H-2→L+1 (14%), H-2→L+2 (75%)	$^1MLCT_{Ru\rightarrow phen\text{-}hpp}$
2.89	427	0.0216	H-2→L+1 (80%), H-2→L+2 (13%)	$^1MLCT_{Ru\rightarrow bistpy}$
3.04	406	0.0726	H-1→L+2 (63%)	$^1MLCT_{Ru\rightarrow phen\text{-}hpp}$
3.15	392	0.0414	H-2→L+3 (10%), H-1→L+3 (82%)	$^1MLCT_{Ru\rightarrow phen\text{-}hpp}$
3.23	382	0.0644	H-2→L+3 (72%)	
3.25	379	0.0828	H→L+4 (65%), H→L+6 (18%)	
3.48	354	0.0049	H→L+6 (25%), H→L+7 (45%)	$^1MLCT_{Ru\rightarrow bistpy}$ (maj.)
3.64	339	0.1138	H-1→L+4 (60%), H-1→L+6 (25%)	$LLCT_{phen\text{-}hpp\rightarrow bistpy}$
3.64	339	0.0011	H→L+5 (98%)	
3.67	336	0.1212	H-6→L (11%), H-5→L (72%)	
3.73	331	0.3066	H-4→L (16%), H-2→L+4 (53%), H-2→L+6 (19%)	$LLCT_{phen\text{-}hpp\rightarrow bistpy}$
3.92	315	0.1647	H-6→L (15%), H-2→L+6 (12%), H-2→L+7 (44%) H-1→L+6 (11%)	$^1MLCT_{Ru\rightarrow bistpy}$ (maj.)
3.94	313	0.2598	H-6→L (32%), H-2→L+7 (10%), H→L+9 (14%)	$LLCT_{phen\text{-}hpp\rightarrow bistpy}$
4.12	300	0.1486	H-4→L+1 (19%), H-4→L+3 (34%)	
4.14	298	0.1681	H-9→L (25%), H-6→L+1 (14%)	
4.21	293	0.1300	H-9→L (29%), H-6→L+1 (46%)	$^1MLCT_{Ru\rightarrow bistpy}$
4.25	290	0.1712	H-3→L+4 (56%), H-2→L+5 (21%)	$^1MLCT_{Ru\rightarrow bistpy}$ $LLCT_{phen\text{-}hpp\rightarrow bistpy}$
4.48	275	0.1691	H-3→L+3 (75%), H-3→L+5 (16%)	$^1MLCT_{Ru\rightarrow bistpy}$
4.49	275	0.5137	H-9→L+1 (15%), H-3→L+3 (24%), H-3→L+5 (47%)	$LLCT_{bistpy\rightarrow phen\text{-}hpp}$
4.59	269	0.1134	H-10→L (37%), H-9→L+2 (12%)	
4.61	268	0.0963	H-9→L+1 (10%), H-2→L+8 (16%), H-2→L+15 (11%)	$^1MLCT_{Ru\rightarrow bistpy}$
4.71	262	0.0816	H→L+13 (48%)	$^1MLCT_{Ru\rightarrow phen\text{-}hpp}$
4.72	262	0.4052	H-6→L+5 (33%), H-5→L+5 (36%)	$^1MLCT_{Ru\rightarrow bistpy}$ $LLCT_{phen\text{-}hpp\rightarrow bistpy}$ (maj.)
5.24	236	0.1091	H-17→L+1 (21%), H-12→L+4 (12%), H-2→L+11 (13%) H-2→L+12 (30%)	$^1MLCT_{Ru\rightarrow bistpy}$

5.27	234	0.1147	H→L+17 (46%)	$^1MLCT_{Ru→bistpy}$ $^1MLCT_{Ru→phen-hpp}$
5.41	228	0.2714	H-14→L+3 (49%)	$^1MLCT_{Ru→bistpy}$
5.43	227	0.0857	H-16→L (13%), H-5→L+8 (41%)	
5.46	226	0.0909	H-9→L+6 (18%), H-9→L+7 (14%), H-5→L+8 (11%)	
5.49	225	0.2332	H-4→L+8 (26%), H-4→L+9 (28%)	$LLCT_{phen-hpp→bistpy}$
5.53	223	0.1065	H-5→L+9 (11%), H-4→L+8 (16%), H-4→L+9 (15%) H-2→L+14 (24%)	
5.73	216	0.0898	H-15→L+4 (39%), H-3→L+9 (12%)	$LLCT_{bistpy→phen-hpp}$

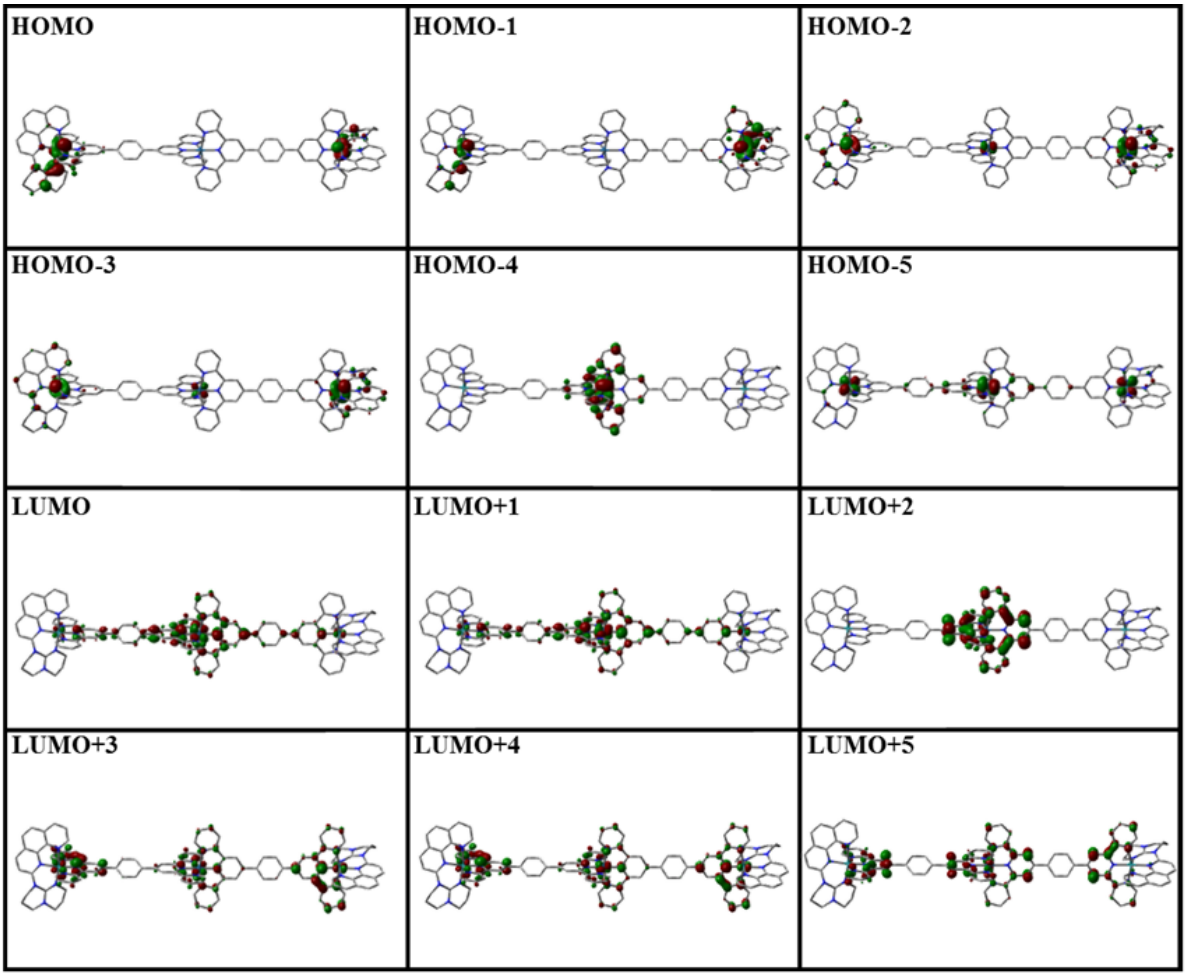

Figure 11.15 - Kohn-Sham electron density illustration of the molecular orbitals for 2 in (S = 0) the ground-state.

Table 11.4 - MO composition of **2** in (*S=0*) ground state.

MO	Energy (eV)	Composition (%)			
		Ruthenium	Osmium	phen-hpp	phenyl-1,4-bistpy
LUMO+5	-2.628	1	2	8	89
LUMO+4	-2.770	5	3	3	89
LUMO+3	-2.775	5	3	3	89
LUMO+2	-2.807	0	0	0	100
LUMO+1	-3.042	3	9	1	87
LUMO	-3.056	3	9	1	87
HOMO	-5.930	55	0	32	13
HOMO-1	-5.930	55	0	32	13
HOMO-2	-6.337	57	4	21	17
HOMO-3	-6.337	58	4	22	17
HOMO-4	-6.395	0	61	0	39
HOMO-5	-6.435	37	27	7	29

Table 11.5 - Selected transitions from TD-DFT calculations of **2** in the singlet ground state (PBE0), CPCM (CH_3CN).

Energy (eV)	**λ (nm)**	**f**	**Transition**	**Character**
1.98	624	0.0677	H-1→L+1 (22%), H-1→L+4 (23%), H→L (21%) H→L+3 (24%)	$^1MLCT_{Ru\rightarrow bistpy}$ (maj.) + $LLCT_{phen\text{-}hpp\rightarrow bistpy}$
1.98	624	0.0078	H-1→L (21%), H-1→L+3 (24%), H→L+1 (22%) H→L+4 (23%)	
2.26	547	0.0194	H-4→L (80%), H-4→L+3 (18%)	$^1MLCT_{Os\rightarrow bistpy}$
2.27	544	0.0192	H-4→L+1 (78%), H-4→L+4 (20%)	
2.31	535	0.0011	H-8→L (15%), H-7→L+1 (14%), H-6→L+1 (19%) H-5→L (21%)	$^1MLCT_{Ru\rightarrow bistpy}$ (maj.) + $^1MLCT_{Os\rightarrow bistpy}$ + $LLCT_{phen\text{-}hpp\rightarrow bistpy}$

2.33	531	0.0223	H-3→L+1 (17%), H-3→L+4 (17%), H-2→L (16%) H-2→L+3 (18%)	$^1MLCT_{Ru\rightarrow bistpy}$ (maj.)
2.33	530	0.0043	H-3→L (15%), H-3→L+3 (18%), H-2→L+1 (16%) H-2→L+4 (17%)	$LLCT_{phen\text{-}hpp\rightarrow bistpy}$
2.39	517	0.0152	H-1→L+6 (18%), H→L+5 (15%), H→L+6 (11%) H→L+7 (10%), H→L+9 (16%)	$^1MLCT_{Ru\rightarrow bistpy}$
2.39	517	0.0048	H-1→L+5 (15%), H-1→L+6 (11%), H-1→L+7 (10%) H-1→L+8 (10%), H→L+6 (18%), H→L+8 (11%)	
2.40	514	0.0075	H-1→L+6 (13%), H-1→L+8 (28%), H→L+9 (28%)	$^1MLCT_{Ru\rightarrow phen\text{-}hpp}$
2.40	514	0.0185	H-1→L+9 (23%), H→L+6 (14%), H→L+8 (23%)	$^1MLCT_{Ru\rightarrow bistpy}$
2.42	511	0.0000	H-8→L+1 (13%), H-7→L (15%), H-6→L (21%) H-5→L+1 (18%)	$^1MLCT_{Ru\rightarrow bistpy}$ (maj.) $^1MLCT_{Os\rightarrow bistpy}$
2.50	494	1.0919	H-6→L+1 (24%), H-5→L (22%)	$LLCT_{phen\text{-}hpp\rightarrow bistpy}$
2.65	466	0.3917	H-8→L (11%), H-7→L+1 (10%), H-4→L+2 (20%)	$^1MLCT_{Ru\rightarrow bistpy}$
2.77	446	0.6177	H-4→L+2 (53%), H-3→L+6 (12%)	$^1MLCT_{Os\rightarrow bistpy}$
3.04	406	0.1099	H-3→L+8 (28%), H-2→L+9 (27%)	$^1MLCT_{Ru\rightarrow bistpy\ and/or\ phen\text{-}hpp}$ (maj.)
3.25	380	0.1207	H-7→L+1 (16%), H-6→L+1 (10%), H-6→L+10 (10%) H-5→L+11 (10%)	$^1MLCT_{Os\rightarrow bistpy\ and/or\ phen\text{-}hpp}$
3.28	376	0.4063	H-8→L+3 (25%), H-7→L+4 (30%), H-6→L+1 (12%)	$^1MLCT_{Ru\rightarrow bistpy}$ $^1MLCT_{Os\rightarrow bistpy}$
3.71	333	0.2004	H-3→L+12 (25%), H-2→L+13 (26%)	$^1MLCT_{Ru\rightarrow bistpy}$ (maj.)
3.74	330	0.2351	H-6→L+12 (27%), H-5→L+13 (27%)	$^1MLCT_{Os\rightarrow bistpy}$
3.85	320	0.1011	H-8→L+13 (16%), H-7→L+12 (16%), H-6→L+16 (16%) H-5→L+15 (16%)	$LLCT_{phen\text{-}hpp\rightarrow bistpy}$
4.00	309	0.1520	H-11→L+6 (15%)	$^1MLCT_{Ru\rightarrow bistpy}$ (maj.)

4.01	308	0.1487	H-3→L+12 (13%), H-3→L+20 (17%), H-2→L+13 (12%) H-2→L+19 (17%)	$LLCT_{phen\text{-}hpp\rightarrow bistpy}$
4.05	305	0.1465	H-17→L (23%), H-4→L+12 (23%), H-4→L+16 (17%)	$^{1}MLCT_{Os\rightarrow bistpy}$
4.05	305	0.1378	H-17→L+1 (17%), H-4→L+13 (24%), H-4→L+15 (20%)	
4.08	302	0.4324	H-12→L (13%)	$^{1}MLCT_{Ru\rightarrow bistpy}$
4.10	301	0.1553	H-12→L+8 (11%), H-11→L+9 (11%)	$LLCT_{phen\text{-}hpp\rightarrow bistpy}$ (maj.)
4.12	299	0.2888	H-17→L (43%), H-4→L+16 (29%)	$^{1}MLCT_{Os\rightarrow bistpy}$
4.13	299	0.3700	H-17→L+1 (41%), H-4→L+15 (26%)	
4.13	299	0.1560	H-6→L+20 (11%), H-5→L+19 (11%)	$^{1}MLCT_{Ru\rightarrow bistpy}$ $^{1}MLCT_{Os\rightarrow bistpy}$ $LLCT_{phen\text{-}hpp\rightarrow bistpy}$
4.20	294	0.4041	H-16→L (25%), H-15→L+1 (22%)	$^{1}MLCT_{Ru\rightarrow bistpy}$ $LLCT_{phen\text{-}hpp\rightarrow bistpy}$ (maj.)
4.47	276	0.1589	H-20→L+2 (11%), H-16→L+3 (31%), H-15→L+4 (35%)	
4.50	274	0.1120	H-20→L+2 (46%), H-14→L (20%)	$LLCT_{bistpy\rightarrow phen\text{-}hpp}$
4.56	271	0.1003	H-15→L+6 (15%), H-14→L+9 (10%), H-13→L+8 (10%)	
4.60	268	0.2927	H-17→L+5 (10%), H-17→L+7 (15%), H-14→L+9 (10%) H-13→L+8 (10%)	$^{1}MLCT_{Ru\rightarrow phen\text{-}hpp}$ $^{1}MLCT_{Os\rightarrow phen\text{-}hpp}$
4.60	268	0.1176	H-2→L+17 (12%)	$^{1}MLCT_{Ru\rightarrow bistpy}$ (maj.) $^{1}MLCT_{Os\rightarrow bistpy}$
4.66	265	0.1370	H-8→L+17 (12%), H-7→L+18 (12%)	$^{1}MLCT_{Ru\rightarrow bistpy}$ (maj.) $^{1}MLCT_{Os\rightarrow bistpy} + LLCT_{phen\text{-}hpp\rightarrow bistpy}$
4.66	265	0.1649	H-19→L+5 (10%), H-18→L+6 (17%)	$^{1}MLCT_{Ru\rightarrow bistpy} + {}^{1}MLCT_{Os\rightarrow bistpy} + LLCT_{phen\text{-}hpp\rightarrow bistpy}$ (maj.)
4.76	260	0.1184	H-19→L+11 (12%), H-18→L+10 (14%), H-13→L+10 (10%)	$^{1}MLCT_{Ru\rightarrow phen\text{-}hpp} + LLCT_{bistpy\rightarrow phen\text{-}hpp}$ (maj.)

11.6. Electrochemistry and photophysical properties

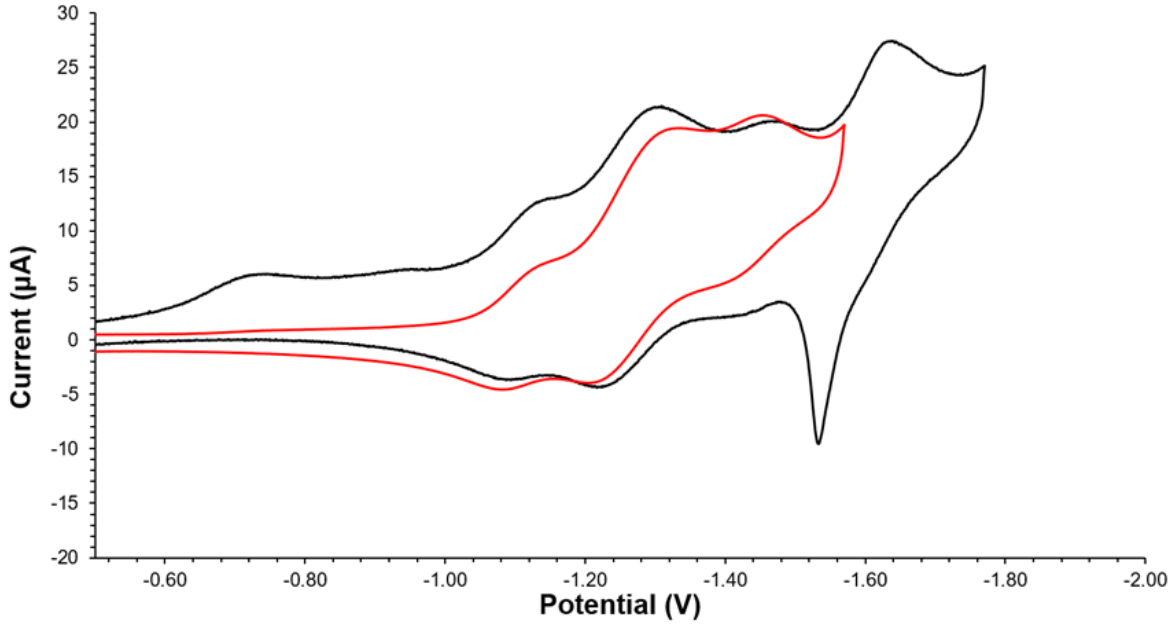

Figure 11.16 - Comparison of the reduction waves of 2 when cycling up to -1.55 V (red) and -1.75 V (black). The three first processes are fully reversible while the fourth one led to adsorption and stripping at the electrode.

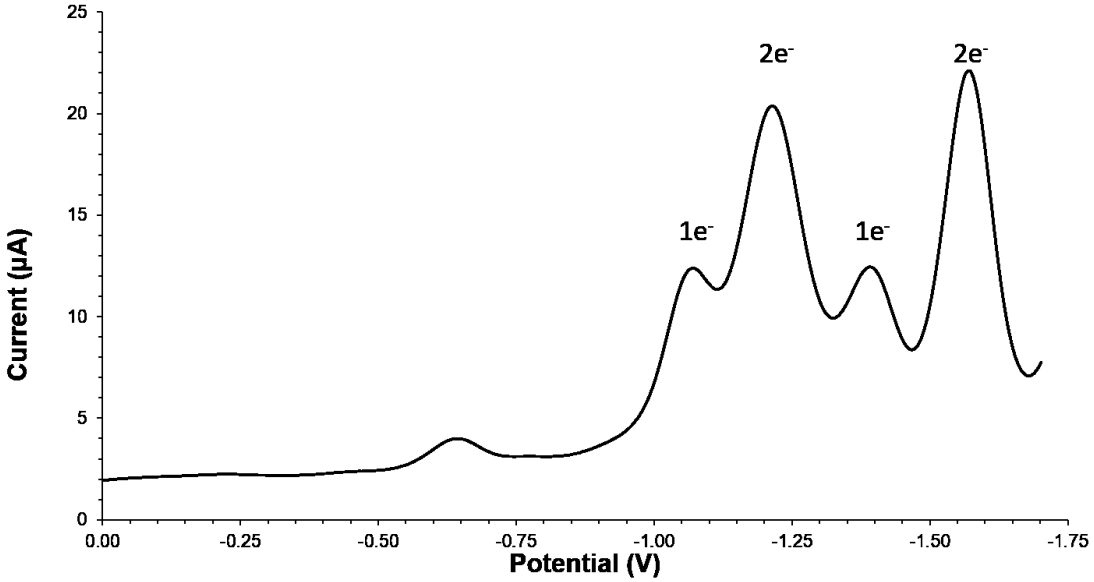

Figure 11.17 - Square-wave voltammetry experiment on **2** displaying the number of electron exchanged during the processes.

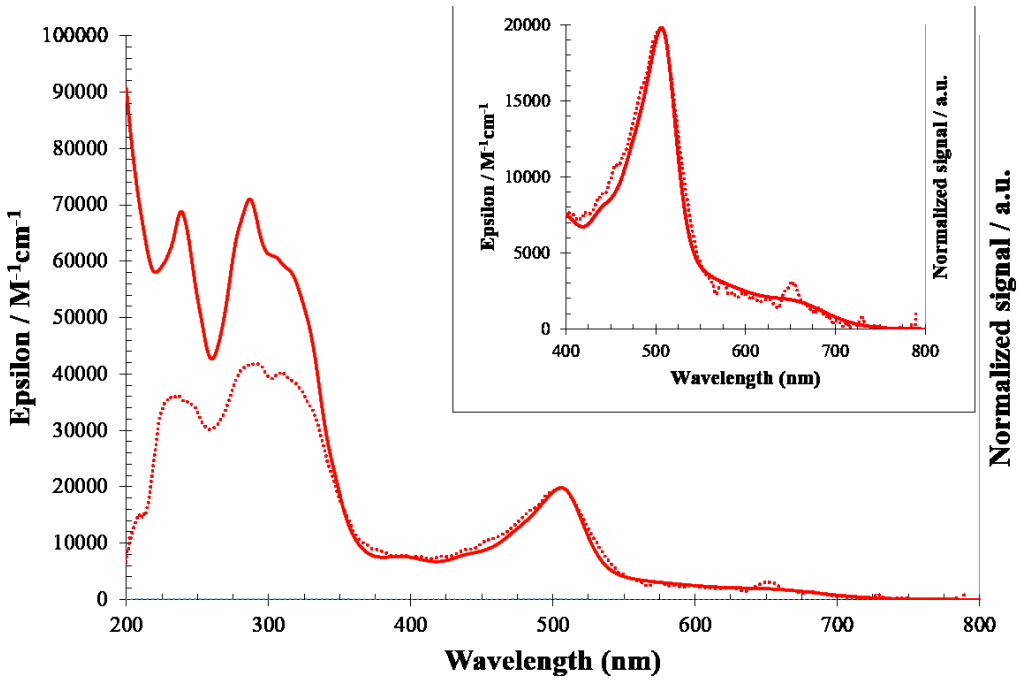

Figure 11.18 - Absorption (plain) and excitation (dots) spectra of **1** in spectrograde acetonitrile solution. The excitation spectrum was recorded with λ_{em} = 805 nm.

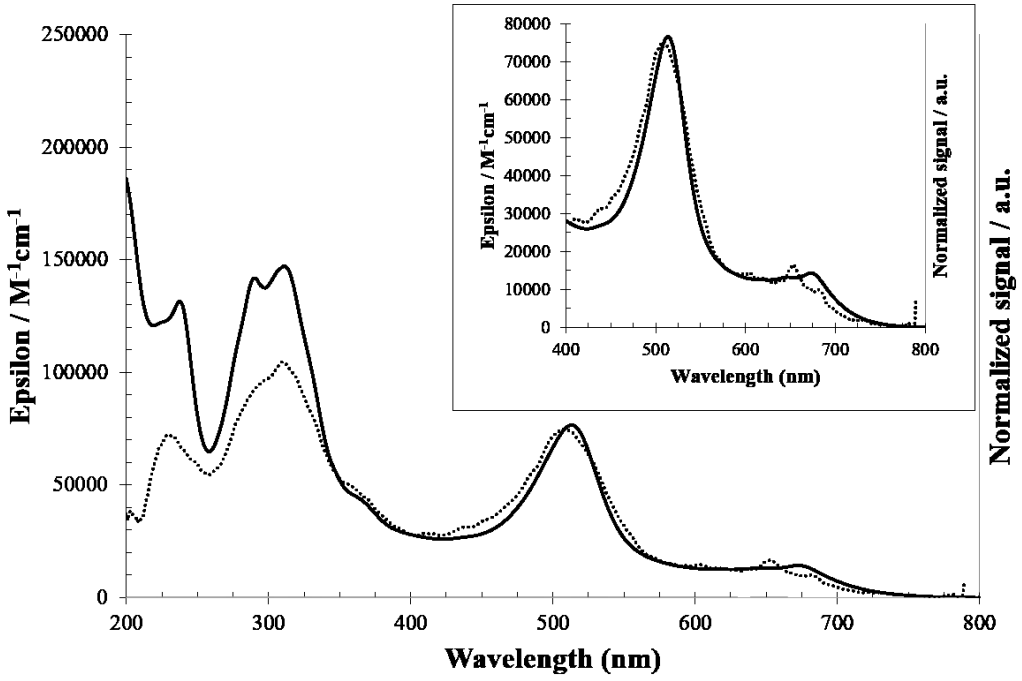

Figure 11.19 - Absorption (plain) and excitation (dots) spectra of **2** in spectrograde acetonitrile solution. The excitation spectrum was recorded with λ_{em} = 805 nm.

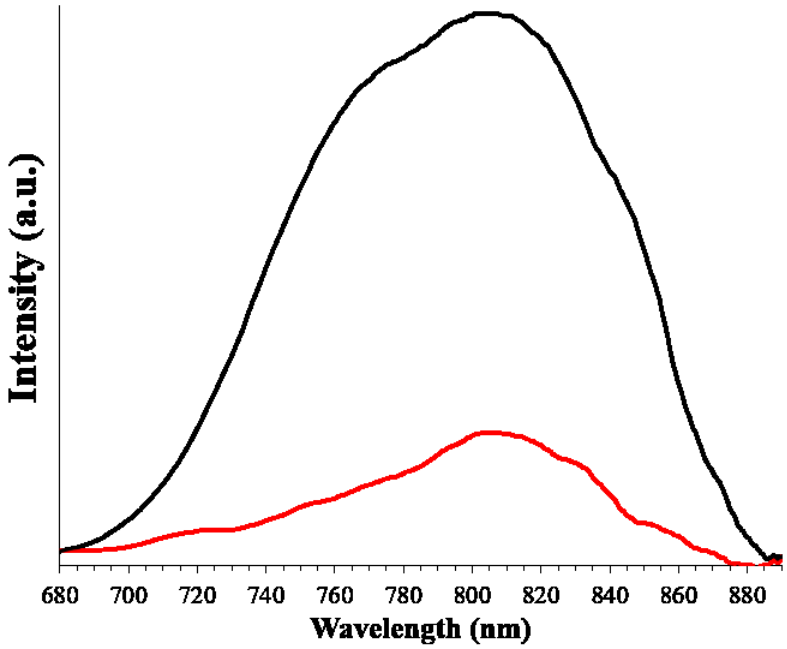

Figure 11.20 - Luminescence spectra of **1** (red) and **2** (black) in deaerated acetonitrile solution at ambient temperature (λex. = 650 nm).

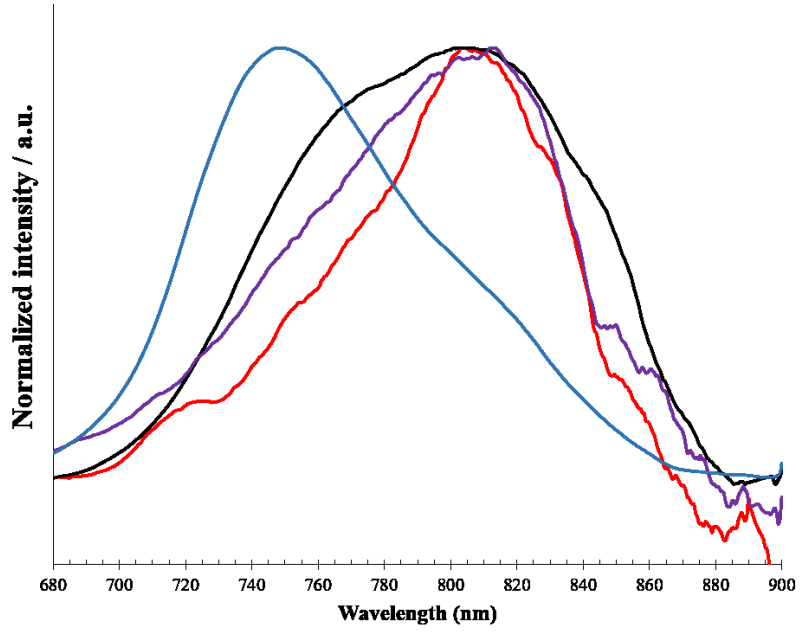

Figure 11.21 - Normalized luminescence spectra of $\mathbf{1}^{2+}$ (red) and $\mathbf{2}^{6+}$ (black), $[\mathbf{Os(ttpy)_2}]^{2+}$ (blue) and $[\mathbf{Ru(phtpy)(phen\text{-}hpp)}]^{2+}$ (purple) recorded in deaerated acetonitrile solution at ambient temperature (λex. = 650 nm).

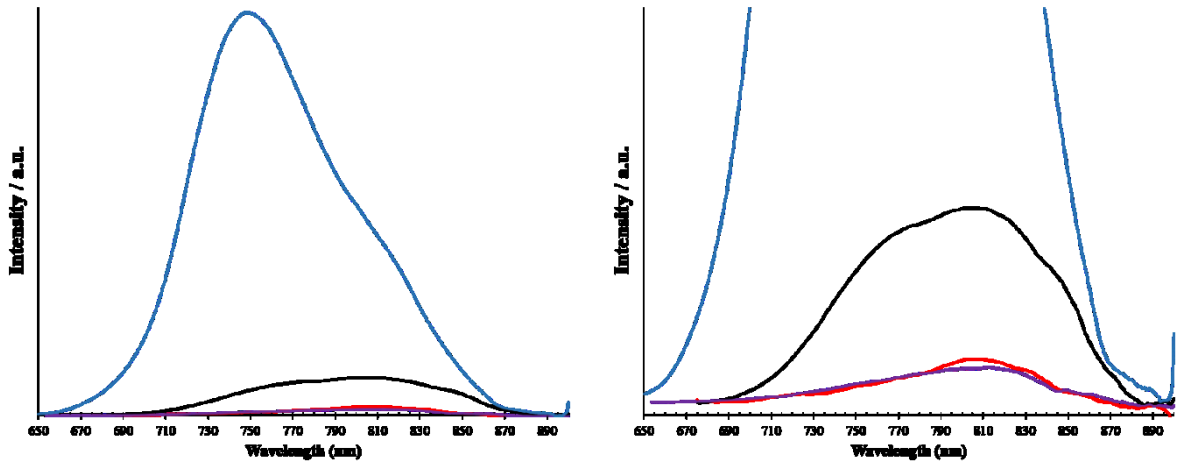

Figure 11.22 - Luminescence spectra of 12+ (red) and 26+ (black), [Os(ttpy)2]2+ (blue) and [Ru(phtpy)(phen-hpp)]2+ (purple) recorded in deaerated acetonitrile solution at ambient temperature (λex. = 650 nm). The spectra on the left is zoomed to put in evidence the intensity of **1** and **2** compared to the Os^{2+} reference.

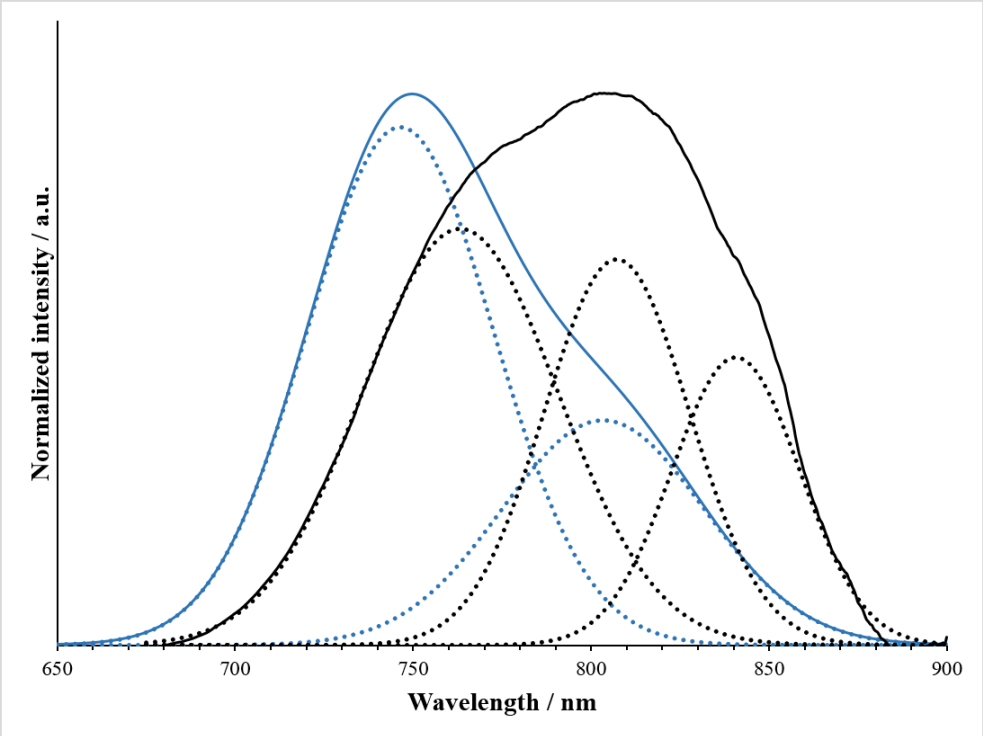

Figure 11.23 - Normalized luminescence spectra of $\mathbf{2}^{6+}$ (black) and $[\mathbf{Os(ttpy)_2}]^{2+}$ (blue) recorded in deaerated acetonitrile solution at ambient temperature and the deconvoluted spectra showing the contributions to the emission.

11.7. References

[1] M. J. Frisch, G. W. Trucks, H. B. Schlegel, G. E. Scuseria, M. A. Robb, J. R. Cheeseman, G. Scalmani, V. Barone, B. Mennucci, G. A. Petersson, H. Nakatsuji, M. Caricato, X. Li, H. P. Hratchian, A. F. Izmaylov, J. Bloino, G. Zheng, J. L. Sonnenberg, M. Hada, M. Ehara, K. Toyota, R. Fukuda, J. Hasegawa, M. Ishida, T. Nakajima, Y. Honda, O. Kitao, H. Nakai, T. Vreven, J. A. Montgomery Jr., J. E. Peralta, F. Ogliaro, M. J. Bearpark, J. Heyd, E. N. Brothers, K. N. Kudin, V. N. Staroverov, R. Kobayashi, J. Normand, K. Raghavachari, A. P. Rendell, J. C. Burant, S. S. Iyengar, J. Tomasi, M. Cossi, N. Rega, N. J. Millam, M. Klene, J. E. Knox, J. B. Cross, V. Bakken, C. Adamo, J. Jaramillo, R. Gomperts, R. E. Stratmann, O. Yazyev, A. J. Austin, R. Cammi, C. Pomelli, J. W. Ochterski, R. L. Martin, K. Morokuma, V. G. Zakrzewski, G. A. Voth, P. Salvador, J. J. Dannenberg, S. Dapprich, A. D. Daniels, Ö. Farkas, J. B. Foresman, J. V. Ortiz, J. Cioslowski, D. J. Fox, Gaussian, Inc., Wallingford, CT, USA, **2009**.

[2] C. Adamo, V. Barone, *J. Chem. Phys.* **1999**, *110*, 6158-6170.

[3] a) J. P. Perdew, K. Burke, M. Ernzerhof, *Phys. Rev. Lett.* **1996**, *77*, 3865-3868; b) J. P. Perdew, K. Burke, M. Ernzerhof, *Phys. Rev. Lett.* **1997**, *78*, 1396-1396.

[4] a) T. H. Dunning, Jr., P. J. Hay, *Modern Theoretical Chemistry, Vol. 3*, Springer US, New York, **1977**; b) T. H. Dunning, Jr., P. J. Hay, *Methods of Electronic Structure Theory, Vol. 2*, Plenum Press, New York, **1977**; c) J. P. Hay, W. R. Wadt, *J. Chem. Phys.* **1985**, *82*, 270; d) W. R. Wadt, J. P. Hay, *J. Chem. Phys.* **1985**, *82*, 284; e) J. P. Hay, W. R. Wadt, *J. Chem. Phys.* **1985**, *82*, 299.

[5] R. Dennington, T. Keith, J. Millam, 5 ed., Semichem Inc., Shawnee Mission, KS, **2009**.

[6] N. M. O'Boyle, A. L. Tenderholt, K. M. Langner, *J. Comput. Chem.* **2008**, *29*, 839-845.

[7] L. Skripnikov, **2005-2014**.

[8] a) G. S. Hanan, J. Wang, *Synlett* **2005**, 1251-1254; b) B. Laramee-Milette, G. S. Hanan, *Dalton Trans.* **2016**, *45*, 12507-12517; c) A. G. Turner, A. F. Clifford, C. N. Ramachandra Rao, *Anal. Chem.* **1958**, *30*, 1708-1709.

Chapitre 12 - Informations supplémentaires : Simple solubilisation of the traditional 2,2' :6',2"-terpyridine ligand in organic solvents by substitution with 4,4"-di-tert-butyl groups

12.1. ^{1}H NMR and ^{13}C NMR

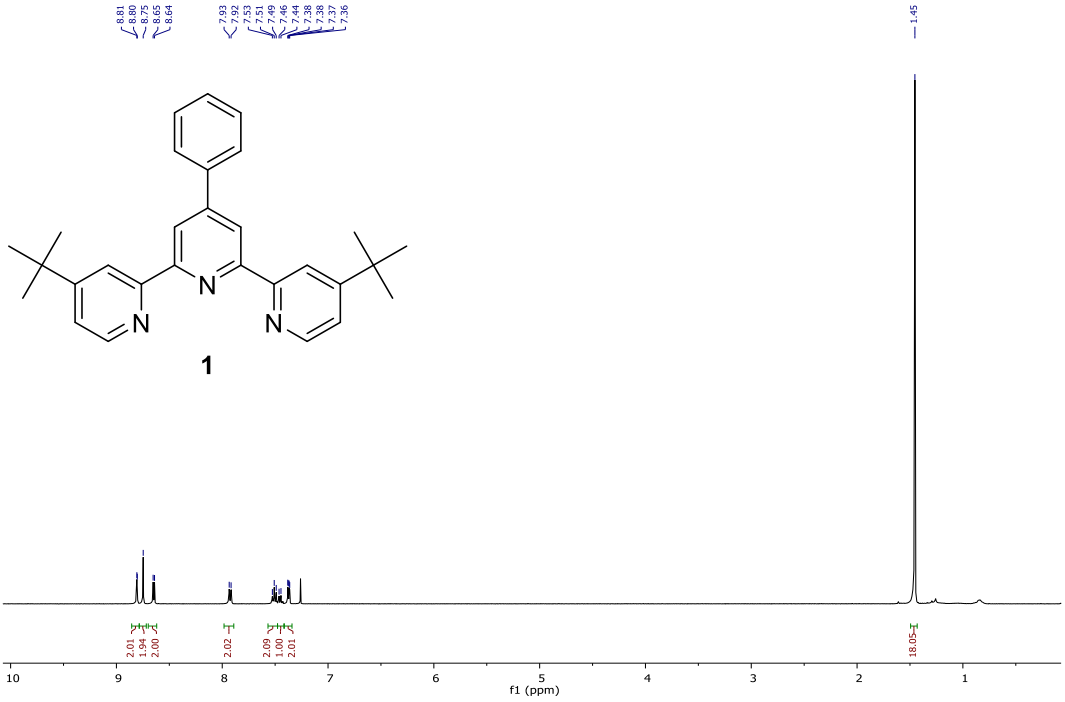

Figure 12.1 - ^{1}H NMR spectrum of 1 in $CDCl_3$.

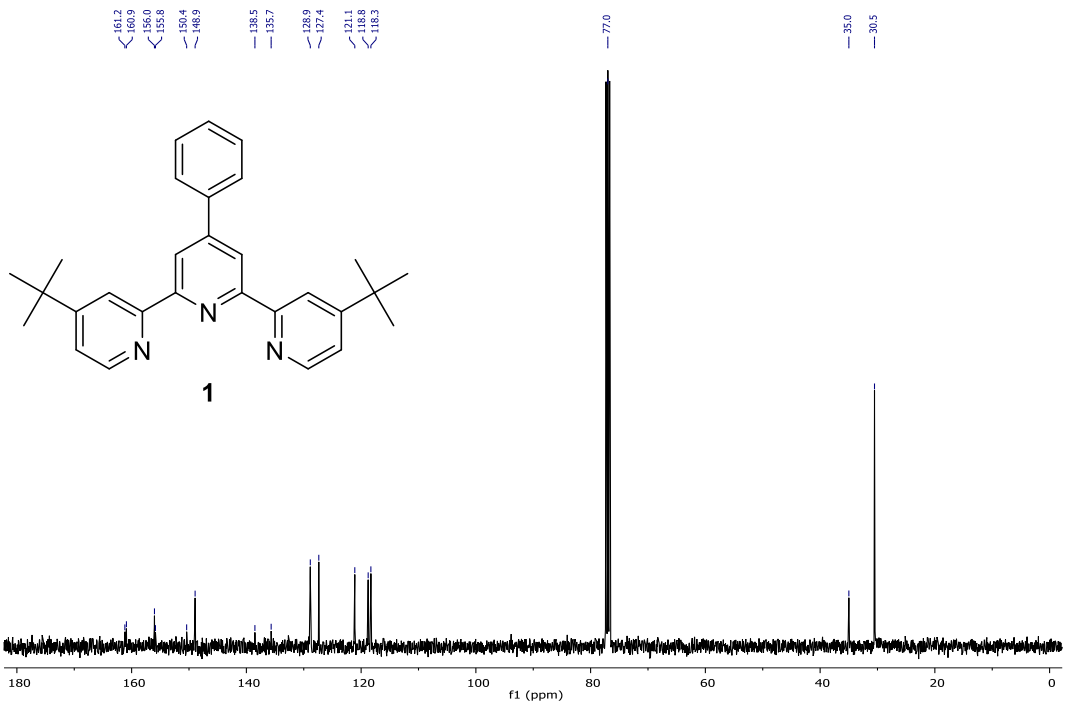

Figure 12.2 - ^{13}C NMR spectrum of **1** in $CDCl_3$.

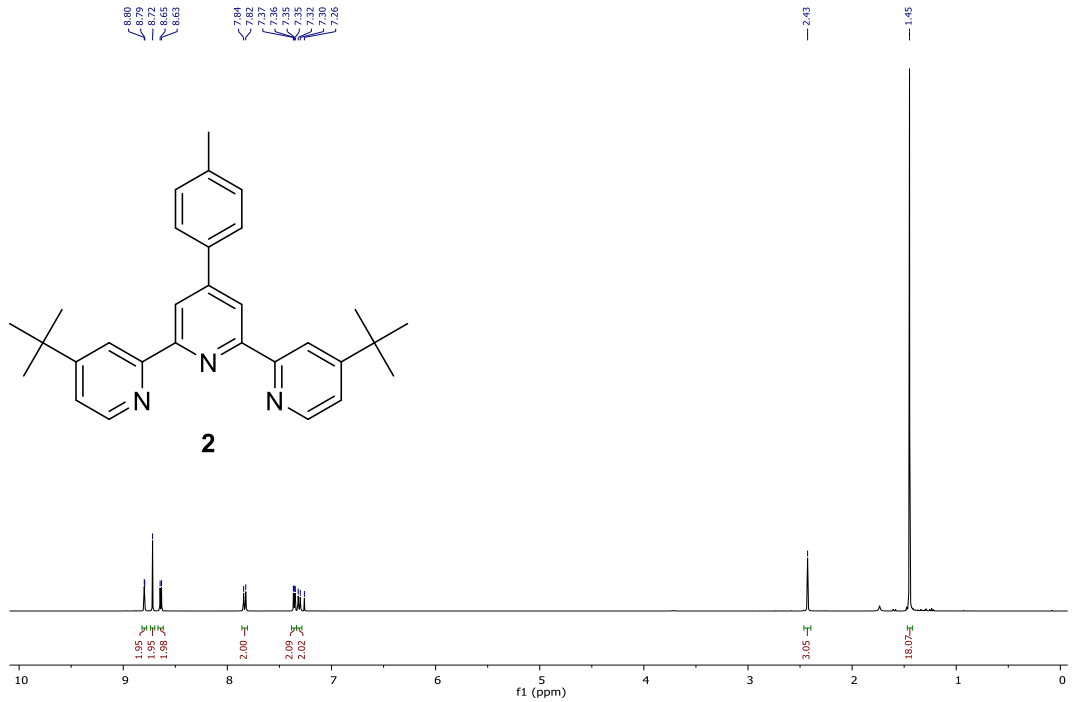

Figure 12.3 - ^{1}H NMR spectrum of **2** in $CDCl_3$.

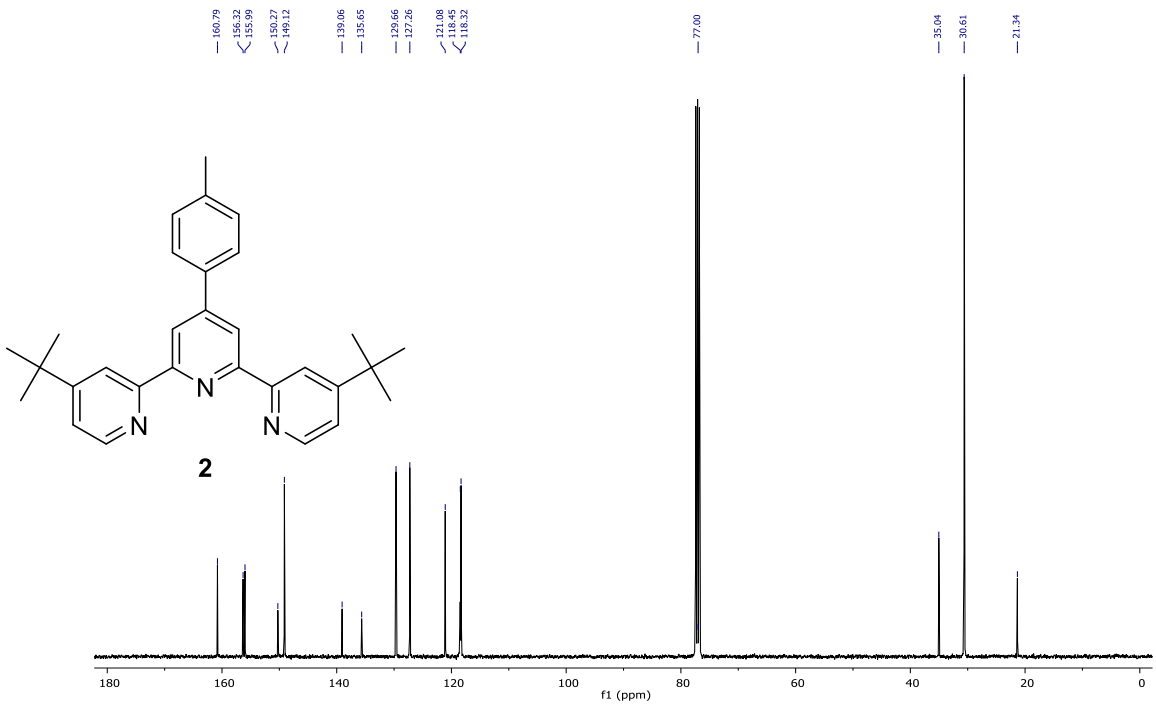

Figure 12.4 - ^{13}C NMR spectrum of **2** in $CDCl_3$.

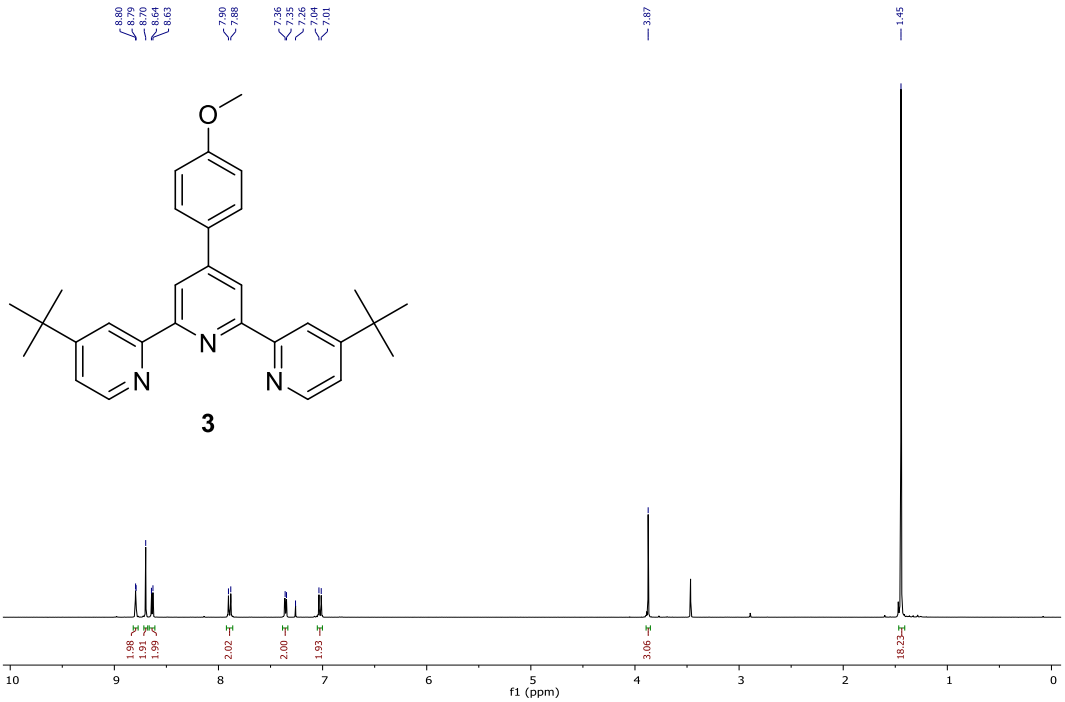

Figure 12.5 - $^{1}HNMR$ spectrum of **3** in $CDCl_3$.

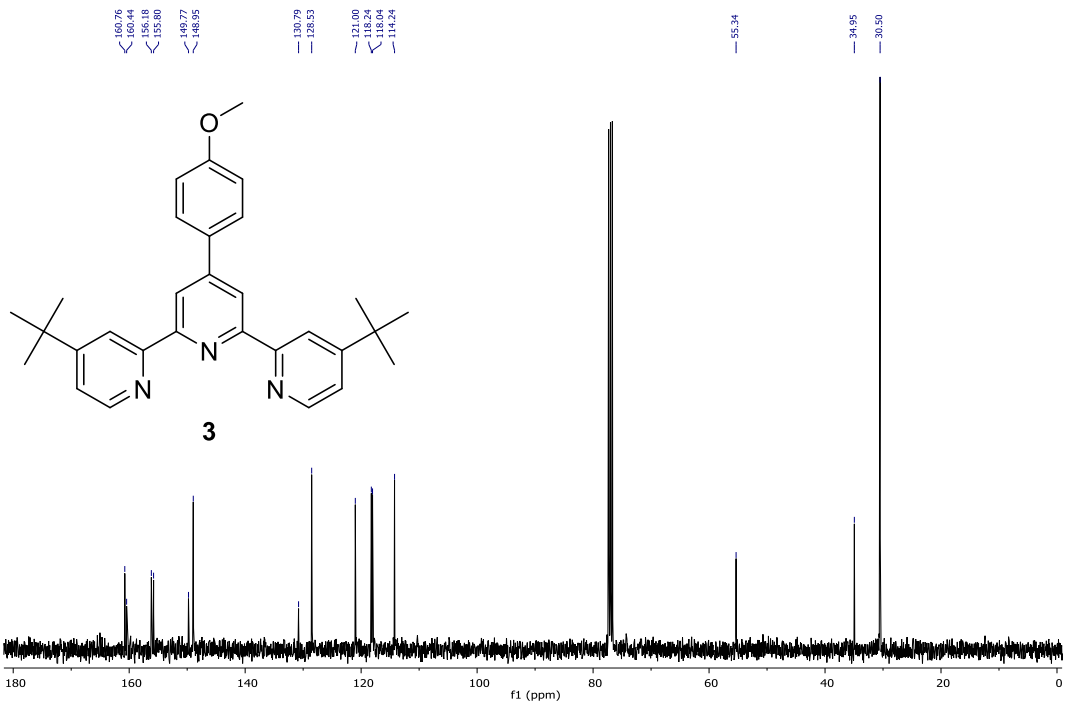

Figure 12.6 - ^{13}C NMR spectrum of **3** in $CDCl_3$.

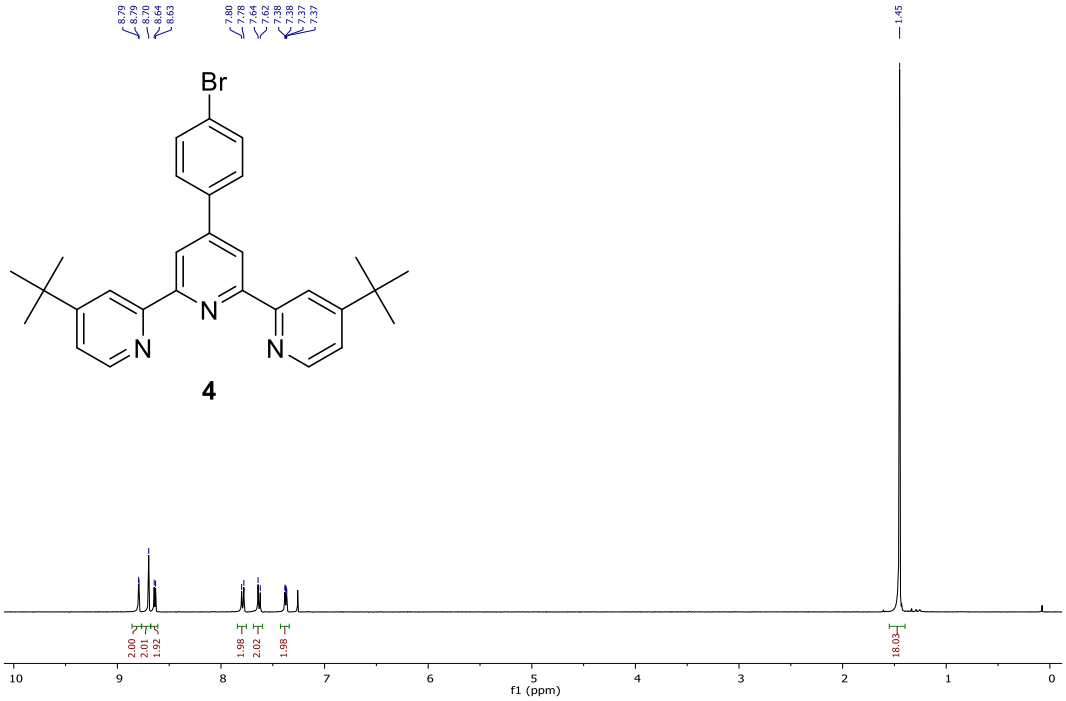

Figure 12.7 - ^{1}H NMR spectrum of **4** in $CDCl_3$.

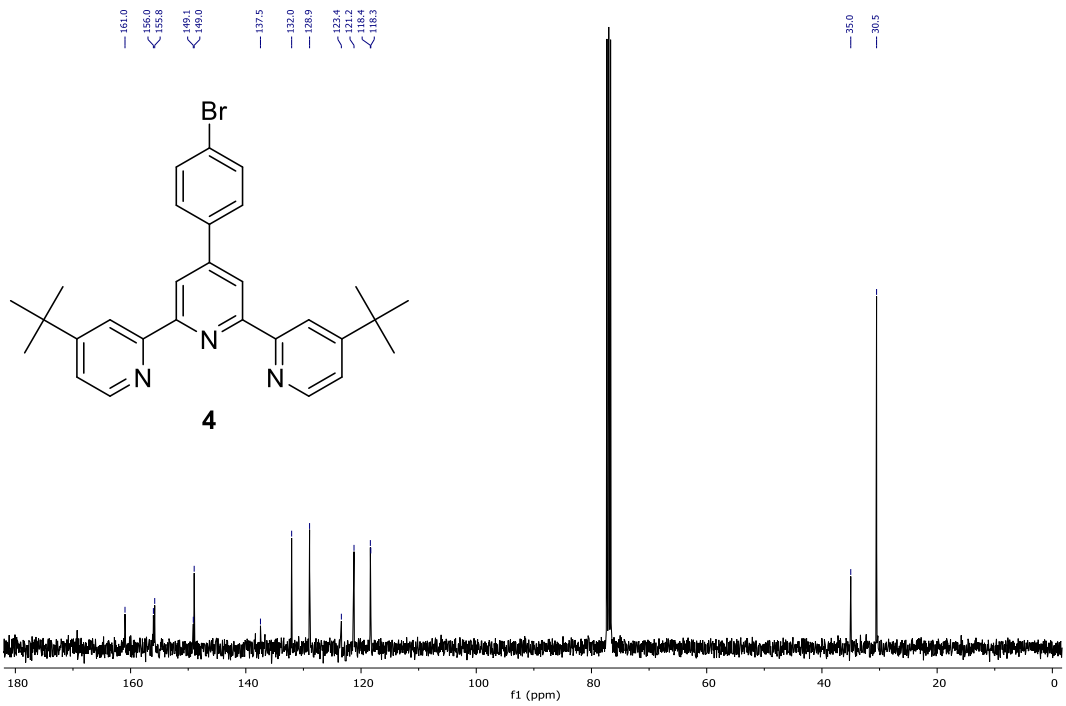

Figure 12.8 - ^{13}C NMR spectrum of **4** in $CDCl_3$.

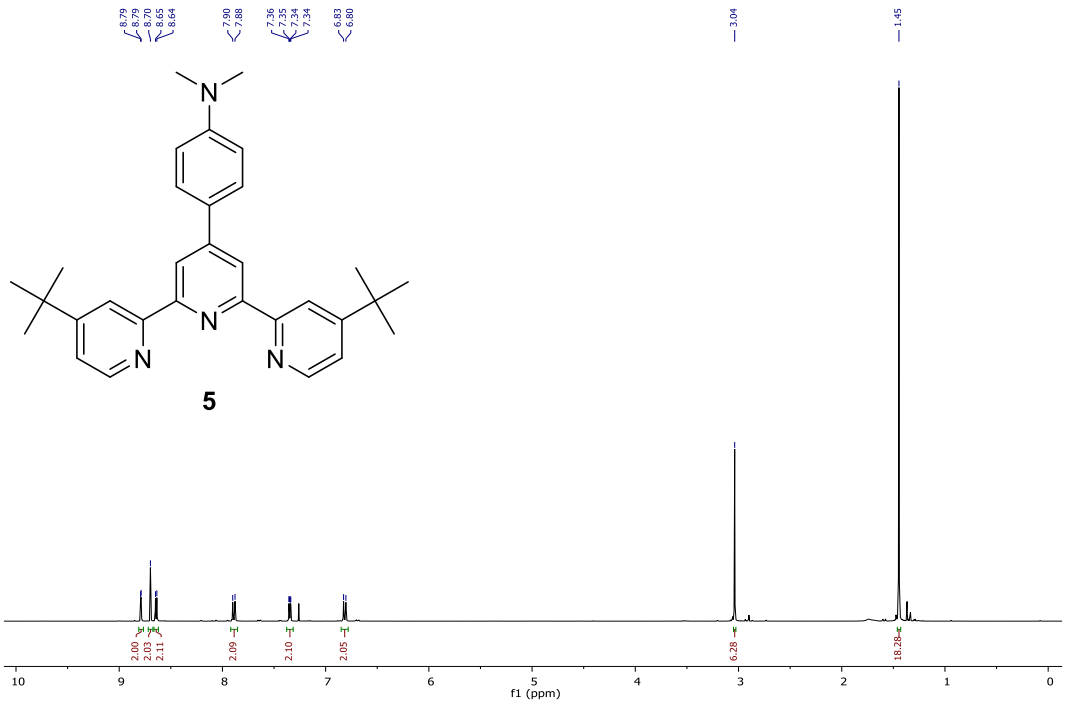

Figure 12.9 - ^{1}H NMR spectrum of **5** in $CDCl_3$.

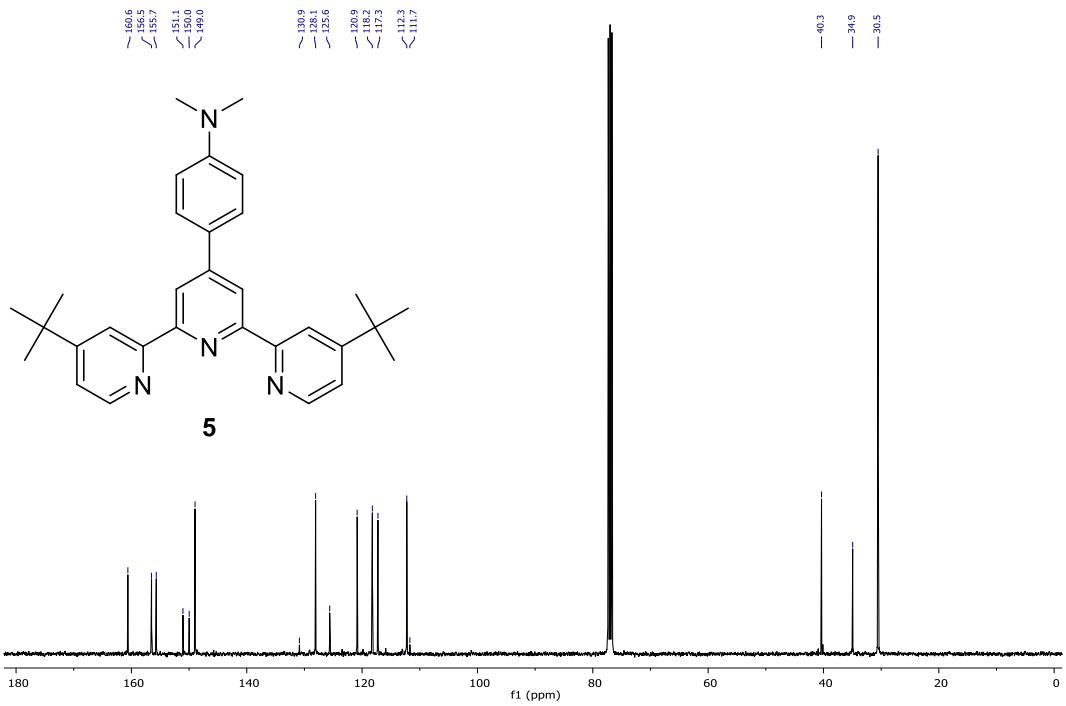

Figure 12.10 - ^{13}C NMR spectrum of **5** in $CDCl_3$.

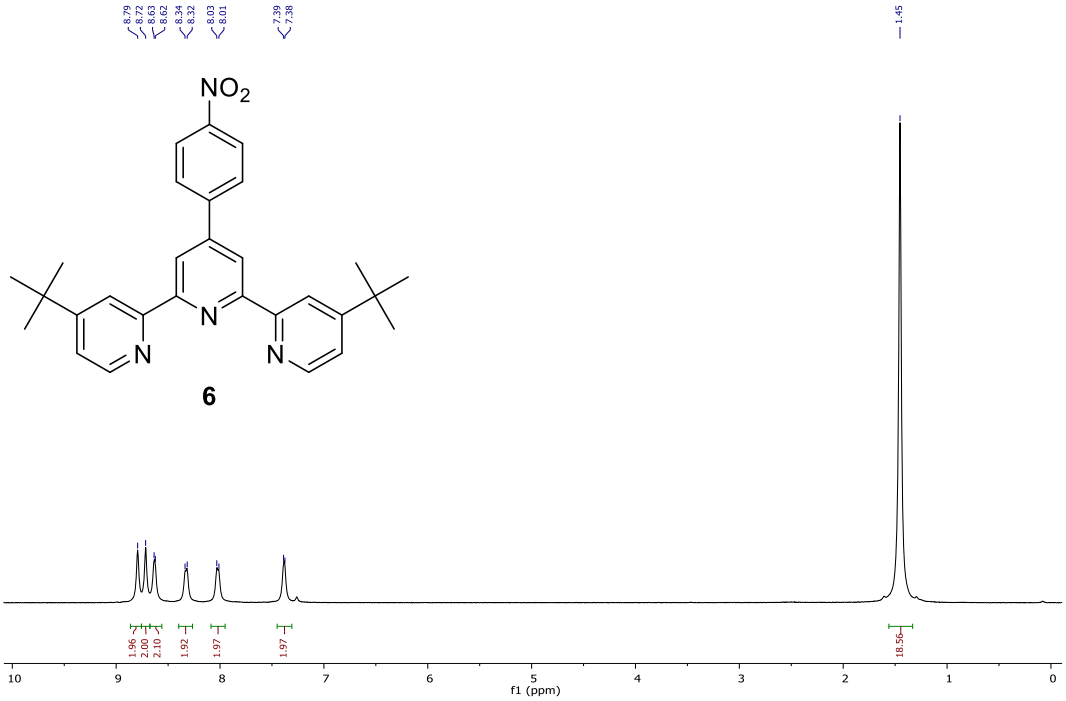

Figure 12.11 - ^{1}H NMR spectrum of **6** in $CDCl_3$.

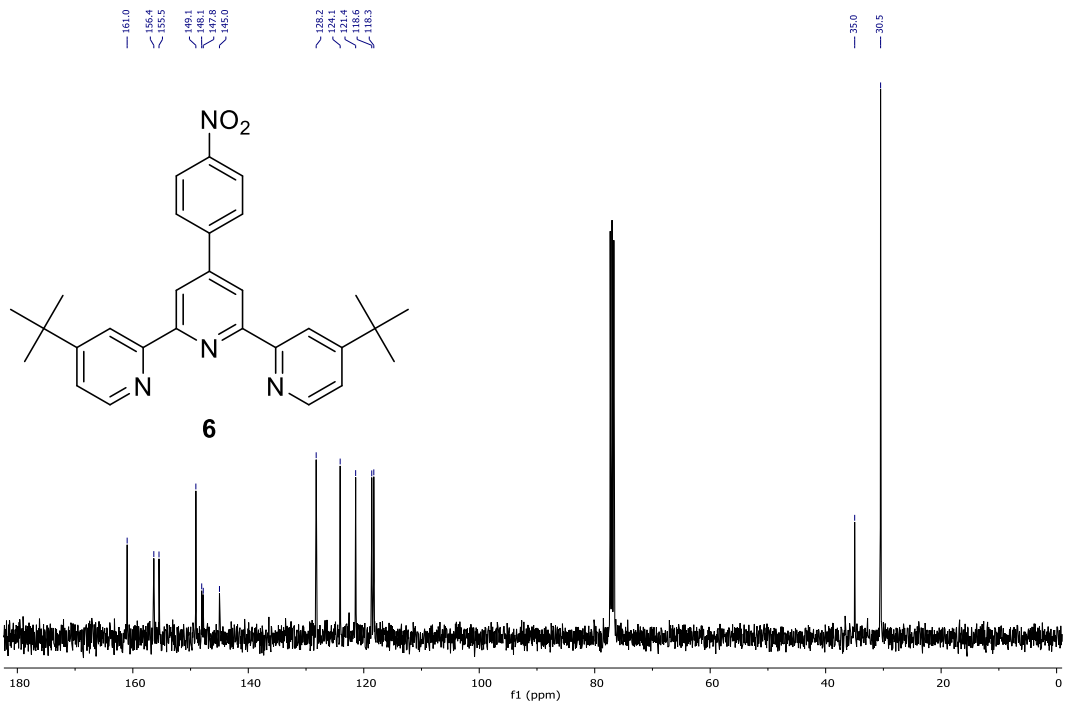

Figure 12.12 - ^{13}C NMR spectrum of **6** in $CDCl_3$.

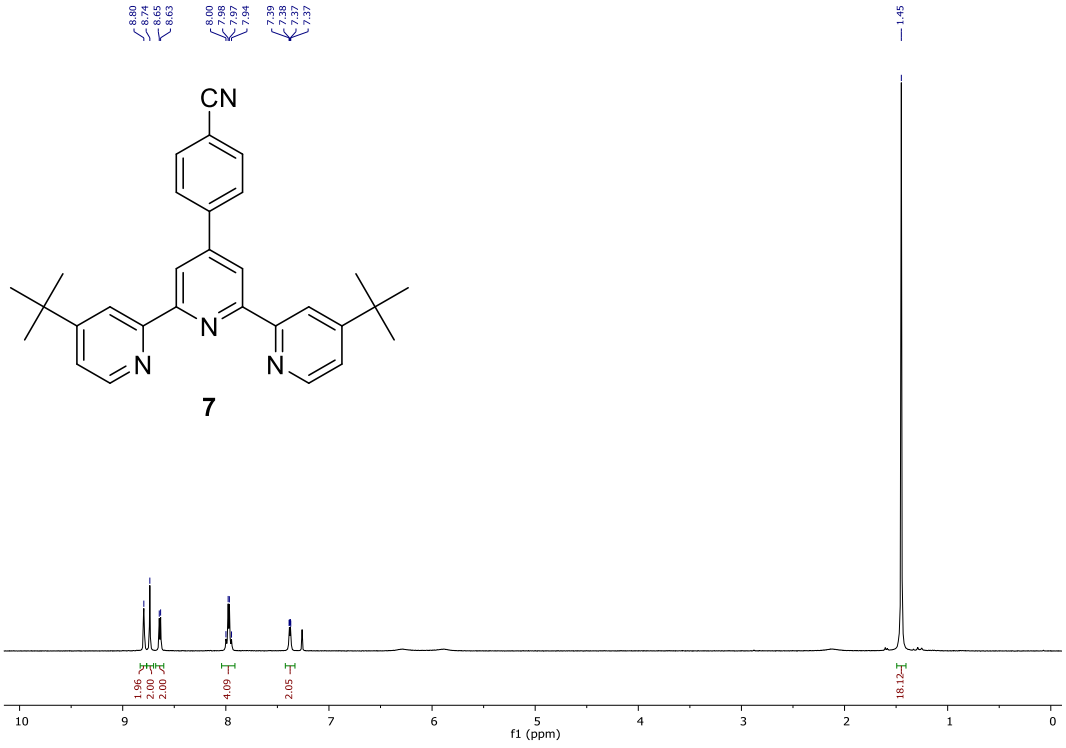

Figure 12.13 - ^{1}H NMR spectrum of **7** in $CDCl_3$.

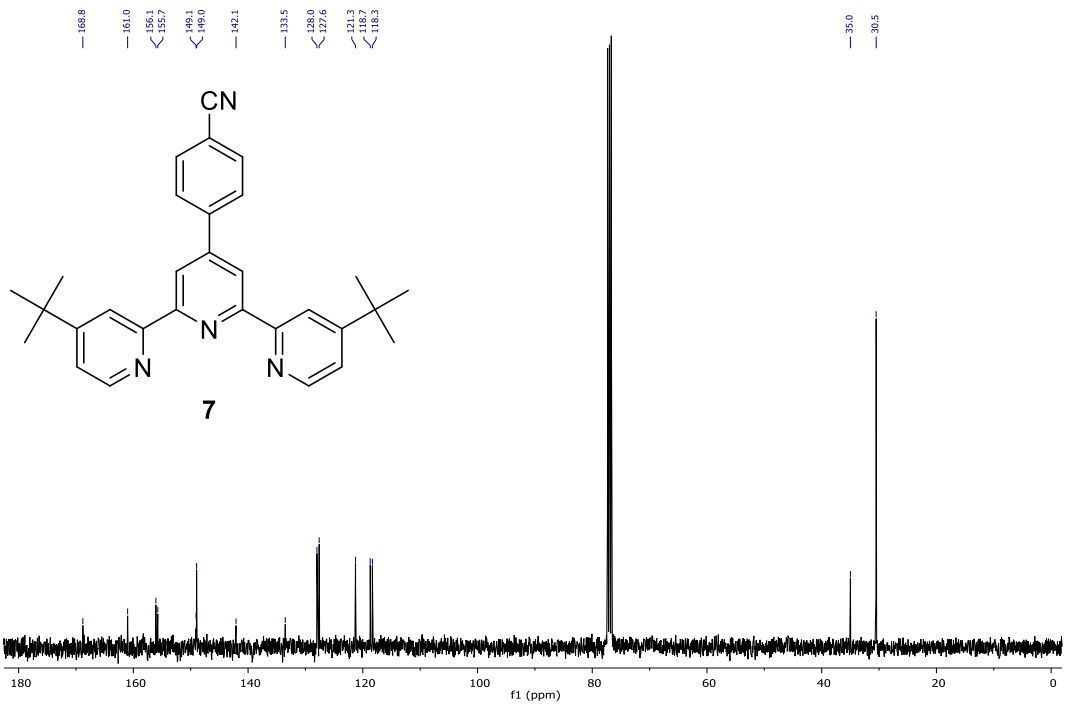

Figure 12.14 - ^{13}C NMR spectrum of **7** in $CDCl_3$.

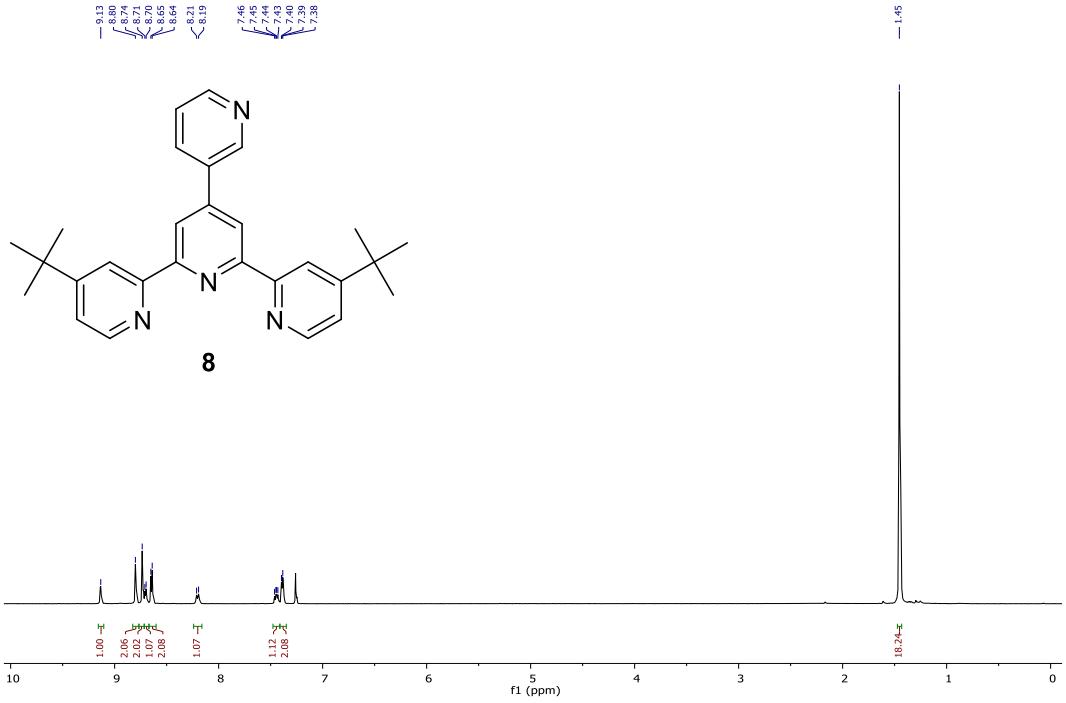

Figure 12.15 - ^{1}H NMR spectrum of **8** in $CDCl_3$.

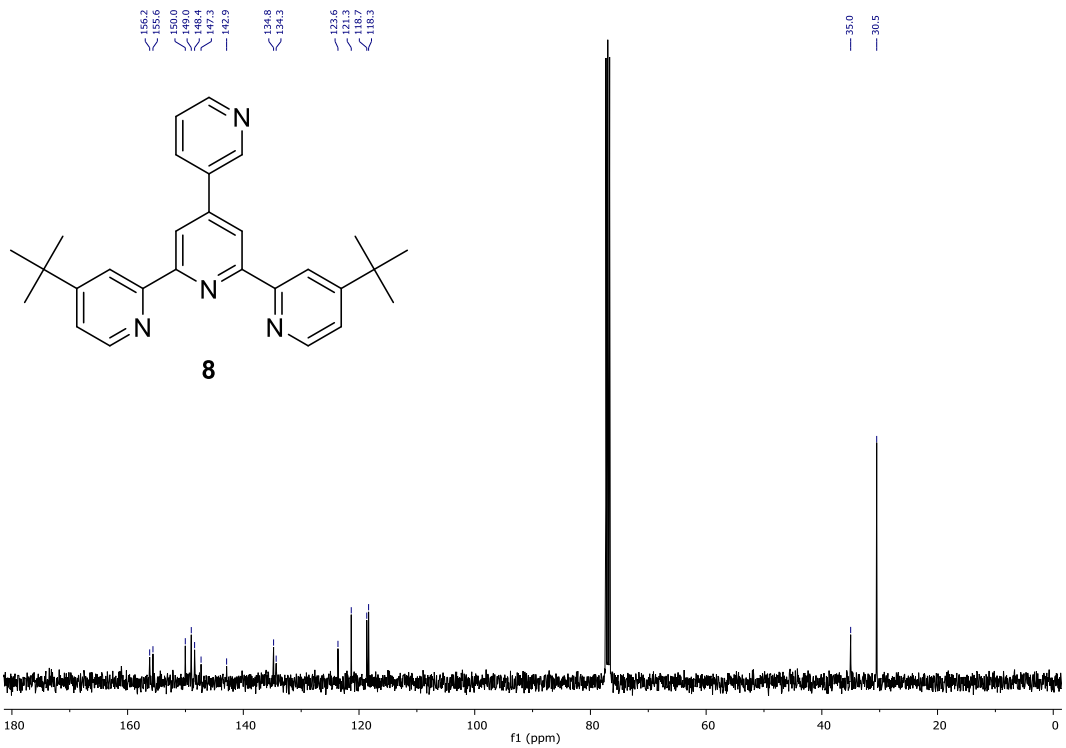

Figure 12.16 - ^{13}C NMR spectrum of **8** in $CDCl_3$.

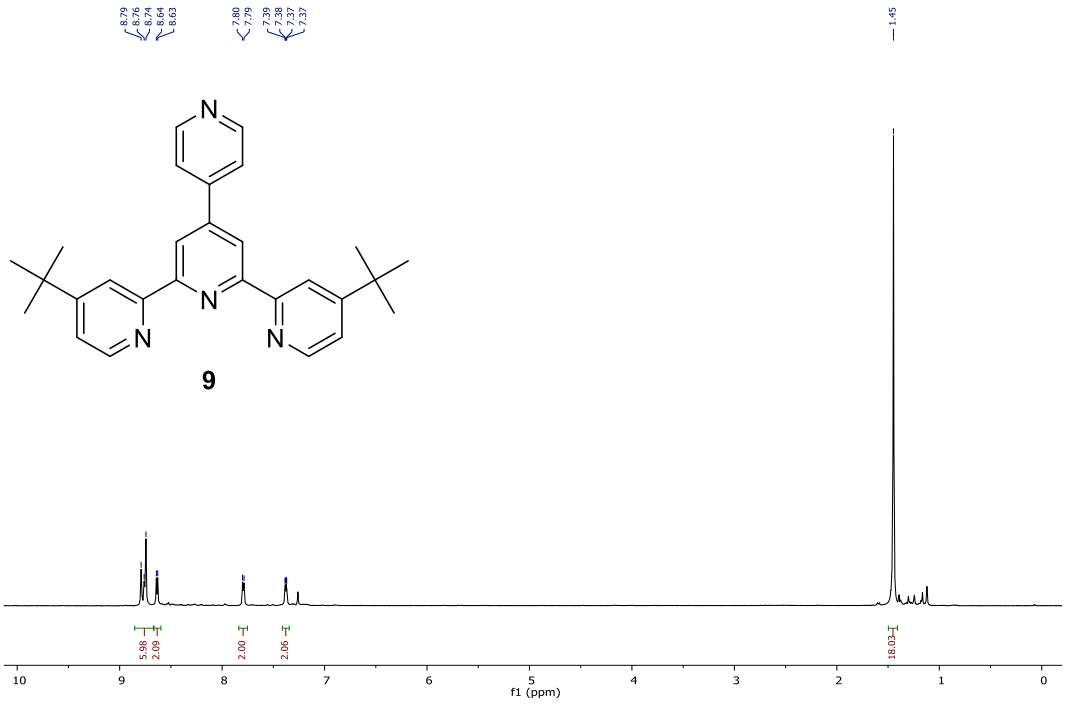

Figure 12.17 - ^{1}H NMR spectrum of **9** in $CDCl_3$.

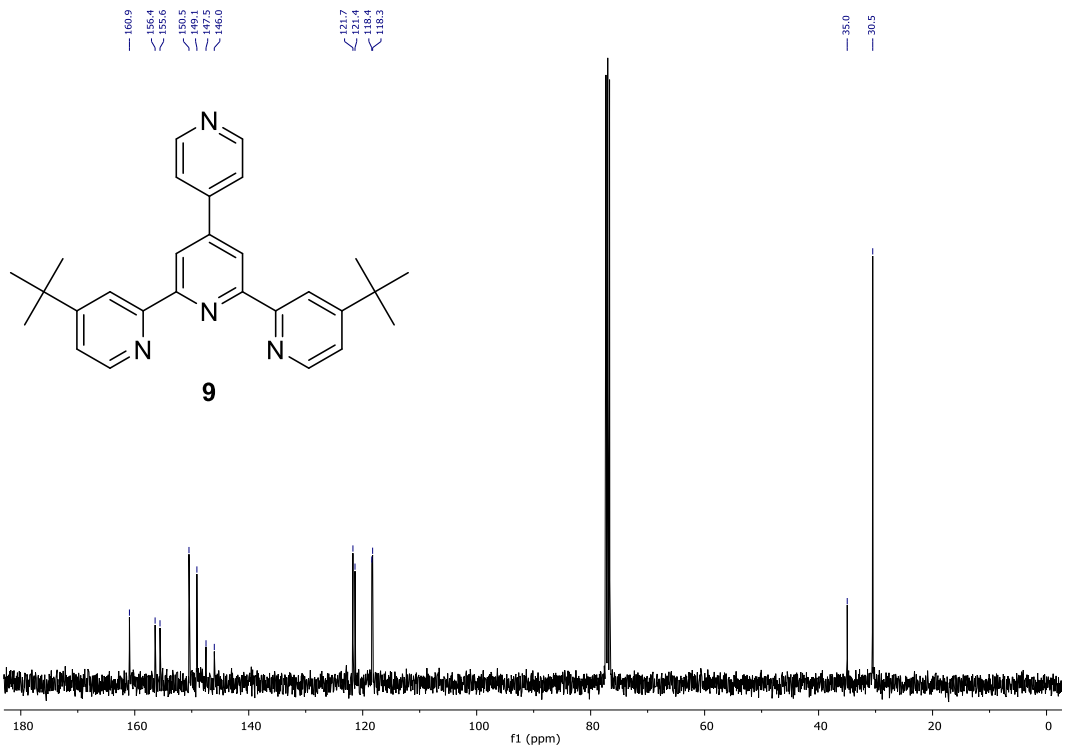

Figure 12.18 - ^{13}C NMR spectrum of **9** in $CDCl_3$.

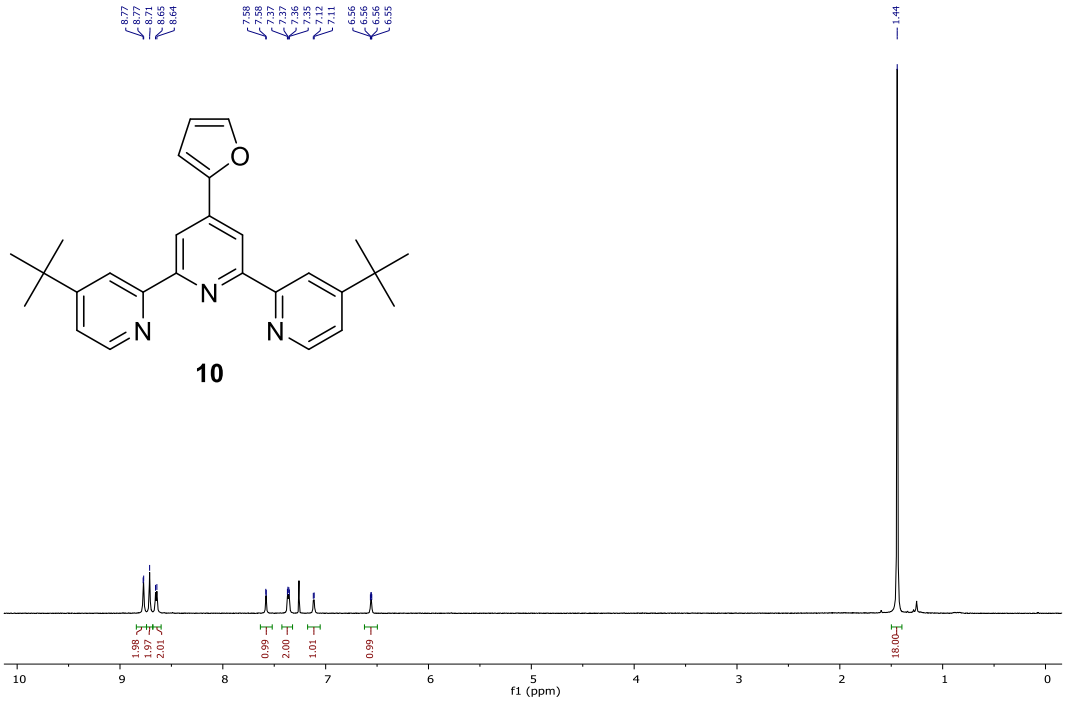

Figure 12.19 - ^{1}H NMR spectrum of **10** in $CDCl_3$.

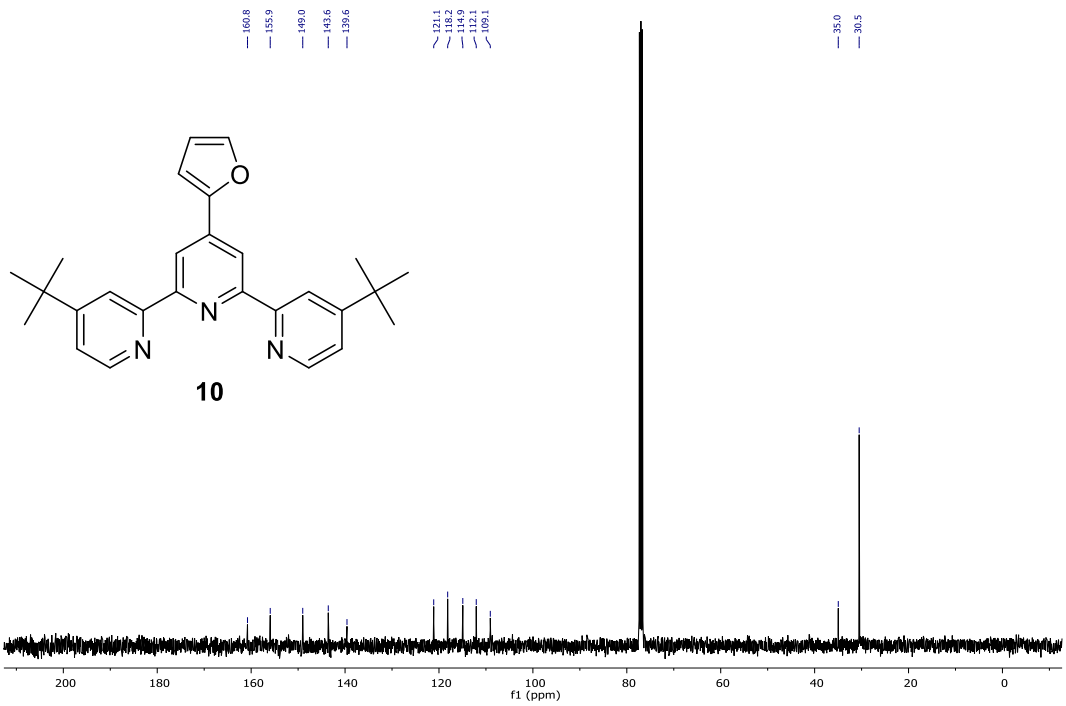

Figure 12.20 - ^{13}C NMR spectrum of **10** in $CDCl_3$.

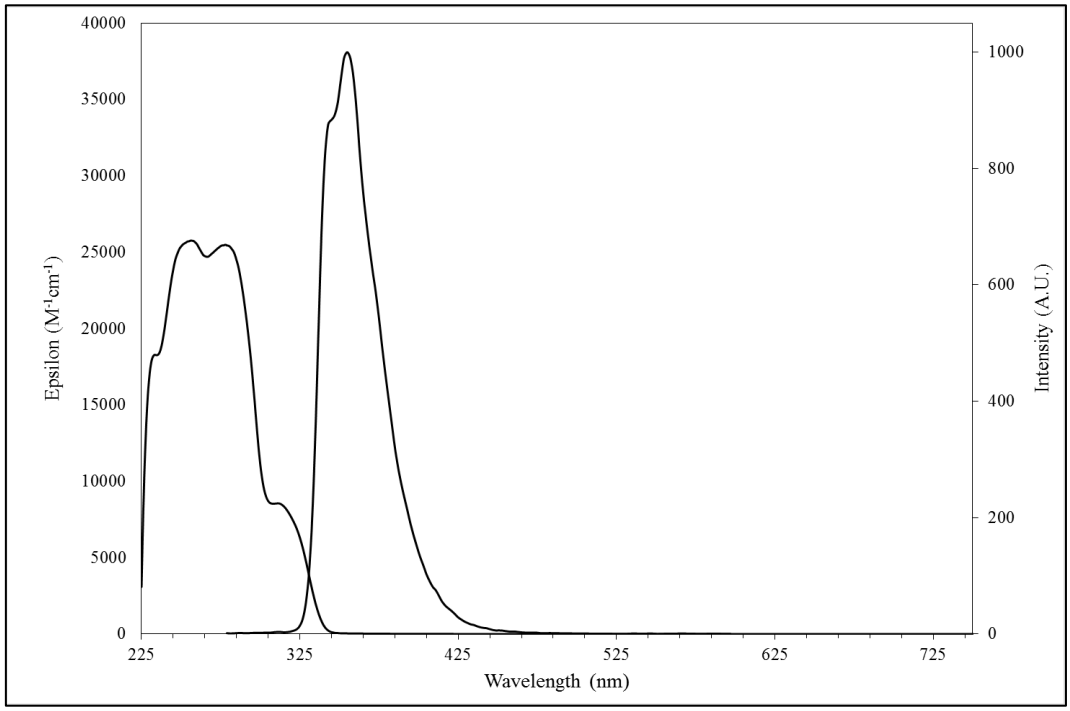

Figure 12.21 - UV-visible and fluorescence spectrum of **1** in CD_2Cl_2.

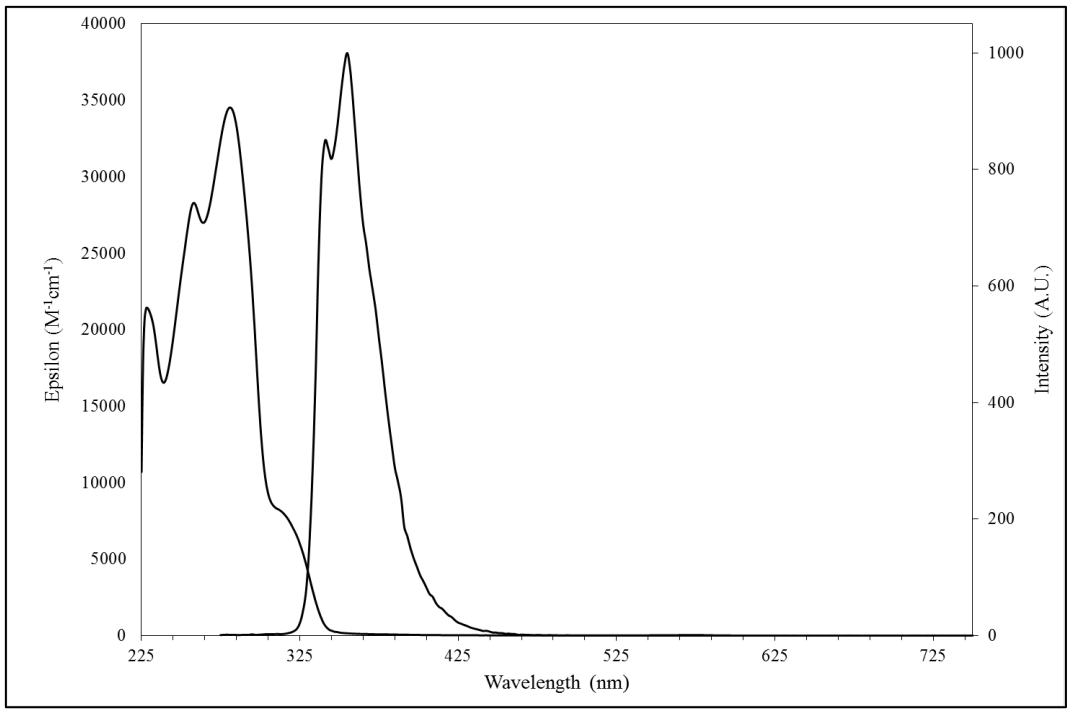

Figure 12.22 - UV-visible and fluorescence spectrum of **2** in CD_2Cl_2.

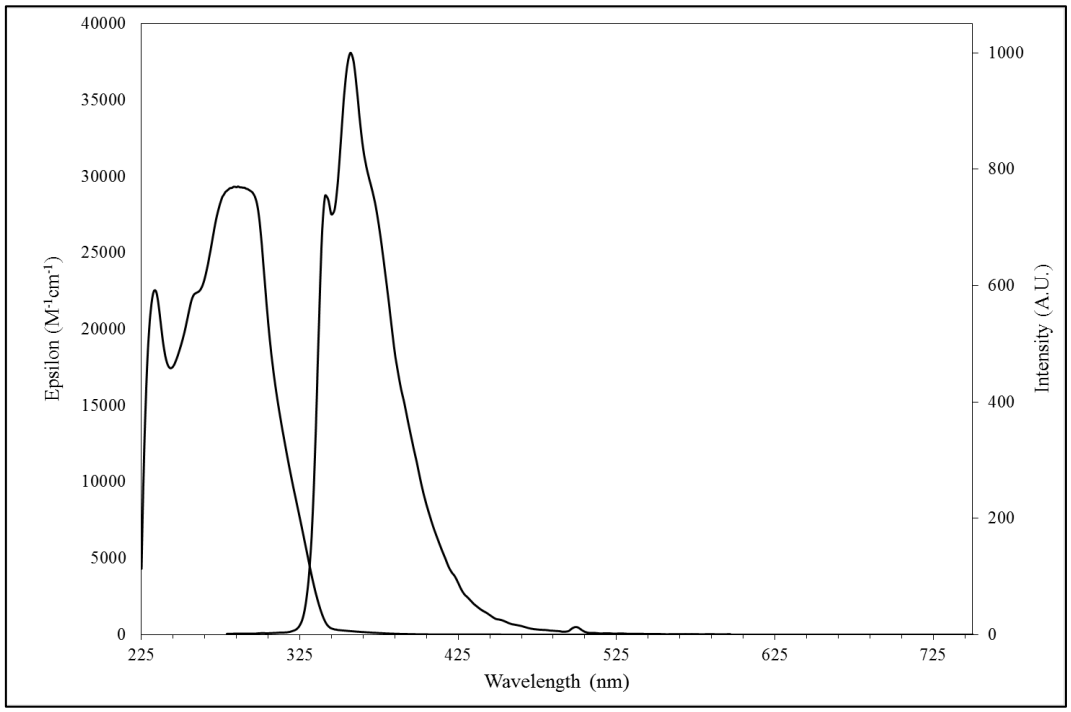

Figure 12.23 - UV-visible and fluorescence spectrum of **3** in CD_2Cl_2.

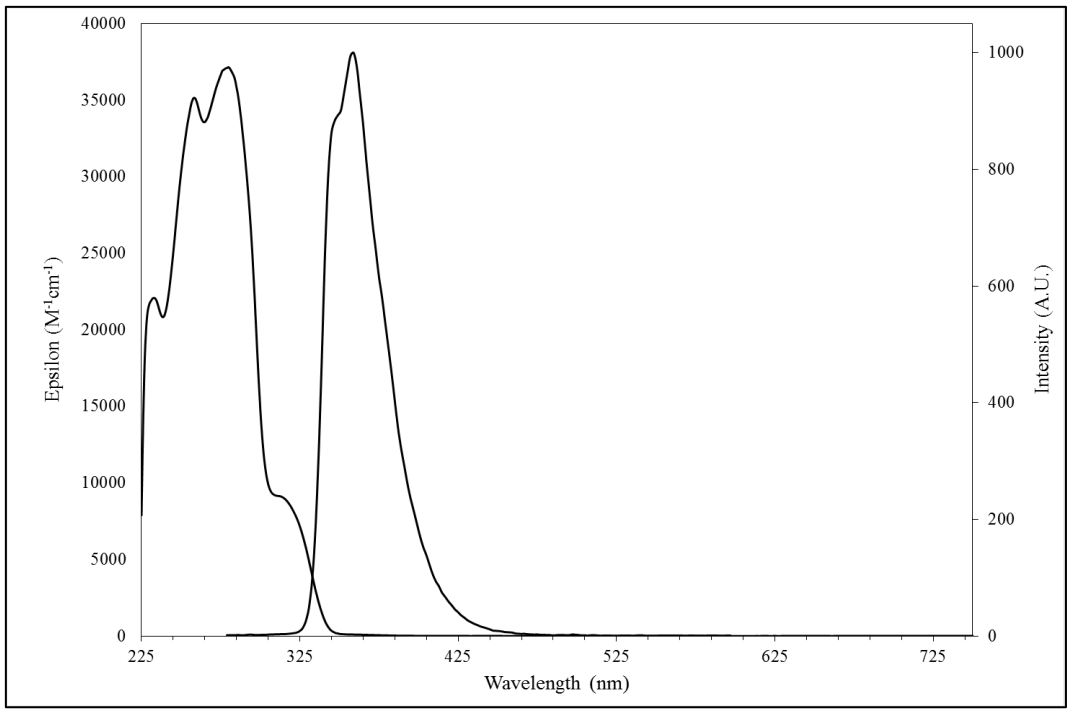

Figure 12.24 - UV-visible and fluorescence spectrum of **4** in CD_2Cl_2.

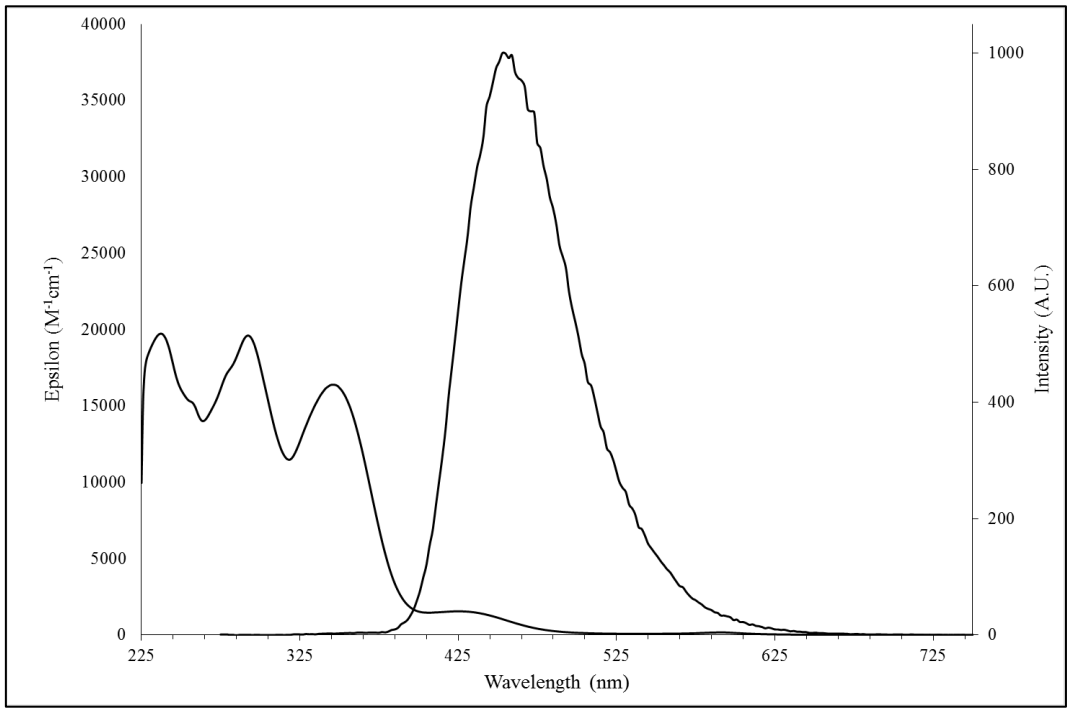

Figure 12.25 - UV-visible and fluorescence spectrum of **5** in CD_2Cl_2.

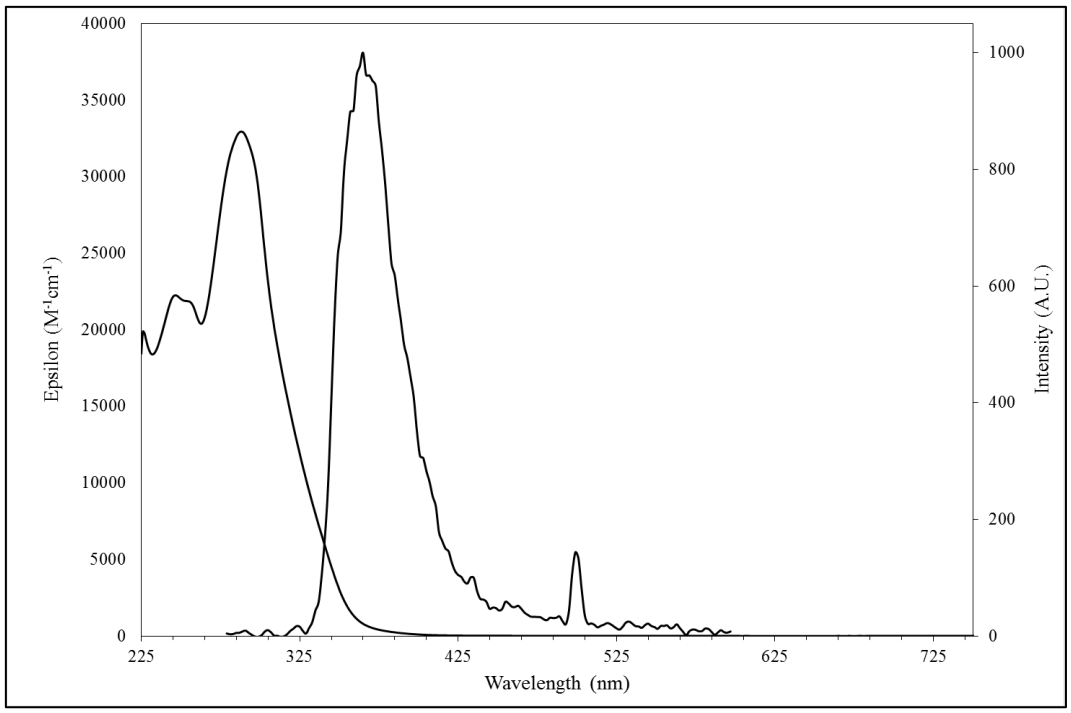

Figure 12.26 - UV-visible and fluorescence spectrum of **6** in CD_2Cl_2.

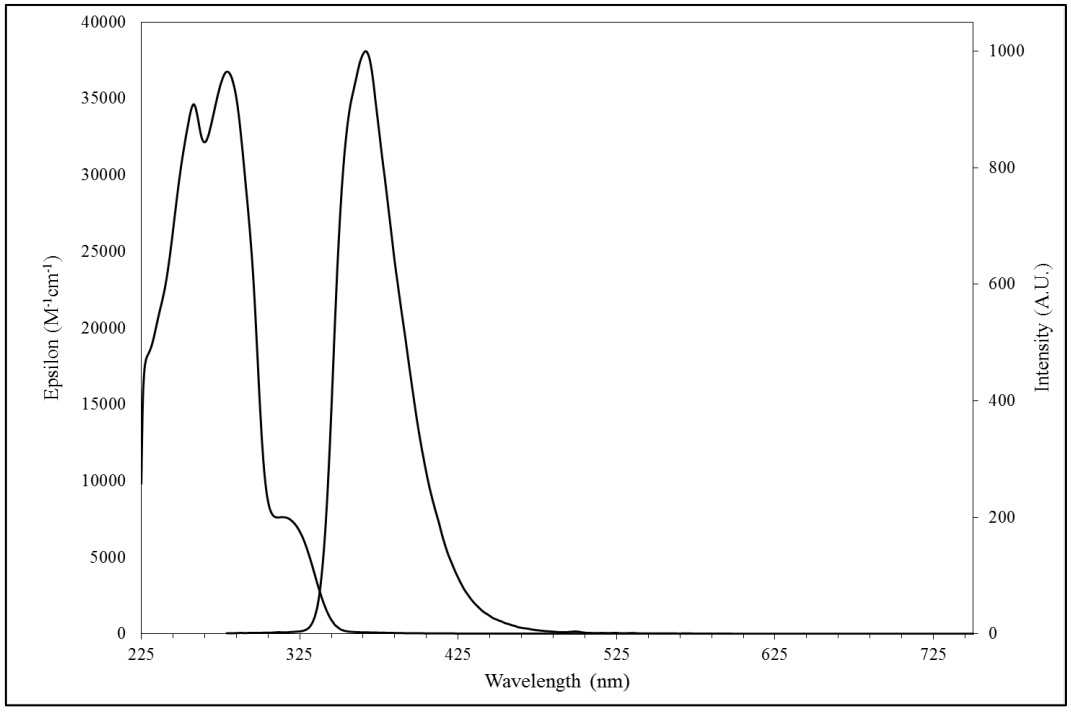

Figure 12.27 - UV-visible and fluorescence spectrum of **7** in CD_2Cl_2.

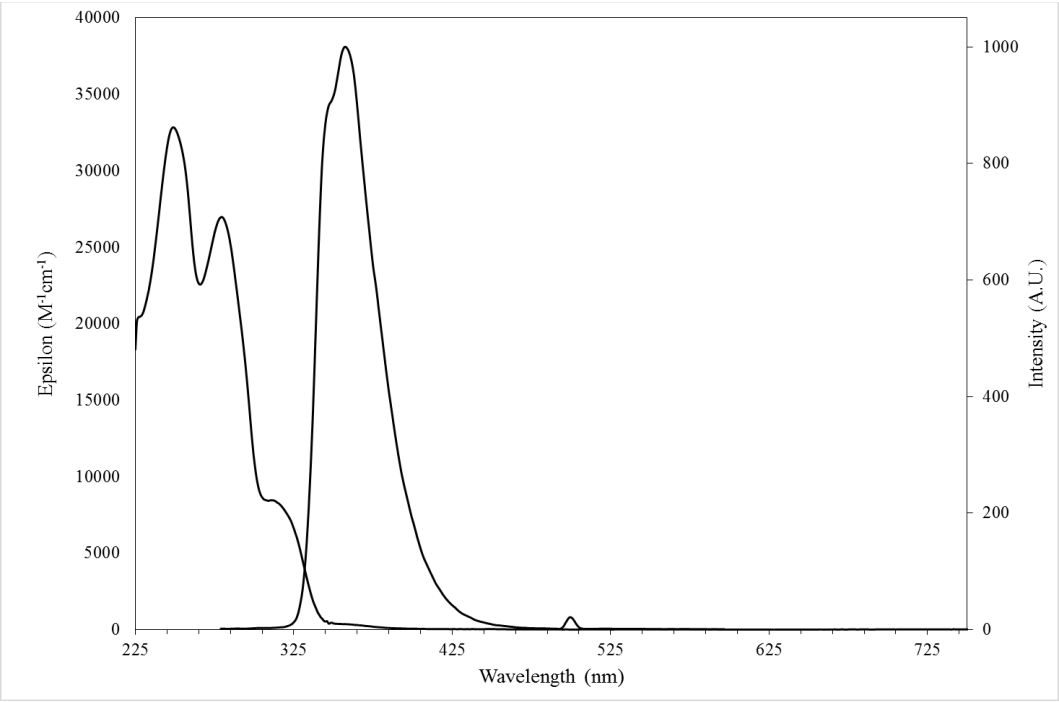

Figure 12.28 - UV-visible and fluorescence spectrum of **8** in CD_2Cl_2.

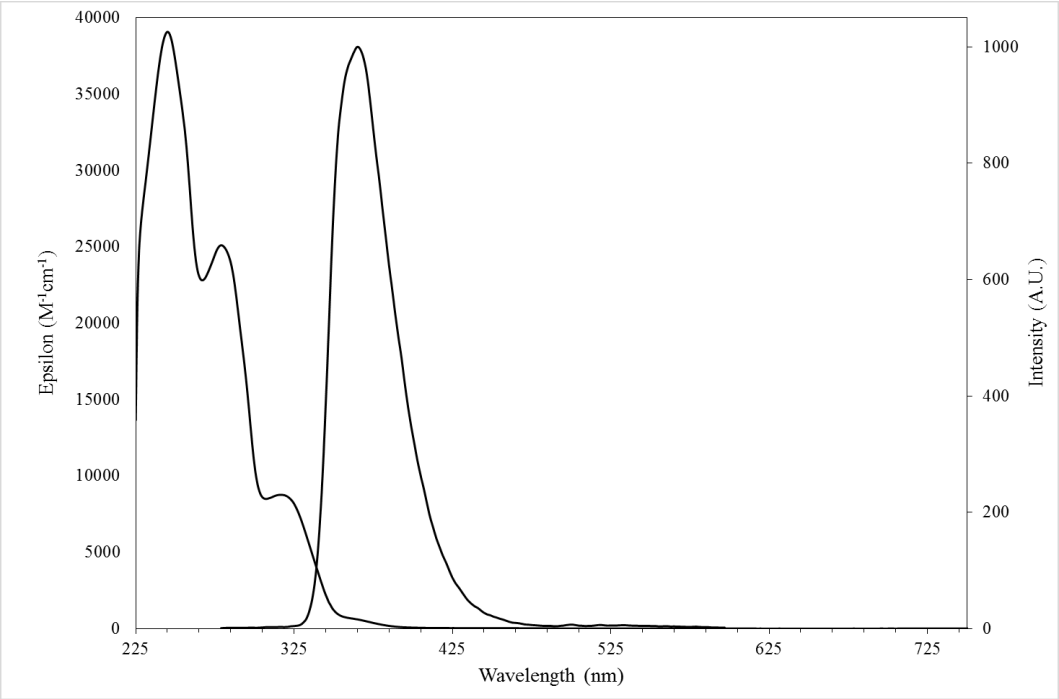

Figure 12.29 - UV-visible and fluorescence spectrum of **9** in CD_2Cl_2.

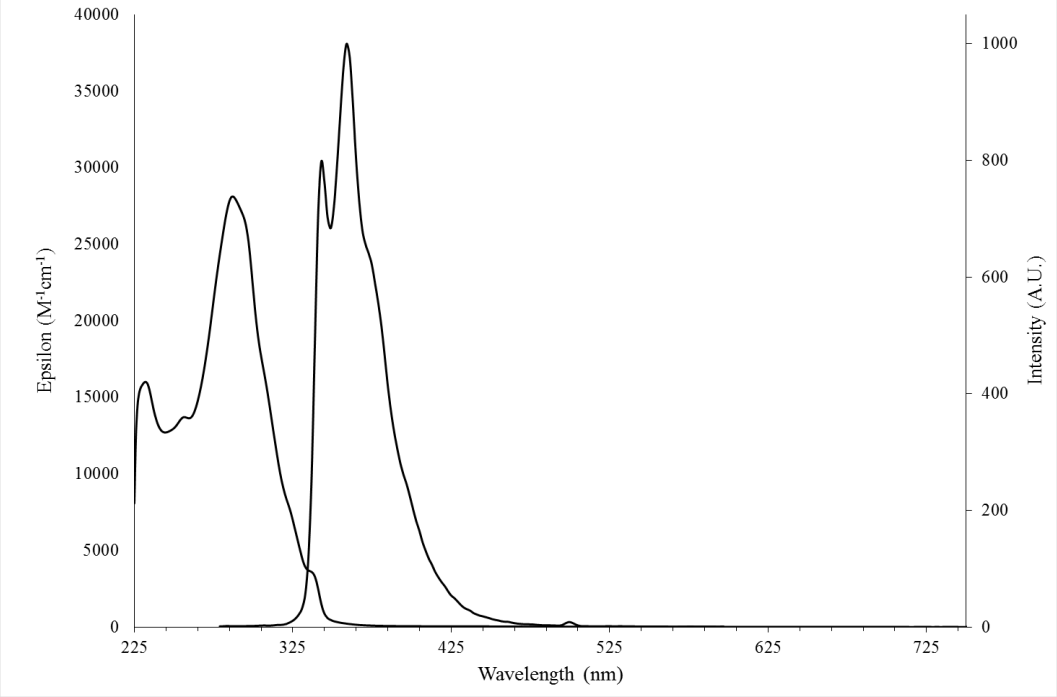

Figure 12.30 - UV-visible and fluorescence spectrum of **10** in CD_2Cl_2.

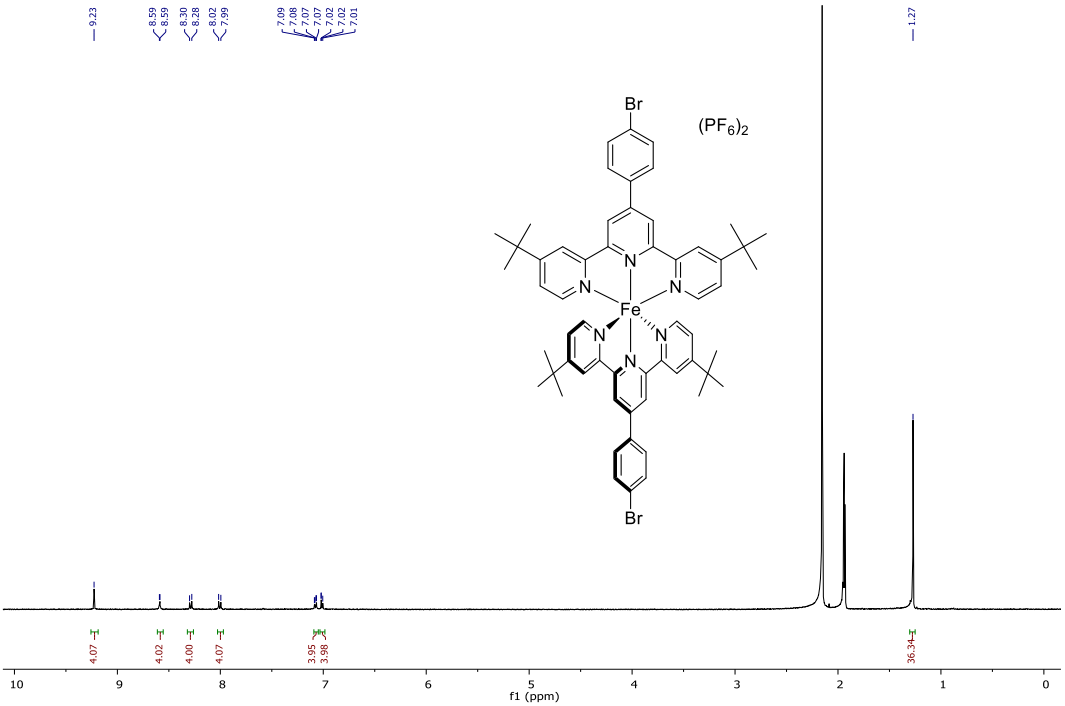

Figure 12.31 - ^1H NMR spectrum of **11** in CD_3CN.

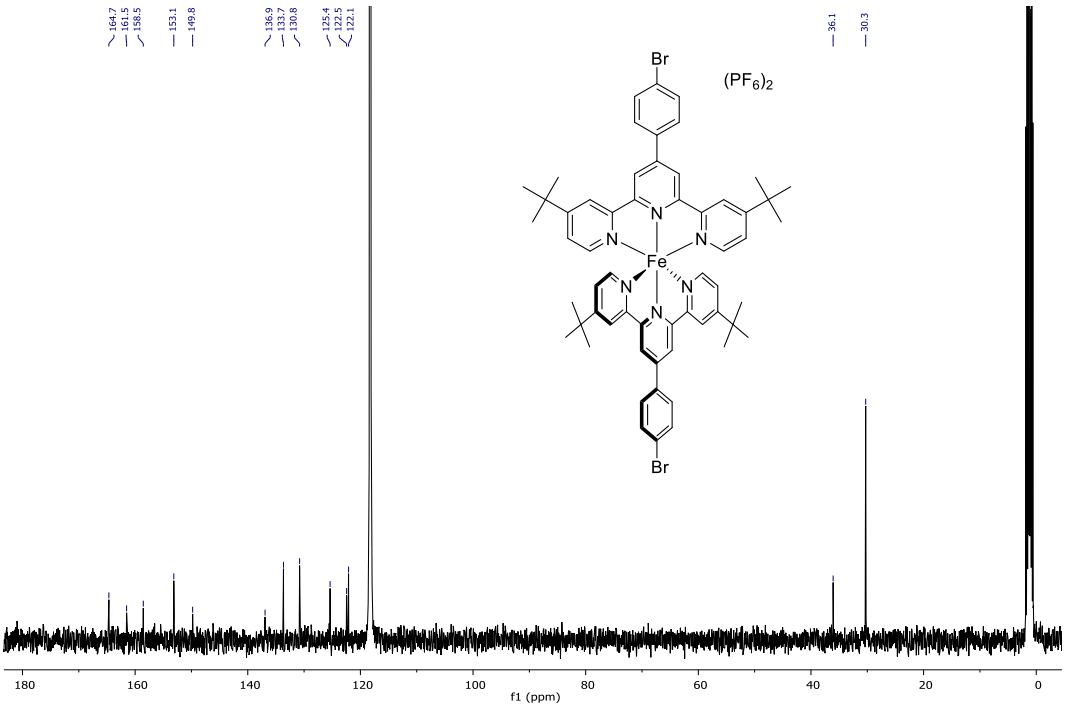

Figure 12.32 - ^{13}C NMR spectrum of **11** in CD_3CN.

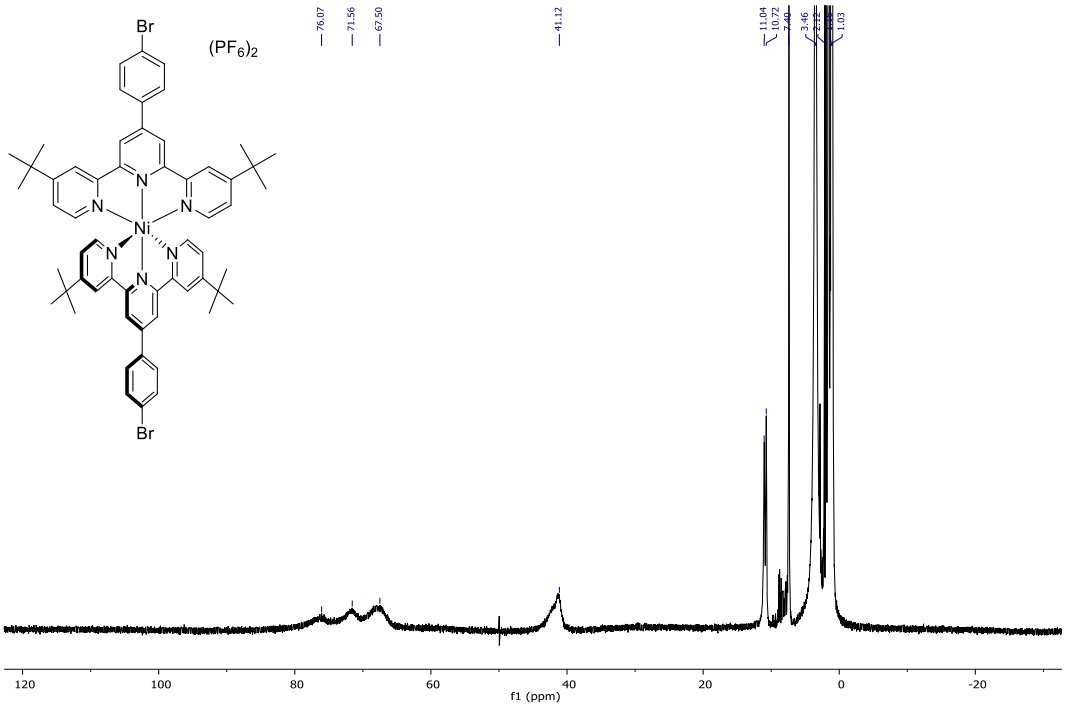

Figure 12.33 - ^{1}H NMR spectrum of **12** in CD_3CN.

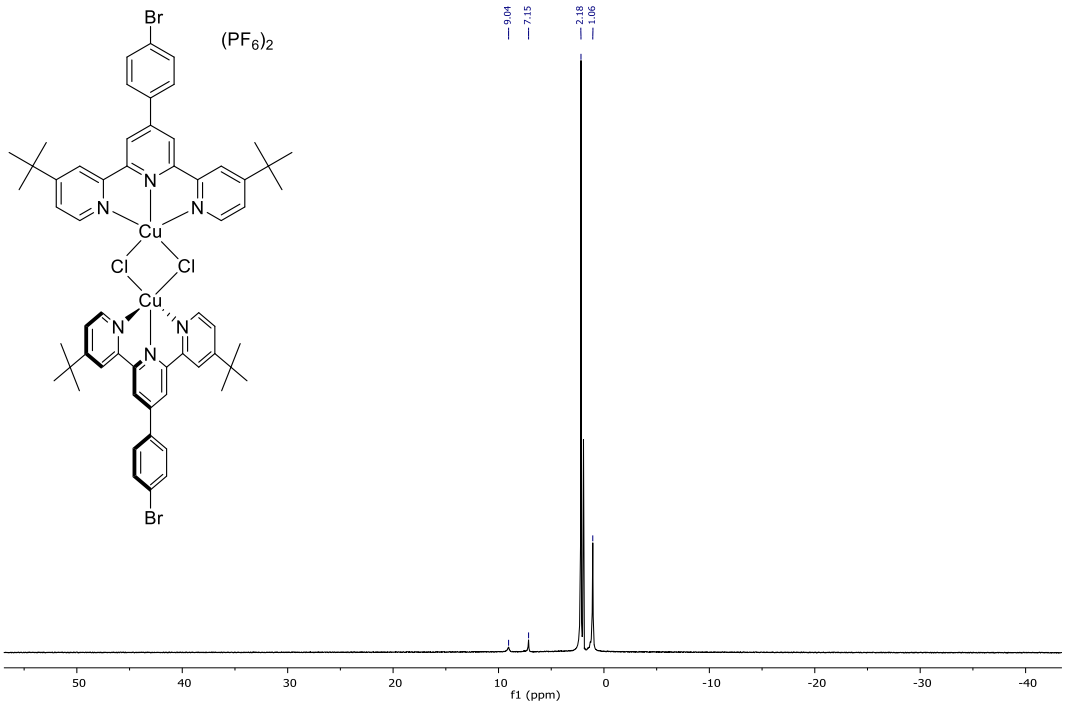

Figure 12.34 - ^{1}H NMR spectrum of **13** in CD_3CN.

Table 12.1 - Solubility of the ligands in common organic solvents.

Solvent	Compound									
	1	**2**	**3**	**4**	**5**	**6**	**7**	**8**	**9**	**10**
Acetone	S	S	S	S	S	SpS	S	S	FS	S
Acetonitrile	SpS	SpS	SpS	SpS	SpS	S	SpS	SpS	FS	SpS
Chloroform	VS	VS	VS	VS	VS	VS	VS	VS	VS	VS
Diethyl ether	S	S	S	S	SpS	S	SS	SS	S	S
Dimethylformamide	FS	FS	VS	VS	FS	VS	VS	VS	VS	VS
Dimethyl sulfoxide	FS	FS	VS	VS	FS	VS	VS	FS	VS	FS
Ethanol	FS	S	FS	S	S	FS	FS	S	FS	FS
Ethyl acetate	S	FS	S	S	FS	FS	SpS	FS	FS	VS
Hexanes	VSS	VSS	VSS	VSS	VSS	VSS	I	VSS	VSS	VSS
Methanol	S	SpS	S	S	S	SS	S	SpS	FS	S
Methylene chloride	VS	VS	VS	VS	VS	VS	VS	VS	VS	VS
Tetrahydrofuran	VS	VS	VS	VS	FS	VS	FS	FS	FS	FS
Toluene	FS	FS	FS	FS	FS	FS	FS	FS	FS	FS
Water	I	I	I	I	I	I	I	I	I	I

Legend:

VS: Very soluble

FS: Freely soluble

S: Soluble

SpS: Sparingly soluble

SS: Slightly soluble

VSS: Very slightly soluble

I: Practically insoluble or Insoluble

Chapitre 13 - Informations supplémentaires: Synthesis of a discrete Re(I) di- and tricarbonyl assemblies using a [4 x 1] directional bonding strategy

13.1. Materials, methods and instrumentation

Nuclear magnetic resonance (NMR) spectra were recorded in acetone-d6 and DMSO-d_6 at room temperature (r.t.) on a Bruker AV400 (400 MHz) spectrometer for ^{1}H NMR, at 100 MHz for ^{13}C NMR and 600 MHz for DOSY experiment, respectively. Chemical shifts are reported in part per million (ppm) relative to residual solvent protons (2.05 ppm for acetone-d_6 and 2.50 ppm for DMSO-d_6) and the carbon resonance (30.83 ppm for acetone-d_6 and 39.43 ppm for DMSO-d_6) of the solvent.

All the photophysical measurements were carried out in deaerated acetonitrile at r.t. in septa sealed quartz cells. Absorption spectra were measured on a Cary 500i UV-Vis-NIR Spectrophotometer. For luminescence spectra a Cary Eclipse Fluorescence spectrofluorimeter was used. Accurate mass measurements were performed on a micrOTOF-Q II mass spectrometer from Bruker Daltonics, in positive electrospray mode. Appropriate $[M\text{-}PF_6]^{n+}$ species were used for empirical formula determination, and exact masses were calculated using the Compass DataAnalysis V4.0 SP5 software package from Bruker Daltonics. Electrochemical measurements were carried out in argon-purged purified dimethylformamide at room temperature with a BAS CV50W multipurpose potentiostat. The working electrode was a glassy carbon electrode. The counter electrode was a Pt wire, and the pseudo-reference electrode was a silver wire. The reference was set using an internal 1 mM ferrocene/ferrocinium sample at 0.450 mV vs. SCE in acetonitrile. The concentration of the compounds was about 1 mM. Tetrabutylammonium hexafluorophosphate (TBAP) was used as supporting electrolyte and its concentration was 0.10 M. Cyclic voltammograms of were obtained at scan rates of 20, 50, 100, 200 and 500 mVs-1, respectively. The criteria for reversibility were the

separation between cathodic and anodic peaks, the close to unity ratio of the intensities of the cathodic and anodic currents, and the constancy of the peak potential on changing scan rate. Differential pulse voltammetry was conducted with a sweep rate of 20 mVs-1 and a pulse amplitude, width and period of 50 mV, 50 ms and 200 ms, respectively.

Experimental uncertainties are as follows: absorption maxima, ±2 nm; molar absorption coefficient, 10%; redox potentials, ± 10 mV, emission maxima, ±2 nm; Diffusion-ordered spectroscopy, ±10 %.

13.2. Experimental

13.2.1. Re(4-pytpy-κ²*N*)(CO)₃Br (1)

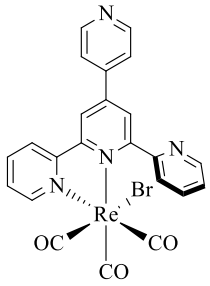

A 250 mL round-bottomed flask was charged with $Re(CO)_5Br$ (1.19 g, 2.93 mmol) and 4-pytpy ligand (1.0 g, 3.22 mmol) and to it 100 mL of toluene was added. The mixture was heated at reflux for 5 hours, after which time the solution was cooled to room temperature. The yellow suspension was filtered and washed with three portions of ether (50 mL) and dried under vacuum. No further purification procedures were needed. Yield = 1.8 g (94%), yellow solid.

^{1}H-NMR: (400 MHz, DMSO-d_6): δ = 9.21 (s, 1H), 9.14-9.09 (m, 2H), 8.85-8.83 (d, *J* = 5.8 Hz, 2H), 8.82-8.80 (d, *J* = 4.4 Hz, 1H), 8.43-8.33 (m, 2H), 8.22-8.20 (d, *J* = 5.9 Hz, 2H), 8.10-8.06 (t, *J* = 7.5 Hz, 1H), 7.92-7.90 (d, *J* = 7.7 Hz, 1H), 7.81-7.78 (t, *J* = 6.4 Hz, 1H), 7.66-7.63 (dd, 1H).

^{13}C-NMR (DMSO-d_6, 100 MHz) : δ 161.8, 157.6, 157.5, 156.0, 152.8, 150.6, 149.2, 148.0, 141.9, 139.9, 137.0, 127.6, 125.6, 125.0, 124.8, 121.8, 121.0.

ESI-MS: Calcd. for $[M+H]^+$: 660.98625, Found: 660.98716, Diff.: 1.39 ppm.

Elemental Analysis: Calcd. for $C_{23}H_{14}N_4ReO_3Br$: C, 41.82; H, 2.14; N, 8.48. Found : C, 41.80; H, 2.11; N, 8.37.

13.2.2. Re(4-pytpy-κ³*N*)(CO)₂Br (2)

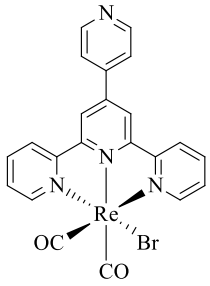

A 20 mL Biotage® microwave vial was loaded with finely grinded powder of precursor **1** (200 mg, 0.3 mmol). The vial was sealed and three cycles of N_2/vacuum were applied in order to remove the oxygen. The vial was heated to 280ºC in a sand bath for 8 hours. After this time, the solid was cooled to room temperature. The solid was dispersed in ether and filter over paper. No further purification procedure needed. Yield = 119 mg (60%), burgundy solid.

^{1}H-NMR (400 MHz, DMSO-d_6): δ = 9.03 (s, 2H), 8.93-8.92 (d, *J* = 5.4 Hz, 2H), 8.90-8.88 (d, *J* = 5.8 Hz, 2H), 8.82-8.80 (d, *J* = 8.1 Hz, 2H), 8.20-8.19 (d, *J* = 5.9 Hz, 2H), 8.10-8.11 (t, *J* = 7.1 Hz, 2H), 7.50-7.49 (t, *J* = 6.4 Hz, 2H).
^{13}C-NMR (DMSO-d_6, 100 MHz) : δ 157.1, 156.6, 150.4, 138.9, 138.5, 137.5, 128.5, 124.8, 122.0, 119.7
ESI-MS: Calcd. for $[M]^+$: 631.98528, Found: 631.98263, Diff.: 4.19 ppm
Elemental Analysis: Calcd. for $C_{22}H_{14}N_4ReO_2Br.H_2O$: C, 40.49; H, 2.78; N, 8.59. Found : C, 40.39; H, 2.09; N, 8.44.

13.2.3. [Re(4-pytpy-κ²*N*)(CO)₃]₄[(PF₆)]₄ (5)

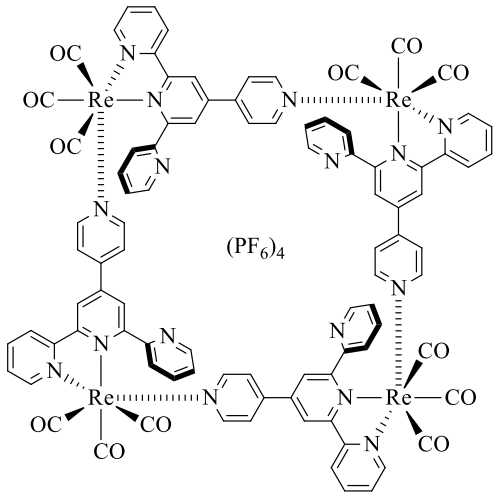

A 250 mL round-bottomed flask was charged with **1** (100 mg, 0.151 mmol), silver triflate (43 mg, 0.166 mmol) and 100 mL of acetonitrile. The solution was heated at reflux under inert atmosphere for 5 hours in the dark. After this time, the AgBr precipitate was removed by filtration. The filtrate was evaporated to dryness under vacuum and 100 mL of a solvent combination of acetone:toluene (1:1) was added to the flask. The solution was heated to reflux for another 12 hours. The solvent was evaporated to dryness under vacuum. The precipitate was carefully dissolved in a minimum amount of acetonitrile and metathesis of the counter-anions was achieved by the addition of an aqueous KPF_6 solution (10 equivalents), leading to the precipitation of a bright yellow compound. Purification was achieved by eluting the compound on Sephadex LH-20 column with a solvent combination of MeOH:MeCN:H_2O (45:45:10). The first band to elute is the desired product. A second metathesis was achieved by the addition of an aqueous solution of KPF_6. The precipitate was isolated by filtration and dried under vacuum. Yield = 155 mg (46%), bright yellow solid.

Due to the 4 possible isomers (Figure 13.1; the arrow indicates the position of the free pyridyl rings), all of the peaks are multiplets and exact ^{1}H NMR assignments are not useful, however, the correct number of protons are present for the title compound.

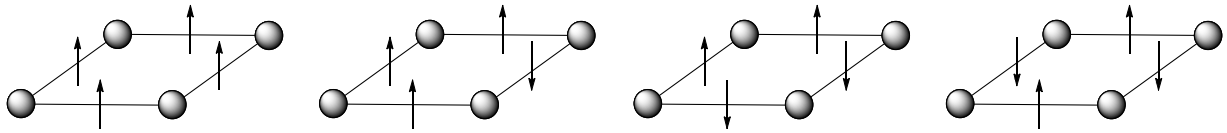

Figure 13.1 - Representation of the four different isomers of molecular square **5**.

^{1}H-NMR (400 MHz, acetone-d_6): δ = 9.55-9.52 (m, 4H), 9.01-8.87 (m, 8H), 8.76-8.73 (dd, 2H), 8.59-8.31 (m, 12H), 8.26-7.89 (m, 26H), 7.80-7.74 (m, 4H).

^{13}C-NMR (DMSO-d_6, 100 MHz) : δ 164.1, 163.9, 163.8, 163.7, 159.0, 158.9, 158.7, 157.6, 157.53, 157.47, 155.7, 155.6, 155.5, 154.2, 154.1, 154.0, 151.80, 151.76, 151.7, 151.6, 149.9, 149.7, 148.1, 147.9, 147.8, 147.6, 146.2, 145.7, 143.1, 142.9, 142.7, 142.6, 139.4, 139.2, 130.7, 130.60, 130.57, 130.3, 129.6, 128.6, 128.5, 128.2, 128.1, 127.94, 127.91, 127.8, 127.6, 127.53, 127.51, 127.4, 127.3, 127.2, 126.8, 126.7, 126.6, 126.5, 126.32, 126.25, 124.4, 124.3, 123.2, 122.5.

ESI-MS: Calcd. for $[M+K]^{+}$: 2941.06736, Found: 2941.06302, Diff.: -1.48 ppm, calcd. for $[M-2PF_6]^{+2}$: 1306.0875, Found: 1306.08541, Diff.: -1.60 ppm, calcd. for $[M-3PF_6]^{+3}$: 822.40342, Found: 822.40391, Diff.: 0.60 ppm

Elemental Analysis: Calcd. for $C_{92}H_{56}N_{16}Re_4O_{12}P_4F_{24}.H_2O$: C, 37.84; H, 2.00; N, 7.67. Found : C, 37.60; H, 1.77; N, 7.45.

13.2.4. [Re(4-pytpy-κ^3*N*)(CO)$_2$]$_4$[(PF$_6$)]$_4$ (6)

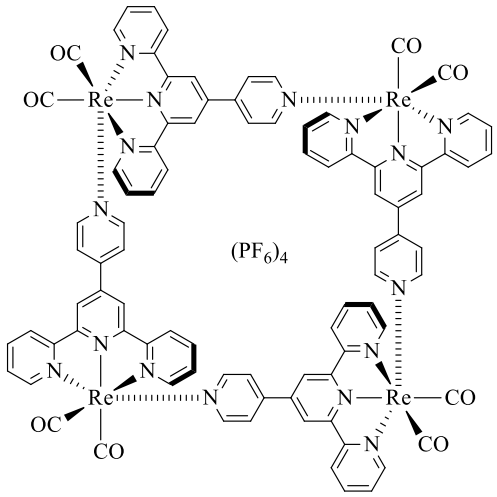

A 250 mL round-bottomed flask was charged with **2** (200 mg, 0.32 mmol), silver triflate (120 mg, 0.47 mmol) and 100 mL of acetonitrile. The solution was heated at reflux under inert atmosphere over 5 hours in the dark. After this time, the AgBr precipitate was removed by filtration. The filtrate was evaporated to dryness under vacuum and 100 mL of a solvent combination of acetone:toluene (1:1) was added to the flask. The solution was heated at reflux for another 10 hours. The solvent was evaporated to dryness under vacuum. The precipitate was carefully dissolved in a minimum amount of acetonitrile and metathesis of the counter-anions was achieved by the addition of an aqueous KPF_6 solution (10 equivalents), leading to the precipitation of a bright yellow compound. Purification was achieved by eluting the compound on Sephadex LH-20 column with a solvent combination of MeOH:MeCN:H_2O (45:45:10). The first band to elute is the desired product. A second metathesis was achieved by the addition of an aqueous solution of KPF_6. The precipitate was isolated by filtration and dried under vacuum. Yield = 183 mg (83%), brown solid.

^{1}H-NMR (400 MHz, acetone-d_6): δ = 9.20-9.18 (d, *J* = 5.2 Hz, 8H), 8.80 (s, 8H), 8.72-8.70 (d, *J* = 8.1 Hz, 8H), 8.34-8.32 (d, *J* = 6.6 Hz, 8H), 8.22-8.18 (t, *J* = 8.1 Hz, 8H), 7.87-7.85 (d, *J* = 6.7 Hz, 8H), 7.78-7.74 (t, *J* = 6.5 Hz, 8H).

^{13}C-NMR (DMSO-d_6, 100 MHz) : δ 168.8, 168.6, 167.6, 167.4, 167.0, 161.8, 161.5, 156.9, 156.4, 149.5, 147.6, 140.7, 140.6, 139.0, 139.8, 136.2, 135.4, 135.3, 134.9, 132.4, 131.8, 131.7, 129.7.

ESI-MS: Calcd. for $[M-2PF_6]^{+2}$: 1250.09763, Found: 1250.10666, Diff.: 7.2 ppm, calcd. for $[M-3PF_6]^{+3}$: 785.07684, Found: 785.08305, Diff.: 7.2 ppm

Elemental Analysis: Calcd. for $C_{88}H_{56}N_{16}Re_4O_8P_4F_{24}.2H_2O$: C, 37.40; H, 2.14; N, 7.93. Found : C, 37.05; H, 1.93.; N, 7.71.

13.3. Crystallographic measurements

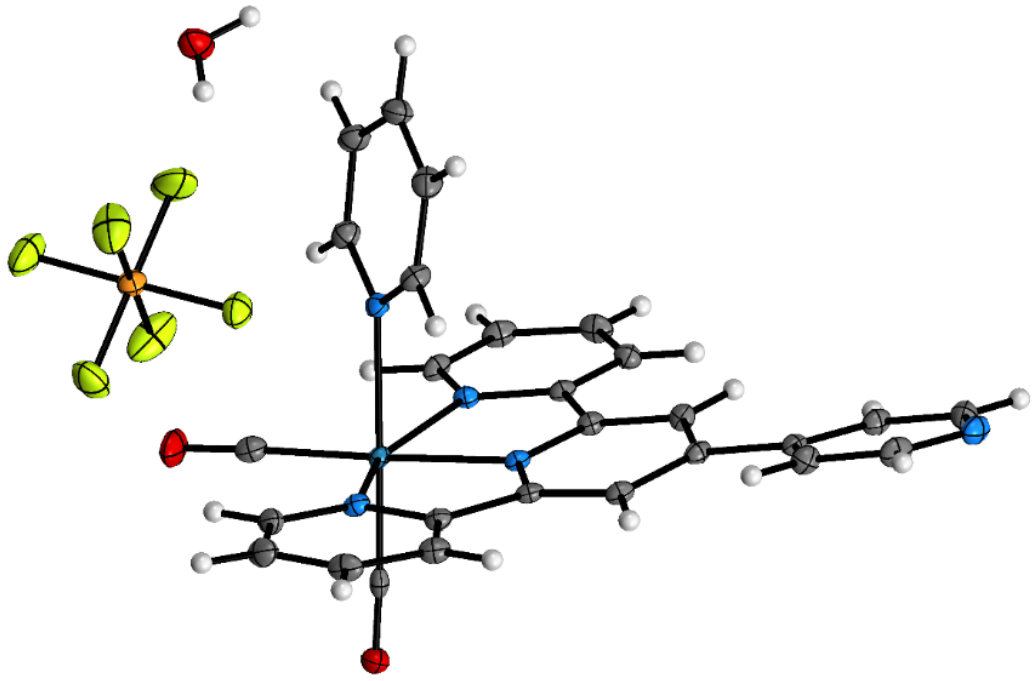

Figure 13.2 - X-ray structure of complexe **4**. Thermal ellipsoids are shown with a 50% probability.

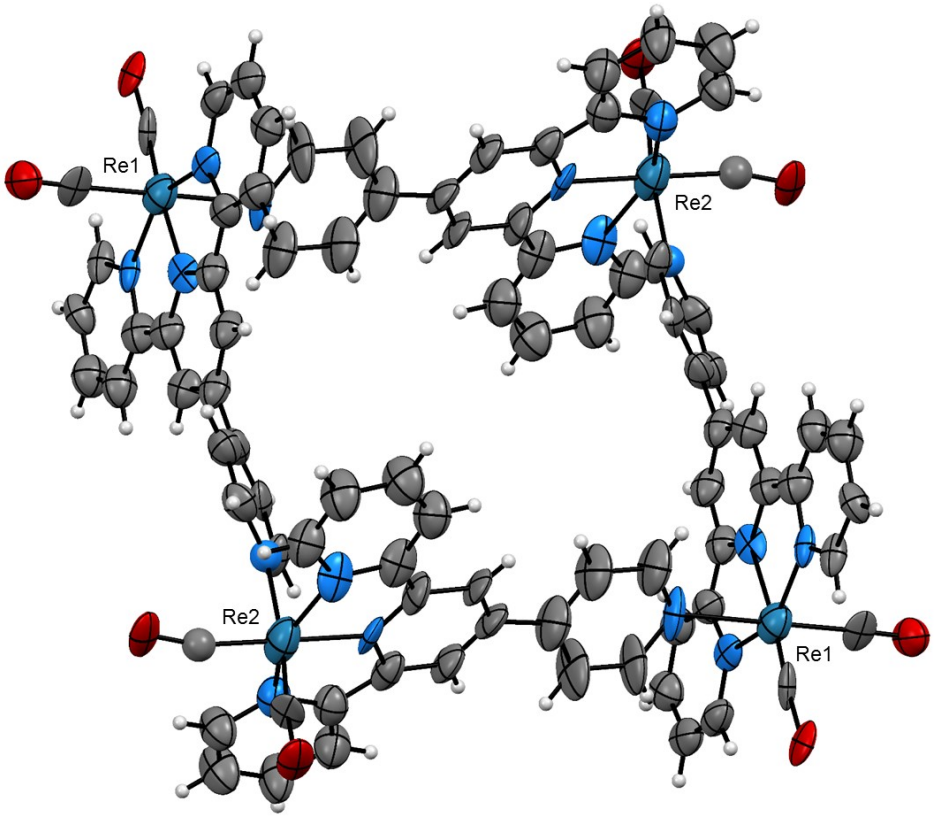

Figure 13.3 - X-ray structure of complexe **6**. Thermal ellipsoids are shown with a 50% probability. Counter-anions (4 PF_6) were omitted for clarity.

Table 13.1 - Crystallographic data for complexes **4** and **6**.

Compound	**4**	**6**
CCDC Number	1017263	1017619
Formula	$[C_{27}H_{19}N_5O_2Re][PF_6](H_2O)$	$[C88H_{56}N_{16}O_8Re_4][(PF_6)_4]$
M_w (g/mol); F(000)	776.64; 1544	2790.21; 5344
T (K); Wavelength	100 ; 1.54178	100 ; 1.54178
Crystal System	Monoclinic	Monoclinic
Space group	$P2_1/n$	C2/c
Unit cell : *a* (Å)	13.9820(2)	27.917(16)
b (Å)	8.17950(10)	12.514(7)
c (Å)	24.0881(4)	32.083(17)
α (°)	90	90
β (°)	104.4190(10)	94.010(9)
γ (°)	90	90

Table 13.2 - Crystallographic data for complexes **4** and **6**.

($Å^3$); Z; $d_{calcd.}$ (g/cm^3)	2668.08(7); 4; 1.978	11181(11); 1.658
θ range (°); completeness	3.34-70.60; 0.973	1.27-16.11; 0.948
Collected reflection; R_σ	99183; 0.0091	9905; 0.1580
Unique reflections; R_{int}	5025; 0.0274	2641; 0.1522
μ (mm^{-1}); Abs. Corr.	10.237; multi-scan	9.638; multi-scan
R1(F); wR(F^2) (I > 2σ(I))	0.0263; 0.0654	0.0916; 0.2344
R1(F); wR(F^2) (all data)	0.0263; 0.0654	0.1474; 0.2646
GoF(F^2)	1.080	0.949
Residual electron density	1.453; -1.267 $e^-/Å^3$	1.110; -0.580 $e^-/Å^3$

13.4 Cyclic voltammetry

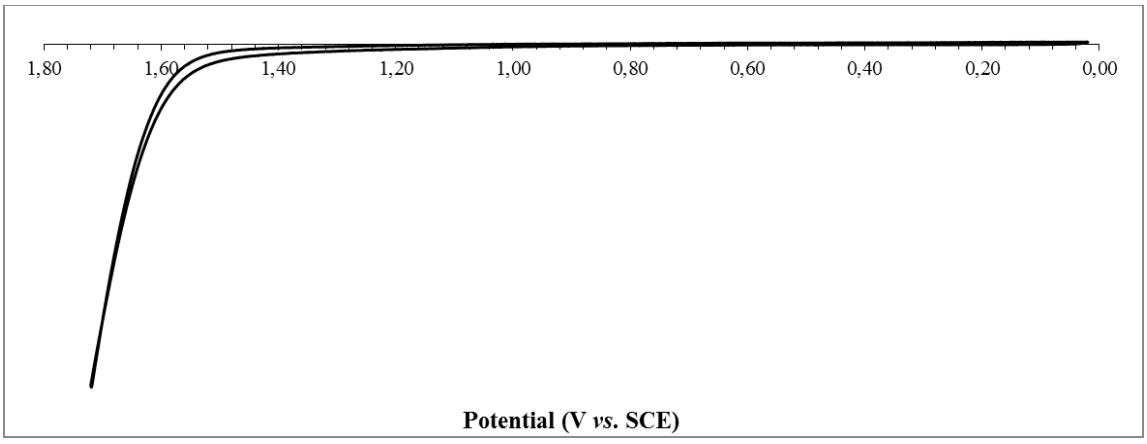

Figure 13.4 - Cyclic voltammogram of complex 5. No evidence of metal-based oxidation at potential lower than the solvent oxidation was found.

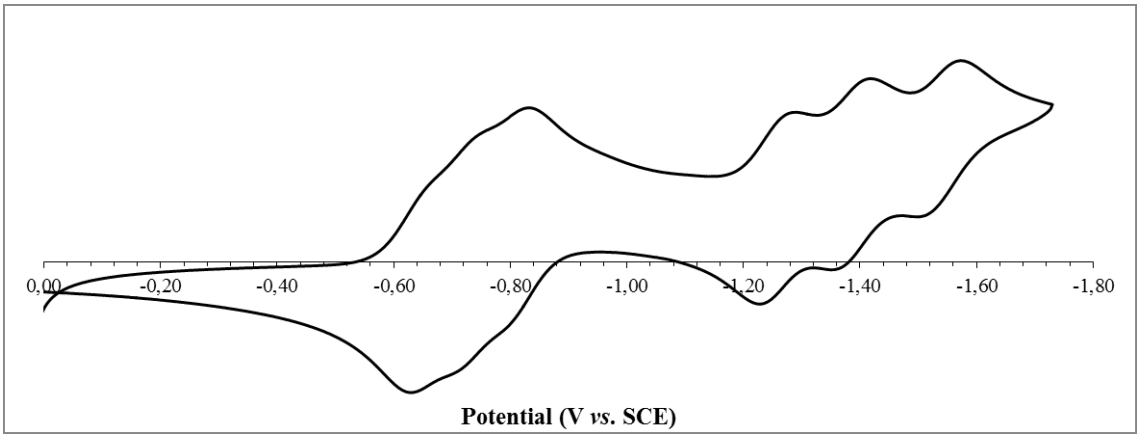

Figure 13.5 - Cyclic voltammogram of complex **5** showing the six fully reversible reduction processes.

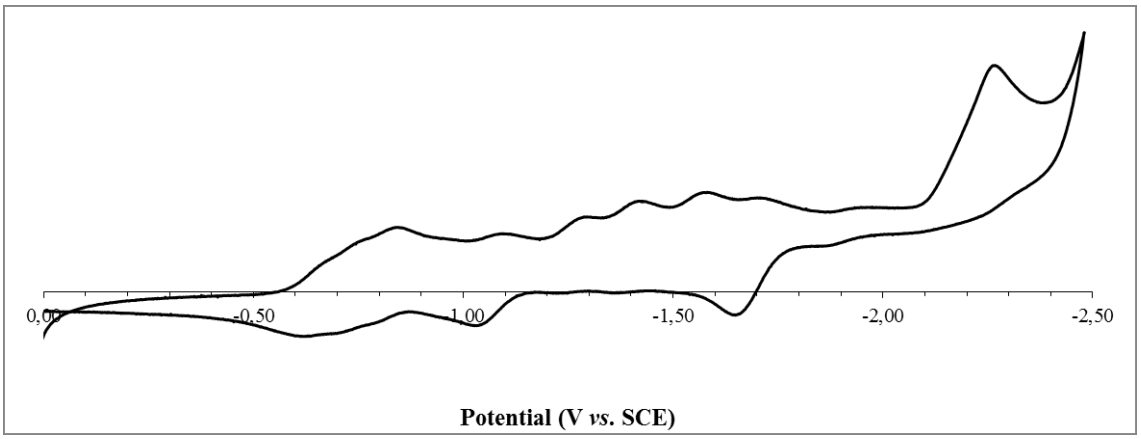

Figure 13.6 - Cyclic voltammogram of complex 5. Upon reduction at high potential (-2.0 and over), degradation related processes are observed.

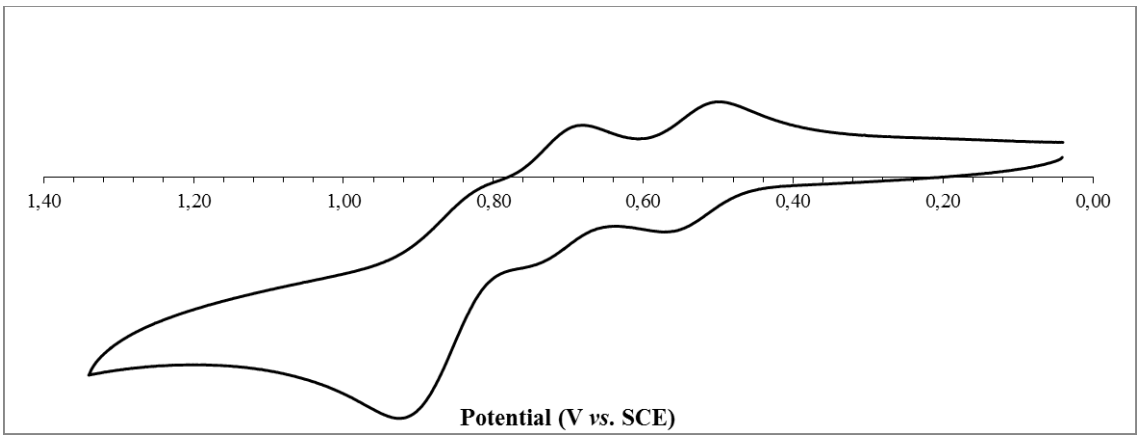

Figure 13.7 - Cyclic voltammogram of complex 6 displaying three metal-based oxidation waves. The first two waves are fully reversible while the last one is quasi-reversible.

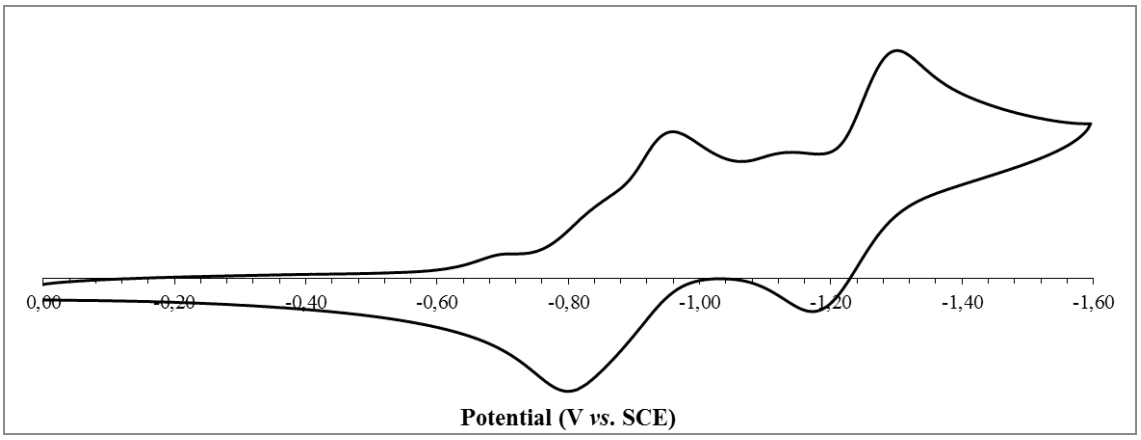

Figure 13.8 - Cyclic voltammogram of complex 6 the ligand-based reduction. The peak at -0.65 V is due to the presence of trace amounts of water.

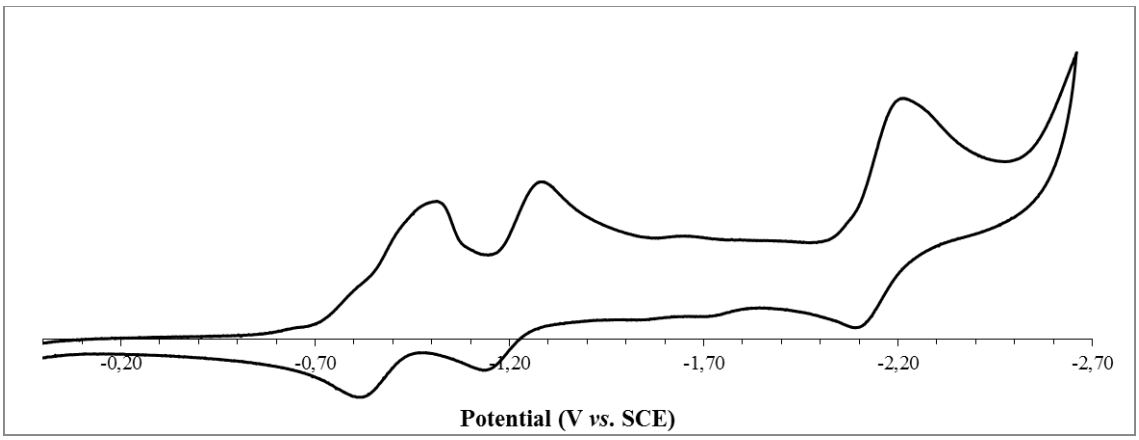

Figure 13.9 - Cyclic voltammogram of complex 6 the ligand-based reduction. Upon reduction at high potential (-2.0 and over), degradation related processes are observed.

Table 13.3 - Experimental C≡O infrared frequencies

Cmpd	*v* (CO)
1	2019, 1936, 1883
2	1889, 1806
3	1903, 1856, 1833
4	1905, 1834
5	2030, 1909
6	1906, 1833
$[Re(py)(CO)_3(2,2'\text{-bpy})][PF_6]$	2040, 1950
$[Re(py)(CO)_2(tpy\text{-}\kappa^3N)][OTf]$	1912, 1841
$[Re(CH_3CN)(CO)_2(tpy\text{-}\kappa^3N)][OTf]$	1921, 1848
$Re(CO)_2(tpy\text{-}\kappa^3N)Cl$	1891, 1798
$Re(CO)_3(tpy\text{-}\kappa^2N)Cl$	2011, 1924, 1902

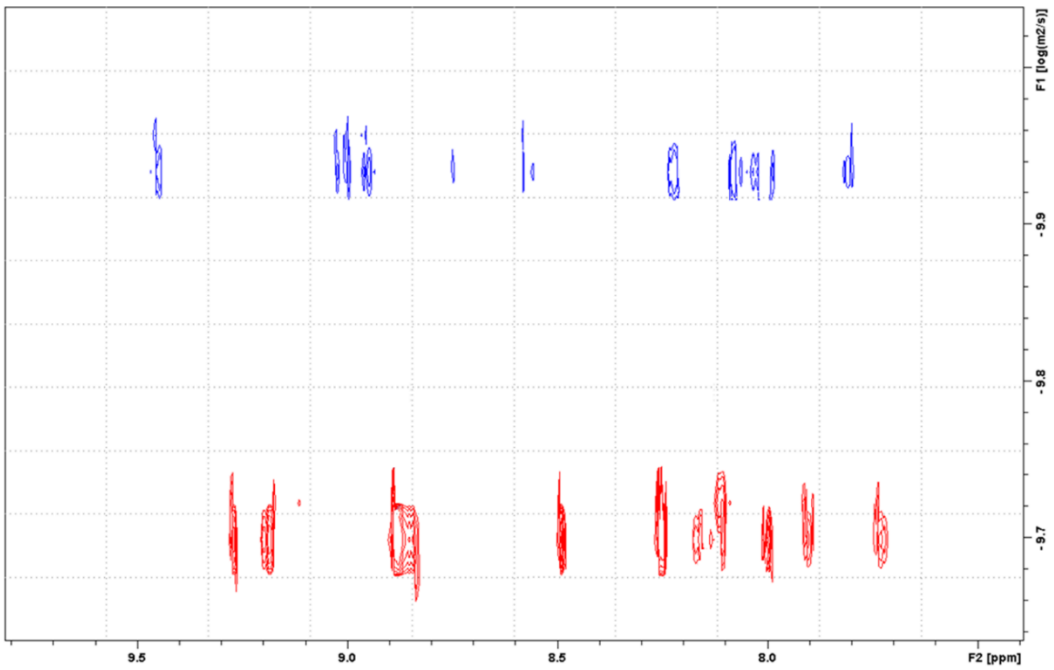

Figure 13.10 -Representative Diffusion-ordered spectroscopy experiment for complexes **1** (red) and **5** (blue) showing the slower diffusion in solution (dmso-d_6) of the supramolecular square compared to its precursor.

Table 13.4 - Experimental DOSY values.

Cmpd	Log D (m^2/s)	D (m^2/s)
1	-9.701	$1.99x10^{-10}$
2	-9.732	$1.85x10^{-10}$
5	-9.941	$1.14x10^{-10}$
6	-10.013	$9.71x10^{-11}$

Chapitre 14 - Informations supplémentaires: Visible and near-IR emission from k^2N- and k^3N-terpyridine rhenium(I) assemblies obtained via a [n x 1] head-to-tail bonding strategy

14.1. Materials, methods and instrumentation

$Re(CO)_5Br$ and 4'-pyridyl-terpyridine starting materials were synthesized as previously described in the literature. Solvents were removed under reduced pressure using a rotary evaporator unless otherwise stated. $Re_2(CO)_{10}$ was purchased from Pressure Chemical. Silver triflate and potassium hexafluorophosphate were purchased from Aldrich. All were used without further purifications. ACS grade solvents were purchased from VWR and Fisher. Nuclear magnetic resonance (NMR) spectra were recorded in acetone-d_6 and DMSO-d_6 at 25ºC on a Bruker AV-400 spectrometer at 400 MHz for ^{1}H NMR and at 100 MHz for ^{13}C NMR. Chemical shifts (δ) are reported in part per million (ppm) relative to TMS, and are referenced to the residual solvent signal (δ = 2.05 ppm for acetone-d_6 and 2.50 ppm for DMSO-d_6). High-Resolution Mass Spectrometry (HR-MS) experiments were conducted on a Bruker Daltonics microTOF spectrometer using electrospray ionization. Absorption spectra and emission spectra were measured in deaerated spectrograde solvent at room temperature on a Cary 500i UV-Vis-NIR Spectrophotometer and a Cary Eclipse Fluorescence Spectrophotometer, respectively. For the luminescence lifetimes, an Edinburgh OB 900 single-photon-counting spectrometer was used, employing a Hamamatsu PLP2 laser diode as pulse (wavelength output, 408 nm; pulse width, 59 ps). The corrected fluorescence emission spectra in the NIR range were recorded with a spectrofluorometer Edinburgh Instruments FLS920 equipped with an Edinburgh Instruments Ge detector (800-1600 nm).[1] Electrochemical

measurements were carried out in argon-purged dimethylformamide at room temperature with a BAS CV50W multipurpose equipment. The working electrode was a glassy carbon electrode. The counter electrode was a Pt wire, and the pseudo-reference electrode was a silver wire. The reference was set using an internal 1 mM ferrocene/ferrocenium sample at 450 mV vs SCE in dimethylformamide. The concentration of the compounds was of about 1 mM. Tetrabutylammonium hexafluorophosphate (NBu_3PF_6) was used as the supporting electrolyte and its concentration was 0.10 M. Cyclic voltammograms were obtained at scan rates of 50, 100, 200, and 500 mV/s. For reversible processes, half-wave potentials (vs SCE) were measured with square wave voltammetry (SWV) experiments performed with a step rate of 4 mV, a pulse height of 25 mV, and a frequency of 15 Hz. For irreversible reduction processes, the cathodic peak was used as *E*. The criteria for reversibility were the close to unity ratio of the intensities of the cathodic and anodic currents, and the constancy of the peak potential on changing scan rate. Experimental uncertainties are as follows: absorption maxima, ±2 nm; molar absorption coefficient, 10%; emission maxima, ± 5 nm; excited state lifetimes, 10%; redox potentials, ± 10 mV. The microanalyses were performed at the Elemental Analysis Service of the Université de Montréal.

14.2. X-ray Structure Determination

X-Ray diffraction data collection for the metal complexes **2** and **5** was carried out on a Bruker Venture Metaljet diffractometer equipped with an Oxford Cryosystem liquid N2 device, using Ga-Kα radiation (λ = 1.34139 Å). The cell parameters were determined (APEX2 software) from reflections taken from three sets of 100 frames, each at 1 s exposure. The structure was solved by direct methods using the program Olex2. The H-atoms were included in calculated positions and treated as riding atoms using Olex2 default parameters. The non-H atoms were refined anisotropically, using weighted full-matrix least-squares on F2. More details are provided in the Supporting Information. CCDC 1493843 and CCDC 1493844 contain the supplementary crystallographic data for this paper. These data can be obtained free of charge from The Cambridge Crystallographic Data Centre via www.ccdc.cam.ac.uk/data_request/cif.

14.3. Computational Details

Gaussian 09, Revision D.01 was used for all theoretical calculations discussed herein.[2] The molecular structure of the metal complexes was fully optimized with CPCM acetonitrile solvation model in absence of constraints at Density Functional Theory (DFT) level, using, when possible, the crystallographic data as the starting point for the optimization. In particular, the hybrid PBE0 functional,[3] casting 25% of HF exchange in the PBE functional was applied.[4] The double zeta valence basis set LANL2DZ was used for all atoms but the Re ones which were described by the Los Alamos pseudo potential and corresponding basis set.[5] No imaginary frequencies were obtained when frequency calculations on optimized geometries were performed. GaussView 5.0.9,[6] GaussSum 3.0[7] and Chemissian 4.30 software were used for data analysis, visualization and surface plots.[8]

14.4. Synthesis of the metal complexes

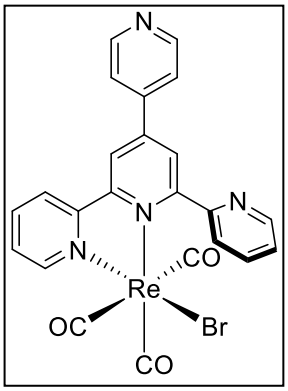

14.4.1. k^2N-Re(4'-pytpy)$(CO)_3$Br, (1)

A 250-mL round-bottomed flask was charged with $Re(CO)_5Br$ (1.19 g, 2.93 mmol) and 4-pytpy ligand (1.0 g, 3.22 mmol) and to it 100 mL of toluene was added. The mixture was heated at reflux for 5 hours, after which time the solution was cooled to room temperature. The yellow suspension was filtered and washed with three portions of ether (50 mL) and dried under vacuum. No further purification procedures were needed.

Yield = 1.8 g (94%), yellow solid.

^{1}H-NMR: (DMSO-d_6, 400 MHz): δ (ppm) = 9.21 (s, 1H), 9.14-9.09 (m, 2H), 8.85-8.83 (d, *J* = 5.8 Hz, 2H), 8.82-8.80 (d, *J* = 4.4 Hz, 1H), 8.43-8.33 (m, 2H), 8.22-8.20 (d, *J* = 5.9 Hz, 2H), 8.10-8.06 (t, *J* = 7.5 Hz, 1H), 7.92-7.90 (d, *J* = 7.7 Hz, 1H), 7.81-7.78 (t, *J* = 6.4 Hz, 1H), 7.66-7.63 (dd, 1H).

^{13}C NMR (DMSO-d_6, 100 MHz) : δ (ppm) 161.8, 157.6, 157.5, 156.0, 152.8, 150.6, 149.2, 148.0, 141.9, 139.9, 137.0, 127.6, 125.6, 125.0, 124.8, 121.8, 121.0.

ESI-MS: Calcd. for $[M+H]^+$: 660.98625, Found: 660.98716, Diff.: 1.39 ppm.

Elemental Analysis: Calcd. for $C_{23}H_{14}N_4ReO_3Br$: C, 41.82; H, 2.14; N, 8.48. Found : C, 41.80; H, 2.11; N, 8.37.

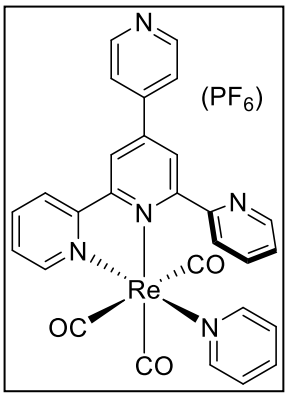

14.4.2. [k^2*N*-Re(4'-pytpy)(py)(CO)$_3$][PF_6], (2)

A 100 mL round-bottomed flask was charged with K^2*N*-Re(4'-pytpy)(CO)$_3$Br (75 mg, 0.11 mmol) and pyridine (50 mL). An aqueous solution of $AgNO_3$ (25 mg, 0.15 mmol dissolve in 0.5 mL of H_2O) was added as a dehalogenating agent to the clear orange solution. The mixture was heated at reflux for 5 hours, after which time the solution was evaporated to dryness. To the resulting yellow precipitate was added a minimum amount of acetone (5-10 mL) and the mixture was sonicated for 10 minutes. The resulting heterogeneous solution was filtered over a bed of Celite to remove the AgBr precipitate which was washed with acetone (25 mL). An aqueous solution of KPF_6 (10 eq.) was added to the filtrate to complete the metathesis of the counter-anion and the acetone was evaporated under vacuum. The resulting aqueous solution was filtered over a frit glass filter and washed with a large amount of water to remove excess KPF_6. The yellow precipitate was dissolved in a minimum amount of acetone and the filtrate was added to a flask containing 50 mL of diethyl ether. The resulting precipitate was filter over a glass filter and dry under vacuum for several minutes. Crystals were grown from the slow evaporation of a water:pyridine solution over several days.

Yield = 45 mg (60%), yellow crystal.

^{1}H-NMR: (acetone-d_6, 400 MHz): δ (ppm) = 9.51 (s, 1H), 9.11 (s, 1H), 9.02 (d, *J* = 8 Hz, 1H), 8.91 (s, 1H), 8.82 (s, 2H), 8.54 (m, 2H), 8.33 (d, *J* = 5 Hz, 2H), 8.19 (m, 1H), 8.12 (d, *J* = 7 Hz, 1H), 8.06 (m, 3H), 7.99 (t, *J* = 8 Hz, 1H), 7.75 (m, 1H), 7.45 (t, *J* = 7 Hz, 2H).

^{13}C NMR (acetone-d_6, 100 MHz) : δ (ppm) 154.9, 154.2, 153.3, 151.9, 151.8, 150.9, 142.2, 140.9, 138.6, 130.2, 130.1, 127.9, 127.5, 127.0, 126.7, 126.0, 122.7.

ESI-MS: Calcd. for $[M+H]^+$: 660.10409, Found: 660.10179, Diff.: 3.48 ppm.

Elemental Analysis: Calcd. for $C_{28}H_{19}N_5ReO_3PF_6$: C, 41.79; H, 2.38; N, 8.70. Found : C, 42.01; H, 2.37; N, 8.69.

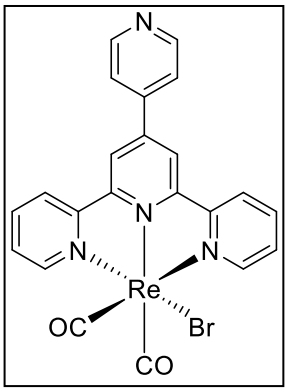

14.4.3. *k*^{3}*N*-Re(4'-pytpy)(CO)$_2$Br, (3)

A 20 mL Biotage® microwave vial was loaded with finely ground powder of precursor **1** (200 mg, 0.3 mmol). The vial was sealed and three cycles of N_2/vacuum were applied in order to remove the oxygen. The vial was heated to 280ºC in a sand bath for 8 hours. After this time, the solid was cooled to room temperature. The solid was dispersed in ether and filtered over paper. No further purification procedure was needed.

Yield = 119 mg (60%), burgundy solid.

^{1}H-NMR (400 MHz, DMSO-d_6): δ (ppm) = 9.03 (s, 2H), 8.93-8.92 (d, *J* = 5.4 Hz, 2H), 8.90-8.88 (d, *J* = 5.8 Hz, 2H), 8.82-8.80 (d, *J* = 8.1 Hz, 2H), 8.20-8.19 (d, *J* = 5.9 Hz, 2H), 8.10-8.11 (t, *J* = 7.1 Hz, 2H), 7.50-7.49 (t, *J* = 6.4 Hz, 2H).

^{13}C NMR (DMSO-d_6, 100 MHz) : δ (ppm) 157.1, 156.6, 150.4, 138.9, 138.5, 137.5, 128.5, 124.8, 122.0, 119.7.

ESI-MS: Calcd. for $[M]^+$: 631.98528, Found: 631.98263, Diff.: 4.19 ppm.

Elemental Analysis: Calcd. for $C_{22}H_{14}N_4ReO_2Br.H_2O$: C, 40.49; H, 2.78; N, 8.59. Found : C, 40.39; H, 2.09; N, 8.44.

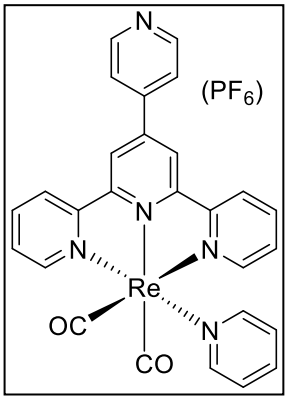

14.4.4. [k^3*N*-Re(4'-pytpy)(py)(CO)$_2$][PF$_6$], (4)

A 50-mL round-bottomed flask was charged with metal complex **3** (150 mg, 0.24 mmol), silver triflate (76 mg, 0.30 mmol) and 25 mL of pyridine. The mixture was heated at reflux for 5 hours under N_2 and protected from light, after which time the solution was cooled to room temperature. The green solution was poured in an aqueous KPF_6 solution (10 eq.). The resulting greenish precipitate was filtered over a glass frit. Purification of the resulting product was achieved over deactivated neutral alumina with CH_2Cl_2:acetone (70:30) as solvent. The pure fractions were combined and evaporated under vacuum to a minimum amount of solvent (5 mL). Further addition of diethyl ether lead to the precipitation of a dark green precipitate which was filtered over glass frit and dried under vacuum.

Yield = 120 mg (65%), greenish solid.

^{1}H-NMR: (acetone-d$_6$, 400 MHz): δ (ppm) = 9.17 (d, *J* = 6 Hz, 2H), 9.09 (s, 2H), 8.90 (broad s, 2H), 8.84 (d, *J* = 8 Hz, 2H), 8.31 (dd, *J* = 7 Hz, 2H), 8.22-8.20 (td, *J* = 8 Hz, 2H), 8.10 (broad s, 2H), 7.91 (m, 1H), 7.71 (m, 2H), 7.36 (m,2H).
^{13}C NMR (acetone-d$_6$, 100 MHz) : δ (ppm) 159.0, 158.0, 157.8, 151.7, 151.4, 150.7, 143.9, 140.1, 139.7, 130.8, 127.4, 126.5, 122.8, 122.0.
ESI-MS: Calcd. for $[M+H]^+$: 632.10917, Found: 632.10697, Diff.: 3.48 ppm.
Elemental Analysis: Calcd. for $C_{27}H_{19}N_5ReO_2PF_6$: C, 41.76; H, 2.47; N, 9.02. Found : C, 42.00; H, 2.26; N, 8.61.

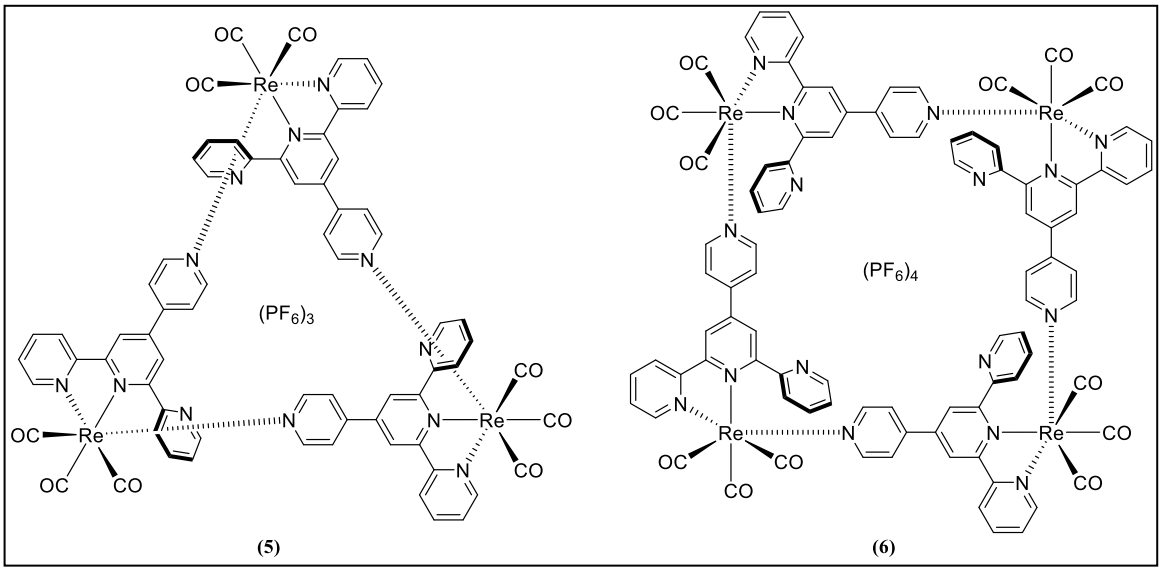

14.4.5. [(k^2N-Re(4'-pytpy)(CO)$_3$)$_3$][(PF$_6$)$_3$], (5) and [(K^2N-Re(4'-pytpy)(CO)$_3$)$_4$][(PF$_6$)$_4$], (6)

A 250-mL round-bottomed flask was charged with **1** (100 mg, 0.151 mmol), silver triflate (43 mg, 0.166 mmol) and 100 mL of acetonitrile. The solution was heated at reflux under an inert atmosphere for 5 hours in the dark. After this time, the AgBr precipitate was removed by filtration. The filtrate was evaporated to dryness under vacuum and 100 mL of a solvent combination of acetone:toluene (1:1) was added to the flask. The solution was heated to reflux for another 12 hours. The solvent was evaporated to dryness under vacuum. The precipitate was carefully dissolved in a minimum amount of acetonitrile and metathesis of the counter-anions was achieved by the addition of an aqueous KPF_6 solution (10 equivalents), leading to the precipitation of a bright yellow compound. Purification was achieved by eluting the compound on Sephadex LH-20 column with a solvent combination of MeOH:MeCN:H_2O (45:45:10). The first band to elute is the square assembly **6** and the second band is the self-assembled triangle **5**. A second metathesis was achieved by the addition of an aqueous solution of KPF_6. The precipitate was isolated by filtration and dried under vacuum.

Yield (**5**; **6**) = 135 mg (40%); 155 mg (46%), yellow solids.

5 and **6**:

^{1}H-NMR (400 MHz, acetone-d_6): δ (ppm) = 9.55-9.52 (m, 4H), 9.01-8.87 (m, 8H), 8.76-8.73 (dd, 2H), 8.59-8.31 (m, 12H), 8.26-7.89 (m, 26H), 7.80-7.74 (m, 4H).
^{13}C NMR (DMSO-d_6, 100 MHz) : δ (ppm) 164.1, 163.9, 163.8, 163.7, 159.0, 158.9, 158.7, 157.6, 157.53, 157.47, 155.7, 155.6, 155.5, 154.2, 154.1, 154.0, 151.80, 151.76, 151.7, 151.6, 149.9, 149.7, 148.1, 147.9, 147.8, 147.6, 146.2, 145.7, 143.1, 142.9, 142.7, 142.6, 139.4, 139.2, 130.7, 130.60, 130.57, 130.3, 129.6, 128.6, 128.5, 128.2, 128.1, 127.94, 127.91, 127.8, 127.6, 127.53, 127.51, 127.4, 127.3, 127.2, 126.8, 126.7, 126.6, 126.5, 126.32, 126.25, 124.4, 124.3, 123.2, 122.5.

5: ESI-MS: Calcd. for $[M\text{-}PF_6]^{+}$: 2031.11258, Found: 2031.11269, Diff.: -0.05 ppm, calcd. for $[M\text{-}2PF_6]^{+2}$: 943.07392, Found: 943.07471, Diff.: -0.84 ppm, calcd. for $[M\text{-}3PF_6]^{+3}$: 580.39437, Found: 580.39593, Diff.: -2.69 ppm.
Elemental Analysis: Calcd. for $C_{69}H_{42}N_{12}Re_3O_9P_3F_{18}$: C, 38.07; H, 1.94; N, 7.72. Found : C, 38.10; H, 2.14; N, 7.61.

6: ESI-MS: Calcd. for $[M+K]^{+}$: 2941.06736, Found: 2941.06302, Diff.: -1.48 ppm, calcd. for $[M\text{-}2PF_6]^{+2}$: 1306.0875, Found: 1306.08541, Diff.: -1.60 ppm, calcd. for $[M\text{-}3PF_6]^{+3}$: 822.40342, Found: 822.40391, Diff.: 0.60 ppm.
Elemental Analysis: Calcd. for $C_{92}H_{56}N_{16}Re_4O_{12}P_4F_{24}.H_2O$: C, 37.84; H, 2.00; N, 7.67. Found : C, 37.60; H, 1.77; N, 7.45.

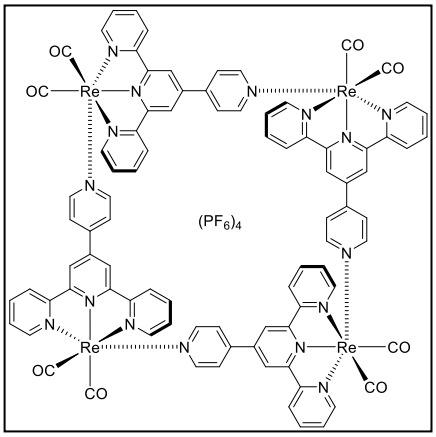

14.4.6. [(k^3*N*-Re(4'-pytpy)(CO)$_2$)$_4$][(PF$_6$)$_4$], (7)

A 250-mL round-bottomed flask was charged with **2** (200 mg, 0.32 mmol), silver triflate (120 mg, 0.47 mmol) and 100 mL of acetonitrile. The solution was heated at reflux under inert atmosphere over 5 hours in the dark. After this time, the AgBr precipitate was removed by filtration. The filtrate was evaporated to dryness under vacuum and 100 mL of a solvent combination of acetone:toluene (1:1) was added to the flask. The solution was heated at reflux for another 10 hours. The solvent was evaporated to dryness under vacuum. The precipitate was carefully dissolved in a minimum amount of acetonitrile and metathesis of the counter-anions was achieved by the addition of an aqueous KPF_6 solution (10 equivalents), leading to the precipitation of a bright yellow compound. Purification was achieved by eluting the compound on Sephadex LH-20 column with a solvent combination of MeOH:MeCN:H_2O (45:45:10). The first band to elute is the desired product. A second metathesis was achieved by the addition of an aqueous solution of KPF_6. The precipitate was isolated by filtration and dried under vacuum.

Yield = 183 mg (83%), brown solid.

^{1}H-NMR (400 MHz, acetone-d$_6$): δ (ppm) = 9.20-9.18 (d, *J* = 5.2 Hz, 8H), 8.80 (s, 8H), 8.72-8.70 (d, *J* = 8.1 Hz, 8H), 8.34-8.32 (d, *J* = 6.6 Hz, 8H), 8.22-8.18 (t, *J* = 8.1 Hz, 8H), 7.87-7.85 (d, *J* = 6.7 Hz, 8H), 7.78-7.74 (t, *J* = 6.5 Hz, 8H).

^{13}C NMR (DMSO-d$_6$, 100 MHz) : δ (ppm) = 168.8, 168.6, 167.6, 167.4, 167.0, 161.8, 161.5, 156.9, 156.4, 149.5, 147.6, 140.7, 140.6, 139.0, 139.8, 136.2, 135.4, 135.3, 134.9, 132.4, 131.8, 131.7, 129.7.

ESI-MS: Calcd. for [M-2PF$_6$]$^{+2}$: 1250.09763, Found: 1250.10666, Diff.: 7.2 ppm, calcd. for [M-3PF$_6$]$^{+3}$: 785.07684, Found: 785.08305, Diff.: 7.2 ppm.

Elemental Analysis: Calcd. for $C_{88}H_{56}N_{16}Re_4O_8P_4F_{24}.2H_2O$: C, 37.40; H, 2.14; N, 7.93. Found : C, 37.05; H, 1.93.; N, 7.71.

14.5. Crystallographic parameters

Table 14.1 - Solid-state structure and refinement data for complexes **2** and **5**.

	2	5
Formula	$[C_{28}H_{19}N_5O_3Re][(PF_6)_2]$	$[C_{69}H_{42}N_{12}Re][C_{69}H_{42}N_{12}Re][(NO_3)_5]$
Color/form	Yellow/block	Yellow/block
M_w [gmol^{-1}]	804.65	3793.61
Temperature [K]	100	100
Wavelength [Å]	1.341139	1.341139
Crystal system	Orthorhombic	Triclinic
a [Å]	10.6739(5)	15.378(3)
b [Å]	12.5684(6)	23.786(5)
c [Å]	20.8906(9)	23.853(5)
α [°]	90	80.33(3)
β [°]	90	82.86(3)
γ [°]	90	72.41(3)
V [Å^3]	2802.6(9)	8174(3)
Space group	$P2_12_12_1$	P-1
Z	4	2
$d_{calcd.}$ [gcm^{-3}]	1.907	1.541
μ [mml^{-1}]	6.343	5.894
F(000)	1560	3658
Reflection collected	79805	35828
Independent reflections	6355	23108
GoF	1.025	1.060
R_1(F) [$I > 2\sigma(I)$]	0.0132	0.0897
$wR(F^2)$ [$I > 2\sigma(I)$]	0.0318	0.2392
R_1(F) (all data)	0.0135	0.1206
wR(F^2) (all data)	0.0319	0.2605
Largest diff. peak/hole [eÅ^{-3}]	1.020	3.240

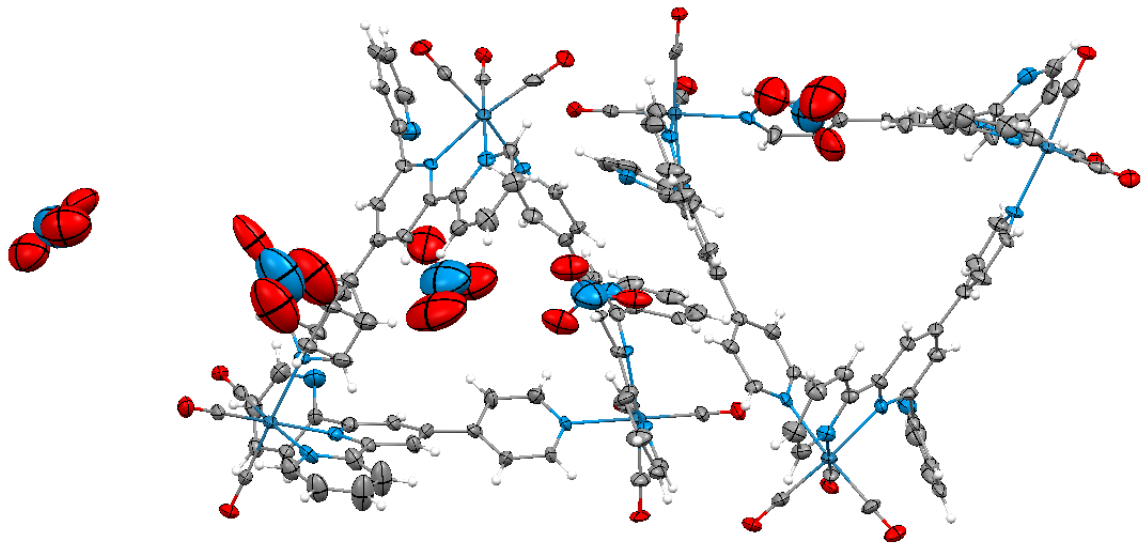

Figure 14.1 - X-ray structure of the k2N-triangle 5 with five of the six counter-anions assigned as NO3-. The sixth counter-anion could not be located. Thermal ellipsoid are shown with a 30% probability.

14.6. DFT and TD-DFT results

Table 14.2 - Atomic coordinates for DFT optimization of ***2*** in ($S = 0$) PBE0/LANL2DZ, CPCM(CH_3CN).

Standard orientation					
Center Number	Atomic Number	Atomic Type	Coordinates (Angstroms)		
			X	Y	Z
1	75	0	-1.776717	0.001726	-0.253836
2	8	0	-2.506694	2.853166	0.716262
3	7	0	0.393002	0.092597	-0.508667
4	7	0	-1.223671	-0.582254	1.787453
5	7	0	-1.229824	-2.000677	-0.802623
6	8	0	-4.760893	-0.642078	0.227663
7	6	0	-0.528266	-1.317064	4.406208

8	6	0	2.577207	1.088492	-0.266015
9	6	0	-2.184126	1.781965	0.332341
10	8	0	-2.418318	0.772050	-3.182799
11	6	0	3.207704	-0.162434	-0.331985
12	6	0	1.000880	-1.133453	-0.623518
13	6	0	-1.669700	-1.748865	2.326259
14	6	0	0.033048	3.104307	-1.544839
15	7	0	0.783310	3.283916	0.752894
16	6	0	-0.380271	4.443762	-1.526133
17	6	0	2.385464	-1.280841	-0.536927
18	6	0	-0.069550	-0.112765	3.854804
19	6	0	1.186547	1.193182	-0.376810
20	6	0	0.561840	-3.565884	-1.170640
21	6	0	-1.343948	-2.145303	3.623497
22	6	0	-2.125985	-2.983156	-1.075516
23	6	0	-3.618572	-0.386441	0.045750
24	6	0	-0.211577	5.191344	-0.352626
25	6	0	0.369998	4.570469	0.762670
26	6	0	-2.170991	0.478338	-2.063698
27	6	0	-0.433737	0.223239	2.550636
28	6	0	0.607261	2.564521	-0.383345
29	6	0	-0.362718	-4.579529	-1.438012
30	6	0	0.106234	-2.278500	-0.857130
31	6	0	-1.730813	-4.281155	-1.396249
32	7	0	7.485647	-0.551642	0.038112
33	6	0	6.769271	-1.389496	-0.748353

34	6	0	5.380012	-1.302121	-0.897499
35	6	0	4.676058	-0.297069	-0.206947
36	6	0	5.418874	0.577640	0.608911
37	6	0	6.805984	0.413263	0.702269
38	1	0	2.824493	-2.267796	-0.591691
39	1	0	4.874602	-1.993882	-1.562535
40	1	0	7.331371	-2.152336	-1.277235
41	1	0	-1.727699	-3.083964	4.004693
42	1	0	-2.303234	-2.368687	1.705349
43	1	0	0.559430	0.563692	4.420930
44	1	0	-0.096941	1.154312	2.109376
45	1	0	1.620473	-3.782834	-1.220831
46	1	0	-0.020642	-5.578736	-1.681896
47	1	0	-2.482154	-5.031996	-1.606839
48	1	0	-3.173561	-2.716788	-1.037177
49	1	0	-0.064396	2.502558	-2.441360
50	1	0	-0.820022	4.891855	-2.410742
51	1	0	0.517132	5.114866	1.689742
52	1	0	-0.516798	6.230185	-0.298345
53	1	0	3.150731	2.001129	-0.160371
54	1	0	4.936899	1.359731	1.185323
55	1	0	7.395965	1.072070	1.331148
56	1	0	-0.260637	-1.600204	5.418323

Table 14.3 - MO composition of ***2*** in (*S=0*) ground state.

MO	Energy (eV)	Composition			
		Rhenium	pytpy	py	CO
LUMO+5	-1.30	13	34	9	44
LUMO+4	-1.57	10	56	3	31
LUMO+3	-1.86	2	68	25	5
LUMO+2	-1.95	1	29	64	5
LUMO+1	-2.31	0	94	4	1
LUMO	**-3.10**	**2**	**93**	**0**	**4**
HOMO	**-7.26**	**62**	**11**	**2**	**26**
HOMO-1	-7.31	58	12	5	25
HOMO-2	-7.50	61	12	1	26
HOMO-3	-7.77	0	100	0	0
HOMO-4	-7.91	3	95	0	2
HOMO-5	-8.00	2	97	0	1

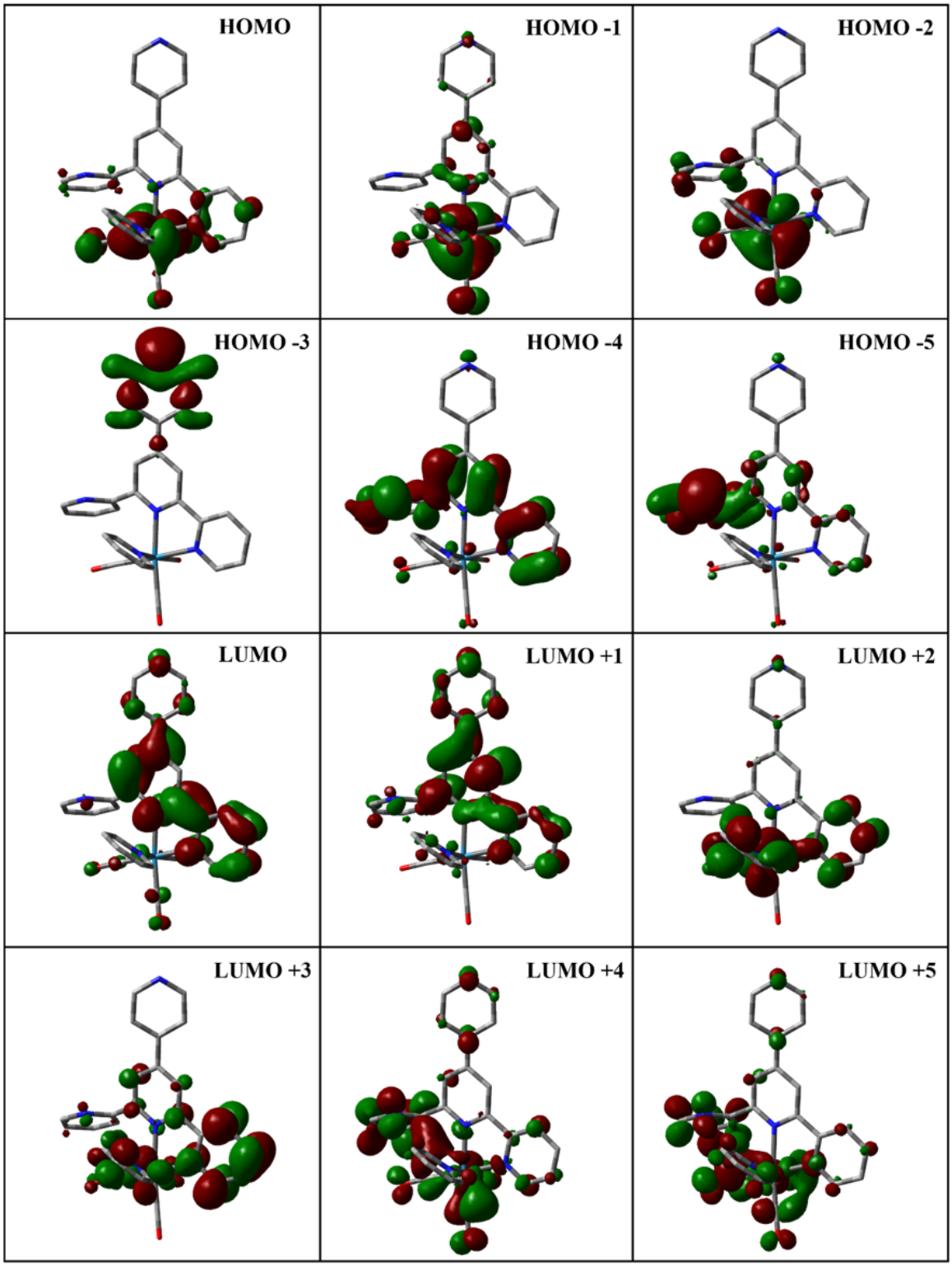

Figure 14.2 - Kohn-Sham electron density illustration of the molecular orbitals of the model complex ***2*** in (*S=0*) ground state.

Table 14.4 - Selected transitions from TD-DFT calculations of **2** in the singlet ground state (PBE0), CPCM (CH_3CN).

Energy (eV)	λ (nm)	f	Transition	Character
3.22	383	0.0124	H→L (91%)	$^1MLCT_{tpy}$ + $^1LLCT_{CO→tpy}$
3,36	367	0,1504	H-1→L (85%)	
3,98	310	0,1577	H-4→L (85%)	$^1MLCT_{tpy}$
4,05	305	0,0317	H-5→L (90%)	$^1MLCT_{CO}$
4,21	293	0,1660	H-1→L+1 (80%)	$^1MLCT_{tpy}$ + $^1LLCT_{CO→tpy}$
4,31	286	0,0232	H→L+2 (46%) H→L+3 (20%)	
4,34	285	0,0243	H-6→L (54%) H-2→L+1 (25%)	
4,46	277	0,0797	H-7→L (14%) H→L+2 (25%) H→L+3 (16%)	$^1MLCT_{tpy}$ and/or $^1MLCT_{py}$ + $^1LLCT_{CO→tpy}$ and/or $^1LLCT_{CO→py}$
4,48	276	0,1128	H-7→L (38%) H-2→L+2 (10%) H-1→L+2 (21%)	
4,51	274	0,0932	H-7→L (29%) H-1→L+2 (19%) H-1→L+4 (11%)	$^1MLCT_{tpy}$ + $^1MLCT_{py}$
4,55	271	0,0254	H-2→L+2 (10%) H-1→L+3 (48%)	$^1MLCT_{tpy}$ and/or $^1MLCT_{py}$ + $^1LLCT_{CO→tpy}$ and/or $^1LLCT_{CO→py}$
4,60	269	0,0331	H-9→L (10%) H-2→L+2 (19%)	

			H→L+3 (16%)	
4,61	268	0,0234	H-9→L (19%) H-3→L+1 (26%) H-2→L+2 (18%)	
4,65	266	0,1175	H-5→L+1 (11%) H-2→L+2 (20%) H-2→L+3 (18%)	
4,66	265	0,0439	H-5→L+1 (27%) H-2→L+3 (11%)	$^{1}MLCT_{tpy} + ^{1}MLCT_{py} + ^{1}MLCT_{CO}$
4,69	263	0,1001	H-9→L (20%) H-8→L (25%) H→L+3 (10%)	$^{1}MLCTt_{py} + ^{1}LLCT_{py\rightarrow tpy}$
4,88	253	0,3248	H-5→L+1 (17%) H-4→L+1 (56%)	
4,91	252	0,0433	H-2→L+5 (29%) H→L+6 (13%)	
4,93	251	0,0922	H-2→L+4 (21%) H-1→L+5 (28%)	
5,10	242	0,0306	H-1→L+6 (10%) H→L+4 (11%) H→L+5 (21%) H→L+6 (11%)	$^{1}MLCT_{tpy} + ^{1}MLCT_{py} + ^{1}MLCT_{CO}$
5,24	236	0,0484	H-1→L+6 (15%) H→L+7 (23%)	
5,24	236	0,0267	H-2→L+4 (15%) H-2→L+5 (14%)	

			H-2→L+6 (12%) H→L+7 (14%)	
5,28	234	0,0418	H→L+6 (18%) H→L+8 (49%)	
5,29	233	0,0679	H-8→L+1 (18%) H-4→L+3 (11%) H-3→L+2 (19%)	$^1MLCT_{py}$ and/or $^1MLCT_{CO}$ + $^1LLCT_{tpy→py}$ and/or $^1LLCT_{tpy→CO}$
5,31	233	0,0472	H-8→L+1 (25%) H-3→L+2 (17%)	
5,66	218	0,0290	H-12→L (17%) H-4→L+5 (14%)	
5,68	217	0,0946	H-10→L+1 (13%) H-9→L+2 (16%)	$^1MLCT_{py}$ + $^1MLCT_{CO}$
5,77	214	0,0427	H→L+14 (13%)	$^1MLCT_{tpy}$ + $^1MLCT_{py}$ + $^1MLCT_{CO}$
5,80	213	0,0289	H-15→L (14%) H-10→L+1 (11%) H-4→L+5 (20%)	$^1LLCT_{tpy→py}$ + $^1LLCT_{tpy→CO}$
5,81	212	0,0280	H-8→L+2 (12%) H-7→L+2 (14%) H→L+14 (14%)	
5,84	211	0,0209	H-9→L+2 (19%) H-9→L+3 (14%) H-8→L+3 (16%) H-7→L+2 (20%)	$^1MLCT_{py}$ and/or $^1MLCT_{CO}$ + $^1LLCT_{tpy→py}$ and/or $^1LLCT_{tpy→CO}$
5,95	208	0,0553	H-14→L (28%)	$^1LLCT_{py→tpy}$ + $^1LLCT_{py→CO}$
5,98	206	0,0229	H-14→L (22%)	

			H-1→L+9 (10%)	$^1MLCT_{CO}$ and/or $^1MLCT_{tpy}$ + $^1LLCT_{py→CO}$ and/or $^1LLCT_{py→tpy}$
6,04	204	0,0215	H-14→L (15%)	

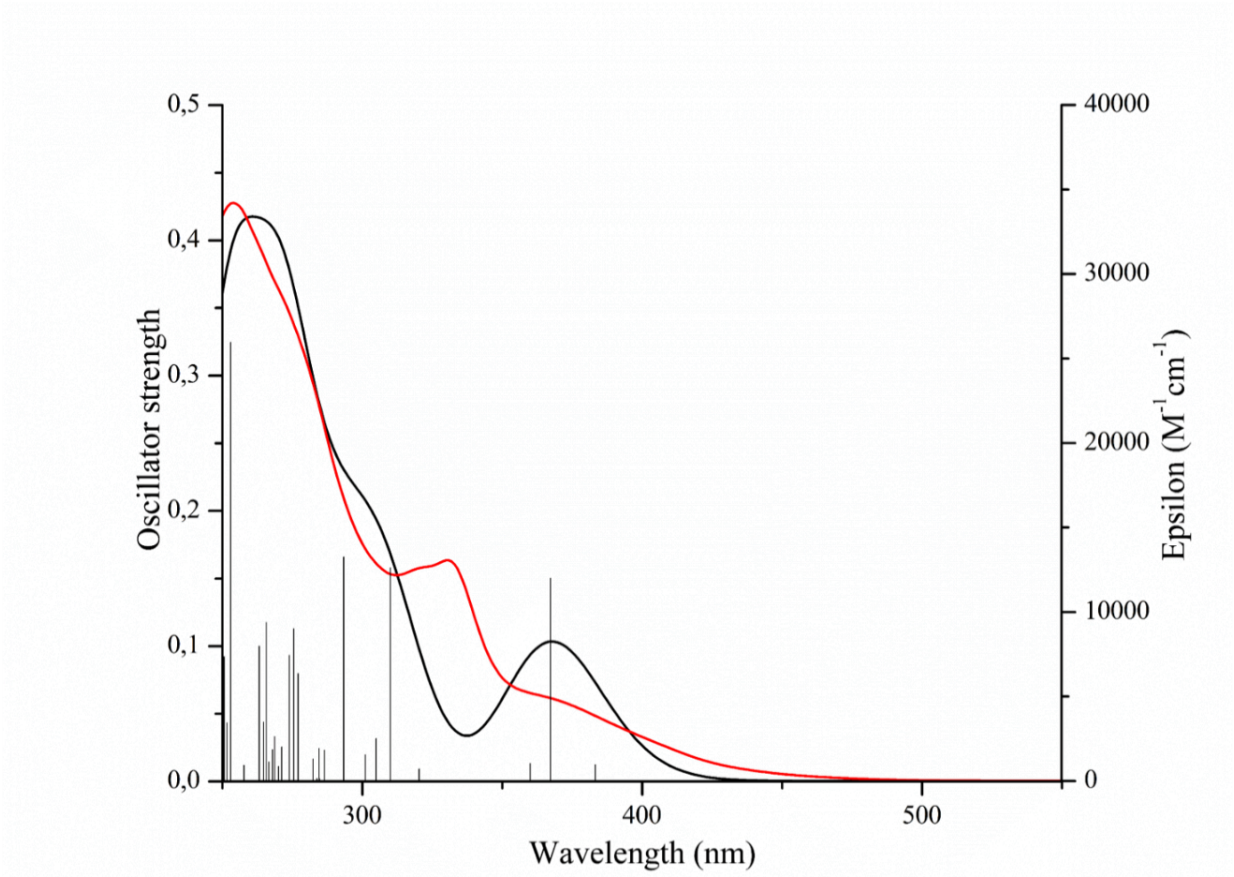

Figure 14.3 - TD-DFT simulated (red) and experimental (black) absorption spectrum (PBE0/LANL2DZ; CPCM: CH_3CN) of model complex **2**.

Table 14.5 - Atomic coordinates for DFT optimization of **5 (**Up-Up-Up isomer) in (*S* = 0) PBE0/LANL2DZ, CPCM(CH_3CN).

Standard orientation					
Center Number	Atomic Number	Atomic Type	Coordinates (Angstroms)		
			X	Y	Z
1	75	0	-4.044412	-5.193218	-0.166778
2	75	0	-2.477633	6.099183	-0.169220
3	75	0	6.524107	-0.908134	-0.174422
4	8	0	-3.267893	6.414940	2.811179
5	8	0	7.191849	-0.340941	2.798982
6	7	0	-4.074031	-4.547135	-2.215178
7	7	0	-4.336764	-3.025941	-0.040384
8	8	0	-3.884966	-6.059138	2.805588
9	7	0	-1.937238	-4.580777	-0.146318
10	8	0	-7.051825	-5.922558	-0.254543
11	7	0	4.788259	-2.238669	-0.050863
12	7	0	-0.458315	5.257103	-0.062342
13	7	0	-3.012846	3.972023	-0.134945
14	6	0	-6.137397	-3.524053	2.511316
15	7	0	-1.929680	5.781891	-2.221294
16	8	0	8.657954	-3.149247	-0.261114
17	8	0	-3.307027	-8.124837	-0.808271
18	8	0	-5.386187	6.943941	-0.783762
19	8	0	8.698014	1.193232	-0.812982

20	6	0	4.812739	-1.926289	-2.442850
21	7	0	5.983400	-1.258380	-2.223222
22	6	0	6.736815	-0.870085	-3.283551
23	6	0	6.349818	-1.118756	-4.599837
24	6	0	5.145202	-1.794279	-4.834235
25	6	0	4.373685	-2.205489	-3.743210
26	6	0	6.106200	-3.552317	2.508944
27	6	0	-3.642070	1.220101	-0.095821
28	6	0	1.346909	4.127835	1.070739
29	6	0	-4.875475	-2.923948	2.377678
30	6	0	-4.107067	-5.391370	-3.277700
31	6	0	-4.240265	-0.905561	1.105713
32	6	0	-2.923347	6.286382	1.687382
33	8	0	-1.588077	9.062262	-0.289022
34	6	0	-4.106457	-2.364376	-1.220917
35	6	0	6.907640	-0.589585	1.678438
36	6	0	1.757639	3.505414	-0.115818
37	6	0	-0.021989	4.707265	-1.242067
38	6	0	2.804194	-2.879648	-1.280256
39	6	0	-3.934528	-0.229814	-0.083517
40	6	0	-3.694050	3.394363	-1.159123
41	6	0	-4.126141	-4.928850	-4.593057
42	6	0	0.052370	7.102510	2.453326
43	6	0	4.102067	-2.368501	-1.232951

44	7	0	-0.347190	4.906299	3.399319
45	6	0	-1.099127	-4.879791	-1.173503
46	6	0	4.959850	-2.754293	2.369180
47	6	0	-1.433447	-3.879660	0.906038
48	6	0	-0.152442	7.692504	3.708258
49	6	0	2.897170	-3.206015	1.091777
50	6	0	1.069107	3.838501	-1.291305
51	6	0	0.759300	-3.748354	-0.112454
52	6	0	-2.955687	1.827890	0.970891
53	6	0	-3.905854	-0.984098	-1.265479
54	6	0	0.236057	-4.483100	-1.190858
55	6	0	-0.108495	-3.456959	0.955479
56	7	0	-4.012916	-2.783410	3.414928
57	6	0	0.261758	5.011814	1.069306
58	6	0	4.206607	-2.711380	1.088104
59	6	0	-0.337936	4.820523	-3.750847
60	6	0	-4.017886	2.039715	-1.174526
61	6	0	-2.652330	6.234397	-3.277387
62	6	0	-4.461834	-2.287710	1.099073
63	6	0	-4.273363	6.624681	-0.536805
64	6	0	-0.464712	6.873421	4.801822
65	6	0	-4.071419	-3.198887	-2.431970
66	6	0	-0.554333	5.487706	4.601303
67	6	0	2.162145	-3.279196	-0.099207

68	6	0	-1.924829	7.930031	-0.241241
69	7	0	4.404800	-2.075358	3.404046
70	6	0	7.840125	-2.296248	-0.226241
71	6	0	-3.593416	-7.005268	-0.551793
72	6	0	6.706395	-3.644163	3.772497
73	6	0	-2.657501	3.186369	0.918582
74	6	0	-5.904273	-5.640601	-0.219141
75	6	0	6.147208	-2.935126	4.844404
76	6	0	7.870117	0.386622	-0.557663
77	6	0	-0.058896	5.707596	2.343580
78	6	0	-1.089861	5.277326	-4.837532
79	6	0	-3.959735	-5.687674	1.685578
80	6	0	-6.518268	-4.004926	3.771801
81	6	0	-0.776279	5.086562	-2.447348
82	6	0	-4.386419	-3.261469	4.622123
83	6	0	-4.112425	-3.547095	-4.824255
84	6	0	-2.264391	6.001746	-4.596296
85	6	0	-5.627831	-3.875474	4.846413
86	6	0	-4.089256	-2.675879	-3.731155
87	6	0	4.999340	-2.161855	4.614037
88	7	0	4.941756	0.612654	-0.155930
89	6	0	4.762627	1.466344	-1.198191
90	6	0	3.748167	2.421000	-1.219548
91	6	0	2.867491	2.527584	-0.128685

92	6	0	3.069806	1.653893	0.954776
93	6	0	4.099246	0.718782	0.907897
94	1	0	4.816419	-2.005954	-5.845127
95	1	0	6.984053	-0.791003	-5.414035
96	1	0	7.663157	-0.356443	-3.065475
97	1	0	3.454369	-2.749863	-3.913548
98	1	0	0.851989	-4.771069	-2.034724
99	1	0	1.349962	3.383109	-2.231501
100	1	0	2.275506	-2.916030	-2.223675
101	1	0	3.675689	3.079998	-2.076837
102	1	0	5.452263	1.384197	-2.027286
103	1	0	7.588265	-4.259563	3.914380
104	1	0	6.499092	-4.104823	1.663013
105	1	0	4.535817	-1.599447	5.417906
106	1	0	6.581440	-2.980088	5.836694
107	1	0	2.484151	-3.550331	2.031953
108	1	0	-1.509115	-5.454540	-1.992816
109	1	0	0.222393	-2.883618	1.813484
110	1	0	-2.107553	-3.651816	1.722997
111	1	0	-4.123068	-6.450912	-3.061722
112	1	0	-4.154343	-5.640142	-5.409103
113	1	0	-4.128785	-3.154026	-5.834173
114	1	0	-4.102618	-1.607089	-3.898544
115	1	0	-6.809500	-3.587522	1.663074

116	1	0	-7.490369	-4.466012	3.909511
117	1	0	-5.884888	-4.234382	5.836539
118	1	0	-3.670478	-3.141500	5.428582
119	1	0	-4.338305	-0.377684	2.046348
120	1	0	-4.575950	1.649952	-2.017695
121	1	0	-3.674850	-0.505233	-2.207777
122	1	0	-3.989037	4.035069	-1.979082
123	1	0	-2.623590	1.256608	1.829801
124	1	0	-2.119252	3.655695	1.733325
125	1	0	0.583256	4.281391	-3.927776
126	1	0	-0.759126	5.080001	-5.850711
127	1	0	-2.872124	6.383330	-5.407226
128	1	0	-3.551106	6.792647	-3.053321
129	1	0	0.316194	7.703262	1.590402
130	1	0	-0.065762	8.767147	3.827118
131	1	0	-0.792804	4.820110	5.422732
132	1	0	-0.629973	7.291109	5.788437
133	1	0	1.869400	3.962197	2.004826
134	1	0	2.422927	1.670331	1.823982
135	1	0	4.251637	0.037890	1.736591

Table 14.6 - Atomic coordinates for DFT optimization of **5** (Up-Up-Down isomer) in (*S* = 0) PBE0/LANL2DZ, CPCM(CH_3CN).

Standard orientation					
Center Number	Atomic Number	Atomic Type	Coordinates (Angstroms)		
			X	Y	Z
1	75	0	-2.495212	6.099083	-0.000614
2	75	0	6.509258	-0.894622	-0.450075
3	75	0	-4.028220	-5.202086	0.285590
4	8	0	7.337798	-0.234772	2.462902
5	7	0	-2.109879	5.732889	-2.080994
6	7	0	-0.476953	5.251998	-0.032666
7	8	0	-3.057087	6.441545	3.028846
8	7	0	-3.049859	3.978347	0.096564
9	8	0	-1.584309	9.048629	-0.226517
10	7	0	-4.326195	-3.037640	0.172137
11	7	0	4.798020	-2.235768	-0.193118
12	7	0	4.914085	0.611249	-0.388384
13	6	0	0.235805	7.159837	2.397784
14	7	0	5.864079	-1.313529	-2.455937
15	8	0	-7.034644	-5.907800	0.503714
16	8	0	-5.427543	6.990509	-0.397847
17	8	0	8.625036	1.204383	-1.266767
18	8	0	-3.299780	-8.145030	0.886752
19	6	0	-4.981257	-2.942748	-2.219279

20	7	0	-4.157285	-2.805161	-3.287877
21	6	0	-4.575489	-3.284836	-4.479715
22	6	0	-5.825397	-3.896970	-4.657065
23	6	0	-6.675890	-4.022734	-3.550264
24	6	0	-6.248376	-3.540248	-2.305524
25	6	0	2.835793	2.519065	-0.280151
26	6	0	2.974137	-3.171998	1.077586
27	6	0	0.110346	5.763921	2.323578
28	6	0	-2.915812	6.154486	-3.088227
29	6	0	1.415104	4.155839	0.983319
30	6	0	6.993145	-0.518774	1.367940
31	8	0	8.649902	-3.126548	-0.585413
32	6	0	-0.132774	4.673204	-1.229110
33	6	0	2.177035	-3.295537	-0.068960
34	6	0	4.053625	-2.414541	-1.332692
35	6	0	-4.310432	-0.919017	-0.979553
36	6	0	1.730786	3.499947	-0.214359
37	6	0	4.658435	1.429574	-1.442907
38	6	0	-2.639791	5.875085	-4.426368
39	6	0	6.254244	-3.456104	2.336430
40	6	0	-4.519840	-2.302263	-0.959035
41	7	0	4.591164	-1.959251	3.269839
42	6	0	-3.888024	3.421252	-0.817186
43	6	0	-2.540613	3.170365	1.065853

44	6	0	6.918463	-3.504583	3.570019
45	6	0	-3.863434	-0.986771	1.370209
46	6	0	2.762673	-2.940982	-1.294617
47	6	0	-3.673793	1.220523	0.175432
48	6	0	3.112694	1.676820	0.811948
49	6	0	0.954423	3.804555	-1.341968
50	6	0	-4.220627	2.069232	-0.804328
51	6	0	-2.822675	1.809173	1.129274
52	7	0	-0.098464	4.984091	3.413728
53	6	0	4.279511	-2.674465	0.988404
54	6	0	-4.041683	-2.370241	1.337929
55	6	0	4.200164	-2.344198	-3.858499
56	6	0	3.638604	2.379065	-1.425536
57	6	0	6.553462	-0.945299	-3.566096
58	6	0	0.331880	5.039390	1.044237
59	6	0	7.820079	0.398967	-0.943667
60	6	0	6.409942	-2.764371	4.646047
61	6	0	-0.982326	5.021416	-2.378820
62	6	0	5.247245	-2.003902	4.449974
63	6	0	-3.955252	-0.232563	0.190056
64	6	0	7.830735	-2.275933	-0.531388
65	6	0	-5.887282	-5.635497	0.419919
66	6	0	-4.305384	6.649962	-0.235651
67	6	0	4.141009	0.743828	0.724446

68	6	0	-1.928754	7.921115	-0.137871
69	6	0	-3.579962	-7.020036	0.647441
70	6	0	5.097011	-2.668576	2.230254
71	6	0	4.907067	-1.956661	-5.000741
72	6	0	-2.798776	6.306273	1.883130
73	6	0	0.130295	7.774455	3.653280
74	6	0	4.697618	-2.010620	-2.592478
75	6	0	-0.210562	5.589049	4.616558
76	6	0	-1.492683	5.134622	-4.739595
77	6	0	6.105895	-1.247376	-4.851674
78	6	0	-0.100800	6.977852	4.783050
79	6	0	-0.655309	4.708844	-3.704153
80	7	0	-1.921685	-4.601504	0.166768
81	6	0	-1.484460	-3.834070	-0.868480
82	6	0	-0.166577	-3.401974	-0.973222
83	6	0	0.775617	-3.766527	0.006539
84	6	0	0.319896	-4.577660	1.062099
85	6	0	-1.016768	-4.966558	1.112748
86	1	0	-7.653342	-4.482009	-3.651197
87	1	0	-6.119597	-4.257040	-5.636362
88	1	0	-3.889424	-3.167636	-5.312098
89	1	0	-6.889305	-3.601223	-1.433346
90	1	0	-4.911888	1.704988	-1.554579
91	1	0	2.210997	-3.061078	-2.216886

92	1	0	-4.415116	-0.409134	-1.928813
93	1	0	0.095510	-2.765346	-1.809293
94	1	0	-2.206005	-3.561013	-1.628974
95	1	0	-3.643786	-0.499994	2.310493
96	1	0	-4.303067	4.075397	-1.572055
97	1	0	-2.348286	1.226457	1.909512
98	1	0	-1.891006	3.624020	1.804370
99	1	0	-3.790378	6.726474	-2.809535
100	1	0	-3.310908	6.233911	-5.196699
101	1	0	-1.248620	4.900186	-5.769302
102	1	0	0.244530	4.155563	-3.937702
103	1	0	0.437144	7.742986	1.506513
104	1	0	0.230958	8.850600	3.744449
105	1	0	-0.188314	7.414921	5.771218
106	1	0	-0.386761	4.938340	5.466767
107	1	0	2.009933	4.015203	1.877327
108	1	0	3.502212	3.009656	-2.296305
109	1	0	1.165821	3.327036	-2.289615
110	1	0	5.290207	1.323908	-2.314272
111	1	0	2.523682	1.715919	1.720651
112	1	0	4.348503	0.085802	1.559626
113	1	0	3.284848	-2.911263	-3.963956
114	1	0	4.532717	-2.211261	-5.985559
115	1	0	6.689866	-0.934421	-5.708181

116	1	0	7.477728	-0.404854	-3.412647
117	1	0	6.608153	-4.033080	1.489586
118	1	0	7.810411	-4.110814	3.686085
119	1	0	4.822164	-1.417466	5.257877
120	1	0	6.894203	-2.775736	5.615861
121	1	0	2.604749	-3.438865	2.059643
122	1	0	0.985279	-4.927943	1.841834
123	6	0	-3.933514	-3.203176	2.546333
124	6	0	-3.847000	-4.932095	4.708135
125	6	0	-3.866666	-2.680050	3.843815
126	7	0	-3.947814	-4.552073	2.331442
127	6	0	-3.911603	-5.395231	3.394445
128	6	0	-3.819075	-3.550369	4.936864
129	6	0	-4.024565	-5.696308	-1.568819
130	8	0	-3.993680	-6.067832	-2.690820
131	1	0	-3.864687	-1.611574	4.012258
132	1	0	-3.821427	-5.642934	5.524640
133	1	0	-3.769378	-3.156297	5.945288
134	1	0	-3.939111	-6.455104	3.181362
135	1	0	-1.373192	-5.588783	1.922692

Table 14.7 - Average MO composition of **5** in (*S=0*) ground state.

MO	Energy (eV)	Composition				
		Rhenium	4-pytpy			CO
			tpy	py	Σ py + tpy	
LUMO+5	-2.613	1	71	26	97	3
LUMO+4	-2.624	1	72	24	96	3
LUMO+3	-2.712	1	75	22	96	2
LUMO+2	-3.371	2	73	22	94	4
LUMO+1	-3.398	2	71	24	95	3
LUMO	**-3.404**	**3**	**67**	**25**	**92**	**6**
HOMO	**-7.379**	**59**	**11**	**5**	**16**	**25**
HOMO-1	-7.384	60	11	5	16	25
HOMO-2	-7.396	61	12	1	13	26
HOMO-3	-7.437	60	11	4	15	26
HOMO-4	-7.441	60	11	4	15	26
HOMO-5	-7.579	63	7	3	10	27

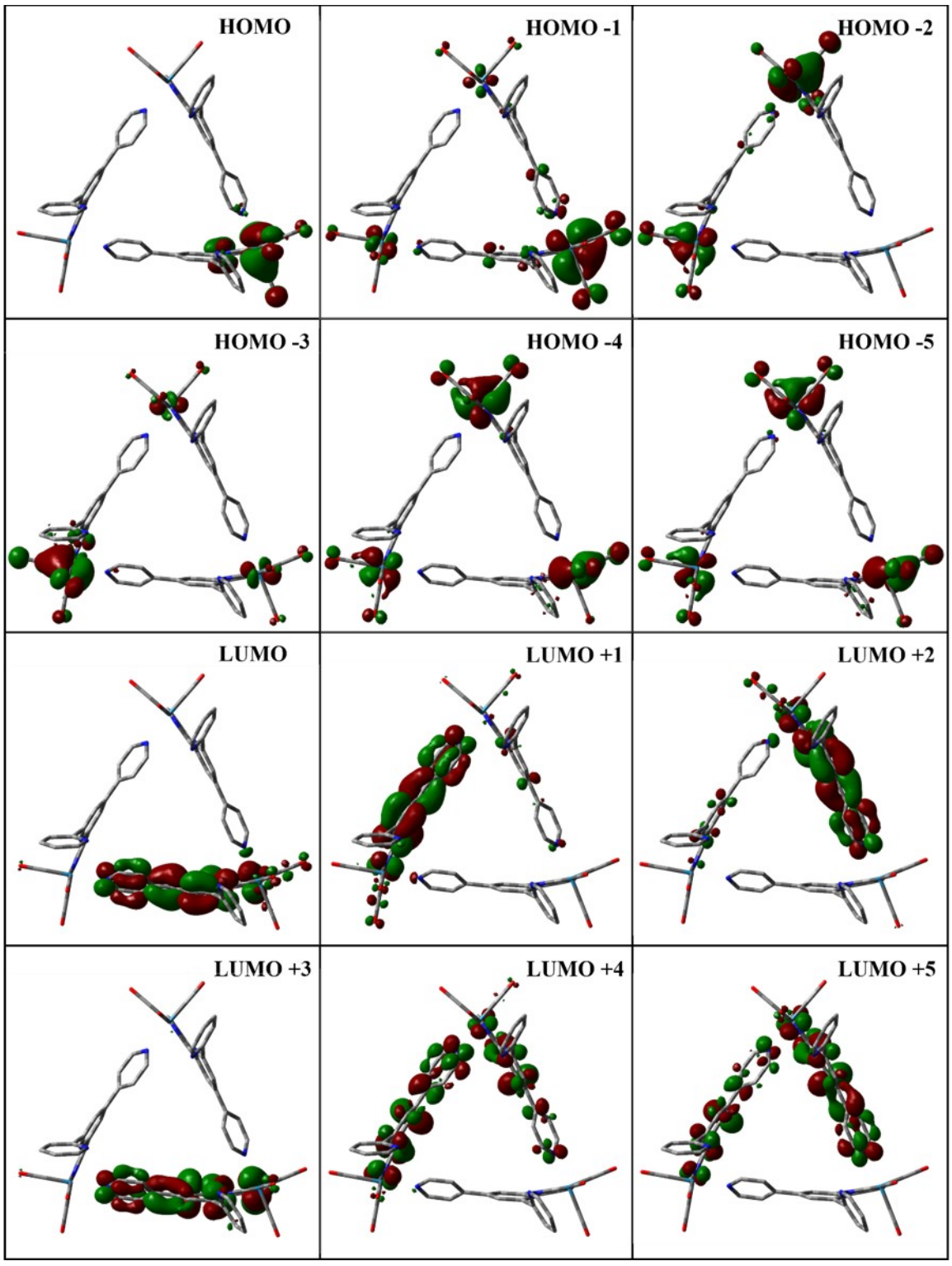

Figure 14.4 - Kohn-Sham electron density illustration of the molecular orbitals of **5 (**Up-Up-Up) in (*S=0*) ground state.

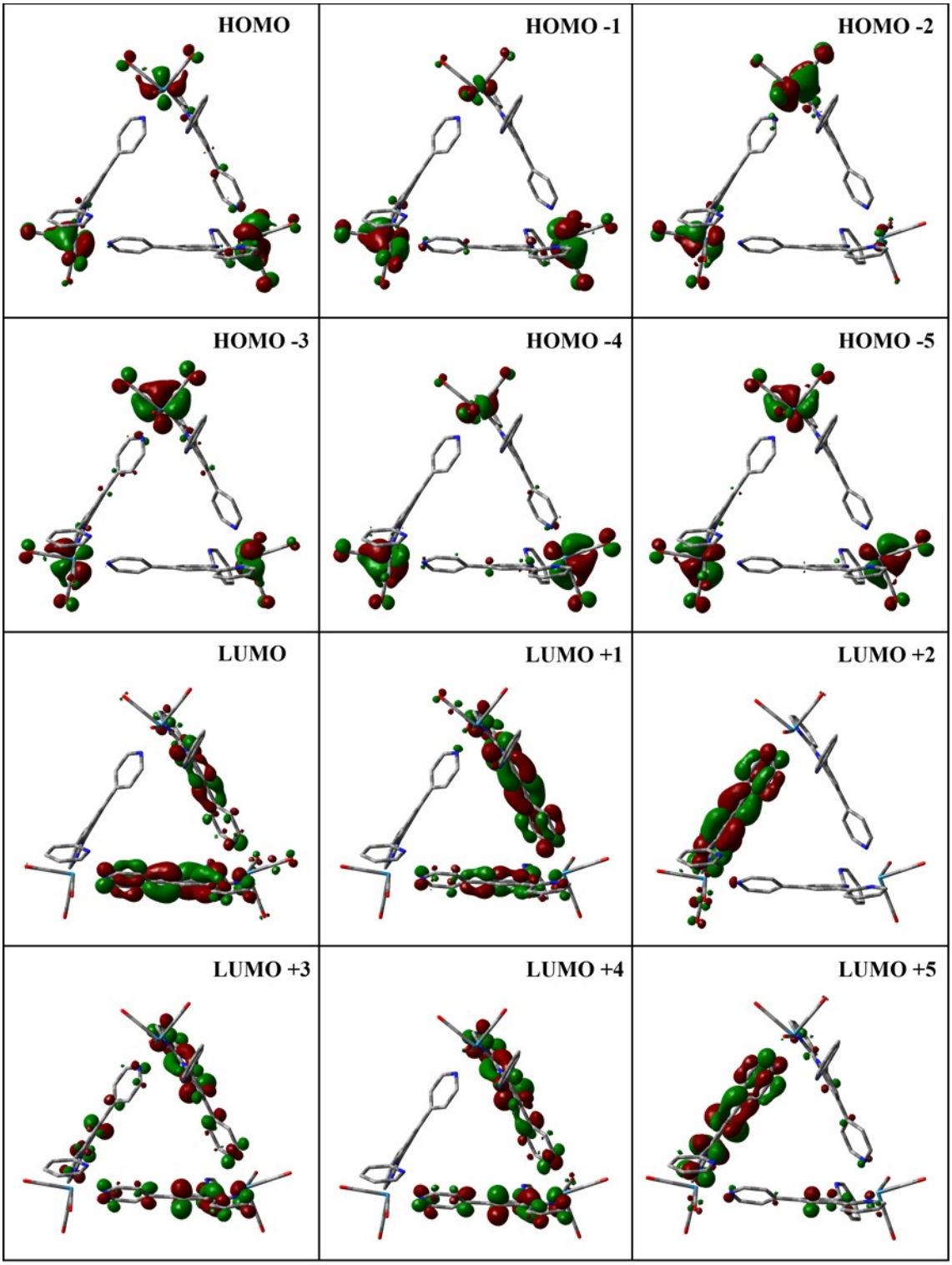

Figure 14.5 - Kohn-Sham electron density illustration of the molecular orbitals of **5 (**Up-Up-Down isomer) in (*S=0*) ground state.

Table 14.8 - Selected transitions from TD-DFT calculations of **5** (Up-Up-Up isomer) in the singlet ground state (PBE0), CPCM (CH_3CN).

Energy (eV)	λ (nm)	f	Transition	Character
3,28	376	0,2982	H-5→L+2 (16%) H-1→L+1 (11%) H→L (15%)	
3,28	376	0,2972	H-5→L+1 (17%) H-4→L+1 (10%) H-3→L+2 (10%) H-1→L (12%) H-1→L+2 (13%) H→L+1 (11%)	$^1MLCT_{tpy} + {}^1LLCT_{CO\rightarrow tpy}$
3,52	351	0,1654	H-5→L+1 (19%) H-3→L (19%) H-3→L+1 (14%) H-1→L (16%) H-1→L+1 (13%)	
3,52	350	0,185	H-5→L+2 (20%) H-4→L (23%) H→L (18%)	
3,85	321	0,2691	H-11→L (20%) H-11→L+1 (25%) H-9→L+2 (11%)	$^1ILCT_{tpy\rightarrow py}$
3,91	316	0,1061	H-14→L (16%) H-14→L+1 (37%) H-13→L+2 (11%)	

4,04	306	0,0853	H-3→L+3 (20%)	
4,04	305	0,0854	H-4→L+3 (21%)	
4,06	304	0,2115	H-5→L+3 (19%) H-4→L+4 (15%) H-3→L+5 (14%) H-1→L+5 (18%) H→L+4 (16%)	
4,38	282	0,0879	H-2→L+6 (10%)	
4,38	282	0,0872	H-2→L+7 (11%)	
4,42	279	0,0694	H-17→L+1 (17%) H-16→L (15%) H-15→L+2 (10%)	$^1MLCT_{tpy} + {}^1LLCT_{CO\rightarrow tpy}$
4,42	279	0,0696	H-16→L+2 (10%) H-15→L (16%)	
4,57	270	0,0758	H-14→L+3 (10%) H-14→L+4 (12%)	
4,72	261	0,1789	H-9→L+3 (16%)	
4,73	261	0,1723	H-11→L+3 (10%) H-11→L+4 (11%)	
4,73	261	0,0808	H-11→L+3 (14%)	
4,80	257	0,0763	H-23→L+2 (10%) H-22→L (23%) H-22→L+1 (11%) H-21→L+2 (19%)	$^1ILCT_{tpy\rightarrow py}$
4,80	257	0,0775	H-23→L (20%)	

			H-23→L+1 (13%) H-22→L+2 (13%) H-21→L+1 (17%)	
4,85	255	0,0799	H-2→L+8 (14%) H-1→L+7 (11%)	$^1MLCT_{tpy} + {}^1LLCT_{CO\rightarrow tpy}$
4,90	252	0,3301	H-24→L+1 (27%) H-21→L+1 (18%)	
4,90	252	0,3459	H-24→L+2 (28%) H-21→L+2 (19%)	
4,92	251	0,0563	H-12→L+3 (11%)	
4,93	251	0,1196	H-13→L+3 (13%)	$^1MLCT_{tpy}$
4,93	251	0,1053	H-14→L+3 (14%)	
5,24	235	0,0553	H-6→L+8 (12%)	
5,24	235	0,0834	H-8→L+8 (10%)	
5,25	235	0,0723	H-11→L+6 (11%) H-7→L+8 (13%)	

Table 14.9 - Selected transitions from TD-DFT calculations of **5** (Up-Up-Down isomer) in the singlet ground state (PBE0), CPCM (CH_3CN).

Energy (eV)	λ (nm)	f	Transition	Character
3,25	380	0,3528	H-5→L+1 (15%) H-4→L (18%) H-3→L+1 (10%) H-1→L+1 (11%) H→L (30%)	
3,28	377	0,2926	H-5→L+2 (14%) H-3→L+2 (24%) H-2→L+2 (11%) H-1→L+2 (22%)	$^1MLCT_{tpy} + {}^1LLCT_{CO\rightarrow tpy}$
3,46	357	0,1694	H-5→L+1 (21%) H-3→L (20%) H-1→L (14%)	
3,46	357	0,0665	H-5→L (27%) H-3→L+1 (14%) H-1→L+1 (12%)	
3,52	351	0,12	H-5→L+2 (21%) H-4→L+2 (24%) H→L+2 (28%)	
3,80	325	0,1393	H-11→L (57%) H-11→L+1 (18%)	$^1MLCT_{py} + {}^1ILCT_{tpy\rightarrow py}$
3,84	322	0,1103	H-10→L+2 (33%) H-9→L+2 (50%)	
3,94	313	0,0584	H-3→L+3 (15%)	$^1MLCT_{tpy} + {}^1LLCT_{CO\rightarrow tpy}$

			H-2→L+3 (24%)
			H-2→L+4 (27%)
3,97	311	0,0748	H-4→L+5 (12%) H-2→L+5 (11%) H-1→L+5 (15%) H→L+3 (21%) H→L+5 (16%)
4,00	309	0,1392	H-4→L+3 (17%) H-3→L+3 (11%)
4,01	308	0,0775	H-5→L+3 (10%) H-4→L+3 (12%) H-4→L+4 (15%) H→L+4 (18%)
4,05	305	0,1229	H-3→L+5 (18%) H-2→L+5 (10%) H-1→L+5 (16%)
4,35	284	0,0577	H→L+12 (14%)
4,35	284	0,1197	H-17→L+1 (13%) H-16→L (18%) H-15→L (17%)
4,36	283	0,0704	H-17→L (18%) H-17→L+1 (11%) H-16→L+1 (24%)
4,42	279	0,0621	H-16→L+2 (11%) H-15→L+2 (23%)
4,59	269	0,0514	H-19→L (22%)

			H-19→L+1 (21%)	
4,70	263	0,0607	H-17→L+2 (34%) H-16→L+2 (28%)	
4,70	262	0,0944	H-11→L+3 (19%) H-11→L+4 (12%)	
4,71	262	0,1976	H-17→L+2 (11%) H-16→L+2 (10%)	
4,72	261	0,1014	H-12→L+5 (13%) H-9→L+5 (15%)	$^1MLCT_{py} + {}^1ILCT_{tpy\rightarrow py}$
4,80	257	0,1222	H-24→L (10%) H-22→L+2 (12%) H-17→L+2 (11%) H-16→L+2 (11%) H-15→L+2 (17%)	
4,83	255	0,3712	H-24→L+1 (17%) H-21→L+1 (21%)	
4,87	253	0,0658	H-11→L+4 (16%)	
4,89	253	0,2574	H-24→L+2 (15%) H-21→L+2 (16%)	$^1MLCT_{tpy}$
5,05	244	0,0528	H-25→L (37%) H-25→L+1 (22%)	
5,13	240	0,0764	H-15→L+5 (10%)	
5,26	235	0,0618	H-26→L+2 (12%) H-25→L+2 (11%)	

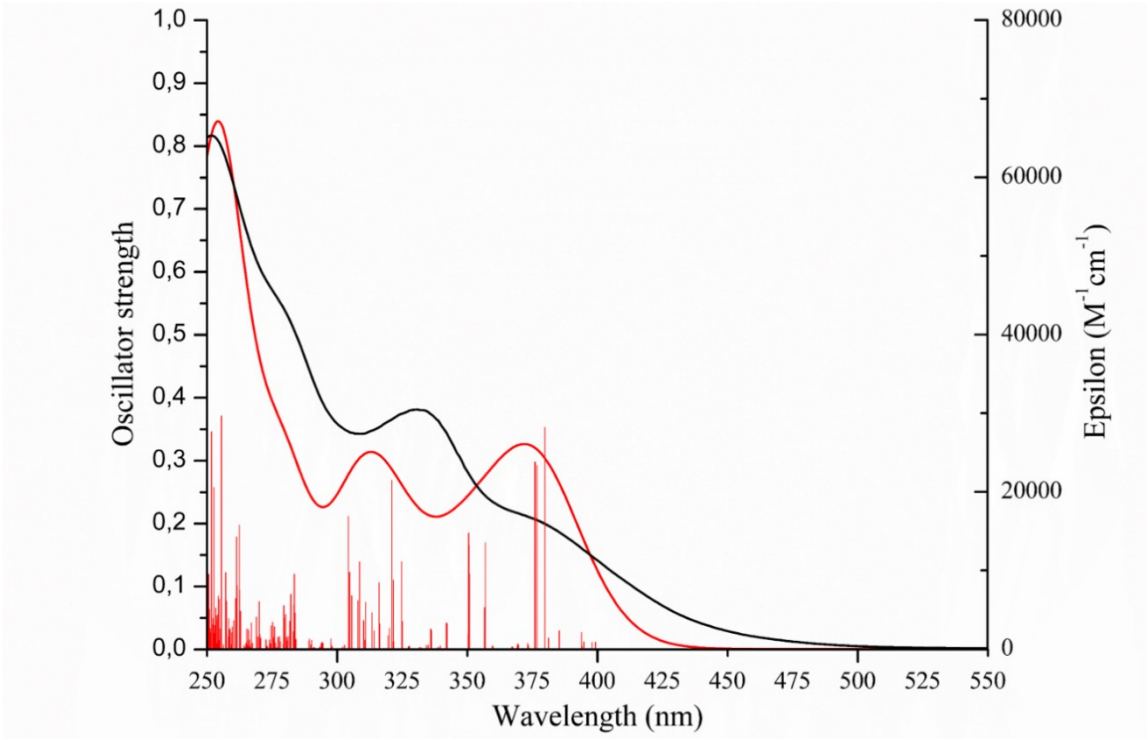

Figure 14.6 - TD-DFT simulated (red) and experimental (black) absorption spectrum (PBE0/LANL2DZ; CPCM: CH3CN) of model complex 5.

Table 14.10 - Atomic coordinates for DFT optimization of **6** (Up-Up-Up-Up isomer) in (S = 0) PBE0/LANL2DZ, CPCM(CH_3CN).

Standard orientation					
Center Number	Atomic Number	Atomic Type	Coordinates (Angstroms)		
			X	Y	Z
1	6	0	7.878290	-1.202849	3.299572
2	6	0	10.555283	-1.568427	2.776911
3	6	0	8.374484	-1.395604	2.000138
4	6	0	8.785082	-1.182559	4.368942
5	6	0	10.148171	-1.370209	4.106035

6	7	0	9.692567	-1.581971	1.739857
7	6	0	7.447984	-1.526984	0.844541
8	6	0	5.814533	-2.015279	-1.327368
9	6	0	6.424522	-2.478190	0.941275
10	7	0	7.624016	-0.785971	-0.288958
11	6	0	6.843135	-1.072104	-1.381441
12	6	0	5.570174	-2.722291	-0.142203
13	6	0	7.188329	-0.364337	-2.626111
14	6	0	8.099165	0.942131	-4.893551
15	6	0	6.608903	-0.654114	-3.868216
16	7	0	8.180122	0.568962	-2.515329
17	6	0	8.630239	1.198673	-3.629799
18	6	0	7.062818	0.007470	-5.013161
19	6	0	4.474065	-3.710765	-0.049870
20	7	0	2.379151	-5.602750	0.116258
21	6	0	4.609923	-4.888992	0.707180
22	6	0	3.252002	-3.509428	-0.714856
23	6	0	2.240161	-4.460592	-0.607312
24	6	0	3.560396	-5.800402	0.764135
25	75	0	0.800314	-7.119233	0.206784
26	7	0	-0.726488	-5.536777	0.220294
27	6	0	-3.167772	-4.121396	-0.004307
28	6	0	-1.312772	-5.325160	-1.005511
29	6	0	-1.311696	-4.978673	1.317948

30	6	0	-2.537372	-4.306283	1.232987
31	6	0	-2.510645	-4.624709	-1.138511
32	6	0	-4.461747	-3.411917	-0.119160
33	7	0	-6.933155	-2.055418	-0.346942
34	6	0	-5.347677	-3.672256	-1.181187
35	6	0	-4.862094	-2.451654	0.828451
36	6	0	-6.086893	-1.805542	0.686815
37	6	0	-6.554629	-2.984265	-1.264242
38	75	0	-8.853969	-1.008593	-0.528070
39	7	0	-7.624132	0.786082	-0.288989
40	6	0	-5.570282	2.722393	-0.142253
41	6	0	-6.843287	1.072239	-1.381500
42	6	0	-7.448065	1.527071	0.844515
43	6	0	-6.424615	2.478289	0.941235
44	6	0	-5.814676	2.015403	-1.327428
45	6	0	-8.374492	1.395584	2.000157
46	6	0	-10.148043	1.370055	4.106167
47	6	0	-7.878197	1.202914	3.299568
48	7	0	-9.692605	1.581820	1.739956
49	6	0	-10.555258	1.568194	2.777062
50	6	0	-8.784917	1.182560	4.368995
51	6	0	-7.188514	0.364486	-2.626168
52	6	0	-8.099379	-0.942018	-4.893572
53	7	0	-8.180162	-0.568951	-2.515327

54	6	0	-6.609274	0.654430	-3.868325
55	6	0	-7.063205	-0.007169	-5.013250
56	6	0	-8.630290	-1.198694	-3.629784
57	6	0	-4.474130	3.710822	-0.049917
58	7	0	-2.379137	5.602718	0.116295
59	6	0	-4.609871	4.888939	0.707328
60	6	0	-3.252129	3.509540	-0.715036
61	6	0	-2.240245	4.460653	-0.607440
62	6	0	-3.560309	5.800304	0.764328
63	75	0	-0.800302	7.119193	0.206829
64	7	0	0.726500	5.536742	0.220279
65	6	0	3.167786	4.121368	-0.004383
66	6	0	1.312745	5.325102	-1.005535
67	6	0	1.311726	4.978636	1.317914
68	6	0	2.537402	4.306245	1.232927
69	6	0	2.510619	4.624654	-1.138570
70	6	0	0.655233	5.019630	2.650860
71	6	0	-0.372358	4.949617	5.204926
72	7	0	1.409362	5.508209	3.666854
73	6	0	-0.616225	4.458297	2.852954
74	6	0	-1.134753	4.422202	4.154624
75	6	0	0.893718	5.481107	4.914432
76	6	0	4.461786	3.411967	-0.119233
77	7	0	6.933272	2.055583	-0.346986

78	6	0	5.347759	3.672417	-1.181196
79	6	0	4.862149	2.451675	0.828333
80	6	0	6.086986	1.805631	0.686724
81	6	0	6.554745	2.984478	-1.264248
82	75	0	8.853993	1.008618	-0.528097
83	6	0	-2.054509	8.520543	-0.095754
84	6	0	0.610765	8.414733	0.200063
85	6	0	9.300724	1.394481	1.296215
86	6	0	10.486973	0.026274	-0.736173
87	6	0	9.768080	2.614984	-0.986741
88	6	0	2.054431	-8.520622	-0.095872
89	6	0	-9.767894	-2.615022	-0.986686
90	6	0	-10.487041	-0.026435	-0.736161
91	6	0	-9.300702	-1.394447	1.296254
92	8	0	-11.503651	0.554324	-0.887853
93	8	0	-10.338726	-3.609303	-1.287691
94	8	0	-9.593669	-1.687204	2.404324
95	8	0	2.821034	-9.398674	-0.304526
96	8	0	11.503551	-0.554496	-0.888024
97	8	0	10.339093	3.609160	-1.287760
98	8	0	9.593666	1.687298	2.404275
99	8	0	-2.821213	9.398510	-0.304388
100	8	0	1.477774	9.216775	0.190965
101	6	0	-0.600243	-5.884274	-2.167719

102	6	0	0.920780	-6.954372	-4.221024
103	7	0	0.472308	-6.679431	-1.871671
104	6	0	-0.951062	-5.615327	-3.496039
105	6	0	-0.187180	-6.157519	-4.534572
106	6	0	1.218269	-7.195581	-2.879438
107	6	0	1.025961	-7.443943	2.085239
108	8	0	1.177232	-7.722217	3.224666
109	6	0	-0.610791	-8.414713	0.200101
110	8	0	-1.477804	-9.216752	0.191096
111	1	0	2.060893	-7.813078	-2.600676
112	6	0	-0.655139	-5.019655	2.650857
113	6	0	0.372584	-4.949621	5.204873
114	6	0	0.616403	-4.458480	2.852860
115	7	0	-1.409277	-5.508083	3.666918
116	6	0	-0.893573	-5.480974	4.914468
117	6	0	1.134996	-4.422367	4.154503
118	6	0	0.600187	5.884218	-2.167729
119	6	0	-0.920867	6.954359	-4.220988
120	7	0	-0.472284	6.679475	-1.871647
121	6	0	0.950890	5.615164	-3.496058
122	6	0	0.186988	6.157375	-4.534569
123	6	0	-1.218253	7.195654	-2.879393
124	1	0	1.798159	4.984863	-3.730471
125	1	0	0.449649	5.955010	-5.566517

126	1	0	-1.544949	7.386789	-4.993049
127	1	0	-2.060807	7.813234	-2.600613
128	6	0	-1.025934	7.443841	2.085313
129	8	0	-1.177167	7.721999	3.224774
130	1	0	-11.601307	1.724011	2.533676
131	1	0	-10.881744	1.367495	4.904259
132	1	0	-8.431991	1.024166	5.382311
133	1	0	-6.404936	-1.073592	1.416603
134	1	0	-6.816369	1.061064	3.471380
135	1	0	-0.737724	4.942593	6.225536
136	1	0	1.519737	5.889146	5.701306
137	1	0	-7.241643	-3.185074	-2.075029
138	1	0	-5.130845	-4.418723	-1.935718
139	1	0	4.232651	2.179774	1.666806
140	1	0	6.405048	1.073680	1.416505
141	1	0	7.241783	3.185386	-2.074991
142	1	0	5.130951	4.418921	-1.935700
143	1	0	2.930952	4.469445	-2.122458
144	1	0	-1.519610	-5.888879	5.701397
145	1	0	0.737997	-4.942586	6.225466
146	1	0	2.111196	-3.987815	4.341270
147	1	0	6.313106	-3.022242	1.871294
148	1	0	6.816493	-1.060861	3.471455
149	1	0	8.432241	-1.024099	5.382277

150	1	0	10.881916	-1.367702	4.904086
151	1	0	11.601301	-1.724360	2.533463
152	1	0	2.973762	3.943628	2.155050
153	1	0	5.822914	-1.391926	-3.956969
154	1	0	6.621755	-0.210321	-5.978995
155	1	0	8.491907	1.467283	-5.755272
156	1	0	9.429342	1.915720	-3.498696
157	1	0	5.218734	-2.215088	-2.207710
158	1	0	5.528389	-5.124459	1.231826
159	1	0	3.062651	-2.614362	-1.295820
160	1	0	1.295153	-4.300481	-1.105544
161	1	0	1.169989	-4.035790	2.023604
162	1	0	3.660174	-6.714358	1.333747
163	1	0	-0.449940	-5.955248	-5.566512
164	1	0	1.544867	-7.386748	-4.993111
165	1	0	-2.931040	-4.469520	-2.122367
166	1	0	-1.798408	-4.985123	-3.730435
167	1	0	-2.973706	-3.943606	2.155094
168	1	0	-4.232610	-2.179842	1.666964
169	1	0	-6.313162	3.022307	1.871271
170	1	0	-2.110891	3.987542	4.341468
171	1	0	-9.429279	-1.915858	-3.498633
172	1	0	-8.492104	-1.467210	-5.755277
173	1	0	-6.622301	0.210754	-5.979127

174	1	0	-5.823431	1.392392	-3.957121
175	1	0	-5.218885	2.215210	-2.207773
176	1	0	-3.062828	2.614528	-1.296102
177	1	0	-5.528267	5.124338	1.232125
178	1	0	-3.659983	6.714159	1.334120
179	1	0	-1.169795	4.035482	2.023747
180	1	0	-1.295276	4.300562	-1.105755

Table 14.11 - Atomic coordinates for DFT optimization of **6** (Up-Up-Up-Down isomer) in (S = 0) PBE0/LANL2DZ, CPCM(CH_3CN).

Standard orientation					
Center Number	Atomic Number	Atomic Type	Coordinates (Angstroms)		
			X	Y	Z
1	6	0	7.355348	-1.448133	3.790965
2	6	0	10.086655	-1.752508	3.644697
3	6	0	8.038900	-1.552664	2.568827
4	6	0	8.096246	-1.488696	4.980883
5	6	0	9.486588	-1.645294	4.909636
6	7	0	9.384224	-1.708315	2.493919
7	6	0	7.297461	-1.615019	1.282042
8	6	0	6.017075	-1.968222	-1.141773
9	6	0	6.265045	-2.555723	1.168554
10	7	0	7.655990	-0.826980	0.227313
11	6	0	7.059499	-1.051830	-0.988691

12	6	0	5.586054	-2.726421	-0.044819
13	6	0	7.629355	-0.316203	-2.130265
14	6	0	8.966958	1.019556	-4.156182
15	6	0	7.291287	-0.573793	-3.465155
16	7	0	8.592333	0.599938	-1.814652
17	6	0	9.253393	1.243856	-2.810005
18	6	0	7.960176	0.103853	-4.489036
19	6	0	4.479884	-3.699272	-0.174205
20	7	0	2.361811	-5.554566	-0.416110
21	6	0	4.537216	-4.958545	0.449993
22	6	0	3.329741	-3.400140	-0.923937
23	6	0	2.300632	-4.335336	-1.014008
24	6	0	3.480352	-5.851176	0.302914
25	75	0	0.748897	-7.028593	-0.596004
26	7	0	-0.735927	-5.437324	-0.280870
27	6	0	-3.166165	-3.994652	-0.203925
28	6	0	-1.345252	-5.014468	-1.438951
29	6	0	-1.287749	-5.069270	0.909698
30	6	0	-2.505745	-4.382456	0.968594
31	6	0	-2.545635	-4.303059	-1.424822
32	6	0	-4.457432	-3.275657	-0.142524
33	7	0	-6.945642	-1.946315	0.035501
34	6	0	-5.439431	-3.423876	-1.138343
35	6	0	-4.758631	-2.425274	0.937090

36	6	0	-5.993095	-1.788633	0.993221
37	6	0	-6.655333	-2.752843	-1.019072
38	75	0	-8.901089	-0.976148	0.261744
39	7	0	-7.679091	0.844169	0.324410
40	6	0	-5.621442	2.764391	0.115760
41	6	0	-7.195174	1.229459	-0.899928
42	6	0	-7.213447	1.484908	1.437121
43	6	0	-6.166879	2.412986	1.357668
44	6	0	-6.181953	2.182986	-1.027945
45	6	0	-7.854608	1.275466	2.761972
46	6	0	-9.109566	1.113123	5.207863
47	6	0	-7.080465	1.009755	3.903011
48	7	0	-9.196985	1.466497	2.816095
49	6	0	-9.803942	1.385785	4.018196
50	6	0	-7.723587	0.920046	5.145826
51	6	0	-7.817485	0.594013	-2.072916
52	6	0	-9.192847	-0.623025	-4.146218
53	7	0	-8.698014	-0.413120	-1.798015
54	6	0	-7.590108	1.013554	-3.389995
55	6	0	-8.279647	0.398135	-4.438813
56	6	0	-9.375210	-1.001768	-2.816620
57	6	0	-4.508864	3.734171	0.015079
58	7	0	-2.375405	5.576530	-0.171225
59	6	0	-4.517193	4.764619	-0.942031

60	6	0	-3.399530	3.654042	0.873120
61	6	0	-2.359093	4.571981	0.743964
62	6	0	-3.455025	5.661830	-0.997581
63	75	0	-0.764253	7.063612	-0.308605
64	7	0	0.733481	5.453954	-0.283218
65	6	0	3.159181	4.024045	-0.057505
66	6	0	1.289788	4.852626	-1.373321
67	6	0	1.337435	5.274809	0.938341
68	6	0	2.530261	4.562091	1.074986
69	6	0	2.510155	4.172275	-1.289574
70	6	0	0.603342	4.847658	-2.691404
71	6	0	-0.486592	4.687393	-5.214860
72	7	0	1.333717	5.296922	-3.742348
73	6	0	-0.672713	4.280916	-2.841705
74	6	0	-1.223910	4.199610	-4.127969
75	6	0	0.787524	5.224959	-4.975046
76	6	0	0.663111	5.901039	2.088938
77	6	0	-0.779169	7.105473	4.125284
78	6	0	1.041702	5.687556	3.419662
79	7	0	-0.400917	6.704683	1.781262
80	6	0	-1.107017	7.288104	2.781455
81	6	0	0.317454	6.297156	4.449451
82	6	0	4.458293	3.322284	0.033511
83	7	0	6.945776	1.991772	0.168418

84	6	0	5.429834	3.485582	-0.969579
85	6	0	4.774246	2.474753	1.110214
86	6	0	6.008401	1.829016	1.140407
87	6	0	6.647594	2.819671	-0.867887
88	75	0	8.893374	0.979730	0.273488
89	6	0	-2.009000	8.483897	-0.050793
90	6	0	0.660877	8.341740	-0.352867
91	6	0	-0.987377	7.330373	-2.195070
92	6	0	9.022587	1.292794	2.159786
93	6	0	10.559643	0.033281	0.310581
94	6	0	9.827260	2.621715	0.032909
95	6	0	1.979223	-8.373510	-1.150681
96	6	0	-9.831724	-2.600110	-0.086899
97	6	0	-10.566308	-0.046642	0.446474
98	6	0	-8.966388	-1.461405	2.114664
99	8	0	-11.600792	0.512910	0.550785
100	8	0	-10.410352	-3.607432	-0.321298
101	8	0	-9.032127	-1.817392	3.241090
102	8	0	2.735254	-9.208316	-1.515600
103	8	0	11.601156	-0.522628	0.314204
104	8	0	10.406385	3.641737	-0.136089
105	8	0	9.125701	1.535684	3.313383
106	8	0	-2.774848	9.368984	0.126284
107	8	0	-1.130123	7.576217	-3.343533

108	8	0	1.535232	9.135625	-0.375121
109	1	0	-10.074035	-1.784286	-2.553589
110	1	0	-9.756965	-1.119957	-4.925606
111	1	0	-8.113334	0.716563	-5.461447
112	1	0	-6.899612	1.817963	-3.605238
113	1	0	-5.800018	2.441367	-2.006688
114	1	0	-5.825316	2.893683	2.266640
115	1	0	-7.152648	0.704855	6.042594
116	1	0	-9.644925	1.058635	6.148958
117	1	0	-10.876898	1.548196	4.026085
118	1	0	-2.918137	-4.174828	1.947943
119	1	0	-2.997769	-3.991932	-2.357222
120	1	0	-5.291802	-4.076545	-1.990666
121	1	0	-7.421610	-2.876073	-1.772493
122	1	0	-4.044547	-2.237683	1.729747
123	1	0	-6.235003	-1.145661	1.828363
124	1	0	7.407702	2.958822	-1.624039
125	1	0	4.069473	2.288410	1.912302
126	1	0	6.259136	1.169617	1.960705
127	1	0	5.264828	4.143378	-1.814795
128	1	0	2.914033	3.737808	-2.195694
129	1	0	2.995636	4.468799	2.047293
130	1	0	1.879972	5.048244	3.662374
131	1	0	0.601931	6.137964	5.483150

132	1	0	-1.372261	7.590153	4.890714
133	1	0	-1.943291	7.910266	2.493916
134	1	0	-3.319729	2.873249	1.620697
135	1	0	-1.494031	4.498800	1.386092
136	1	0	-5.348466	4.896185	-1.624994
137	1	0	-3.461715	6.471968	-1.713801
138	1	0	-2.204862	3.760465	-4.275281
139	1	0	-0.877031	4.645021	-6.225300
140	1	0	1.394732	5.601772	-5.791685
141	1	0	10.020406	1.946515	-2.513098
142	1	0	9.521426	1.554432	-4.917167
143	1	0	7.707001	-0.088125	-5.525337
144	1	0	6.530465	-1.300674	-3.715813
145	1	0	5.556769	-2.111439	-2.110453
146	1	0	6.005721	-3.148788	2.037412
147	1	0	3.208242	-2.441487	-1.414742
148	1	0	5.401719	-5.265635	1.026871
149	1	0	3.522157	-6.828357	0.764317
150	1	0	1.405830	-4.099448	-1.570972
151	1	0	10.095990	-1.686837	5.805249
152	1	0	11.159901	-1.881103	3.547667
153	1	0	7.596683	-1.398953	5.939476
154	1	0	-6.007608	0.867763	3.825120
155	1	0	-1.201667	3.886040	-1.983189

156	1	0	6.277884	-1.324020	3.813348
157	6	0	-0.655369	-5.366118	-2.692589
158	6	0	0.816314	-6.084104	-4.927280
159	7	0	0.401570	-6.224730	-2.559833
160	6	0	-1.007873	-4.847244	-3.943995
161	6	0	-0.268475	-5.210971	-5.074465
162	6	0	1.121325	-6.570602	-3.655633
163	6	0	0.966735	-7.685181	1.193990
164	8	0	1.104285	-8.163443	2.267089
165	6	0	-0.686037	-8.277516	-0.821211
166	8	0	-1.565915	-9.052198	-0.965691
167	1	0	-1.835051	-4.157413	-4.045921
168	1	0	-0.531903	-4.813993	-6.048049
169	1	0	1.419532	-6.386800	-5.774108
170	1	0	1.950636	-7.247987	-3.504846
171	6	0	-0.602670	-5.338893	2.200387
172	6	0	0.486827	-5.704504	4.702736
173	6	0	0.683805	-4.838569	2.457339
174	7	0	-1.343619	-5.972162	3.143446
175	6	0	-0.797925	-6.157580	4.364294
176	6	0	1.235018	-5.025058	3.732536
177	1	0	-1.414172	-6.676153	5.091558
178	1	0	0.876651	-5.871726	5.700368
179	1	0	2.224152	-4.643033	3.961370

180	1	0	1.221840	-4.291838	1.693137

Table 14.12 - Atomic coordinates for DFT optimization of **6** (Up-Up-Down-Down isomer) in ($S = 0$) PBE0/LANL2DZ, CPCM(CH_3CN).

Standard orientation					
Center Number	Atomic Number	Atomic Type	Coordinates (Angstroms)		
			X	Y	Z
1	6	0	6.114146	-2.388514	1.096669
2	6	0	4.859167	-3.067244	-1.251124
3	6	0	5.106522	-3.355062	1.112521
4	7	0	6.510266	-1.770224	-0.066331
5	6	0	5.870374	-2.100547	-1.222373
6	6	0	4.454074	-3.711700	-0.075715
7	6	0	3.350198	-4.695518	-0.091539
8	7	0	1.203410	-6.537160	-0.133442
9	6	0	3.355367	-5.841840	0.723578
10	6	0	2.237997	-4.505003	-0.928820
11	6	0	1.197068	-5.428956	-0.919881
12	6	0	2.284704	-6.730691	0.672934
13	75	0	-0.447412	-7.985994	-0.160040
14	7	0	-1.839129	-6.294643	-0.042854
15	6	0	-3.905761	-4.372868	-0.177746
16	6	0	-2.346945	-5.884635	-1.253527
17	6	0	-2.342575	-5.732846	1.092077

18	6	0	-3.396376	-4.811644	1.050255
19	6	0	-3.351873	-4.919888	-1.342681
20	6	0	-4.944767	-3.321460	-0.232900
21	7	0	-6.832171	-1.218567	-0.240097
22	6	0	-4.836038	-2.247084	-1.131357
23	6	0	-6.047842	-3.329311	0.639201
24	6	0	-6.964689	-2.282884	0.600195
25	6	0	-5.778952	-1.221767	-1.098555
26	75	0	-8.251157	0.457829	-0.141152
27	7	0	-6.510231	1.770368	0.066972
28	6	0	-4.454289	3.712119	0.076287
29	6	0	-6.114211	2.388689	-1.096046
30	6	0	-5.870349	2.100786	1.222994
31	6	0	-4.859307	3.067662	1.251723
32	6	0	-5.106687	3.355335	-1.111936
33	6	0	-6.191074	1.440156	2.520823
34	6	0	-6.611702	0.419834	5.041805
35	6	0	-5.711315	0.154943	2.816576
36	7	0	-6.836473	2.210742	3.430115
37	6	0	-7.047449	1.698461	4.662310
38	6	0	-5.927651	-0.362195	4.101895
39	6	0	-6.784321	1.941920	-2.329990
40	6	0	-8.078201	0.899443	-4.548193
41	7	0	-7.720146	0.956738	-2.167135

42	6	0	-6.488084	2.447666	-3.601490
43	6	0	-7.141533	1.925402	-4.722392
44	6	0	-8.344586	0.444146	-3.256592
45	6	0	-3.350483	4.696020	0.092005
46	7	0	-1.203602	6.537575	0.133328
47	6	0	-3.355595	5.842093	-0.723464
48	6	0	-2.238348	4.505788	0.929445
49	6	0	-1.197381	5.429700	0.920232
50	6	0	-2.284880	6.730893	-0.673119
51	75	0	0.447497	7.986092	0.159084
52	7	0	1.838946	6.294453	0.042385
53	6	0	3.905618	4.372761	0.177748
54	6	0	2.342137	5.732107	-1.092389
55	6	0	2.347011	5.885006	1.253146
56	6	0	3.351922	4.920260	1.342549
57	6	0	3.395987	4.810973	-1.050354
58	6	0	1.760953	6.015251	-2.434116
59	6	0	0.880029	6.360626	-5.018613
60	7	0	2.586350	6.620375	-3.322667
61	6	0	0.486648	5.538774	-2.782126
62	6	0	0.042287	5.714601	-4.099961
63	6	0	2.141735	6.796491	-4.586241
64	6	0	1.758475	6.508700	2.450932
65	6	0	0.475552	7.726996	4.583738

66	6	0	2.139486	6.186919	3.759198
67	7	0	0.778287	7.432916	2.212485
68	6	0	0.148169	8.020756	3.259694
69	6	0	1.494933	6.801399	4.837559
70	6	0	4.944700	3.321439	0.233133
71	7	0	6.832229	1.218657	0.240685
72	6	0	6.047626	3.329074	-0.639152
73	6	0	4.836199	2.247363	1.131974
74	6	0	5.779171	1.222088	1.099342
75	6	0	6.964541	2.282717	-0.599965
76	75	0	8.251228	-0.457749	0.141869
77	6	0	-0.755445	9.413024	0.546925
78	6	0	1.920531	9.205945	0.252128
79	6	0	0.250896	8.458767	-1.689494
80	6	0	9.434401	-1.962417	0.102232
81	6	0	9.705877	0.684424	0.607753
82	6	0	0.755880	-9.412525	-0.548283
83	6	0	-9.705840	-0.684327	-0.606970
84	6	0	-9.434336	1.962493	-0.101451
85	6	0	-8.714087	0.127558	1.689819
86	8	0	-10.167061	2.888875	-0.082075
87	8	0	-10.603791	-1.392278	-0.912640
88	8	0	-9.094579	-0.079862	2.790857
89	8	0	1.499309	-10.296625	-0.807339

90	8	0	10.167124	-2.888802	0.082888
91	8	0	10.603795	1.392400	0.913462
92	8	0	-1.498625	10.297425	0.805673
93	8	0	0.124577	8.844705	-2.800723
94	8	0	2.826267	9.961497	0.315388
95	1	0	-9.070627	-0.337991	-3.083931
96	1	0	-8.600721	0.459485	-5.388428
97	1	0	-6.919318	2.311155	-5.710626
98	1	0	-5.757611	3.234741	-3.731269
99	1	0	-4.805259	3.806756	-2.047598
100	1	0	-4.405302	3.305247	2.206156
101	1	0	-5.564058	-1.350791	4.361341
102	1	0	-6.797554	0.058647	6.046967
103	1	0	-7.572624	2.338299	5.363986
104	1	0	-3.761852	-4.405314	1.985603
105	1	0	-3.721504	-4.607305	-2.310084
106	1	0	-4.007824	-2.172368	-1.826581
107	1	0	-5.681010	-0.381448	-1.769350
108	1	0	-6.208649	-4.140686	1.339661
109	1	0	-7.821421	-2.284956	1.259781
110	1	0	7.821155	2.284636	-1.259704
111	1	0	4.008114	2.172826	1.827371
112	1	0	5.681401	0.381990	1.770438
113	1	0	6.208256	4.140226	-1.339909

114	1	0	3.761296	4.404240	-1.985591
115	1	0	3.721711	4.608067	2.310021
116	1	0	2.924209	5.467303	3.949368
117	1	0	1.782965	6.558641	5.853906
118	1	0	-0.055907	8.220638	5.387756
119	1	0	-0.624589	8.740057	3.027284
120	1	0	-2.153575	3.635322	1.569211
121	1	0	-0.340523	5.273392	1.557597
122	1	0	-4.187477	6.067106	-1.380759
123	1	0	-2.285772	7.620528	-1.288154
124	1	0	-0.934594	5.350786	-4.400182
125	1	0	0.574496	6.516641	-6.047028
126	1	0	2.823539	7.292156	-5.269639
127	1	0	4.405118	-3.304739	-2.205560
128	1	0	4.805051	-3.806512	2.048156
129	1	0	2.153174	-3.634319	-1.568283
130	1	0	4.187283	-6.067027	1.380772
131	1	0	2.285675	-7.620555	1.287637
132	1	0	0.340154	-5.272422	-1.557112
133	1	0	-5.160014	-0.410103	2.074146
134	1	0	-0.124540	5.020587	-2.052699
135	6	0	-1.758142	-6.507737	-2.451490
136	6	0	-0.474827	-7.725079	-4.584602
137	7	0	-0.777985	-7.432045	-2.213273

138	6	0	-2.138873	-6.185322	-3.759684
139	6	0	-1.494126	-6.799330	-4.838198
140	6	0	-0.147682	-8.019425	-3.260629
141	6	0	-0.250944	-8.459394	1.688362
142	8	0	-0.124829	-8.845774	2.799460
143	6	0	-1.920176	-9.206118	-0.253832
144	8	0	-2.825747	-9.961832	-0.317523
145	1	0	-2.923510	-5.465565	-3.949692
146	1	0	-1.781941	-6.556090	-5.854492
147	1	0	0.056773	-8.218371	-5.388742
148	1	0	0.625040	-8.738822	-3.028399
149	6	0	-1.761768	-6.016738	2.433815
150	6	0	-0.881651	-6.363552	5.018389
151	6	0	-0.487696	-5.540172	2.782562
152	7	0	-2.587310	-6.622664	3.321683
153	6	0	-2.143085	-6.799482	4.585298
154	6	0	-0.043751	-5.716732	4.100439
155	1	0	-2.824991	-7.295778	5.268135
156	1	0	-0.576435	-6.520136	6.046812
157	1	0	0.932935	-5.352867	4.401234
158	1	0	0.123628	-5.021394	2.053669
159	6	0	6.784272	-1.941829	2.330635
160	6	0	8.078211	-0.899527	4.548887
161	7	0	7.720148	-0.956688	2.167826

162	6	0	6.488007	-2.447617	3.602112
163	6	0	7.141485	-1.925441	4.723038
164	6	0	8.344620	-0.444182	3.257308
165	1	0	5.757493	-3.234660	3.731852
166	1	0	6.919251	-2.311230	5.711254
167	1	0	8.600757	-0.459639	5.389142
168	1	0	9.070702	0.337923	3.084683
169	6	0	8.714277	-0.127504	-1.689074
170	8	0	9.094826	0.079912	-2.790093
171	6	0	6.191339	-1.440088	-2.520235
172	6	0	6.612446	-0.420174	-5.041302
173	7	0	6.837015	-2.210777	-3.429246
174	6	0	5.711541	-0.154966	-2.816319
175	6	0	5.928125	0.361964	-4.101681
176	6	0	7.048220	-1.698696	-4.661484
177	1	0	5.160033	0.410165	-2.074108
178	1	0	5.564511	1.350487	-4.361380
179	1	0	6.798487	-0.059149	-6.046487
180	1	0	7.573610	-2.338610	-5.362931

Table 14.13 - Atomic coordinates for DFT optimization of **6** (Up-Down-Up-Down isomer) in ($S = 0$) PBE0/LANL2DZ, CPCM(CH_3CN).

Standard orientation					
Center Number	Atomic Number	Atomic Type	Coordinates (Angstroms)		
			X	Y	Z
1	6	0	6.069974	-0.883928	4.072224
2	6	0	8.729826	-1.542274	4.328604
3	6	0	6.855618	-1.290488	2.982351
4	6	0	6.670047	-0.796289	5.337039
5	6	0	8.023115	-1.133126	5.470551
6	7	0	8.165315	-1.622072	3.105712
7	6	0	6.245855	-1.513255	1.643139
8	6	0	5.197868	-2.196964	-0.813337
9	6	0	5.200518	-2.443007	1.565964
10	7	0	6.741725	-0.900388	0.528658
11	6	0	6.234023	-1.268396	-0.692848
12	6	0	4.656793	-2.806614	0.326663
13	6	0	6.901967	-0.698161	-1.875375
14	6	0	8.408345	0.322054	-3.966918
15	6	0	6.588533	-1.059293	-3.192614
16	7	0	7.922361	0.170864	-1.611847
17	6	0	8.665764	0.657756	-2.638369
18	6	0	7.342328	-0.541585	-4.249737

19	6	0	3.628924	-3.864813	0.201071
20	7	0	1.841451	-6.021677	-0.177693
21	6	0	3.625435	-4.973775	1.066296
22	6	0	2.665176	-3.845181	-0.824030
23	6	0	1.797726	-4.923893	-0.978942
24	6	0	2.732559	-6.019786	0.848651
25	75	0	0.692174	-7.834572	-0.665411
26	7	0	-1.077657	-6.548045	-0.586270
27	6	0	-3.192220	-4.719818	-0.153735
28	6	0	-1.736181	-5.982267	-1.640260
29	6	0	-1.504760	-6.246873	0.683255
30	6	0	-2.548637	-5.348620	0.918890
31	6	0	-2.764736	-5.051921	-1.446154
32	6	0	-4.312285	-3.777812	0.060085
33	7	0	-6.464622	-1.983270	0.443050
34	6	0	-4.469102	-2.640839	-0.750041
35	6	0	-5.272228	-3.991202	1.066638
36	6	0	-6.322591	-3.091519	1.222296
37	6	0	-5.537516	-1.775138	-0.528386
38	6	0	-0.843461	-6.969741	1.782529
39	6	0	0.393780	-8.545632	3.697151
40	7	0	0.137135	-7.842905	1.406202
41	6	0	-1.215096	-6.842024	3.127484
42	6	0	-0.589117	-7.631386	4.096447

43	6	0	0.731176	-8.621318	2.346377
44	6	0	-1.454078	-6.391551	-3.043457
45	6	0	-1.188838	-7.197777	-5.662157
46	6	0	-1.117545	-5.434839	-4.013952
47	7	0	-1.667520	-7.697503	-3.343620
48	6	0	-1.535881	-8.083875	-4.629851
49	6	0	-0.974054	-5.850279	-5.345713
50	75	0	-8.138167	-0.599251	0.776333
51	7	0	-6.665417	1.014674	0.691775
52	6	0	-4.979244	3.257599	0.341367
53	6	0	-6.563070	1.640499	-0.528697
54	6	0	-5.925722	1.497441	1.728164
55	6	0	-5.100520	2.617060	1.581110
56	6	0	-5.738249	2.749828	-0.721926
57	6	0	-5.922060	0.842967	3.068161
58	6	0	-5.762188	-0.136487	5.634335
59	6	0	-5.161615	-0.313613	3.301867
60	7	0	-6.566800	1.511078	4.055270
61	6	0	-6.491129	1.017830	5.310991
62	6	0	-5.082677	-0.809942	4.610781
63	6	0	-7.332392	1.040721	-1.632895
64	6	0	-8.757066	-0.290638	-3.601522
65	7	0	-8.040304	-0.085066	-1.311454
66	6	0	-7.338292	1.544630	-2.938968

67	6	0	-8.058743	0.876307	-3.934151
68	6	0	-8.728782	-0.737986	-2.280241
69	6	0	-4.033658	4.377778	0.151580
70	7	0	-2.139189	6.439099	-0.249733
71	6	0	-4.277471	5.428596	-0.751486
72	6	0	-2.820150	4.406080	0.859404
73	6	0	-1.910325	5.433825	0.635032
74	6	0	-3.324278	6.429392	-0.921578
75	75	0	-0.644243	8.000328	-0.617109
76	7	0	0.874796	6.419294	-0.571909
77	6	0	3.094112	4.690413	-0.295793
78	6	0	1.327786	5.692670	-1.631933
79	6	0	1.508458	6.268230	0.639892
80	6	0	2.596905	5.410102	0.799358
81	6	0	2.445425	4.855767	-1.525474
82	6	0	0.629875	5.706636	-2.948285
83	6	0	-0.455381	5.562830	-5.473342
84	7	0	1.325219	6.241071	-3.981789
85	6	0	-0.608971	5.067329	-3.114760
86	6	0	-1.157530	4.993868	-4.402745
87	6	0	0.779895	6.176465	-5.216288
88	6	0	0.957184	7.044458	1.764536
89	6	0	-0.281412	8.501723	3.769707
90	6	0	1.453944	6.977857	3.071871

91	7	0	-0.115853	7.836663	1.461176
92	6	0	-0.724230	8.540861	2.447281
93	6	0	0.832734	7.714836	4.085344
94	6	0	4.239317	3.766145	-0.149169
95	7	0	6.428616	2.009851	0.141106
96	6	0	5.223414	3.657788	-1.146858
97	6	0	4.378478	2.956560	0.992498
98	6	0	5.466641	2.094919	1.097968
99	6	0	6.294261	2.785879	-0.966678
100	75	0	8.195601	0.738753	0.437663
101	6	0	-1.932388	9.382607	-0.364524
102	6	0	0.719068	9.321713	-0.870417
103	6	0	-1.035258	8.120746	-2.491616
104	6	0	8.307874	1.265264	2.277374
105	6	0	9.699544	-0.425683	0.671513
106	6	0	9.371134	2.189644	0.064528
107	6	0	-0.348530	-9.389522	-1.077312
108	6	0	2.231673	-8.934261	-0.445827
109	6	0	1.208969	-7.678239	-2.504696
110	6	0	-9.409787	-2.003605	0.556169
111	6	0	-9.563244	0.659080	1.006339
112	6	0	-8.227697	-0.956661	2.658316
113	8	0	-10.444583	1.433471	1.143636
114	8	0	-10.198998	-2.872199	0.401463

115	8	0	-8.379635	-1.202973	3.805501
116	8	0	-0.973598	-10.361555	-1.319031
117	8	0	1.594666	-7.607340	-3.620727
118	8	0	3.180529	-9.628955	-0.298412
119	8	0	10.640762	-1.126928	0.799674
120	8	0	10.103054	3.088138	-0.183136
121	8	0	8.409460	1.647384	3.392527
122	8	0	-2.725442	10.243992	-0.188847
123	8	0	-1.293706	8.288804	-3.633677
124	8	0	1.558591	10.138677	-1.021830
125	1	0	-9.268086	-1.627263	-1.985416
126	1	0	-9.320253	-0.845426	-4.341524
127	1	0	-8.069979	1.259268	-4.948013
128	1	0	-6.791736	2.443246	-3.191090
129	1	0	-5.653937	3.193689	-1.704509
130	1	0	-4.557098	2.966962	2.450220
131	1	0	-4.498546	-1.698915	4.823734
132	1	0	-5.724679	-0.485842	6.659937
133	1	0	-7.024005	1.572240	6.076640
134	1	0	1.484778	-9.316955	2.003301
135	1	0	0.894848	-9.188514	4.410026
136	1	0	-0.870324	-7.539402	5.139133
137	1	0	-1.986929	-6.147029	3.428730
138	1	0	-2.851427	-5.125932	1.932971

139	1	0	-3.265159	-4.646288	-2.317216
140	1	0	-3.760947	-2.403395	-1.535334
141	1	0	-5.650263	-0.896238	-1.144838
142	1	0	-5.233786	-4.859882	1.713548
143	1	0	-7.073275	-3.256880	1.982897
144	1	0	7.070932	2.716790	-1.715816
145	1	0	3.644644	2.970257	1.789950
146	1	0	5.582641	1.463123	1.968252
147	1	0	5.187775	4.262917	-2.045293
148	1	0	2.759338	4.304973	-2.403763
149	1	0	3.073834	5.314980	1.765524
150	1	0	2.309177	6.360836	3.311897
151	1	0	1.210443	7.670173	5.100264
152	1	0	-0.799289	9.080772	4.524095
153	1	0	-1.574144	9.146660	2.165663
154	1	0	-2.551881	3.622179	1.557256
155	1	0	-0.973617	5.441418	1.170190
156	1	0	-5.201384	5.492367	-1.314506
157	1	0	-3.503380	7.242786	-1.611545
158	1	0	-2.109722	4.499659	-4.563552
159	1	0	-0.844487	5.527524	-6.484592
160	1	0	1.357947	6.621680	-6.019532
161	1	0	9.478421	1.323872	-2.382264
162	1	0	9.029519	0.733485	-4.752661

163	1	0	7.107218	-0.815886	-5.271660
164	1	0	5.777753	-1.742733	-3.405190
165	1	0	4.840815	-2.479879	-1.793929
166	1	0	4.844594	-2.891338	2.485728
167	1	0	2.578791	-3.008153	-1.507215
168	1	0	4.340348	-5.065739	1.875110
169	1	0	2.752620	-6.891269	1.488652
170	1	0	1.068040	-4.926813	-1.777528
171	1	0	-1.096596	-7.559456	-6.679980
172	1	0	-0.704300	-5.135468	-6.115638
173	1	0	-1.717997	-9.133524	-4.836712
174	1	0	8.523515	-1.086741	6.431140
175	1	0	9.777358	-1.818401	4.392740
176	1	0	6.090844	-0.474858	6.195954
177	1	0	-4.625779	-0.793195	2.490610
178	1	0	-0.967639	-4.396269	-3.738056
179	1	0	-1.113603	4.616192	-2.268400
180	1	0	5.022101	-0.637633	3.936589

Table 14.14 - Average MO composition of ***6*** isomers in (*S=0*) ground state.

MO	Energy (eV)	Composition				
		Rhenium	4-pytpy			CO
			tpy	py	Σ py + tpy	
LUMO+5	-2.700	1	70	27	96	3
LUMO+4	-2.721	1	70	27	97	2
LUMO+3	-3.370	3	73	21	93	5
LUMO+2	-3.386	2	73	21	94	4
LUMO+1	-3.421	2	72	22	94	4
LUMO	**-3.442**	**2**	**71**	**23**	**94**	**4**
HOMO	**-7.272**	**58**	**10**	**8**	**17**	**25**
HOMO-1	-7.298	60	11	4	15	25
HOMO-2	-7.306	61	12	3	15	25
HOMO-3	-7.345	60	9	6	15	25
HOMO-4	-7.443	60	10	5	15	25
HOMO-5	-7.491	61	10	4	14	26

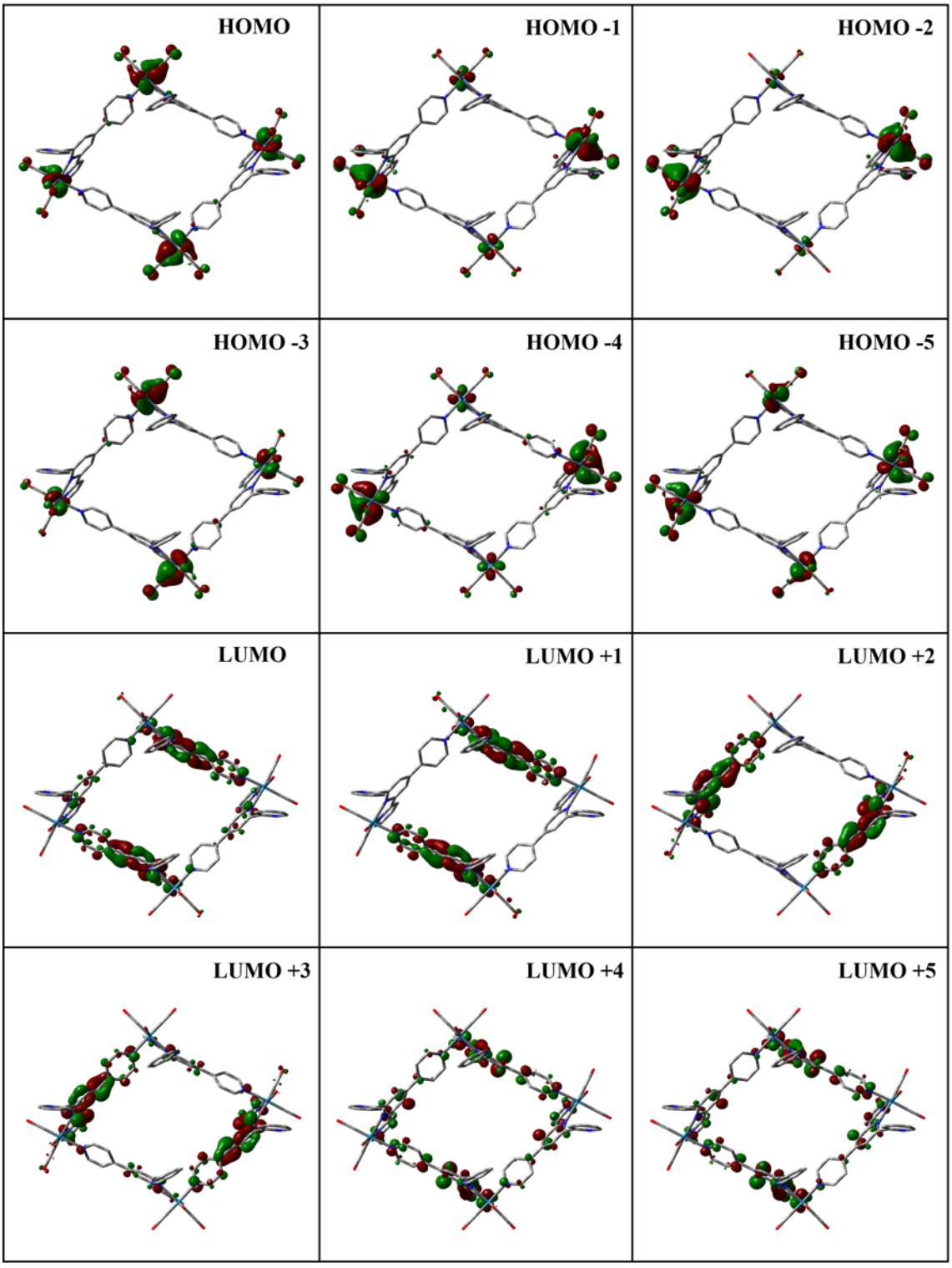

Figure 14.7 - Kohn-Sham electron density illustration of the molecular orbitals of **6** (Up-Up-Up-Up isomer) in (*S=0*) ground state.

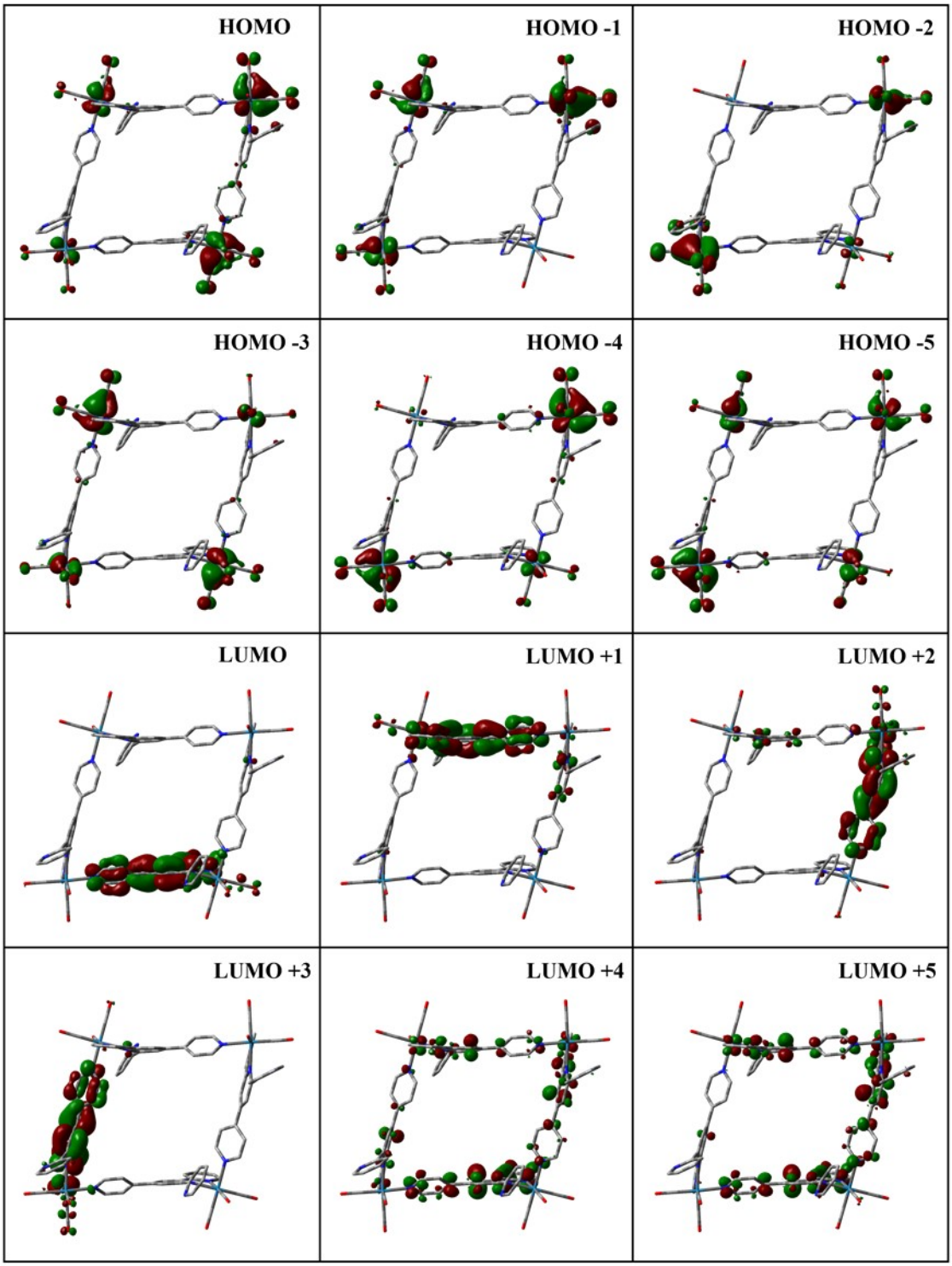

Figure 14.8 - Kohn-Sham electron density illustration of the molecular orbitals of **6** (Up-Up-Up-Down isomer) in (*S=0*) ground state.

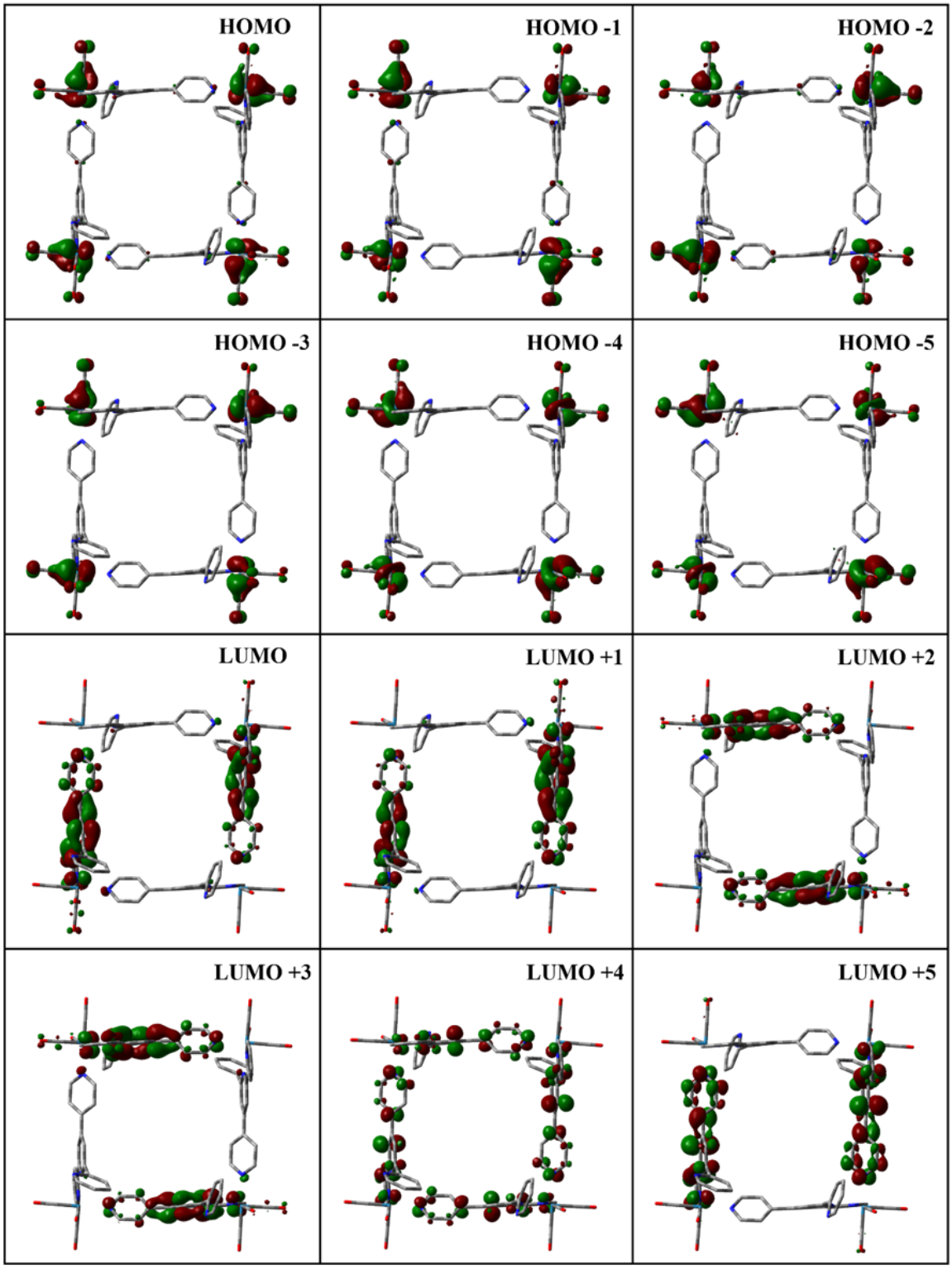

Figure 14.9 – Kohn-Sham electron density illustration of the molecular orbitals of **6** (Up-Up-Down-Down isomer) in (*S=0*) ground state.

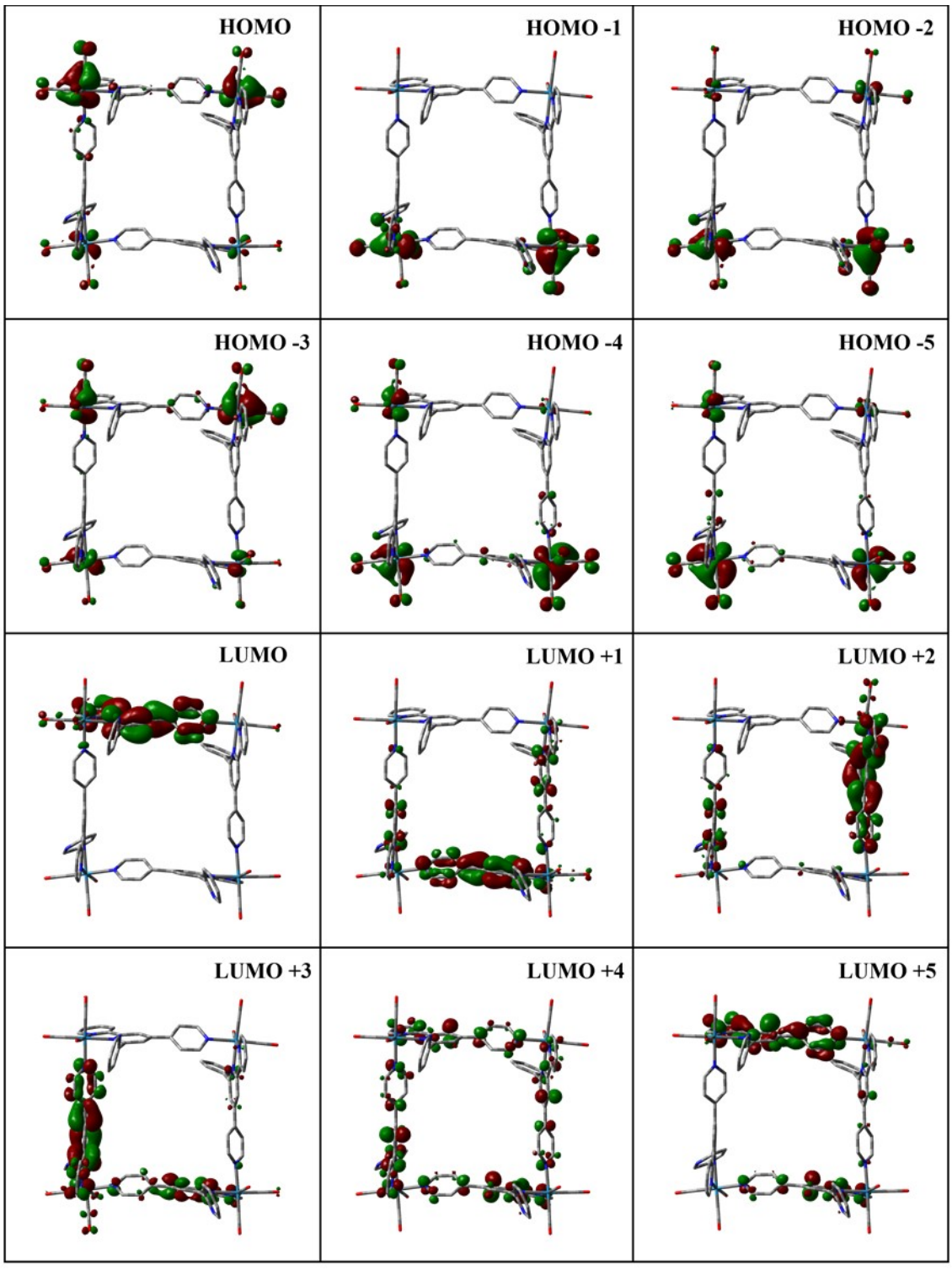

Figure 14.10 - Kohn-Sham electron density illustration of the molecular orbitals of **6** (Up-Down-Up-Down isomer) in (*S=0*) ground state.

Table 14.15 - Selected transitions from TD-DFT calculations of 6 (Up-Down-Up-Down isomer) in S=0 ground state (PBE0), CPCM (CH3CN).

Energy (eV)	λ (nm)	f	Transition	Character
3,16	390	0,1562	H-5→L+3 (11%) H-4→L+1 (32%) H→L+1 (14%)	
3,21	384	0,3261	H-5→L+1 (19%) H-4→L+1 (13%) H-4→L+3 (12%) H→L+3 (16%)	
3,25	380	0,0851	H-7→L (71%)	
3,26	378	0,2123	H-10→L (10%) H-8→L+2 (10%) H-6→L+2 (21%) H-3→L (16%) H→L (10%)	$^{1}MLCT_{tpy} + {}^{1}LLCT_{CO\rightarrow tpy}$
3,29	375	0,1828	H-8→L+2 (15%) H-6→L+2 (14%) H-3→L (15%)	
3,38	365	0,2824	H-11→L+2 (10%) H-10→L (15%) H-5→L+2 (11%) H-4→L+3 (13%)	
3,44	359	0,0948	H-10→L (36%) H-7→L (13%)	
3,45	358	0,1044	H-5→L+1 (27%)	

			H-5→L+3 (23%) H-3→L+1 (11%) H→L+1 (11%)	
3,83	322	0,1135	H-12→L+1 (43%) H-12→L+3 (15%)	$^{1}MLCT_{tpy}$
3,89	317	0,0821	H-18→L+2 (11%) H-7→L+1 (10%) H-7→L+2 (17%)	
3,94	313	0,0816	H-19→L (46%) H-11→L+1 (13%)	
3,95	313	0,0798	H-18→L+2 (11%) H-9→L+2 (33%)	
3,95	313	0,0756	H-18→L+2 (14%) H-9→L+2 (29%) H-8→L+2 (10%)	
3,97	311	0,1934	H-12→L+1 (11%) H-4→L+4 (17%) H-4→L+5 (10%) H-4→L+7 (11%)	$^{1}MLCT_{tpy} + {}^{1}LLCT_{CO\rightarrow tpy}$
3,98	310	0,1916	H-13→L+3 (10%) H-5→L+4 (11%) H→L+6 (13%)	
4,04	305	0,1241	H-3→L+4 (12%) H-3→L+5 (35%) H→L+5 (14%)	
4,13	299	0,1027	H-4→L+6 (15%)	

			H-4→L+7 (18%)	
4,70	263	0,1204	H-13→L+4 (19%) H-13→L+6 (28%)	
4,71	262	0,0817	H-26→L+1 (12%) H-12→L+4 (11%)	
4,78	258	0,0824	H-30→L (20%)	
4,79	258	0,0858	H-30→L (17%) H-19→L+4 (13%) H-19→L+5 (25%)	
4,80	257	0,1091	H-28→L+1 (16%)	
4,83	255	0,0865	H-31→L+1 (10%) H-31→L+2 (10%) H-31→L+3 (30%) H-23→L+3 (10%)	$^1MLCT_{tpy}$
4,93	250	0,0885	H-33→L (13%) H-32→L (16%)	
4,94	250	0,2715	H-32→L (10%) H-32→L+1 (12%)	
4,98	248	0,1954	H-34→L+2 (12%) H-32→L+1 (15%) H-32→L+2 (22%)	$^1MLCT_{tpy} + {}^1ILCT_{py\rightarrow tpy}$
4,99	248	0,0847	H-19→L+6 (13%)	$^1MLCT_{tpy}$

Table 14.16 - Selected transitions from TD-DFT calculations of **6** (Up-Up-Down-Down isomer) in *S*=0 ground state (PBE0), CPCM (CH_3CN).

Energy (eV)	λ (nm)	f	Transition	Character
3,27	378	0,0604	H-8→L (10%) H-7→L (22%) H-6→L+1 (26%) H-4→L (11%)	
3,29	375	0,1476	H-7→L+3 (14%) H-6→L+2 (10%) H-5→L+2 (23%) H-4→L+3 (18%)	
3,32	372	0,5949	H-9→L+1 (11%) H-3→L (15%) H-2→L+1 (13%) H-1→L+1 (12%) H→L (14%)	$^1MLCT_{tpy} + {}^1LLCT_{CO\rightarrow tpy}$
3,36	367	0,5659	H-10→L+2 (12%) H-3→L+3 (15%) H-2→L+2 (15%) H-1→L+2 (12%) H→L+3 (13%)	
3,45	358	0,0867	H-9→L+1 (20%) H-8→L (15%)	
3,48	355	0,0498	H-11→L+3 (14%) H-10→L+2 (23%)	
3,85	321	0,0715	H-13→L+3 (41%)	$ILCT_{tpy\rightarrow py}$

			H-12→L+2 (35%)	
3,89	318	0,0809	H-1→L+4 (16%) H→L+5 (20%)	
3,89	318	0,1594	H-2→L+4 (17%) H→L+6 (23%)	
3,94	313	0,2697	H-17→L+2 (14%) H-17→L+3 (14%) H-16→L+2 (13%) H-16→L+3 (12%)	
3,96	311	0,4262	H-19→L+1 (28%) H-18→L (25%)	
4,04	305	0,2004	H-3→L+6 (24%) H-1→L+7 (21%) H→L+6 (12%)	$^{1}MLCT_{tpy} + {}^{1}LLCT_{CO\rightarrow tpy}$
4,05	305	0,2424	H-3→L+5 (24%) H-2→L+7 (18%) H-1→L+4 (10%) H→L+5 (13%)	
4,22	293	0,0563	H-9→L+4 (14%) H-8→L+5 (17%)	
4,22	293	0,0497	H-17→L (11%) H-17→L+1 (14%) H-9→L+4 (11%) H-8→L+5 (10%)	
4,23	292	0,0968	H-11→L+6 (19%) H-10→L+4 (20%)	

			H-10→L+7 (17%) H-8→L+6 (16%)	
4,40	280	0,0735	H-23→L+3 (10%) H-22→L+2 (10%) H-3→L+5 (16%)	
4,41	280	0,0569	H-1→L+7 (13%)	
4,42	279	0,1559	H-23→L+3 (13%) H-22→L+2 (13%) H-3→L+5 (10%)	
4,65	265	0,0745	H-6→L+7 (11%)	
4,76	259	0,2551	H-27→L+2 (13%) H-26→L+3 (12%)	
4,79	258	0,2162	H-19→L+4 (14%) H-18→L+5 (19%)	$^{1}MLCT_{tpy}$
4,90	252	0,0494	H-2→L+9 (11%)	
4,98	248	0,5606	H-33→L+1 (18%) H-32→L (39%)	$ILCT_{tpy\rightarrow py}$
5,01	247	0,1638	H-32→L+3 (11%)	$^{1}MLCT_{tpy}$
5,02	246	0,0512	H-15→L+4 (24%) H-14→L+6 (33%)	$ILCT_{tpy\rightarrow py}$
5,03	246	0,1321	H-32→L+3 (14%) H-14→L+6 (13%)	$^{1}MLCT_{tpy}$

Table 14.17 - Selected transitions from TD-DFT calculations of **6** (Up-Up-Up-Down isomer) in *S*=0 ground state (PBE0), CPCM (CH_3CN).

Energy (eV)	λ (nm)	f	Transition	Character
3,27	378	0,0604	H-8→L (10%) H-7→L (22%) H-6→L+1 (26%) H-4→L (11%)	
3,29	375	0,1476	H-7→L+3 (14%) H-6→L+2 (10%) H-5→L+2 (23%) H-4→L+3 (18%)	
3,32	372	0,5949	H-9→L+1 (11%) H-3→L (15%) H-2→L+1 (13%) H-1→L+1 (12%) H→L (14%)	$^1MLCT_{tpy} + {}^1LLCT_{CO\rightarrow tpy}$
3,36	367	0,5659	H-10→L+2 (12%) H-3→L+3 (15%) H-2→L+2 (15%) H-1→L+2 (12%) H→L+3 (13%)	
3,45	358	0,0867	H-9→L+1 (20%) H-8→L (15%)	
3,48	355	0,0498	H-11→L+3 (14%) H-10→L+2 (23%)	
3,85	321	0,0715	H-13→L+3 (41%)	$ILCT_{tpy\rightarrow py}$

			H-12→L+2 (35%)	
3,89	318	0,0809	H-1→L+4 (16%) H→L+5 (20%)	
3,89	318	0,1594	H-2→L+4 (17%) H→L+6 (23%)	
3,94	313	0,2697	H-17→L+2 (14%) H-17→L+3 (14%) H-16→L+2 (13%) H-16→L+3 (12%)	
3,96	311	0,4262	H-19→L+1 (28%) H-18→L (25%)	
4,04	305	0,2004	H-3→L+6 (24%) H-1→L+7 (21%) H→L+6 (12%)	$^{1}MLCT_{tpy} + {}^{1}LLCT_{CO\rightarrow tpy}$
4,05	305	0,2424	H-3→L+5 (24%) H-2→L+7 (18%) H-1→L+4 (10%) H→L+5 (13%)	
4,22	293	0,0563	H-9→L+4 (14%) H-8→L+5 (17%)	
4,22	293	0,0497	H-17→L (11%) H-17→L+1 (14%) H-9→L+4 (11%) H-8→L+5 (10%)	
4,23	292	0,0968	H-11→L+6 (19%) H-10→L+4 (20%)	

			H-10→L+7 (17%) H-8→L+6 (16%)	
4,40	280	0,0735	H-23→L+3 (10%) H-22→L+2 (10%) H-3→L+5 (16%)	
4,41	280	0,0569	H-1→L+7 (13%)	
4,42	279	0,1559	H-23→L+3 (13%) H-22→L+2 (13%) H-3→L+5 (10%)	
4,65	265	0,0745	H-6→L+7 (11%)	
4,76	259	0,2551	H-27→L+2 (13%) H-26→L+3 (12%)	$^1MLCT_{tpy}$
4,79	258	0,2162	H-19→L+4 (14%) H-18→L+5 (19%)	
4,90	252	0,0494	H-2→L+9 (11%)	$^1MLCT_{tpy} + {}^1ILCT_{py\rightarrow tpy}$
4,98	248	0,5606	H-33→L+1 (18%) H-32→L (39%)	$^1MLCT_{tpy}$
5,01	247	0,1638	H-32→L+3 (11%)	
5,02	246	0,0512	H-15→L+4 (24%) H-14→L+6 (33%)	$^1ILCT_{tpy\rightarrow py}$
5,03	246	0,1321	H-32→L+3 (14%) H-14→L+6 (13%)	$^1MLCT_{tpy}$

Table 14.18 - Selected transitions from TD-DFT calculations of **6** (Up-Up-Up-Up isomer) in *S*=0 ground state (PBE0), CPCM (CH_3CN).

Energy (eV)	λ (nm)	f	Transition	Character
3,17	390	0,5029	H-5→L+2 (14%) H-4→L (11%) H-4→L+3 (16%) H→L+2 (31%)	
3,23	382	0,1219	H-2→L+1 (41%) H-1→L (28%)	
3,25	380	0,0768	H-9→L+1 (19%) H-8→L (19%) H-7→L (11%) H-6→L+1 (18%)	
3,32	372	0,6065	H-11→L+1 (14%) H-10→L (14%) H-5→L+1 (17%) H-4→L (15%) H→L+1 (10%)	$^1MLCT_{tpy} + {}^1LLCT_{CO\rightarrow tpy}$
3,38	365	0,1296	H-5→L+2 (21%) H-4→L+3 (24%) H-3→L (13%) H→L+1 (10%)	
3,43	360	0,1005	H-11→L+1 (20%) H-10→L (18%) H-7→L (12%) H-6→L+1 (12%)	

3,56	347	0,0554	H-9→L+1 (25%) H-8→L (15%) H-7→L (15%) H-6→L+1 (14%)	
3,73	331	0,1628	H-13→L (34%) H-12→L+1 (38%)	$ILCT_{tpy\rightarrow py}$
3,79	326	0,0866	H-15→L+2 (27%) H-14→L+3 (22%)	
3,80	325	0,1767	H-19→L (21%) H-18→L+1 (25%)	
3,83	322	0,0998	H-7→L (10%) H-6→L+1 (14%) H→L+5 (14%)	
3,93	314	0,2172	H-15→L+2 (10%) H-4→L+6 (14%) H→L+4 (11%) H→L+7 (14%)	$^1MLCT_{tpy} + {}^1LLCT_{CO\rightarrow tpy}$
3,93	314	0,1036	H-14→L+2 (10%) H-4→L+7 (13%) H→L+6 (16%)	
4,31	286	0,0615	H-2→L+6 (10%) H-1→L+7 (11%)	
4,32	286	0,0708	H-21→L+2 (12%) H-4→L+4 (11%)	
4,37	283	0,0904	H-23→L+1 (23%) H-22→L (22%)	

4,65	265	0,1991	H-23→L+2 (29%) H-22→L+3 (26%)	$^1MLCT_{tpy} + {}^1ILCT_{tpy\rightarrow tpy}$
4,66	265	0,0885	H-23→L+2 (10%) H-22→L+3 (10%)	$^1MLCT_{tpy} + {}^1LLCT_{CO\rightarrow tpy}$
4,69	263	0,1109	H-2→L+9 (11%) H-1→L+8 (10%)	$^1MLCT_{tpy} + {}^1ILCT_{tpy\rightarrow py+} {}^1LLCT_{CO\rightarrow tpy}$
4,73	261	0,0563	H-3→L+14 (11%) H→L+10 (10%), H→L+15 (15%)	$^1MLCT_{tpy} + LLCT_{CO\rightarrow tpy}$
4,79	258	0,1646	H-31→L+2 (29%) H-30→L+3 (20%) H-29→L+3 (10%) H-28→L+2 (11%)	$^1ILCT_{tpy\rightarrow py} + {}^1LLCT_{tpy\rightarrow CO}$
4,88	253	0,0888	H-32→L (11%)	
4,89	253	0,0899	H-32→L+1 (13%) H-19→L+5 (14%)	
4,89	253	0,4194	H-33→L (13%) H-32→L+1 (26%)	
4,94	250	0,0961	H-4→L+8 (19%) H-4→L+11 (10%) H→L+9 (13%)	$^1MLCT_{tpy} + {}^1LLCT_{CO\rightarrow tpy}$
4,96	249	0,0627	H-13→L+5 (10%)	$^1MLCT_{tpy}$
4,96	249	0,0986	H-28→L+2 (10%)	

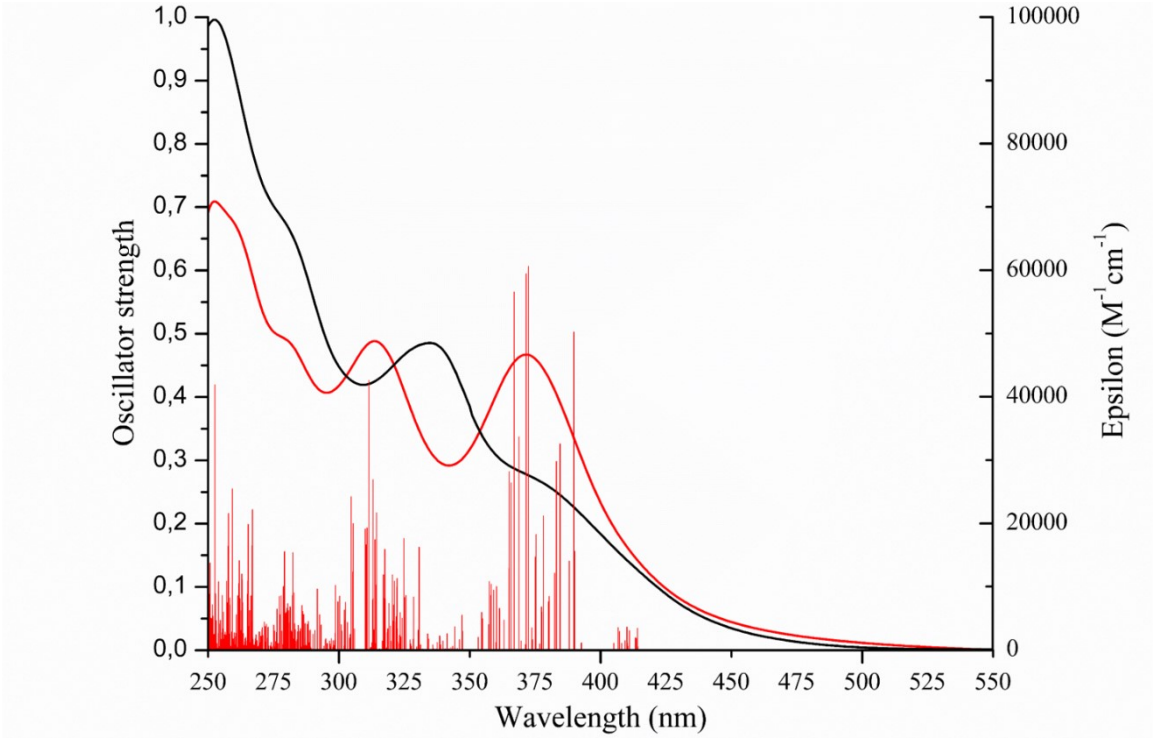

Figure 14.11 - TD-DFT simulated (red) and experimental (black) absorption spectrum (PBE0/LANL2DZ; CPCM: CH3CN) of model complex 6.

Table 14.19 - Atomic coordinates for DFT optimization of **4** in ($S = 0$) PBE0/LANL2DZ, CPCM(CH_3CN).

Standard orientation					
Center Number	Atomic Number	Atomic Type	Coordinates (Angstroms)		
			X	Y	Z
1	6	0	-0.757391	3.681366	-0.461824
2	6	0	1.948129	3.146016	-0.476245
3	6	0	-0.277792	2.370390	-0.407707
4	6	0	0.145768	4.748805	-0.525876
5	6	0	1.519237	4.473369	-0.531727
6	7	0	1.079328	2.103061	-0.421227

7	6	0	-1.149134	1.182341	-0.346793
8	6	0	-2.483353	-1.244250	-0.216322
9	6	0	-2.539737	1.176371	-0.230788
10	7	0	-0.465364	0.011639	-0.407519
11	6	0	-1.094389	-1.188832	-0.340326
12	6	0	-3.232357	-0.050223	-0.164987
13	6	0	-0.174088	-2.337203	-0.425381
14	6	0	1.692409	-4.362786	-0.708695
15	6	0	-0.602480	-3.667353	-0.464705
16	7	0	1.166039	-2.014670	-0.512296
17	6	0	2.068964	-3.020440	-0.655330
18	6	0	0.335369	-4.696000	-0.604794
19	6	0	-4.710542	-0.079787	-0.036756
20	7	0	-7.542510	-0.131657	0.220704
21	6	0	-5.429482	1.037771	0.432880
22	6	0	-5.461772	-1.223955	-0.375053
23	6	0	-6.853648	-1.205832	-0.233284
24	6	0	-6.822542	0.968955	0.544807
25	75	0	1.601135	0.052027	-0.483689
26	6	0	1.763492	0.141839	-2.361194
27	6	0	3.482720	0.087383	-0.353045
28	1	0	2.999386	2.892550	-0.479224
29	1	0	2.254242	5.267734	-0.578783
30	1	0	-0.216007	5.769582	-0.571033
31	1	0	-1.823159	3.874084	-0.458149

32	1	0	-3.078655	2.114219	-0.205384
33	1	0	-4.933837	1.952307	0.737603
34	1	0	-7.384303	1.822065	0.911444
35	1	0	-7.441164	-2.079698	-0.495858
36	1	0	-4.998694	-2.120728	-0.769064
37	1	0	-2.973791	-2.204529	-0.134337
38	1	0	-1.656923	-3.903922	-0.394425
39	1	0	0.012970	-5.730353	-0.637557
40	1	0	2.453705	-5.124358	-0.826353
41	1	0	3.106837	-2.724826	-0.729184
42	7	0	1.506055	-0.046755	1.739522
43	6	0	1.508202	-0.216912	4.549842
44	6	0	0.996260	0.953695	2.503603
45	6	0	2.020562	-1.133047	2.378753
46	6	0	2.039013	-1.251236	3.768940
47	6	0	0.978822	0.903861	3.898983
48	1	0	0.599919	1.817492	1.991504
49	1	0	0.560871	1.734973	4.454529
50	1	0	1.510535	-0.280939	5.632572
51	1	0	2.465546	-2.138843	4.221155
52	1	0	2.434998	-1.913001	1.757597
53	8	0	1.866892	0.198814	-3.554064
54	8	0	4.677627	0.108313	-0.249249

Table 14.20 - MO composition of **4** in (*S=0*) ground state.

MO	Energy (eV)	Composition			
		Rhenium	pytpy	py	CO
LUMO+5	-1.45	1	98	1	0
LUMO+4	-1.62	2	91	2	5
LUMO+3	-1.76	2	3	91	4
LUMO+2	-1.94	0	98	1	0
LUMO+1	-2.62	2	96	1	1
LUMO	**-3.13**	**3**	**91**	**1**	**5**
HOMO	**-6.07**	**64**	**18**	**1**	**17**
HOMO-1	-6.34	67	7	0	26
HOMO-2	-6.70	55	15	4	26
HOMO-3	-7.75	0	100	0	0
HOMO-4	-7.82	1	99	0	0
HOMO-5	-8.14	0	100	0	0

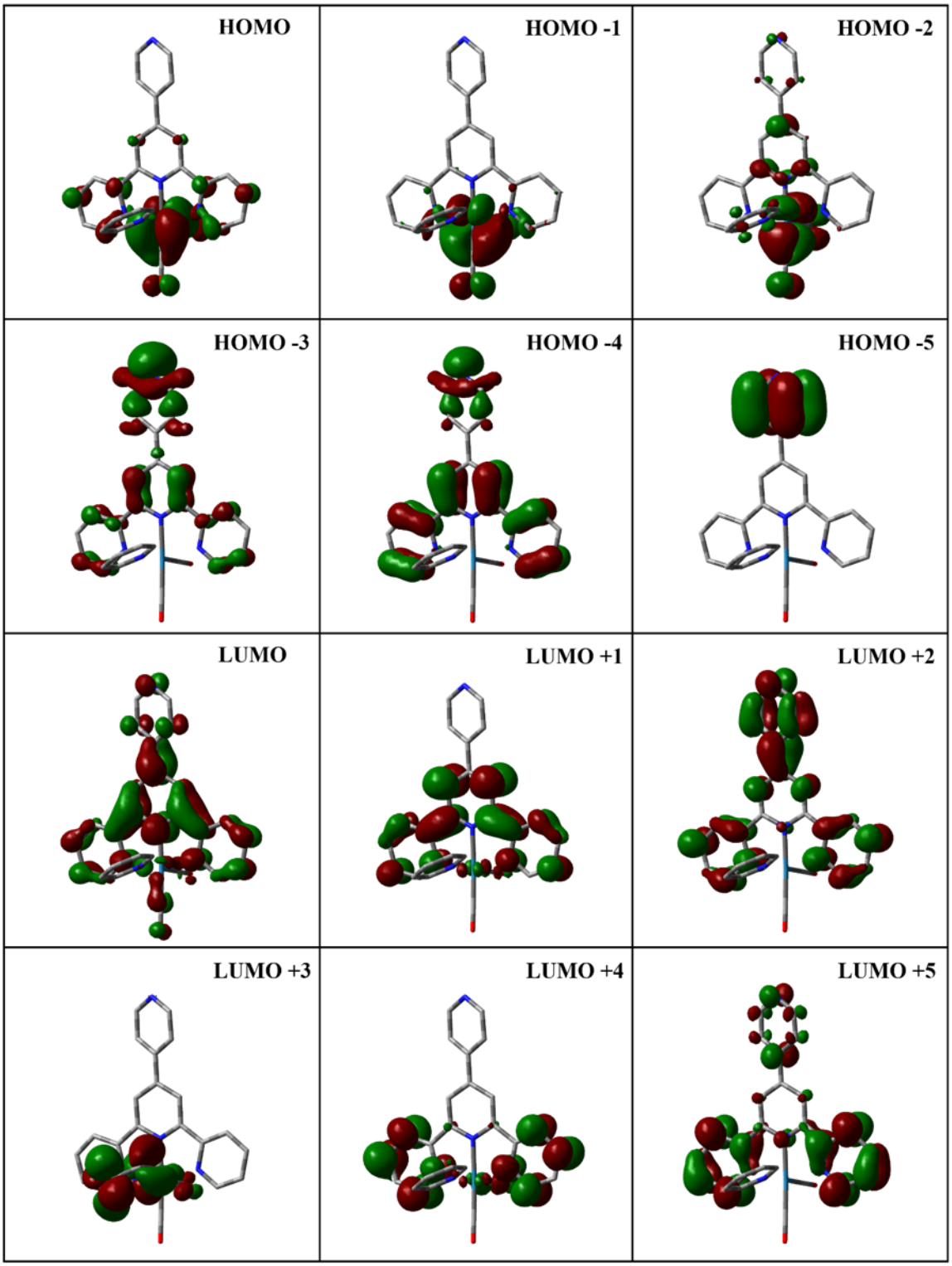

Figure 14.12 - Kohn-Sham electron density illustration of the molecular orbitals of the model complex **4** in (*S=0*) ground state.

Table 14.21 - Selected transitions from TD-DFT calculations of **4** in the singlet ground state (PBE0), CPCM (CH_3CN).

Energy (eV)	**λ (nm)**	**f**	**Transition**	**Character**
2,76	447	0,0408	H-2→L (26%) H-1→L+1 (66%)	
2,88	429	0,1817	H-2→L (43%) H-1→L+1 (32%) H→L+1 (18%)	$^1MLCT_{tpy}$ + $^1LLCT_{CO\rightarrow tpy}$
3,32	372	0,0479	H→L+2 (28%) H→L+3 (64%)	
3,38	366	0,0693	H→L+2 (57%) H→L+3 (30%)	$^1MLCT_{tpy}$ and/or $^1MLCT_{py}$ + $^1LLCT_{CO\rightarrow tpy}$ and/or $^1LLCT_{CO\rightarrow py}$
3,75	329	0,0288	H→L+5 (74%)	
3,93	314	0,4428	H-4→L (66%) H→L+5 (14%)	
3,98	310	0,1269	H-2→L+2 (91%)	$^1MLCT_{tpy}$ + $^1LLCT_{CO\rightarrow tpy}$
4,05	305	0,0331	H-2→L+3 (43%) H→L+6 (31%)	
4,10	301	0,0566	H-2→L+3 (19%) H-2→L+4 (24%) H→L+6 (33%) H→L+8 (12%)	
4,16	297	0,0425	H-2→L+3 (25%) H-2→L+4 (65%)	$^1MLCT_{tpy}$ and/or $^1MLCT_{py}$ + $^1LLCT_{CO\rightarrow tpy}$ and/or $^1LLCT_{CO\rightarrow py}$
4,32	286	0,0404	H-5→L (95%)	$^1MLCT_{tpy}$ + $^1LLCT_{CO\rightarrow tpy}$

4,44	278	0,0597	H-2→L+5 (93%)	
4,50	275	0,3200	H-7→L (40%) H-6→L (45%)	$^1LLCT_{py\rightarrow tpy}$
4,60	268	0,1466	H-4→L+1 (57%) H→L+10 (22%)	$^1MLCT_{CO}$
4,61	268	0,1007	H-4→L+1 (35%) H→L+10 (40%)	
4,88	253	0,0276	H-6→L+1 (11%) H-4→L+2 (17%) H-3→L+2 (11%) H→L+9 (11%) H→L+12 (28%)	$^1MLCT_{tpy}$
4,91	252	0,0366	H-6→L+1 (46%) H→L+12 (21%)	$^1LLCT_{py\rightarrow tpy}$
5,12	241	0,0386	H-4→L+2 (30%)	$^1MLCT_{tpy}$ + $^1LLCT_{py\rightarrow tpy}$
5,19	238	0,1553	H-8→L+1 (79%)	$^1MLCT_{tpy}$
5,46	226	0,0625	H-5→L+2 (56%) H-2→L+7 (26%)	$^1MLCT_{tpy}$
5,53	223	0,0389	H-11→L (21%) H-10→L (17%), H-4→L+5 (15%)	$^1MLCT_{tpy}$ + $^1LLCT_{py\rightarrow tpy}$
5,56	222	0,0270	H-11→L (11%) H-10→L (20%) H-4→L+5 (13%) H-1→L+11 (23%)	$^1MLCT_{tpy}$
5,58	221	0,1046	H-9→L+6 (10%)	$^1LLCT_{py\rightarrow tpy}$

			H-7→L+3 (53%) H-6→L+3 (15%)	
5,59	221	0,0320	H-10→L (11%) H-1→L+11 (47%)	$^1MLCT_{tpy} + {}^1LLCT_{py\rightarrow tpy} + {}^1LLCT_{CO\rightarrow tpy}$
5,71	216	0,0281	H-12→L (33%) H-3→L+4 (15%) H-2→L+13 (23%)	$^1MLCT_{tpy}$ and/or $^1MLCT_{CO} + {}^1LLCT_{py\rightarrow tpy}$
5,72	216	0,0860	H-6→L+2 (48%) H-4→L+4 (14%) H-3→L+4 (29%)	
5,73	215	0,0966	H-6→L+2 (32%) H-4→L+4 (25%) H-3→L+4 (14%)	
5,76	214	0,0386	H-12→L (14%) H-11→L (15%) H-3→L+5 (46%)	$^1LLCT_{py\rightarrow tpy}$
5,78	214	0,0319	H-9→L+1 (72%)	
5,80	213	0,0516	H-11→L (18%) H-9→L+1 (12%) H-4→L+5 (42%)	
5,96	207	0,0495	H-2→L+9 (48%)	$^1MLCT_{py\rightarrow tpy}$
6,17	200	0,0458	H-12→L+1 (57%)	$^1LLCT_{py\rightarrow tpy}$

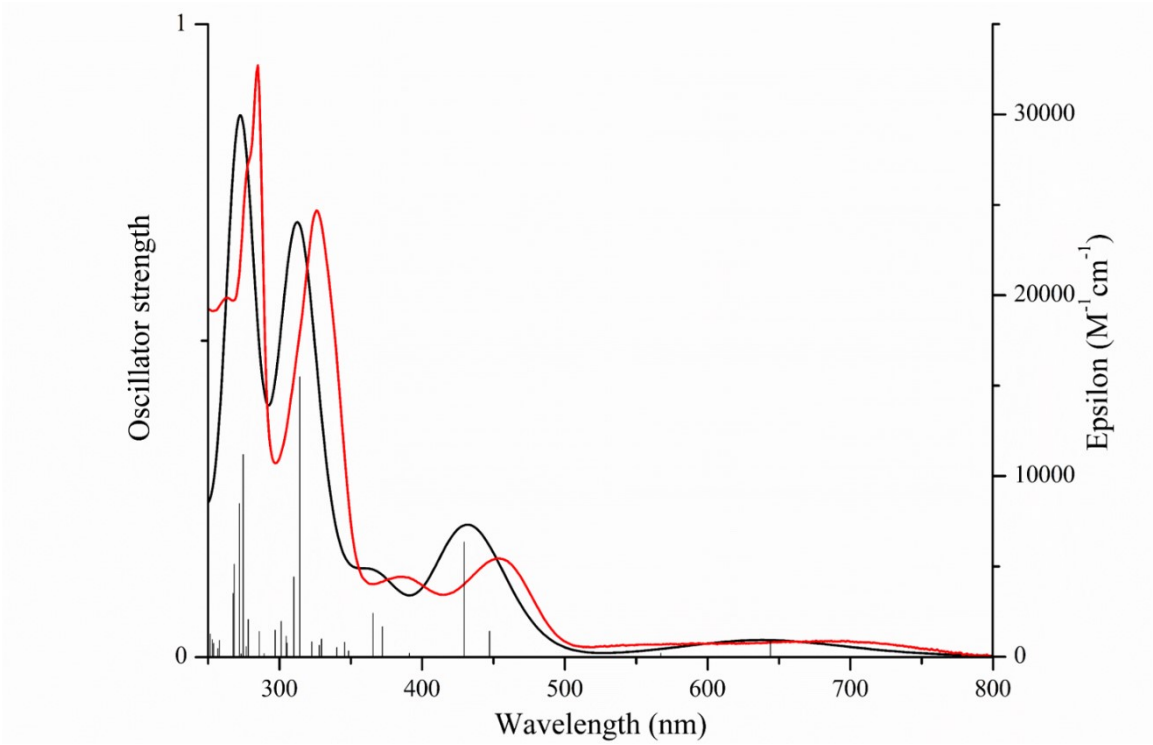

Figure 14.13 - TD-DFT simulated (red) and experimental (black) absorption spectrum (PBE0/LANL2DZ; CPCM: CH_3CN) of model complex **4**.

Table 14.22 - Atomic coordinates for DFT optimization of **7** (S = 0) PBE0/LANL2DZ, CPCM(CH_3CN).

Standard orientation					
Center Number	Atomic Number	Atomic Type	Coordinates (Angstroms)		
			X	Y	Z
1	7	0	7.792250	0.358935	-2.015802
2	6	0	6.884032	1.356834	-2.322665
3	6	0	6.668667	1.758406	-3.643443
4	1	0	5.959446	2.546179	-3.865522
5	6	0	7.373428	1.137473	-4.681591

6	1	0	7.215859	1.443056	-5.709453
7	6	0	8.279307	0.116924	-4.366796
8	1	0	8.842468	-0.395880	-5.137123
9	6	0	8.461777	-0.245726	-3.030241
10	1	0	9.156231	-1.024454	-2.746875
11	7	0	7.610138	0.224356	2.096663
12	6	0	8.230980	-0.395430	3.133561
13	1	0	9.032866	-1.073470	2.873919
14	6	0	7.872925	-0.169728	4.464190
15	1	0	8.403531	-0.690192	5.252236
16	6	0	6.833220	0.724242	4.749136
17	1	0	6.528963	0.915566	5.771665
18	6	0	6.194289	1.375413	3.687779
19	1	0	5.394419	2.077318	3.888072
20	6	0	6.595747	1.120621	2.373440
21	7	0	1.513511	6.365421	0.021881
22	6	0	1.483501	5.325710	0.895333
23	1	0	0.667974	5.293403	1.603372
24	6	0	2.453092	4.326043	0.912666
25	1	0	2.352885	3.518944	1.629019
26	6	0	3.517534	4.366543	-0.005767
27	6	0	3.536873	5.437038	-0.919129
28	1	0	4.334734	5.549176	-1.643999
29	6	0	2.534786	6.402491	-0.876047

30	1	0	2.549442	7.237506	-1.563113
31	7	0	6.572463	1.418556	0.023433
32	6	0	6.010879	1.794309	1.200821
33	6	0	5.000285	2.758351	1.212942
34	1	0	4.563755	3.083516	2.148705
35	6	0	4.577059	3.333009	-0.001592
36	6	0	5.176180	2.912979	-1.205156
37	1	0	4.843812	3.321035	-2.151417
38	6	0	6.177548	1.939138	-1.167309
39	6	0	0.375743	8.228618	-3.047245
40	1	0	1.073992	9.007296	-2.771108
41	6	0	0.131992	7.913682	-4.385746
42	1	0	0.659969	8.453330	-5.162577
43	6	0	-0.790112	6.905557	-4.692835
44	1	0	-0.996814	6.635653	-5.722007
45	6	0	-1.448976	6.252530	-3.644690
46	1	0	-2.171621	5.475892	-3.861988
47	6	0	-1.174213	6.609518	-2.321664
48	7	0	-0.251772	7.594175	-2.023657
49	6	0	-4.435062	3.504765	0.009495
50	6	0	-4.465859	2.484998	0.977173
51	1	0	-3.707004	2.412838	1.747761
52	6	0	-5.471103	1.521264	0.935311
53	1	0	-5.491260	0.734340	1.675440

54	7	0	-6.452318	1.521360	-0.003948
55	6	0	-6.427763	2.508274	-0.939657
56	1	0	-7.222016	2.504438	-1.673442
57	6	0	-5.448566	3.497426	-0.966574
58	1	0	-5.504285	4.265001	-1.729852
59	6	0	-3.382780	4.545851	0.017947
60	6	0	-1.848225	6.002478	-1.160302
61	6	0	-1.067911	7.139324	4.755647
62	1	0	-1.358609	6.948754	5.782254
63	6	0	9.341062	-1.412246	0.050779
64	6	0	-1.708967	6.473553	3.704185
65	1	0	-2.497646	5.761977	3.914833
66	6	0	0.295262	8.275955	3.120331
67	1	0	1.072885	8.976166	2.848483
68	6	0	-2.915447	5.076201	1.235758
69	1	0	-3.332729	4.733090	2.174179
70	6	0	-0.047130	8.049917	4.455563
71	1	0	0.480876	8.584001	5.236264
72	6	0	-1.931681	6.068229	1.216263
73	6	0	-1.326393	6.731024	2.385330
74	6	0	-2.838142	5.016974	-1.192470
75	1	0	-3.170060	4.599919	-2.134972
76	6	0	9.502896	1.210214	0.131562
77	7	0	-1.433800	6.505433	0.030586

78	7	0	-0.328968	7.644334	2.093626
79	8	0	10.140101	-2.307473	0.046989
80	8	0	10.432158	1.959507	0.189646
81	75	0	0.012803	7.986794	0.035547
82	75	0	8.068094	-0.012367	0.047994
83	8	0	2.313097	10.052350	0.079127
84	8	0	-1.947826	10.364617	-0.003632
85	6	0	1.416861	9.254517	0.058177
86	6	0	-1.202882	9.430336	0.014055
87	7	0	-7.796172	-0.358633	2.008029
88	6	0	-6.888626	-1.356550	2.316796
89	6	0	-6.675792	-1.757900	3.638054
90	1	0	-5.967077	-2.545710	3.861624
91	6	0	-7.382457	-1.136700	4.674750
92	1	0	-7.226872	-1.442108	5.702966
93	6	0	-8.287617	-0.116102	4.358051
94	1	0	-8.852168	0.396921	5.127214
95	6	0	-8.467527	0.246313	3.021086
96	1	0	-9.161337	1.025087	2.736262
97	7	0	-7.606000	-0.224433	-2.104079
98	6	0	-8.224650	0.395406	-3.142247
99	1	0	-9.026937	1.073598	-2.884255
100	6	0	-7.864000	0.169534	-4.472150
101	1	0	-8.392941	0.690042	-5.261285

102	6	0	-6.823937	-0.724695	-4.754965
103	1	0	-6.517721	-0.916188	-5.776877
104	6	0	-6.187231	-1.375900	-3.692294
105	1	0	-5.387127	-2.078007	-3.890938
106	6	0	-6.591218	-1.120901	-2.378775
107	7	0	-1.513534	-6.365443	-0.016542
108	6	0	-1.482423	-5.326458	-0.890818
109	1	0	-0.665998	-5.294708	-1.597845
110	6	0	-2.451968	-4.326793	-0.910208
111	1	0	-2.350786	-3.520278	-1.627078
112	6	0	-3.517628	-4.366551	0.006848
113	6	0	-3.538093	-5.436271	0.921106
114	1	0	-4.336863	-5.547821	1.645063
115	6	0	-2.535907	-6.401713	0.880169
116	1	0	-2.551340	-7.236099	1.567981
117	7	0	-6.572573	-1.418624	-0.028699
118	6	0	-6.008714	-1.794536	-1.204948
119	6	0	-4.998133	-2.758615	-1.214988
120	1	0	-4.559824	-3.083878	-2.149884
121	6	0	-4.577199	-3.333074	0.000441
122	6	0	-5.178642	-2.912854	1.202785
123	1	0	-4.848067	-3.320700	2.149761
124	6	0	-6.179963	-1.939056	1.162874
125	6	0	-0.375716	-8.222227	3.056146

126	1	0	-1.074195	-9.001281	2.781666
127	6	0	-0.131778	-7.904598	4.393983
128	1	0	-0.659855	-8.442486	5.171966
129	6	0	0.790666	-6.896134	4.698924
130	1	0	0.997543	-6.624182	5.727521
131	6	0	1.449639	-6.245454	3.649388
132	1	0	2.172542	-5.468594	3.865018
133	6	0	1.174654	-6.605067	2.327124
134	7	0	0.251915	-7.590082	2.031214
135	6	0	4.435349	-3.505138	-0.010659
136	6	0	4.465092	-2.486441	-0.979495
137	1	0	3.705471	-2.415250	-1.749419
138	6	0	5.470237	-1.522506	-0.939638
139	1	0	5.489566	-0.736345	-1.680601
140	7	0	6.452379	-1.521497	-0.001347
141	6	0	6.428902	-2.507457	0.935392
142	1	0	7.223918	-2.502810	1.668340
143	6	0	5.449811	-3.496658	0.964394
144	1	0	5.506327	-4.263394	1.728456
145	6	0	3.383064	-4.546242	-0.016904
146	6	0	1.848629	-6.000459	1.164470
147	6	0	1.066652	-7.148294	-4.749139
148	1	0	1.357037	-6.959635	-5.776187
149	6	0	-9.340949	1.412327	-0.061626

150	6	0	1.708009	-6.480558	-3.699107
151	1	0	2.496610	-5.769347	-3.911294
152	6	0	-0.296044	-8.281886	-3.111309
153	1	0	-1.073604	-8.981575	-2.837935
154	6	0	2.915325	-5.078758	-1.233609
155	1	0	3.332334	-4.737380	-2.172787
156	6	0	0.045966	-8.058335	-4.447057
157	1	0	-0.482268	-8.593870	-5.226608
158	6	0	1.931490	-6.070677	-1.211998
159	6	0	1.325839	-6.735612	-2.379661
160	6	0	2.838742	-5.015080	1.194541
161	1	0	3.170998	-4.596317	2.136168
162	6	0	-9.502724	-1.210104	-0.142607
163	7	0	1.433850	-6.505592	-0.025374
164	7	0	0.328497	-7.648367	-2.085967
165	8	0	-10.140002	2.307549	-0.059362
166	8	0	-10.431904	-1.959358	-0.202457
167	75	0	-0.012876	-7.986841	-0.027182
168	75	0	-8.068023	0.012416	-0.056331
169	8	0	-2.313014	-10.052655	-0.066657
170	8	0	1.947754	-10.364589	0.016533
171	6	0	-1.416868	-9.254678	-0.047254
172	6	0	1.202824	-9.430334	-0.002974

Table 14.23 - MO composition of **7** in (*S=0*) ground state.

MO	Energy (eV)	Composition				
		Rhenium	4-pytpy			CO
			tpy	py	Σ py + tpy	
LUMO+5	-2.802	2	96	1	97	1
LUMO+4	-2.804	2	95	1	96	1
LUMO+3	-3.325	4	74	15	89	7
LUMO+2	-3.337	3	75	16	91	5
LUMO+1	-3.350	3	74	17	91	5
LUMO	**-3.363**	**3**	**76**	**18**	**94**	**4**
HOMO	**-6.232**	**64**	**17**	**2**	**19**	**16**
HOMO-1	-6.476	64	17	2	19	16
HOMO-2	-6.477	64	17	2	19	16
HOMO-3	-6.477	64	17	2	19	16
HOMO-4	-6.808	66	8	0	8	26
HOMO-5	-6.893	66	8	0	8	26

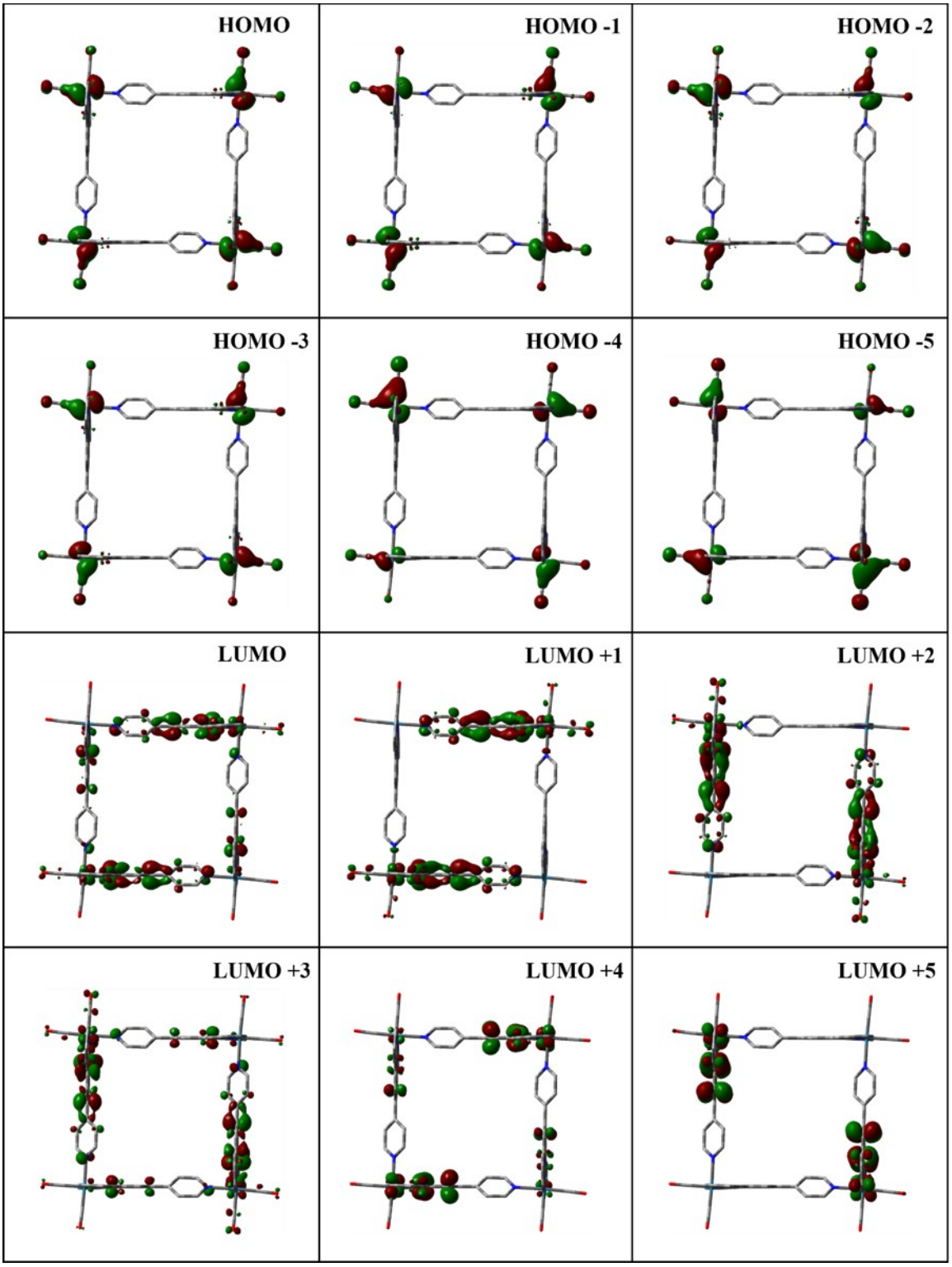

Figure 14.14 - Kohn-Sham electron density illustration of the molecular orbitals of the **7** in (*S=0*) ground state.

Table 14.24 - Selected transitions from TD-DFT calculations of **7** in the singlet ground state (PBE0), CPCM (CH_3CN).

Energy (eV)	**λ (nm)**	**f**	**Transition**	**Character**
2,34	527	0,2038	H-3→L+1 (21%) H-2→L (20%) H-1→L (16%) H→L+1 (22%)	
2,36	523	0,1651	H-3→L+2 (23%) H-2→L+3 (13%) H-1→L+3 (16%) H→L+2 (22%)	
2,72	453	0,0656	H-7→L+6 (19%) H-6→L+4 (11%) H-5→L+4 (12%) H-4→L+6 (10%)	$^1MLCT_{tpy} + {}^1LLCT_{CO\rightarrow tpy}$
2,73	453	0,0533	H-7→L+5 (12%) H-5→L+7 (18%) H-4→L+5 (19%)	
2,84	435	0,0462	H-7→L+2 (24%) H-6→L (20%) H-6→L+3 (11%) H-4→L+2 (15%)	
2,86	432	0,3765	H-9→L (18%) H-8→L+1 (19%)	
2,86	431	0,4064	H-10→L (13%)	

			H-8→L+2 (21%)	
3,27	378	0,1174	H-2→L+11 (35%) H→L+10 (35%)	
3,27	377	0,1058	H-3→L+9 (18%) H-2→L+8 (21%)	
3,27	377	0,1066	H-3→L+10 (27%) H-1→L+11 (26%)	
3,85	320	0,1695	H-11→L+5 (14%) H-10→L+7 (13%) H-9→L+8 (21%) H-8→L+9 (22%)	
3,88	318	0,2368	H-11→L+5 (32%) H-10→L+7 (12%) H-8→L+9 (10%)	
3,88	318	0,5427	H-13→L+2 (10%)	
3,89	317	0,1466	H-11→L+6 (17%) H-10→L+11 (14%) H-8→L+10 (23%) H-6→L+11 (11%)	
3,95	312	1,1069	H-7→L+17 (11%) H-6→L+16 (11%) H-5→L+19 (11%) H-4→L+18 (10%)	
4,58	269	0,5737	H-15→L+4 (17%) H-14→L+6 (31%) H-12→L+4 (15%)	$^1MLCT_{tpy}$

4,59	269	0,6173	H-13→L+5 (33%) H-12→L+7 (22%)	
4,68	264	0,1243	H-3→L+25 (13%) H-2→L+24 (15%) H-1→L+24 (12%) H→L+25 (14%)	
4,69	263	0,4298	H-23→L+1 (10%) H-22→L (24%) H-20→L+1 (19%)	$^1MLCT_{tpy} + {}^1MLCT_{CO}$
4,70	263	0,3801	H-21→L+3 (15%) H-20→L+2 (16%)	
4,71	262	0,1764	H-21→L+3 (11%)	$^1MLCT_{tpy}$
4,86	254	0,3287	H-24→L+1 (24%) H-23→L+1 (22%) H-21→L (17%)	$^1MLCT_{CO} + {}^1LLCT_{tpy\rightarrow CO}$
4,87	253	0,1534	H-24→L+2 (13%)	$^1MLCT_{tpy} + {}^1LLCT_{CO\rightarrow tpy}$
4,94	250	0,1324	H-24→L+1 (19%) H-21→L (14%) H-20→L+1 (14%)	$^1MLCT_{tpy} + {}^1LLCT_{tpy\rightarrow CO}$
4,95	249	0,1045	H-13→L+10 (14%) H-12→L+11 (12%)	$^1MLCT_{tpy} + {}^1MLCT_{CO}$

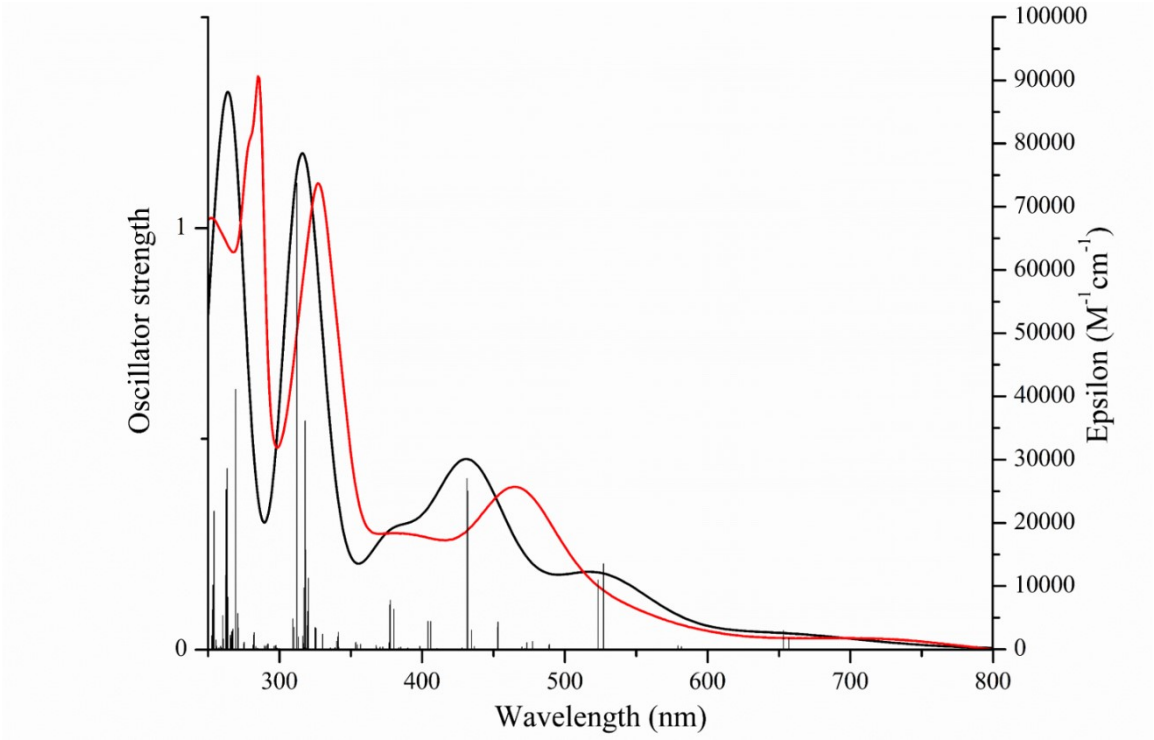

Figure 14.15 - TD-DFT simulated (red) and experimental (black) absorption spectrum (PBE0/LANL2DZ; CPCM: CH_3CN) of model complex **7**.

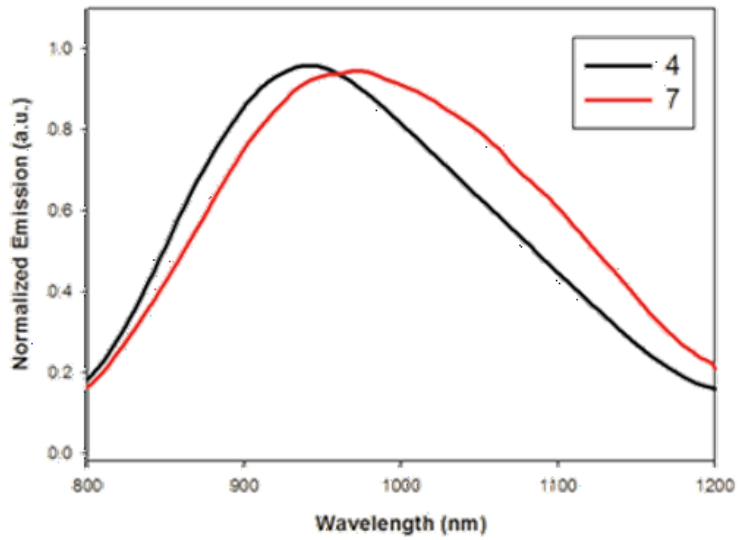

Figure 14.16 - Normalized emission spectra of the k^3N-series compound **4** and **7** recorded in acetonitrile solutions at room temperature.

Table 14.25 - Emission photophysical data of metal complexes **4** and **7**

Complex	$\lambda_{em@298K}$ (nm)	Φ	$\lambda_{em@77K}$ (nm)
4	940	$2x10^{-4}$	830
7	980	$1x10^{-4}$	825

Table 14.26 - Predicted phosphorescence energies employing different approaches.[a]

Complex	**Theoretical**[b]			**Experimental**
	λ_{TDDFT} (nm)	$\lambda_{0,0}$ (nm)	λ_{AE}(nm)	$\lambda_{em@298K}$ (nm)
2	450	474	611	564
4	706	856	993	940
5	460	491	617	546
6	469	497	629	563
7	714	871	1040	980

[a]λ_{TDDFT}= wavelength of $S_0 \rightarrow T_1$ transition obtained by TDDFT at the S_0 optimized geometry. $\lambda_{0,0}$= 1240/[E(T_1)–E(S_0)] at their respective optimized geometries obtained by DFT. λ_{AE}= 1240/[E(T_1)–E(S_0)] at the T_1 optimized geometry (adiabatic electronic emission) obtained by DFT. See Exp. Sect. for computational details. All values were determined with MeCN as solvent. [b] The calculated values for the k^2N-macrocycles are an average of the different isomers.

14.7. References

[1] A. Credi and L. Prodi, *Spectroc. Acta A*, 1998, **54**, 159.

[2] M. J. Frisch, G. W. Trucks, H. B. Schlegel, G. E. Scuseria, M. A. Robb, J. R. Cheeseman, G. Scalmani, V. Barone, B. Mennucci, G. A. Petersson, H. Nakatsuji, M. Caricato, X. Li, H. P. Hratchian, A. F. Izmaylov, J. Bloino, G. Zheng, J. L. Sonnenberg, M. Hada, M. Ehara, K. Toyota, R. Fukuda, J. Hasegawa, M. Ishida, T. Nakajima, Y.

Honda, O. Kitao, H. Nakai, T. Vreven, J. A. Montgomery Jr., J. E. Peralta, F. Ogliaro, M. J. Bearpark, J. Heyd, E. N. Brothers, K. N. Kudin, V. N. Staroverov, R. Kobayashi, J. Normand, K. Raghavachari, A. P. Rendell, J. C. Burant, S. S. Iyengar, J. Tomasi, M. Cossi, N. Rega, N. J. Millam, M. Klene, J. E. Knox, J. B. Cross, V. Bakken, C. Adamo, J. Jaramillo, R. Gomperts, R. E. Stratmann, O. Yazyev, A. J. Austin, R. Cammi, C. Pomelli, J. W. Ochterski, R. L. Martin, K. Morokuma, V. G. Zakrzewski, G. A. Voth, P. Salvador, J. J. Dannenberg, S. Dapprich, A. D. Daniels, Ö. Farkas, J. B. Foresman, J. V. Ortiz, J. Cioslowski and D. J. Fox, *Gaussian 09*, (2009) Gaussian, Inc., Wallingford, CT, USA.

[3] C. Adamo and V. Barone, *J. Chem. Phys.*, 1999, **110**, 6158.

[4] (a) J. P. Perdew, K. Burke and M. Ernzerhof, *Phys. Rev. Lett.*, 1996, **77**, 3865; (b) J. P. Perdew, K. Burke and M. Ernzerhof, *Phys. Rev. Lett.*, 1997, **78**, 1396.

[5] (a) T. H. Dunning, Jr. and P. J. Hay, *Modern Theoretical Chemistry*, Springer US, New York, 1977; (b) T. H. Dunning, Jr. and P. J. Hay, *Methods of Electronic Structure Theory*, Plenum Press, New York, 1977; (c) J. P. Hay and W. R. Wadt, *J. Chem. Phys.*, 1985, **82**, 270; (d) W. R. Wadt and J. P. Hay, *J. Chem. Phys.*, 1985, **82**, 284; (e) J. P. Hay and W. R. Wadt, *J. Chem. Phys.*, 1985, **82**, 299.

[6] R. Dennington, T. Keith and J. Millam, *GaussView V. 5.0.9*, (2009) Semichem Inc., Shawnee Mission, KS.

[7] N. M. O'Boyle, A. L. Tenderholt and K. M. Langner, *J. Comput. Chem.*, 2008, **29**, 839.

[8] L. Skripnikov, *Chemissian, V 4.30*, (2005-2014).

Chapitre 15 - Informations supplémentaires : Light-induced self-assembly of a luminescent tetraruthenium square

15.1. Materials, methods and instrumentation

All solvent and reagents were used as purchased without further purification before the reactions. $RuCl_3.3H_2O$ was purchased from Pressure Chemical Corporation. All other reagents were purchased from Sigma-Aldrich. ACS grade solvents were purchased from VWR and Fisher.

Nuclear magnetic resonance (NMR) spectra were recorded in acetone-d_6 at room temperature (r.t.) on a Bruker AV400 (400 MHz) spectrometer for ^{1}H NMR, at 100 MHz for ^{13}C NMR and 600 MHz for DOSY experiment, respectively. Chemical shifts (δ) are reported in part per million (ppm) relative to TMS, and are referenced to the residual solvent protons (δ = 2.05 ppm for acetone-d_6) and the carbon resonance (δ = 30.83 ppm for acetone- d_6) of the solvent.

All the photophysical measurements were carried out in deaerated acetonitrile at r.t. in sealed quartz cells. Absorption spectra were measured on a Cary 500i UV-Vis-NIR Spectrophotometer from Agilent Technologies. For steady-state luminescence measurements, a Jobin Yvon-Spex Fluoromax P spectrofluorimeter was used, equipped with a Hamamatsu R3896 photomultiplier. The spectra were corrected for photomultiplier response by using a program purchased with the fluorimeter. For the luminescence lifetimes, an Edinburgh OB 900 time-correlated single-photon-counting spectrometer was used. A Hamamatsu PLP 2 laser diode (59 ps pulse width at 408 nm) and/or nitrogen discharge (pulse width 2 ns at 337 nm) were employed as excitation sources.

Time-resolved transient absorption experiments were performed using a pump–probe setup based on the Spectra-Physics MAI-TAI Ti:sapphire system as the laser source and the Ultrafast Systems Helios spectrometer as the detector. The pump pulse was generated using a Spectra-Physics 800 FP OPA instrument. The probe pulse was

obtained by continuum generation on a sapphire plate (spectral range 450–800 nm). The effective time resolution was around 200 fs, and the temporal chirp over the white-light 450–750 nm range around 150 fs; the temporal window of the optical delay stage was 0–3200 ps. In order to cancel out orientation effects on the dynamics, the polarization direction of the linearly polarized probe pulse was set at a magic angle of 54.7° with respect to that of the pump pulse. Please note that all the transient spectra shown in the present paper are chirp corrected. The chirp correction was done by using the pump induced absorption signals themselves in the same conditions (same cuvette, solvent, temperature, stirring frequency, etc.) used for each single experiment. All the time-resolved data were analyzed with the Ultrafast Systems Surface Explorer Pro software (http://www.ultrafastsystems.com/surfexp.html).

Accurate high-resolution mass spectrometry experiments (HR-MS) was performed on a micrOTOF-Q II mass spectrometer from Bruker Daltonics, in positive electrospray mode. Appropriate $[M\text{-}PF_6]^{n+}$ species were used for empirical formula determination, and exact masses were calculated using the Compass DataAnalysis V4.0 SP5 software package from Bruker Daltonics.

Electrochemical measurements were carried out in argon-purged purified dimethylformamide at room temperature with a BAS CV50W multipurpose potentiostat. The working electrode was a 3-mm diameter glassy carbon electrode from CH Instruments. The counter electrode was a Pt wire, and the pseudo-reference electrode was a silver wire. The reference was set using an internal 1 mM ferrocene/ferrocinium sample at 0.450 mV vs. SCE in acetonitrile. The concentration of the compounds was about 1 mM. Tetrabutylammonium hexafluorophosphate (TBAP) was used as supporting electrolyte and its concentration was 0.10 M. Cyclic voltammograms of were obtained at scan rates of 50, 100, 200 and 500 mVs^{-1}, respectively. The criteria for reversibility were the separation between cathodic and anodic peaks, the close to unity ratio of the intensities of the cathodic and anodic currents, and the constancy of the peak potential on changing scan rate. Square wave voltammetry was conducted with a sweep rate of 20 mVs^{-1} and a pulse amplitude, width and period of 50 mV, 50 ms and 200 ms, respectively.

X-Ray diffraction data collection for the metal complexes **3** and **5** was carried out on a Bruker Venture Metaljet diffractometer equipped with an Oxford Cryosystem liquid

N2 device, using Ga-Kα radiation (λ = 1.34139 Å). The cell parameters were determined (APEX2 software) from reflections taken from three sets of 100 frames, each at 1 s exposure. The structure was solved by direct methods using the program Olex2. The H-atoms were included in calculated positions and treated as riding atoms using Olex2 default parameters. The non-H atoms were refined anisotropically, using weighted full-matrix least-squares on F2. CCDC 1542678 and CCDC 1542679 contain the supplementary crystallographic data for this paper. These data can be obtained free of charge from The Cambridge Crystallographic Data Centre via www.ccdc.cam.ac.uk/data_request/cif.

Experimental uncertainties are as follows: absorption maxima, ±2 nm; molar absorption coefficient, 10%; redox potentials, ± 10 mV, emission maxima, ±2 nm; Diffusion-ordered spectroscopy, ±10 %. The microanalyses were performed at the Elemental Analysis Service of the Université de Montréal.

15.2 Synthesis of the ligands and the metal complexes

The 4,4”-di-*tert*-butyl-4’-(pyridine-4-yl)-2,2’:6’,2”-terpyridine ligand (4-pytpy) was synthesized as previously described.[1] Unless otherwise stated, the solvents were removed under reduced pressure using a rotary evaporator.

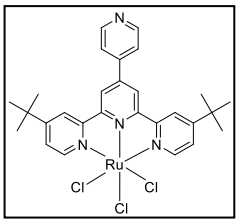

15.2.1. (4-pytpy)$RuCl_3$ (1)

A 100 mL round-bottomed flask charged with ligand 4-pytpy (425 mg, 1 mmol) and $RuCl_3.3H_2O$ (260 mg, 1 mmol) in a mixture of DCM:EtOH 95:5 (50 mL). The reaction mixture was left under reflux conditions for 3 hours. After this time, the solution was evaporated to dryness. A minimum amount of ethanol (10 mL) was added to wash the precipitate. The resulting suspension was sonicated for 5 minutes before being poured into an excess amount of water (200 mL). The suspension was then filtered over a fine porosity glass filter and dried overnight, leaving a deep brown powder, which was used without further purification (535 mg, 85 %).

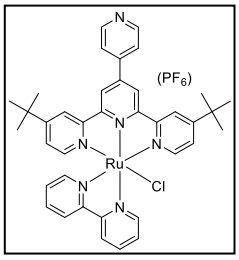

15.2.2. [(4-pytpy)(2,2'-bpy)RuCl][(PF_6)] (2)

A 20-mL microwave vial was charged with precursor 1 (100 mg, 0.16 mmol), 2,2'-bpy (37 mg, 0.24 mmol) and LiCl (20 mg, 0.48 mmol) in ethylene glycol (20 mL) with 4-ethylmorpholine (16 drops). The reaction mixture was left under microwave irradiation (400W) for 30 minutes. After this time, a few drops of hydrazine were added to convert any Ru(III) to Ru(II). The resulting purple solution was poured into an aqueous solution of KPF_6 (10 eq.) leading to instant precipitation of a deep purple precipitate. The heterogeneous solution was filtered over Celite®. The precipitate was washed with plenty of water and then dissolve in a minimum amount of acetonitrile. The organic fraction was then evaporated to dryness. The residue was purified on a neutral alumina column, deactivated with 5% p/p water, using a MeCN:toluene mixture in a 1:2 ratio. The recovered purple solution was evaporated to dryness. The residue was dissolved in a minimum amount of acetone and precipitated by the addition of an excess amount of diethyl ether (50 mL). The burgundy precipitate was recovered by filtration over a PTFE membrane (50 mg, 37 %).

^{1}H NMR (400 MHz, $(CD_3)_2O$): δ (ppm) = 10.37 (d, *J* = 6 Hz, 1H), 9.23 (s, 2H), 8.91-8.85 (m, 5H), 8.62 (d, *J* = 8 Hz, 1H), 8.41 (td, *J* = 8 Hz, 1H), 8.11-8.08 (m, 3H), 7.81 (td, *J* = 8 Hz, 1H), 7.72 (d, *J* = 6 Hz, 2H), 7.65 (d, *J* = 6 Hz, 1H), 7.44 (dd, *J* = 8 Hz, 2H), 7.10 (td, *J* = 6 Hz, 1H), 1.38 (s, 18H).

^{13}C NMR (100 MHz, $(CD_3)_2O$): δ (ppm) = 162.5, 159.9, 159.5, 157.2, 154.9, 153.5, 152.9, 152.6, 151.8, 145.3, 143.5, 137.6, 136.5, 127.7, 127.2, 125.4, 124.5, 124.3, 122.7, 122.3, 121.1, 36.1.

HR-MS (ESI): m/z $[M]^+$ calcd for $C_{38}H_{38}N_6RuCl$: 715.18913; found: 715.19149; difference: 3.30 ppm.

Calc. for $C_{38}H_{38}N_6RuClPF_6 \cdot 3H_2O$: C, 49.92; H, 4.85; N, 9.19. Found: C, 50.26; H, 4.37; N, 9.17%.

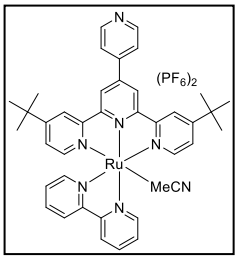

15.2.3. [(4-pytpy)(2,2'-bpy)(CH_3CN)Ru][(PF_6)$_2$] (3)

A 100 mL round-bottomed flask was charged with metal complex 2 (100 mg, 0.12 mmol) and silver triflate (90 mg, 0.35 mmol) in acetonitrile (50 mL). The reaction mixture was left at reflux for 72 h. After this time, the reaction mixture was cooled to room temperature and few drops of hydrazine hydrate were added to precipitate the remaining excess of silver triflate and convert any Ru(III) to Ru(II). The resulting slurry was filtered over Celite®. The filtrate was evaporated to minimum amount (5 mL) and poured into an aqueous solution of KPF_6 (10 eq.). The precipitate was extracted with chloroform and evaporated under vacuum. The residue was dissolve in a minimum amount of acetone and precipitated by the addition of diethyl ether. The orange precipitate was filtered over a PTFE membrane (112 mg, 96 %).

^{1}H NMR (400 MHz, $(CD_3)_2O$): δ (ppm) = 9.91 (d, *J* = 6 Hz, 1H), 9.32 (s, 2H), 8.93-8.91 (m, 4H), 8.66 (d, *J* = 8 Hz, 1H), 8.46 (td, *J* = 8 Hz, 1H), 8.17 (s (broad), 2H), 8.11 (ddd, *J* = 8 Hz, 2H), 7.96 (td, *J* = 8 Hz, 1H), 7.86 (d, *J* = 6 Hz, 2H), 7.67 (d, *J* = 6 Hz, 1H), 7.55 (dd, *J* = 6 Hz, 2H), 7.22 (td, *J* = 8 Hz, 1H), 1.39 (s, 18H).

^{13}C NMR (100 MHz, $(CD_3)_2O$): δ (ppm) = 164.2, 159.3, 158.9, 158.6, 156.7, 153.4, 152.0, 138.6, 138.4, 128.6, 127.7, 126.5, 126.0, 125.1, 124.5, 123.3, 122.4, 36.3.

HR-MS (ESI): m/z $[M\text{-}PF_6]^+$ calcd for $C_{40}H_{41}N_7RuPF_6$: 866.21138; found: 866.20876; difference: 3.02 ppm.

Calc. for $C_{40}H_{41}N_7RuP_2F_{12}\cdot 3H_2O$: C, 45.12; H, 4.45; N, 9.21. Found: C, 45.02; H, 4.10; N, 9.34%.

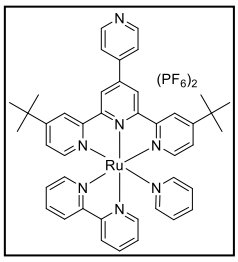

15.2.4. [(4-pytpy)(2,2'-bpy)(py)Ru][$(PF_6)_2$] (4)

A 100 mL round-bottomed flask was charged with metal complex 2 (100 mg, 0.12 mmol) and silver triflate (90 mg, 0.35 mmol) in pyridine (50 mL). The reaction mixture was left at reflux for 120 h. After this time, the reaction mixture was cooled to room temperature and few drops of hydrazine hydrate were added to precipitate the remaining excess of silver triflate and convert any Ru(III) to Ru(II). The resulting slurry was filtered over Celite®. The filtrate was evaporated to dryness and solubilized in a minimum amount of acetone (5 mL) and then poured into an aqueous solution of KPF_6 (10 eq.). The precipitate was extracted with chloroform and evaporated under vacuum. The residue was dissolve in a minimum amount of acetone and precipitated by the addition of diethyl ether. The orange precipitate was filtered over a PTFE membrane (102 mg, 84 %).

^{1}H NMR (400 MHz, $(CD_3)_2O$): δ (ppm) = 9.30 (s, 2H), 8.98-8.93 (m, 5H), 8.71 (d, *J* = 8 Hz, 1H), 8.45 (dt, *J* = 8 Hz, 1H), 8.20 (s (broad), 2H), 8.04-8.00 (m, 5H), 7.96 (t, *J* = 8 Hz, 1H), 7.89 (t, *J* = 8 Hz, 1H), 7.68 (d, *J* = 6 Hz, 1H), 7.61 (dd, *J* = 6 Hz, 2H), 7.35 (t, *J* = 6 Hz, 2H), 7.22 (t, *J* = 6 Hz, 1H), 1.38 (s, 18H).

^{13}C NMR (100 MHz, $(CD_3)_2O$): δ (ppm) = 164.2, 163.7, 159.3, 158.7, 158.3, 157.1, 153.3, 153.0, 152.5, 152.1, 139.1, 138.6, 138.3, 128.7, 127.7, 127.3, 126.7, 125.3, 124.5, 123.7, 122.7, 36.2.

HR-MS (ESI): m/z $[M\text{-}PF_6]^+$ calcd for $C_{43}H_{42}N_7RuPF_6$: 904.22712; found: 904.22618; difference: 1.04 ppm.

Calc. for $C_{43}H_{43}N_7RuP_2F_{12}.(C_2H_5)_2O$: C, 50.27; H, 4.76; N, 8.73. Found: C, 50.01; H, 5.03; N, 8.42%.

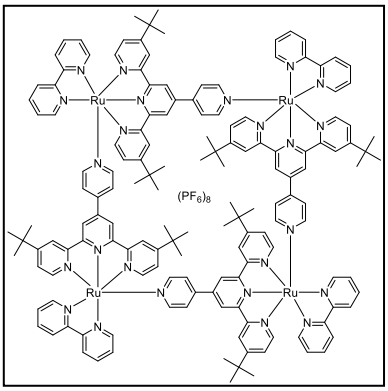

15.2.5. [((4-pytpy)(2,2'-bpy)Ru)$_4$][(PF_6)$_8$] (5)

A NMR tube was charged with metal complex 3 (21.3 mg, 0.005 mmol) in acetone (0.6 mL). The tube was irradiated at 452 nm for 24h. After this time, the solvent was evaporated under vacuum. The residue was then purified on Sephadex LH-20 column using 45:45:10 (acetone:MeOH:H_2O). The counter-anions were exchanged with a solution of KPF_6 in water (10 eq.), resulting in the precipitation of an orange-red solid. The solid was extracted with chloroform (5 x 25 mL) and the organic fraction was evaporated to near-dryness (~5mL). Diethyl ether (50 mL) was added, leading to the precipitation of an orange-red solid, which was further filtered over a PTFE membrane (16.3 mg, 80 %).

^{1}H NMR (400 MHz, $(CD_3)_2O$): δ (ppm) = 9.09-9.07 (m, 8H), 8.96 (t, *J* = 8 Hz, 8H), 8.87 (d, *J* = 6 Hz, 4H), 8.82 (s, 8H), 8.71 (d, *J* = 8 Hz, 4H), 8.45 (t, *J* = 8 Hz, 4H), 8.17 (d, *J* = 6 Hz, 4H), 8.04-7.95 (m, 28H), 7.63 (m, 8H), 7.21 (t, *J* = 6 Hz, 4H) 1.37 (s, 72H).

^{13}C NMR (100 MHz, $(CD_3)_2O$): δ (ppm) = 164.6, 159.5, 158.5, 157.2, 154.0, 153.4, 152.5, 152.2, 152.0, 146.7, 144.4, 139.0, 138.9, 138.6, 138.5, 129.0, 128.0, 127.2, 127.1, 125.6, 124.7, 124.0, 123.9, 122.8, 122.7, 36.4.

HR-MS (ESI): m/z $[M-2PF_6]^{+2}$ calcd for $C_{152}H_{152}N_{24}Ru_4P_6F_{36}$: 1794.8362; found: 1794.8377; difference: 0.84 ppm; $[M-3PF_6]^{+3}$ calcd for $C_{152}H_{152}N_{24}Ru_4P_5F_{30}$: 1148.2359; found: 1148.2343; difference: 1.39 ppm

Calc. for $C_{152}H_{152}N_{24}Ru_4P_8F_{48}\cdot 2CHCl_3$: C, 44.92; H, 3.77; N, 8.16. Found: C, 44.54; H, 4.13; N, 7.88%.

Table 15.1 - Solid-state structure and refinement data for complexes **3** and **5**.

	3	**5**
Formula	$[C_{40}H_{41}N_7Ru][(PF_6)_2]$ $\cdot 2.67CH_3CN$	$[C_{152}H_{152}N_{24}Ru_4][(PF_6)_8]$
Color/form	Red/block	red/block
M_w [gmol^{-1}]	1120.42	3878.41
Temperature [K]	100.0	100.0
Wavelength [Å]	1.341139	1.341139
Crystal system	Triclinic	Monoclinic
a [Å]	8.854(2)	15.7071(8)
b [Å]	15.812(3)	19.5715(9)
c [Å]	17.958(2)	39.546(2)
α [°]	81.988(7)	90
β [°]	89.181(7)	98.830(3)
γ [°]	89.061(7)	90
V [Å^3]	2489.1(8)	12013(1)
Space group	*P*-1	$P2_1/c$
Z	2	2
$d_{calcd.}$ [gcm^{-3}]	1.495	1.072
μ [mml^{-1}]	2.626	2.096
F(000)	1141	3919
Reflection collected	63303	72982
Independent reflections	11378	12925
GoF	1.047	1.043
R_1(F) [$I > 2\sigma(I)$]	0.0716	0.1388
$wR(F^2)$ [$I > 2\sigma(I)$]	0.1921	0.4417
R_1(F) (all data)	0.0743	0.1413
wR(F^2) (all data)	0.1959	0.4459
Largest diff. peak/hole [eÅ^{-3}]	1.540	1.845

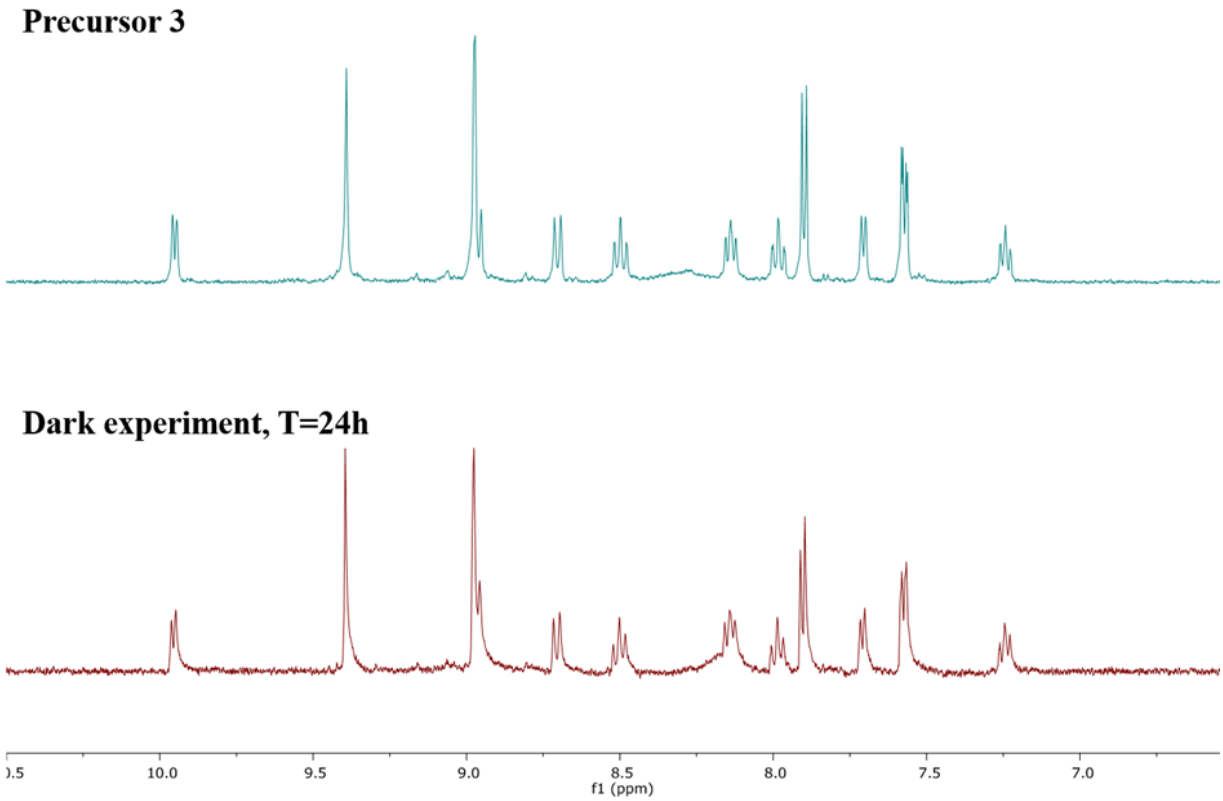

Figure 15.1 - Comparison of the 1H NMR spectra of the starting material 3 (top) and the dark experiment after 24 hours of irradiation, with the sample protected from light. The experiment was performed in acetone-d_6 at 20ºC. No changes were observed at all.

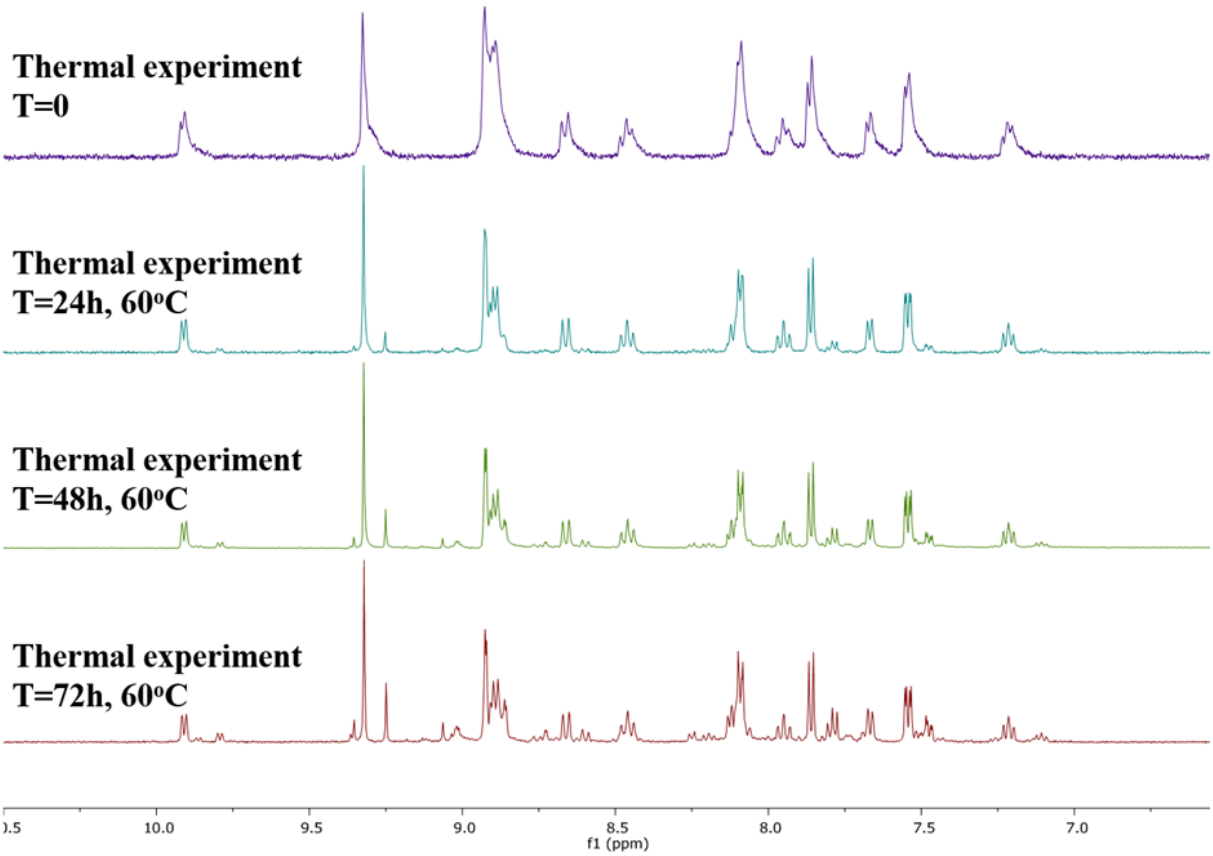

Figure 15.2 - 1H NMR study over time of the thermal attempt to convert 3 (top) into 5. The experiment was performed in acetone-d_6 at 60°C. Very slight changes can be observed over 72 hours, however no traces of species **4** were detected.

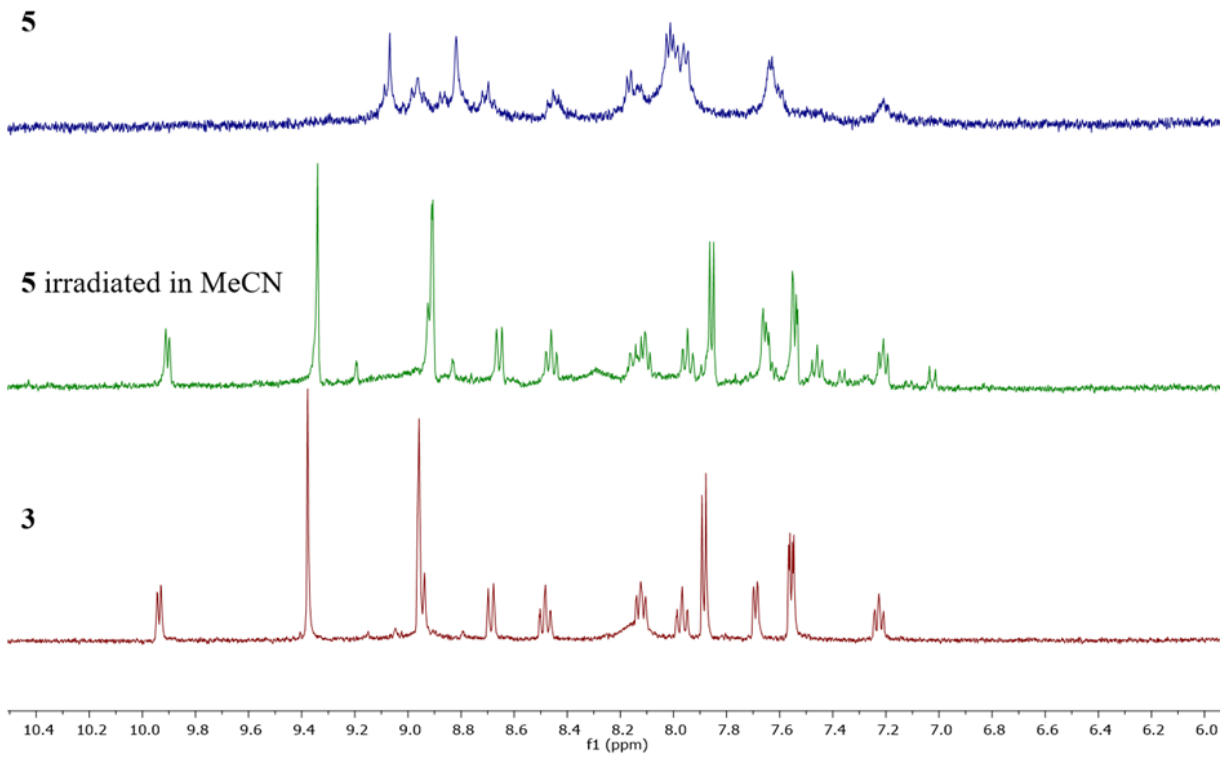

Figure 15.3 - ^{1}H NMR of the conversion of **5** (blue) to **3** (green) and comparison to **3** obtained by thermal (red).

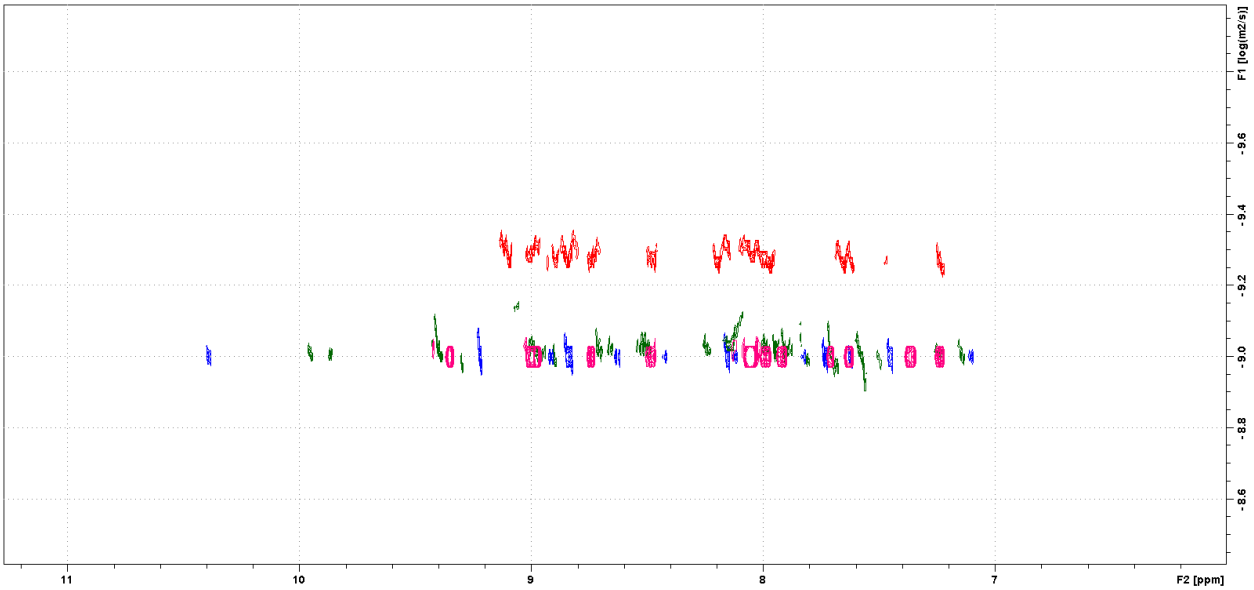

Figure 15.4 - DOSY NMR experiment on precursor 2 (blue) and 3 (green), model complex 4 (pink) and self-assembled metallosquare 5 (red).

Table 15.2 - Experimental DOSY values.

Cmpd	Log D (m^2/s)	D (m^2/s)
2	**-8.998**	**$10.0x10^{-10}$**
3	**-9.003**	**$9.93x10^{-10}$**
4	**-9.001**	**$9.98x10^{-10}$**
5	**-9.285**	**$5.19x10^{-10}$**

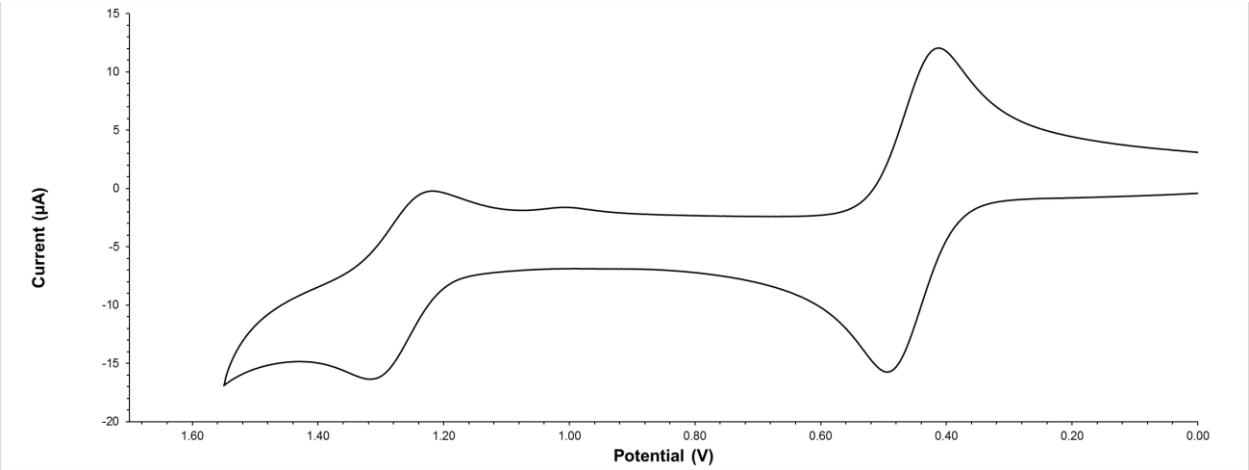

Figure 15.5 - Cyclic voltammogram in DMF displaying the oxidation of **2**, with ferrocene added.

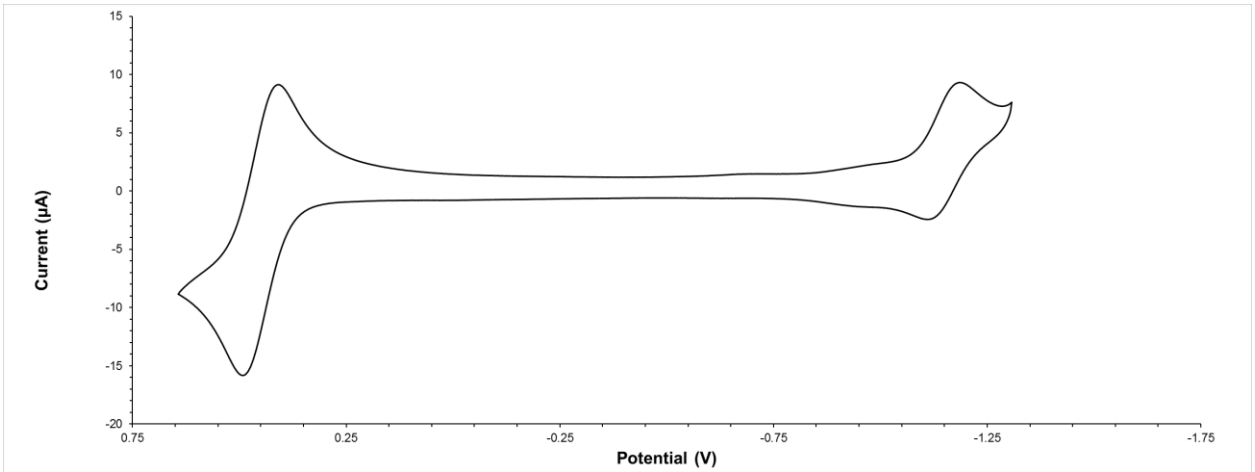

Figure 15.6 - Cyclic voltammogram in DMF displaying the reduction of 2, with ferrocene added.

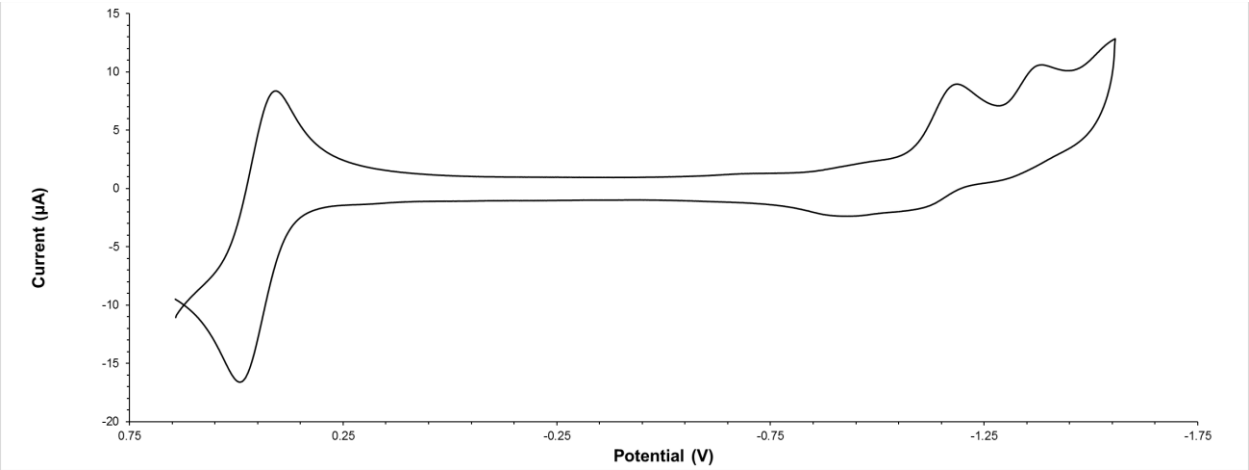

Figure 15.7 - Cyclic voltammogram in DMF displaying the reduction of **2**, with ferrocene added. At potential higher than -1.35 V, decomposition of the species was observed.

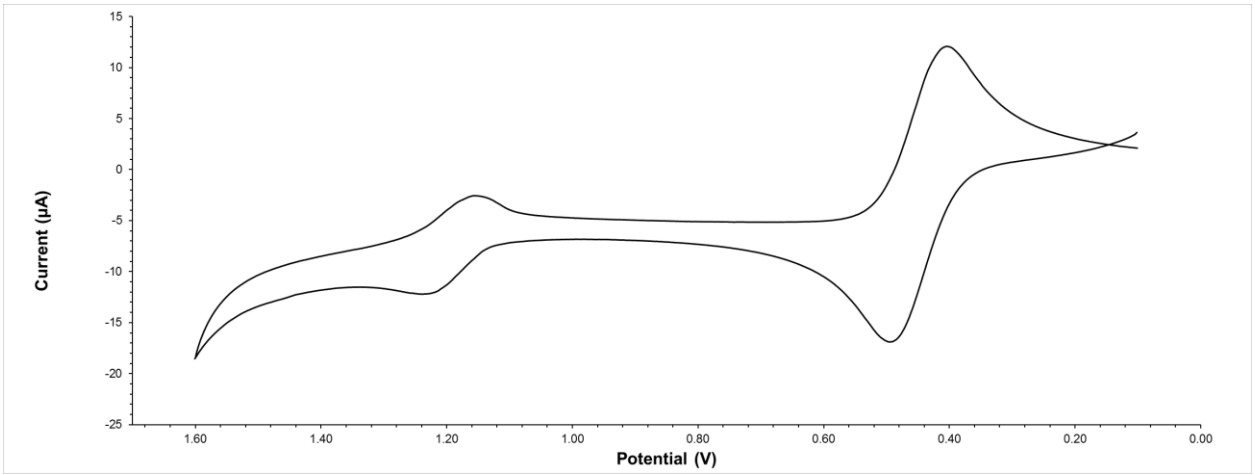

Figure 15.8 - Cyclic voltammogram in DMF displaying the oxidation of **3**, with ferrocene added.

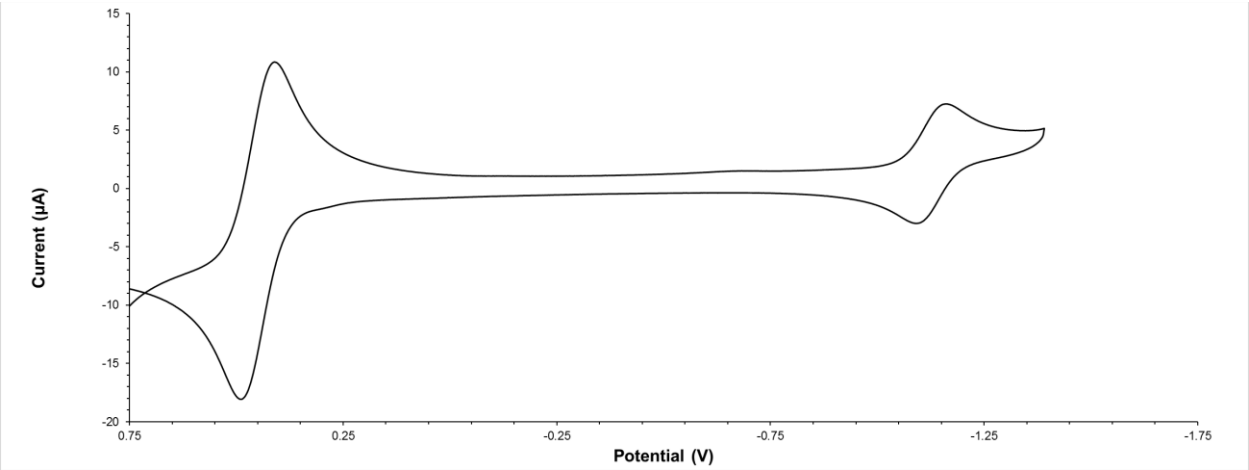

Figure 15.9 yclic voltammogram in DMF displaying the reduction of **3**, with ferrocene added.

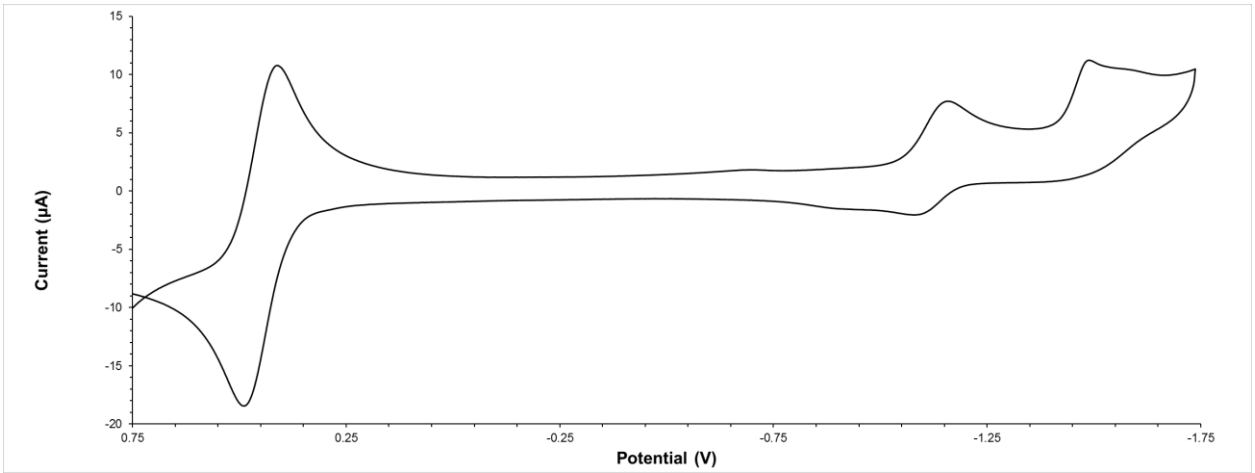

Figure 15.10 - Cyclic voltammogram in DMF displaying the reduction of 3, with ferrocene added. At potential higher than -1.30 V, decomposition of the species was observed.

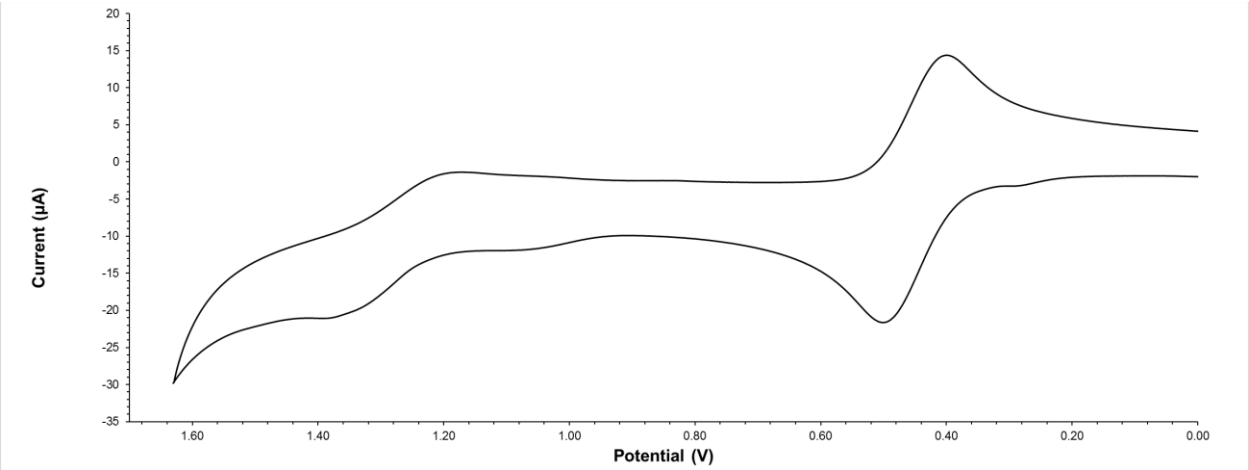

Figure 15.11 - Cyclic voltammogram in DMF displaying the oxidation of **5**, with ferrocene added.

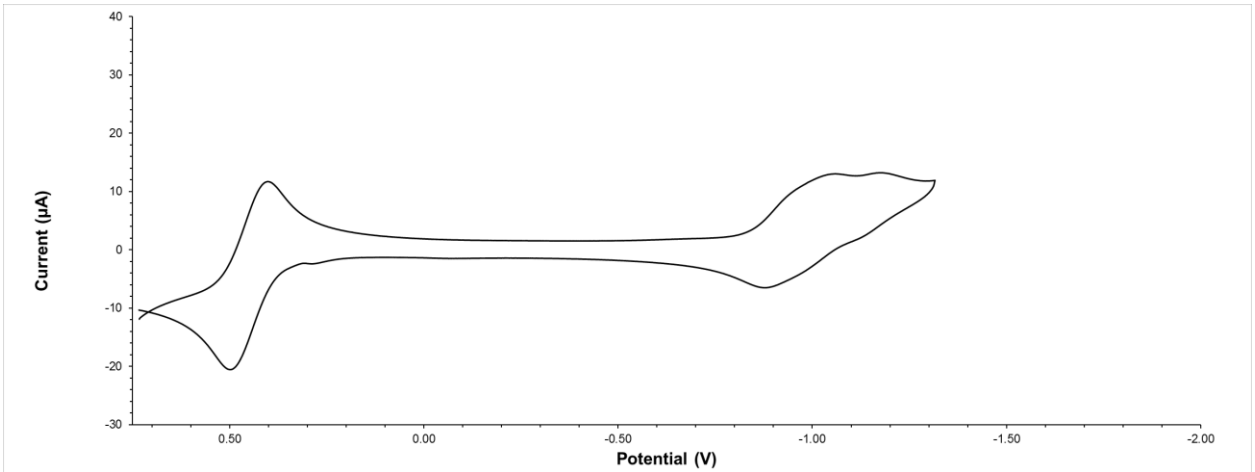

Figure 15.12 - Cyclic voltammogram in DMF displaying the reduction of **5**, with ferrocene added.

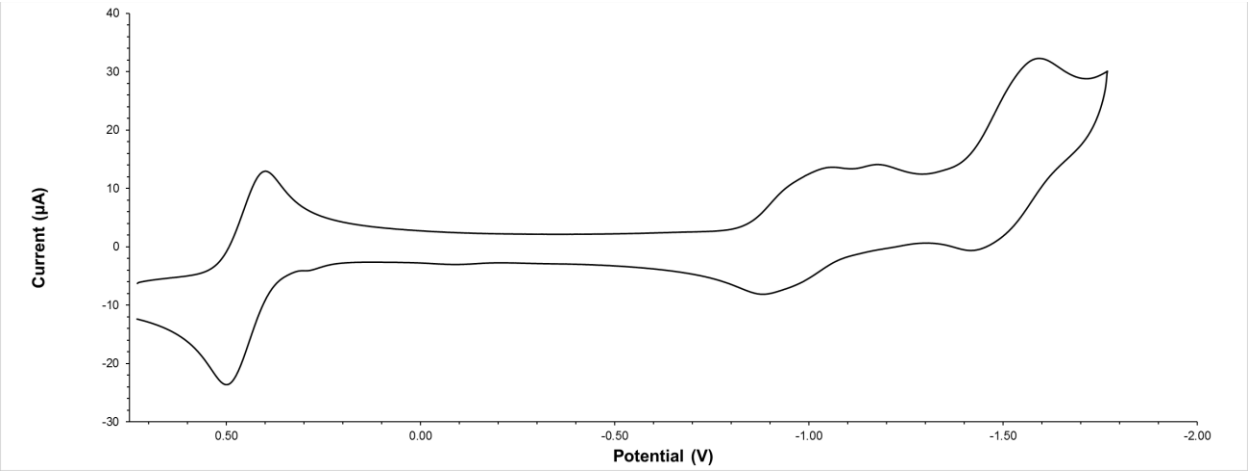

Figure 15.13 - Cyclic voltammogram in DMF displaying the reduction of **5**, with ferrocene added.

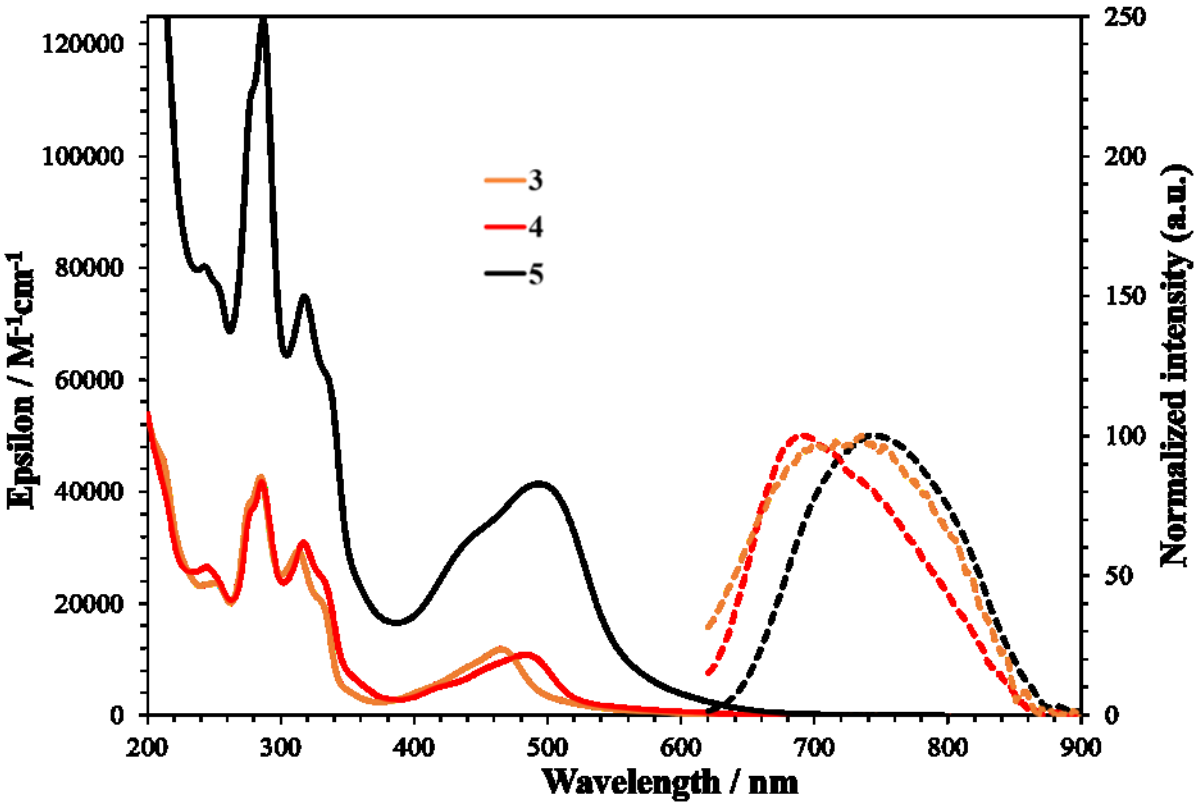

Figure 15.14 - Absorption (plain) and normalized luminescence (dash) spectra of the precursor (**3**), model complex (**4**) and assembly (**5**) in deaerated MeCN solution, at ambient temperature.

Table 15.3 - Atomic coordinates for DFT optimization of **3** in ($S = 0$) PBE0/LANL2DZ, CPCM(CH_3CN).

Standard orientation					
Center Number	Atomic Number	Atomic Type	Coordinates (Angstroms)		
			X	Y	Z
1	44	0	0.001117	-1.210875	0.328824
2	7	0	-0.004486	0.754844	0.096703
3	6	0	-0.012623	3.510377	-0.132925
4	6	0	1.185601	1.409260	0.053312
5	6	0	-1.198453	1.401168	0.041194
6	6	0	-1.225073	2.792790	-0.077913
7	6	0	1.204028	2.801037	-0.064027
8	6	0	-2.357114	0.489542	0.120528
9	6	0	-4.392601	-1.357361	0.293160
10	6	0	-3.686001	0.918971	0.059688
11	7	0	-2.043607	-0.841674	0.265090
12	6	0	-3.053170	-1.736955	0.349277
13	6	0	-4.745902	-0.000323	0.144580
14	6	0	2.349578	0.506681	0.154599
15	6	0	4.395857	-1.324464	0.363380
16	7	0	2.043818	-0.826472	0.297335
17	6	0	3.676014	0.945892	0.112990
18	6	0	4.741298	0.034828	0.216929
19	6	0	3.058584	-1.713985	0.399307

20	7	0	0.018865	-1.702905	-1.659478
21	6	0	0.044083	-2.565399	-4.320428
22	6	0	0.022451	-0.805626	-2.675220
23	6	0	0.027731	-3.043517	-1.948214
24	6	0	0.040378	-3.493499	-3.274987
25	6	0	0.034924	-1.197385	-4.013723
26	6	0	0.022708	-3.931537	-0.779220
27	6	0	0.011122	-5.417287	1.556605
28	7	0	0.009331	-3.286691	0.430901
29	6	0	0.030750	-5.330575	-0.854663
30	6	0	0.024928	-6.084258	0.322847
31	6	0	0.003616	-4.021902	1.571240
32	6	0	-0.016497	4.986977	-0.257021
33	7	0	-0.022178	7.812467	-0.495241
34	6	0	0.994545	5.663398	-0.967087
35	6	0	-1.030223	5.768561	0.330627
36	6	0	-0.992890	7.160725	0.188353
37	6	0	0.951568	7.059483	-1.060043
38	1	0	1.718661	7.596787	-1.608439
39	1	0	1.792872	5.124097	-1.465235
40	1	0	-1.826306	5.317476	0.913046
41	1	0	-1.762222	7.779099	0.639568
42	1	0	-2.169994	3.317379	-0.147177
43	1	0	2.145907	3.335470	-0.075835

44	1	0	3.875561	2.003107	-0.002039
45	1	0	2.780986	-2.754455	0.512655
46	1	0	5.156555	-2.091799	0.450257
47	1	0	-3.891727	1.975053	-0.054828
48	1	0	-5.148775	-2.130611	0.366276
49	1	0	-2.769512	-2.775517	0.464888
50	1	0	0.014923	0.241179	-2.402891
51	1	0	0.037288	-0.442860	-4.790992
52	1	0	0.053845	-2.902435	-5.350712
53	1	0	0.047242	-4.553693	-3.494008
54	1	0	0.041574	-5.830003	-1.815253
55	1	0	0.031057	-7.167391	0.278553
56	1	0	0.006153	-5.961900	2.493174
57	1	0	-0.007126	-3.469336	2.500979
58	6	0	-6.216286	0.416138	0.082097
59	6	0	-6.385777	1.936052	-0.083618
60	6	0	-6.886314	-0.290639	-1.121209
61	6	0	-6.917667	-0.019962	1.391189
62	6	0	6.209326	0.462388	0.176705
63	6	0	6.369820	1.983217	0.010555
64	6	0	6.893149	0.034186	1.497685
65	6	0	6.903911	-0.241460	-1.014316
66	1	0	-5.953650	2.490123	0.758685
67	1	0	-6.462614	0.466830	2.261949

68	1	0	-7.975138	0.266726	1.351626
69	1	0	-6.869612	-1.104478	1.539410
70	1	0	-7.453996	2.176429	-0.122608
71	1	0	-5.931032	2.299290	-1.013351
72	1	0	-6.412201	0.005301	-2.064527
73	1	0	-7.945150	-0.010279	-1.166445
74	1	0	-6.831853	-1.381711	-1.036907
75	1	0	5.919476	2.535726	0.844293
76	1	0	7.436662	2.231789	-0.011137
77	1	0	5.927859	2.341003	-0.927426
78	1	0	6.420211	0.518565	2.360213
79	1	0	7.948719	0.329493	1.474475
80	1	0	6.851668	-1.050471	1.647008
81	1	0	7.961529	0.045749	-1.042190
82	1	0	6.855154	-1.332777	-0.929643
83	1	0	6.443648	0.050356	-1.965740
84	7	0	-0.015596	-0.900656	2.349275
85	6	0	-0.024908	-0.674684	3.496680
86	6	0	-0.036298	-0.407143	4.924745
87	1	0	0.856230	0.157076	5.210470
88	1	0	-0.052062	-1.346797	5.484858
89	1	0	-0.922015	0.176239	5.192681

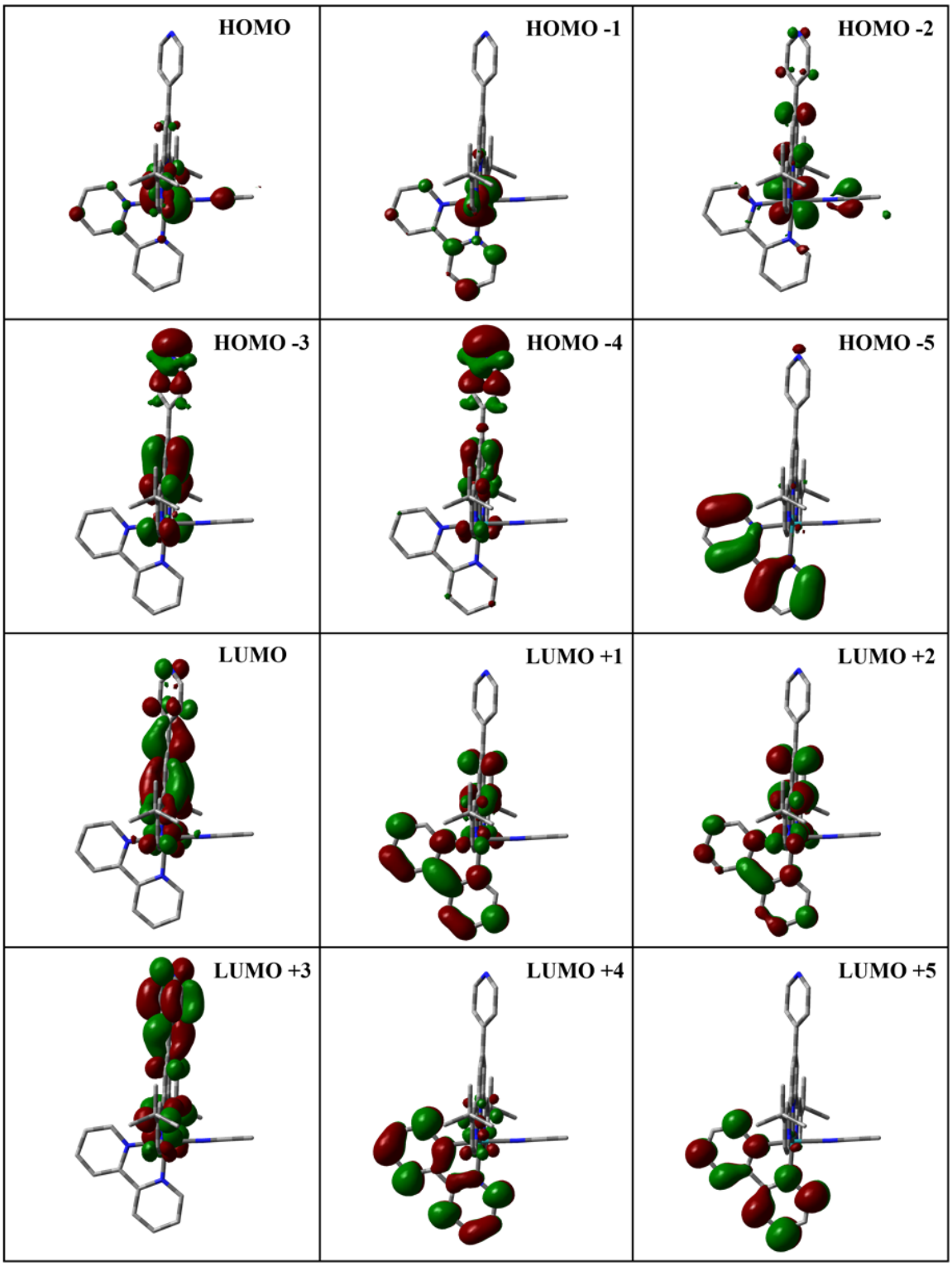

Figure 15.15 - Kohn-Sham electron density illustration of the molecular orbitals for **3** in (*S*=0) the ground-state

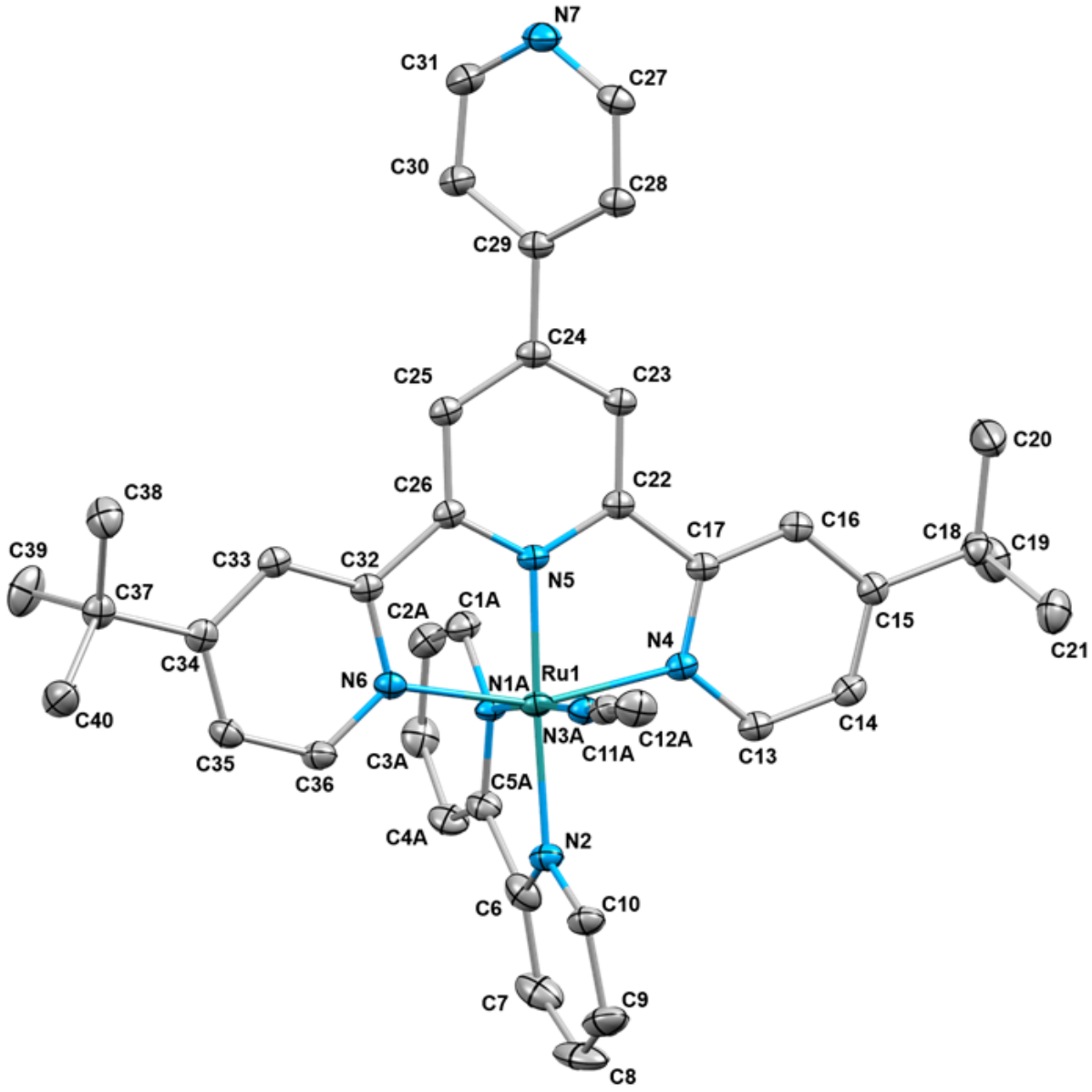

Figure 15.16 - Single-crystal X-ray structure of **3** with the numbering of the atoms showing one of the two possible position for the acetonitrile ligand on the metal core. The ellipsoids were plotted at a 30% probability level. The solvent molecules (acetonitrile), the hydrogen atoms as well as the PF_6 counter-anions have been omitted for clarity.

Table 15.4 - Selected bond distances (Å) and angles (°) of **3**

Bond Length			Angle		
	Obs. (X-ray)	Calc. (DFT)		Obs. (X-ray)	Calcl. (DFT)
N1A-Ru1	1.988(4)	2.04835	N1A-Ru1-N2	79.90(17)	78.914
			N1B-Ru1-N2	77.0(3)	
			N1A-Ru1-N3A	176.0(2)	174.830
N1B-Ru1	1.961(5)		N1B-Ru1-N3B	169.2(4)	
			N1A-Ru1-N4	91.9(2)	91.215
			N1B-Ru1-N4	93.1(3)	
N2-Ru1	2.067(3)	2.07834	N1A-Ru1-N5	100.14(16)	97.166
			N1B-Ru1-N5	103.0(3)	
			N1A-Ru1-N6	91.7(2)	91.228
N3A-Ru1	2.115(6)	2.04420	N1B-Ru1-N6	91.7(3)	
			N2-Ru1-N3A	96.16(19)	95.915
			N2-Ru1-N3B	92.3(4)	
N3B-Ru1	2.126(14)		N2-Ru1-N4	97.68(13)	100.460
			N2-Ru1-N5	177.58(12)	176.080
			N2-Ru1-N6	103.65(13)	100.532
N4-Ru1	2.068(3)	2.07879	N3A-Ru1-N4	89.41(18)	89.710
			N3B-Ru1-N4	88.8(5)	
			N3A-Ru1-N5	83.82(18)	88.004
N5-Ru1	1.973(3)	1.97938	N3B-Ru1-N5	87.7(4)	
			N3A-Ru1-N6	88.37(18)	89.731
			N3B-Ru1-N6	90.3(5)	
N6-Ru1	2.075(3)	2.07877	N4-Ru1-N5	79.90(13)	79.477
			N4-Ru1-N6	158.67(13)	158.946
			N5-Ru1-N6	78.77(13)	79.469

Table 15.5 - MO composition of **3** in (*S=0*) ground state.

MO	Energy (eV)	Composition (%)			
		Ruthenium	**4-pytpy**	**MeCN**	**2,2'-bipyridyl**
LUMO+5	-1.481	1	1	98	0
LUMO+4	-1.687	1	13	0	86
LUMO+3	-1.727	0	100	0	0
LUMO+2	-2.545	4	62	1	33
LUMO+1	-2.611	2	36	0	62
LUMO	**-2.885**	**6**	**93**	**1**	**0**
HOMO	**-6.451**	**71**	**17**	**5**	**7**
HOMO-1	-6.610	75	0	11	14
HOMO-2	-6.703	72	20	6	3
HOMO-3	-7.710	1	96	0	2
HOMO-4	-7.794	0	95	0	5
HOMO-5	-7.847	1	7	0	92

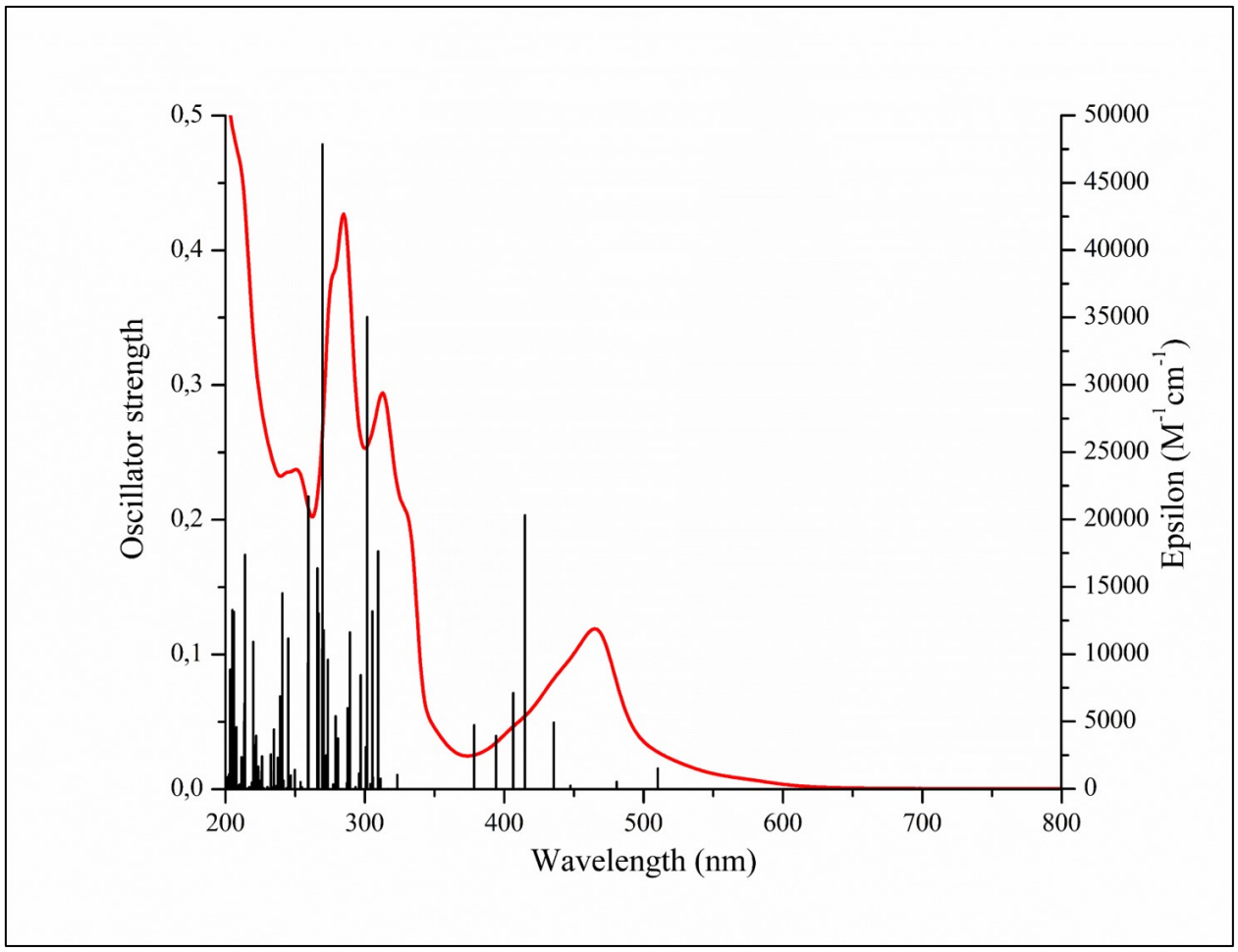

Figure 15.17 - Comparison of the experimental (red) absorption spectra recorded in acetonitrile and TD-DFT (black) simulated (PBE0/LANL2DZ; CPCM: CH_3CN) absorption spectrum for the precursor complex **3**.

Table 15.6 - Selected transitions from TD-DFT calculations of **3** in the singlet ground state (PBE0), CPCM (CH_3CN).

Energy (eV)	**λ (nm)**	**f**	**Transition**	**Character**
2.42	510	0.0153	H→L (93%)	$^1MLCT_{tpy}$
2.83	436	0.0494	H-2→L (55%) H→L+1 (15%) H→L+2 (27%)	
2.98	415	0.2034	H-2→L (17%) H-1→L+2 (43%) H→L+1 (21%) H→L+2 (13%)	$^1MLCT_{tpy}$ + $^1MLCT_{bpy}$
3.04	407	0.0715	H-1→L+1 (83%) H-1→L+2 (14%)	
3.99	310	0.1766	H-3→L (47%) H-1→L+3 (21%) H→L+3 (12%)	$^1MLCT_{tpy}$
4.04	305	0.1321	H→L+5 (79%)	$^1MLCT_{bpy}$
4.09	302	0.3505	H-4→L (32%) H-1→L+3 (16%) H→L+3 (19%)	$^1MLCT_{tpy}$
4.16	297	0.0847	H-2→L+3 (85%)	
4.27	289	0.1165	H-5→L (14%) H→L+6 (67%)	$^1MLCT_{tpy}$ + $LLCT_{bpy→tpy}$

4.29	288	0.0602	H-5→L (81%) H→L+6 (14%)	
4.42	279	0.0542	H-1→L+7 (29%) H→L+7 (37%)	$^1MLCT_{tpy} + {}^1MLCT_{bpy}$
4.51	274	0.0961	H-2→L+6 (86%)	$^1MLCT_{tpy}$
4.56	270	0.1180	H-5→L+1 (24%) H-3→L+1 (14%) H-3→L+2 (44%)	$^1MLCT_{tpy} + {}^1MLCT_{MeCN}$
4.58	270	0.1047	H-2→L+7 (16%) H-1→L+10 (21%) H-1→L+15 (20%)	
4.63	267	0.1305	H-5→L+2 (44%) H-4→L+1 (16%) H-4→L+2 (28%)	
4.64	266	0.1639	H-5→L+1 (18%) H-5→L+2 (31%) H-4→L+1 (16%) H-4→L+2 (22%)	$LLCT_{bpy\rightarrow tpy}$
4.76	259	0.2173	H-7→L (56%) H-2→L+13 (14%)	
4.76	259	0.0940	H-7→L (28%) H-2→L+10 (10%) H-2→L+13 (26%) H-2→L+15 (17%)	$^1MLCT_{MeCN}$

5.04	245	0.1118	H-7→L+1 (30%) H-7→L+2 (35%) H-4→L+3 (12%)	
5.13	241	0.1454	H-8→L+1 (65%)	
5.16	239	0.0689	H-8→L+2 (43%) H-6→L+1 (22%) H-6→L+2 (18%)	$LLCT_{tpy\rightarrow bpy}$
5.61	220	0.1094	H-9→L+1 (22%) H-9→L+2 (26%) H-5→L+4 (11%) H-5→L+5 (20%)	
5.77	214	0.1739	H-12→L (18%) H-3→L+6 (47%)	$^1MLCT_{tpy}$
5.78	214	0.0635	H-2→L+9 (67%)	
5.79	213	0.0500	H-12→L (71%) H-3→L+6 (17%)	$LLCT_{bpy\rightarrow tpy}$
6.02	205	0.1331	H-8→L+3 (29%) H-2→L+13 (10%) H→L+12 (10%)	$^1MLCT_{MeCN}$
6.07	204	0.0803	H-16→L (14%) H-8→L+4 (53%)	$LLCT_{tpy\rightarrow bpy}$
6.07	203	0.0889	H-8→L+3 (24%) H-8→L+4 (11%)	$^1MLCT_{MeCN}$

Table 15.7 - Atomic coordinates for DFT optimization of **4** in (S = 0) PBE0/LANL2DZ, CPCM(CH_3CN).

Standard orientation					
Center Number	Atomic Number	Atomic Type	Coordinates (Angstroms)		
			X	Y	Z
1	44	0	-0.001550	-1.169516	0.179308
2	7	0	0.024039	0.794961	-0.010041
3	6	0	0.061931	3.559843	-0.178183
4	6	0	1.225010	1.433782	-0.059747
5	6	0	-1.158469	1.465851	-0.056194
6	6	0	-1.161597	2.859749	-0.137235
7	6	0	1.265853	2.827559	-0.144292
8	6	0	-2.331392	0.571038	-0.054316
9	6	0	-4.393703	-1.251790	-0.153903
10	6	0	-3.649215	1.023532	-0.170516
11	7	0	-2.040907	-0.771076	0.029466
12	6	0	-3.065817	-1.653773	-0.032360
13	6	0	-4.722876	0.118252	-0.218629
14	6	0	2.374913	0.510875	-0.004386
15	6	0	4.389787	-1.361624	0.128455
16	7	0	2.045844	-0.817452	0.154470
17	6	0	3.707211	0.922326	-0.102352
18	6	0	4.757074	-0.010013	-0.037957
19	6	0	3.047887	-1.724510	0.218781
20	7	0	0.040062	-1.619788	-1.831914

21	6	0	-0.002485	-2.414681	-4.513130
22	6	0	0.075319	-0.698354	-2.824864
23	6	0	-0.009513	-2.950723	-2.153082
24	6	0	-0.034797	-3.367681	-3.490980
25	6	0	0.056743	-1.055867	-4.172995
26	6	0	-0.011526	-3.868236	-1.006435
27	6	0	0.089019	-5.426932	1.278206
28	7	0	0.016769	-3.258664	0.222728
29	6	0	-0.010129	-5.264530	-1.125091
30	6	0	0.034065	-6.055931	0.026250
31	6	0	0.080160	-4.032896	1.335889
32	6	0	0.081116	5.039105	-0.258305
33	7	0	0.119261	7.870720	-0.410234
34	6	0	1.098575	5.721140	-0.953853
35	6	0	-0.916714	5.818579	0.358873
36	6	0	-0.857986	7.213643	0.258824
37	6	0	1.077547	7.119882	-1.003717
38	1	0	1.850126	7.661473	-1.540086
39	1	0	1.885100	5.184965	-1.473685
40	1	0	-1.716828	5.362799	0.932076
41	1	0	-1.614918	7.829934	0.733301
42	1	0	-2.098103	3.400825	-0.192759
43	1	0	2.217335	3.344843	-0.155708
44	1	0	3.923082	1.974760	-0.231123
45	1	0	2.754434	-2.758832	0.346280

46	1	0	5.137807	-2.143991	0.187852
47	1	0	-3.834260	2.087972	-0.229386
48	1	0	-5.160087	-2.017283	-0.193588
49	1	0	-2.803502	-2.703690	0.019348
50	1	0	0.116159	0.340371	-2.526030
51	1	0	0.086114	-0.283063	-4.931600
52	1	0	-0.022072	-2.725890	-5.551409
53	1	0	-0.077555	-4.420965	-3.737493
54	1	0	-0.037123	-5.732976	-2.100699
55	1	0	0.034973	-7.137116	-0.052246
56	1	0	0.139533	-5.999317	2.196672
57	1	0	0.133380	-3.516610	2.284436
58	6	0	-6.181508	0.561495	-0.341102
59	6	0	-6.322279	2.091853	-0.406565
60	6	0	-6.784663	-0.046776	-1.630533
61	6	0	-6.966579	0.045148	0.889039
62	6	0	6.230520	0.386164	-0.141360
63	6	0	6.415984	1.902700	-0.320733
64	6	0	6.960057	-0.052025	1.151545
65	6	0	6.858904	-0.336647	-1.357530
66	1	0	-5.934389	2.576999	0.497506
67	1	0	-6.564299	0.467631	1.817469
68	1	0	-8.017829	0.344389	0.803453
69	1	0	-6.933930	-1.047235	0.966194
70	1	0	-7.383195	2.351955	-0.490527

71	1	0	-5.808666	2.513304	-1.279333
72	1	0	-6.245235	0.302374	-2.518999
73	1	0	-7.833008	0.259933	-1.723252
74	1	0	-6.756068	-1.142047	-1.619707
75	1	0	6.014719	2.467353	0.529760
76	1	0	7.485906	2.127885	-0.390592
77	1	0	5.940890	2.266898	-1.239855
78	1	0	6.534862	0.446197	2.030888
79	1	0	8.019975	0.219661	1.082550
80	1	0	6.901035	-1.134860	1.307727
81	1	0	7.919019	-0.068339	-1.434428
82	1	0	6.794938	-1.426365	-1.263294
83	1	0	6.361971	-0.042327	-2.289550
84	7	0	-0.127023	-0.914215	2.279867
85	6	0	-0.374527	-0.561489	5.061819
86	6	0	-1.205852	-1.395529	2.956443
87	6	0	0.826282	-0.253809	2.990094
88	6	0	0.736858	-0.061836	4.370248
89	6	0	-1.361398	-1.240946	4.333915
90	1	0	1.678746	0.121264	2.442432
91	1	0	1.528877	0.470176	4.884089
92	1	0	-0.468746	-0.426555	6.133727
93	1	0	-2.241223	-1.648159	4.818047
94	1	0	-1.952791	-1.916571	2.373367

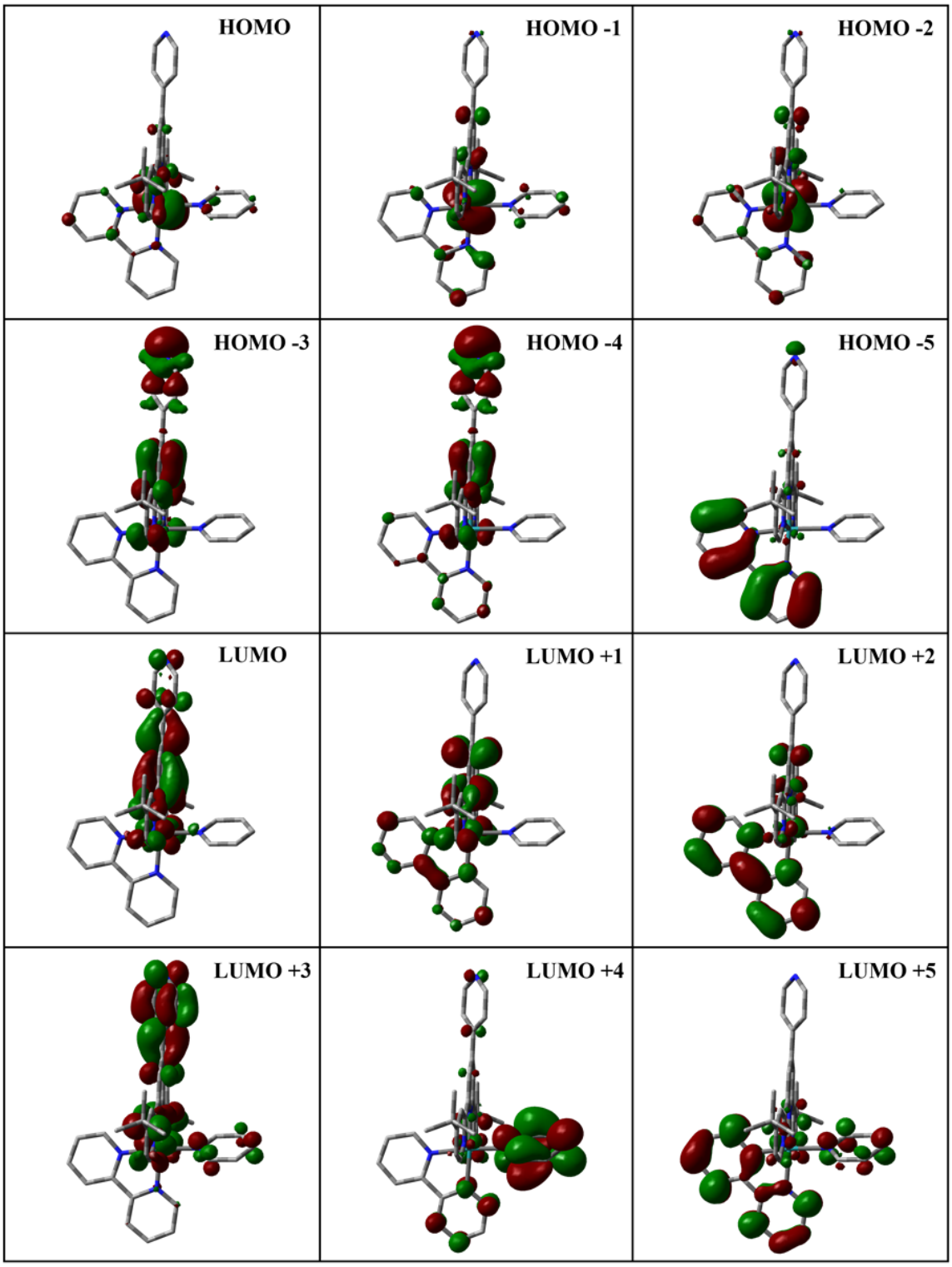

Figure 15.18 - Kohn-Sham electron density illustration of the molecular orbitals for **4** in (*S*=0) the ground-state

Table 15.8 - MO composition of **4** in (*S=0*) ground state.

MO	Energy (eV)	Composition (%)			
		Ruthenium	**4-pytpy**	**pyridine**	**2,2'-bipyridyl**
LUMO+5	-1.684	2	13	13	73
LUMO+4	-1.734	3	14	69	14
LUMO+3	-1.764	0	88	9	3
LUMO+2	-2.564	5	20	2	74
LUMO+1	-2.608	1	78	0	21
LUMO	**-2.895**	**7**	**91**	**1**	**1**
HOMO	**-6.364**	**73**	**18**	**3**	**6**
HOMO-1	-6.555	74	14	3	9
HOMO-2	-6.579	74	17	1	8
HOMO-3	-7.719	0	97	0	2
HOMO-4	-7.796	0	91	0	9
HOMO-5	-7.833	1	10	0	89

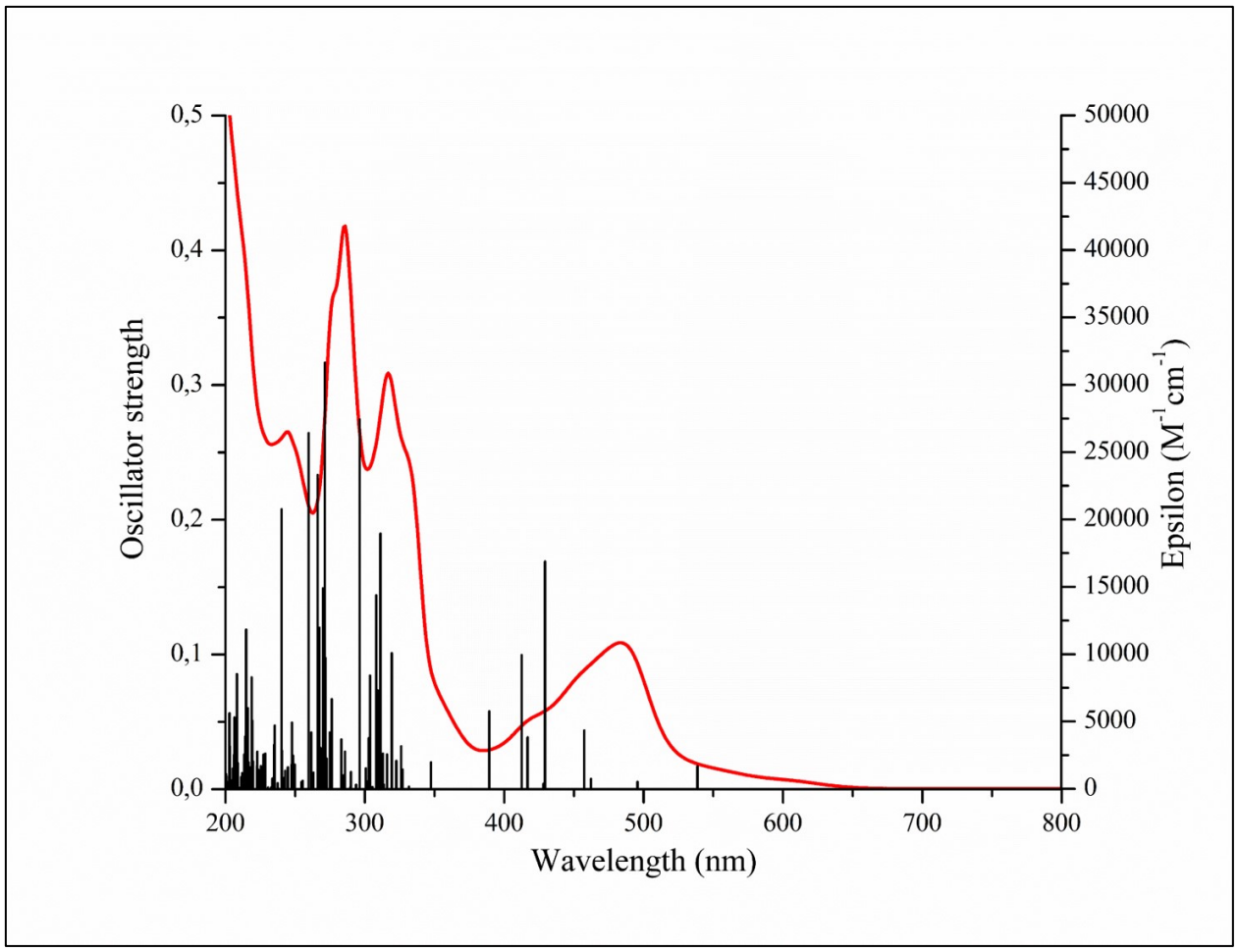

Figure 15.19 - Comparison of the experimental (red) absorption spectra recorded in acetonitrile and TD-DFT (black) simulated (PBE0/LANL2DZ; CPCM: CH_3CN) absorption spectrum for the model Ru(II) complex **4**.

Table 15.9 - Selected transitions from TD-DFT calculations of **4** in the singlet ground state (PBE0), CPCM (CH_3CN).

Energy (eV)	**λ (nm)**	**f**	**Transition**	**Character**
2,29	539	0,0171	H→L (94%)	
2,49	496	0,0056	H-2→L (43%) H-1→L (51%)	$^1MLCT_{tpy}$
2,67	462	0,0077	H→L+2 (84%)	$^1MLCT_{tpy}$ + $^1MLCT_{bpy}$
2,70	457	0,0437	H-2→L (26%) H-1→L (20%) H→L+1 (47%)	$^1MLCT_{tpy}$
2,88	429	0,1690	H-2→L (12%) H-2→L+2 (14%) H-1→L+2 (17%) H→L+1 (38%)	$^1MLCT_{tpy}$ + $^1MLCT_{bpy}$
2,99	413	0,0996	H-2→L+1 (87%)	
3,17	389	0,0578	H-2→L+2 (38%) H-1→L+2 (19%)	$^1MLCT_{tpy}$ + $^1MLCT_{bpy}$
3,87	319	0,1011	H-1→L+4 (34%) H→L+6 (15%) H→L+13 (15%)	$^1MLCT_{bpy}$ + $^1MLCT_{py}$
3,97	311	0,1898	H-2→L+3 (14%) H-1→L+3 (16%) H-1→L+4 (10%)	$^1MLCT_{tpy}$ + $^1MLCT_{bpy}$ + $^1MLCT_{py}$

			H→L+6 (29%)	
3,99	309	0,0733	H-3→L (19%), H-1→L+3 (18%) H→L+6 (22%) H→L+8 (17%)	$^1MLCT_{tpy}$ + $^1MLCT_{bpy}$
4,01	308	0,1440	H-3→L (22%) H-2→L+3 (39%)	$^1MLCT_{tpy}$
4,06	304	0,0844	H-4→L (24%) H-1→L+6 (23%)	$^1MLCT_{tpy}$ + $^1MLCT_{bpy}$
4,17	296	0,2744	H-4→L (14%) H→L+7 (52%) H→L+8 (14%)	$^1MLCT_{tpy}$
4,47	276	0,0669	H-4→L+2 (14%) H-3→L+2 (29%) H-2→L+8 (11%) H→L+8 (10%) H→L+9 (11%)	$^1MLCT_{tpy}$ and/or $^1MLCT_{py}$ + $LLCT_{tpy→bpy}$ and/or $LLCT_{tpy→py}$
4,54	272	0,0973	H-3→L+1 (53%) H-3→L+2 (25%)	$LLCT_{tpy→bpy}$
4,55	271	0,3167	H-5→L+1 (15%) H-5→L+2 (29%) H-1→L+9 (37%)	$^1MLCT_{tpy}$ and/or $^1MLCT_{py}$ + $LLCT_{bpy→tpy}$ and/or $LLCT_{bpy→py}$
4,57	270	0,1492	H-5→L+2 (31%) H-2→L+9 (29%)	$^1MLCT_{py}$

			H-1→L+9 (18%)	
4,64	266	0,2333	H-5→L+1 (10%) H-2→L+9 (22%) H-1→L+9 (19%)	
4,76	260	0,2643	H-8→L (87%)	$LLCT_{py→tpy}$
5,14	240	0,2078	H-9→L+1 (39%)	$LLCT_{tpy→bpy}$ + $LLCT_{py→bpy}$
5,63	219	0,0509	H-11→L+2 (19%) H-10→L+2 (10%) H-5→L+6 (19%) H-4→L+4 (11%)	$LLCT_{tpy→bpy}$
5,64	219	0,0830	H-8→L+4 (13%) H-7→L+4 (30%)	$LLCT_{tpy→py}$
5,72	216	0,0603	H-12→L+1 (13%) H-3→L+7 (21%) H-2→L+14 (18%)	$^1MLCT_{tpy}$
5,75	215	0,1185	H-4→L+7 (10%) H-3→L+7 (28%) H-2→L+14 (20%)	
5,93	208	0,0855	H-14→L+2 (11%) H-12→L+2 (16%) H-7→L+3 (28%)	$LLCT_{py→tpy}$
5,98	207	0,0533	H-8→L+3 (44%)	
6,09	203	0,0564	H-14→L+1 (17%) H-9→L+5 (30%)	$LLCT_{tpy→bpy}$

Table 15.10 - Atomic coordinates for DFT optimization of **5** in ($S = 0$) PBE0/LANL2DZ, CPCM(CH_3CN).

Standard orientation					
Center Number	Atomic Number	Atomic Type	Coordinates (Angstroms)		
			X	Y	Z
1	44	0	-1.454917	-7.762329	-0.059820
2	7	0	-2.575030	-6.137288	-0.031983
3	6	0	-4.105019	-3.830446	0.013048
4	6	0	-2.878798	-5.528829	-1.210699
5	6	0	-3.006595	-5.658785	1.167568
6	6	0	-3.778735	-4.495555	1.211930
7	6	0	-3.645051	-4.361674	-1.209357
8	6	0	-2.586952	-6.493069	2.310008
9	6	0	-1.704585	-8.168762	4.309256
10	6	0	-2.958202	-6.243099	3.634233
11	7	0	-1.785995	-7.564693	1.981463
12	6	0	-1.360578	-8.377943	2.975629
13	6	0	-2.524099	-7.081120	4.675960
14	6	0	-2.357907	-6.250765	-2.387424
15	6	0	-1.417468	-7.795533	-4.465332
16	7	0	-1.646886	-7.393429	-2.102014
17	6	0	-2.593915	-5.853118	-3.707008
18	6	0	-2.122876	-6.617720	-4.787822
19	6	0	-1.201075	-8.146717	-3.135153

20	7	0	-3.001632	-9.123431	-0.179419
21	6	0	-4.958224	-11.105158	-0.437700
22	6	0	-4.315438	-8.794386	-0.216625
23	6	0	-2.637443	-10.441249	-0.264311
24	6	0	-3.603659	-11.447827	-0.396470
25	6	0	-5.319749	-9.754064	-0.343542
26	6	0	-1.193250	-10.695763	-0.185171
27	6	0	1.547681	-10.972644	0.079056
28	7	0	-0.413752	-9.574455	-0.053380
29	6	0	-0.625164	-11.976587	-0.208511
30	6	0	0.759353	-12.120865	-0.081785
31	6	0	0.927807	-9.722786	0.089489
32	6	0	-4.931639	-2.603215	0.036100
33	7	0	-6.544290	-0.269126	0.093635
34	6	0	-5.813766	-2.290322	-1.015567
35	6	0	-4.882590	-1.698910	1.112889
36	6	0	-5.687063	-0.561620	1.107768
37	6	0	-6.589121	-1.136367	-0.954388
38	1	0	-7.275318	-0.900278	-1.755570
39	1	0	-5.931677	-2.944493	-1.871635
40	1	0	-4.212760	-1.851323	1.951339
41	1	0	-5.648206	0.129495	1.936770
42	1	0	-4.145247	-4.122110	2.159938
43	1	0	-3.870244	-3.857694	-2.140867

44	1	0	-3.154356	-4.946176	-3.891157
45	1	0	-0.658606	-9.048531	-2.877947
46	1	0	-1.029713	-8.448802	-5.238432
47	1	0	-3.589741	-5.391758	3.851735
48	1	0	-1.325916	-8.862271	5.051203
49	1	0	-0.730812	-9.208857	2.683975
50	1	0	-4.559648	-7.743151	-0.145810
51	1	0	-6.356911	-9.442445	-0.368836
52	1	0	-5.713875	-11.875591	-0.540358
53	1	0	-3.308970	-12.487110	-0.465544
54	1	0	-1.250194	-12.853680	-0.317403
55	1	0	1.210695	-13.106273	-0.098748
56	1	0	2.622830	-11.036679	0.195711
57	1	0	1.505889	-8.818916	0.222739
58	6	0	-2.903008	-6.853667	6.139871
59	6	0	-3.786360	-5.608357	6.326891
60	6	0	-3.677465	-8.091895	6.653878
61	6	0	-1.609854	-6.672561	6.971047
62	6	0	-2.354977	-6.227783	-6.248137
63	6	0	-3.142093	-4.912962	-6.383561
64	6	0	-0.983515	-6.056971	-6.945458
65	6	0	-3.151743	-7.356255	-6.946682
66	1	0	-3.276325	-4.692680	6.003355
67	1	0	-1.042910	-5.797975	6.630465

68	1	0	-1.871424	-6.522854	8.025010
69	1	0	-0.957185	-7.550426	6.909747
70	1	0	-4.025900	-5.494566	7.389833
71	1	0	-4.734765	-5.693678	5.782412
72	1	0	-4.602546	-8.240970	6.084476
73	1	0	-3.943008	-7.945373	7.707345
74	1	0	-3.079512	-9.007281	6.583497
75	1	0	-2.612702	-4.069846	-5.922775
76	1	0	-3.271779	-4.680196	-7.446187
77	1	0	-4.141842	-4.986383	-5.938153
78	1	0	-0.399464	-5.257811	-6.473701
79	1	0	-1.139655	-5.792225	-7.997711
80	1	0	-0.391389	-6.978323	-6.916418
81	1	0	-3.309724	-7.093888	-7.999218
82	1	0	-2.618878	-8.313113	-6.916101
83	1	0	-4.132560	-7.493919	-6.476311
84	44	0	-7.768465	1.456349	0.098299
85	7	0	-6.141275	2.573286	0.068236
86	6	0	-3.830295	4.098440	0.030846
87	6	0	-5.579169	2.883420	-1.131787
88	6	0	-5.614432	2.996445	1.250328
89	6	0	-4.449507	3.767079	1.252880
90	6	0	-4.410544	3.646466	-1.172064
91	6	0	-6.401668	2.569528	2.423065

92	6	0	-7.992561	1.672360	4.484270
93	6	0	-6.098009	2.933039	3.738188
94	7	0	-7.485245	1.769451	2.133924
95	6	0	-8.256488	1.336938	3.158190
96	6	0	-6.891262	2.490598	4.810912
97	6	0	-6.350184	2.374071	-2.282158
98	6	0	-7.984003	1.457540	-4.301786
99	7	0	-7.482739	1.664753	-1.955460
100	6	0	-6.006128	2.618848	-3.615176
101	6	0	-6.816411	2.159123	-4.667196
102	6	0	-8.280810	1.231600	-2.960051
103	7	0	-9.131770	3.004886	0.043497
104	6	0	-11.120419	4.965368	-0.110293
105	6	0	-8.803070	4.318759	0.004851
106	6	0	-10.452439	2.642454	0.011461
107	6	0	-11.462568	3.610731	-0.067726
108	6	0	-9.766133	5.324977	-0.071055
109	6	0	-10.704951	1.197544	0.084335
110	6	0	-10.972543	-1.547196	0.317337
111	7	0	-9.579862	0.416069	0.158990
112	6	0	-11.986105	0.630048	0.106139
113	6	0	-12.125940	-0.756237	0.218042
114	6	0	-9.722889	-0.927683	0.285276
115	6	0	-2.602094	4.923736	0.011465

116	7	0	-0.267866	6.537699	-0.007833
117	6	0	-2.315339	5.793255	-1.058069
118	6	0	-1.669264	4.885551	1.064342
119	6	0	-0.533829	5.691231	1.022393
120	6	0	-1.159919	6.568604	-1.035269
121	1	0	-0.942827	7.243826	-1.851197
122	1	0	-2.989941	5.901253	-1.899454
123	1	0	-1.798154	4.223970	1.913118
124	1	0	0.177690	5.661488	1.834308
125	1	0	-4.039455	4.128016	2.187673
126	1	0	-3.943982	3.876444	-2.121741
127	1	0	-5.104863	3.176817	-3.832111
128	1	0	-9.173229	0.690231	-2.669842
129	1	0	-8.670680	1.079299	-5.050248
130	1	0	-5.239569	3.564719	3.924709
131	1	0	-8.654154	1.288061	5.251988
132	1	0	-9.098166	0.708175	2.896988
133	1	0	-7.749464	4.561461	0.032973
134	1	0	-9.454715	6.362112	-0.099810
135	1	0	-11.893724	5.722543	-0.172053
136	1	0	-12.504222	3.317604	-0.095133
137	1	0	-12.866481	1.256773	0.043204
138	1	0	-13.111522	-1.207176	0.235799
139	1	0	-11.032469	-2.624142	0.418623

140	1	0	-8.814488	-1.507832	0.369706
141	6	0	-6.601564	2.857968	6.266787
142	6	0	-5.356964	3.751130	6.405914
143	6	0	-7.821650	3.615401	6.845206
144	6	0	-6.370808	1.558048	7.075087
145	6	0	-6.484066	2.398498	-6.140450
146	6	0	-5.174187	3.184339	-6.322956
147	6	0	-6.342864	1.030271	-6.850864
148	6	0	-7.637542	3.200339	-6.790576
149	1	0	-4.451896	3.251887	6.038636
150	1	0	-5.507199	1.003417	6.689195
151	1	0	-6.175887	1.810120	8.123979
152	1	0	-7.244369	0.897441	7.046207
153	1	0	-5.198671	3.983641	7.464694
154	1	0	-5.474468	4.702654	5.873013
155	1	0	-8.005798	4.544248	6.292453
156	1	0	-7.628427	3.872438	7.893215
157	1	0	-8.733776	3.009354	6.811948
158	1	0	-4.314532	2.650691	-5.899128
159	1	0	-4.983186	3.320302	-7.393078
160	1	0	-5.228081	4.181370	-5.868720
161	1	0	-5.528060	0.441891	-6.412430
162	1	0	-6.117344	1.191335	-7.911488
163	1	0	-7.263941	0.440022	-6.790479

164	1	0	-7.415170	3.364422	-7.851360
165	1	0	-8.593021	2.667924	-6.726962
166	1	0	-7.756195	4.178356	-6.309366
167	44	0	1.454799	7.762727	-0.058793
168	7	0	2.574089	6.137143	-0.031085
169	6	0	4.104128	3.830352	0.013493
170	6	0	2.877991	5.529021	-1.209931
171	6	0	3.005395	5.658271	1.168407
172	6	0	3.777604	4.495076	1.212532
173	6	0	3.644255	4.361877	-1.208826
174	6	0	2.585412	6.492135	2.311033
175	6	0	1.702096	8.166774	4.310723
176	6	0	2.957129	6.242243	3.635141
177	7	0	1.783392	7.563073	1.982834
178	6	0	1.357589	8.375868	2.977211
179	6	0	2.522564	7.079742	4.677093
180	6	0	2.357090	6.251326	-2.386428
181	6	0	1.416291	7.796722	-4.463693
182	7	0	1.645256	7.393367	-2.100553
183	6	0	2.593615	5.854515	-3.706170
184	6	0	2.122421	6.619467	-4.786668
185	6	0	1.199350	8.147036	-3.133371
186	7	0	3.002084	9.123163	-0.178476
187	6	0	4.959478	11.104007	-0.437241

188	6	0	4.315759	8.793574	-0.215376
189	6	0	2.638413	10.441082	-0.263936
190	6	0	3.605040	11.447229	-0.396356
191	6	0	5.320465	9.752809	-0.342504
192	6	0	1.194295	10.696177	-0.185089
193	6	0	-1.546554	10.974235	0.078752
194	7	0	0.414319	9.575212	-0.053166
195	6	0	0.626737	11.977230	-0.208736
196	6	0	-0.757735	12.122100	-0.082221
197	6	0	-0.927193	9.724123	0.089536
198	6	0	4.930771	2.603131	0.036305
199	7	0	6.543643	0.269159	0.093401
200	6	0	5.812946	2.290514	-1.015393
201	6	0	4.881757	1.698582	1.112894
202	6	0	5.686332	0.561361	1.107561
203	6	0	6.588406	1.136621	-0.954433
204	1	0	7.274659	0.900797	-1.755636
205	1	0	5.930847	2.944873	-1.871315
206	1	0	4.211897	1.850763	1.951364
207	1	0	5.647489	-0.129931	1.936404
208	1	0	4.143945	4.121344	2.160497
209	1	0	3.869514	3.858151	-2.140460
210	1	0	3.154527	4.947928	-3.890667
211	1	0	0.656303	9.048402	-2.875792

212	1	0	1.028354	8.450199	-5.236529
213	1	0	3.589388	5.391362	3.852341
214	1	0	1.323024	8.859851	5.052867
215	1	0	0.727097	9.206335	2.685862
216	1	0	4.559526	7.742259	-0.144187
217	1	0	6.357509	9.440778	-0.367545
218	1	0	5.715447	11.874105	-0.540088
219	1	0	3.310774	12.486600	-0.465873
220	1	0	1.252134	12.854057	-0.317670
221	1	0	-1.208668	13.107692	-0.099429
222	1	0	-2.621691	11.038741	0.195258
223	1	0	-1.505644	8.820516	0.222937
224	6	0	2.901877	6.852355	6.140911
225	6	0	3.786564	5.607933	6.327581
226	6	0	3.675065	8.091279	6.655137
227	6	0	1.608973	6.669699	6.972143
228	6	0	2.355075	6.230448	-6.247141
229	6	0	3.142807	4.916053	-6.383065
230	6	0	0.983914	6.059427	-6.944988
231	6	0	3.151565	7.359684	-6.944783
232	1	0	3.277464	4.691778	6.003929
233	1	0	1.042988	5.794524	6.631476
234	1	0	1.870778	6.520149	8.026070
235	1	0	0.955312	7.546840	6.910991

236	1	0	4.026339	5.494187	7.390473
237	1	0	4.734817	5.694365	5.783012
238	1	0	4.599941	8.241443	6.085692
239	1	0	3.940843	7.944804	7.708551
240	1	0	3.076144	9.006048	6.585003
241	1	0	2.613698	4.072472	-5.922799
242	1	0	3.272817	4.683871	-7.445779
243	1	0	4.142431	4.989699	-5.937416
244	1	0	0.400081	5.259734	-6.473872
245	1	0	1.140510	5.795347	-7.997340
246	1	0	0.391355	6.980486	-6.915613
247	1	0	3.309890	7.098060	-7.997452
248	1	0	2.618308	8.316309	-6.913696
249	1	0	4.132223	7.497441	-6.474105
250	44	0	7.768285	-1.456057	0.097795
251	7	0	6.141484	-2.573513	0.067424
252	6	0	3.829827	-4.097584	0.029556
253	6	0	5.579349	-2.883156	-1.132684
254	6	0	5.614660	-2.997059	1.249380
255	6	0	4.449318	-3.767061	1.251683
256	6	0	4.410273	-3.645493	-1.173227
257	6	0	6.402484	-2.571405	2.422183
258	6	0	7.994582	-1.676581	4.483474
259	6	0	6.098689	-2.935140	3.737217

260	7	0	7.487073	-1.772671	2.133137
261	6	0	8.258841	-1.341210	3.157451
262	6	0	6.892505	-2.493818	4.809989
263	6	0	6.351053	-2.374212	-2.282763
264	6	0	7.986586	-1.459579	-4.301836
265	7	0	7.485121	-1.667482	-1.955599
266	6	0	6.006548	-2.617586	-3.615917
267	6	0	6.817670	-2.158734	-4.667664
268	6	0	8.283934	-1.235133	-2.959965
269	7	0	9.132083	-3.004223	0.043101
270	6	0	11.121381	-4.964073	-0.110496
271	6	0	8.803769	-4.318166	0.003255
272	6	0	10.452674	-2.641418	0.012185
273	6	0	11.463134	-3.609371	-0.066845
274	6	0	9.767161	-5.324073	-0.072579
275	6	0	10.704705	-1.196467	0.085886
276	6	0	10.971327	1.548271	0.320152
277	7	0	9.579334	-0.415309	0.159679
278	6	0	11.985677	-0.628630	0.109192
279	6	0	12.125033	0.757653	0.221704
280	6	0	9.721873	0.928427	0.286658
281	6	0	2.601456	-4.922618	0.009966
282	7	0	0.267300	-6.536699	-0.009235
283	6	0	2.314652	-5.792093	-1.059593

284	6	0	1.668652	-4.884483	1.062875
285	6	0	0.533237	-5.690189	1.020962
286	6	0	1.159297	-6.567542	-1.036713
287	1	0	0.942308	-7.242950	-1.852519
288	1	0	2.989276	-5.900168	-1.900951
289	1	0	1.797599	-4.223005	1.911719
290	1	0	-0.178168	-5.660559	1.832980
291	1	0	4.039267	-4.128310	2.186356
292	1	0	3.943681	-3.875026	-2.122999
293	1	0	5.104278	-3.173808	-3.833158
294	1	0	9.177488	-0.695767	-2.669509
295	1	0	8.673936	-1.082157	-5.050095
296	1	0	5.239668	-3.566068	3.923626
297	1	0	8.656636	-1.293175	5.251242
298	1	0	9.101231	-0.713372	2.896316
299	1	0	7.750205	-4.561173	0.030280
300	1	0	9.456049	-6.361272	-0.102287
301	1	0	11.894937	-5.721000	-0.172149
302	1	0	12.504736	-3.315965	-0.093345
303	1	0	12.866282	-1.255095	0.046994
304	1	0	13.110479	1.208839	0.240648
305	1	0	11.030863	2.625195	0.421903
306	1	0	8.813235	1.508272	0.370587
307	6	0	6.602501	-2.861158	6.265816

308	6	0	5.358460	-3.755158	6.404618
309	6	0	7.822808	-3.617575	6.845048
310	6	0	6.370474	-1.561131	7.073618
311	6	0	6.484846	-2.396533	-6.141067
312	6	0	5.172652	-3.178381	-6.324116
313	6	0	6.347844	-1.027643	-6.850993
314	6	0	7.636061	-3.201573	-6.791280
315	1	0	4.453136	-3.256573	6.037087
316	1	0	5.506585	-1.007280	6.687233
317	1	0	6.175372	-1.812995	8.122529
318	1	0	7.243559	-0.899891	7.044775
319	1	0	5.200001	-3.987741	7.463358
320	1	0	5.476792	-4.706602	5.871754
321	1	0	8.007887	-4.546429	6.292619
322	1	0	7.629186	-3.874489	7.893009
323	1	0	8.734560	-3.010943	6.812188
324	1	0	4.314504	-2.642265	-5.900345
325	1	0	4.981507	-3.313446	-7.394325
326	1	0	5.223418	-4.175703	-5.870165
327	1	0	5.534741	-0.437008	-6.412433
328	1	0	6.121978	-1.187650	-7.911703
329	1	0	7.270665	-0.440161	-6.790270
330	1	0	7.413455	-3.364523	-7.852190
331	1	0	8.593123	-2.672063	-6.727201

332	1	0	7.751664	-4.180154	-6.310472

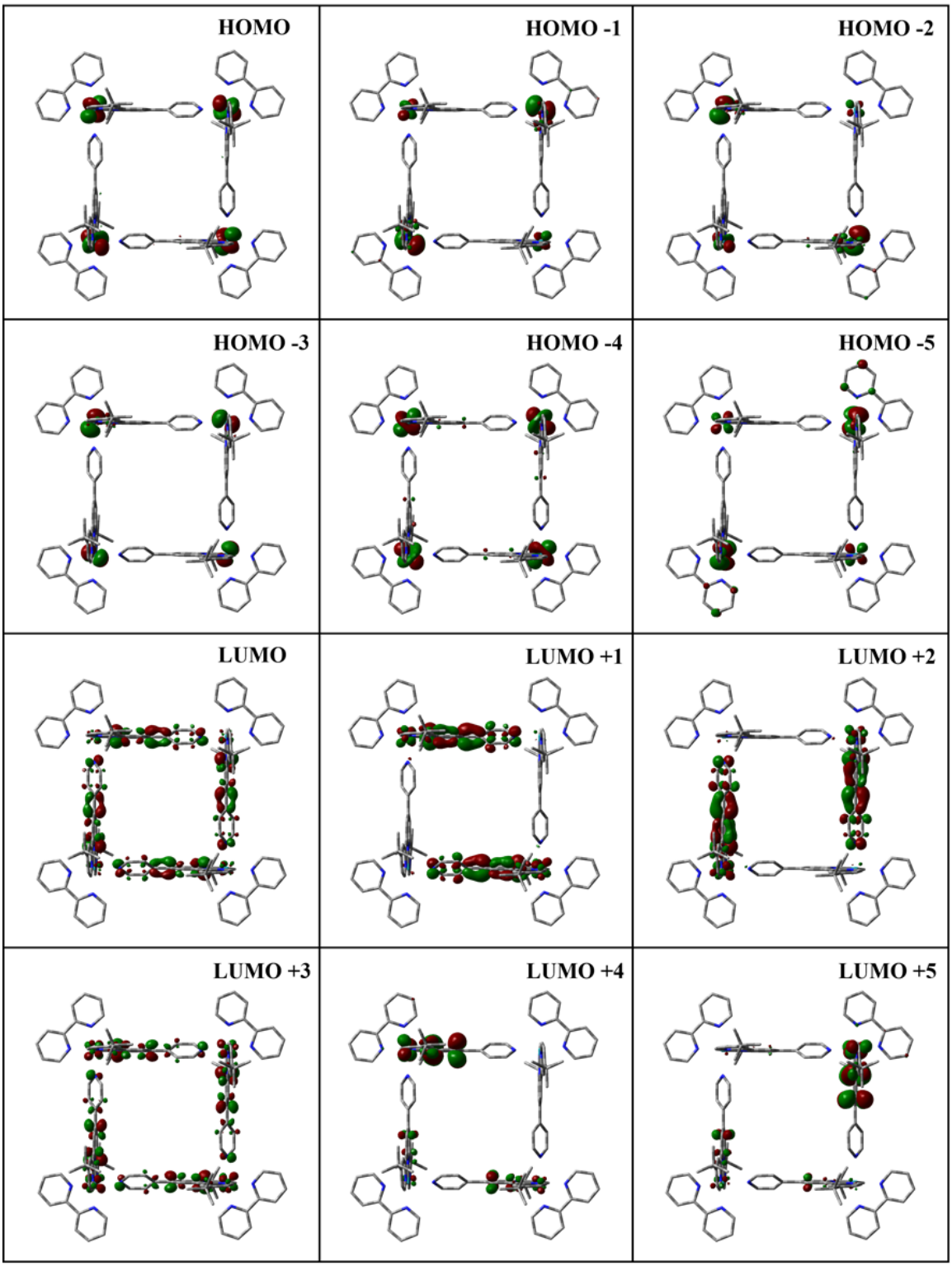

Figure 15.20 - Kohn-Sham electron density illustration of the molecular orbitals for **5** in (*S*=0) the ground-state

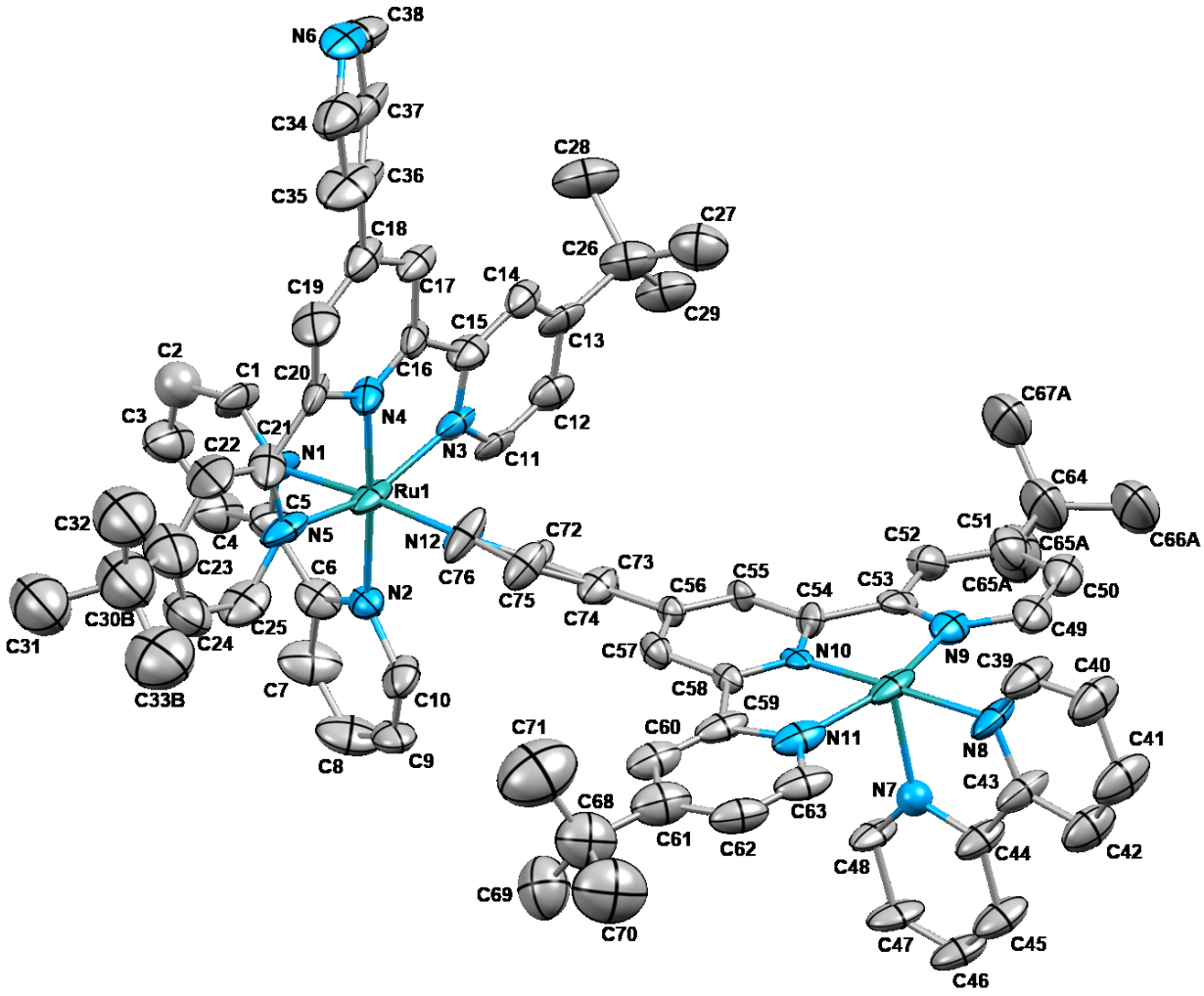

Figure 15.21 - Asymmetric unit of **5** with the numbering of the atoms. The ellipsoids are plot at a 30% probability level. The hydrogen atoms as well as the PF_6 counter-anions have been omitted for clarity.

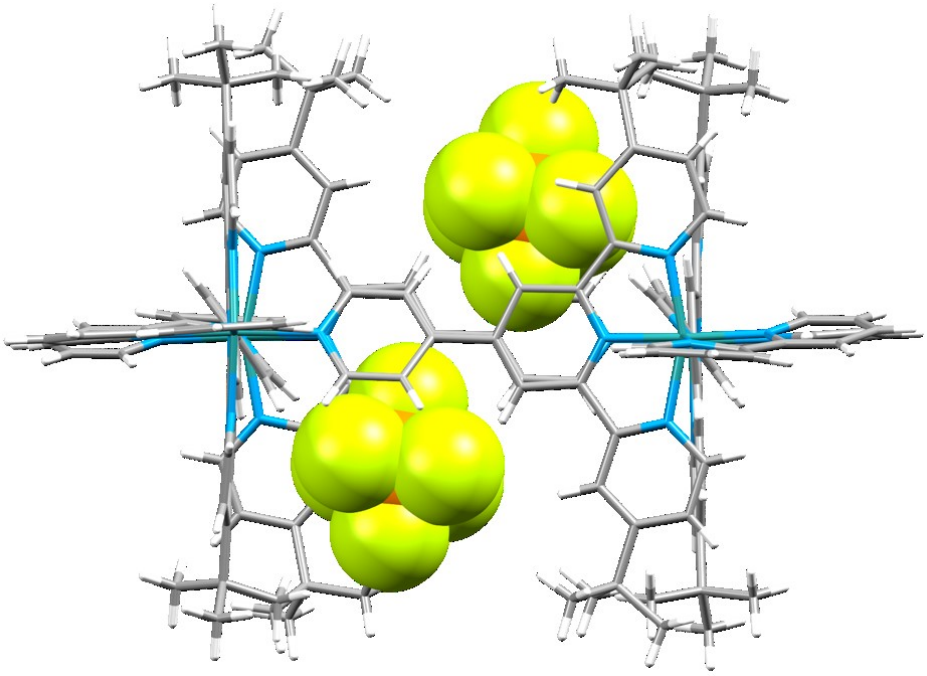

Figure 15.22 - Side view of the molecular square displaying the cavity filled with two PF_6^- counter-anions.

Table 15.11 - Selected bond distances and angles of **5**

Bond Length			Angle		
	Obs. (X-ray)	Calc. (DFT)		Obs. (X-ray)	Calcl. (DFT)
Ru1-N1	2.142(8)	2.06387 2.06378	N1-Ru1-N2	79.0(4)	78.564 78.563
Ru2-N7	2.03(1)	2.06379 2.06392	N7-Ru2-N8	79.5(4)	78.562 78.562
Ru1-N2	2.078(9)	2.08974 2.08991	N3-Ru1-N4	78.6(4)	79.477 79.393
Ru2-N8	2.05(1)	2.08971 2.08994	N4-Ru1-N5	80.6(4)	79.478 79.361
Ru1-N3	2.13(1)	2.08399 2.07895	N9-Ru2-N10	79.3(3)	79.478 79.387
Ru1-N5	2.072(9)	2.08362 2.07752	N10-Ru2-N11	78.8(3)	79.476 79.361
Ru2-N9	2.090(7)	2.08358 2.07893	N3-Ru1-N5	159.2(3)	158.668 158.626
Ru2-N11	2.05(1)	2.08411 2.07738	N9-Ru2-N11	157.9(3)	158.645 158.593
Ru1-N4	1.967(9)	1.97386 1.97388	N4-Ru1-N12	88.7(4)	89.115 89.113
Ru2-N10	1.992(9)	1.97388 1.97385	N6-Ru2-N10	87.3(3)	89.110 89.121
Ru2-N6	2.113(6)	2.11442 2.11563			
Ru1-N12	2.069(9)	2.11444 2.11569			

Table 15.12 - MO composition of **5** in (*S=0*) ground state.

MO	Energy (eV)	Composition (%)		
		Ruthenium	4-pytpy	2,2'-bipyridyl
LUMO+5	-2.858	1	93	6
LUMO+4	-2.858	1	94	5
LUMO+3	-3.168	11	87	1
LUMO+2	-3.259	8	91	1
LUMO+1	-3.264	8	91	1
LUMO	**-3.360**	**3**	**96**	**1**
HOMO	**-6.576**	**72**	**24**	**5**
HOMO-1	-6.613	73	21	6
HOMO-2	-6.615	73	21	6
HOMO-3	-6.625	74	20	6
HOMO-4	-6.721	74	21	5
HOMO-5	-6.805	75	13	12

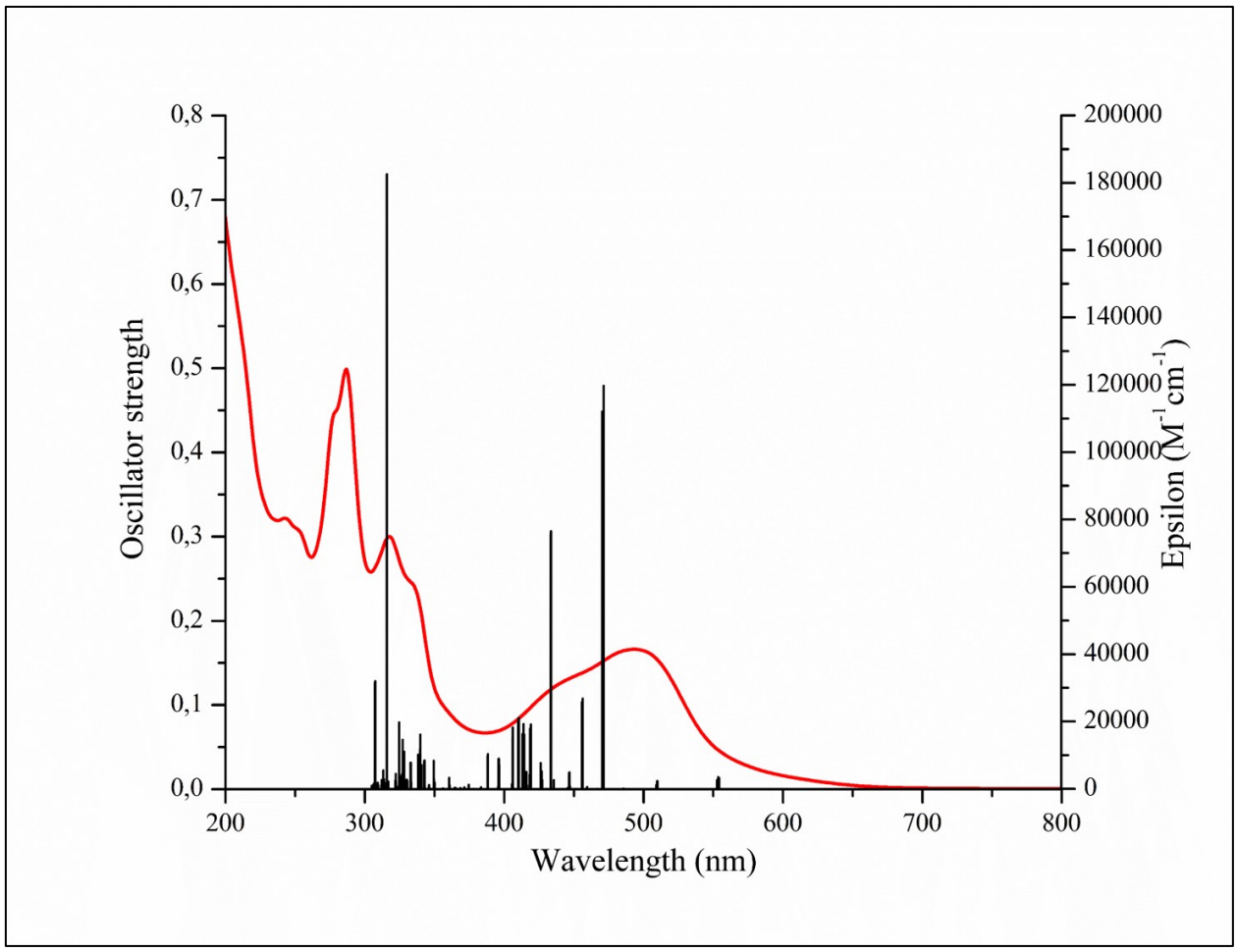

Figure 15.23 - Comparison of the experimental (red) absorption spectra recorded in acetonitrile and TD-DFT (black) simulated (PBE0/LANL2DZ; CPCM: CH3CN) absorption spectrum for the model Ru(II) complex 5.

Table 15.13 - Selected transitions from TD-DFT calculations of **5** in the singlet ground state (PBE0), CPCM (CH_3CN).

Energy (eV)	λ (nm)	f	Transition	Character
2.23	554	0.0130	H-2→L (14%) H-2→L+1 (24%) H-2→L+3 (11%)	
2.23	554	0.0144	H-3→L+1 (16%) H-2→L (10%) H-2→L+1 (16%)	
2.23	553	0.0103	H-1→L (12%) H-1→L+2 (21%)	
2.23	553	0.0111	H-3→L+2 (12%) H-1→L (11%) H-1→L+2 (20%) H-1→L+3 (10%)	$^1MLCT_{tpy}$
2.62	471	0.4792	H-9→L (12%) H→L+1 (20%)	
2.63	470	0.4484	H-10→L (13%) H→L+2 (18%)	
2.70	456	0.1076	H-4→L+1 (13%) H-3→L+1 (10%) H-1→L (11%)	$^1MLCT_{bpy} + {}^1MLCT_{tpy}$
2.71	456	0.1035	H-4→L+2 (12%)	

			H-3→L+2 (10%) H-2→L (11%)	
2.76	447	0.0200	H-1→L+10 (12%) H→L+8 (12%)	
2.95	419	0.0716	H-8→L+2 (11%) H-6→L (11%)	
2.98	414	0.0648	H-1→L (16%) H→L+1 (10%) H→L+2 (10%)	
2.98	414	0.0773	H-2→L (14%) H→L+1 (10%)	
2.99	413	0.0657	H-1→L+1 (12%) H→L (17%)	$^1MLCT_{tpy}$
3.01	410	0.0810	H-8→L+6 (10%)	
3.04	406	0.0732	H-3→L+1 (14%)	
3.04	406	0.0611	H-3→L+2 (13%)	
3.18	388	0.0417	H-10→L (12%) H-5→L (10%) H-4→L+1 (32%)	$^1MLCT_{bpy} + {}^1MLCT_{tpy}$
3.63	340	0.0649	H-3→L+8 (13%) H-1→L+12 (12%) H→L+13 (14%)	
3.63	340	0.0483	H-3→L+9 (18%)	
3.65	338	0.0410	H-3→L+13 (14%)	

3.76	328	0.0445	H-9→L+11 (10%) H-4→L+9 (18%)	$^1MLCT_{bpy}$
3.76	328	0.0418	H-5→L+11 (10%) H-4→L+8 (21%)	
3.77	327	0.0587	H-5→L+11 (22%) H-4→L+14 (11%)	
3.80	325	0.0786	H-11→L+4 (17%) H-10→L+11 (13%) H-4→L+14 (11%)	$^1MLCT_{bpy} + {}^1MLCT_{tpy}$
3.80	325	0.0794	H-11→L+5 (19%) H-4→L+13 (12%)	
3.91	316	0.7304	H-12→L+2 (11%)	$^1MLCT_{tpy} + LLCT_{bpy→tpy}$
4.02	307	0.1283	H-2→L+23 (12%)	$^1MLCT_{bpy} + {}^1MLCT_{tpy}$